Development of Metabolomics Workflows in Clinical Bioanalysis by Ultra-High-Performance Liquid Chromatography Tandem Mass Spectrometry

Dissertation

der Mathematisch-Naturwissenschaftlichen Fakultät

der Eberhard Karls Universität Tübingen

zur Erlangung des Grades eines

Doktors der Naturwissenschaften

(Dr. rer. nat.)

vorgelegt von

Kristian Serafimov

aus Veliko Tarnovo, Bulgarien

Tübingen

2024

Gedruckt mit Genehmigung der Mathematisch-Naturwissenschaftlichen Fakultät der Eberhard Karls Universität Tübingen.

Tag der mündlichen Qualifikation:	06.12.2024
Dekan:	Prof. Dr. Thilo Stehle
1. Berichterstatter/-in:	Prof. Dr. Michael Lämmerhofer
2. Berichterstatter/-in:	Prof. Dr. Stefan Laufer

The research described in this thesis was conducted between November 1st 2020 and November 1st 2024 at the Institute of Pharmaceutical Sciences, Division Pharmaceutical (Bio-)Analysis, Eberhard Karls Universität Tübingen under the supervision of Prof. Dr. Michael Lämmerhofer.

Table of Contents

I. Summary of the Dissertation

Throughout the recent years, the field of metabolomics has seen interest from the life science community, as it is able to provide valuable information about the quantitative and qualitative alterations of endogenous polar metabolites upon specific pertubations. Coupled with the substantial technological innovations in mass spectrometry (MS) over the last decades, MS-based metabolomics has attained the role of a valuable tool in bioanalysis and diagnosis, enabling us to detect the early manifestations of certain diseases and metabolic disorders and their progress. With regard to the bioanalytical aspect, often a tradeoff between sufficient sensitivity (triple quadrupole/linear ion trap systems) and sufficient analyte coverage (hybrid quadrupole time-of-flight QToF systems or Q-orbitrap mass spectrometry systems) is a necessity. QToF and Q-orbitrap systems are the first choice when it comes to broad analyte coverage, as their rapid acquisition rates allow to combine high-resolution mass spectra with the hyphenation to ultra-high-performance liquid chromatography. Along with the introduction of sequential window acquisition of all theoretical fragment ion mass spectra (SWATH), a powerful tool for true comprehensive analysis was made available. Ultra-high-performance liquid chromatography coupled to linear ion trap systems and triple quadrupole mass spectrometry systems on the other hand, provide superior sensitivity and a wider linear ranger, allowing superior accurate quantification while minimizing the risk of possible isobaric interferences from other compounds.

In this thesis, advanced targeted and untargeted MS approaches coupled to liquid chromatography were developed with the aim of obtaining further insight into various biological matrices (cell culture, urine, plasma). In the first project, a targeted approach with wide metabolite coverage was developed for cellular, urinary and plasma metabolomic analysis using a UHPLC-QTrap-MS system operated in the scheduled multiple reaction monitoring (sMRM) mode. In the course of the method development, HeLa cell samples were analyzed via UHPLC-QToF-MS with SWATH acquisition and an updated in-house bioinformatics script transformed the acquired high-resolution MS data to MRM ion pairs for the following targeted QTrap analysis (SWATH-to-MRM). One hundred sixty-one (161) metabolites were successfully detected in ESI^+ mode of the untargeted QToF-MS/MS with SWATH acquisition, whereas 92 were detected in negative ionization mode, totaling to a number of 253 compounds in three different biological matrices covered by the two HILIC methods developed in this study. Both established HILIC-QTrap-MS/MS methods with sMRM acquisition were calibrated and validated based on 105 authentic chemical standards and U-^{13}C-labeled *Pichia pastoris* (*Komagataella phaffii*) yeast extract as internal standard for cellular matrix (HeLa cells).

Further work was conducted to extend the metabolite coverage. Sugar phosphates are a set of specific metabolites, which play a crucial role in the pentose phosphate and glycolysis pathways. From an analytical perspective, these metabolites cause problems due to their multiple negatively charged phosphate groups, high hydrophilicity, poor chromatographic performance and numerous isomers. For this reason, there were no good accurate methods available that could have coped with our requirement of comprehensive accurate analysis of all isomers with adequate assay specificity. Chromatographic conditions were evaluated with the aim of achieving separation of the isomeric glycolytic phosphorylated carbohydrate metabolites free from isomeric interferences and thus allowing for selective targeted analysis by liquid chromatography with tandem mass spectrometry (MS/MS) using multiple reaction monitoring acquisition. Separation of 7 biologically relevant hexose monophosphate metabolites turned out to be challenging by HILIC-MS/MS, with the Waters Premier Acquity BEH Amide providing the best individual results for such a separation. However, fructose 6-phosphate and glucose 1-phosphate co-eluted. Therefore, an on-line heart-cutting HILIC-Mixed Mode 2D-LC-QToF method was developed, allowing the separation of this critical isomer pair. In this setup, the BEH Amide column in the first dimension (^{1}D) separated the majority of target metabolites, while a heart-cut of the peak from totally coeluted fructose 6-phosphate and glucose 1-phosphate was separated in the second

dimension (^{2}D) with a HILICpak VT50-2D column, thus allowing undisturbed determination of the glycolytic phosphorylated carbohydrate metabolites due to their chromatographic separation from hexose monophosphate metabolites.

In the third project of this thesis, the redox-active thiol metabolites related to the glutathione (GSH) pathway were the focal point of method development for extending the metabolite coverage. Glutathione, its biosynthesis intermediates and other thiol metabolites are of central relevance for the redox homeostasis of cells. Their analysis is critical due to the rapid interconversion of redox pairs during sampling, sample preparation, and data acquisition, in particular in the electrospray ionization interface. In this study, a fast, targeted LC-MS/MS method was developed with the aim to accurately quantify 14 metabolites from the glutathione pathway for monitoring metabolite alterations in the course of ferroptosis, a kind of an iron-dependent programmed cell death in which glutathione depletion plays a role. Derivatization of free thiols with N-ethylmaleimide during the extraction step instantly stabilized the thiol-redox state in a Michael-Addition type of reaction. Liquid chromatographic separation of the analytes was performed on a sub-2µm superficially porous HILIC column with sulfobetaine chemistry. Tandem MS with triple-quadrupole mass spectrometry in multiple-reaction monitoring acquisition mode allowed sensitive detection of the targeted metabolites and run times of 2.5 min enable a high throughput analysis of cellular samples. A ^{13}C-labelled cell extract was used as internal standard, strengthening the performance of the developed assay.

The next project in this thesis elaborated on the retention time repeatability issue of polar metabolites in HILIC. Various studies have pointed out the poor retention time repeatability of HILIC, which has often been attributed to the insufficient re-equilibration time at the end of each gradient elution chromatographic run to establish the sensitive semi-immobilized water layer at the interface of the polar stationary phase and the bulk mobile phase. In the course of this study it was demonstrated that the poor retention time repeatability in HILIC is caused by the use of for borosilicate glass solvent bottles. Their replacement by PFA (co-polymer of tetrafluoroethylene and perfluoroalkoxyethylene) solvent bottles drastically improved the retention time repeatability. A characteristic pattern was observed in peak retention time behavior shifting towards higher retention times for metabolites with progressing analysis time when standard borosilicate glass bottles were used as solvent reservoirs. Hypothesis for this phenomenon was that release of ions (sodium, potassium, borate, etc.) from the borosilicate glass bottles leads up to alterations in the semi-immobilized water layer

which is adsorbed to the polar stationary phase surface under acetonitrile-rich eluents in HILIC. With increasing time more ions are accumulated in this water layer which leads to a thickening and hence increase of the phase ratio, thus higher retention of polar analytes. By exchanging the borosilicate glass bottles with PFA solvent bottles retention time repeatability was significantly improved and changed from an average of 8.4% RSD for the tested metabolites with borosilicate glass bottles to 0.14% RSD for the PFA solvent bottles (30 injections over 12h).

Since above sugar phosphate method showed suboptimal performance and was technically complex in its setup, thus not suitable for clinical analysis of a larger number of samples, another study focused again on the development of a HILIC-UHPLC-MS/MS assay to comprehensively cover all sugar phosphate derivatives relevant to the pentose phosphate and glycolysis pathways. The aim was to optimize the chromatographic separation of these metabolites and allowing their selective and reliable quantification, without the interference of any isomeric compounds. The developed method involved the usage of a BEH Amide column with polymer-coated hardware employing HILIC in alkaline conditions (pH 11) at high ammonium formate concentrations. Quantification of 24 metabolites relevant to these pathways was achieved and a ^{13}C-labelled cell extract was used as internal standard. After validation, application was demonstrated in HeLa cell samples and in HEK293 samples, where ferroptosis was catalyted via Erastin, which acts as an inhibitor of the glutamate/cystine antiporter system (system XC^-). As a result, fructose-1,6-bis-phosphates, 2,3-bis-phosphoglycerate, 2- and 3-phosphoglycerate were upregulated compared to controls.

A further urinary metabolomics project involved the analysis of patient samples with Alkaptonuria. Alkaptonuria (AKU) is a rare autosomal-recessive disease which is characterized through black urine and ochronosis. It is caused by deficiency of the enzyme Homogentisate 1,2-dioxygenase in the Phenylalanine/Tyrosine degradation pathway which leads to the accumulation of Homogentisic acid (HGA). Urine was provided by AKU patients and healthy controls. Several different methods were developed in this study each with a specific goal: 1) A simple and inexpensive UHPLC-UV method for routine monitoring of HGA as a key metabolite employing a Phenylhexyl stationary phase chemistry. Validation was performed in accordance to FDA guidelines and method selectivity was further evaluated via on-line high-resolution sampling 2D-LC-QToF-MS, coupling the Phenylhexyl phase in the first dimension with a C18 phase in the second dimension. 2) A targeted and accurate UHPLC-MRM-QTrap method, providing quantitative analysis of the relevant pathway metabolites based on a

Phenylhexyl stationary phase, and 3) an untargeted HILIC-UHPLC-QToF-MS/MS with SWATH acquisition employing a HILIC-Z superficially porous particle column, with the aim of uncovering more details about the metabolic profile of this genetic disorder. Untargeted analysis allowed to annotate 204 metabolites detected in positive and negative ESI mode in total. By combining the aforementioned methods, a comprehensive workflow was developed, allowing the effective analysis of both patient and control urine samples.

II. Zusammenfassung

In den letzten Jahren stand das Gebiet von Metabolomics im Mittelpunkt des anhaltenden Interesses in den Biowissenschaften, da es wertvolle Informationen über die Veränderungen von quantitativen und qualitativen Aspekten endogener polarer Metabolite liefern kann. In Verbindung mit den erheblichen technologischen Innovationen in der Massenspektrometrie (MS) in den letzten Jahrzehnten ist Metabolomics zu einer wertvollen Technik geworden, mit der wir die frühen Manifestationen bestimmter Krankheiten und Stoffwechselstörungen sowie deren Verlauf erkennen können. Im Hinblick auf bioanalytischen Anwendungen ist oft ein Kompromiss zwischen ausreichender Empfindlichkeit (Triple-Quadrupol-/Linear-Ionenfallen-MS-Systeme) und ausreichender Analytabdeckung (Hybrid-Quadrupol-Flugzeit-QToF-Systeme oder Q-Orbitrap-MS-Systeme) erforderlich. QToF- und Q-Orbitrap-MS-Systeme sind die erste Wahl, wenn es um eine breite Analytabdeckung geht, da ihre schnellen Erfassungsraten es ermöglichen, hochauflösende Massenspektren mit der Kopplung an die Ultrahochleistungsflüssigkeitschromatographie zu kombinieren. Mit der Einführung der sequentiellen Fenstererfassung aller theoretischen Fragmentionen-Massenspektren (SWATH) wurde ein leistungsstarkes Werkzeug für eine umfassende Analyse verfügbar gemacht. Lineare Ionenfallen MS-Systeme und Triple-Quadrupol-MS-Systeme bieten dagegen eine überlegene Empfindlichkeit und einen weiteren linearen Bereich. Sie haben Vorteile bei der genauen Quantifizierung. Durch Kopplung an eine Hochleistungsflüssigkeitschromatographie sowie durch spezifische Ionenübergänge wird Assayspezifität gewährleistet und so können mögliche Interferenzen durch andere Verbindungen vermieden werden.

In dieser Arbeit wurden targeted und untargeted MS-Assays in Verbindung mit Flüssigkeitschromatographie entwickelt, um polare Metabolite in verschiedenen

biologischen Proben (Zellkultur, Urin, Plasma) zu bestimmen. Im Laufe des ersten Projekts wurde ein targeted UHPLC-MS/MS Assay mit breiter Metabolitenabdeckung für die zelluläre, Urin- und Plasmametabolomanalyse entwickelt, wobei ein UHPLC-QTrap-MS-System verwendet wurde, das im Multiple-Reaction-Monitoring-Modus (sMRM) betrieben wurde. HeLa-Zellproben wurden zuerst mit untargeted UHPLC-QToF-MS mit SWATH-Erfassung analysiert, und ein aktualisiertes internes Bioinformatik-Skript wandelte die erfassten hochauflösenden MS-Daten in MRM-Ionenpaare für die folgende targeted QTrap-Analyse um. Einhunderteinundsechzig (161) Metaboliten wurden erfolgreich im ESI^+-Modus mittels der untargeted UHPLC-QToF-MS Methode annotiert, während 92 im negativen Ionisierungsmodus annotiert werden konnten, was insgesamt eine Anzahl von 253 Verbindungen in drei verschiedenen biologischen Systemen ergibt, die von den beiden in dieser Studie entwickelten HILIC-Methoden abgedeckt werden. Beide etablierten HILIC-MS/MS Methoden wurden mittels 105 authentischen chemischen Standards und U-^{13}C-markiertem Hefeextrakt von *Pichia pastoris* (*Komagataella phaffii*) als internem Standard für die Zellmatrix (HeLa-Zellen) kalibriert und validiert.

Um die Metabolitenabdeckung zu erweitern, wurden weitere Methoden entwickelt. Zuckerphosphate sind eine Reihe spezifischer Metaboliten, die eine entscheidende Rolle im Glykolyse- und Pentosephosphatweg spielen. Aus analytischer Sicht bereiten diese Metaboliten aufgrund ihrer mehrfach negativ geladenen Phosphatgruppen, ihrer hohen Hydrophilie, ihrer schlechten chromatographischen Performance und ihrer zahlreichen Isomere Probleme. Aus diesem Grund standen keine guten und akkuraten LC-MS/MS Methoden zur Verfügung, die unseren Anforderungen einer umfassenden, genauen Analyse aller Isomere mit angemessener Assay-Spezifität hätten gerecht werden können. Daher wurden verschiedene chromatographischen Bedingungen evaluiert mit dem Ziel eine Trennung der isomeren phosphorylierten Kohlenhydratmetaboliten von Glykolyse und Pentosephosphat Weg mit adäquater Assay Spezifität frei von isomeren Interferenzen zu erreichen und so eine selektive Analyse durch Flüssigkeitschromatographie mit Tandem-Massenspektrometrie (MS/MS) zu ermöglichen. Die Trennung von 7 biologisch relevanten Hexosemonophosphat-Metaboliten erwies sich mittels HILIC-MS/MS als schwierig, wobei die Premier Acquity BEH Amid Säule die besten Einzelergebnisse für eine solche Trennung lieferte. Allerdings wurden Fructose-6-phosphat und Glucose-1-phosphat gemeinsam eluiert. Daher wurde eine Online-Heart-Cutting-HILIC-Mixed-Mode-2D-LC-QToF-Methode entwickelt, welche die Trennung dieses kritischen Isomerenpaars in

einer 2. Trenndimension ermöglichte. In diesem Aufbau trennte die BEH-Amid-Säule in der ersten Dimension (1D) die Mehrheit der Zielmetaboliten, während ein Heart-Cut des Peaks aus vollständig gemeinsam eluiertem Fructose-6-phosphat und Glucose-1-phosphat in der zweiten Dimension (2D) mit einer HILICpak VT50-2D-Säule getrennt wurde, wodurch eine ungestörte Bestimmung der phosphorylierten Kohlenhydratmetaboliten der Glykolyse aufgrund ihrer chromatographischen Trennung von den Hexosemonophosphat-Metaboliten ermöglicht wurde.

Im dritten Projekt dieser Arbeit standen die redoxaktiven Thiolmetaboliten im Mittelpunkt, die mit dem Glutathionstoffwechselweg (GSH) in Zusammenhang stehen. Glutathion, seine Biosynthesezwischenprodukte und andere Thiolmetaboliten sind von zentraler Bedeutung für die Redoxhomöostase von Zellen. Ihre Analyse ist aufgrund der schnellen Umwandlung von Redoxpaaren während der Probenentnahme, Probenvorbereitung und Datenerfassung, insbesondere an der Schnittstelle der Elektrospray-Ionisation, problematisch. In dieser Studie wurde eine schnelle LC-MS/MS-Methode entwickelt, um 14 Metabolite aus dem Glutathionstoffwechselweg genau zu quantifizieren. Die Derivatisierung von Thiolmetaboliten mit N-Ethylmaleimid während des Extraktionsschritts stabilisierte den Thiol-Redoxzustand durch eine Michael-Additionsreaktion. Die flüssigchromatographische Trennung der Analyten erfolgte auf einer HILIC-Säule mit Sulfobetainchemie. Tandem-MS mit Triple-Quadrupol-Massenspektrometrie im MRM-Modus ermöglichte eine empfindliche Erkennung der Zielmetaboliten mit kurzen Laufzeiten um einen Hochdurchsatz zu erreichen. Ein U-^{13}C-markierter Zellextrakt wurde als interner Standard verwendet, was die analytische Leistung des entwickelten Tests verbesserte.

Das nächste Projekt dieser Arbeit befasste sich mit dem Problem der Wiederholbarkeit der Retentionszeit von polaren Metaboliten in HILIC. Verschiedene Studien haben auf die schlechte Wiederholbarkeit der Retentionszeit von HILIC hingewiesen, die oft auf die unzureichende Re-Equilibrationszeit am Ende jedes chromatographischen Laufs zurückgeführt wurde, um die empfindliche Wasserschicht an der Schnittstelle der polaren stationären Phase und der mobilen Phase aufzubauen. Im Verlauf dieser Studie wurde ein Vergleich zwischen der Wiederholbarkeit der Retentionszeit in HILIC für Lösungsmittelflaschen aus Borosilikatglas und PFA (Copolymer aus Tetrafluorethylen und Perfluoralkoxyethylen) durchgeführt. Bei Verwendung von Standard-Borosilikatglasflaschen als Lösungsmittelreservoirs wurde ein signifikanter Retentionszeit-Shift von polaren Metaboliten mit fortschreitender Analysezeit zu längerer Retentionszeit beobachtet. Die Hypothese für dieses Phänomen war, dass die

Freisetzung von Ionen (Natrium, Kalium, Borat usw.) aus den Borosilikatglasflaschen zu Veränderungen in der semiimmobilisierten Wasserschicht führt, die unter acetonitrilreichen Eluenten in HILIC an der polaren Oberfläche der stationären Phase adsorbiert wird. Die Ionen aus den Borosilikatglasflaschen reichern sich in der semi-immobilisierten Wasserschicht zunehmends an. Dadurch wird diese Wasserschicht dicker und das Phasenverhältnis größer, was zu zunehmender Retention führt. Durch Austausch der Borosilikatglasflaschen gegen PFA-Lösungsmittelflaschen konnte die Wiederholbarkeit der Retentionszeit deutlich verbessert und von durchschnittlich 8,4 % RSD für die getesteten Metaboliten mit Borosilikatglasflaschen auf 0,14 % RSD mit den PFA-Lösungsmittelflaschen (30 Injektionen über 12 Stunden) verringert werden. Ähnliche Verbesserungen wurden bei Peptiden und Oligonukleotiden beobachtet.

Im weiteren Verlauf der Doktorareit wurde eine verbesserte akkurate quantitative Methode für Zuckerphosphatderivate, die aus dem Pentosephosphat- und Glykolyseweg, entwickelt. Die Arbeit wurde mit dem Ziel fortgesetzt, die chromatographische Trennung dieser Metabolite zu optimieren, d.h. das starke Peaktailing zu reduzieren und die Auftrennung zwischen den Zuckerphosphat-Isomeren zu verbessern. Ausserdem sollte eine selektive und zuverlässige Quantifizierung ohne Interferenz von isomeren Verbindungen aus anderen Pathways (Mannose und Lactose Metabolismus) ermöglicht werden. Augenmerk wurde in dem Zusammenhang auch auf eine geeignete Probenvorbereitung gelegt. Die entwickelte Methode beinhaltete die Verwendung einer BEH-Amidsäule unter alkalischen HILIC Bedingungen. Die Probenvorbereitung basierte auf einer sauren Metalloxid-Affinitätsextraktion mit TiO_2 beads. Es wurde eine Quantifizierung von 24 für diese Wege relevanten Metaboliten erreicht und ein ^{13}C-markierter Zellextrakt wurde als interner Standard verwendet. Nach der Validierung wurde die Anwendbarkeit in HeLa-Zellproben demonstriert und in HEK293-Zellproben, wo Ferroptose exprimiert wurde mittels Erastin, was als Inhibitor von dem Glutamat/Cystin Antiportersystem (system XC^-) funktioniert.

Ein weiteres Projekt umfasste die Analyse von Patientenproben mit Alkaptonurie. Alkaptonurie (AKU) ist eine seltene autosomal-rezessive Erkrankung, die durch schwarzen Urin und Ochronose gekennzeichnet ist. Ursache ist ein Mangel des Enzyms Homogentisat-1,2-Dioxygenase im Phenylalanin/Tyrosin-Abbauprozess, der zur Ansammlung von Homogentisinsäure (HGA) führt. Der Urin wurde von AKU-Patienten und gesunden Kontrollpersonen bereitgestellt. In dieser Studie wurden mehrere verschiedene Methoden entwickelt, jede mit einem bestimmten Ziel: 1) Eine

einfache und kostengünstige UHPLC-UV-Methode zur routinemäßigen Überwachung von HGA als Schlüsselmetabolit unter Verwendung einer Phenylhexyl-Stationärphasenchemie. Die Validierung erfolgte gemäß den FDA-Richtlinien und die Methodenselektivität wurde zusätzlich durch Online-Sampling mit 2D-LC-QToF-MS bewertet, wobei die Phenylhexyl-Phase in der ersten Dimension mit einer C18-Phase in der zweiten Dimension gekoppelt wurde. 2) Eine UHPLC-MRM-QTrap-Methode, die eine quantitative Analyse der relevanten Stoffwechselwegmetaboliten auf der Grundlage einer stationären Phenylhexylphase ermöglicht, und 3) eine HILIC-UHPLC-QToF-MS/MS Methode mit SWATH-Erfassung unter Verwendung einer HILIC-Z-Säule mit oberflächlich porösen Partikeln, mit dem Ziel, mehr Details über das Stoffwechselprofil dieser genetischen Störung aufzudecken. Durch die untargeted UHPLC-QToF-MS/MS Analytik konnten insgesamt 204 Metaboliten annotiert werden, die im positiven und negativen ESI-Modus erkannt wurden. Durch die Kombination der oben genannten Methoden wurde ein Workflow entwickelt, der die effektive Analyse von Patienten- und Kontrollurinproben ermöglicht.

III. List of publications

Publication I

Serafimov, K.; Lämmerhofer, M. Metabolic profiling workflow for urine, plasma and cell extracts by targeted hydrophilic interaction liquid chromatography-tandem mass spectrometry. J. Chromatogr. A, 1684 (2022) 463556, DOI: 10.1016/j.chroma.2022.463556.

Publication II

Su, M.; Serafimov, K.; Li, P.; Knappe, C.; Lämmerhofer, M. Isomer selectivity of mixed-mode and hydrophilic interaction liquid chromatography coupled to tandem mass spectrometry for sugar phosphates of glycolysis and pentose phosphate pathways. J. Chromatogr. A, (2022) 463727, DOI: 10.1016/j.chroma.2022.463727.

Publication III

Serafimov, K.; Aydin, Y.; Lämmerhofer, M. Quantitative analysis of the glutathione pathway cellular metabolites by targeted liquid chromatography-tandem mass spectrometry. J. Sep. Sci., (2023), DOI: 10.1002/jssc.202300780

Publication IV

Serafimov K, Knappe C, Li F, Sievers-Engler A, Lämmerhofer M. Solving the retention time repeatability problem of hydrophilic interaction liquid chromatography. J Chromatogr A. 2024 Aug 16;1730:465060. doi: 10.1016/j.chroma.2024.465060

Publication V

Serafimov K, Lämmerhofer M. Comprehensive coverage of glycolysis and pentose phosphate metabolic pathways by isomer-selective accurate targeted hydrophilic interaction liquid chromatography-tandem mass spectrometry assay. Anal. Chem. 2024 Article ASAP. doi: 10.1021/acs.analchem.4c03490

IV. Manuscripts currently under revision/to be published

Publication VI

Serafimov, K., Tischlarik, J-R., Lämmerhofer, M. Targeted and untargeted urinary metabolomics of alkaptonuria patients using ultra high-performance liquid chromatography-tandem mass spectrometry

V. Author contributions

Publication I

Metabolic profiling workflow for urine, plasma and cell extracts by targeted hydrophilic interaction liquid chromatography-tandem mass spectrometry.

Kristian Serafimov:

General idea generation

Method development

Sample preparation and analysis

Data processing and interpretation

Main writing of the manuscript

Prof. Dr. Michael Lämmerhofer:

Generation, initiation, coordination and financing of the project

Discussion of results and interpretation

Partial writing and editing of the manuscript

Proofreading and final approval of the manuscript

Corresponding Author

Publication II

Isomer selectivity of mixed-mode and hydrophilic interaction liquid chromatography coupled to tandem mass spectrometry for sugar phosphates of glycolysis and pentose phosphate pathways.

Min Su:

Method development

Sample preparation and analysis

Data processing and interpretation

Main writing of the manuscript

Kristian Serafimov:

Method development

Sample preparation and analysis

Data processing and interpretation

Main writing of the manuscript

Prof. Dr. Michael Lämmerhofer:

Generation, initiation, coordination and financing of the project

Discussion of results and interpretation

Partial writing and editing of the manuscript

Proofreading and final approval of the manuscript

Corresponding Author

Publication III

Quantitative analysis of the glutathione pathway cellular metabolites by targeted liquid chromatography-tandem mass spectrometry.

Kristian Serafimov:

General idea generation

Method development

Sample preparation and analysis

Data processing and interpretation

Main writing of the manuscript

Yüsra Aydin

Sample preparation and analysis

Data processing and interpretation

Prof. Dr. Michael Lämmerhofer:

Generation, initiation, coordination and financing of the project

Discussion of results and interpretation

Partial writing and editing of the manuscript

Proofreading and final approval of the manuscript

Corresponding Author

Publication IV

Solving the retention time repeatability problem of hydrophilic interaction liquid chromatography

Kristian Serafimov:

General idea generation

Method development

Sample preparation and analysis

Data processing and interpretation

Main writing of the manuscript

Cornelius Knappe:

General idea generation

Method development

Sample preparation and analysis

Data processing and interpretation

Main writing of the manuscript

Fei-Yang Li:

Sample preparation and analysis

Data processing and interpretation

Adrian Sievers-Engler:

Discussion of results and interpretation

Proofreading and approval of the manuscript

Prof. Dr. Michael Lämmerhofer:

Generation, initiation, coordination and financing of the project

Discussion of results and interpretation

Partial writing and editing of the manuscript

Proofreading and final approval of the manuscript

Corresponding Author

Publication V

Comprehensive coverage of glycolysis and pentose phosphate metabolic pathways by isomer-selective accurate targeted hydrophilic interaction liquid chromatography-tandem mass spectrometry assay

Kristian Serafimov:

General idea generation

Method development

Sample preparation and analysis

Data processing and interpretation

Main writing of the manuscript

Prof. Dr. Michael Lämmerhofer:

Generation, initiation, coordination and financing of the project

Discussion of results and interpretation

Partial writing and editing of the manuscript

Proofreading and final approval of the manuscript

Corresponding Author

Publication VI

Targeted and untargeted urinary metabolomics of alkaptonuria patients using ultra high-performance liquid chromatography-tandem mass spectrometry

Kristian Serafimov:

General idea generation

Method development

Sample preparation and analysis

Data processing and interpretation

Main writing of the manuscript

Johanna-Ruth Tischlarik

Sample preparation and analysis

Data processing and interpretation

Prof. Dr. Michael Lämmerhofer:

Generation, initiation, coordination and financing of the project

Discussion of results and interpretation

Partial writing and editing of the manuscript

Proofreading and final approval of the manuscript

Corresponding Author

VI. Poster Presentations

Advances in Chromatography and Electrophoresis Chiranal 2022, Olomouc, Czech Republic, June 13th – 16th.

Targeted metabolic profiling workflow for urine, plasma and cell extracts by hydrophilic interaction liquid chromatography mass spectrometry.

Kristian Serafimov, Michael Lämmerhofer

International Symposium on Chromatography (ISC) 2022, Budapest, Hungary, September 18th –22nd.

Targeted metabolic profiling workflow for urine, plasma and cell extracts by hydrophilic interaction liquid chromatography tandem mass spectrometry.

Kristian Serafimov, Michael Lämmerhofer

HPLC 2023, Düsseldorf, Germany, June 18th – 22nd.

Analysis of urine samples of patients with alkaptonuria by targeted and untargeted ultra-high-performance liquid chromatography-tandem mass spectrometry

Kristian Serafimov, Michael Lämmerhofer

International Symposium on Separation Sciences (ISSS) 2023, Cluj-Napoca, Romania, September 24th – 27th.

Targeted metabolic profiling workflow for urine, plasma and cell extracts by hydrophilic interaction liquid chromatography mass spectrometry.

Kristian Serafimov, Michael Lämmerhofer awarded with a Best Poster Award

DPhG (German Pharmaceutical Society) Annual Meeting 2023, Tübingen, Germany, October 7th – 10th.

Analysis of urine samples of patients with alkaptonuria by targeted and untargeted ultra-high-performance liquid chromatography-tandem mass spectrometry

Kristian Serafimov, Michael Lämmerhofer

International Symposium on Chromatography (ISC) 2022, Liverpool, United Kingdom, October 6th –10th.

Comprehensive coverage of glycolysis and pentose phosphate metabolic pathways by isomer-selective accurate targeted hydrophilic interaction liquid chromatography-tandem mass spectrometry assay

Kristian Serafimov, Michael Lämmerhofer

VII. Oral Presentations

Metabolomics Society Annual Meeting 2024, Osaka, Japan, June 16th – 20th.

Comprehensive coverage of glycolysis and pentose phosphate metabolic pathways by isomer-selective targeted hydrophilic interaction liquid chromatography tandem mass spectrometry

Kristian Serafimov, Michael Lämmerhofer

VIII. Abbreviations

2D-LC	Two-dimensional liquid chromatography
AAPS	American Association of Pharmaceutical Scientists
ACN	Acetonitrile
ADC	Analog-to-digital converter
AIF	All-ion-fragmentation
APCI	Atmospheric pressure chemical ionization
CCS	Collisional cross section
CE	Collision energy
CEM	Channel electron multiplier
cps	Counts per second
DDA	Data-dependent acquisition
DP	Declustering potential
EIC	Extracted ion chromatogram

ESI	Electrospray ionization
FDA	United States Food and Drug Administration
FT-ICR	Fourier transform ion cyclotron resonance
fwhm	Full width at half maximum
HILIC	Hydrophilic interaction liquid chromatography
HR	High resolution
Hz	Hertz
IDA	Information-dependent acquisition (Sciex term for DDA)
IMS	Ion mobility spectrometry
IPA	Isopropanol
IRD	Ion release delays
IRW	Ion release width
IS	Internal standard
ITC	Ion transmission control
LC	Liquid chromatography
LLOQ	Lower limit of quantification
MeOH	Methanol
MRM	Multiple Reaction Monitoring
MS	Mass Spectrometry
MS/MS	Free fatty acid
MS-DIAL	Mass Spectrometry Data-Independent Analysis
NMR	Nuclear Magnetic Resonance
PCA	Principal Component Analysis
PG	Phosphatidylglycerole
ppm	Parts per Million
QC	Quality Control

QqQ	Triple Quadrupole
QToF	Quadrupole Time-of-Flight
RP	Reversed Phase
S/N	Signal to Noise
SD	Standard Deviation
SRM	Selected Reaction Monitoring
TIC	Total Ion Current
t_R	Retention Time
UHPLC	Ultra-high-performance liquid chromatography
ULOQ	Upper Limit of Quantification
XIC	Extracted Ion Chromatogram (Sciex term for EIC)

1. Introduction

1.1. Metabolomics

Metabolomics deals with the analysis of metabolites, which are biologically present small molecules, with a molecular weight up to 1500 Da. Metabolites are extremely diverse, with various classes such as amino acids, lipids, sugars, organic acids, phosphorylated analytes (sugar phosphates, nucleotides) present in every biological system. Metabolomics as a study, focuses on the biochemical entirety in a system, aiming to analyze all features at a system-wide level. Analytical chemistry constantly develops at fast pace with respect to in both hard- and software aspects. Metabolomics' role in the study of biological systems greatly benefits from this development and has become extremely popular, which is evident by annually increasing research work published in this field (**Figure 1**)

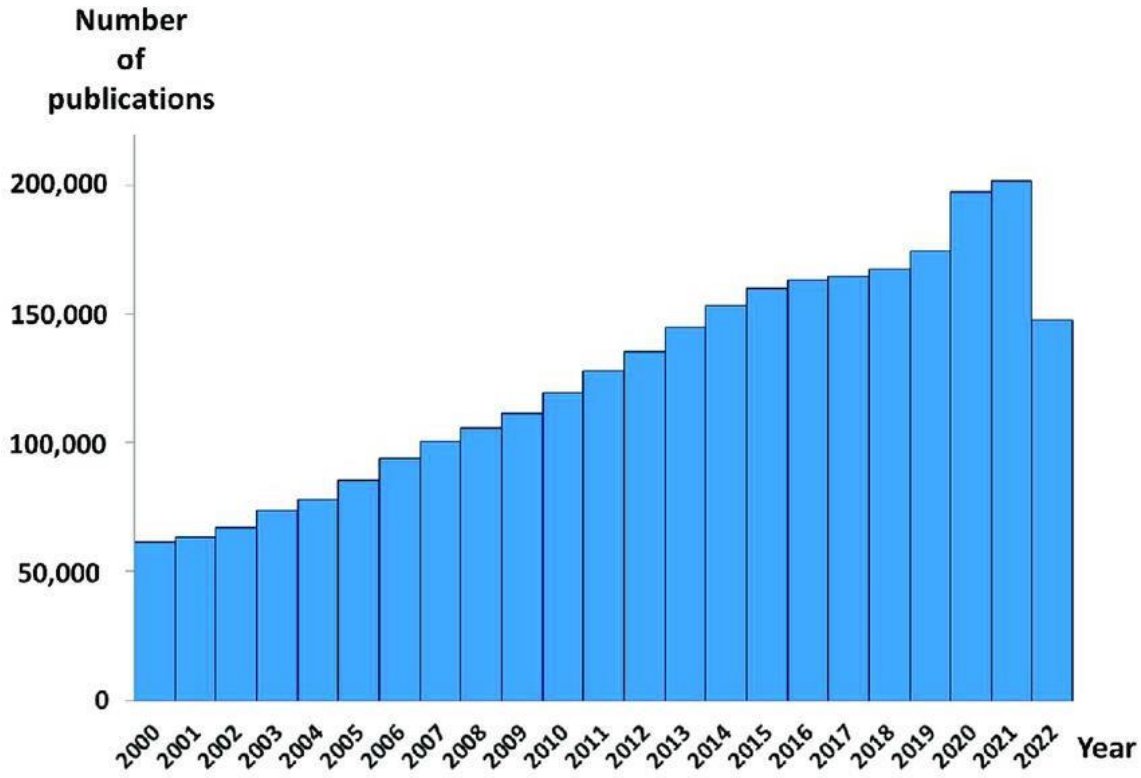

Figure 1*:* Current trend in research articles published belonging to the field of metabolomics. [**Trifonova OP, Maslov DL, Balashova EE, Lokhov PG. Current State and Future Perspectives on Personalized Metabolomics. Metabolites. 2023 Jan 1;13(1):67. doi: 10.3390/metabo13010067.]**

Metabolomics possesses the ability to reveal alterations in certain metabolic pathways under specific case-control conditions, pertubations or disorders, which makes it a powerful tool in hypothesis generation. This, however, is challenging, as one can see from **Figure 2** the sheer complexity of a biological system, coupled with the fact that the concentration ranges from metabolite to metabolite vary immensely.

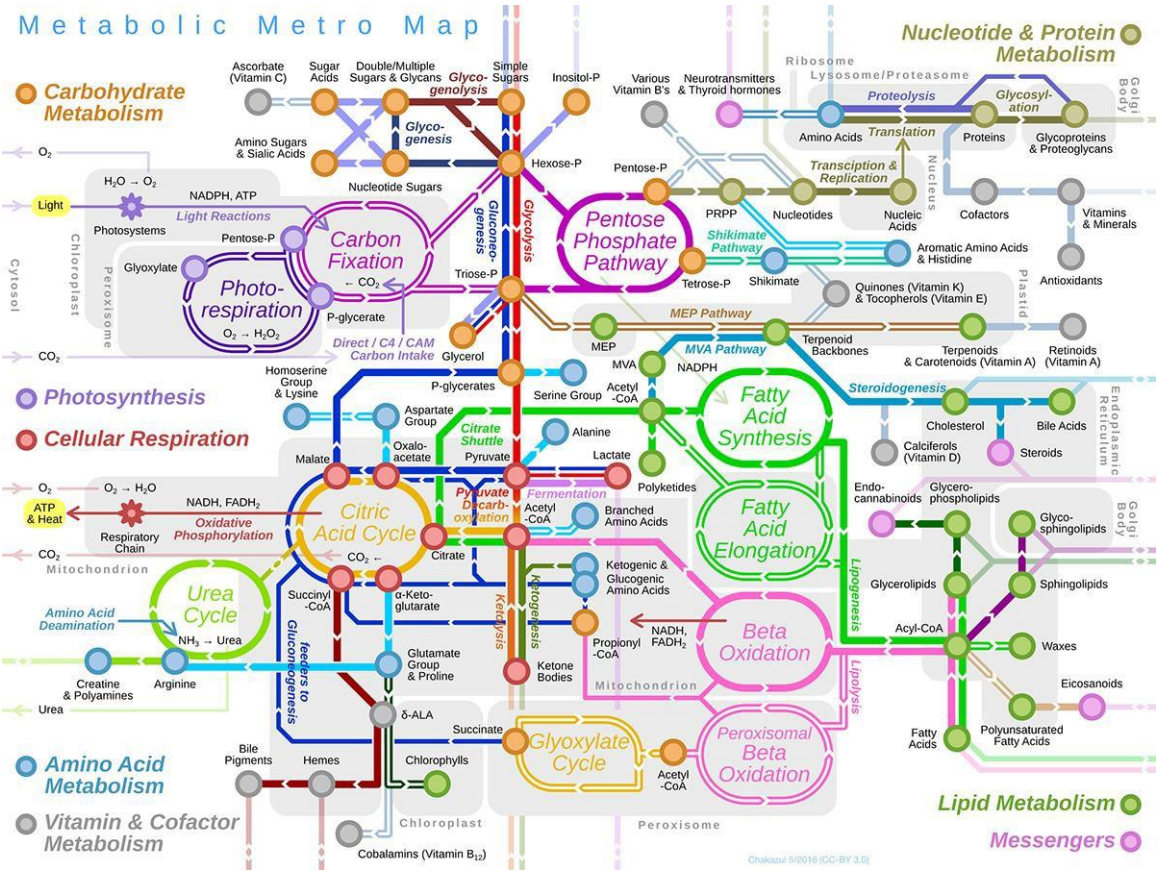

Figure 2*:* The human metabolome and its complexity displayed as an overview of all relevant pathways. [**https://www.behance.net/gallery/38270165/Metro-Map-of-Metabolism-The-Overview]**

A standard metabolomics workflow consists of a few major steps, in which strict quality assurance strategies are necessary during the entire process in order to avoid pitfalls (**Figure 3**). These individual steps comprise the design of experiments, sample generation including quenching, extraction, data acquisition, data processing with identification, statistical evaluation and biochemical interpretation [**1**]. The possibilities in data acquisition are numerous, with nuclear magnetic resonance spectroscopy (NMR) [**2-4**], gas chromatography tandem mass spectrometry (GC-MS) [**5,6**] and liquid chromatography tandem mass spectrometry (LC-MS) [**7,8,9**]. The main challenge in metabolomics remains proper feature i.e. metabolite identification as well as untargeted quantification. To address this issue, the

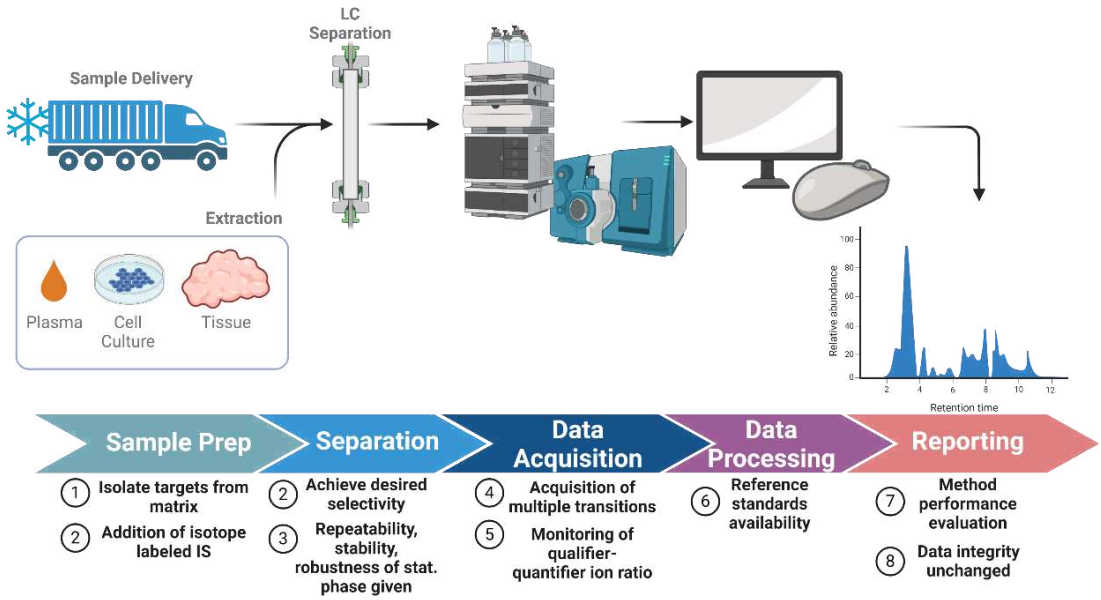

Figure 3*:* Metabolomics workflow overview with important aspects in terms of quality assurance.

development in computational metabolomics has seen exponential and rapid increase in the former years. Due to the fact that authentic chemical standards are often limited due to their availability and costs, online databases for spectral matching have received a keyrole such as the human metabolome database (HMDB) [**10**], MassBank [**11**], Manchester Metabolomics Database (MMD) [**12**], and Tandem MS Database (METLIN) [**13,14**], Golm Metabolome Database (GMD) [**15**], FiehnLib [**16**], and NIST Database [**17**]. After the identification and detection process under different conditions, structurally annotated and in particular differential metabolites have to be subjected to revision and validation, specifically also in view of matching to dedicated biochemical pathways. In this stage, pathway databases like Kyoto Encyclopedia of Genes and Genomes (KEGG) [**18**], MetaCyc [**19**], etc can be implemented. In certain cases where metabolites are involved that play a key role in certain pathways, metabolic flux analysis can be performed to determine the metabolite turnover rate, with stable isotopic tracers often used in this approach [**20**].

1.1.1. Sample preparation

The steps to be taken and considered before the instrumental analysis itself, involving the study design, sample collection and storage are of vital importance during every metabolomics study. Sampling and sample preparation have to be tailored to the respective matrix in which a sample, i.e. specific set of analytes is to be analyzed. Classical sample matrices are biofluids (such as plasma, serum, urine, saliva, cerebro-spinal fluid), tissues and cultured cells. One has to consider that depending on the matrix, the abundancy of the desired metabolites can and will vary. This may require specific adaptations of sample preparation, including e.g. an enrichment step by SPE or evaporation-reconstitution (in small volume) of metabolite extracts. The process of sample collection has to follow carefully optimized standard operating procedures (SOPs), so that the procedure is fully reproducible, reliable and comparable results can be obtained during multiple sample batches. Factors such as sample collection time and biological variances are to be drawn into consideration, as the metabolite profile represents the current status of a biologic system (specifically when one is analyzing the redox state of a system). Elements such as nutrition and circadian/biologic rhytm are to be considered during sample collection, as this can introduce further bias in the hypothesis generation. The entire sampling and sample preparation process should ideally be conducted under a low temperature, light protection and the possibility to work under an inert gas cover should always be drawn into consideration. Multiple freeze-thaw cycles are to be avoided, as it can hamper metabolite stability. Ideally, once collected, samples are to be stored under proper conditions, typically -80 °C or lower for long term purposes. The Metabolomics-Standards-Initiative (MSI) generally recommends the collection, preparation and storage of samples on ice, their immediate flash-freezing in liquid nitrogen and long-term storage to be at -150°C - -80°C [**21**]. Sample preparation needs also specific adaptations to the biological matrix. For example, tissue needs to be homogenized and cells lysed in order to fully release the endogenous present metabolites in the system. There are two main possibilities how this can be achieved, either by physical or biochemical methods. Physical options include pressure, temperature, ultrasonication, electric field and bead impact. Cell disruption by chemicals utilizes acid/alkaline conditions, ionic or supercritical fluids, detergents, oxidizing agents, and further. Chemical options provide the advantage that they are low-energy consuming and more selective. However, the quality and cost as well as the compatibility with the set LC-MS platform should also be considered. Lysis utilizing various buffers is a common practice in proteomics, however, not usually employed in the metabolomics field, as a multitude of steps are required to remove

these MS-incompatible compounds. When it comes to large-scale studies, options such as bead homogenization, high-speed homogenization or high-pressure homogenization are usually preferred, due to their high throughput and readily compatibility with MS. An issue with such physical factors is that temperature can often hamper analyte stability, as due to the increased mechanic stress temperatures can rise. For this reason, efficient homogenizers with a temperature control function are preferred, like used in the current work. Low temperature (typically 4 °C) with the help of a dry ice compartment was always maintained to keep the enzyme activity and compound degradation throughout the process to a minimum. Post release from the designated sample matrix, metabolites are extracted and transferred into the interferent-free phase. Liquid-liquid extraction (LLE) and solid phase extraction (SPE) are options commonly employed. Depending on the polarity of the target analytes, various solvents and mixtures are used for their extraction. In the case that additional sample clean-up is required, biphasic LLE is performed by using a water-immiscible organic solvent such as chloroform (CHCl3), hexane, or methyl tert-butyl ether (MTBE) together with an aqueous phase, with the organic layer then being used for the analysis of lipophilic metabolites, whilst analysis of the polar metabolome is performed from the aqueous phase. Another possibility that offers sample clean-up is SPE, which involves distinct interaction mechanisms of the metabolites with the stationary phase such as reversed phase, ion exchange interactions or mixed-mode RP/ion-exchange. A special case represents the extraction of phosphorylated analytes, as it is highly challenging due to the fact that they are prone to bind to proteins. Therefore, several acids including acetic acid, perchloric acid, trichloroacetic acid, and hydrochloric acid were reported to protonate analytes to achieve satisfying recovery. Additionally, metal oxide affinity chromatography (MOAC) is interesting for phosphorylated metabolites/lipids [**22**,**23,24**].

1.1.2. Derivatization strategies

Chemical derivatization represents a versatile approach in liquid chromatography-tandem mass spectrometry. By effectively chemically modifying certain moieties in a metabolite, i.e. functional groups, problematic issues involving insufficient sensitivity, inadequate selectivity, limited stability and insufficient chromatographic retention can successfully be solved. **Figure 4** provides an overview of a few well-known derivatization strategies often employed when it comes to the derivatization of functional groups in metabolites [**64**].

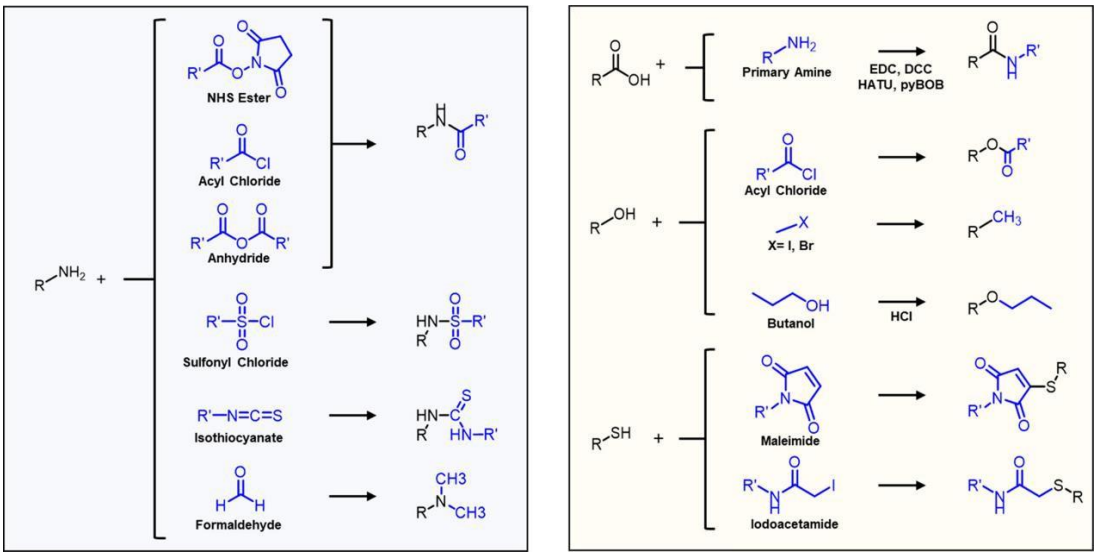

Figure 4*:* Common derivatization options in analytical chemistry for different functional groups. [Huang T, Armbruster MR, Coulton JB, Edwards JL. Chemical Tagging in Mass Spectrometry for Systems Biology. Anal Chem. 2019 Jan 2;91(1):109-125. doi: 10.1021/acs.analchem.8b04951. Epub 2018 Nov 14.] Reprinted with permission of Huang et. al. from ref doi: 10.1021/acs.analchem.8b04951.

There are a few points to consider when one intends to conduct chemical derivatization. The derivatization kinetics should be fast and quantitative (within a few minutes) to facilitate automation in the autosampler. The reaction should proceed under mild conditions, to avoid chemical degradation unstable metabolites during derivatization. The reaction yield is of importance as it improves the sensitivity and accuracy if the reaction is quantitative. For targeted methods the chemical selectivity of the derivatization reagent may be beneficial while for derivatization in untargeted metabolomics a reagent with wide coverage of distinct functional groups at the same time is certainly beneficial. In any case, the originating products should be stable, especially when the derivatization occurs before the analysis of the sample batch and the time between derivatization and injection is different for the distinct samples. In situ derivatization in the autosampler can be of advantage in this regard. Interfering by-products must not be formed during derivatization. Regarding real sample application, one has to consider that the extraction and derivatization protocol are compatible with one another, i.e. pH value, buffer ionic strength and solvent miscibility properties. This thesis dealt with two main compound classes commonly derivatized – phosphorylated analytes and thiols. In the case of phosphorylated metabolites, derivatization is worth considering, due to their problematic performance in LC-MS. The phosphate group increases the polarity of the metabolite significantly, making retention and separation with classical reversed-phase chromatography not possible. The negatively charged groups exhibit high interaction potential with glass and stainless-steel surfaces, which are commonly employed during sample preparation and instrumentation leading to

severe peak tailing and low recovery [**25-27**]. Several possibilities exist how to address the derivatization of the highly reactive phosphate group, those being amine-based and diazo-based approaches [**28**]. In the amine-based scenario, the phosphate moiety is modified with an amino group with N-(3-Dimethylaminopropyl)-N′-ethylcarbodiimide (EDC) as a catalyst. The drawback of the reaction is the necessity for high temperatures and the often high duration until the process is completed. With the diazo approach (e.g. diazomethane, trimethylsilyldiazomethane), alkylation is conducted under nitrogen release in a rapid reaction. In this thesis, the analysis of sugar phosphates was aimed at to be performed without the necessity of an extra derivatization step, which might also introduce additional variances and some bias. Derivatization was, however, employed in the case of the analysis of the thiol metabolites in order to cap the reactive sulfhydryl moiety and thus freeze the redox state, as thiols have been shown to be highly reactive in the ESI-source, showing rapid interconversion between their reduced and oxidized disulfide forms [**29-31**].

1.1.3. Quenching and extraction of cell samples

An important aspect in metabolomics in general is rapid quenching of the metabolism quickly after sampling and the quantitative metabolite extraction. In this thesis, the prime focus was laid specifically on the analysis of cell samples and thus cell culture played an important part during the course of the experimental work. Generally, metabolomic profiling of cells can be divided into two subgroups, with those being i) analysis of extracellular metabolites and ii) analysis of intracellular metabolites [**32, 33**]. Cell growth can also be conducted in two different ways, either adherent or in suspension, with both ways differing vastly when it comes to passaging, seeding and counting the culture. Whilst the analysis of the exometabolome is more convenient and less demanding to conduct in terms of sample preparation, cellular metabolite leakage must be prevented. On the other hande, it is challenging to draw a connection between the concentration of the exometabolome and actual biological state of the cell culture [**32**]. This being the reason why intracellular metabolites are primarily analysed to study cellular metabolism, due to the fact that they represent a more accurate picture of the actual status of the cells [**32**]. Analyzing endogenous metabolites is, however, quite difficult, not only due to the complexity of their chemical nature, but also due to their vast differences in their concentration ranges, often spanning over multiple orders of magnitudes. When it comes to quenching of cellular metabolism, one should carefully consider the protocol used in this case, as certain metabolites, specifically the adenylate charge molecules, are known to have a high turnover [**32, 34-39**]. Thus, it is

crucial to quench the metabolism as fast and efficient as possible after sampling to be able to analyse the actual status of the cells and not artifacts due to continuing metabolic reactions. There are various options to quench metabolism already described in the literature [**37,38,39**]. Options include drastic temperature changes, pH changes or the usage of organic solvents as methanol or acetonitrile. An issue during quenching is that cells often burst during this process, which leads to a loss of metabolites beforehand extraction. For this reason, organic solvents are often preferred in order to prevent such rapid changes in temperature or pH. Separating the cells from the media in which they were grown (mostly DMEM supplemented with FBS), is another critical aspect, as one does not want metabolic interferences from the media to occur. In the case of adherently grown cells, the separation is the easiest step during extraction [**40,41**]. The media can simply be removed with a serologic pipette or with a pump, with the remaining cells left intact. After washing wit hice-cold PBS buffer, cell detachment is usually conducted with trypsin/ethylene diamine tetraacetic acid (EDTA) solution [**36**]. However, studies showed metabolite loss and changes in the metabolome due to treatment with trypsin/EDTA [**41,42,43**]. What should be also considered is that the detachment process takes time, as it depends on the cell line how long the trypsinization should be performed. This means that the quenching can only be performed after detachment. It leads to the problem that biochemical and enzymatic processes in the cell culture continue to take place and hence do not represent the actual metabolic status of the cells during sampling anymore when metabolite extraction and the metabolomics analysis is performed. An alternative would be detaching the cells with a cell scraper after quenching with liquid nitrogen has been performed. The remaining cells can then be simply scraped off and transferred into a vessel of choice for extraction. Other difficulties occur by using cells, which are grown in suspension. The challenging step is the removal of the media. Centrifugation is a possibility, however, this is time consuming and the effect of centrifugal forces on the cells with a significant risk for metabolite leakage and cell lysis has to be considered. Fast filtration is another possibility by employing specific filters with varying diameters, as every cell culture has different individual cell sizes. A limitation here is that fast filtration can only be used for small quantities as the cell number is limited due to the possibility of blocking the filter [**32,44**]. In order to be able to analyze the intracellular metabolome, a proper extraction protocol has to be implemented. A critical point in metabolomics, is the removal of proteins, which is always necessary, as proteins can easily lead to chromatographic system contamination during analysis or column clogging. Solvents commonly employed in metabolomics extraction protocols include water, methanol and acetonitrile, with options available to perform either acidic or basic

extraction in case one is aiming for specific compound classes. Nevertheless, there is no universal extraction method which covers the whole metabolome and is suitable for all cell lines [**32, 34**]. What should also be considered is the way cell lysis is conducted, meaning the rupture of the cell membranes in order to release the intracellular metabolites. Common options involve ultrasonication or freeze/thaw cycles with liquid nitrogen. In this thesis, a CellLyser device (Precellys Evolution using Cryolys Evolution cooling unit with dry ice), which involves the usage of zirconia/glass beads, was employed. With this cell lyser, the homogenization takes place in timed rotating cycles, which are programmable on the device to the specific sample requirements. It can also be used for tissue samples. Of course, there are other options regarding cell lysis, such as deproteinization using heat or inorganic acids. This, however, has been shown to lead to lower metabolite coverage [**45,46**]. To conclude, the majority of variance and highest risk for metabolite loss in a metabolomics analysis occurs during sample processing. Therefore, only minimal sample pre-treatment is recommended [**47**]. Specifically, samples acquired from cell culture require a good sample work-up strategy. One aspect being cell density, which is critical, as it highly affects the intracellular and extracellular metabolite concentration [**32**]. Furthermore, one should also consider the fact that one single extraction protocol does not sufficiently cover the entire metabolome. Therefore, in any metabolomics studies based on using cells as a sample matrix, it is a necessity to consider a multitude of aspects. Specifically, cultivation conditions have to be standardized in order to prevent any possible changes in the metabolic processes, which may occur due to confounding factors. Standardization during cultivation is absolutely necessary in order to achieve reproducible and reliable results. Workflows should be continuously improved and optimized, in order to maximize metabolite extraction coverage and yield. And lastly, the implementation of internal standards and quality control samples/strategies is a vital point, in order to control and track the entire process throughout the metabolomics study [**32**]. It is of utmost importance to normalize the cell extracts obtained, for example, with isotopic labeled internal standards, because the raw data likely does not reflect the changes in concentration [**29,32**].

1.2. Liquid Chromatography in Metabolomics

MS-based data acquisition of prepared metabolite extracts can be performed by various methodologies, either by hyphenation of MS with a chromatographic separation method (GC or LC) or through direct infusion of the sample in the MS device, commonly described as shotgun metabolomics. The advantage of such direct-infusion methods is their high throughput, allowing for fast sample analysis with high analyte coverage. However, it is required to have high resolution instruments (preferentially orbitrap or FT-ICR MS). The drawback, however, of such direct infusion approaches is the high matrix effect (ion suppression) present [**84**]. Furthermore, there is the possibility of detector saturation, especially on an MS1 level (e.g. with Q-TOF instruments). In case of DI with orbitrap mass analyzers, low abundant metabolites will not be detected due to ion suppression in the ESI source and limited ion abundance in the analyzer to avoid *space-charge effects. Furthermore, numerous isomers make problems in DI-MS. For this reason,* hyphenation to LC or GC has been widely adopted in bioanalytical chemistry, providing an extra orthogonal separation mode to MS. This thesis mainly dealt with LC-tandem mass spectrometry, with possible interactions between analytes and the RPLC employed stationary phase shown in **Figure 5**. Depending on the chemical nature of the analytes, various separation modes are used and are discussed hereafter in more detail.

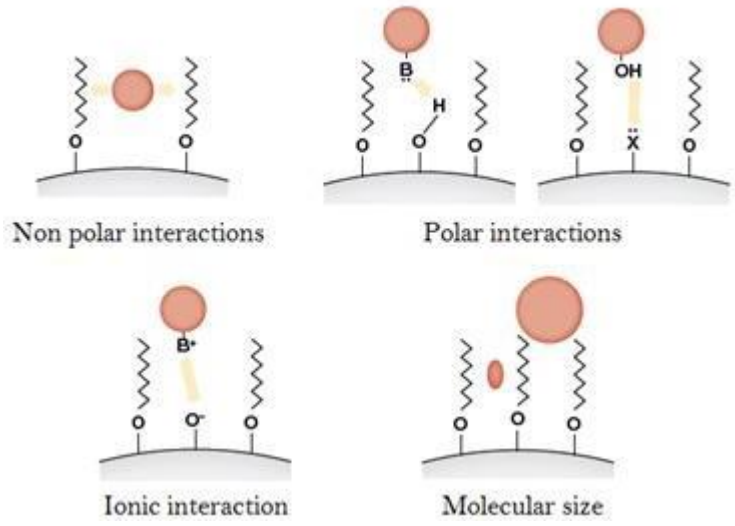

Figure 5*:* Different interaction possibilities between column stationary phase and analyte in chromatography. [**https://theory.labster.com/column-type-interaction/**]

1.2.1. Reversed phase liquid chromatography

Reversed-phase liquid chromatography (RP-LC) has established itself as the gold-standard separation technique in bioanalysis. During this separation mode, the mobile phase is mostly polar, with the elution strength increasing continuously by increasing a non-polar solvent as organic modifier in the aqueous based eluent. Water miscible solvents such as acetonitrile, isopropanol and methanol are commonly used as strong eluting components. **Figure 6** shows a traditional design of a non-polar stationary phase in reversed-phase liquid chromatography, with C18 moieties bonded to the silanols groups of the porous spherical silica particles. A multitude of further surface chemistries exist, for example the modification with a phenyl-hexyl moiety, as also shown in **Figure 6**, or different lengths of alkyl chains, which would modify the interaction potential with non-polar analytes. Essentially, the longer the alkyl chain, the stronger the interactions between the stationary phase and non-polar analytes become as the hydrophobicity of the modified silica increases. The modification with a phenyl-hexyl moiety offers alternative selectivities, as it provides the extra possibility to exert π−π interactions with analytes having aromatic groups. Free silanols of bonded silica phases are further modified with small alkyl silanes, a phenomenon known as endcapping, to minimize detrimental interactions of analytes with residual silanol groups. Such phases show enhanced chromatographic performance. The endcapping can also be performed with silanes having a polar group. Besides polar functional groups like amides, carbamates sulfonamides can be embedded in the alkyl chain. Both concepts, polar endcapping and embedded polar group, can provide stronger retention for polar analytes that are not sufficiently retained on common C18 phases. They show also better compatibility with highly aqueous eluents and samples. On the contrary, common C18 phases require at least 5-10% organic modifier in the mobile phase in order to prevent the collapsing of the alkyl strands of the silica phase which is accompanied by a loss in retention. This can be specifically useful in scenarios when a focusing step in the beginning of the gradient is required [**48**]. Most metabolites, however, are chemically highly polar and thus show limited retention capabilities and interaction potential in reversed-phase liquid chromatography. Nonetheless, RP-LC is still common practice in metabolomics, due to its ability to generate reproducible and robust data. The issue with low retention can be readily solved with the process of chemical derivatization of analytes, which is further discussed in section 1.1.2. In this thesis, reversed phase chromatography was employed specifically with a phenyl-hexyl phase in the case of urinary metabolomics.

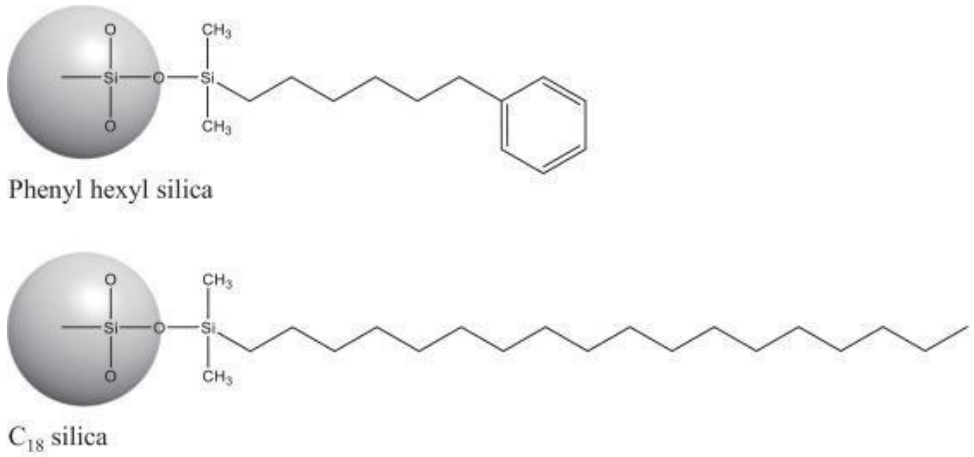

Figure 6*:* Representative example of a C18 and phenylhexyl stationary phase in RP-LC. [Nakamura K, Saito S, Shibukawa M. Intrinsic difference between phenyl hexyl- and octadecyl-bonded silicas in the solute retention selectivity in reversed-phase liquid chromatography with aqueous mobile phase. J Chromatogr A. 2020 Sep 27;1628:461450. doi: 10.1016/j.chroma.2020.461450.] Reprinted with permission of Nakamura et. al. from ref. doi: 10.1016/j.chroma.2020.461450.

1.2.2. Hydrophilic interaction liquid chromatography

As discussed above, RP-LC is actually dedicated to separate hydrophobic compounds. Hydrophilic interaction (liquid) chromatography, on the other hand, is an alternative separation mode highly suitable for the analysis of hydrophilic compounds like metabolites. Initially the term HILIC was coined by *Alpert et al.* in the early 90s [**49-57**]. Previously, such chromatographic applications were described as aqueous normal-phase (NP) chromatography, as HILIC uses stationary phases that are polar and usually found in NP chromatography. However, HILIC has significant advantages over NP chromatography as well as over RP chromatography. In HILIC, the stationary is polar (silica or polar functionalized silica). The mobile phase consists of water-miscible organic solvent (mostly acetonitrile) and water. The water percentage in the mobile phase usually accounts for at least 2.5% to form the semi-immobilized water layer on the stationary phase which permits retention of neutral polar analytes by partitioning into this water layer [**58,59**]. Due to the high content of organic solvent (acetonitrile) as mobile phase, the ionization efficiency and sensitivity are superior compared to RP-LC [**58,60**]. Furthermore, the high organic content in the mobile phase and the resulting low viscosity both lead to low back pressure in the column, which means that higher flow rates and a faster and more efficient separation [**50,52,57-59,61**] can be utilized. (Neutral) analytes are separated according to their partitioning between the water layer (the actual stationary phase) and mobile phase (**Figure 7**).

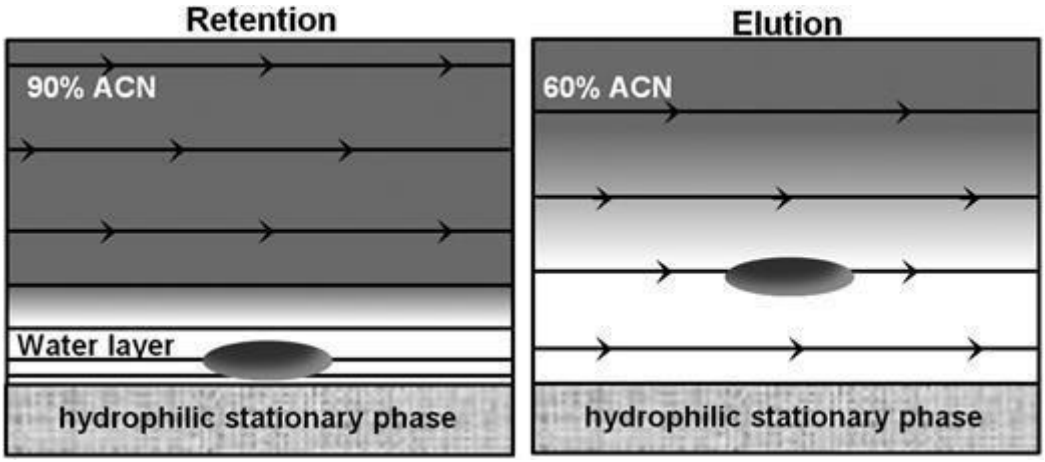

Figure 7*:* HILIC partitioning principle overview. [Greco, G., & Letzel, T. (2013). Main interactions and influences of the chromatographic parameters in HILIC separations. Journal of chromatographic science, 51(7), 684–693. https://doi.org/10.1093/chromsci/bmt015]. Reprinted with permission from Greco et. al. from doi.org/10.1093/chromsci/bmt015.

Apart from the distribution of the analytes between the organic and aqueous layer, ionic interactions and the direct adsorption of the analytes to the stationary phase via hydrogen bonding and dipole-dipole interactions play a further role in the separation mechanism [**49,51,54,59-63**]. This allows certain separation properties to be controlled by the type of stationary phase of a HILIC column as well as composition of the mobile phase which allows to disrupt specific type of interactions (e.g. ionic interactions by high buffer concentration). rRegarding stationary phase chemistry, various HILIC phases have been developed over the years – DIOL [**64,65**], Amide [**66,67**], sulfobetaine coated [68,69], polymer phases [**70**], bare silica [**71**], amino [**71**], cyano [**72**], amongst others, with particle morphology also varying (e.g. fully porous or superficially porous). Depending on the stationary phase's chemistry, further interactions can take place apart from the distribution between adsorbed water layer and bulk mobile phase, and influence the separation of the analytes. The thickness of the water layer is depending on the stationary phase's chemical properties [**49,52,59**]. The higher the polarity of the phase, the more water is bound and thus the water layer is thicker. It has been documented that in particular polymer type HILIC phases allow to build up a thicker water layer and hence exhibit stronger retention. The thickness of this polar water layer is also influenced by the properties of the mobile phase, i.e. the amount of organic solvent present [**51**]. Depending whether or not an organic solvent can be used in HILIC, there are certain requirements that have to be met – specifically the solvent should be miscible with water, but should not have strong hydrogen acceptor or donor properties. Acetonitrile meets the requirements and has become the common choice in HILIC. Generally, the higher the acetonitrile content, the thinner the polar water layer is, it is thus that at least 2.5% of water should be present in the mobile phase at all

times. Aqueous buffer solutions are often present in the mobile phase during analysis, specifically in the case of analysis of highly ionic compounds [**65,66,67**]. Salt additives as ammonium formate and ammonium acetate are common choices, due to their volatility and thus compatibility with MS, however, ammonium bicarbonate can also be used [**67**]. The pH value of the mobile phase plays a further important role, as it influences the charge state of the analytes and stationary phase, and thus the ionic interactions between the analytes and the stationary phase are influenced. As a conclusion, HILIC provides a complementary alternative to normal-phase chromatography, while at the same time offering the advantage of working with solvents commonly employed in RP-LC, specifically acetonitrile and water, thus eliminating the necessity of using toxic solvents like hexane, as in the case of NP-LC. HILIC, however, reportedly has the drawback of difficulties to reproduce retention times. Therefore, column re-equilibration is a critical point in this separation technique [**74**]. Nevertheless, in the field of metabolomics, HILIC has established itself as the preferred mode of separation, with numerous studies already described in the literature [**65-69**].

1.3. Mass Spectrometry in Metabolomics

MS is the first choice in metabolomics studies, with the development in MS devices and analysis over the last years having undergone significant development in both resolving power and sensitivity [**74-76**]. In brief, post the ionization process of the individual analytes in the ion source, separation takes place according to the *m/z* value, with a subsequent detection. Fragmentation can occur depending on design of the experiment and the hardware of the instrumented implemented, with MS1 and MS2 analysis available.

1.3.1. Ionization

For detection and separation of individual atoms or molecules to occur via MS, ions must be present in the gas-phase. Possibilities exist how ionization can occur, be it by electron ejection, capture, protonation, deprotonation or the formation of adducts with charged ions [**77**]. In present, most ionization modes take place under atmospheric pressure conditions so that a combination to liquid chromatography can be possible, i.e. ESI or APCI. MALDI, also known as matrix-assisted laser desorption/ionization is a popular choice, specifically in MS imaging [**78**]. In this thesis, the projects conducted operated under the ionization technique of ESI. Essentially, a flow which is variable depending on the choice of LC system (nano/micro/standard) flows through a capillary

on which a high voltage is applied (approx. 5000 Volt) [**79**]. Depending on the choice of solvent, a minimum onset voltage is required as the physico-chemical properties of every solvent differ, specifically in this case the surface tension being the critical parameter. The originally formed spherical drops formed in the nebulization sprayer process are elongated with an increasing voltage until the Rayleigh limit is reached (**Figure 8**).

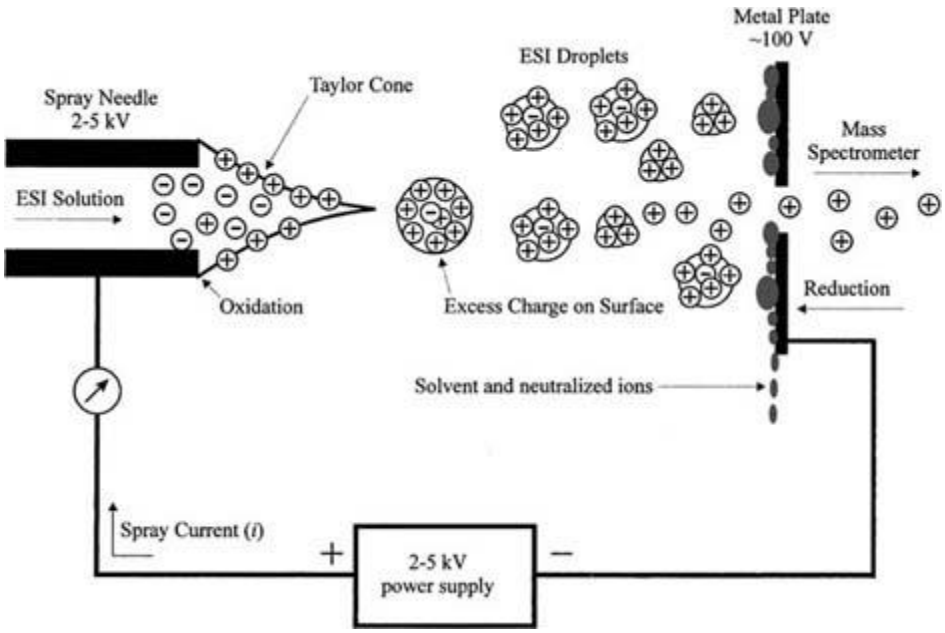

Figure 8*:* Schematic of the electrospray ionization process. [Cech NB, Enke CG. Practical implications of some recent studies in electrospray ionization fundamentals. Mass Spectrom Rev. 2001 Nov-Dec;20(6):362-87. doi: 10.1002/mas.10008]. Reprinted with permission of Cech et. al. from doi: 10.1002/mas.10008.

What happens when the Rayleigh limit is reached is that the flow is transformed into a spray due to Coulomb explosion occurring, as a result of the electrostatic repulsion taking place on the drop's surface (solvent evaporates, charge density increases, explosion) [**77**]. This leads to the formation of a Taylor cone which constantly releases drops carrying a charge. An inert gas, mostly nitrogen or zero grade air, flows during the entire process which is heated and supports the entire nebulization process. This leads to an even more efficient solvent evaporation process from the smallest of droplets, for which also Coulomb explosion occurs and thus analyte loss is minimized from the sample. The process repeats until the solvent is completely evaporated [**77,79**]. A nebulizer gas, again either nitrogen or zero grade air, leads the ions to the orifice plate of the MS device, where they are drawn into the ion pathway. Originally the setup of the spray was axial and the orifice is nowadays predominantly replaced with an orthogonal setup, which avoids any unwanted contamination, whilst allowing the diameter of the orifice to be modulated, delivering better sensitivity and robustness [**77**]. ESI is an ionization mode which in most cases provides single charged ions, with the

tendency to form adducts apart from $[M+H]^+$, $[M-H]^-$ depending on the conditions used in the mobile phase i.e. buffer and pH. In the case of the analysis of large molecules, e.g. proteins or oligonucleotides, ions carrying multiple charges are present, which has the advantage of shifting the *m/z* value to ranges in which the specific instrument can operate. ESI's sensitivity depends furthermore to the concentration of a specific analyte present and not the total mass [**80**]. It is therefore that when coupled to liquid chromatography, higher sensitivity can be achieved at lower flow rates, i.e. with micro or nano LC. The lower flow rates, however, require adequate chromatographic conditions, specifically proper column geometry (smaller inner diameter) in order to prevent peak broadening effects due to the increased longitudinal diffusion [**81**]. One has also to consider that essentially the ESI source is a redox active chamber, with the specific electrochemical processes occurring at the topmost point of the ESI electrode [**82**]. During analysis, reduction and oxidation processes take place in the ESI source, which can limit the amounts of ions that can be extracted due to the electrical current generated by these reactions [**83**]. A further factor effecting how efficient the ionization process takes places is the simultaneous presence of compounds that either effect the formation of the drops or compete for ionization [**84**]. This phenomenon is known as matrix effects, with both the possibility of the signal either being enhanced or negatively affected. Due to its different ionization principle, APCI has been described in the literature to be less prone to matrix effects [**85**]. In the case of APCI, the flow passes through a heated ceramic tube and a gas current is utilized to conduct the nebulization process. The gaseous phase is transferred to a high voltage corona discharge needle, where the formation of the ionized plasma takes place [**77**]. APCI can be favourable in cases where ESI is not the go-to mechanism of choice, specifically with non-polar compounds APCI excels and can provide better signal intensity. MALDI, as a comparison, is traditionally regarded as the method of choice in imaging studies with large analytes i.e. proteins or RNA/DNA material. MALDI offers the advantage that it is less prone to contamination and sample preparation is less complicated than the traditional MS approaches. Essentially, the analyte is embedded in a liquid matrix, containing molecules with a high absorption coefficient for the wavelength the laser has been adjusted to. Post the drying process, the analyte is further exposed to the laser, but with stronger pulses. While this occurs, evaporation of the absorbing molecules takes places and ionization via proton transfer is conducted [**86**].

1.3.2. Mass analyzers

Having successfully transformed the analytes into charged ions, they are efficiently directed through the orifice plate of the instrument via an electromagnetic field. In order to keep the ions on stable trajectories and avoid unwanted fragmentation through collision in the ion pathway (post collision chamber), high vacuum field conditions are a necessity, achieved by so-called “turbo pumps”, able to provide vacuum conditions between 10^{-3} - 10^{-7} Torr. When planning how to conduct a specific MS based analysis, scientists nowadays have an array of available mass analyzers available, each of them having their own unique properties regarding mass range, sensitivity, resolution, instrument acquisition frequency and mass accuracy [**77,87**]. Instruments used in this thesis were based on the quadrupole time-of-flight (QToF) and triple quadrupole principles and are herein further discussed.

1.3.2.1. Triple Quadrupole Mass Spectrometry

The quadrupole is undoubtedly the most popular choice as a mass analyzer. Its advantages including a wide dynamic linear range, increased sensitivity, whilst simultaneously being a budget-friendly option requiring little space minus complex operating procedures, make it a standard go-to-choice among analytical chemists. The typical structure and scan principle are illustrated in **Figure 9**. The essential operation principle of a quadrupole is based on a radiofrequency (RF) and direct current (DC), which are applied to four parallel metal rods, of which basically the quadrupole consists. Ions, based on their *m/z* values are directed on specific trajectories in an electromagnetic field, with the RF and DC values varying depending on the *m/z* of the target ion, allowing it thus to pass through the quadrupole towards the detector system.

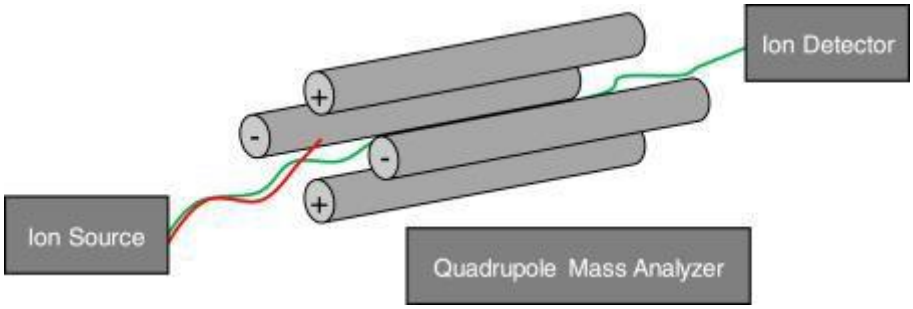

Figure 9*:* Physical design of a quadrupole. [R. W. Smith; Encyclopedia of Forensic Sciences, Third Edition 2023]. Reprinted with permission from R. W. Smith. from doi.org/10.1016/B978-0-12-823677-2.00054-4

Figure 10 shows a quadrupole operated in a standard MRM mode (discussed further in this chapter), but specifically also that different ions with different *m/z* have certain stable trajectories in the quadrupole. The offset and slope (or gain) of the scan line are two parameters that can be used to tune the MS performance regarding resolution and sensitivity. The area divided by the scan line represents the total amount of ions passing through the quadrupole, meaning that by increasing the offset and slope, an increase in resolution and a decrease in sensitivity will be observed, and vice versa. As a rule of thumb, quadrupoles are accordingly tuned to yield 0.6 to 0.8 peak width values, which represent a trade-off between resolution and sensitivity. Single quadrupoles are also used as ion guides and collision chambers in tandem mass spectrometry. In the case that a quadrupole is used as an ion guide, it operates without a DC current (RF only mode) and ions comprised of a wide *m/z* range can pass through. With the implementation of an inert gas (e.g., nitrogen or zero-grade air) and a collision energy (CE) value is applied, ion fragmentation can take place, also known in this case as collision-induced dissociation (CID). Due to the flexibility of a quadrupole with regard to the roles it can play during analysis, it is suitable to be used in combination with other quadrupoles or mass analyzers in more complex systems (e.g., QqQ, QTOF). A classic example of quadrupoles being employed in mass spectrometry is in triple quadrupole instruments (QToF discussed in 1.3.2.3.). A triple quadrupole instrument, much as the name already reveals, utilizes 3 quadrupoles, with Q1 and Q3 often being used to select the precursor and product ions in a targeted analysis, with Q2 acting as a collision chamber. This, is what is known as a targeted MRM acquisition in mass spectrometry and an overview is provided in **Figure 10**.

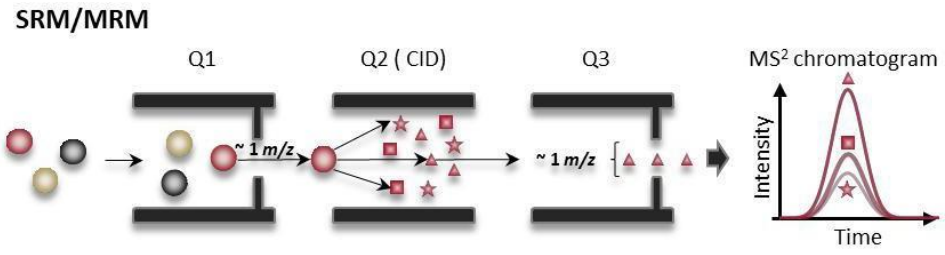

Figure 10*:* Schematic depiction of a triple quadrupole MS system operated in MRM mode, detecting three transitions from the same precursor.

The generation of the desired transition, i.e. combination of precursor and product ion is performed beforehand (pairs of m/z in Q1 and third quadrupole, Q3). Apart from triple quadrupoles, linear ion trap (in this thesis QTRAP4500 by Sciex) instruments are also used, due to their high sensitivity, high specificity and fast scan speeds available. Multiple scan modes are available in such instruments. The product-ion scan being one of them, during which the Q1 filters one specific precursor ion mass and Q3 scans all of the originating product ions from the set precursor ion. The neutral loss scan sets the Q1 to radio-frequency (RF) leading up to the fact that all precursor ions in the specific mass range are scanned. Q3 is also used in scan mode and detects all fragments with a set mass difference (*Δm*) between Q1 and Q3. With the case of the well-known MRM acquisition, it is normally performed on triple quadrupole systems with both Q1 and Q3 set to unit mass resolution [**88**], meaning that the desired precursor ions are selected in Q1, fragmentation taking place in the collision cell (Q2) and one or multiple fragment ions being selected in Q3 (**Figure 10**) [**89**]. It is a rule of thumb, that multiple MRM transitions are measured during analysis, in order to avoid possible isobaric interferences. Generally, 2 transitions called quantifier and qualifier are acquired in every analysis, as long as fragmentation of the specific compound allows that. What also is monitored during analysis is the ion-ratio of both quantifier-qualifier fragments, which has to remain constant, otherwise that would point towards an interfering ion present [**90**]. There is a limitation, however, in MRM acquisition and that is in the number of selected precursor ions due to the needed time for switching between different masses, cycle time and settling time, which essentially is the re-equilibration of the electronics after switching to new compound specific settings, as well as the width of the chromatographic peak [**91,92**]. Furthermore, authentic chemical standards are a pre-requisite during targeted LC-MS method development, in order to optimize the chromatographic separation and the individual compound specific parameters for the MRM transitions [**93,94**]. Compound specific parameters are the declustering potential (DP), collision energy (CE), entrance potential (EP) and cell exit potential (CXP). This is, of course, the case with Sciex instruments, as every vendor provides differently built and programmed mass spectrometers. DP is a voltage, which is applied to the orifice of the MS-device, with the aim of dissociating clusters of target ions, so that the target can navigate to the ion path as a single monomeric gas-phase ion. The voltage furthermore supports the desolvation process in order to release analyte ions and regulates their acceleration into the orifice. During their way, the ions come to collision with the residual gas molecules, leading to the reduction of undesired adducts or solvent clusters. One thing which should always be taken into consideration is the possibility of in-source fragmentation, especially if the declustering potential value is set

too high. This is specifically the case with compounds such as nucleotides, which can lead to a drastic loss of sensitivity [**95,96**]. The CE is another key value to be individually adjusted for each MRM transition. By selecting the optimal CE, the specific fragment masses of an analyte are generated as the highest abundant fragment masses. As already mentioned, the necessity of authentic standards in MRM method development, together with their unavailability commercially and their high cost is a limiting factor in this analysis [**94,97**]. This can be accounted for by the introduction of the so-called new pseudo-targeted approaches [**98,99,100**], which do not necessarily rely on the availability of an authentic standard. Source specific parameters as previously discussed are optimized via computational approaches, with platforms such as CFMID [**101**] leading the way in this approach. Absolute quantification is, however, still not possible to achieve with this approach, as only a relative one is possible with the approximate estimation of the compound specific response factor. As previously mentioned, the cycle time of the analysis and individual compound dwell time can be limiting factors, as with high dwell times come high cycle times, leading often not to the generation of enough data points per peak [**102**]. An option to circumvent this issue is the utilization of the so-called Scheduled MRM feature [**92**]. During scheduled MRM, time windows during acquisition are set for the individual analytes [**92**], which results in higher dwell times possible for the individual compounds, whilst simultaneously utilizing shorter cycle times.

1.3.2.2. Quadrupole linear ion trap mass spectrometry

With the difference regarding the 3D ion trap, the linear quadrupole ion traps is essentially operated as a 2D device. The difference with the quadrupole mass filter is that ions with *m/z* values found on unstable trajectories are detected in the linear ion trap, as they are selectively ejected by a changing alternating current (AC). The linear ion trap provides the advantages of having a wider dynamic linear ranger, coupled together with better sensitivity. In this thesis, specifically the QTrap 4500 by Sciex was utilized for the studies conducted. A linear ion trop provides more flexibility in analysis options, as the possibility to conduct MS^n analysis (MS3 for example, where MS2 fragments are accumulated in the trap and fragmented once more), which provides extra selectivity and represents a useful tool in structure elucidation. However, there is a certain drawback in the case when one uses ion traps, with that being the low mass cut-off, also known as the one-third rule, meaning that fragments with *m/z* values less than 30% of the *m/z* value of the precursor cannot be effectively trapped.

1.3.2.3. Quadrupole Time of flight Mass Spectrometry

The hardware setup of a QToF begins with a quadrupole, which essentially is made from four parallel hyperbolic metal rods, aligned in a square. A radio frequency current (RF) together with a superimposed direct current (DC) are applied to this element (**Figure 9**). After the ionization process has taken place, the ions pass through the quadrupole, as they are attracted by an existing voltage potential difference at its lead end. While passing through, interaction takes place between the ions and the electromagnetic fields, which are generated by the electric currents. By varying the amplitude and frequency of the RF, as well as the offset potential of the DC and the set position and passing velocity, only a set of specific ions with a *m/z* value will traverse through the quadrupole, as they traverse on stable trajectories [**74**]. The case with the other ions (i.e. other *m/z* values) is that they undergo increasing oscillation and are essentially filtered out when encountering the metal rods of the quadrupole [**76**]. By effectively selecting an RF and DC value, a *m/z* filter is essentially established for chosen ions. The stability areas below given m/z ratios represent possible combinations of RC and DC values that will result in stable trajectories through the quadrupole. One should, however, consider that certain *m/z* values have identical stability areas, thus the necessity of RF and DC being carefully set in order to prevent overlapping interferences between *m/z* values. It is therefore that during acquisition and scanning, the values for RF and DC are increased in a linear rate, with the intersection of this linear function and the stability areas being proportional to the acquired peak width and as a connection also to the peak resolution. In order to obtain the necessary resolving power, one has to carefully tune the quadrupole so that values between 0.6 to 0.8 units at full width at half maximum for the individual peaks are obtained. However, higher resolution comes with the price in sensitivity loss and vice versa [**103,104**]. Often quadrupoles are merely used as ion guides or collision cells when operated in “RF-only” mode. If DC is not present as a current, wider *m/z* transmission windows can be controlled via RF settings in order to obtain a quadrupole acting as a focused ion beam for the ion optics system. The ions passing through the quadrupole can be fragmented in MS/MS by the encounter with an inert gas (N2 or zero grade air) into an RF-only quadrupole and collision-induced dissociation (CID). How strong the effect of fragmentation is, depends solely on the kinetic energy that the ions carry, which can further be adjusted by an additional electric potential dubbed collision energy (CE). A QToF instrument essentially contains two quadrupoles, with the first one (Q1) being used as a mass filter and the second one (Q2) as a collision chamber (**Figure 11**). There is, however, the possibility to operate both in RF only mode to process the

unfiltered precursor ions to the ToF drift tube. The physical principle behind a ToF instrument is based on the varying ion flight times (t) in a region, which is field-free, after the ions have been accelerated by a specific electric potential (V) [**105**]. The principle can be characterized by the following equation:

$$E_{kin} = \frac{1}{2}mv^2 = qV = zEV \quad \textbf{Equation 1}$$

Essentially, ions with a specific mass (m) and a total charge q (defined as the product of the charge number z and the elementary charge e) show certain velocities (v) after acceleration in a field (V) to reach a set kinetic energy (E_{kin}). Calculation of the velocities can be conducted by the following equation:

$$v = \sqrt{\frac{2zeV}{m}} \quad \textbf{Equation 2}$$

With the flight time of the ions being dependent on the length of the ToF drift tube (L) and the ion velocity (v):

$$t = \frac{L}{v} \quad \textbf{Equation 3}$$

By combining equation 2 and 3:

$$\frac{m}{z} = 2eV\left(\frac{t}{L}\right)^2 \quad \textbf{Equation 4}$$

What equation 4 provides as information is that the *m/z* ratio of a specific ion can be calculated, if the drift time (t) of the ion, the length of the drift tube (L) and the amplitude of the potential (V) are known values. Evidently, ions with an increasing *m/z* value will display higher drift times when compared with ones with lower *m/z* values. A critical point is that spontaneous changes in the length of the flight trajectory or potential amplitude can negatively alter the measurement accuracy. The main culprit for such issues are temperature fluctuations. It is therefore that such instruments should be kept in strictly temperature-controlled environments and mass calibrations are to be conducted regularly on a more often scale compared to quadrupoles [**105**]. The resolving power of a ToF instrument can be improved with a higher drift duration, however, increasing the length of the drift tube or reducing the acceleration voltage has been proven to be detrimental [**105**]. Poor resolution is often caused by starting

conditions for the ions which are not identical, due to kinetic and spatial dispersion [**105**]. It is how the introduction of the reflectron took place, as both of these factors were significantly minimized [**105**], together with the implementation of delayed pulsed extraction elements [**106, 107**]. The principle of a reflectron is in its mirroring qualities for ions (**Figure 11**).

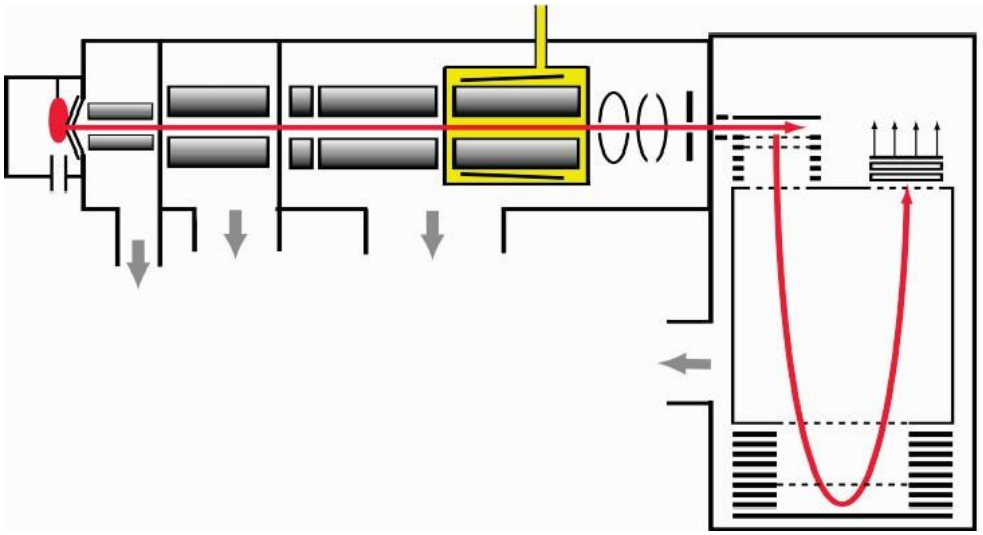

Figure 11. Scheme of the SCIEX 5600+ TripleToF instrument. [Andrews GL, Simons BL, Young JB, Hawkridge AM, Muddiman DC. Performance characteristics of a new hybrid quadrupole time-of-flight tandem mass spectrometer (TripleTOF 5600). Anal Chem. 2011 Jul 1;83(13):5442-6. doi: 10.1021/ac200812d.] Reprinted with permission of Andrews et. al. from ref doi: 10.1021/ac200812d.

It additionally provides a correction to the kinetic spread of ions carrying identical *m/z* values. The element's principle is based on the longer driftway of ions carrying a higher initial velocity, due to the fact that they reach deeper in the reflectron before being reflected. The position of the detector is critical, as it has to be located conveniently in order to record ions with identical *m/z* values as soon as the fast ions reach the slower ones. Ions with identical *m/z* values can nevertheless show a varying spatial distribution, despite being in a homogenous ion beam, due to diverse velocities and/or lacking homogeneity in the beam angle. In order to account for the missing resolution, the ions are collected once more in a field-free region before being "pushed" to an acceleration by an ion pusher. Ions which are found in closer proximity to the pulse (and thus essentially further away from the detector) are more drastically affected and thus experience a higher acceleration. The ions drift towards the detector and at a certain point join the originally separated ones, which earlier on were subjected to a lower acceleration, and are then recorded together with their flight time. The way a QToF functions is that this delayed pulsing takes place in an orthogonal direction, post the passage of the ions through the collision chamber [**108**]. By doing so the ion beam is transformed to an ion pulse. Furthermore, the detection axis is independent like this

from the ion beam, which leads to the fact that values such as resolution, acquisition speed and sensitivity are improved [**109**]. The distribution in terms of usage of QToF instruments is now vast, as they are employed with different aims, due to their flexibility and fast acquisition speeds, making comprehensive analysis of complex samples, in conjuction specifically with high-throughput UHPLC state-of-the-art methods. Newer generations of instruments have benefited from qualities similar to those of targeted MS instruments, specifically a wider dynamic range and higher sensitivity, thus providing simultaneously the benefits of a triple quadrupole instrument, whilst utilizing the power of untargeted acquisition. The most critical part in a MS instrument is undoubtedly the detector. No matter how well the ionization process takes place, resolving and filtering takes place, every acquisition is inferior without a proper ion-to-signal connection.

Obtaining an adequate signal-to-noise (S/N) ratio for a singularity of ions represents a challenge due to the low electric current they induce [**77**]. It is therefore that amplification is required, with a few exceptions [**110**]. Electron multipliers [**111**] represent a possibility to amplify the electric current induced by ions. After the ions pass through the ToF drift tube, they are accelerated in the direction of the electron multiplier dynode, by a voltage applied of the opposite polarity. In this manner, ions reach the electron multiplier with a higher kinetic energy and release multiple charged secondary particles (in negative mode those being positive ions and in positive mode those being negative ions and electrons) [**77**]. Through a following impact with the dynode, these secondary particles are converted into electrons, which on their end release further electrons in a chain reaction matter. The applied voltage‘s intensity and the form of the surface of the dynode influence the signal and by this way multiplication factors of $>10^6$ can be reached. Microchannel plates (MCPs) are the major electron multipliers used in QToF instruments. Those are essentially plates with a multitude of cylinder shaped holes, all functioning as single amplifying dynodes. A QToF instrument with regard to application has valuable qualities such as the swift response time, as the electron part is short and the larger detection area, which is perfect for large arriving ion beams. A further element down the detector system of a QToF is a digital converter for the released electron signals of the MCP. Two possibilities exist, with one being either an analog-to-digital converter (ADC), which has the advantage of a wider linear range and the ability to record signal amplitudes, or a time-to-digital converter (TDC). TDCs have the advantage of a higher sensitivity, thus resulting in a better S/N ratio [**105**]. Throughout the acquisition process the TDC is synchronized with the pulsating signals of the accelerator. Post amplification, the released ion signals are directed by a discriminator, provided that a certain threshold is reached. The arrival time of the ion signals is then registered by the TDC since the last pulse has occurred [**105**]. An *m/z*

value can be calculated through Equation 4 from this acquisition. The TDC, however, harbors the drawback that it is unable to record any further ion events during a span of a few nanoseconds knows as deadtime [**105**]. Therefore, if multiple ions with identical *m/z* values arrive at the detector system at the same time during the same pulse cycle, they are essentially recorded only as a single ion. This results in a limitation of the linear range of the detector system. It is therefore that a mathematical correction is a necessity through probability statistics, for example Poisson distribution models can be used to predict the amount of ions not acquired during instrument dead time [**105**]. This signal correction mechanism can be used to enhance the linear dynamic range by over 10-fold. Multi-channel alignment is another possibility to overcome the TDC drawbacks. The QToF instrument used in this thesis has four TDC channels [**113**]. Provided that a uniform spread of the ion bean is assumed, the ion counting capacity can be increased by 4-times. Furthermore, automated ion gating is offered by the system, meaning transmission control of the ions (ITC). An extra lens in the Q0 region (**Figure 11**) modulates the transmission of the ions in a dynamic matter depending on the total intensity of the total ion current (TIC). Vice versa, by a decrease in the ion current TDC saturation is less likely to happen. A correction factor is always used and applied to the signal intensities recorded with reduced ITC. In the case of MS/MS experiments, the ion current is vastly reduced, meaning that ITC is only activated in ToF-MS acquisition modes, but not during MS/MS experiments. Ideally, the goal of untargeted MS analysis is to acquire all analytes which can be detected, in order to further progress biomarker discovery and analysis. It is therefore that absolute quantification is not the main objective in this form of acquisition, but a more qualitative approach of the features detected, together with their identification and relative quantification. Due to the complexity of the matrices that the analytes are contained in, instruments with high resolving power are required. In this thesis, a TripleToF 5600+ by Sciex was employed and in the following text the fundamental acquisition modes of the instrument are described. Beginning with the ToF-MS survey scan, in which a complete high-resolution precursor ion spectrum is acquired. Both quadrupoles (Q1 and Q2 as a collision chamber) are operated in the RF and thus “open” mode, with the CE value set to a minimum (-5 or +5 V depending on the ionization mode used) in order to prevent any unwanted fragmentation. The acquisition mode has a nominated resolution of ≥30,000fwhm (@ m/z 829.5393 in ESI^+ and @ m/z 933.6363 in ESI^-). Having obtained the precise *m/z* values, together with metabolite specific isotopic patterns, sum formulas can be predicted. This is, however, not sufficient to provide a high enough level of confidence for metabolite identification [**113,114**]. It is therefore that further data is required in order to strengthen the metabolite identification process. Further

experiments can be appended by the addition of product ion scans, delivering a combination of targeted and untargeted analysis [**115**], called MRM-HR. Narrow Q1 transmission ranges, usually with *m/z* values of roundabout 0.7 are employed to isolate certain precursor ions, which are then fragmented in the collision chamber via CID. Due to the similarities with a classic MRM acquisition in triple quadrupole instruments, but the difference being in the high mass accuracy, this scan mode has been dubbed MRM-HR. The obtained highly selective spectra can be used for structure elucidation and proper metabolite identification. Furthermore, as the acquisition process is dynamic, the extraction of ion chromatograms (EICs), can be beneficial for quantification be it on a MS1 or MS2 level. When employing tandem mass spectrometry, one has to consider variables such as cycle time, which is essentially the summed value of experimental accumulation times and system times such as instrument settling time. It is a general consensus that a minimum of 10 data points per peak are required [**102**]. The peak width is a value, which is therefore closely connected with the accumulation time in an experiment. As with increasing accumulation time the signal to noise value is improved [**116**], it should always be held at the highest possible value for the least abundant metabolites. The analytical run can be split into multiple periods different in their MS and MS/MS acquisition parameters [**117**]. Such period experiments are designed with the aim of monitoring a set of target analytes only during their elution time periods. It is in a manner comparable with scheduled multiple reaction monitoring (sMRM) analysis in triple quadrupole instruments, where accumulation times can be more efficiently distributed throughout the target metabolites. Compared to a triple quadrupole, the analysis of fragment ion ratios is automatically enabled without the necessity of any further MS experiments. The monitoring of these ion ratios is a good marker for the selectivity of the analysis, as the ratios should remain constant, provided no isobaric interferences are present [**116**]. Product ion analysis scans can either be conducted in high-resolution or high-sensitivity mode of action. In high-sensitivity, a focusing of the ions after their release from the collision chamber takes places, which increases the yield of the ions in the accelerator. However, the linear correlation between the initial ion velocity and the ion position in the pulser, on which the compensation by delayed pulsed extraction and reflection is based, is hereby distorted. It is therefore that this increase in sensitivity comes together with a lower resolution (resolving power ≥15,000fwhm). During the high-resolution acquisition mode, the ion optics system is off and a loss of ions occurs at the tip of the skimmer towards the entrance of the accelerator. Thus, sensitivity is lower due to the reduced duty cycle. However, a resolution as in during a ToF-MS survey scan (resolving power ≥30,000fwhm) is reached owing to the correction of velocity and spatial spreads [**118**]. Other than these

two acquisition options, signal intensity can be modulated by enhancing set *m/z* values via pre-tuning of the ion optic potentials, which leads to a momentarily ion trapping and accumulation in the collision chamber, with a following rapid ion release into the accelerator and optimized timing of the ToF ion pulse [**105**]. IRD values, meaning ideal ion release delays, as in the time between ion release and the conduction of the ToF pulse, and IRW values, as in the duration of the ToF pulse releasing the ion beam. By optimizing these values, a ≥3-fold gain in sensitivity for a *m/z* region of about 400 units around the set value can be achieved. By optimizing the experiment cycle, sensitivities compared to those achieved with instruments designed for targeted analysis, i.e. triple quadrupoles can be achieved. Despite that the ToF-MS survey scan acquires untargeted MS data on a MS1 level, acquiring comprehensive data on a MS2-level is much more challenging. A possibility to increase the comprehensiveness of MS/MS data is the implementation of information-dependent acquisition (IDA, which is a form of data dependent acquisition (DDA)) [**119, 120**]. In brief, it showcases a form of a dynamic product ion scan, triggered after certain set criteria are met in the ToF-MS scan. IDA is versatile and is used to acquire the product ion spectra of the most abundant metabolites in an analytical run. A further option to customize the IDA analysis is the utilization of so-called inclusion and/or exclusion lists. A limitation of IDA is the number of product ion scans that can be recorded during a single cycle, and this is set by the acquisition frequency of the individual instrument, which in this case is 100 Hz for the Sciex TripleToF 5600+, which leads to the fact that often only the top 10 – 20 most abundant ions per cycle are chosen for further fragmentation and analysis. IDA provides an advantageous result with the amount of high-quality MS/MS spectra acquired, leading to a more reliable metabolite identification process. However, this highly selective result on a MS2 level cannot be fully relied upon for quantitative analysis, as often the amount of data points per peak is not sufficient. It is therefore that one is restricted to the data obtained in the ToF-MS survey scan, which is however, present with a certain risk to it, as interferences can occur. Despite the increased comprehensiveness provided by IDA, there is still a possibility to miss certain metabolites, which can be of high importance. Specifically, low abundant metabolites are not always acquired in IDA, which leads to missing information on a MS2 level. It is therefore that truly full comprehensive data can only be acquired by data-independent acquisition (DIA) modes. A simple, yet flexible possibility to achieve this is MS^E, which has been originally reported in its use on the QTof instruments provided by Waters. It has often been also coined as All-ion-fragmentation (AIF), with this technique being implemented in the QTof system of Agilent Technologies and the Orbitraps designed by Thermo Fisher Scientific [**121,122**]. Essentially, two ToF-MS scans take place, one

with a lower collision energy value for precursor isolation and detection and the second one with a higher one in order to provide adequate fragmentation. It is of utmost importance to achieve good chromatographic separation, otherwise the acquired spectra require the process of deconvolution [**122**]. MS/MS^{ALL} is another possibility for DIA acquisition [**123**], which relies on small unit mass resolution Q1 precursor window steps, so that sequential fragmentation is achieved. A limitation of this mode is its incompatibility with LC or GC techniques, as the cycle times are simply not compatible together. It is therefore that this DIA mode of analysis is only available when it comes to direct infusion, also known as shotgun acquisition. Experiments with sequential fragmentation via Q1 isolation have been reported in the scientific literature [**124**]. In this scenario, every MS2 experiment involved a *m/z* width of 10 units. The issue here was, however, that the acquisition rates of the instruments were not fast enough to record the complexity of the range acquired, especially when coupled with chromatographic separation techniques. This remained an issue until the introduction of the DIA acquisition mode called SWATH (sequential windows acquisition of all theoretical fragment-ion mass spectra) [**121,125**]. SWATH is based on setting the Q1 transmission windows in variable widths. The precursor ions are then collectively fragmented in the collision chamber, which yields significantly more composite MS2 spectra with a higher degree of selectivity compared to MS^{E} (AIF). The drawback is that the quality of the spectra is more prone to interferences than the ones obtained in IDA, together with the requirement of deconvolution, which is a complex process. Despite this, it has been shown that SWATH data leads to better and more accurate metabolite identification, together with a much higher metabolome coverage [**121,126,127**]. A further advantage is the possibility to generate extracted ion chromatograms on both MS1 and MS2 levels, which provides an option to quantify via various ions. The comprehensive spectra acquired can be easily deconvoluted in the MS-DIAL software (Mass Spectrometry - Data-Independent Analysis) [**128**], which was also used in numerous projects in this thesis. Another tool utilized in this thesis is swathTUNER [**129**], which allows the more flexible design of SWATH experiments. As a conclusion, it can be regarded certainly that SWATH is the superior acquisition mode in terms of untargeted MS, with the qualitative and quantitative data obtained being of high reproducible quality [**130**].

2. References

[1] Moss, G. P.; Smith, P. A. S.; Tavernier, D. In Pure and Applied Chemistry, 1995, p 1307.

[2] Emwas AH, Roy R, McKay RT, Tenori L, Saccenti E, Gowda GAN, Raftery D, Alahmari F, Jaremko L, Jaremko M, Wishart DS. NMR Spectroscopy for Metabolomics Research. Metabolites. 2019 Jun 27;9(7):123. doi: 10.3390/metabo9070123.

[3] Wishart DS, Cheng LL, Copié V, Edison AS, Eghbalnia HR, Hoch JC, Gouveia GJ, Pathmasiri W, Powers R, Schock TB, Sumner LW, Uchimiya M. NMR and Metabolomics-A Roadmap for the Future. Metabolites. 2022 Jul 23;12(8):678. doi: 10.3390/metabo12080678.

[4] Nagana Gowda GA, Raftery D. NMR-Based Metabolomics. Adv Exp Med Biol. 2021;1280:19-37. doi: 10.1007/978-3-030-51652-9_2.

[5] Beale DJ, Pinu FR, Kouremenos KA, Poojary MM, Narayana VK, Boughton BA, Kanojia K, Dayalan S, Jones OAH, Dias DA. Review of recent developments in GC-MS approaches to metabolomics-based research. Metabolomics. 2018 Nov 17;14(11):152. doi: 10.1007/s11306-018-1449-2.

[6] Kanani H, Chrysanthopoulos PK, Klapa MI. Standardizing GC-MS metabolomics. J Chromatogr B Analyt Technol Biomed Life Sci. 2008 Aug 15;871(2):191-201. doi: 10.1016/j.jchromb.2008.04.049. Epub 2008 May 21.

[7] Theodoridis GA, Gika HG, Want EJ, Wilson ID. Liquid chromatography-mass spectrometry based global metabolite profiling: a review. Anal Chim Acta. 2012 Jan 20;711:7-16. doi: 10.1016/j.aca.2011.09.042. Epub 2011 Nov 4.

[8] Xiao JF, Zhou B, Ressom HW. Metabolite identification and quantitation in LC-MS/MS-based metabolomics. Trends Analyt Chem. 2012 Feb 1;32:1-14. doi: 10.1016/j.trac.2011.08.009.

[9] Chen CJ, Lee DY, Yu J, Lin YN, Lin TM. Recent advances in LC-MS-based metabolomics for clinical biomarker discovery. Mass Spectrom Rev. 2023 Nov-Dec;42(6):2349-2378. doi: 10.1002/mas.21785. Epub 2022 May 29. PMID: 35645144.

[10] Zamboni, N.; Fendt, S.-M.; Rühl, M.; Sauer, U. 13 C-Based Metabolic Flux Analysis. Nat. Protoc. 2009, 4 (6), 878–892.

[11] Horai, H.; Arita, M.; Kanaya, S.; Nihei, Y.; Ikeda, T.; Suwa, K.; Ojima, Y.; Tanaka, K.; Tanaka, S.; Aoshima, K.; et al. MassBank: A Public Repository for Sharing Mass Spectral Data for Life Sciences. J. Mass Spectrom. 2010, 45 (7), 703–714. https://doi.org/10.1002/jms.1777.

[12] Brown, M.; Dunn, W. B.; Dobson, P.; Patel, Y.; Winder, C. L.; Francis Mcintyre, S.; Begley, P.; Carroll, K.; Broadhurst, D.; Tseng, A.; et al. Mass Spectrometry Tools and Metabolite-Specific Databases for Molecular Identification in Metabolomics. Analyst 2009, 134 (7), 1322–1332. https://doi.org/10.1039/b901179j.

[13] Guijas, C.; Montenegro-Burke, J. R.; Domingo-Almenara, X.; Palermo, A.; Warth, B.; Hermann, G.; Koellensperger, G.; Huan, T.; Uritboonthai, W.; Aisporna, A. E.; et al. METLIN: A Technology Platform for Identifying Knowns and Unknowns. Anal. Chem. 2018, 90 (5), 3156–3164. https://doi.org/10.1021/acs.analchem.7b04424.

[14] Montenegro-Burke, J. R.; Guijas, C.; Siuzdak, G. METLIN: A Tandem Mass Spectral Library of Standards. Methods Mol. Biol. 2020, 2104, 149 163. https://doi.org/10.1007/978-1-0716-0239-3_9

[15] Hummel, J.; Selbig, J.; Walther, D.; Kopka, J. The Golm Metabolome Database: A Database for GC-MS Based Metabolite Profiling. In Metabolomics; Springer, 2007; pp 75–95.

[16] Kind, T.; Wohlgemuth, G.; Lee, D. Y.; Lu, Y.; Palazoglu, M.; Shahbaz, S.; Fiehn, O. FiehnLib: Mass Spectral and Retention Index Libraries for Metabolomics Based on Quadrupole and Time-of-Flight Gas Chromatography/Mass Spectrometry. Anal. Chem. 2009, 81 (24), 10038 10048.

[17] Sisco, E.; Moorthy, A. S.; Watt, L. M. Creation and Release of an Updated NIST DART-MS Forensics Database. J. Am. Soc. Mass Spectrom. 2021, 32 (3), 685–689. https://doi.org/10.1021/jasms.0c00416., Heller, S. The History of the NIST/EPA/NIH Mass Spectral Database. Today's Chem. Work 1999, 8 (2), 45–46.

[18] Kanehisa, M.; Goto, S. KEGG: Kyoto Encyclopedia of Genes and Genomes. Nucleic Acids Res. 2000, 28 (1), 27–30.

[19] Caspi, R.; Billington, R.; Keseler, I. M.; Kothari, A.; Krummenacker, M.; Midford, P. E.; Ong, W. K.; Paley, S.; Subhraveti, P.; Karp, P. D. The MetaCyc Database of Metabolic Pathways and Enzymes-a 2019 Update. Nucleic Acids Res. 2020, https://doi.org/10.1093/nar/gkz862.

[20] Zamboni, N.; Fendt, S.-M.; Rühl, M.; Sauer, U. 13 C-Based Metabolic Flux Analysis. Nat. Protoc. 2009, 4 (6), 878–892.

[21] Liebisch, G.; Ahrends, R.; Arita, M.; Arita, M.; Bowden, J. A.; Ejsing, C. S.; Griffiths, W. J.; Holčapek, M.; Köfeler, H.; Mitchell, T. W.; et al. Lipidomics Needs More Standardization. Nat. Metab. 2019, 1 (8), 745–747. https://doi.org/10.1038/s42255-019-0094-z.

[22] D'Hondt, E.; Martín-Juárez, J.; Bolado, S.; Kasperoviciene, J.; Koreiviene, J.; Sulcius, S.; Elst, K.; Bastiaens, L. Cell Disruption Technologies. Microalgae-Based Biofuels Bioprod. From Feed. Cultiv. to End-Products 2017, 133–154. https://doi.org/10.1016/B978-0-08-101023-5.00006-6.

[23] Leitner, A. Phosphopeptide Enrichment Using Metal Oxide Affinity Chromatography. TrAC Trends Anal. Chem. 2010, 29 (2), 177–185. https://doi.org/https://doi.org/10.1016/j.trac.2009.08.007.

[24] Connor, P. A.; McQuillan, A. J. Phosphate Adsorption onto TiO2 from Aqueous Solutions: An in Situ Internal Reflection Infrared Spectroscopic Study. Langmuir 1999, https://doi.org/10.1021/la980894p. 15 (8), 2916–2921.

[25] A. Wakamatsu, K. Morimoto, M. Shimizu, S. Kudoh, A severe peak tailing of phosphate compounds caused by interaction with stainless steel used for liquid chromatography and electrospray mass spectrometry, J. Sep. Sci. 28 (2005) 1823–1830. https://doi.org/10.1002/jssc.200400027.

[26] Y. Asakawa, N. Tokida, C. Ozawa, M. Ishiba, O. Tagaya, N. Asakawa, Suppression effects of carbonate on the interaction between stainless steel and phosphate groups of phosphate compounds in high-performance liquid chromatography and electrospray ionization mass spectrometry, J. Chromatogr. A. 1198–1199 (2008) 80–86. https://doi.org/10.1016/j.chroma.2008.05.015.

[27] R. Tuytten, F. Lemière, E. Witters, W. Van Dongen, H. Slegers, R.P. Newton, H. Van Onckelen, E.L. Esmans, Stainless steel electrospray probe: A dead end for phosphorylated organic compounds?, J. Chromatogr. A. 1104 (2006) 209–221. https://doi.org/10.1016/j.chroma.2005.12.004.

[28] Zhang, T. Y.; Li, S.; Zhu, Q. F.; Wang, Q.; Hussain, D.; Feng, Y. Q. Derivatization for Liquid Chromatography-Electrospray Ionization-Mass Spectrometry Analysis of Small-Molecular Weight Compounds. TrAC - Trends Anal. Chem. 2019, 119. https://doi.org/10.1016/j.trac.2019.07.019.

[29] Ortmayr, K., et al., An integrated metabolomics workflow for the quantification of sulfur pathway intermediates employing thiol protection with N-ethyl maleimide and hydrophilic interaction liquid chromatography tandem mass spectrometry. Analyst, 2015. 140(22): p. 7687-95.

[30] Hansen, R.E. and J.R. Winther, An introduction to methods for analyzing thiols and disulfides: Reactions, reagents, and practical considerations. Anal Biochem, 2009. 394(2): p. 147-58.6. Morgan, B., et al., Multiple glutathione disulfide removal pathways mediate cytosolic redox homeostasis. Nature chemical biology, 2013. 9(2): p. 119-125.

[31] Serafimov K, Aydin Y, Lämmerhofer M. Quantitative analysis of the glutathione pathway cellular metabolites by targeted liquid chromatography-tandem mass spectrometry. J Sep Sci. 2024 Jan;47(1):e2300780. doi: 10.1002/jssc.202300780.

[32] Z. León, J.C. García-Cañaveras, M.T. Donato, A. Lahoz, Mammalian cell metabolomics: Experimental design and sample preparation, Electrophoresis. 34 (2013) 2762–2775. doi:10.1002/elps.201200605.

[33] A. Zhang, H. Sun, P. Wang, Y. Han, X. Wang, Modern analytical techniques in metabolomics analysis, Analyst. 137 (2012) 293–300. doi:10.1039/C1AN15605E

[34] F. Courant, J.-P. Antignac, G. Dervilly-Pinel, B. Le Bizec, Basics of mass spectrometry based metabolomics, Proteomics. 14 (2014) 2369–2388. doi:10.1002/pmic.201400255

[35] I. Kohler, A. Verhoeven, R.J. Derks, M. Giera, Analytical pitfalls and challenges in clinical metabolomics, Bioanalysis. 8 (2016) 1509–32. doi:10.4155/bio-2016 0090

[36] P. Yin, G. Xu, Current state-of-the-art of nontargeted metabolomics based on liquid chromatography-mass spectrometry with special emphasis in clinical applications, J. Chromatogr. A. 1374 (2014) 1–13. doi:10.1016/j.chroma.2014.11.050

[37] Wang T, Wang X, Zhuang Y, Wang G. A systematic evaluation of quenching and extraction procedures for quantitative metabolome profiling of HeLa carcinoma cell under 2D and 3D cell culture conditions. Biotechnol J. 2023 May;18(5):e2200444. doi: 10.1002/biot.202200444.

[38] Sellick CA, Hansen R, Maqsood AR, Dunn WB, Stephens GM, Goodacre R, Dickson AJ. Effective quenching processes for physiologically valid metabolite profiling of suspension cultured Mammalian cells. Anal Chem. 2009 Jan 1;81(1):174-83. doi: 10.1021/ac8016899.

[39] Pabst M, Grass J, Fischl R, Léonard R, Jin C, Hinterkörner G, Borth N, Altmann F. Nucleotide and nucleotide sugar analysis by liquid chromatography-electrospray ionization-mass spectrometry on surface-conditioned porous graphitic carbon. Anal Chem. 2010 Dec 1;82(23):9782-8. doi: 10.1021/ac101975k.

[40] Pabst M, Grass J, Fischl R, Léonard R, Jin C, Hinterkörner G, Borth N, Altmann F. Nucleotide and nucleotide sugar analysis by liquid chromatography-electrospray ionization-mass spectrometry on surface-conditioned porous graphitic carbon. Anal Chem. 2010 Dec 1;82(23):9782-8. doi: 10.1021/ac101975k.

[41] A. Hutschenreuther, A. Kiontke, G. Birkenmeier, C. Birkemeyer, Comparison of extraction conditions and normalization approaches for cellular metabolomics of adherent growing cells with GC-MS, Anal. Methods. 4 (2012) 1953–1963. doi:10.1039/c2ay25046b.

[42] K. Dettmer, N. Nürnberger, H. Kaspar, M.A. Gruber, M.F. Almstetter, P.J. Oefner, Metabolite extraction from adherently growing mammalian cells for metabolomics studies: Optimization of harvesting and extraction protocols, Anal. Bioanal. Chem. 399 (2011) 1127–1139. doi:10.1007/s00216-010-4425-x.

[43] Y. Wu, L. Li, Sample normalization methods in quantitative metabolomics, J. Chromatogr. A. 1430 (2016) 80–95. doi:10.1016/j.chroma.2015.12.007

[44] S. Dietmair, N.E. Timmins, P.P. Gray, L.K. Nielsen, J.O. Krömer, Towards quantitative metabolomics of mammalian cells: Development of a metabolite extraction protocol, Anal. Biochem. 404 (2010) 155–164. doi:10.1016/j.ab.2010.04.031.

[45] R.J. Raterink, P.W. Lindenburg, R.J. Vreeken, R. Ramautar, T. Hankemeier, Recent developments in sample-pretreatment techniques for mass spectrometry-based metabolomics, Trends Anal. Chem. 61 (2014) 157–167. doi:10.1016/j.trac.2014.06.003.

[46] E.J. Want, G. O'Maille, C.A. Smith, T.R. Brandon, W. Uritboonthai, C. Qin, S.A. Trauger, G. Siuzdak, Solvent-dependent metabolite distribution, clustering, and protein extraction for serum profiling with mass spectrometry, Anal. Chem. 78 (2006) 743–752. doi:10.1021/ac051312t.

[47] A. Agin, D. Heintz, E. Ruhland, J.M. Chao de la Barca, J. Zumsteg, V. Moal, A.S. Gauchez, I.J. Namer, Metabolomics - an overview. From basic principles to potential biomarkers (part 1), Med. Nucl. 40 (2016) 4–10. doi:10.1016/j.mednuc.2015.12.006

[48] A. Rühling, D. Wang, J.B. Ernst, S. Wulff, R. Honeker, C. Richter, A. Ferry, H.J. Galla, F. Glorius, Influence of the Headgroup of Azolium-Based Lipids on Their Biophysical Properties and Cytotoxicity, Chem. - A Eur. J. 23 (2017) 5920 5924. doi:10.1002/chem.201604182.

[49] G. Marrubini, P. Appelblad, M. Maietta, A. Papetti, Hydrophilic interaction chromatography in food matrices analysis: An updated review, Food Chem. 257 (2018) 53–66. doi:10.1016/j.foodchem.2018.03.008

[50] D. V. McCalley, Hydrophilic Interaction Chromatography, LCGC North Am. Suppl. 26 (2008) 53–58. doi:10.1002/9781118495247.

[51] Y. Guo, Recent progress in the fundamental understanding of hydrophilic interaction chromatography (HILIC), Analyst. 140 (2015) 6452–6466. doi:10.1039/c5an00670h

[52] D. V. McCalley, Understanding and manipulating the separation in hydrophilic interaction liquid chromatography, J. Chromatogr. A. 1523 (2017) 49–71. doi:10.1016/j.chroma.2017.06.026

[53] A.J. Alpert, Hydrophilic-interaction chromatography for the separation of peptides, nucleic acids and other polar compounds, J. Chromatogr. 499 (1990) 177–196. doi:10.1016/S0021-9673(00)96972-3

[54] P. Jandera, Stationary and mobile phases in hydrophilic interaction chromatography: a review, Anal. Chim. Acta. 692 (2011) 1–25. doi:http://dx.doi.org/10.1016/j.aca.2011.02.047

[55] K. Spagou, H. Tsoukali, N. Raikos, H. Gika, I.D. Wilson, G. Theodoridis, Hydrophilic interaction chromatography coupled to MS for metabonomic/metabolomic studies, J. Sep. Sci. 33 (2010) 716–727. doi:10.1002/jssc.200900803.

[56] L. Qiao, X. Shi, G. Xu, Recent advances in development and characterization of stationary phases for hydrophilic interaction chromatography, Trends Anal. Chem. 81 (2016) 23–33. doi:http://dx.doi.org/10.1016/j.trac.2016.03.021.

[57] P. Hemström, K. Irgum, Hydrophilic interaction chromatography, J. Sep. Sci. 29 (2006) 1784–1821. doi:10.1002/jssc.200600199.

[58] S. Hendrickx, E. Adams, D. Cabooter, Recent advances in the application of hydrophilic interaction chromatography for the analysis of biological matrices., Bioanalysis. 7 (2015) 2927–2945. doi:10.4155/bio.15.200.

[59] G. Greco, T. Letzel, Main interactions and influences of the chromatographic parameters in HILIC separations, J. Chromatogr. Sci. 51 (2013) 684–693. doi:10.1093/chromsci/bmt015.

[60] B. Buszewski, S. Noga, Hydrophilic interaction liquid chromatography (HILIC)-a powerful separation technique, Anal. Bioanal. Chem. 402 (2012) 231–247. doi:10.1007/s00216-011-5308-5

[61] Z. Li, J. Han, S. Sun, K. Chen, D. Tang, Hydrophilic Interaction Liquid Chromatography Tandem Mass Spectrometry: An Attractive and Prospective Method for Quantitative Bioanalysis in Drug Metabolism, Curr. Drug Metab. 17 (2016) 386–400. doi:10.2174/1389200217666151210141757.

[62] D.S. Bell, Retention and Selectivity of Stationary Phases Used in HILIC, LCGC North Am. 33 (2015) 90–101. http://www.chromatographyonline.com/retention and-selectivity-stationary-phases-used-hilic

[63] P. Jandera, T. Hájek, Mobile phase effects on the retention on polar columns with special attention to the dual hydrophilic interaction–reversed-phase liquid chromatography mechanism, a review, J. Sep. Sci. 41 (2018) 145–162. doi:10.1002/jssc.201701010.

[64] Virgiliou C, Sampsonidis I, Gika HG, Raikos N, Theodoridis GA. Development and validation of a HILIC-MS/MS multitargeted method for metabolomics applications. Electrophoresis. 2015 Sep;36(18):2215-2225. doi: 10.1002/elps.201500208. Erratum in: Electrophoresis. 2016 Jul;37(14):2113. doi: 10.1002/elps.201670125.

[65] Preinerstorfer B, Schiesel S, Lämmerhofer M, Lindner W. Metabolic profiling of intracellular metabolites in fermentation broths from beta-lactam antibiotics production by liquid chromatography-tandem mass spectrometry methods. J Chromatogr A. 2010 Jan 15;1217(3):312-28. doi: 10.1016/j.chroma.2009.11.051.

[66] Serafimov K, Lämmerhofer M. Metabolic profiling workflow for cell extracts by targeted hydrophilic interaction liquid chromatography-tandem mass spectrometry. J Chromatogr A. 2022 Nov 22;1684:463556. doi: 10.1016/j.chroma.2022.463556.

[67] Su M, Serafimov K, Li P, Knappe C, Lämmerhofer M. Isomer selectivity of one- and two-dimensional approaches of mixed-mode and hydrophilic interaction liquid chromatography coupled to tandem mass spectrometry for sugar phosphates of glycolysis and pentose phosphate pathways. J Chromatogr A. 2023 Jan 11;1688:463727. doi: 10.1016/j.chroma.2022.463727.

[68] Lioupi A, Virgiliou C, Walter TH, Smith KM, Rainville P, Wilson ID, Theodoridis G, Gika HG. Application of a hybrid zwitterionic hydrophilic interaction liquid chromatography column in metabolic profiling studies. J Chromatogr A. 2022 Jun 7;1672:463013. doi: 10.1016/j.chroma.2022.463013.

[69] Pascali JP, Fais P, Vaiano F, Ciolini A, Bertol E. Zwitterionic HILIC stationary phase as a valuable alternative in separative techniques: Application to the analysis of gamma-hydroxybutyric acid and its metabolite in hair. J Chromatogr B Analyt Technol Biomed Life Sci. 2019 Dec 15;1134-1135:121876. doi: 10.1016/j.jchromb.2019.121876.

[70] Fu X, Cebo M, Ikegami T, Lämmerhofer M. Retention characteristics of poly(N-(1H-tetrazole-5-yl)-methacrylamide)-bonded stationary phase in hydrophilic interaction chromatography. J Chromatogr A. 2020 Jan 4;1609:460500. doi: 10.1016/j.chroma.2019.460500.

[71] Sonnenberg RA, Naz S, Cougnaud L, Vuckovic D. Comparison of underivatized silica and zwitterionic sulfobetaine hydrophilic interaction liquid chromatography stationary phases for global metabolomics of human plasma. J Chromatogr A. 2019 Dec 20;1608:460419. doi: 10.1016/j.chroma.2019.460419.

[72] Vass A, Robles-Molina J, Pérez-Ortega P, Gilbert-López B, Dernovics M, Molina-Díaz A, García-Reyes JF. Study of different HILIC, mixed-mode, and other aqueous normal-phase approaches for the liquid chromatography/mass spectrometry-based determination of challenging polar pesticides. Anal Bioanal Chem. 2016 Jul;408(18):4857-69. doi: 10.1007/s00216-016-9589-6.

[73] Serafimov K, Knappe C, Li F, Sievers-Engler A, Lämmerhofer M. Solving the retention time repeatability problem of hydrophilic interaction liquid chromatography. J Chromatogr A. 2024 Aug 16;1730:465060. doi: 10.1016/j.chroma.2024.465060.

[74] Miller, P. E.; Denton, M. B. Journal of Chemical Education 1986, 63, 617.

[75] Somogyi, Á. In Medical Applications of Mass Spectrometry, Vékey, K.; Telekes, A.; Vertes, A., Eds.; Elsevier: Amsterdam, 2008, pp 93-140.

[76] Henchman, M.; Steel, C. Journal of Chemical Education 1998, 75, 1049.

[77] de Hoffmann, E.; Stroobant, V. Mass Spectrometry - Principles and Appication, 3rd ed.; John Wiley & Sons, Ltd, 2007

[78] Buchberger AR, DeLaney K, Johnson J, Li L. Mass Spectrometry Imaging: A Review of Emerging Advancements and Future Insights. Anal Chem. 2018 Jan 2;90(1):240-265. doi: 10.1021/acs.analchem.7b04733. Epub 2017 Dec 13
[79] Wait R. Introduction to mass spectrometry. Methods Mol Biol. 1993;17:191-213. doi: 10.1385/0-89603-215-9:191.

[80] Tang, L.; Kebarle, P. Analytical Chemistry 1993, 65, 3654-3668.

[81] Hopfgartner, G.; Bean, K.; Henion, J.; Henry, R. J Chromatogr A 1993, 647, 51-61.

[82] Van Berkel GJ, Kertesz V. Using the electrochemistry of the electrospray ion source. Anal Chem. 2007 Aug 1;79(15):5510-20. doi: 10.1021/ac071944a.

[83] Van Berkel, G. J.; Zhou, F. Analytical Chemistry 1995, 67, 3958-3964.

[84] Matuszewski BK, Constanzer ML, Chavez-Eng CM. Strategies for the assessment of matrix effect in quantitative bioanalytical methods based on HPLC-MS/MS. Anal Chem. 2003 Jul 1;75(13):3019-30. doi: 10.1021/ac020361s.

[85] Trufelli H, Palma P, Famiglini G, Cappiello A. An overview of matrix effects in liquid chromatography-mass spectrometry. Mass Spectrom Rev. 2011 May-Jun;30(3):491-509. doi: 10.1002/mas.20298.

[86] Dreisewerd K. The desorption process in MALDI. Chem Rev. 2003 Feb;103(2):395-426. doi: 10.1021/cr010375i.

[87] Haag AM. Mass Analyzers and Mass Spectrometers. Adv Exp Med Biol. 2016;919:157-169. doi: 10.1007/978-3-319-41448-5_7.

[88] R. Bonner, G. Hopfgartner, SWATH data independent acquisition mass spectrometry for metabolomics, TrAC - Trends Anal. Chem. 120 (2019). doi:10.1016/j.trac.2018.10.014.

[89] Zhou, Y. Yin, Strategies for large-scale targeted metabolomics quantification by liquid chromatography-mass spectrometry, Analyst. 141 (2016) 6362–6373. doi:10.1039/C6AN01753C.

[90] Dell'mour, L. Jaitz, E. Oburger, M. Puschenreiter, G. Koellensperger, S. Hann, Hydrophilic interaction LC combined with electrospray MS for highly sensitive analysis of underivatized amino acids in rhizosphere research, J Sep Sci. 33 (2010) 911–922. doi:10.1002/jssc.200900743.

[91] Chen, Z. Zhou, W. Yang, N. Bi, J. Xu, J. He, R. Zhang, L. Wang, Z. Abliz, Development of a Data-Independent Targeted Metabolomics Method for Relative Quantification Using Liquid Chromatography Coupled with Tandem Mass Spectrometry, Anal. Chem. 89 (2017) 6954–6962. doi:10.1021/acs.analchem.6b04727

[92] Bonner, G. Hopfgartner, SWATH data independent acquisition mass spectrometry for metabolomics, TrAC - Trends Anal. Chem. 120 (2019). doi:10.1016/j.trac.2018.10.014.

[93] S.J. Lehotay, Y. Sapozhnikova, H.G.J. Mol, Current issues involving screening and identification of chemical contaminants in foods by mass spectrometry, TrAC - Trends Anal. Chem. 69 (2015) 62–75. doi:10.1016/j.trac.2015.02.012

[94] J. Zhou, Y. Yin, Strategies for large-scale targeted metabolomics quantification by liquid chromatography-mass spectrometry, Analyst. 141 (2016) 6362–6373. doi:10.1039/C6AN01753C.

[95] Siegel D, Permentier H, Reijngoud DJ, Bischoff R. Chemical and technical challenges in the analysis of central carbon metabolites by liquid-chromatography mass spectrometry. J Chromatogr B Analyt Technol Biomed Life Sci. 2014 Sep 1;966:21-33. doi: 10.1016/j.jchromb.2013.11.022.

[96] Giera M, Aisporna A, Uritboonthai W, Siuzdak G. The hidden impact of in-source fragmentation in metabolic and chemical mass spectrometry data interpretation. Nat Metab. 2024 Jun 25. doi: 10.1038/s42255-024-01076-x. Epub ahead of print.

[97] O. Begou, H.G. Gika, I.D. Wilson, G. Theodoridis, Hyphenated MS-based targeted approaches in metabolomics, Analyst. 142 (2017) 3079–3100. doi:10.1039/c7an00812k.

[98] Xu J, Li J, Zhang R, He J, Chen Y, Bi N, Song Y, Wang L, Zhan Q, Abliz Z. Development of a metabolic pathway-based pseudo-targeted metabolomics method using liquid chromatography coupled with mass spectrometry. Talanta. 2019 Jan 15;192:160-168. doi: 10.1016/j.talanta.2018.09.021.

[99] Liu B, Du Z, Zhang W, Guo X, Lu Y, Jiang Y, Tu P. A pseudo-targeted metabolomics for discovery of potential biomarkers of cardiac hypertrophy in rats. J Chromatogr B Analyt Technol Biomed Life Sci. 2024 Jun 1;1240:124133. doi: 10.1016/j.jchromb.2024.124133.

[100] Zheng F, Zhao X, Zeng Z, Wang L, Lv W, Wang Q, Xu G. Development of a plasma pseudotargeted metabolomics method based on ultra-high-performance liquid chromatography-mass spectrometry. Nat Protoc. 2020 Aug;15(8):2519-2537. doi: 10.1038/s41596-020-0341-5.

[101] Wang F, Liigand J, Tian S, Arndt D, Greiner R, Wishart DS. CFM-ID 4.0: More Accurate ESI-MS/MS Spectral Prediction and Compound Identification. Anal Chem. 2021 Aug 31;93(34):11692-11700. doi: 10.1021/acs.analchem.1c01465.

[102] Hopfgartner G, Bourgogne E. Quantitative high-throughput analysis of drugs in biological matrices by mass spectrometry. Mass Spectrom Rev. 2003 May-Jun;22(3):195-214. doi: 10.1002/mas.10050.

[103] Glish GL, Burinsky DJ. Hybrid mass spectrometers for tandem mass spectrometry. J Am Soc Mass Spectrom. 2008 Feb;19(2):161-72. doi: 10.1016/j.jasms.2007.11.013.

[104] Griffiths WJ, Wang Y. Mass spectrometry: from proteomics to metabolomics and lipidomics. Chem Soc Rev. 2009 Jul;38(7):1882-96. doi: 10.1039/b618553n.

[105] Chernushevich IV, Loboda AV, Thomson BA. An introduction to quadrupole-time-of-flight mass spectrometry. J Mass Spectrom. 2001 Aug;36(8):849-65. doi: 10.1002/jms.207.

[106] Vestal, M. L.; Juhasz, P.; Martin, S. A. Rapid Communications in Mass Spectrometry 1995, 9, 1044-1050.

[107] Wiley, W. C.; McLaren, I. H. Review of Scientific Instruments 1955, 26, 1150-1157.

[108] Dawson, J. H. J.; Guilhaus, M. Rapid Communications in Mass Spectrometry 1989, 3, 155-159.

[109] Guilhaus, M.; Selby, D.; Mlynski, V. Mass Spectrometry Reviews 2000, 19, 65-107.

[110] Koppenaal, D. W.; Barinaga, C. J.; Denton, M. B.; Sperline, R. P.; Hieftje, G. M.; Schilling, G. D.; Andrade, F. J.; Barnes, J. H.; Iv, I. V. Analytical Chemistry 2005, 77, 418 A-427 A.

[111] Collins, R. D. Vacuum 1969, 19, 105-111.

[112] Andrews GL, Simons BL, Young JB, Hawkridge AM, Muddiman DC. Performance characteristics of a new hybrid quadrupole time-of-flight tandem mass spectrometer (TripleTOF 5600). Anal Chem. 2011 Jul 1;83(13):5442-6. doi: 10.1021/ac200812d

[113] Kirwan JA, Gika H, Beger RD, Bearden D, Dunn WB, Goodacre R, Theodoridis G, Witting M, Yu LR, Wilson ID; metabolomics Quality Assurance and Quality Control Consortium (mQACC). Quality assurance and quality control reporting in untargeted metabolic phenotyping: mQACC recommendations for analytical quality management. Metabolomics. 2022 Aug 27;18(9):70. doi: 10.1007/s11306-022-01926-3.

[114] Mosley JD, Schock TB, Beecher CW, Dunn WB, Kuligowski J, Lewis MR, Theodoridis G, Ulmer Holland CZ, Vuckovic D, Wilson ID, Zanetti KA. Establishing a framework for best practices for quality assurance and quality control in untargeted metabolomics. Metabolomics. 2024 Feb 12;20(2):20. doi: 10.1007/s11306-023-02080-0.

[115] Cajka T, Fiehn O. Toward Merging Untargeted and Targeted Methods in Mass Spectrometry-Based Metabolomics and Lipidomics. Anal Chem. 2016 Jan 5;88(1):524-45. doi: 10.1021/acs.analchem.5b04491.

[116] Drotleff B, Hallschmid M, Lämmerhofer M. Quantification of steroid hormones in plasma using a surrogate calibrant approach and UHPLC-ESI-QTOF-MS/MS with SWATH-acquisition combined with untargeted profiling. Anal Chim Acta. 2018 Aug 31;1022:70-80. doi: 10.1016/j.aca.2018.03.040.

[117] Zhou J, Liu C, Si D, Jia B, Zhong L, Yin Y. Workflow development for targeted lipidomic quantification using parallel reaction monitoring on a quadrupole-time of flight mass spectrometry. Anal Chim Acta. 2017 Jun 15;972:62-72. doi: 10.1016/j.aca.2017.04.008.

[118] Laiko, V. V.; Dodonov, A. F.; Cotter, R. J. Resolution and spectral-line shapes in the reflecting time-of-flight mass spectrometer with orthogonally injected ions. Rapid Communications in Mass Spectrometry 1994, 8, 720-726. doi: 10.1002/rcm.1290080912

[119] Fitzgerald RL, Rivera JD, Herold DA. Broad spectrum drug identification directly from urine, using liquid chromatography-tandem mass spectrometry. Clin Chem. 1999 Aug;45(8 Pt 1):1224-34.

[120] Decaestecker TN, Clauwaert KM, Van Bocxlaer JF, Lambert WE, Van den Eeckhout EG, Van Peteghem CH, De Leenheer AP. Evaluation of automated single mass spectrometry to tandem mass spectrometry function switching for comprehensive drug profiling analysis using a quadrupole time-of-flight mass spectrometer. Rapid Commun Mass Spectrom. 2000;14(19):1787-92. doi: 10.1002/1097-0231(20001015)14:19<1787::AID-RCM94>3.0.CO;2-S.

[121] Hopfgartner G, Tonoli D, Varesio E. High-resolution mass spectrometry for integrated qualitative and quantitative analysis of pharmaceuticals in biological matrices. Anal Bioanal Chem. 2012 Mar;402(8):2587-96. doi: 10.1007/s00216-011-5641-8.

[122] Plumb RS, Johnson KA, Rainville P, Smith BW, Wilson ID, Castro-Perez JM, Nicholson JK. UPLC/MS(E); a new approach for generating molecular fragment information for biomarker structure elucidation. Rapid Commun Mass Spectrom. 2006;20(13):1989-94. doi: 10.1002/rcm.2550. Erratum in: Rapid Commun Mass Spectrom. 2006;20(14):2234.

[123] Simons B, Kauhanen D, Sylvänne T, Tarasov K, Duchoslav E, Ekroos K. Shotgun Lipidomics by Sequential Precursor Ion Fragmentation on a Hybrid Quadrupole Time-of-Flight Mass Spectrometer. Metabolites. 2012 Feb 20;2(1):195-213. doi: 10.3390/metabo2010195.

[124] Venable JD, Dong MQ, Wohlschlegel J, Dillin A, Yates JR. Automated approach for quantitative analysis of complex peptide mixtures from tandem mass spectra. Nat Methods. 2004 Oct;1(1):39-45. doi: 10.1038/nmeth705.

[125] Gillet LC, Navarro P, Tate S, Röst H, Selevsek N, Reiter L, Bonner R, Aebersold R. Targeted data extraction of the MS/MS spectra generated by data-independent acquisition: a new concept for consistent and accurate proteome analysis. Mol Cell Proteomics. 2012 Jun;11(6):O111.016717. doi: 10.1074/mcp.O111.016717.

[126] Álvarez-Ruiz R, Picó Y. Sequential window acquisition of all theoretical fragments versus information dependent acquisition for suspected-screening of pharmaceuticals in sediments and mussels by ultra-high pressure liquid chromatography-quadrupole time-of-flight-mass spectrometry. J Chromatogr A. 2019 Jun 21;1595:81-90. doi: 10.1016/j.chroma.2019.02.041.

[127] Whitman JD, Lynch KL. Optimization and Comparison of Information-Dependent Acquisition (IDA) to Sequential Window Acquisition of All Theoretical Fragment Ion Spectra (SWATH) for High-Resolution Mass Spectrometry in Clinical Toxicology. Clin Chem. 2019 Jul;65(7):862-870. doi: 10.1373/clinchem.2018.300756.

[128] Tsugawa H, Cajka T, Kind T, Ma Y, Higgins B, Ikeda K, Kanazawa M, Van der Gheynst J, Fiehn O, Arita M. MS-DIAL: data-independent MS/MS deconvolution for comprehensive metabolome analysis. Nat Methods. 2015 Jun;12(6):523-6. doi: 10.1038/nmeth.3393. Epub 2015 May 4.

[129] Zhang Y, Bilbao A, Bruderer T, Luban J, Strambio-De-Castillia C, Lisacek F, Hopfgartner G, Varesio E. The Use of Variable Q1 Isolation Windows Improves Selectivity in LC-SWATH-MS Acquisition. J Proteome Res. 2015 Oct 2;14(10):4359-71. doi: 10.1021/acs.jproteome.5b00543.

[130] Collins BC, Hunter CL, Liu Y, Schilling B, Rosenberger G, Bader SL, Chan DW, Gibson BW, Gingras AC, Held JM, Hirayama-Kurogi M, Hou G, Krisp C, Larsen B, Lin L, Liu S, Molloy

MP, Moritz RL, Ohtsuki S, Schlapbach R, Selevsek N, Thomas SN, Tzeng SC, Zhang H, Aebersold R. Multi-laboratory assessment of reproducibility, qualitative and quantitative performance of SWATH-mass spectrometry. Nat Commun. 2017 Aug 21;8(1):291. doi: 10.1038/s41467-017-00249-5.

3. List of Figures

4. Objectives of the thesis

The aim of this thesis was to develop new methods and optimize existing workflows for metabolomics in clinical bioanalysis. On the one hand, the focus was to improve both targeted and untargeted assays, which allow broad metabolite profiling in each sample. Focus was laid upon the quantification capabilities of such assays, whilst at the same time allowing broad metabolite coverage. The developed methods were implemented in various types of biological matrix (cell culture, plasma and urine) and successfully displayed the desired outcome. The thesis is built upon four topics in bioanalytical chemistry, namely those being:

1. The development of targeted quantitative assays in metabolomics with the aim of providing a broad metabolite coverage.

2. Developing specific targeted assays for metabolic pathways and metabolite classes, which were generally not sufficiently covered by the initial methods (i.e. thiols and phosphorylated compounds).

3. Improving the retention time reproducibility challenge faced in HILIC metabolomics methods.

4. The development of an untargeted assay as a complementary basis to the previous targeted methods, allowing post-acquisition retrospective data-mining and relative quantification of metabolites, which were not covered by the initially developed targeted methods.

The publications included in this thesis deal specifically with these 4 points and are included in the following section.

Journal of Chromatography A 1684 (2022) 463556

Contents lists available at ScienceDirect

Journal of Chromatography A

journal homepage: www.elsevier.com/locate/chroma

Metabolic profiling workflow for cell extracts by targeted hydrophilic interaction liquid chromatography-tandem mass spectrometry

Kristian Serafimov, Michael Lämmerhofer*

Institute of Pharmaceutical Sciences, Pharmaceutical (Bio-)Analysis, University of Tübingen, Auf der Morgenstelle 8, Tübingen 72076, Germany

article info

Article history:
Received 22 July 2022
Revised 4 October 2022
Accepted 7 October 2022
Available online 8 October 2022

Keywords:
Targeted metabolomics
Hydrophilic interaction liquid chromatography
Stable isotope-labelled internal standards
13C-cell extract
UHPLC

abstract

In this study, a targeted approach with wide metabolite coverage was developed for cellular metabolomic analysis using a UHPLC-QTrap-MS system operated in the scheduled multiple reaction monitoring (sMRM) mode. MRM ion pairs were acquired from HeLa cell samples through untargeted analysis using UHPLC-QTOF-MS with SWATH acquisition complemented by missing metabolites from pathway databases. Four different cell extraction protocols were studied and compared based on an experiment series involving the calculation of individual metabolite recoveries (pre/post extraction spiking U-^{13}C isotope-labeled standards), with a Methanol/Water extraction mixture (1:1; v/v) showing the best results. Two HILIC-MS methods employing a Waters Premier BEH Amide column were developed, utilizing two different chromatographic conditions (20 mM ammonium formate as buffer additive adjusted to a pH = 3.5 with formic acid in ESI$^+$ mode and 20 mM ammonium acetate adjusted to a pH = 7.5 with acetic acid in ESI$^-$ mode. One hundred sixty-one (161) metabolites were successfully detected in ESI+ mode, whereas 92 were detected in negative ionization mode, totaling to a number of 253 compounds in three different biological matrices covered by the analytical system employed. Both established HILIC methods were calibrated and validated based on 105 authentic chemical standards and U-^{13}C-labeled *Pichia pastoris* (*Komagataella phaffii*) yeast extract as internal standards for cellular matrix (HeLa cells). Within-day and between-day precision was determined on three different QC concentration levels and was below 15% for the entirety of the analytes. Inter- and intra-day accuracies showed values in the range between 85 and 115% (assessed as % recovery) in the entire range. Matrix effects, extraction recoveries and process efficiencies were evaluated following the Matuszewski protocol with U-^{13}C-labeled *Pichia pastoris* metabolite extract as internal standards. Eventually, the method was utilized to quantify metabolites in HeLa cell extracts.

© 2022 Elsevier B.V. All rights reserved.

1. Introduction

The aim of metabolomics is to thoroughly study small molecule metabolites found in biological systems and their cellular responses perturbed by either endogenous or exogenous stimulus [1–3]. The resultant information complements other omics technologies in biomarker discovery, disease diagnosis, biotechnology, bioprocess optimization, cellular biology, drug development and other fields. Undoubtedly, mass spectrometry (MS), using quadrupole-time-of-flight (QTOF), Fourier transform ion cyclotron resonance (FT-ICR), triple quadrupole (QqQ), Orbitrap and quadrupole linear ion trap (QTRAP) instruments, is the leading analytical platform for metabolic analysis, due to its excellent molecular specificity and sensitivity [4,5]. To resolve the complexity of metabolite extracts, reduce ion suppression and avoid (isobaric, isomeric, isotopic, and in-source fragmentation) interferences, MS is commonly hyphenated to separation techniques [6], such as liquid chromatography (LC), gas chromatography (GC) or capillary electrophoresis (CE). Recently, ion-mobility spectrometry (IMS) has been introduced as an additional separation dimension to LC-MS enhancing selectivity of the entire analytical workflow and providing with collisional cross section (CCS) values an additional parameter for identification [7]. Two distinct strategies are pursued in metabolomics, untargeted and target analysis. Untargeted metabolomics does not preselect specific metabolites for analysis and aims at a broad coverage of detected molecular features and discovery of significant alterations between sample groups. This approach, however, is significantly limited by a narrower dynamic range and lower sensitivity. It commonly performs relative quantification rather than accurate quantitative analysis with authentic standards. On the contrary, targeted metabolomics selects predefined metabolites which are measured typically using

* Corresponding author.
E-mail address: Michael.laemmerhofer@uni-tuebingen.de (M. Lämmerhofer).

https://doi.org/10.1016/j.chroma.2022.463556
0021-9673/© 2022 Elsevier B.V. All rights reserved.

multiple-reaction monitoring (MRM) acquisition with QqQ and QTRAP instruments relative to authentic calibrants leading to accurate quantification [8]. Such assays are commonly more robust, have wider linear range, and lower LOQs.

The choice of chromatographic conditions plays a major role in metabolomic analysis. Separation methods commonly used have been reviewed recently [9]. Reversed-phase liquid chromatography (RPLC) due to its compatibility with aqueous biological samples, excellent chromatographic efficiency, and its ability to separate a large number of metabolites from diverse chemical classes is still the most popular LC mode in metabolomics [8,10]. Strategies to overcome the limited retention of very polar metabolites comprise pre-column derivatization providing more efficient analyte retention and dedicated detection properties [11,12] or addition of ion-pairing reagents to the mobile phase under RP conditions [13]. Hydrophilic interaction liquid chromatography (HILIC), on the other hand, provides extended retention for hydrophilic analytes without ion-pairing agent and without derivatization, and moreover is well compatible with ESI-MS detection. Therefore, HILIC represents a useful approach to increase the coverage of the polar metabolome [14–20]. Various HILIC stationary phases with regard to their chemical structure have been developed and are classified according to the ionic character of the functional group as neutral phases (amide, diol), charged phases (amino, silica) and zwitterionic phases (e.g., sulfobetaine-modified) [21]. A significant drawback often in large-scale metabolomic studies is the limited availability of such large number of authentic metabolite standards. In order to overcome this bottleneck, pseudo-targeted metabolic profiling, in which MRM transitions are measured without standards for quantification, is sometimes suggested as alternative with even wider coverage, but allow relative quantification only [22].

In this study, we present a workflow which utilizes targeted hydrophilic interaction liquid chromatography-tandem mass spectrometry for metabolic profiling of biological samples, specifically cell extracts. We have thoroughly evaluated new Premier hybrid, sub-2 μm, UHPLC–HILIC columns with two distinct surface chemistries, viz. zwitterionic sulfobetaine and neutral amide bondings, based on ethylene-bridged hybrid silica particles, which are stable from pH 2–10. These Premier columns utilize dedicated polymer-modified column hardware to minimize the interactions of highly hydrophilic analytes (such as e.g. hydroxy acids and phosphates etc.) with metal surfaces through a high-performance surface coating [23,24]). A zwitterionic sulfobetaine core-shell particle (2.7 μm) HILIC column was evaluated as well. In this study, the chromatographic performance of these three HILIC columns were examined using different chromatographic conditions with both reference standards and biological samples. Included in this investigation were chromatographic properties such as retention time, general metabolite distribution throughout the chromatographic run, peak widths and peak tailing factors. After full method optimization with the best performing Premier BEH Amide column, a validated UHPLC-MS/MS assay for accurate quantitative analysis of a large number of metabolites based on authentic standards and another subset by pseudo-targeted analysis (for relative quantification) was obtained. Its applicability to cellular samples was documented by application to HeLa cells.

2. Experimental

2.1. Materials

Formic acid, acetic acid, acetonitrile and methanol of Ultra LC-MS grade were supplied by Carl Roth (Karlsruhe, Germany). Trypan blue solution and ammonium hydroxide solution (Suprapur® quality 28.0 - 30.0% NH_3 basis) were purchased from Sigma-Aldrich (Merck, Taufkirchen, Germany). Deionized water was purified by a Purelab ultrapurification system (ELGA LabWater, Celle, Germany). Uniformly (U-) ^{13}C-labeled yeast extract of more than 2×10^9 Pichia pastoris cells (~15 mg; strain CBS 7435) was obtained from ISOtopic Solutions (Vienna, Austria). All standards used in this study were provided by Sigma-Aldrich (Merck). NIST SRM1950 plasma was also provided by Sigma-Aldrich (Merck). Stock solutions of the individual calibrants were prepared at concentrations of 1 mg mL^{-1} and used for further dilution. The individual stocks were stored at −80 °C until use. Three different chromatographic columns (all of the same dimension of 150×2.1 mm) were used for further evaluation during method development. A direct comparison was drawn between a Poroshell 120 HILIC-Z (2.7 μm, superficially porous particle SPP) column, Acquity Premier BEH Amide (1.7 μm, fully porous particle FPP) column and an Atlantis Premier Z-HILIC (1.7 μm, FPP) column.

2.2. Instrumentation

Targeted LC-MS analysis was performed using an Agilent 1290 Infinity II series UHPLC system from Agilent Technologies (Waldbronn, Germany) equipped with a binary pump, autosampler, thermostated column compartment and a QTrap 4500 mass spectrometer with a TurboIonSpray Source from SCIEX (Ontario, Canada). For untargeted analysis, an Agilent 1290 Infinity I series LC system from Agilent Technologies equipped with a binary pump, thermostated column compartment and an HTC-xt PAL (CTC Analytics AG, Zwingen, CH) autosampler and a TripleToF 5600+ mass spectrometer with DuoSpray Source, operated in TurboIonSpray mode, from SCIEX (Ontario, Canada) was used.

2.3. Preparation of HeLa cells

The human cervical HeLa cells adapted to serum-free conditions (AC free, ECACC 08,011,102) were grown in a humidified incubator at 37 °C with 5% CO_2. Cells were fed with EX-CELL Hela serum-free media (SigmaAldrich) with 2 mM l-glutamine (Sigma-Aldrich), 12 U mL^{-1} penicillin, and 12 μg mL^{-1} streptomycin until the cell density reached around 1×10^6.

Cell counting was performed in triplicate with a hemocytometer. Aliquots of 3×10^6 HeLa cells were transferred into 15 mL falcon tubes and spun down for 5 min at 100 g. After removing the supernatant, cell pellets were washed twice with ice-cold Dulbecco's phosphate-buffered saline (PBS) (Sigma-Aldrich) with repeated centrifugation. Cell samples were snap-frozen in liquid nitrogen and kept at −80 °C till use.

For the extraction of the analytes, 1 mL of the ice-cold extraction solvent (50% methanol and 50% water) was added to the cell pellets (which were slowly thawed on ice) and the cells were lysed with the handheld ultrasonic cell disruptor Branson Sonifier (Cell Disruptor B15, Danbury, USA) at level five for one minute. After the cell lysis, the extract was centrifuged at 1968 rcf for 10 min. The collected supernatants (extracts) were evaporated to dryness overnight under nitrogen using a high-performance evaporator (Genevac EZ-2) (Genevac, Ipswich, UK). The dry residue of the extract was reconstituted in 10 μL methanol and 90 μL mobile phase B, followed by 3 cycles of vortexing and sonication (each 30 s). The samples were vortexed centrifuged at 18,928 rcf for 5 min and the supernatant further analyzed.

2.4. Cell extraction protocol optimization

Four different extraction protocols were carefully tested in this study regarding further method optimization: 1. Methanol/acetonitrile/water (MeOH/ACN/H_2O – 45/10/45; v/v/v); 2. Pure methanol (MeOH); 3. Methanol/water (MeOH/H_2O – 50/50; v/v/);

and 4. Methanol/isopropanol/water (MeOH/IPA/H_2O – 45/10/45; v/v/v). Cell pellets were thawed on ice. Extraction solvents were kept on ice before their addition to the cell samples. Evaluation of each extraction protocol's performance was based on the extraction of 10 aliquots of cell samples (pellets containing 3×10^6 cells). For the determination of metabolite extraction recoveries, 3 of these samples were spiked before the extraction (pre-extraction spiking) with 10 µL of methanolic internal standard solution (^{13}C-labeled yeast extract of *Pichia pastoris* cells, synonymous with *Komagataella phaffii*), whereas for the other 3 samples, 10 µL of the internal standard solution were added as a post-extraction spike. Extraction recoveries were calculated as the ratio of average peak areas for internal standards in the pre-extraction and post extraction spiked sample.

2.5. Human plasma sample preparation

NIST SRM1950 human plasma was used as reference material in this study. The blood plasma was thawed on ice. ACN (1 mL) and 100 µL of a methanolic fraction containing the ^{13}C isotopic labeled *Pichia pastoris* extract was added to each plasma aliquot of 100 µL. The samples were vortexed for 30 s, centrifuged at 18,928 rcf for 5 min and the supernatant evaporated to dryness under nitrogen in a GeneVac system. The dry residue was then reconstituted in a total volume of 100 µL (10:90; v/v) methanol and mobile phase B. Three (3) cycles of vortexing and sonication (each 30 s) were conducted followed by sample centrifugation at 18,928 rcf for 5 min. The supernatants were further analyzed. Samples were stored at −80 °C until analysis.

2.6. Urine sample preparation

Pooled urine (first morning mid-stream), stored at 4 °C until use, was used for sample preparation. To each urine aliquote, a 100 µL methanolic fraction containing the ^{13}C isotopic labeled *Pichia pastoris* extract was added before sample preparation. As urine represents a medium susceptible for bacterial growth, a 0.22 µm sterile filter was used to filter the samples. Samples were then centrifuged at 4 °C, 20,784 rcf x 15 min to remove cell debris and unwanted precipitants. Each 1 mL sample aliquot was preserved at −80 °C until further metabolomic analysis. Samples were freeze dried in a Labconco (Kansas City, MO, USA) FreeZone 4.5 L Benchtop Freeze Dry System for 24 h and subsequently reconstituted in 100 µL methanol and 900 µL mobile phase B. Analogous as before, 3 cycles of vortexing and sonication (each 30 s) were conducted following sample centrifugation at 18,928 rcf for 5 min and analysis of the supernatant.

2.7. MRM Analysis with UHPLC-QTrap-MS

Chromatographic separation was performed on a Waters (Eschborn, Germany) Premier BEH Amide column (150×2.1 mm, 1.7 µm). For metabolite analysis in ESI$^+$ mode, mobile phases A and B were adjusted to a pH of 3.5 with formic acid and consisted of 20 mM ammonium formate in water and acetonitrile, respectively. In ESI-, the chromatographic conditions differed. Mobile phase A and B were adjusted to a pH of 7.5 with acetic acid and consisted of 20 mM ammonium acetate in water and acetonitrile respectively. The gradient elution profile was the same for both positive and negative ionization mode (0.0 min, 100% B; 13 min 70% B; 15 min 70% B; 15.1 min 100% B; 20 min 100% B) and was carried out at a flow rate of 0.25 mL min^{-1} and a constant column temperature of 35 °C was maintained throughout the entire run. Injection volume was 10 µL. The autosampler was kept at 4 °C. Ion source parameters were as follows: nebulizer gas (GS1, zero grade air) 50 psi, heater gas (GS2, zero grade air) 30 psi, curtain gas (CUR, nitrogen) 30 psi, source temperature (TEM) 450 °C, ion source voltage +5500 V (positive mode) and −4500 V (negative mode). Compound specific parameters were optimized individually through direct infusion MS (**Table S-4 and Table S-5**). Due to the large amount of transitions monitored simultaneously, the Scheduled-MRM function was enabled. A window of 30 s was set around the designated metabolite specific retention time and the total cycle time was 1 s. Blank solvents (mobile phase A and B) followed by QCs in quintuplicate ($n = 5$) were injected in the beginning of the chromatographic batch to ensure proper column and system equilibration.

2.8. UHPLC-QToF-MS with swath acquisition

LC-ESI+ and LC-ESI- conditions were the same as specified above for the UHPLC-QTrap-MS method. Injection volume was 10 µL. The experimental MS-setup consisted of a TOF-MS survey scan for precursor detection in the mass range of *m/z* 60–1000 (ESI+) and m/z 70–900 (ESI-), respectively.

For comprehensive recording of MS/MS spectra, SWATH acquisition was utilized with a collision energy of ± 30 V and a spread of ± 20 V. A total number of 20 SWATH-MS/MS experiments were created for both positive and negative ion mode (**Table S-1**). Variable SWATH window widths were optimized by swathTUNER based on preliminary measurements of cell culture extracts using IDA [25]. SWATH-experiment parameters were as follows - accumulation time was set to 30 ms. The total cycle time summed up to 750 ms, which yielded a minimum of 10 data points per peak with an average peak width at the base of 8 s. The MS instrument was run in high sensitivity mode achieving a TOF-MS resolution of 30,000 (FWHM @ *m/z* 829.5393) and a SWATH-MS/MS resolution of 15,000 (FWHM @ *m/z* 397.2122).

Ion source parameters were as follows: nebulizer gas (GS1, zero grade air) 50 psi, heater gas (GS2, zero grade air) 30 psi, curtain gas (CUR, nitrogen) 30 psi, source temperature (TEM) 450 °C, ion source voltage +5500 V (positive mode) and −4500 V (negative mode). Samples were first analyzed in positive and subsequently in negative ionization mode. Mass calibration was performed before every run via the Calibrant Delivery System (Sciex, Ontario, Canada). The analytical system was controlled by the Analyst 1.7 TF software (Sciex, Ontario, Canada).

2.9. Data processing and evaluation (SWATH-MS)

Data processing comprising peak finding, blank subtraction, feature alignment, normalization, MS/MS spectral deconvolution and score-based metabolite identification, which relies primarily on MS/MS similarity of deconvoluted experimental MS2 spectra of the analytes to those of metabolite libraries, was performed with MS-DIAL software (version 4.7.0) [26]. A similarity score of 80% was chosen as threshold for reliable metabolite identification. For peak finding an intensity threshold of 100 counts per second (cps) was selected. Further detailed information on data processing with MS-DIAL is provided in **Table-S2**. The raw QToF data files (*.wiff*) obtained were later converted to mzXML files using the "msconvert" program from ProteoWizard [27] (version 3.0.21211). The data files were grouped together in one file directory and processed by the R-Package SWATHtoMRM [28], in order to generate the MRM-ion pairs for UHPLC-QTRAP-MS analysis.

All further data processing steps and evaluations were executed with MS-DIAL, PeakView 2.2 (Sciex), MultiQuant 3.0 (Sciex), Excel 2016 (Microsoft, Redmond, WA, USA), Origin 2021 (OriginLab, Northampton, MA, USA), and R Studio 1.4.1717 (R Foundation for Statistical Computing, Vienna, Austria).

2.10. Metabolite quantification and method validation

Matrix-matched calibration curves were constructed using weighted least-square linear regression (weighting factor: 1/x) by spiking five different calibrant levels in a standard addition experiment to a pooled HeLa cell extract and by plotting the peak area ratio of analyte to IS versus the nominal concentration of each analyte. The endogenous metabolite concentrations were derived from the x-axis intercept multiplied by −1. The resulting calibration functionswere used to determine target analyte concentrations in real samples (HeLa cell extracts). Integration and data processing were conducted with the MultiQuant 3.0 software (Sciex) via an automated algorithm employing a Gaussian smoothing (1 Point), noise percentage of 90%, baseline subtraction window of 0.1 min and a peak splitting factor of 2. Excel 20,019 (Microsoft, Redmond, WA; USA) and Origin 2017 (OriginLab, Northampton, MA, USA) were used for further data processing. One hundred and five (105) authentic chemical standards were used to calibrate and validate the methods. Validation was performed in accordance to FDA (United States Food and Drug Administration Agency) guidelines for bioanalytical method validation with modifications. Matrix effects, extraction recoveries, and process efficiencies were determined in accordance to the Matuszewski protocol [29] **(Table S-8)**, with consideration of the endogenously present metabolite concentrations in the cell extracts, as there is no stripped matrix available. As mentioned previously, pre-determination of the individual metabolites was conducted via LC-MS and standard addition. The determined concentration of the individual metabolite was accounted for by background subtraction (i.e. subtraction of the endogenously present concentration A_0 from the determined concentration to the matrix). Thus, signal suppression or enhancement due to matrix effect was calculated as follows:

$$ME\% = \frac{A_{determined} - A_0}{A_{neat}}$$

Where $A_{determined}$ is the area of spiked cell extracts after extraction, A_0 the peak area of the analyte endogenously present in the extract and A_{neat} being the peak area of the selected metabolite in neat solution. Similarly, individual metabolite accuracies (Acc) were calculated in quality controls as% recovery as follows:

$$ACC\% = \frac{c_{found} - c_0}{c_{spiked}}$$

With c_{spiked} is the concentration of spiked cell extracts after extraction, c_0 the endogenously present amount and c_{found} the concentration of the selected metabolite found in the spiked sample.

3. Results and discussion

3.1. MS/MS optimization and MRM list generation

The MRM transitions for the targeted UHPLC-MS/MS analysis were selected by two strategies: (1) Untargeted metabolomic UHPLC-QTOF-MS/MS analysis with SWATH acquisition and data processing through the R-Package SWATHtoMRM [28]; (2) missing key metabolites of various biological pathways were collected from KEGG (http://www.genome.jp/kegg/pathway.html) and HMDB (http://hmdb.ca/) databases to supplement the MRM transition list. SWATHtoMRM is an R package used to construct a large-scale set of MRM transitions from the generated SWATH-MS data files. There are 4 steps for the analysis of SWATH-MS data: (1) MS^1 peak detection and alignment; (2) extraction of MS^2 peaks and chromatograms; (3) MS^1 and MS^2 peak grouping; (4) generation of consensus MS^2 spectra. As a result, a csv file containing all generated transitions can be obtained by the SWATHtoMRM script.

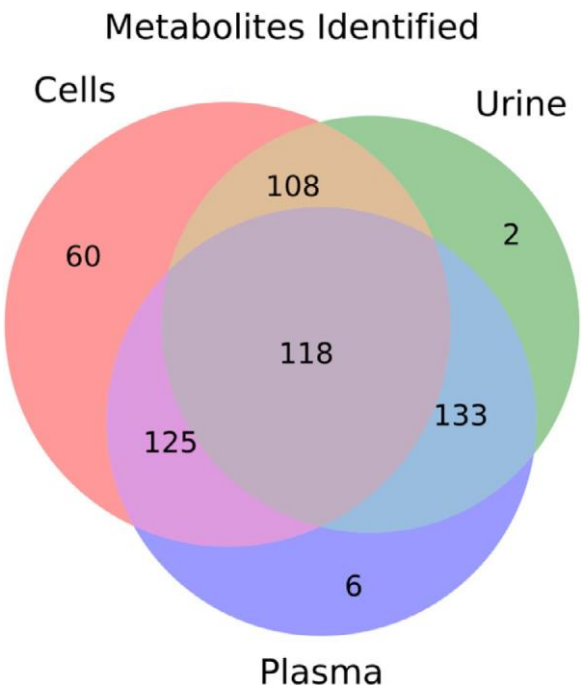

Fig. 1. Venn diagrams representing the method's metabolite coverage in positive and negative ionization mode in the different biological matrices.

A minimum of 2 MRM transitions (quantifier and qualifier) were monitored for the majority of the metabolites, in order to allow for method selectivity evaluation and verification regarding potential interferences from isobaric matrix components by quantifier/qualifier ratio monitoring. In **Tables S-4** and **S-5**, precursor and product ions of the target metabolites, as well as the compound-specific optimized MS/MS parameters including DP, EP, CE and CXP, are summarized.

Overall 253 metabolites were successfully detected with the presented analytical platform in three different biological matrices (Fig. 1). The identity of the peaks detected in the cell extract was confirmed by authentic standards, which were available for 105 metabolites (**Table S-6 and Table S-7**), through retention time (RT), precursor mass and MS/MS spectra match (level 1 identification according to MSI). For the other detected targets for which no standards were available, level 2 identification by UHPLC-QToF-SWATH-MS analysis and MS spectral matching of deconvoluted experimental MS spectra with spectra from two publicly available MSP-Databanks (*Riken Institute, All Public MS/MS*) containing over 290.000 and 36.000 metabolites in positive and negative ionization mode, respectively, was employed. These compounds were finally measured only in a pseudo-targeted manner (i.e. allowing relative quantification e.g. when different sample groups are compared).

For a few low molecular metabolites, the intensity of the product ions was too low or the generated fragment ions were not specific enough for reliable qualitative and quantitative analysis. Thus, so-called pseudo-MRM transitions were employed for which the *m/z* of the intact precursor ion was measured also in the third quadrupole (e.g. Glycine, Pyruvic Acid, GABA).

Some metabolite classes exhibit class-specific fragment ions, such as nucleotides. The detection of nucleotides by MRM was achieved in ESI^- mode with $[M\text{-}H]^-$ precursor ion and the group-characteristic fragment ion with *m/z* of 79. For this reason, attention was paid to a sufficient chromatographic separation of corresponding mono-, di- and triphosphates to avoid interferences in case of in-source fragmentation [30,31].

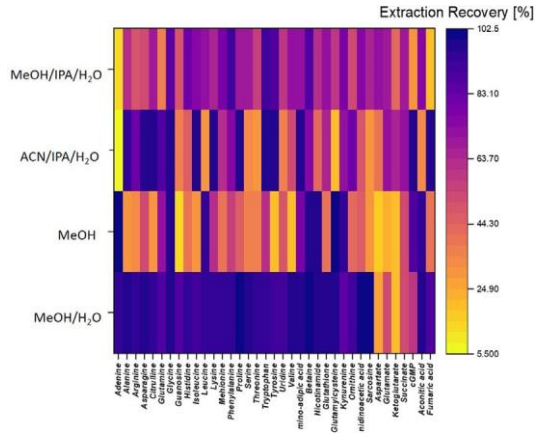

Fig. 2. Heatmap displaying an overview of extraction recoveries of a representative set of metabolites for extraction protocol comparison. Individual metabolite recoveries evaluated with ^{13}C *Pichia Pastoris* yeast extract.

3.2. Optimization of cell extraction protocol

As described in Section 2.4, four different solvent compositions were evaluated for their extraction recoveries and metabolite coverage. Aliquots of washed HeLa cell pellets (each 3×10^6 cells) were suspended in the extraction solvents (MeOH/ACN/H_2O 45/10/45, v/v/v; MeOH; MeOH/H_2O 50/50, v/v; or MeOH/IPA/H_2O 45/10/45, v/v/v) and cell lysis induced by sonication for 1 min. Supernatants were dried and reconstituted in the 10 µL MeOH (containing the post-extraction ^{13}C-IS spike) and 90 µL mobile phase B before analysis by UHPLC-ESI-MS/MS. The performance of the distinct extraction solvents was assessed by extraction recoveries of the spiked internal standards (^{13}C-cell extract) (Figs. 2 and **suppl. S1**). In terms of extraction recovery, out of the four different extraction protocols tested, the methanol-water mixture performed best. Pure methanol performed also sufficiently. However, it proved to be a poor choice for the extraction of amino acids and their derivatives. The MeOH/ACN/H_2O and MeOH/IPA/H_2O mixtures showed similar performance. The addition of ACN or IPA did not seem to improve further metabolite recovery, compared to MeOH/H_2O. On contrary, it impaired extraction recoveries of highly polar metabolites like amino acids and their derivatives.

3.3. Column performance comparison

Chromatographic runs on 3 HILIC columns (FPP-based Premier Z-HILIC and Premier BEH-Amide, as well as SPP-based HILIC-Z) were evaluated with respect to retention time, peak width and peak tailing factors of individual analytes in order to obtain a comprehensive data matrix of these chromatographic performance parameters of the metabolites. The individual factors were calculated from triplicate injections of all the examined analytes. All of the 253 metabolites covered in this analytical platform were used for the further assessment of each individual column's performance. The distribution of the individual metabolites in both ionization modes is shown in **Fig. S-2A, S-2B** (for the HILIC-Z column) **Fig. S-3A, S-3B** (for the Z-HILIC column) and **Fig. S-4A, S-4B** (for the BEH Amide column). All four columns generally provided a similar distribution pattern, specifically class-wise, which was also confirmed by parity plots of normalized retention times shown in Fig. 3**A, B** and **C**. The spread of the data points closely around the 45° parity line indicates a similar chromatographic behavior in terms of retention between all columns. Substantial differences were, however, observed between the columns when the peak widths and peak tailing factors were evaluated (Fig. 4**A and B**). It was observed that the values for the peak widths and peak tailing factors were significantly higher in the case of the zwitterionic HILIC-Z and Z-HILIC columns when compared with the BEH Amide column. Some metabolites exhibit higher tailing factors in the range between 1.2 and 1.7 which are mainly phosphorylated ones that are known to interact with stainless steel surfaces of LC systems esp. column inlet and outlet frits and the inner wall of electrospray probes leading to tailing, partly irreversible adsorption and even loss of analytes [32,33]. The currently used Premier BEH Amide columns shows reduced tailing as can be seen in (Fig. 4**A and B**), partly probably also due to its polymer coated frits and column hardware, respectively. Consequently, the Premier BEH Amide column was chosen for further method validation and analysis.

3.5. Method validation

Two HILIC methods were finally developed based on the Premier BEH Amide column, one employing acidic conditions (positive ionization mode; pH = 3.5) and the other one neutral conditions (negative ionization mode; pH = 7.5). The corresponding retention times of all metabolites which could reliably and reproducibly be determined with these developed methods are given in **Tables S-4** and **S-5** of the Supplementary Material. Under acidic conditions, in particular amino acids and nucleobases performed well. Negative ionization mode under neutral conditions was preferred specifically for nucleotide and organic acid analysis

3.5.1. Assay specificity

A critical parameter of bioanalytical methods is assay specificity, i.e. the ability to differentiate the analytes from components of similar structure present in the respective complex biological matrix. Both methods were evaluated with respect to compounds that

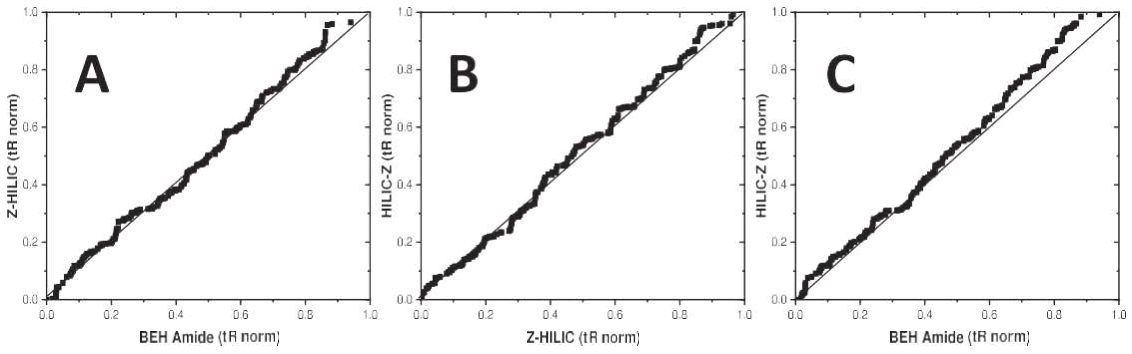

Fig. 3. Parity plots showing the chromatographic behavior of metabolites in terms of normalized retention times on the different stationary phases employed. Comparison between Atlantis Premier Z-HILIC and Acquity Premier BEH Amide (A). Comparison between Agilent HILIC-Z and Atlantis Premier Z-HILIC (B), and comparison between Agilent HILIC-Z and Acquity Premier BEH Amide (C).

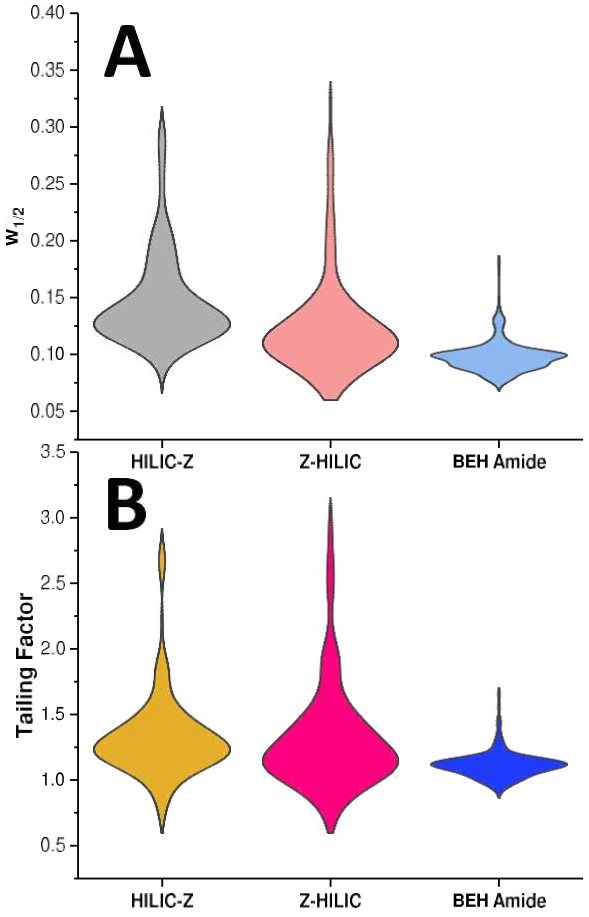

Fig. 4. Violin plots providing comparison of peak widths at half maximum (A) and tailing factors (B) between 2.7 µm SPP HILIC-Z Column, 1.7 µm FPP Premier Z-HILIC Column and 1.7 µm FPP Premier BEH-Amide Column.

can possibly interfer with other targets in MS/MS detection (such as isobaric compounds, isomers, in-source fragmentation products) and need to be separated chromatographically when no specific MRM transitions are available. Some examples are presented in Fig. 5. Under the employed chromatographic conditions, redox active critical analytes e.g. NAD^+ and NADH are separated from each other, because oxidation in the ESI process could lead to an interference (Fig. 5A). Similarly, cysteine was fully separated from cystine, as in-source oxidation could lead to assay specificity problems (Fig. 5B) [34]. The adenylate energy charge molecules (AMP, ADP and ATP) are providing important information but are critical not only due to peak tailing, but also due to tentative interferences from in-source fragmentation. In the provided chromatographic method, they were separated from one another (Fig. 5C), thus avoiding signal interferences. Chromatographic separation is also required for isobaric and isomeric metabolites, such as Isoleucine (Ile), Creatine, Leucine (Leu) and 3-guanidinopropionic acid (3-GPA) which all have the same *m/z* of precursor and product ions in the present study, these four isobaric metabolites were successfully distinguished from each other by full baseline chromatographic separation (Fig. 5D).

3.5.2. *Matrix effects, extraction recoveries and process efficiencies*

Matrix effects (ME), extraction recoveries (ER) and process efficiencies (PE) were evaluated at an intermediate concentration level of each target analyte by comparison of the peak areas of post-extraction spiked cell extract vs standard solution, pre-extraction spike vs post-extraction spiked cell extract, and pre-extraction-spiked cell extract vs standard solution, respectively [31]. Values close to 100% represent minimum matrix effect, quantitative extraction and optimal process efficiency, respectively. The results are summarized in **Table S-8**.

MEs ranged between 42% (Serine) and 110% (Threonine). It indicates that for several analytes isotope labelled IS are recommended which were considered in this work by the use of the

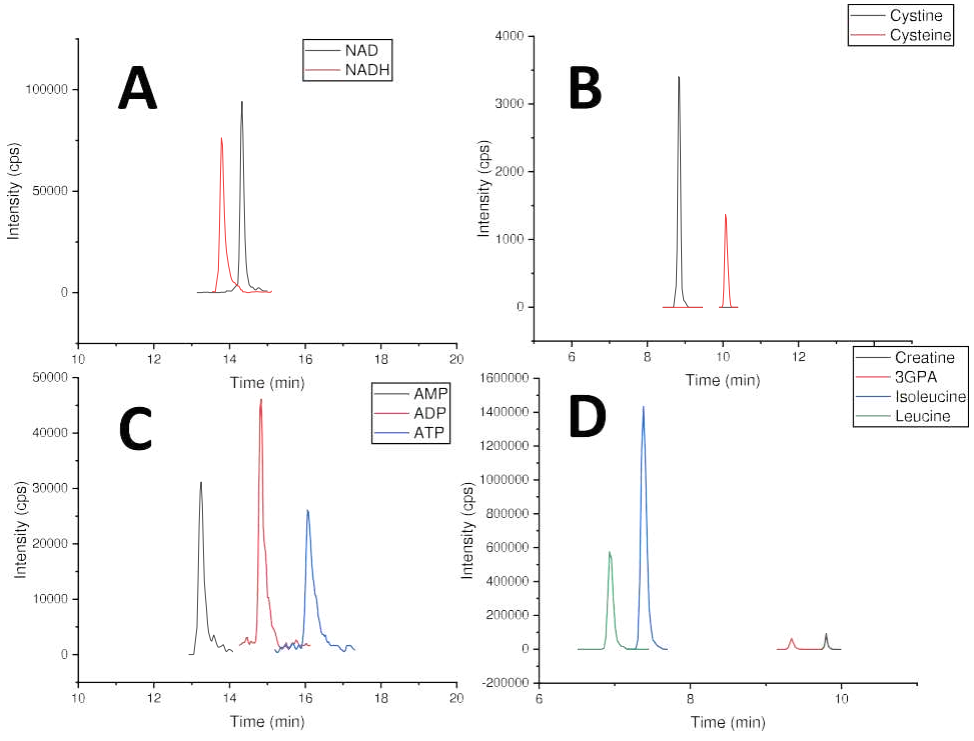

Fig. 5. Extracted ion chromatograms showing method selectivity for selected metabolites. (A) Oxidized and reduced forms of nicotinamide adenine dinucleotide (NAD^+ /NADH), (B) cysteine and cystine (Cys/CysCys), (C) the adenylate energy charge molecules (AMP, ADP and ATP), and (D) isobaric and isomeric compounds with *m/z* = 132 (D) (Leucine, Isoleucine, Creatine, and 3-guanidinopropionic acid).

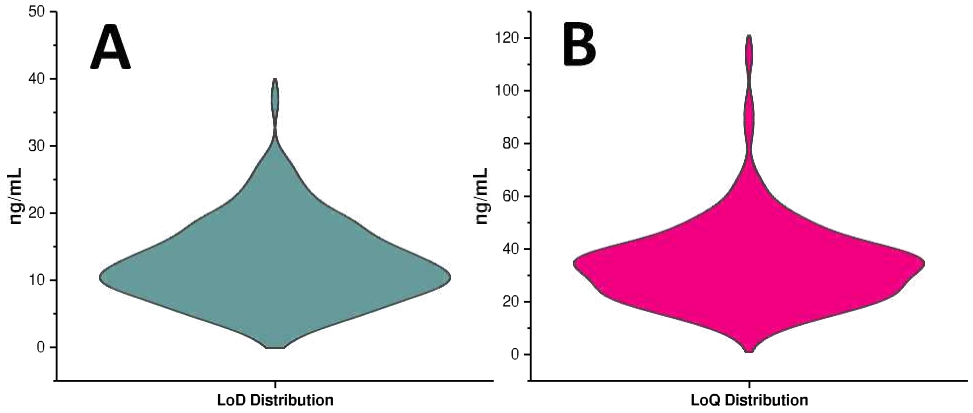

Fig. 6. Violin plots providing distribution of metabolite LoDs (A) and LoQs (B) values.

U^{13}C-labelled cell extract that allowed proper compensation of ion-suppression. ER between 77.4 and 98.1% were found which is in the acceptable range. PE was determined to be between 33.3 and 104.1%. Detailed results for each individual analyte's ME, PE and RE are provided in **Table S-8**. Based on these results it was concluded to use a ^{13}C-labelled cell extract for compensating of MEs and losses during sample preparation. It is possible when a limited number of samples is analyzed, for large scale metabolomics studies it may be too costly.

3.5.3. Calibration, linearity and method sensitivity

External calibration functions were established by plotting peak area ratios of analytes and their internal standards versus the concentration of standard solutions. Weighted linear regression (1/x) was used to derive slopes, intercepts and correlation coefficients of the calibration curves (**Tables S-6** and **S-7**). Linearity was evaluated by the correlation coefficients (r) of the external calibration functions for each metabolite and were, as can be seen form **Table S-6** (positive mode) and **Table S-7** (negative mode), always $r \geq 0.99$. indicating good linearity. Apart from external calibration, matrix matched calibration was performed as well by spiking series of 5 concentration levels to the biological matrix (HeLa cell extract), as described in Section 2.9. Also, the matrix-matched calibration functions showed $r \geq 0.99$) (data not shown). LoDs and LoQs were determined through the external calibration function for the individual metabolites as follows:

$$LoD = \frac{3.3\ x\ \sigma}{m}$$

With σ being the standard error of the calibration function's slope and m the slope value itself. Analogous for the LoQ determination, the following equation was used:

$$LoQ = \frac{10\ x\ \sigma}{m}$$

Tables S-6 and **S-7** provide further information on this. The results prove that this multi-target metabolite assay shows adequate sensitivity for determining cellular metabolite concentrations in HeLa cells. Fig. 6 provides a graphical representation of the distribution of the individual LoD and LoQ values in form of violin plots across the metabolites analyzed in this study. An additional experiment was conducted, which investigated the effect of cell count and number of metabolites detected. Apart from 3.0×10^6 cells, four further aliquots were measured, those being 1.0×10^6, 0.5×10^6, 1.0×10^5 and 1.0×10^4 cells. As expected, the lower the cell count, the lower the number of metabolites above LoD detected. **Fig. S-5** displays the results obtained from this measurement series and the tabular results are provided as **Tables S-13** and **S-14**. It turns out that a significant loss of sensitivity is observed if less than 3.0×10^6 cells are used. If only lower cell numbers are available, it is advice to further optimized the sensitivity e.g. by using more sensitive MS instruments, exclude the qualifier transitions and increase the dwell time of the quantifier transitions, at least of the metabolite that give less sensitivity.

3.5.4. Intra-assay and inter-day accuracy and precision

Precision and accuracy were evaluated and the results are given in **Tables S-8** and **S-9**. For this purpose, the intra-assay and inter-day precision and accuracy were assessed in cell matrix by using three quality controls prepared by spiking cell extract with different concentrations using calibrants at 3 distinct levels: QC_{Low} (50 ng mL^{-1}), QC_{Mid} (100 ng mL^{-1}), QC_{High} (200 ng mL^{-1}). These three QCs were measured in quintuplicate ($n = 5$) on three different days to determine the within-day and between-day precision and accuracy, respectively. Precision was below 5% CV for the majority of the analytes and below 15% in the entire analyte range, both within-day (Fig. 7**A** and **B**) and between-day. Inter- and intra-day accuracies showed values in the range between 85 and 115% (assessed as% recovery) in the entire range. This, together with the precision levels found, proved the adequate performance of the methods.

3.5.5. Stability

Analyte stability during freeze-thaw cycles and autosampler stability was verified as well. Therefore, fresh QC samples at three levels (50 ng mL^{-1} QC_{Low}, 100 ng mL^{-1} QC_{Mid} and 200 ng mL^{-1} QC_{High}) were prepared and measured in quintuplicate ($n = 5$) for all stability experiments. A total number of 4 freeze-thaw cycles were conducted, with the QC samples being kept frozen for 12 h between each cycle. To study extract stability, QCs were reanalyzed that were kept in an autosampler tray (4 °C) for 10 h, 24 h and 48 h. All prepared QC samples for stability assays were compared with freshly prepared QCs. The results of the stability tests are summarized in **Tables S-9** and **S-10**. It becomes evident that the analytes can be considered stable in the stock solutions. Changes in analyte concentration for autosampler and freeze/thaw stability were all within common acceptance limits for accuracy (±15%) and hence can be considered sufficiently stable. For certain compounds, autosampler stability values were outside common acceptance limits. This was specifically the case with the reduced form of Glutathione, Cysteine, Cysteinyl-Glycine and *N*-Acetyl-Cysteine. For this reason, it may be advisable to derivatize the reactive sulfhydryls of these oxidation-prone metabolites if accurate quantification is required as suggested in previous studies [34].

3.5.6. Carryover

To ensure absence of any carryover, blanks were injected subsequently to a QC or a calibrant at highest concentration according

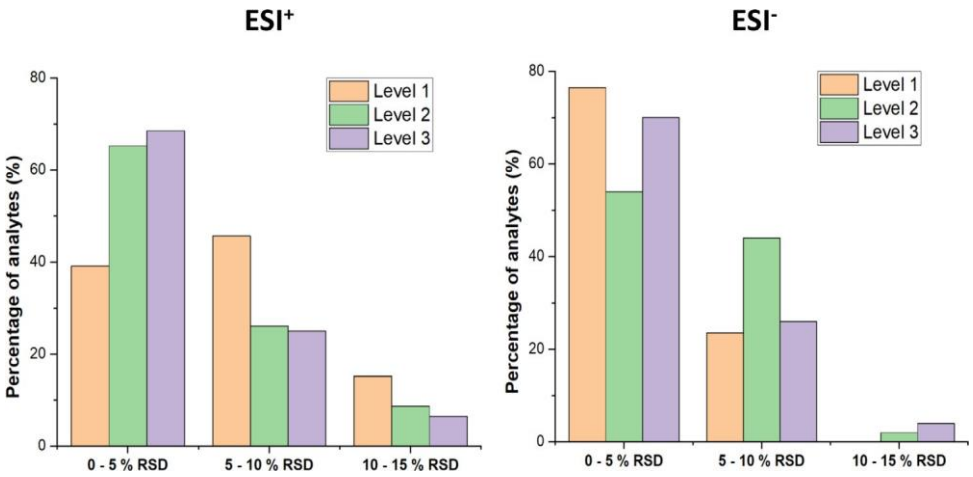

Fig. 7. Intra-day precision determined for the acidic HILIC (ESI^+) (A) and neutral (B) HILIC method (ESI^-).

to the FDA guideline. No carryover was observed and thus the acceptance criteria requested by the FDA guideline for carryover was met [35].

3.6. Comparison to previous methods

There are several published methods showing the successful application of targeted HILIC-MS for the quantitative determination of metabolites in biological samples. In their work, Xu et al. [31] have developed a targeted metabolomics method employing a Q-Orbitrap MS to initially generate the MRM ion pairs required for the tandem MS assay performed on QqQ. Despite providing a broader metabolite coverage compared to our developed assaysh, a full method validation wa not conducted in the aforementioned study and the distribution of precision values obtained as RSD was also shifted to higher RSDs. Further investigation into key analytical performance parameters such as linearity, LoD and LoQ has also not been conducted. Preinerstorfer et al. [15] focused on the development of targeted LC-MS methods employing HILIC (with ZIC–HILIC, 3 μm column) in fermentation broths from beta-lactam antibiotics. When comparing the methods, our UHPLC assays provide a wider metabolite coverage with better precision (RSD) values. LoD and LoQ values between both works are similar. Contrary to this former work, herein ^{13}C labeled isotopic standards were used which better compensate for matrix effects. The utility of HILIC-MS is widely recognized, however, in most works focus on certain pathways or metabolite classes only, e.g. on histamine and its main metabolites in urine samples by Nelis et al. [36]. A

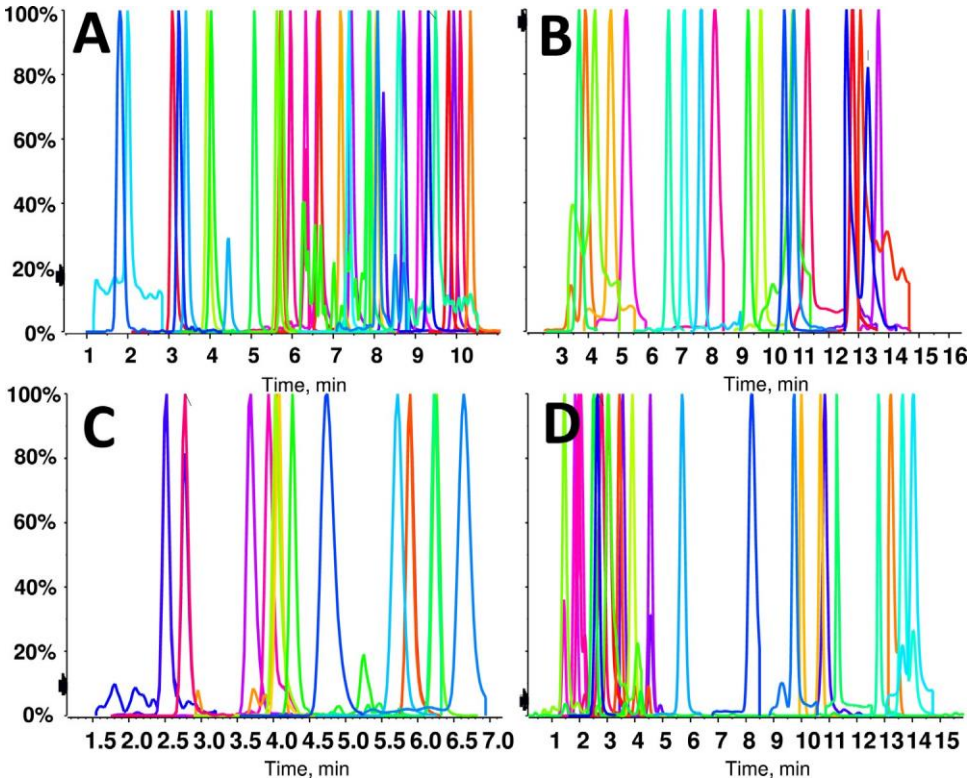

Fig. 8. XICs of metabolites according to classes found in real sample (HeLa cell extract). (A) Amino acids and derivatives. (B) Organic acids and nucleotides. (C) Nucleobases and nucleosides. (D) Vitamins, selenocompounds and miscellaneous.

most recent work published by Lioupi et al. [37] investigated the performance of the new zwitterionic Premier Atlantis Z-HILIC column by Waters during the metabolic profiling of mouse liver extracts. The method provided coverage for 88 hydrophilic metabolites with targeted and untargeted metabolic profiling, however, no quantification of the set metabolites was conducted. Our study reveals that Premier BEH Amide gives better chromatographic performance than Premier Atlantis Z-HILIC phase in this former study., Herein, a wider metabolite coverage with quantification including ^{13}C-labeled internal standards and full method validation. Recently, a novel approach employing stable isotope labeled standards to quantify endogenous present metabolites was discussed by Visconti et al. [38]. This technique, however, is not possible to implement at present in our workflow, as to do so a specified concentration of the individually present U-^{13}C metabolites used as IS is required and this is not the case in the *Pichia pastoris* extract, as only a range for each individual metabolite is listed by the supplier, this making accurate quantification impossible. However, for the metabolites available as authentic standards, the concentrations of the U-^{13}C metabolites in the *Pichia pastoris* extract could be determined analytically to make this approach a simplification and advancement of this workflow.

3.7. Method application

The validated UHPLC-ESI-MS/MS methods were applied to quantify metabolites in a HeLa cell extract. The sample extract was measured in quintuplicate (n = 5). Quantification of 105 endogenous metabolites was achieved by standard addition with ^{13}C-labeled *Pichia pastoris* (*Komagataella phaffii*) yeast extract [39–42] included to ensure good precision, correct for sample losses during sample preparation and correct for matrix effects. Detailed results are listed in **Tables S-6** and **S-7** for both ionization modes, respectively. Endogenous amounts detected varied between 10 ng mL^{-1} and 500 ng mL^{-1}. Representative chromatograms of metabolite classes found in the cell culture extract are shown in Fig. 8**A, B, C and D**.

4. Conclusion

In this study, a wide-coverage targeted metabolomics method was developed and validated, which benefits from the high specificity and sensitivity of UHPLC-MS/MS with scheduled MRM acquisition. Besides 107 key metabolites which can be accurately quantified by calibration with authentic standards another 146 metabolites can be monitored by selective MRM transitions for relative quantification (no standards currently available in this study for calibration) (pseudo-targeted assay). To allow for monitoring assay specificity throughout analytical batches, for the majority of metabolites besides the quantifier transition a qualifier transition was acquired as well. Precision and accuracy was assured by the incorporation of a U-^{13}C-labeled cell extract which enables to correct for matrix effects and analyte losses during sample preparation. The validation confirmed a good performance in terms of precision and accuracy. The assay was sufficiently sensitive to allow for accurate quantitative analysis of the 107 target metabolites in HeLa cell extracts. The initial screening of new sub-2 µm FPP and 2.7 µm SPP HILIC columns revealed the sub-2 µm FPP Premier BEH Amide column with neutral bonding-chemistry provides better efficiency and less peak tailing compared to sub-2 µm FPP Premier BEH Z-HILIC and 2.7 µm SPP HILIC-Z with the zwitterionic sulfobetaine bonding. Overall, it can be concluded that the new targeted metabolomics assay is suitable for analysing cellular metabolite concentrations with good coverage of major metabolite classes.

Declaration of Competing Interest

The authors declare that they have no known competing financial interests or personal relationships that could have appeared to influence the work reported in this paper.

CRediT authorship contribution statement

Kristian Serafimov: Investigation, Methodology, Formal analysis, Data curation, Visualization, Writing – original draft, Writing – review & editing. **Michael Lämmerhofer:** Conceptualization, Methodology, Supervision, Writing – review & editing, Resources.

Data Availability

Data will be made available on request.

Supplementary materials

Supplementary material associated with this article can be found, in the online version, at doi:10.1016/j.chroma.2022.463556.

References

[1] J.R. Idle, F.J. Gonzalez, Metabolomics, Cell Metab. 6 (2007) 348–351.
[2] S. Chen, H. Kong, X. Lu, Y. Li, P. Yin, Z. Zeng, G. Xu, Pseudotargeted metabolomics method and its application in serum biomarker discovery for hepatocellular carcinoma based on ultra high-performance liquid chromatography/triple quadrupole mass spectrometry, Anal. Chem. 17 (2013) 391 8326-8333.
[3] M. Baker, Metabolomics: from small molecules to big ideas, Nat. Methods 8393 (2011) 117–121.
[4] T. Cajka, O. Fiehn, Toward merging untargeted and targeted methods in mass spectrometry-based metabolomics and lipidomics, Anal. Chem. 88 (1) (2016) 524–545 Jan 5Epub 2015 Dec 16. PMID: 26637011, doi:10.1021/acs.analchem.5b04491.
[5] A.A. Aksenov, R. da Silva, R. Knight, N. P.MLopes, P.C. Dorrestein, Global chemical analysis of biology by mass spectrometry, Nat. Rev. Chem. 1 (2017) 1–20 (13) C. H. Johnson, J. Ivanisevic, G. Siuzdak, Metabolomics: beyond biomarkers and towards mechanisms. Nat Rev Mol Cell Bio, 17 (2016) 451-459.
[6] O. Begou, H.G. Gika, I.D. Wilson, G. Theodoridis, Hyphenated MS-based targeted approaches in metabolomics, Analyst 142 (17) (2017) 3079–3100 Aug 21PMID: 28792021, doi:10.1039/c7an00812k.
[7] M.L. Feuerstein, R.T. Kurulugama, S. Hann, T. Causon, Novel acquisition strategies for metabolomics using drift tube ion mobility-quadrupole resolved all ions time-of-flight mass spectrometry (IM-QRAI-TOFMS), Anal. Chim. Acta 1163 (2021) 338508 Jun 8Epub 2021 Apr 12. PMID: 34024419, doi:10.1016/j.aca.2021.338508.
[8] W.B. Dunn, D. Broadhurst, P. Begley, E. Zelena, S. Francis-McIntyre, N. Anderson, M. Brown, J.D. Knowles, A. Halsall, J.N. Haselden, A.W. Nicholls, I.D. Wilson, D.B. Kell, R. Goodacre, The Human Serum Metabolome (HUSERMET) Consortium, Procedures for large-scale metabolic profiling of serum and plasma using gas chromatography and liquid chromatography coupled to mass spectrometry, Nat. Protoc. 6 (2011) 1060–1083, doi:10.1038/nprot.2011.335.
[9] E.M. Harrieder, F. Kretschmer, S. Böcker, M. Witting, Current state-of-the-art of separation methods used in LC-MS based metabolomics and lipidomics, J. Chromatogr. B Analyt. Technol. Biomed. Life Sci. 1188 (2022) 123069 Jan 1Epub 2021 Nov 27. PMID: 34879285, doi:10.1016/j.jchromb.2021.123069.
[10] E.J. Want, P. Masson, F. Michopoulos, I.D. Wilson, G. Theodoridis, R.S. Plumb, J. Shockcor, N. Loftus, E. Holmes, J.K. Nicholson, Global metabolic profiling of animal and human tissues via UPLC-MS, Nat. Protoc. 8 (2013) 17–32, doi:10.1038/nprot.2012.135.
[11] D. Siegel, A.C. Meinema, H. Permentier, G. Hopfgartner, R. Bischoff, Integrated quantification and identification of aldehydes and ketones in biological samples, Anal. Chem. 86 (10) (2014) 5089–5100 May 20Epub 2014 May 5. PMID: 24745975, doi:10.1021/ac500810r.
[12] S. Zhao, L. Liang, Chemical derivatization in LC-MS based metabolomics study, TrAC Trends Analyt. Chem. (2020) 0165–9936 October, doi:10.1016/j.trac.2020.115988.
[13] F. Michopoulos, N. Whalley, G. Theodoridis, I.D. Wilson, T.P. Dunkley, S.E. Critchlow, Targeted profiling of polar intracellular metabolites using ion-pair-high performance liquid chromatography and -ultra high performance liquid chromatography coupled to tandem mass spectrometry: applications to serum, urine and tissue extracts, J. Chromatogr. A 1349 (2014) 60–68 Jul 4Epub 2014 May 12. PMID: 24861786, doi:10.1016/j.chroma.2014.05.019.
[14] Y. Gagnebin, J. Pezzatti, P. Lescuyer, J. Boccard, B. Ponte, S. Rudaz, Toward a better understanding of chronic kidney disease with complementary chromatographic methods hyphenated with mass spectrometry for improved polar metabolome coverage, J. Chromatogr. B Analyt. Technol. Biomed. Life Sci. 1116

(2019) 9–18 May 15Epub 2019 Mar 26. PMID: 30951967, doi:10.1016/j.jchromb.2019.03.031.

[15] B. Preinerstorfer, S. Schiesel, M. Lämmerhofer, W. Lindner, Metabolic profiling of intracellular metabolites in fermentation broths from beta-lactam antibiotics production by liquid chromatography-tandem mass spectrometry methods, J. Chromatogr. A 1217 (3) (2010) 312–328 Jan 15Epub 2009 Nov 20. PMID: 19954781, doi:10.1016/j.chroma.2009.11.051.

[16] C. Virgiliou, I. Sampsonidis, H.G. Gika, N. Raikos, G.A. Theodoridis, Development and validation of a HILIC-MS/MS multitargeted method for metabolomics applications, Electrophoresis 36 (18) (2015) 2215–2225 SepErratum in: Electrophoresis. 2016 Jul;37(14):2113. PMID: 26180020, doi:10.1002/elps.201500208.

[17] C. Virgiliou, H.G. Gika, G.A Theodoridis, HILIC-MS/MS multi-targeted method for metabolomics applications, Methods Mol. Biol. 1738 (2018) 65–81 PMID: 29654583, doi:10.1007/978-1-4939-7643-0_5.

[18] S.U. Bajad, W. Lu, E.H. Kimball, J. Yuan, C. Peterson, J.D. Rabinowitz, Separation and quantitation of water soluble cellular metabolites by hydrophilic interaction chromatography-tandem mass spectrometry, J. Chromatogr. A 1125 (1) (2006) 76–88 Aug 25Epub 2006 Jun 6. PMID: 16759663, doi:10.1016/j.chroma.2006.05.019.

[19] F. Fei, D.M. Bowdish, B.E. McCarry, Comprehensive and simultaneous coverage of lipid and polar metabolites for endogenous cellular metabolomics using HILIC-TOF-MS, Anal. Bioanal. Chem. 406 (15) (2014) 3723–3733 JunEpub 2014 Apr 10. PMID: 24714971; PMCID: PMC4026627, doi:10.1007/s00216-014-7797-5.

[20] K. Klavins, H. Drexler, S. Hann, G. Koellensperger, Quantitative metabolite profiling utilizing parallel column analysis for simultaneous reversed-phase and hydrophilic interaction liquid chromatography separations combined with tandem mass spectrometry, Anal. Chem. 86 (9) (2014) 4145–4150 May 6Epub 2014 Apr 8. PMID: 24678888, doi:10.1021/ac5003454.

[21] B. Buszewski, S. Noga, Hydrophilic interaction liquid chromatography (HILIC) – a powerful separation technique, Anal. Bioanal. Chem. 402 (2012) 231–247, doi:10.1007/s00216-011-5308-5.

[22] J. Xu, J. Li, R. Zhang, J. He, Y. Chen, N. Bi, Y. Song, L. Wang, Q. Zhan, Z. Abliz, Development of a metabolic pathway-based pseudo-targeted metabolomics method using liquid chromatography coupled with mass spectrometry, Talanta 192 (2019) 160–168 Jan 15Epub 2018 Sep 11. PMID: 30348373, doi:10.1016/j.talanta.2018.09.021.

[23] G.J. Guimaraes, J.M. Sutton, M. Gilar, M. Donegan, M.G. Bartlett, Impact of non-specific adsorption to metal surfaces in ion pair-RP LC-MS impurity analysis of oligonucleotides, J. Pharm. Biomed. Anal. 208 (2022) 114439 Jan 20Epub 2021 Oct 23. PMID: 34742118, doi:10.1016/j.jpba.2021.114439.

[24] D.V. McCalley, Influence of metals in the column or instrument on performance in hydrophilic interaction liquid chromatography, J. Chromatogr. A 1663 (2022) 462751 Jan 25Epub 2021 Dec 16. PMID: 34995861, doi:10.1016/j.chroma.2021.462751.

[25] Y. Zhang, A. Bilbao, T. Bruderer, J. Luban, C. Strambio-De-Castillia, F. Lisacek, G. Hopfgartner, E. Varesio, The use of variable Q1 isolation windows improves selectivity in LC-SWATH-MS acquisition, J. Proteome Res. 14 (10) (2015) 4359–4371 Oct 2Epub 2015 Sep 3. PMID: 26302369, doi:10.1021/acs.jproteome.5b00543.

[26] H. Tsugawa, T. Cajka, T. Kind, Y. Ma, B. Higgins, K. Ikeda, M. Kanazawa, J. VanderGheynst, O. Fiehn, M. Arita, MS-DIAL: data-independent MS/MS deconvolution for comprehensive metabolome analysis, Nat. Methods 12 (6) (2015) 523–526 JunEpub 2015 May 4. PMID: 25938372; PMCID: PMC4449330, doi:10.1038/nmeth.3393.

[27] M.C. Chambers, B. Maclean, R. Burke, D. Amodei, D.L. Ruderman, S. Neumann, L. Gatto, B. Fischer, B. Pratt, J. Egertson, K. Hoff, D. Kessner, N. Tasman, N. Shulman, B. Frewen, T.A. Baker, M.Y. Brusniak, C. Paulse, D. Creasy, L. Flashner, K. Kani, C. Moulding, S.L. Seymour, L.M. Nuwaysir, B. Lefebvre, F. Kuhlmann, J. Roark, P. Rainer, S. Detlev, T. Hemenway, A. Huhmer, J. Langridge, B. Connolly, T. Chadick, K. Holly, J. Eckels, E.W. Deutsch, R.L. Moritz, J.E. Katz, D.B. Agus, M. MacCoss, D.L. Tabb, P. Mallick, A cross-platform toolkit for mass spectrometry and proteomics, Nat. Biotechnol. 30 (10) (2012) 918–920 OctPMID: 23051804; PMCID: PMC3471674, doi:10.1038/nbt.2377.

[28] H. Zha, Y. Cai, Y. Yin, Z. Wang, K. Li, Z.J. Zhu, SWATHtoMRM: development of high-coverage targeted metabolomics method using SWATH technology for biomarker discovery, Anal. Chem. 90 (6) (2018) 4062–4070 Mar 20Epub 2018 Mar 2. PMID: 29485856, doi:10.1021/acs.analchem.7b05318.

[29] B.K. Matuszewski, M.L. Constanzer, C.M. Chavez-Eng, Strategies for the assessment of matrix effect in quantitative bioanalytical methods based on HPLC-MS/MS, Anal. Chem. 75 (13) (2003) 3019–3030 Jul 1PMID: 12964746, doi:10.1021/ac020361s.

[30] D. Siegel, H. Permentier, D.J. Reijngoud, R. Bischoff, Chemical and technical challenges in the analysis of central carbon metabolites by liquid-chromatography mass spectrometry, J. Chromatogr. B Analyt. Technol. Biomed. Life Sci. 966 (2014) 21–33 Sep 1Epub 2013 Nov 26. PMID: 24326023, doi:10.1016/j.jchromb.2013.11.022.

[31] Y.F. Xu, W. Lu, J.D. Rabinowitz, Avoiding misannotation of in-source fragmentation products as cellular metabolites in liquid chromatography-mass spectrometry-based metabolomics, Anal. Chem. 87 (4) (2015) 2273–2281 Feb 17Epub 2015 Jan 27. PMID: 25591916; PMCID: PMC4354698, doi:10.1021/ac504118y.

[32] Y. Asakawa, N. Tokida, C. Ozawa, M. Ishiba, O. Tagaya, N. Asakawa, Suppression effects of carbonate on the interaction between stainless steel and phosphate groups of phosphate compounds in high-performance liquid chromatography and electrospray ionization mass spectrometry, J. Chromatogr. A (2008) 1198–1199 Jul 1180-6Epub 2008 May 13. PMID: 18541253, doi:10.1016/j.chroma.2008.05.015.

[33] Szabolcs Fekete, Mathew DeLano, AndrewBates Harrison, StephenJ. Shiner, JonathanLeon Belanger, KevinD. Wyndham, MatthewA. Lauber, Size exclusion and ion exchange chromatographic hardware modified with a hydrophilic hybrid surface, Anal. Chem. 94 (7) (2022) 3360–3367, doi:10.1021/acs.analchem.1c05466.

[34] K. Ortmayr, M. Schwaiger, S. Hann, G. Koellensperger, An integrated metabolomics workflow for the quantification of sulfur pathway intermediates employing thiol protection with N-ethyl maleimide and hydrophilic interaction liquid chromatography tandem mass spectrometry, Analyst 140 (22) (2015) 7687–7695 Nov 21PMID: 26451393, doi:10.1039/c5an01629k.

[35] F. and D.A., U.S. department of health and human services, bioanalytical method validation guidance for industry 1043, U.S. Dep. Health Hum. Serv. Food Drug Adm (2018) 1e41 https://www.fda.gov/files/drugs/published/Bioanalytical-Method-Validation-Guidance-for-Industry.pdf.

[36] M. Nelis, L. Decraecker, G. Boeckxstaens, P. Augustijns, D. Cabooter, Development of a HILIC-MS/MS method for the quantification of histamine and its main metabolites in human urine samples, Talanta 220 (2020) 121328 Dec 1Epub 2020 Jul 11. PMID: 32928382, doi:10.1016/j.talanta.2020.121328.

[37] A. Lioupi, C. Virgiliou, T.H. Walter, K.M. Smith, P. Rainville, I.D. Wilson, G. Theodoridis, H.G. Gika, Application of a hybrid zwitterionic hydrophilic interaction liquid chromatography column in metabolic profiling studies, J. Chromatogr. A 1672 (2022) 463013 Jun 7Epub 2022 Mar 31. PMID: 35436684, doi:10.1016/j.chroma.2022.463013.

[38] G. Visconti, E. Olesti, V. González-Ruiz, G. Glauser, D. Tonoli, P. Lescuyer, N. Vuilleumier, S. Rudaz, Internal calibration as an emerging approach for endogenous analyte quantification: application to steroids, Talanta 240 (2022) 123149 Apr 1Epub 2021 Dec 15. Erratum in: Talanta. 2022 Mar 15;:123288. PMID: 34954616, doi:10.1016/j.talanta.2021.123149.

[39] G. Hermann, M. Schwaiger, P. Volejnik, G. Koellensperger, ^{13}C-labelled yeast as internal standard for LC-MS/MS and LC high resolution MS based amino acid quantification in human plasma, J. Pharm. Biomed. Anal. 155 (2018) 329–334 Jun 5Epub 2018 Mar 27. PMID: 29704823, doi:10.1016/j.jpba.2018.03.050.

[40] C. Haberhauer-Troyer, M. Delic, B. Gasser, D. Mattanovich, S. Hann, G. Koellensperger, Accurate quantification of the redox-sensitive GSH/GSSG ratios in the yeast Pichia pastoris by HILIC-MS/MS, Anal. Bioanal. Chem. 405 (6) (2013) 2031–2039 FebEpub 2012 Dec 22. PMID: 23263514, doi:10.1007/s00216-012-6620-4.

[41] S. Neubauer, C. Haberhauer-Troyer, K. Klavins, H. Russmayer, M.G. Steiger, B. Gasser, M. Sauer, D. Mattanovich, S. Hann, G. Koellensperger, U13C cell extract of Pichia pastoris–a powerful tool for evaluation of sample preparation in metabolomics, J. Sep. Sci. 35 (22) (2012) 3091–3105 NovEpub 2012 Oct 22. PMID: 23086617, doi:10.1002/jssc.201200447.

[42] H. Wasito, G. Hermann, V. Fitz, C. Troyer, S. Hann, G. Koellensperger, Yeast-based reference materials for quantitative metabolomics, Anal. Bioanal. Chem. 414 (15) (2022) 4359–4368 JunEpub 2021 Oct 13. PMID: 34642781; PMCID: PMC9142427, doi:10.1007/s00216-021-03694-w.

Supporting information

Metabolic profiling workflow for cell extracts by targeted hydrophilic interaction liquid chromatography-tandem mass spectrometry

Kristian Serafimov[a]† Michael Lämmerhofer[a]*

[a] Institute of Pharmaceutical Sciences, Pharmaceutical (Bio-)Analysis, University of Tübingen, Auf der Morgenstelle 8, 72076 Tübingen, Germany

Corresponding Authors:

Prof. Michael Lämmerhofer

Email: Michael.laemmerhofer@uni-tuebingen.de; Telephone: +49 7071 29 78793; Fax: +49 7071 29 4565

Contents

Table S-1. MS Experiment Design

Experiment	*m/z* range	
	Positive mode	**Negative mode**
TOF-MS	60 - 1000	70 – 900
SWATH-MS/MS 1	59.5 – 83.6	69.5 – 143.5
SWATH-MS/MS 2	82.6 – 132.6	142.5 – 167.5
SWATH-MS/MS 3	131.6 – 166.6	166.5 – 199.7
SWATH-MS/MS 4	165.6 – 202.6	198.7 – 241.7
SWATH-MS/MS 5	201.6 – 259.6	240.7 – 269.7
SWATH-MS/MS 6	258.6 – 289.6	268.7 – 286.6
SWATH-MS/MS 7	288.6 – 315.7	285.6 – 301.7
SWATH-MS/MS 8	314.7 – 329.5	300.7 – 332.6
SWATH-MS/MS 9	328.5 – 369.9	331.6 – 346.6
SWATH-MS/MS 10	368.9 – 429.5	345.6 – 349.6
SWATH-MS/MS 11	428.5 – 478.8	348.6 – 379.8
SWATH-MS/MS 12	477.8 – 550.0	378.8 – 436.7
SWATH-MS/MS 13	549.0 – 596.5	435.7 – 510.6
SWATH-MS/MS 14	595.5 – 623.9	509.6 – 577.8
SWATH-MS/MS 15	622.9 – 677.7	576.8 – 632.3
SWATH-MS/MS 16	676.7 – 721.1	631.3 – 688.7
SWATH-MS/MS 17	720.1 – 760.1	687.7 – 741.0
SWATH-MS/MS 18	759.1 – 810.1	740.0 – 791.1
SWATH-MS/MS 19	809.1 – 876.6	790.1 – 841.1
SWATH-MS/MS 20	875.6 – 1000.5	840.1 – 900.5

Table S-2. MS Dial Processing Settings

Parameter	Setting	
	Positive mode	**Negative mode**
Data collection range	0.5 – 19 min	0.5 – 19 min
Mass range	60 - 1000	70 – 900
MS^1 Tolerance	0.01 Da	0.01 Da
MS/MS Tolerance	0.025 Da	0.025 Da
Smoothing level	2	2
Minimum peak width	5	5
Minimum peak height [cps]	100	100
Mass slice width	0.1 Da	0.1 Da

Table S-3. Extraction recoveries investigated with U^{13}C metabolites.

Compound	MeOH / H_2O (50/50)	MeOH	MeOH/ACN/H_2O (45/10/45)	MeOH/IPA/H_2O (45/10/45)
(U-^{13}C) Adenine	93.7 ± 2.2	99.4 ± 0.9	5.9 ± 0.2	13.5 ± 0.2
(U-^{13}C) Alanine	97.6 ± 2.7	30.6 ± 1.5	95.4 ± 3.3	62.7 ± 2.2
(U-^{13}C) Arginine	92.9 ± 2.6	31.8 ± 1.6	80.5 ± 1.1	47.8 ± 2.9
(U-^{13}C) Asparagine	97.9 ± 1.9	51.3 ± 1.3	96.7 ± 2.3	51.3 ± 3.3
(U-^{13}C) Citrulline	95.1 ± 3.1	29.9 ± 0.7	97.6 ± 2.2	69.1 ± 0.7
(U-^{13}C) Glutamine	88.4 ± 2.5	70.5 ± 2.4	88.5 ± 0.9	34.6 ± 1.9
(U-^{13}C) Glycine	96.8 ± 2.7	96.6 ± 3.9	98.8 ± 3.9	84.3 ± 3.6
(U-^{13}C) Guanosine	88.5 ± 4.5	14.2 ± 1.6	35.9 ± 1.9	48.6 ± 2.8
(U-^{13}C) Histidine	95.8 ± 2.2	41.1 ± 0.8	46.5 ± 3.6	80.2 ± 2.6
(U-^{13}C) Isoleucine	90.2 ± 2.5	28.2 ± 0.4	99.1 ± 0.2	73.7 ± 3.8
(U-^{13}C) Leucine	93.5 ± 1.8	93.8 ± 2.5	28.8 ± 0.8	72.9 ± 0.9
(U-^{13}C) Lysine	95.2 ± 2.2	61.2 ± 2.7	96.7 ± 2.4	66.2 ± 0.9
(U-^{13}C) Methionine	93.4 ± 2.8	39.5 ± 2.9	61.2 ± 2.8	79.2 ± 1.4
(U-^{13}C) Phenylalanine	92.8 ± 2.3	54.6 ± 2.1	75.7 ± 4.9	92.3 ± 0.7
(U-^{13}C) Proline	99.3 ± 2.7	45.7 ± 2.1	97.8 ± 2.7	67.4 ± 1.7
(U-^{13}C) Serine	96.7 ± 2.4	36.7 ± 0.3	34.6 ± 2.3	67.9 ± 0.8
(U-^{13}C) Threonine	95.3 ± 2.7	37.6 ± 1.8	30.9 ± 1.9	55.6 ± 1.5
(U-^{13}C) Tryptophan	95.2 ± 0.6	60.7 ± 2.2	97.2 ± 2.9	90.8 ± 2.9
(U-^{13}C) Tyrosine	90.1 ± 0.6	20.7 ± 2.9	98.9 ± 2.6	87.6 ± 3.3
(U-^{13}C) Uridine	90.3 ± 0.6	50.7 ± 1.2	34.6 ± 0.6	59.4 ± 1.5
(U-^{13}C) Valine	96.2 ± 0.7	20.9 ± 0.7	53.8 ± 1.5	70.6 ± 0.9
(U-^{13}C) 2-amino-adipic acid	97.6 ± 0.8	77.4 ± 1.3	96.6 ± 2.5	70.2 ± 2.4
(U-^{13}C) Betaine	99.3 ± 2.3	97.2 ± 1.2	74.2 ± 6.1	88.3 ± 1.2
(U-^{13}C) Nicotinamide	98.5 ± 1.5	99.1 ± 5.9	44.1 ± 3.7	62.6 ± 1.4
(U-^{13}C) Glutathione	96.3 ± 0.9	40.7 ± 2.2	65.1 ± 1.1	72.3 ± 1.5
(U-^{13}C) γ-Glutamylcysteine	97.2 ± 1.6	101.6 ± 4.1	20.7 ± 1.7	60.3 ± 1.7
(U-^{13}C) Kynurenine	85.4 ± 2.7	95.3 ± 2.7	72.7 ± 3.6	78.1 ± 1.9
(U-^{13}C) Ornithine	90.8 ± 3.1	43.3 ± 2.3	80.6 ± 1.1	52.8 ± 1.2
(U-^{13}C) Guanidinoacetic acid	102.1 ± 2.7	46.3 ± 1.4	49.1 ± 0.9	74.4 ± 1.6
(U-^{13}C) Sarcosine	99.3 ± 1.4	29.2 ± 1.8	30.7 ± 0.2	65.4 ± 1.3
(U-^{13}C) Aspartic acid	25.6 ± 2.3	16.7 ± 3.7	40.3 ± 4.1	73.2 ± 3.2
(U-^{13}C) Glutamic acid	53.6 ± 0.9	22.8 ± 1.3	71.5 ± 4.7	67.7 ± 1.8
(U-^{13}C) Ketoglutarate	18.9 ± 0.5	20.6 ± 0.9	64.7 ± 4.5	41.1 ± 2.3
(U-^{13}C) Succinate	52.7 ± 8.9	51.3 ± 5.8	73.3 ± 7.9	69.4 ± 0.9
(U-^{13}C) cGMP	60.2 ± 1.6	89.2 ± 4.4	97.7 ± 0.9	29.1 ± 1.2
(U-^{13}C) Aconitic acid	96.1 ± 0.3	94.1 ± 2.4	34.3 ± 3.2	75.2 ± 3.4
(U-^{13}C) Fumaric acid	86.9 ± 0.9	38.5 ± 1.4	97.8 ± 3.1	20.3 ± 0.5

Table S-4. Metabolites identified in ESI$^+$ ionization mode.

Compound	Precursor ion [m/z]	Product ion [m/z]	t_R [min]	DP [V]	EP [V]	CE [V]	CXP [V]	Sum formula	Identified in cells	Identified in urine	Identified in plasma	Identification Level	Pathway
Ethanolamine	62.0	45.0	8.34	31	10	21	10	C2H7NO	+	-	+	2	Glycerophospholipid metabolism
Glycine	76.0	76.0	9.61	16	10	5	10	C2H5NO2	+	+	+	1	Glycine, serine and threonine metabolism
Trimethylamine-N-oxide	76.1	58	8.18	25	10	29	10	C3H9NO	-	+	+	2	Glycine, serine and threonine metabolism
Cysteamine	78	61	3.27	31	10	17	10	C2H7NS	+	-	+	2	Cysteine and methionine metabolism
Putrescine	89.0	72.0	12.25	31	10	13	10	C4H12N2	+	+	+	2	Arginine and proline metabolism
Alanine	90.0	44.0	8.71	31	10	21	10	C3H7NO2	+	+	+	1	Alanine, aspartate and glutamate metabolism
beta-Alanine	90.0	73.0	8.21	39	10	25	10	C3H7NO2	+	-	-	1	Pyrimidine metabolism
Sarcosine	90.0	44.0	8.33	31	10	21	10	C3H7NO2	+	+	+	1	Glycine, serine and threonine metabolism
Cadaverine	103.0	86.0	11.22	26	10	15	10	C5H14N2	+	-	-	2	Lysine metabolism
Choline	105.0	105.0	4.74	15	10	20	10	C5H14NO	+	+	+	1	Glycine, serine and threonine metabolism
Serine	106.0	60.0	9.95	16	10	15	10	C3H7NO3	+	+	+	1	Glycine, serine and threonine metabolism
Hypotaurine	110.0	92.0	8.85	31	10	13	10	C2H7NO2S	-	+	+	2	Taurine and hypotaurine metabolism
Cytosine	112.0	95.0	4.80	45	10	25	10	C4H5N3O	+	+	+	1	Pyrimidine metabolism
Histamine	112.0	112.0	8.60	22	10	5	10	C5H9N3	+	+	+	1	Histidine metabolism
Histamine	112.0	95.0	8.60	22	10	12	10	C5H9N3	+	+	+	1	Histidine metabolism
Uracil	113.0	96.0	4.06	56	10	25	10	C4H4N2O2	+	+	+	1	Pyrimidine metabolism
Uracil	113.0	70.0	4.06	56	10	23	10	C4H4N2O2	+	+	+	1	Pyrimidine metabolism
Creatinine	114.0	86.1	1.99	26	10	10	10	C4H7N3O	+	+	+	2	Arginine and proline metabolism
Creatinine	114.0	114.0	1.99	26	10	7	10	C4H7N3O	+	+	+	2	Arginine and proline metabolism

Dihydrouracil	115.0	73.0	2.41	16	10	10	10	C4H6N2O2	+	-	-	1	Pyrimidine metabolism
Dihydrouracil	115.0	115.0	2.41	16	10	5	10	C4H6N2O2	+	-	-	1	Pyrimidine metabolism
Proline	116.0	70.0	7.52	26	10	25	10	C5H9NO2	+	+	+	1	Arginine and proline metabolism
Betaine	118.0	118.0	6.72	31	10	5	10	C5H11NO2	+	+	+	1	Glycine, serine and threonine metabolism
Valine	118.0	72.0	7.31	31	10	17	10	C5H11NO2	+	+	+	1	Valine, leucine and isoleucine metabolism
Threonine	120.0	74.0	9.11	49	10	17	10	C4H9NO3	+	+	+	1	Glycine, serine and threonine metabolism
Cysteine	122.1	76.1	7.99	25	10	25	10	C3H7NO2S	+	+	+	1	Cysteine and methionine metabolism
Cysteine	122.1	104.9	7.99	25	10	25	10	C3H7NO2S	+	+	+	1	Cysteine and methionine metabolism
Nicotinamide	123.0	79.0	6.65	11	10	15	10	C6H6N2O	+	+	+	1	Nicotinate and nicotinamide metabolism
4-Hydroxybenzaldehyde	123	95.1	7.35	25	10	10	10	C7H6O2	+	-	-	2	Tyrosine metabolism
Nicotinic acid	124.0	80.0	2.40	46	10	31	10	C6H5NO2	+	-	+	2	Nicotinate and nicotinamide metabolism
5-Methylcytosine	126.0	126.0	4.90	56	10	5	10	C5H7N3O	+	+	-	1	Pyrimidine metabolism
1-methylhistamine	126.1	82.1	7.07	25	10	25	10	C6H11N3	+	+	+	2	Histidine metabolism
1-methylhistamine	126.1	68.0	7.07	25	10	25	10	C6H11N3	+	+	+	2	Histidine metabolism
Thymine	127.0	110.0	2.46	21	10	20	10	C5H6N2O2	+	+	+	1	Pyrimidine metabolism
Pipecolic acid	130.1	70.1	7.65	38	10	22	10	C6H11NO2	+	+	+	2	Lysine metabolism
N-Acetylputrescine	131.0	114.0	6.25	16	10	15	10	C6H14N2O	+	+	+	2	Arginine and proline metabolism
Agmatine	131.1	72.1	10.61	25	10	15	10	C5H14N4	-	-	+	2	Arginine and proline metabolism
Agmatine	131.1	114.1	10.61	25	10	10	10	C5H14N4	-	-	+	2	Arginine and proline metabolism
Creatine	132.0	44.0	9.02	51	10	35	10	C4H9N3O2	+	+	+	2	Arginine and proline metabolism
3-Guanidinopropionic acid	132.0	72.0	8.81	51	10	23	10	C4H9N3O2	+	-	-	2	Arginine and proline metabolism
Isoleucine	132.0	69.0	6.41	46	10	25	10	C6H13NO2	+	+	+	1	Valine, leucine and isoleucine metabolism

Leucine	132.0	44.0	6.05	51	10	35	10	C6H13NO2	+	+	+	1	Valine, leucine and isoleucine metabolism
Asparagine	133.0	74.0	10.10	41	10	21	10	C4H8N2O3	+	+	+	1	Alanine, aspartate and glutamate metabolism
Ornithine	133.0	116.0	13.47	36	10	10	10	C5H12N2O2	+	+	+	1	Arginine and proline metabolism
Ornithine	133.0	70.0	13.47	36	10	31	10	C5H12N2O2	+	+	+	1	Arginine and proline metabolism
Adenine	136.0	92.0	3.73	16	10	30	10	C5H5N5	+	+	+	1	Purine metabolism
Adenine	136.0	119.0	3.73	16	10	33	10	C5H5N5	+	+	+	1	Purine metabolism
2-Phenylacetamide	136.1	91.1	7.39	25	10	20	10	C8H9NO3	+	-	-	2	Phenylalanine metabolism
Hypoxanthine	137.0	119.0	3.99	61	10	25	10	C5H4N4O	+	+	+	1	Purine metabolism
Hypoxanthine	137.0	110.0	3.99	61	10	29	10	C5H4N4O	+	+	+	1	Purine metabolism
1-Methylnicotinamide	137.1	94.1	5.57	25	10	30	10	C7H9N2O	+	+	+	2	Nicotinate and nicotinamide metabolism
Anthranilic acid	138.0	91.9	1.68	31	10	30	10	C7H7NO2	+	+	+	1	Tryptophan metabolism
Anthranilic acid	138.0	120.0	1.68	31	10	17	10	C7H7NO2	+	+	+	1	Tryptophan metabolism
Trigonelline	138.1	92.1	7.04	25	10	30	10	C7H7NO2	+	+	+	2	Nicotinate and nicotinamide metabolism
Tyramine	138.1	121.1	3.85	25	10	15	10	C8H11NO	+	-	-	2	Tryptophan metabolism
Tyramine	138.1	103.1	3.85	25	10	20	10	C8H11NO	+	-	-	2	Tryptophan metabolism
O-Phosphoethanolamine	142.1	44.2	12.53	25	10	13	10	C2H8NO4P	-	-	+	2	Glycerophospholipid metabolism
4-Methyl-5-thiazoleethanol	144.8	126	6.48	25	10	20	10	C6H9NOS	+	+	+	2	Thiamine metabolism
4-Methyl-5-thiazoleethanol	144.8	113.1	6.48	25	10	30	10	C6H9NOS	+	+	+	2	Thiamine metabolism
Homoleucine	146.1	86.1	3.03	25	10	15	10	C7H15NO2	+	+	+	1	Valine, leucine and isoleucine metabolism
Spermidine	146.2	72.1	15.41	50	10	22	10	C7H19N3	+	+	+	2	Arginine and proline metabolism
Acetylcholine	147.0	88.0	3.03	26	10	20	10	C7NH16O2	+	+	+	1	Glycine, serine and threonine metabolism
Glutamine	147.0	130.0	9.91	36	10	10	10	C5H10N2O3	+	+	+	1	Alanine, aspartate and glutamate metabolism

Glutamine	147.0	84.0	9.91	36	10	29	10	C5H10N2O3	+	+	+	1	Alanine, aspartate and glutamate metabolism
Lysine	147.0	130.0	13.00	36	10	10	10	C6H14N2O2	+	+	+	1	Lysine metabolism
Lysine	147.0	84.0	13.00	36	10	29	10	C6H14N2O2	+	+	+	1	Lysine metabolism
O-Acetyl-serine	148.0	106.1	7.75	26	10	15	10	C5H9NO4	+	+	+	1	Cysteine and methionine metabolism
O-Acetyl-serine	148.0	88.0	7.75	26	10	15	10	C5H9NO4	+	+	+	1	Cysteine and methionine metabolism
Methylaspartic acid	148.1	102	11.56	25	10	10	10	C5H9NO4	-	-	+	2	Valine, leucine and isoleucine metabolism
Methylaspartic acid	148.1	88.0	11.56	25	10	10	10	C5H9NO4	-	-	+	2	Alanine, aspartate and glutamate metabolism
p-Coumaraldehyde	149.1	103.1	5.75	25	10	10	10	C9H8O2	+	+	+	2	Alanine, aspartate and glutamate metabolism
Methionine	150.0	104.0	6.74	56	10	10	10	C5H11NO2S	+	+	+	1	Cysteine and methionine metabolism
Methionine	150.0	133.0	6.74	56	10	15	10	C5H11NO2S	+	+	+	1	Cysteine and methionine metabolism
Guanine	152.0	111.0	2.91	31	10	25	10	C5H5N5O	+	-	-	1	Purine metabolism
Guanine	152.0	135.0	2.91	31	10	29	10	C5H5N5O	+	-	-	1	Purine metabolism
Xanthine	153.0	136.0	2.84	46	10	25	10	C5H4N4O2	+	+	-	1	Purine metabolism
Xanthine	153.0	110.0	2.84	46	10	27	10	C5H4N4O2	+	+	-	1	Purine metabolism
3-OH-anthranilate	154.3	108.0	8.90	30	10	25	10	C7H7NO3	+	-	-	2	Tryptophan metabolism
3-OH-anthranilate	154.3	136.2	8.90	30	10	18	10	C7H7NO3	+	-	-	2	Tryptophan metabolism
Histidine	156.0	83.0	11.49	46	10	25	10	C6H9N3O2	+	+	+	1	Histidine metabolism
Histidine	156.0	110.0	11.49	46	10	21	10	C6H9N3O2	+	+	+	1	Histidine metabolism
Dihydroorotic acid	158.9	113.1	7.51	25	10	11	10	C5H6N2O4	+	+	+	1	Pyrimidine metabolism
Dihydroorotic acid	158.9	131.0	7.51	25	10	10	10	C5H6N2O4	+	+	+	1	Pyrimidine metabolism
Allantoin	159.0	99.0	16.30	31	10	25	10	C4H6N4O3	+	-	-	2	Purine metabolism
Allantoin	159.0	116.0	16.30	31	10	11	10	C4H6N4O3	+	-	-	2	Purine metabolism
Tryptamine	161.0	91.0	3.02	26	10	40	10	C10H12N2	+	-	-	2	Tryptophan metabolism

Tryptamine	161.0	144.0	3.02	26	10	15	10	C10H12N2	+	-	-	2	Tryptophan metabolism
Carnitine	162.0	85.0	8.78	46	10	30	10	C7H15NO3	+	+	+	1	Carnitine shuttle metabolism
Carnitine	162.0	103.0	8.78	46	10	25	10	C7H15NO3	+	+	+	1	Carnitine shuttle metabolism
2-amino-adipic acid	162.2	55.15	10.32	25	10	28	10	C6H11NO4	+	-	-	2	Lysine metabolism
2-amino-adipic acid	162.2	116.2	10.32	25	10	14	10	C6H11NO4	+	-	-	2	Lysine metabolism
N-Acetyl-Cysteine	164.1	122.1	4.62	25	10	14	10	C5H9NO3S	+	+	+	1	Cysteine and methionine metabolism
N-Acetyl-Cysteine	164.1	59.05	4.62	25	10	30	10	C5H9NO3S	+	+	+	1	Cysteine and methionine metabolism
Phenylalanine	166.0	103.0	5.81	51	10	15	10	C9H11NO2	+	+	+	1	Phenylalanine metabolism
Phenylalanine	166.0	120.0	5.81	51	10	11	10	C9H11NO2	+	+	+	1	Phenylalanine metabolism
Methionine sulfoxide	166.2	74.1	9.81	25	10	14	10	C5H11NO3S	+	+	+	1	Cysteine and methionine metabolism
Methionine sulfoxide	166.2	55.9	9.81	25	10	25	10	C5H11NO3S	+	+	+	1	Cysteine and methionine metabolism
Pyridoxal	168.0	94.0	2.79	31	10	25	10	C8H9NO3	+	-	+	2	Vitamin B6 metabolism
Pyridoxal	168.0	150.0	2.79	31	10	17	10	C8H9NO3	+	-	+	2	Vitamin B6 metabolism
Norharmane	169.1	142.1	2.17	25	10	12	10	C11H8N2	-	-	+	2	Tryptophan metabolism
Norharmane	169.1	115	2.17	25	10	35	10	C11H8N2	-	-	+	2	Tryptophan metabolism
Pyridoxamine	169.1	134	8.76	25	10	25	10	C8H12N2O2	-	-	+	2	Vitamin B6 metabolism
Pyridoxamine	169.1	152	8.76	25	10	25	10	C8H12N2O2	-	-	+	2	Vitamin B6 metabolism
Cysteic Acid	170.2	124	10.40	46	10	10	10	C3H7NO5S	+	-	-	2	Cysteine and methionine metabolism
Pyridoxine	170.0	134.0	3.04	41	10	25	10	C8H11NO3	-	-	+	1	Vitamin B6 metabolism
Pyridoxine	170.0	152.0	3.04	41	10	19	10	C8H11NO3	-	-	+	1	Vitamin B6 metabolism
Selenocysteine	170.1	123.9	2.79	25	10	20	10	C3H7NO2Se	+	-	+	2	Selenocompound metabolism
Selenocysteine	170.1	106.9	2.79	25	10	20	10	C3H7NO2Se	+	-	+	2	Selenocompound metabolism
N-Acetyl-ornithine	175.0	115.3	14.78	31	10	20	10	C7H14N2O3	+	+	+	2	Arginine and proline metabolism
N-Acetyl-ornithine	175.0	70.0	14.78	31	10	39	10	C7H14N2O3	+	+	+	2	Arginine and proline metabolism
Arginine	175.0	116.0	12.69	31	10	10	10	C6H14N4O2	+	+	+	1	Arginine and proline metabolism

Arginine	175.0	70.0	12.69	31	10	39	10	C6H14N4O2	+	+	+	1	Arginine and proline metabolism
N-Acetyl-aspartic acid	175.9	134.1	8.95	25	10	12	10	C6H9NO5	+	-	-	2	Alanine, aspartate and glutamate metabolism
N-Acetyl-aspartic acid	175.9	88.1	8.95	25	10	16	10	C6H9NO5	+	-	-	2	Alanine, aspartate and glutamate metabolism
Indole-3-acetic acid	176.2	130.1	1.69	46	10	25	10	C10H9NO2	+	+	+	2	
Citrulline	176.0	70.1	10.45	36	10	30	10	C6H13N3O3	+	+	+	1	Arginine and proline metabolism
Citrulline	176.0	159.0	10.45	36	10	15	10	C6H13N3O3	+	+	+	1	Arginine and proline metabolism
N-carbamoyl aspartate	177.1	88.0	8.45	25	10	20	10	C5H8N2O5	+	-	-	2	Pyrimidine metabolism
N-carbamoyl aspartate	177.1	116.0	8.45	25	10	20	10	C5H8N2O5	+	-	-	2	Pyrimidine metabolism
CysteinylGlycine	179.1	162.0	9.60	25	10	12	10	C5H10N2O3S	+	-	-	1	Cysteine and methionine metabolism
CysteinylGlycine	179.1	76.0	9.60	25	10	18	10	C5H10N2O3S	+	-	-	1	Cysteine and methionine metabolism
Glucosamine	180.0	144.0	10.28	31	10	13	10	C6H13NO5	+	-	+	1	Amino sugar and nucleotide sugar metabolism
Glucosamine	180.0	162.0	10.28	31	10	13	10	C6H13NO5	+	-	+	1	Amino sugar and nucleotide sugar metabolism
Theobromine	181.1	108.0	2.36	25	10	25	10	C7H8N4O2	+	+	+	2	Tryptophan metabolism
Theobromine	181.1	163.0	2.36	25	10	13	10	C7H8N4O2	+	+	+	2	Tryptophan metabolism
Tyrosine	182.0	165.0	7.34	46	10	10	10	C9H11NO3	+	+	+	1	Tyrosine metabolism
Tyrosine	182.0	136.0	7.34	46	10	21	10	C9H11NO3	+	+	+	1	Tyrosine metabolism
Methionine sulfone	182.3	136	7.85	25	10	15	10	C5H11NO4S	+	-	+	2	Cysteine and methionine metabolism
Methionine sulfone	182.3	56.1	7.85	25	10	25	10	C5H11NO4S	+	-	+	2	Cysteine and methionine metabolism
Selenohomocysteine	184.1	137.9	2.74	25	10	20	10	C4H9NO2Se	+	-	-	2	Selenocompound metabolism
Selenohomocysteine	184.1	120.9	2.74	25	10	20	10	C4H9NO2Se	+	-	-	2	Selenocompound metabolism
Se-Methylselenocysteine	184.1	123.0	3.00	25	10	20	10	C4H9NO2Se	+	-	-	2	Selenocompound metabolism
Se-Methylselenocysteine	184.1	167.1	3.00	25	10	20	10	C4H9NO2Se	+	-	-	2	Selenocompound metabolism

O-Phospho-serine	186.0	70.0	13.00	36	10	25	10	C3H8NO6P	+	-	-	2	Glycine, serine and threonine metabolism
O-Phospho-serine	186.0	88.0	13.00	36	10	35	10	C3H8NO6P	+	-	-	2	Glycine, serine and threonine metabolism
N8-Acetyl-Spermidine	188.2	171.3	10.69	25	10	10	10	C9H21N3O	+	-	+	2	Polyamine metabolism
N-Acetyl-glutamine	189.0	84.0	8.16	16	10	28	10	C7H12N2O4	+	-	+	1	Alanine, aspartate and glutamate metabolism
N-Acetyl-glutamine	189.0	130.0	8.16	16	10	21	10	C7H12N2O4	+	-	+	1	Alanine, aspartate and glutamate metabolism
Nε, Nε, Nε - Trimethyllysine	189.2	130.1	11.67	25	10	10	10	C9H21N2O2	+	-	-	2	Lysine metabolism
N-Acetyl-glutamic acid	190.0	130.2	8.42	26	10	20	10	C7H11NO5	+	-	+	1	Alanine, aspartate and glutamate metabolism
N-Acetyl-glutamic acid	190.0	84.0	8.42	26	10	33	10	C7H11NO5	+	-	+	1	Alanine, aspartate and glutamate metabolism
Kynurenic Acid	190.1	146.1	2.78	25	10	20	10	C10H7NO3	+	-	+	2	Tryptophan metabolism
Kynurenic Acid	190.1	172.0	2.78	25	10	30	10	C10H7NO3	+	-	+	2	Tryptophan metabolism
N-Acetyl-methionine	192.0	104.0	3.97	21	10	20	10	C7H13NO3S	+	+	+	1	Cysteine and methionine metabolism
N-Acetyl-methionine	192.0	144.0	3.97	21	10	15	10	C7H13NO3S	+	+	+	1	Cysteine and methionine metabolism
Phenylacetylglycine	194.1	76.0	3.33	25	10	10	10	C10H11NO3	+	-	+	2	Phenylalanine metabolism
Phenylacetylglycine	194.1	91.0	3.33	25	10	20	10	C10H11NO3	+	-	+	2	Phenylalanine metabolism
Selenomethionine	198	56.4	3.63	25	10	20	10	C5H11NO2Se	+	-	-	2	Selenocompound metabolism
Selenomethionine	198	180.9	3.63	25	10	9	10	C5H11NO2Se	+	-	-	2	Selenocompound metabolism
Hercynine	198.1	139.1	9.90	25	10	20	10	C9H15N3O2	+	-	+	2	Histidine metabolism
Hercynine	198.1	95.1	9.90	25	10	20	10	C9H15N3O2	+	-	+	2	Histidine metabolism
N, N-Dimethylarginine	203.2	158.1	10.88	25	10	12	10	C8H18N4O2	+	-	-	2	Arginine and proline metabolism
Tryptophan	205.0	146.0	5.70	51	10	25	10	C11H12N2O2	+	+	+	1	Tryptophan metabolism
Tryptophan	205.0	188.0	5.70	51	10	15	10	C11H12N2O2	+	+	+	1	Tryptophan metabolism
AcetylCarnitine	205.0	84.1	3.30	34	10	19	10	C9H17NO4	+	-	+	1	Carnitine shuttle metabolism

AcetylCarnitine	205.0	145.0	3.30	34	10	19	10	C9H17NO4	+	-	+	1	Carnitine shuttle metabolism
N-Acetylphenylalanine	208.1	148.1	5.55	25	10	20	10	C11H13NO3	+	+	+	2	Phenylalanine metabolism
N-Acetylphenylalanine	208.1	120.1	5.55	25	10	20	10	C11H13NO3	+	+	+	2	Phenylalanine metabolism
Kynurenine	209.0	146.0	5.84	31	10	25	10	C10H12N2O3	+	+	+	1	Tryptophan metabolism
Kynurenine	209.0	192.0	5.84	31	10	13	10	C10H12N2O3	+	+	+	1	Tryptophan metabolism
Cyclo(Leu-Pro)	211.1	70.1	1.78	25	10	15	10	C11H18N2O2	+	+	+	2	Valine, leucine and isoleucine metabolism
Cyclo(Leu-Pro)	211.1	183.1	1.78	25	10	15	10	C11H18N2O2	+	+	+	2	Valine, leucine and isoleucine metabolism
Panthothenic acid	220.1	90.2	3.93	25	10	15	10	C9H17NO5	+	+	+	2	Pantothenate and CoA biosynthesis
Panthothenic acid	220.1	72.2	3.93	25	10	23	10	C9H17NO5	+	+	+	2	Pantothenate and CoA biosynthesis
5-Hydroxy-tryptophan	221.0	162.1	7.01	36	10	20	10	C11H12N2O3	+	-	-	1	Tryptophan metabolism
5-Hydroxy-tryptophan	221.0	204.0	7.01	36	10	15	10	C11H12N2O3	+	-	-	1	Tryptophan metabolism
GlcNAc	222.0	138.1	6.53	26	10	10	10	C8H15NO6	+	-	+	2	Amino sugar and nucleotide sugar metabolism
GlcNAc	222.0	204.0	6.53	26	10	11	10	C8H15NO6	+	-	+	2	Amino sugar and nucleotide sugar metabolism
Cystathionine	223.0	134.0	6.48	36	10	10	10	C7H14N2O4S	+	-	-	2	Cysteine and methionine metabolism
Cystathionine	223.0	88.0	6.48	36	10	41	10	C7H14N2O4S	+	-	-	2	Cysteine and methionine metabolism
Carnosine	227.0	209.9	12.55	31	10	10	10	C9H14N4O3	+	-	-	2	Histidine metabolism
Carnosine	227.0	110.0	12.55	31	10	33	10	C9H14N4O3	+	-	-	2	Histidine metabolism
2'-deoxycytidine	228.0	94.9	2.36	31	10	40	10	C9H13N3O4	+	-	-	2	Pyrimidine metabolism
2'-deoxycytidine	228.0	112.0	2.36	31	10	15	10	C9H13N3O4	+	-	-	2	Pyrimidine metabolism
Proline-hydroxyproline	229.2	211.1	10.54	25	10	10	10	C5H9NO3	+	-	-	2	Arginine and proline metabolism
Proline-hydroxyproline	229.2	70.1	10.54	25	10	20	10	C5H9NO3	+	-	-	2	Arginine and proline metabolism
Melatonin	233.1	174.3	5.08	30	10	18	10	C13H16N2O2	-	+	+	2	Tryptophan metabolism

Cystine	241.0	74.0	6.70	46	10	37	10	C6H12N2O4S2	+	-	+	1	Cysteine and methionine metabolism
Tetrahydrobiopterin	242.1	149.0	7.36	25	10	30	10	C9H15N5O3	+	-	-	2	Folate biosynthesis
Tetrahydrobiopterin	242.1	166.1	7.36	25	10	20	10	C9H15N5O3	+	-	-	2	Folate biosynthesis
Thymidine	243.0	110.0	2.45	26	10	25	10	C10H14N2O5	+	+	+	1	Pyrimidine metabolism
Thymidine	243.0	127.0	2.45	26	10	15	10	C10H14N2O5	+	+	+	1	Pyrimidine metabolism
Cytidine	244.0	94.8	4.67	26	10	40	10	C9H13N3O5	+	+	+	1	Pyrimidine metabolism
Cytidine	244.0	112.0	4.67	26	10	19	10	C9H13N3O5	+	+	+	1	Pyrimidine metabolism
Biotin	245.0	97.0	2.42	46	10	43	10	C10H16N2O3S	+	-	+	1	Biotin metabolism
Uridine	245.0	113.0	3.98	31	10	15	10	C9H12N2O6	+	+	+	1	Pyrimidine metabolism
gamma Glutamylcysteine	251.1	122.1	9.46	25	10	25	10	C8H14N2O5S	+	-	-	1	Cysteine and methionine metabolism
gamma Glutamylcysteine	251.1	130.1	9.46	25	10	30	10	C8H14N2O5S	+	-	-	1	Cysteine and methionine metabolism
2'-Deoxyadenosine	252.0	235.2	3.91	36	10	10	10	C10H13N5O3	+	-	-	2	Purine metabolism
2'-Deoxyadenosine	252.0	136.0	3.91	36	10	21	10	C10H13N5O3	+	-	-	2	Purine metabolism
Linatine	260.1	214.1	2.32	25	10	20	10	C10H17N3O5	+	-	-	2	Arginine and proline metabolism
Linatine	260.1	242.1	2.32	25	10	10	10	C10H17N3O5	+	-	-	2	Arginine and proline metabolism
Biotin sulfoxide	261.1	243.1	5.45	25	10	10	10	C10H16N2O4S	-	-	+	2	Biotin metabolism
Biotin sulfoxide	261.1	215.1	5.45	25	10	20	10	C10H16N2O4S	-	-	+	2	Biotin metabolism
Adenosine	268.0	136.0	4.02	25	10	51	10	C10H13N5O4	+	+	+	1	Purine metabolism
2'-Deoxyguanosine	268.0	152.0	4.56	41	10	15	10	C10H13N5O4	+	+	+	1	Purine metabolism
Homocystine	269.0	136.0	4.07	26	10	15	10	C8H16N2O4S2	+	-	+	2	Cysteine and methionine metabolism
Inosine	269.0	110.0	5.17	36	10	30	10	C10H12N4O5	+	+	+	1	Purine metabolism
Inosine	269.0	137.0	5.17	36	10	15	10	C10H12N4O5	+	+	+	1	Purine metabolism
Biotin Sulfone	277.1	259.1	3.13	25	10	10	10	C10H16N2O5S	+	-	+	2	Biotin metabolism
Biotin Sulfone	277.1	231.1	3.13	25	10	20	10	C10H16N2O5S	+	-	+	2	Biotin metabolism
Saccharopine	277.1	130.1	2.79	25	10	12	10	C11H20N2O6	+	-	-	2	Lysine degradation

Saccharopine	277.1	213.1	2.79	25	10	12	10	C11H20N2O6	+	-	-	2	Lysine degradation
1-Methyladenosine	282.1	150.1	7.08	25	10	40	10	C11H15N5O4	+	+	+	2	Purine metabolism
Guanosine	284.0	152.0	6.30	36	10	19	10	C10H13N5O5	+	+	+	1	Purine metabolism
Xanthosine	285.0	136.0	6.28	46	10	30	10	C10H12N4O6	+	-	+	1	Purine metabolism
Xanthosine	285.0	153.0	6.28	46	10	17	10	C10H12N4O6	+	-	+	1	Purine metabolism
S Methylthioadenosine	298.1	136	2.52	25	10	20	10	C11H15N5O3S	+	+	+	2	Cysteine and methionine metabolism
S Methylthioadenosine	298.1	163.0	2.52	25	10	13	10	C11H15N5O3S	+	+	+	2	Cysteine and methionine metabolism
S Methylthioinosine	299.1	167.0	2.86	25	10	13	10	C11H14N4O4S	+	+	+	2	Cysteine and methionine metabolism
S Methylthioinosine	299.1	137.0	2.86	25	10	20	10	C11H14N4O4S	+	+	+	2	Cysteine and methionine metabolism
d-Sphingosine	300.0	282.0	2.39	31	10	17	10	C18H37NO2	+	+	+	2	Sphingolipid metabolism
Glutathione	308.1	130.1	11.78	71	10	10	10	C10H17N3O6S	+	-	+	1	Cysteine and methionine metabolism
Glutathione	308.1	179.1	11.78	71	10	13	10	C10H17N3O6S	+	-	+	1	Cysteine and methionine metabolism
NANA	310.0	121.0	10.95	31	10	25	10	C11H19NO9	+	-	+	1	Amino sugar and nucleotide sugar metabolism
NANA	310.0	274.0	10.95	31	10	15	10	C11H19NO9	+	-	+	1	Amino sugar and nucleotide sugar metabolism
PQQ	331.0	285.0	1.70	51	10	27	10	C14H6N2O8	+	-	-	2	Amino sugar and nucleotide sugar metabolism
Riboflavin	377.0	243.0	4.63	71	10	35	10	C17H20N4O6	+	+	+	1	Riboflavin metabolism
S-(5'-adenosyl)-l-homocysteine	385.0	136.1	10.45	51	10	27	10	C14H20N6O5S	+	-	-	2	Cysteine and methionine metabolism
S-(5'-adenosyl)-l-homocysteine	385.0	134.0	10.45	51	10	27	10	C14H20N6O5S	+	-	-	2	Cysteine and methionine metabolism
Ergocalciferol	397.4	69.1	1.45	25	10	28	10	C28H44O	+	-	+	2	Steroid biosynthesis
Ergocalciferol	397.4	379.3	1.45	25	10	12	10	C28H44O	+	-	+	2	Steroid biosynthesis

S-(5'-adenosyl)-l-methionine	399.0	135.9	13.17	51	10	30	10	C15H22N6O5S	+	-	+	2	Cysteine and methionine metabolism
S-(5'-adenosyl)-l-methionine	399.0	250.0	13.17	51	10	23	10	C15H22N6O5S	+	-	+	2	Cysteine and methionine metabolism
Palmitoylcarnitine	400.3	85.0	2.33	25	10	20	10	C23H45NO4	-	+	+	2	Carnitine shuttle metabolism
Folic acid	442.0	295.0	9.32	41	10	23	10	C19H19N7O6	-	-	+	1	Folate biosynthesis
5-Methyl-THF	460.0	311.0	14.27	51	10	29	10	C20H25N7O6	-	-	+	2	Riboflavin metabolism
5-Methyl-THF	460.0	313.0	14.27	51	10	29	10	C20H25N7O6	-	-	+	2	Riboflavin metabolism
Glutathione oxidized	613.0	231.0	1.22	71	10	40	10	C20H32N6O12S2	+	-	+	1	Cysteine and methionine metabolism
Glutathione oxidized	613.0	355.0	1.22	71	10	33	10	C20H32N6O12S2	+	-	+	1	Cysteine and methionine metabolism
NAD^+	664.4	664.0	14.29	24	10	5	10	C21H27N7O14P2	+	-	+	1	Nicotinate and nicotinamide metabolism
NAD^+	664.4	136.0	14.29	24	10	39	10	C21H27N7O14P2	+	-	+	1	Nicotinate and nicotinamide metabolism
NADH	666.0	649.0	13.77	23	10	23	10	C21H29N7O14P2	+	-	+	1	Nicotinate and nicotinamide metabolism
$NADP^+$	744.0	604.0	12.51	51	10	35	10	C21H29N7O17P3	+	-	+	1	Nicotinate and nicotinamide metabolism
$NADP^+$	744.0	136.0	12.51	51	10	79	10	C21H29N7O17P3	+	-	+	1	Nicotinate and nicotinamide metabolism
NADPH	746.0	509.0	11.57	24	10	23	10	C21H31N7O17P3	+	-	+	1	Nicotinate and nicotinamide metabolism
NADPH	746.1	136.0	11.57	24	10	22	10	C21H31N7O17P3	+	-	+	1	Nicotinate and nicotinamide metabolism
NADPH	746.1	625.0	11.57	24	10	23	10	C21H31N7O17P3	+	-	+	1	Nicotinate and nicotinamide metabolism
FAD	786.0	348.0	11.37	76	10	31	10	C27H33P2N9O15	+	-	+	1	Riboflavin metabolism

Table S-5. Metabolites identified in ESI^- ionization mode.

Compound	Precursor ion [m/z]	Product ion [m/z]	t_R [min]	DP [V]	EP [V]	CE [V]	CXP [V]	Sum formula	Identified in cells	Identified in urine	Identified in plasma	Identification Level	Pathway
Glycolic acid	75.0	75.0	9.41	-30	-10	-5	-10	C2H4O3	+	+	-	1	Glyoxylate and dicarboxylate metabolism
Pyruvic acid	87.1	87.1	5.27	-30	-10	-5	-10	C3H4O3	+	+	+	1	Citrate cycle
Lactic acid	89.3	89.3	8.20	-45	-10	-5	-10	C3H6O3	+	+	+	1	Citrate cycle
gamma-Aminobutyric acid	102.2	102.2	11.30	-10	-10	-5	-10	C4H9NO2	+	-	-	1	Alanine, aspartate and glutamate metabolism
Hydroxybutyric acid	103.1	59.0	8.05	-25	-10	-18	-25	C4H8O3	+	+	+	2	Butanoate and propanoate metabolism
Malonic acid	103.1	41.1	11.94	-25	-10	-36	-10	C3H4O4	+	+	+	1	Fatty acid biosynthesis
Fumaric acid	115.2	71.1	13.83	-35	-10	-12	-10	C4H4O4	-	+	+	1	Citrate cycle
Succinic acid	117.4	73.0	12.73	-35	-10	-16	-10	C4H6O4	+	+	+	1	Citrate cycle
Taurine	124.1	80.0	9.57	-25	-10	-12	-10	C2H7NO3S	+	+	-	2	Taurine and hypotaurine metabolism
Pyroglutamic acid	127.9	83.9	9.73	-25	-10	-13	-10	C5H7NO3	+	+	+	1	Glutathione metabolism
Pyroglutamic acid	127.9	81.9	9.73	-25	-10	-17	-10	C5H7NO3	+	+	+	1	Glutathione metabolism
Citraconic acid	129.0	85.0	11.66	-15	-10	-14	-10	C5H6O4	+	-	+	1	Valine, leucine and isoleucine metabolism
Itaconic acid	129.0	85.0	5.25	-15	-10	-14	-10	C5H6O4	+	+	+	1	Citrate cycle
Oxaloacetic Acid	131.0	87.0	11.68	-15	-10	-10	-10	C4H4O5	+	+	-	2	Glycolysis
Aspartic acid	132.2	88.1	15.20	-15	-10	-20	-10	C4H7NO4	+	+	+	1	Alanine, aspartate and glutamate metabolism
Aspartic acid	132.2	71.3	15.20	-15	-10	-33	-10	C4H7NO4	+	+	+	1	Alanine, aspartate and glutamate metabolism
Threonic acid	135.2	75.0	10.50	-15	-10	-14	-10	C4H8O5	+	+	+	2	Ascorbate and aldarate metabolism
O-Phosphorylethanolamine	140.0	79.0	15.07	-20	-10	-15	-10	C2H8NO4P	+	-	+	2	Glycerophospholipid metabolism
Octanoic acid	143.1	143.1	2.01	-65	-10	-5	-10	C8H16O2	+	-	+	1	Fatty acid biosynthesis
alpha-Ketoglutaric acid	145.0	57.0	12.47	-20	-10	-25	-10	C5H6O5	+	+	+	2	Citrate cycle
alpha-Ketoglutaric acid	145.0	101.0	12.47	-20	-10	-12	-10	C5H6O5	+	+	+	2	Citrate cycle

N-Acetyl-DL-serine	146.0	128.2	11.53	-15	-10	-20	-10	C5H9NO4	+	+	+	2	Glycine, serine and threonine metabolism
Glutamic acid	146.2	131.0	13.26	-30	-10	-10	-10	C5H9NO4	+	+	+	1	Alanine, aspartate and glutamate metabolism
Glutamic acid	146.2	102.1	13.26	-30	-10	-20	-10	C5H9NO4	+	+	+	1	Alanine, aspartate and glutamate metabolism
Cinnamic acid	147.1	131.0	3.92	-60	-10	-23	-10	C9H8O2	+	+	+	1	Phenylalanine metabolism
Cinnamic acid	147.1	103.0	3.92	-60	-10	-16	-10	C9H8O2	+	+	+	1	Phenylalanine metabolism
p-Coumaric acid	163.0	119.1	4.75	-60	-10	-19	-10	C9H8O3	+	+	-	1	Tyrosine metabolism
Phenylpyruvic acid	163.0	91.1	2.56	-25	-10	-15	-10	C9H8O3	+	+	+	2	Phenylalanine metabolism
Quinolinate	166.5	78.2	2.25	-30	-10	-25	-10	C10H7NO2	-	-	+	2	Tryptophan metabolism
Quinolinate	166.5	122.0	2.25	-30	-10	-13	-10	C10H7NO2	-	-	+	2	Tryptophan metabolism
Uric acid	167.0	124.0	11.27	-50	-10	-22	-10	C5H4N4O3	-	+	+	1	Purine metabolism
Homogentisate	167.0	107.9	4.21	-50	-10	-35	-10	C8H8O4	+	+	+	1	Tyrosine metabolism
Homogentisate	167.0	123.0	4.21	-50	-10	-23	-10	C8H8O4	+	+	+	1	Tyrosine metabolism
Dihydroxyacetone phosphate	169.0	79.0	14.29	-40	-10	-36	-10	C3H7O6P	+	-	-	2	Glycolysis
Glycerol 3-phosphate	171.0	79.0	14.16	-40	-10	-26	-10	C3H9O6P	+	-	-	2	Glycolysis
N-Acetylleucine	172.1	130.1	5.78	-15	-10	-20	-10	C8H15NO3	+	+	+	1	Valine, leucine and isoleucine metabolism
Shikimic Acid	173.1	119.1	1.52	-75	-10	-10	-10	C7H10O5	+	+	+	2	Phenylalanine, tyrosine and tryptophan metabolism
Shikimic Acid	173.1	93.0	1.52	-75	-10	-15	-10	C7H10O5	+	+	+	2	Phenylalanine, tyrosine and tryptophan metabolism
Aconitic acid	173.0	129.0	13.65	-25	-10	-10	-10	C6H6O6	+	+	+	2	Citrate cycle
Aconitic acid	173.0	85.0	13.65	-25	-10	-18	-10	C6H6O6	+	+	+	2	Citrate cycle
N-Acetylaspartate	174.2	130.0	13.38	-15	-10	-20	-10	C6H9NO5	+	+	+	2	Alanine, aspartate and glutamate metabolism
N-Acetylaspartate	174.2	88.2	13.38	-15	-10	-20	-10	C6H9NO5	+	+	+	2	Alanine, aspartate and glutamate metabolism
Allantoic acid	175.0	115.2	10.50	-25	-10	-10	-10	C4H8N4O4	-	+	-	2	Purine metabolism
Allantoic acid	175.0	132.0	10.50	-25	-10	-12	-10	C4H8N4O4	-	+	-	2	Purine metabolism

Hippurate	178.1	77.1	5.70	-50	-10	-25	-10	C9H9NO3	+	+	+	2	Phenylalanine metabolism
Hippurate	178.1	134.0	5.70	-50	-10	-16	-10	C9H9NO3	+	+	+	2	Phenylalanine metabolism
Inositol	179.1	179.1	14.09	-25	-10	-5	-10	C6H12O6	-	+	+	1	Galactose metabolism
Inositol	179.1	81.0	14.09	-50	-10	-15	-10	C6H12O6	-	+	+	1	Galactose metabolism
Glucose	179.1	89.1	13.64	-15	-10	-28	-10	C6H12O6	+	-	+	1	Glycolysis
Glucose	179.1	59.1	13.64	-15	-10	-13	-10	C6H12O6	+	-	+	1	Glycolysis
Sorbitol	181.1	89.0	9.64	-60	-10	-20	-10	C6H14O6	+	+	+	2	Galactose metabolism
Homovanillate	181.1	137.1	5.77	-50	-10	-12	-10	C9H10O4	-	+	+	1	Tyrosine metabolism
4-hydroxyphenyllactic acid	181.1	163.0	6.15	-25	-10	-14	-10	C9H10O4	+	+	+	2	Tyrosine metabolism
4-hydroxyphenyllactic acid	181.1	135.1	6.15	-25	-10	-16	-10	C9H10O4	+	+	+	2	Tyrosine metabolism
4-Pyridoxic acid	182.1	108.2	2.34	-40	-10	-21	-10	C8H9NO4	+	+	+	2	Vitamin B6 metabolism
4-Pyridoxic acid	182.1	138.0	2.34	-40	-10	-21	-10	C8H9NO4	+	+	+	2	Vitamin B6 metabolism
Phosphoglyceric acid	185.0	79.0	9.82	-45	-10	-32	-10	C3H7O7P	+	-	-	2	Glycolysis
Phosphoglyceric acid	185.0	97.0	9.82	-45	-10	-21	-10	C3H7O7P	+	-	-	2	Glycolysis
Azelaic acid	187.0	169.0	10.80	-50	-10	-22	-10	C9H16O4	+	+	+	1	Fatty acid biosynthesis
Azelaic acid	187.0	125.0	10.80	-50	-10	-22	-10	C9H16O4	+	+	+	1	Fatty acid biosynthesis
5-Hydroxyindole-3-acetate	190.1	157.2	6.38	-50	-10	-18	-10	C10H9NO3	-	+	-	2	Tryptophan metabolism
5-Hydroxyindole-3-acetate	190.1	146.0	6.38	-50	-10	-16	-10	C10H9NO3	-	+	-	2	Tryptophan metabolism
Citric acid	191.1	191.0	8.32	-25	-10	-5	-10	C6H8O7	+	+	+	1	Citrate cycle
Citric acid	191.1	87.0	8.32	-25	-10	-12	-10	C6H8O7	+	+	+	1	Citrate cycle
Glucuronic acid	193.0	113.0	14.12	-45	-10	-18	-10	C6H10O7	+	+	+	1	Amino sugar and nucleotide sugar metabolism
Gluconic acid	195.0	195.0	11.81	-50	-10	-5	-10	C6H12O7	+	-	-	2	Pentose phosphate pathway
Gluconic acid	195.0	129.0	11.81	-50	-10	-20	-10	C6H12O7	+	-	-	2	Pentose phosphate pathway
Xanthurenic acid	204.0	160.0	6.42	-45	-10	-20	-10	C10H7NO4	+	+	+	1	Tryptophan metabolism
Lipoic acid	205.0	171.0	2.56	-45	-10	-12	-10	C8H14O2S2	+	+	+	2	Citrate cycle

Myristic acid	227.2	227.2	1.76	-15	-10	-5	-10	C14H28O2	+	-	+	2	Fatty acid biosynthesis
Neopterin	252.1	252.1	6.63	-40	-10	-5	-10	C9H11N5O4	+	+	-	2	Folate metabolism
Neopterin	252.1	192.0	6.63	-40	-10	-22	-10	C9H11N5O4	+	+	-	2	Folate metabolism
Palmitic Acid	255.2	255.2	1.71	-15	-10	-5	-10	C16H32O2	+	+	+	2	Fatty acid biosynthesis
Linoleic acid	279.2	279.2	1.66	-15	-10	-5	-10	C18H32O2	+	-	+	2	Fatty acid biosynthesis
Oleic acid	281.2	281.2	1.72	-15	-10	-5	-10	C18H34O2	+	-	+	2	Fatty acid biosynthesis
Stearic acid	283.3	283.3	1.67	-15	-10	-5	-10	C18H36O2	+	-	+	2	Fatty acid biosynthesis
cTMP	303.2	241.2	6.67	-65	-10	-20	-10	C10H13N2O7P	+	-	-	2	Pyrimidine metabolism
cTMP	303.2	125.0	6.67	-65	-10	-28	-10	C10H13N2O7P	+	-	-	2	Pyrimidine metabolism
cCMP	304.0	261.0	5.00	-70	-10	-20	-10	C9H12N3O7P	+	+	+	2	Pyrimidine metabolism
cCMP	304.0	110.1	5.00	-23	-10	-5	-10	C9H12N3O7P	+	+	+	2	Pyrimidine metabolism
dCMP	306.1	195.1	13.30	-70	-10	-56	-10	C9H14N3O7P	+	-	-	2	Pyrimidine metabolism
dCMP	306.1	79.0	13.30	-22	-10	-36	-10	C9H14N3O7P	+	-	-	2	Pyrimidine metabolism
Geranyl PP	313.0	79.0	14.65	-25	-10	-45	-10	C10H20O7P2	+	-	-	2	Ubiquinone and other terpenoid-quinone biosynthesis
TMP	321.1	79.0	14.91	-65	-10	-44	-10	C10H15N2O8P2	+	-	+	1	Pyrimidine metabolism
TMP	321.1	195.1	14.91	-65	-10	-24	-10	C10H15N2O8P2	+	-	+	1	Pyrimidine metabolism
CMP	322.0	195.1	15.24	-75	-10	-25	-10	C9H14N3O8P	+	-	-	1	Pyrimidine metabolism
CMP	322.0	79.0	15.24	-75	-10	-62	-10	C9H14N3O8P	+	-	-	1	Pyrimidine metabolism
UMP	323.2	195.1	15.77	-60	-10	-25	-10	C9H13N2O9P	+	-	-	1	Pyrimidine metabolism
UMP	323.2	79.0	15.77	-60	-10	-60	-10	C9H13N2O9P	+	-	-	1	Pyrimidine metabolism
cAMP	328.0	107.0	8.10	-85	-10	-36	-10	C10H11N5O6P	+	-	-	2	Purine metabolism
cAMP	328.0	134.0	8.10	-85	-10	-36	-10	C10H11N5O6P	+	-	-	2	Purine metabolism
dAMP	330.1	134.0	14.28	-60	-10	-20	-10	C10H14N5O6P	+	-	-	2	Purine metabolism
dAMP	330.1	79.0	14.28	-60	-10	-62	-10	C10H14N5O6P	+	-	-	2	Purine metabolism
Lactose	341.0	161.0	14.24	-65	-10	-12	-10	C12H22O11	+	-	-	1	Galactose metabolism
cGMP	344.0	133.0	10.68	-75	-10	-34	-10	C10H12N5O7P	+	-	-	1	Purine metabolism
cGMP	344.0	150.0	10.68	-75	-10	-34	-10	C10H12N5O7P	+	-	-	1	Purine metabolism

AMP	346.1	211.1	13.33	-73	-10	-50	-10	C10H14N5O7P	+	-	-	1	Purine metabolism
AMP	346.1	79.0	13.33	-73	-10	-65	-10	C10H14N5O7P	+	-	-	1	Purine metabolism
GMP	362.0	211.1	15.29	-65	-10	-25	-10	C10H14N5O8P	+	-	+	1	Purine metabolism
GMP	362.0	79.0	15.29	-65	-10	-62	-10	C10H14N5O8P	+	-	+	1	Purine metabolism
XMP	363.0	151.0	13.11	-35	-10	-25	-10	C10H13N4O9P	+	-	+	2	Purine metabolism
XMP	363.0	79.0	13.11	-35	-10	-36	-10	C10H13N4O9P	+	-	+	2	Purine metabolism
Farnesyl Ppi	381.0	79.0	14.61	-25	-10	-45	-10	C15H28O7P2	+	-	-	2	Steroid biosynthesis
dCDP	386.2	159.0	11.34	-65	-10	-25	-10	C9H15N3O10P2	+	-	-	2	Pyrimidine metabolism
dCDP	386.2	79.0	11.34	-65	-10	-72	-10	C9H15N3O10P2	+	-	-	2	Pyrimidine metabolism
CDP	402.0	159.0	15.91	-65	-10	-25	-10	C9H15N3O11P2	+	-	-	2	Pyrimidine metabolism
CDP	402.0	79.0	15.91	-65	-10	-78	-10	C9H15N3O11P2	+	-	-	2	Pyrimidine metabolism
ADP	426.3	159.0	15.11	-75	-10	-25	-10	C10H15N5O10P2	+	-	-	1	Purine metabolism
ADP	426.3	79.0	15.11	-75	-10	-88	-10	C10H15N5O10P2	+	-	-	1	Purine metabolism
CDP-ethanolamine	445.0	79.0	14.52	-45	-10	-82	-10	C11H20N4O11P2	+	-	-	2	Glycerophospholipid metabolism
dUTP	467.0	159.0	12.23	-24	-10	-25	-10	C9H15N2O14P3	+	-	-	2	Pyrimidine metabolism
dUTP	467.0	79.0	12.23	-24	-10	-44	-10	C9H15N2O14P3	+	-	-	2	Pyrimidine metabolism
TTP	481.0	159.0	14.48	-60	-10	-25	-10	C10H17N2O14P3	+	-	-	1	Pyrimidine metabolism
TTP	481.0	79.0	14.48	-60	-10	-60	-10	C10H17N2O14P3	+	-	-	1	Pyrimidine metabolism
ATP	506.1	159.0	16.14	-70	-10	-25	-10	C10H16N5O13P3	+	-	-	1	Purine metabolism
ATP	506.1	79.0	16.14	-70	-10	-90	-10	C10H16N5O13P3	+	-	-	1	Purine metabolism
ITP	507.0	159.0	14.97	-60	-10	-25	-10	C10H15N4O14P3	+	-	-	1	Pentose phosphate pathway
ITP	507.0	79.0	14.97	-60	-10	-90	-10	C10H15N4O14P3	+	-	-	1	Pentose phosphate pathway
UDP-GalNAc	606.2	79.0	15.00	-85	-10	-85	-10	C17H27N3O17P2	+	-	+	2	Pentose phosphate pathway
UDP-GalNAc	606.2	385.0	15.00	-85	-10	-38	-10	C17H27N3O17P2	+	-	+	2	Pentose phosphate pathway
CMP-NANA	613.0	79.0	15.30	-60	-10	-85	-10	C20H31N4O16P	+	-	+	2	Pentose phosphate pathway
CMP-NANA	613.0	322.0	15.30	-60	-10	-28	-10	C20H31N4O16P	+	-	+	2	Pentose phosphate pathway

Table S-6: Data on method validation for the individual metabolites analyzed in positive ionization mode.

Metabolite	t_R [min]	LOD [ng/mL]	LOQ [ng/mL]	Linearity [r]	Precision [%]			Accuracy [%]			Slope	Intercept	Amount detected [ng/mL]	^{13}C IS used
					QC_{low}	QC_{mid}	QC_{high}	QC_{low}	QC_{mid}	QC_{high}				
Glycine	9.21	18.9	34.6	0.9941	7.35	4.65	5.99	92.5	93.4	92.1	7.72×10^2	2.72×10^4	246.96 ± 25.22	Glycine
Alanine	8.81	10.5	36.2	0.9923	9.66	0.83	3.25	101.1	98.6	95.6	6.01×10^2	1.63×10^4	107.37 ± 13.21	Alanine
beta-Alanine	7.83	9.6	28.4	0.9869	7.97	1.59	1.79	105.6	99.9	98.7	6.02×10^2	1.42×10^4	123.51 ± 14.18	Alanine
Sarcosine	8.22	7.9	36.6	0.9976	1.1	5.94	4.38	108.9	99.1	111.6	1.40×10^3	2.14×10^4	36.60 ± 8.85	Sarcosine
Choline	4.61	16.8	31.8	0.9950	7.61	4.78	6.18	93.3	96.5	104.3	7.90×10^1	5.03×10^3	415.60 ± 23.98	Choline
Serine	4.61	11.5	32.5	0.9914	3.26	1.33	2.26	98.6	107.5	95.6	2.79×10^2	1.56×10^4	316.39 ± 14.33	Serine
Cytosine	4.60	11.1	35.1	0.9916	2.04	5.14	3.36	96.6	103.4	109.9	1.12×10^4	1.04×10^6	39.19 ± 6.93	Serine
Uracil	4.58	8.4	21.2	0.9893	1.46	1.44	4.15	97.7	107.6	113.4	8.49×10^2	4.09×10^4	22.67 ± 3.44	Serine
Dihydrouracil	2.45	9.1	28.5	0.9965	5.09	1.91	6.84	96.6	98.9	94.3	2.40×10^1	1.21×10^3	57.48 ± 1.56	Biotin
Dihydrouracil	2.45	5.0	12.8	0.9926	2.15	2.26	5.54	96.4	99.1	94.3	5.04×10^2	1.06×10^3	56.89 ± 5.31	Biotin
Proline	7.25	12.1	27.3	0.9976	7.05	4.82	1.96	99.1	101.1	95.4	1.00×10^4	4.14×10^5	253.19 ± 21.84	Proline
Betaine	6.40	9.8	20.3	0.9979	7.27	4.16	2.61	93.2	98.7	104.3	6.08×10^4	5.89×10^6	20.48 ± 1.32	Betaine
Valine	7.10	10.6	32.6	0.9978	2.08	2.69	5.24	105.4	98.1	99.9	2.53×10^3	2.50×10^4	206.55 ± 27.41	Valine
Threonine	9.08	17.5	44.1	0.9948	2.93	1.28	3.84	110.3	94.4	104.5	4.41×10^2	1.09×10^4	420.24 ± 31.22	Threonine

Nicotinamide	2.33	19.9	35.4	0.9969	4.61	10.61	5.96	101.3	98.8	107.7	1.02×10^{1}	6.18×10^{2}	223.50 ± 16.58	Nicotinamide
Thymine	2.44	7.6	23.6	0.9982	10.86	1.49	2.85	99.1	104.4	95.6	2.61×10^{2}	5.50×10^{2}	27.74 ± 3.32	Biotin
Isoleucine	6.14	16.1	39.1	0.9970	3.13	5.25	4.41	95.9	98.3	101.4	6.49×10^{2}	1.61×10^{4}	164.89 ± 11.14	Isoleucine
Leucine	5.79	14.1	33.1	0.9973	8.08	3.3	4.32	105.4	97.7	102.3	2.54×10^{2}	6.63×10^{2}	441.28 ± 22.65	Leucine
Asparagine	9.99	14.2	36.3	0.9933	11.71	3.74	0.38	101.6	96.5	104.3	4.79×10^{2}	1.36×10^{4}	554.46 ± 31.23	Asparargine
Ornithine	13.10	13.1	36.7	0.9936	3.79	1.35	0.92	98.8	101.4	104.7	1.42×10^{3}	7.20×10^{4}	281.09 ± 17.56	Ornithine
Ornithine	13.10	15.8	38.4	0.9971	2.06	1.71	0.45	99.0	101.1	104.9	1.35×10^{3}	1.59×10^{5}	278.88 ± 12.23	Ornithine
Adenine	3.59	13.1	31.5	0.9881	10.24	2.01	0.73	113.3	97.7	103.2	1.93×10^{3}	1.63×10^{5}	50.31 ± 8.75	Adenine
Adenine	3.59	9.1	22.4	0.9886	1.95	1.7	2.56	113.1	97.8	103.3	8.52×10^{3}	8.13×10^{5}	48.88 ± 4.43	Adenine
Hypoxanthine	3.81	18.6	38.4	0.9825	2.06	3.45	1.01	101.1	99.9	102.5	2.52×10^{3}	3.87×10^{5}	265.77 ± 18.87	Adenine
Hypoxanthine	3.81	19.8	31.9	0.9857	1.99	0.58	0.76	101.3	99.7	102.5	2.47×10^{3}	4.12×10^{5}	262.08 ± 21.12	Adenine
Acetylcholine	3.01	5.2	14.1	0.9945	3.52	1.58	1.23	97.7	104.3	99.1	1.05×10^{4}	2.87×10^{5}	19.75 ± 0.89	Adenine
Glutamine	9.65	7.9	24.9	0.9967	8.46	4.41	1.58	95.6	107.7	99.8	2.15×10^{3}	3.16×10^{4}	235.23 ± 7.55	Glutamine
Glutamine	9.65	11.1	32.7	0.9926	8.46	3.62	3.96	95.7	107.6	99.8	1.59×10^{3}	2.52×10^{4}	230.09 ± 11.35	Glutamine
Lysine	13.19	15.1	38.9	0.9941	1.93	1.51	1.21	101.3	97.7	102.1	1.33×10^{3}	7.75×10^{4}	284.95 ± 16.94	Lysine
Lysine	13.19	11.2	32.9	0.9953	1.14	0.91	0.34	101.3	97.8	102.0	1.90×10^{3}	7.07×10^{4}	280.19 ± 23.32	Lysine
Methionine	6.50	11.1	44.5	0.9961	5.99	9.26	2.08	99.4	98.7	101.2	5.56×10^{2}	4.62×10^{4}	349.38 ± 28.85	Methionine
Methionine	6.50	12.2	45.8	0.9966	5.74	7.87	3.81	99.3	98.7	101.3	5.57×10^{2}	4.41×10^{4}	343.45 ± 28.87	Methionine
Histidine	11.12	7.2	21.7	0.9999	1.57	2.7	0.43	104.4	98.8	103.4	2.08×10^{3}	1.79×10^{4}	190.12 ± 7.76	Histidine
Histidine	11.12	3.1	15.1	0.9975	3.06	0.42	1.32	104.5	98.9	103.3	1.17×10^{4}	2.81×10^{5}	188.90 ± 6.65	Histidine

Phenylalanine	5.57	8.5	21.8	0.9957	2.12	6.01	3.51	110.2	98.6	101.2	1.84×10^3	1.34×10^4	134.92 ± 8.87	Phenylalanine
Phenylalanine	5.57	5.4	18.2	0.9975	2.16	1.63	3.87	110.0	98.7	101.3	1.18×10^4	1.93×10^3	137.18 ± 11.14	Phenylalanine
Arginine	10.70	36.9	92.5	0.9927	1.23	4.59	2.89	104.3	98.8	102.1	8.21×10^1	4.73×10^3	277.48 ± 18.87	Arginine
Arginine	10.70	18.5	46.9	0.9947	9.69	1.95	1.02	104.1	98.9	102.1	1.38×10^3	6.37×10^4	273.78 ± 23.32	Arginine
Citrulline	10.33	9.5	41.2	0.9822	2.25	8.07	2.56	110.1	93.2	96.5	1.18×10^3	4.98×10^4	43.02 ± 18.87	Citrulline
Citrulline	10.33	11.1	41.5	0.9886	7.32	4.84	3.18	110.0	93.3	96.6	2.27×10^3	6.44×10^4	42.56 ± 11.19	Citrulline
Glucosamine	10.37	5.6	12.9	0.9966	4.2	6.78	4.95	101.1	96.5	97.8	1.94×10^2	4.66×10^3	14.29 ± 1.28	Citrulline
Glucosamine	10.37	6.6	11.9	0.9969	10.57	6.28	5.43	101.1	96.4	97.8	1.42×10^3	3.32×10^4	13.23 ± 2.21	Citrulline
Tyrosine	7.22	14.7	55.5	0.9954	10.27	2.21	5.44	99.8	97.7	94.3	3.69×10^2	9.18×10^3	237.18 ± 8.89	Tyrosine
Tyrosine	7.22	10.2	41.8	0.9963	9.67	5.16	4.61	100.0	97.6	94.3	4.70×10^2	1.01×10^4	235.79 ± 14.43	Tyrosine
N-Acetyl-Glutamine	7.87	7.7	22.9	0.9989	7.98	1.38	6.12	99.1	101.3	99.8	1.57×10^3	4.88×10^4	24.46 ± 6.65	Tyrosine
N-Acetyl-Glutamine	7.87	5.9	19.1	0.9970	4.91	1.63	2.07	99.0	101.1	99.8	2.62×10^3	8.26×10^4	24.21 ± 4.43	Tyrosine
N-Acetyl-Glutamic Acid	8.11	7.1	12.1	0.9983	4.31	4.59	2.5	94.3	98.8	108.7	1.29×10^3	2.49×10^4	26.70 ± 5.54	Sarcosine
N-Acetyl-Glutamic Acid	8.11	8.9	19.6	0.9988	10.78	6.26	8.51	94.2	98.9	108.8	9.89×10^2	1.19×10^4	27.31 ± 2.23	Sarcosine
N-Acetyl-Methionine	3.84	7.7	34.3	0.9967	9.91	4.54	4.24	104.3	103.2	109.8	3.10×10^3	5.64×10^4	48.70 ± 8.98	Adenine
N-Acetyl-Methionine	3.84	8.7	27.1	0.9981	8.23	4.48	7.87	104.1	103.1	109.8	4.11×10^3	6.20×10^4	47.55 ± 6.64	Adenine

Tryptophan	5.48	7.1	32.1	0.9983	11.65	8.25	3.31	98.8	101.3	104.6	4.74×10^3	1.09×10^5	200.22 ± 16.65	Tryptophan
Tryptophan	5.48	5.8	25.5	0.9972	5.06	11.19	5.34	98.8	101.2	104.7	9.79×10^3	2.15×10^5	197.40 ± 17.43	Tryptophan
Kynurenine	5.63	19.2	49.2	0.9949	10.07	9.05	5.13	97.6	99.6	104.3	1.88×10^3	1.93×10^4	23.22 ± 7.76	Tryptophan
Kynurenine	5.63	11.7	45.9	0.9977	11.08	10.34	7.88	97.6	99.5	104.3	6.22×10^3	1.08×10^5	20.98 ± 3.34	Tryptophan
5-OH-Tryptophan	6.82	6.7	31.2	0.9969	7.81	5.38	1.39	101.2	99.8	105.6	6.14×10^2	8.92×10^3	33.69 ± 2.27	Tryptophan
5-OH-Tryptophan	6.82	4.6	28.7	0.9975	6.79	4.28	5.51	101.1	99.9	105.7	1.96×10^3	1.46×10^4	33.56 ± 5.12	Tryptophan
Cystine	7.26	17.2	112.6	0.9968	4.54	3.65	6.65	106.6	98.8	104.3	1.47×10^2	7.03×10^4	385.56 ± 18.85	Tyrosine
Thymidine	2.70	2.9	9.2	0.9995	9.55	4.53	14.31	99.7	101.3	110.5	3.25×10^2	2.36×10^3	12.71 ± 2.21	Biotin
Thymidine	2.70	1.8	7.7	0.9965	4.41	8.7	12.93	99.5	101.2	110.6	9.11×10^3	9.26×10^4	12.25 ± 1.54	Biotin
Cytidine	5.75	12.6	39.8	0.9912	7.61	13.35	2.77	104.3	110.2	92.3	1.05×10^3	1.20×10^4	42.48 ± 6.65	Tryptophan
Cytidine	5.75	10.1	32.2	0.9890	11.65	10.66	3.98	104.3	110.1	92.4	1.85×10^4	1.57×10^5	45.20 ± 5.54	Tryptophan
Biotin	2.57	6.1	18.6	0.9993	6.61	0.31	2.91	110.6	97.6	94.3	5.42×10^3	5.11×10^4	19.19 ± 6.81	Biotin
Uridine	3.98	10.7	33.3	0.9886	5.8	6.81	3.71	105.4	98.8	103.2	1.24×10^3	9.12×10^4	136.50 ± 11.95	Uridine
Adenosine	3.94	10.7	39.6	0.9837	6.41	4.08	4.28	101.2	97.7	98.9	1.81×10^4	2.29×10^6	134.42 ± 9.94	Uridine
2'-Deoxyguanosine	5.14	13.9	33.4	0.9934	2.86	8	1.92	104.5	107.8	101.2	2.40×10^4	9.01×10^5	40.84 ± 3.32	Serine
Homocystine	3.72	14.8	35.9	0.9954	5.63	6.58	2.58	103.2	96.5	107.7	5.89×10^2	8.53×10^4	114.60 ± 2.56	Uridine
Guanosine	6.16	12.6	38.5	0.9988	1.04	4.91	6.95	92.3	103.4	105.6	3.83×10^3	9.27×10^4	39.93 ± 1.93	Guanosine

N-Acetyl-Neuraminic Acid	10.67	16.4	29.9	0.9983	4.26	11.44	5.49	98.8	101.5	109.4	1.01×10^2	3.98×10^3	44.61 ± 8.85	Citrulline
N-Acetyl-Neuraminic Acid	10.67	11.6	28.5	0.9914	8.24	8.34	7.49	98.9	101.5	109.3	6.42×10^2	1.74×10^4	46.36 ± 6.64	Citrulline
Riboflavin	4.43	4.2	16.9	0.9996	8.49	4.9	1.52	102.1	97.8	103.4	4.02×10^3	3.16×10^4	17.44 ± 5.99	Serine
Folic Acid	9.18	5.5	16.9	0.9993	4.09	3.61	5.622	96.6	98.8	102.1	6.52×10^2	6.93×10^3	17.83 ± 2.01	Glutamine
Glutathione Oxidized	7.33	8.7	23.6	0.9991	3.27	4.23	2.59	103.1	102.4	97.7	5.23×10^2	3.03×10^2	24.33 ± 1.74	Tyrosine
NAD	14.29	6.1	16.8	0.9929	8.94	9.92	10.23	101.2	96.6	98.8	1.23×10^2	7.41×10^4	17.77 ± 1.03	NAD
NADH	13.77	5.2	13.9	0.9954	9.21	10.52	8.72	100.4	100.1	98.8	5.78×10^1	7.10×10^4	17.41 ± 2.94	NADH
NADP	12.51	4.9	15.4	0.9912	10.88	2.83	4.69	94.5	98.8	101.2	1.89×10^2	6.04×10^4	18.56 ± 1.85	NADP
NADPH	11.17	4.2	15.5	0.9948	6.71	3.95	5.64	103.1	105.5	98.8	4.63×10^1	7.05×10^4	18.86 ± 2.12	NADPH
FAD	11.37	8.5	18.8	0.9966	8.54	9.41	7.69	97.7	98.1	103.2	1.38×10^3	7.32×10^4	22.98 ± 1.58	NADPH
Glutathione Reduced	11.51	19.6	67.9	0.9964	5.49	3.41	4.67	101.1	96.6	95.4	4.71×10^2	6.99×10^4	406.35 ± 19.98	Glutathione
Methionine Sulfoxide	9.53	10.3	31.8	0.9978	12.82	4	2.42	99.1	98.8	103.2	2.56×10^3	1.38×10^4	103.58 ± 8.87	Methionine
Methionine Sulfoxide	9.53	12.2	32.8	0.9959	4.12	0.89	0.85	98.8	98.9	103.2	6.87×10^2	6.53×10^3	114.65 ± 11.43	Methionine
N-Acetyl-Cysteine	4.92	17.7	34.4	0.9967	5.93	6.13	8.72	101.1	95.4	98.8	8.61×10^2	1.21×10^4	43.99 ± 8.97	Serine
N-Acetyl-Cysteine	4.92	19.2	39.3	0.9921	8.41	4.07	4.19	101.0	95.4	98.7	7.40×10^1	1.25×10^3	46.18 ± 10.12	Serine

Homoleucine	3.00	18.3	46.9	0.9895	4.68	4.35	2.09	104.2	97.7	93.4	3.83×10^2	1.12×10^4	166.83 ± 21.34	Leucine
Cysteine	7.72	10.1	48.9	0.9919	8.45	6.95	3.73	103.2	105.4	109.1	1.15×10^2	1.57×10^3	117.10 ± 11.43	Tyrosine
Cysteinyl-Glycine	9.34	11.9	36.9	0.9976	8.12	7.69	4.91	98.8	101.2	109.6	3.76×10^2	4.53×10^3	40.43 ± 7.76	Methionine
Cysteinyl-Glycine	9.34	10.1	35.9	0.9943	9.51	4.39	10.92	98.9	101.1	109.7	3.62×10^2	5.06×10^3	43.63 ± 5.56	Methionine
5-Methyl-Cytosine	4.29	5.2	22.7	0.9889	7.95	1.04	3.16	101.1	99.6	95.4	6.94×10^4	5.28×10^6	69.58 ± 8.44	Serine
Histamine	8.44	2.4	14.5	0.9859	7.57	0.78	2.91	103.2	98.7	104.1	9.09×10^4	1.05×10^7	28.48 ± 6.65	Histidine
Histamine	8.44	3.9	18.7	0.9801	8.87	2.66	5.67	103.1	98.6	104.2	3.87×10^4	4.08×10^6	21.43 ± 4.43	Histidine
Dihydroorotic Acid	6.34	11.1	33.9	0.9989	4.97	2.74	1.41	96.3	97.1	101.2	2.17×10^2	5.71×10^3	35.42 ± 3.98	Methionine
O-Acetyl-Serine	7.19	11.1	24.2	0.9977	2.66	4.61	1.57	103.1	98.6	99.4	8.92×10^2	2.24×10^4	35.89 ± 3.12	Tyrosine
O-Acetyl-Serine	7.19	8.8	20.9	0.9995	9.64	7.61	2.79	103.2	98.5	99.4	1.06×10^3	2.41×10^4	37.21 ± 2.77	Tyrosine

Table S-7: Data on method validation for the individual metabolites analyzed in negative ionization mode.

Metabolite	t_R [min]	LOD [ng/mL]	LOQ [ng/mL]	Linearity [r]	Precision [%]			Accuracy [%]			Slope	Intercept	Amount detected [ng/mL]	^{13}C IS used
					QC_{low}	QC_{mid}	QC_{high}	QC_{low}	QC_{mid}	QC_{high}				
Glycolic Acid	9.41	22.9	61.2	0.9847	4.12	5.36	1.08	94.4	97.4	108.7	3.13×10^3	2.56×10^4	293.59 ± 3.3	Glycolic Acid
Pyruvic Acid	5.21	12.7	38.4	0.9996	2.49	1.50	1.34	93.2	91.4	96.9	4.99×10^4	1.69×10^6	107.01 ± 10.12	Pyruvic Acid
Lactic Acid	8.10	23.3	62.5	0.9846	3.39	1.58	1.14	101.2	105.6	98.7	8.22×10^3	1.03×10^6	392.32 ± 15.54	Lactic Acid
GABA	11.27	14.1	23.7	0.9956	1.59	0.58	1.92	96.6	99.8	103.2	4.37×10^3	7.14×10^4	118.67 ± 8.99	GABA
Malonic Acid	11.80	27.5	84.3	0.9926	1.83	2.63	1.29	95.7	99.1	104.4	8.50×10^2	1.24×10^5	261.76 ± 13.45	Malonic Acid
Fumaric Acid	11.80	13.5	48.6	0.9995	2.49	2.15	1.66	98.8	96.6	99.1	1.70×10^3	7.15×10^4	320.78 ± 22.43	Fumaric Acid
Succinic Acid	12.82	21.8	61.3	0.9909	1.39	6.01	3.51	97.7	102.1	106.5	1.14×10^3	9.01×10^4	118.47 ± 18.65	Succinic Acid
Citraconic Acid	5.45	14.4	29.4	0.9876	1.21	0.11	2.12	99.3	103.4	97.6	1.97×10^5	2.31×10^7	34.91 ± 9.91	Pyruvic Acid
Itaconic Acid	11.76	9.9	21.4	0.9944	2.66	1.15	1.10	92.2	101.3	99.6	2.41×10^4	2.35×10^6	28.99 ± 7.75	Fumaric Acid
Glutaric Acid	13.00	19.1	39.1	0.9922	2.21	1.39	3.47	103.4	98.8	102.8	8.40×10^2	1.13×10^5	310.12 ± 19.21	Succinic Acid
Cinnamic Acid	3.33	14.7	24.8	0.9986	5.13	1.73	1.47	96.6	101.1	99.6	7.08×10^4	1.38×10^5	36.03 ± 6.64	Pyruvic Acid
Coumaric Acid	4.66	12.1	26.9	0.9989	2.26	3.11	0.70	107.3	98.8	103.2	1.18×10^5	3.16×10^6	35.28 ± 3.45	Pyruvic Acid
Uric Acid	10.60	9.6	19.6	0.9980	2.15	1.59	2.91	101.1	99.3	96.2	3.79×10^3	2.18×10^5	252.41 ± 17.75	Aspartic Acid
Citric Acid	10.60	26.9	52.1	0.9950	1.17	1.82	3.11	95.4	94.9	102.7	1.68×10^3	3.79×10^6	374.74 ± 23.41	Citric Acid

Glucuronic Acid	13.00	27.3	43.7	0.9926	1.35	3.84	2.33	101.1	98.8	99.3	8.24×10^{2}	2.59×10^{5}	355.93 ± 25.66	Succinic Acid
Xanthurenic Acid	4.66	9.5	24.7	0.9955	3.71	3.50	1.76	103.7	102.1	99.5	1.91×10^{5}	4.64×10^{6}	28.05 ± 6.61	Pyruvic Acid
Lactose	12.46	15.4	37.6	0.9953	4.59	3.88	2.27	101.2	99.7	96.8	9.53×10^{1}	2.71×10^{4}	398.93 ± 31.31	Glucose
cGMP	10.42	16.9	51.3	0.9993	6.86	6.62	4.55	103.7	105.8	109.1	6.46×10^{2}	5.37×10^{3}	252.55 ± 26.77	cGMP
cGMP	10.42	17.7	53.7	0.9993	8.44	7.33	3.99	103.5	105.8	109.0	2.26×10^{3}	1.55×10^{4}	248.43 ± 18.91	cGMP
AMP	13.33	14.8	35.5	0.9972	7.79	8.34	5.56	101.1	96.6	98.9	2.68×10^{1}	7.55×10^{3}	45.29 ± 6.61	AMP
GMP	15.50	18.6	36.9	0.9966	6.34	7.39	4.85	95.6	102.8	109.1	2.00×10^{2}	2.77×10^{3}	165.50 ± 9.91	GMP
GMP	15.50	14.0	33.8	0.9934	6.91	7.15	11.01	95.4	102.9	109.1	5.51×10^{2}	3.01×10^{4}	158.54 ± 7.73	GMP
UDP	4.66	15.4	39.4	0.9867	5.91	5.14	11.15	108.1	94.5	99.1	1.47×10^{2}	1.36×10^{4}	36.38 ± 3.41	UDP
UDP	4.66	16.4	31.3	0.9862	6.81	6.56	7.51	107.9	94.6	99.2	1.97×10^{2}	1.41×10^{4}	33.69 ± 8.84	UDP
ADP	15.11	18.4	35.8	0.9998	7.32	1.21	6.03	101.3	98.8	103.4	4.71×10^{2}	4.04×10^{4}	177.44 ± 7.71	ADP
ADP	15.11	25.9	49.2	0.9974	6.91	6.44	7.23	101.2	99.5	103.3	2.15×10^{2}	9.39×10^{3}	173.82 ± 14.41	ADP
TTP	14.39	15.1	27.3	0.9905	6.32	5.85	5.91	97.7	98.9	106.5	9.55×10^{2}	4.04×10^{3}	158.71 ± 16.88	TTP
TTP	14.39	22.2	38.4	0.9913	5.79	8.15	7.75	97.6	98.9	106.5	1.94×10^{2}	2.99×10^{3}	154.79 ± 13.59	TTP
CTP	10.38	20.9	43.9	0.9978	9.81	7.65	3.92	98.8	99.1	102.1	1.20×10^{2}	7.20×10^{1}	61.47 ± 8.43	cGMP
CTP	10.38	13.9	23.5	0.9995	7.65	5.59	8.71	98.7	99.0	102.0	1.81×10^{1}	1.72×10^{3}	58.80 ± 7.91	cGMP
UTP	14.51	24.4	44.7	0.9933	5.41	4.91	7.77	103.4	97.7	102.1	1.82×10^{1}	3.81×10^{3}	130.80 ± 11.43	UTP
ATP	16.14	23.8	48.7	0.9950	4.67	6.77	8.54	99.1	97.6	103.4	9.74×10^{1}	6.83×10^{3}	163.84 ± 12.54	ATP

ITP	14.98	19.2	38.3	0.9989	8.91	5.58	0.59	105.6	104.3	98.8	7.45×10^{0}	1.07×10^{4}	312.63 ± 28.83	TTP
Glucose	13.56	13.1	31.4	0.9923	4.91	3.54	1.81	102.1	99.5	107.7	5.34×10^{2}	1.81×10^{5}	112.34 ± 8.31	Glucose
pGlu	9.65	8.8	26.8	0.9998	2.49	5.08	0.79	98.8	97.7	95.4	6.13×10^{1}	1.14×10^{3}	363.85 ± 18.31	Glycolic Acid
pGlu	9.65	12.7	29.3	0.9959	0.96	4.76	1.30	98.9	97.5	95.6	6.69×10^{1}	9.68×10^{2}	344.71 ± 24.49	Glycolic Acid
Inositol	14.10	9.4	20.2	0.9918	1.27	9.93	2.38	101.2	103.5	99.6	5.31×10^{4}	1.77×10^{7}	330.14 ± 25.91	Glucose
Homogentisate	4.18	9.3	17.6	0.9982	0.59	2.53	1.51	98.8	101.2	97.6	1.79×10^{4}	9.47×10^{5}	20.42 ± 1.23	Pyruvic Acid
Homogentisate	4.18	7.1	11.1	0.9982	0.74	1.68	1.46	98.7	101.3	97.5	8.31×10^{4}	4.71×10^{6}	20.28 ± 0.87	Pyruvic Acid
N-Acetyl-Leucine	5.64	9.3	28.1	0.9998	1.79	1.78	0.67	101.2	99.5	105.8	8.81×10^{4}	6.12×10^{5}	31.76 ± 2.21	Glycolic Acid
Azelaic Acid	10.73	15.3	23.4	0.9953	8.24	3.95	2.64	97.6	104.5	108.7	1.39×10^{3}	1.11×10^{4}	36.25 ± 3.14	cGMP
Azelaic Acid	10.73	13.8	20.7	0.9964	7.61	4.81	4.02	97.7	104.6	108.9	2.47×10^{4}	1.94×10^{5}	32.94 ± 3.56	cGMP
CMP	12.92	23.5	52.2	0.9834	7.25	3.41	4.82	106.6	105.4	99.4	1.41×10^{2}	6.32×10^{3}	58.81 ± 4.41	CMP
Glutamic Acid	13.93	9.9	22.1	0.9950	3.32	2.58	1.24	103.2	97.3	108.9	1.67×10^{2}	8.80×10^{3}	338.89 ± 19.91	Glutamic Acid
Aspartic Acid	14.80	9.8	22.9	0.9948	2.17	1.55	3.23	104.5	103.2	101.8	1.89×10^{2}	7.19×10^{3}	304.80 ± 24.44	Aspartic Acid
GDP	15.45	21.3	55.1	0.9961	6.84	5.49	7.91	109.5	106.5	104.3	1.44×10^{2}	2.61×10^{3}	93.45 ± 13.31	GDP
Homovanillate	5.68	11.9	36.3	0.9996	1.11	1.48	1.06	96.5	99.1	103.2	8.52×10^{3}	3.58×10^{4}	43.79 ± 8.91	Pyruvic Acid
UMP	15.51	13.8	22.4	0.9897	5.66	4.92	3.31	98.3	102.3	97.5	2.63×10^{1}	1.73×10^{3}	100.07 ± 5.56	UMP
TMP	12.98	12.9	20.2	0.9937	4.42	5.44	7.59	99.2	103.7	109.5	1.03×10^{2}	7.45×10^{3}	404.69 ± 21.74	TMP

Table S-8. Matrix effect, extraction recovery, process efficiency.

Compound	ME	ER	PE
Glycine	78.4	88.5	69.4
Alanine	59.6	86.1	51.3
beta-Alanine	51.6	89.3	46.1
Sarcosine	65.5	91.4	59.9
Choline	69.5	95.6	66.4
Serine	42.0	94.1	39.5
Cytosine	94.9	92.2	87.5
Uracil	87.0	93.6	81.4
Dihydrouracil	82.0	84.0	68.9
Dihydrouracil	82.0	83.7	68.6
Proline	91.3	92.4	84.4
Betaine	88.7	83.3	73.9
Valine	106.1	98.1	104.1
Threonine	109.5	95.3	104.4
Nicotinamide	74.9	88.1	66.0
Thymine	102.1	96.5	98.5
Isoleucine	93.2	94.4	88.0
Leucine	59.2	93.6	55.4
Asparagine	78.6	83.3	65.5
Ornithine	86.2	88.5	76.3
Ornithine	87.3	88.2	77.0
Adenine	103.7	85.5	88.7
Adenine	99.3	85.8	85.2
Hypoxanthine	90.7	89.3	81.0
Hypoxanthine	89.6	89.0	79.7
Acetylcholine	102.4	87.3	89.4
Glutamine	59.5	78.8	46.9
Glutamine	60.0	79.1	47.5
Lysine	99.1	95.4	94.5
Lysine	100.0	95.4	95.4
Methionine	60.7	88.4	53.7
Methionine	60.5	88.3	53.4
Histidine	54.0	85.4	46.1
Histidine	54.2	85.4	46.3
Phenylalanine	86.4	91.2	78.8
Phenylalanine	85.9	91.0	78.2
Arginine	91.9	93.3	85.7
Arginine	91.8	93.2	85.6
Citrulline	86.7	95.4	82.7
Citrulline	86.1	95.3	82.1
Glucosamine	71.6	81.2	58.1
Glucosamine	72.7	81.0	58.9

Tyrosine	82.4	88.6	73.0
Tyrosine	83.9	88.6	74.3
N-Acetyl-Glutamine	78.7	91.1	71.7
N-Acetyl-Glutamine	76.6	91.2	69.9
N-Acetyl-Glutamic Acid	64.3	89.5	57.5
N-Acetyl-Glutamic Acid	63.6	89.4	56.9
N-Acetyl-Methionine	90.3	90.3	81.5
N-Acetyl-Methionine	90.9	90.2	82.0
Tryptophan	62.7	85.4	53.5
Tryptophan	63.9	85.3	54.5
Kynurenine	99.2	88.1	87.4
Kynurenine	102.1	87.9	89.7
5-OH-Tryptophan	72.9	86.5	63.1
5-OH-Tryptophan	73.6	86.3	63.5
Cystine	89.2	86.6	77.2
Thymidine	90.6	89.9	81.4
Thymidine	90.7	90.0	81.6
Cytidine	101.7	91.4	93.0
Cytidine	101.0	91.5	92.4
Biotin	95.0	85.5	81.2
Uridine	67.0	84.4	56.5
Adenosine	100.1	96.6	96.7
2'-Deoxyguanosine	100.6	95.4	96.0
Homocystine	100.1	89.1	89.2
Guanosine	98.9	97.6	96.5
N-Acetyl-Neuraminic Acid	67.3	81.2	54.6
N-Acetyl-Neuraminic Acid	67.1	81.1	54.4
Riboflavin	68.6	88.4	60.6
Folic Acid	44.3	89.1	39.5
Glutathione Oxidized	87.5	86.4	75.6
Glutathione Oxidized	88.3	86.3	76.2
NAD	89.3	89.1	79.6
NADH	90.2	86.5	78.0
NADP	92.8	85.4	79.3
NADPH	82.5	83.2	68.6
FAD	84.5	81.1	68.5

Glutathione Reduced	96.6	77.4	74.8
Methionine Sulfoxide	65.6	81.2	53.3
Methionine Sulfoxide	64.4	81.1	52.2
N-Acetyl-Cysteine	66.8	76.5	51.1
N-Acetyl-Cysteine	66.2	76.4	50.6
Homoleucine	93.6	84.1	78.7
Cysteine	54.9	67.7	37.2
Cysteinyl-Glycine	65.0	55.4	36.0
Cysteinyl-Glycine	65.2	55.1	35.9
5-Methyl-Cytosine	99.0	83.4	82.6
Histamine	87.6	91.2	79.9
Histamine	88.6	91.1	80.7
Dihydroorotic Acid	72.2	88.5	63.9
O-Acetyl-Serine	53.8	85.5	46.0
O-Acetyl-Serine	53.0	85.1	45.1
Glycolic Acid	102.2	91.3	93.3
Pyruvic Acid	92.3	91.0	84.0
Lactic Acid	98	87.8	86.0
GABA	83.5	94.4	78.8
Malonic Acid	91.6	93.3	85.5
Fumaric Acid	42.5	95.5	40.6
Succinic Acid	76.9	96.1	73.9
Citraconic Acid	57.8	96.0	55.5
Itaconic Acid	99.4	89.1	88.6
Glutaric Acid	89.8	88.6	79.6
Cinnamic Acid	85.3	93.4	79.7
Coumaric Acid	93.3	93.0	86.8
Uric Acid	98.5	88.9	87.6
Citric Acid	81.9	91.1	74.6
Glucuronic Acid	79.6	90.4	72.0
Xanthurenic Acid	60.5	90.7	54.9
Lactose	65.8	85.5	56.3
cGMP	63.2	88.1	55.7
cGMP	64	88.2	56.4
AMP	71.8	89.1	64.0
GMP	70.1	85.5	59.9
GMP	69.4	85.5	59.3
UDP	49.8	91.1	45.4
UDP	49.7	91.0	45.2
ADP	93.3	84.4	78.7
ADP	92.2	84.3	77.7
TTP	61.1	81.1	49.6

TTP	61.5	81.0	49.8
CTP	44.8	80.5	36.1
CTP	45.8	80.5	36.9
UTP	42.7	86.6	37.0
ATP	84.4	79.0	66.7
ITP	49.3	81.3	40.1
Glucose	69.1	91.1	26.5
pGlu	56.4	88.6	50.0
pGlu	55.1	88.5	48.8
Inositol	37.8	94.1	35.6
Homogentisate	78.7	87.6	68.9
Homogentisate	79.4	87.7	69.6
N-Acetyl-Leucine	85.5	95.5	81.7
Azelaic Acid	55.5	93.3	51.8
Azelaic Acid	55.6	93.3	51.9
CMP	38.1	87.5	33.3
Glutamic Acid	99.6	93.3	92.9
Aspartic Acid	88.7	91.1	80.8
GDP	64.8	87.7	56.8
Homovanillate	80.8	94.4	76.3
UMP	56	89.5	50.1
TMP	98.4	85.4	84.0

Table S-9. Freeze-thaw analyte stability. QC samples consisted of spiked cell extract matrix on three different concentration levels (low/mid/high).

Compound	1 Cycle	2 Cycles	3 Cycles	4 Cycles
Glycine	98.9 ± 5.7	98.2 ± 2.4	97.6 ± 2.5	98.1 ± 1.2
Alanine	99.3 ± 3.3	98.5 ± 3.5	98.3 ± 1.4	97.9 ± 2.3
beta-Alanine	99.6 ± 4.4	99.1 ± 4.7	98.4 ± 3.3	98.8 ± 1.4
Sarcosine	99.4 ± 2.5	99.0 ± 3.6	98.6 ± 4.2	99.1 ± 4.4
Choline	99.7 ± 6.2	99.4 ± 3.4	98.4 ± 8.2	98.7 ± 2.7
Serine	99.5 ± 5.3	98.4 ± 4.3	98.3 ± 5.9	99.3 ± 6.2
Cytosine	99.3 ± 3.4	98.6 ± 2.2	99.1 ± 2.1	99.4 ± 5.1
Uracil	99.5 ± 1.5	98.4 ± 3.2	98.8 ± 0.7	99.0 ± 6.7
Dihydrouracil	98.7 ± 2.6	98.0 ± 5.5	99.1 ± 3.4	97.5 ± 5.8
Dihydrouracil	99.8 ± 8.2	98.1 ± 6.4	98.7 ± 2.5	98.5 ± 4.6
Proline	98.4 ± 5.3	97.5 ± 3.6	98.8 ± 1.6	98.1 ± 3.5
Betaine	99.5 ± 4.4	98.1 ± 5.7	99.1 ± 07.5	97.3 ± 4.4
Valine	99.8 ± 3.3	97.9 ± 2.6	98.4 ± 5.4	96.6 ± 2.7
Threonine	99.6 ± 4.1	97.6 ± 1.5	98.1 ± 6.3	97.5 ± 1.7
Nicotinamide	98.4 ± 2.4	98.1 ± 0.5	99.4 ± 4.2	97.3 ± 2.8
Thymine	99.3 ± 1.8	97.7 ± 0.6	98.3 ± 6.0	96.5 ± 3.7
Isoleucine	99.7 ± 2.7	98.1 ± 3.4	98.6 ± 4.9	97.5 ± 4.6
Leucine	99.5 ± 3.7	98.4 ± 4.7	98.3 ± 3.4	97.3 ± 5.5
Asparagine	98.9 ± 5.1	98.1 ± 3.6	99.1 ± 8.5	97.7 ± 6.8
Ornithine	99.4 ± 6.2	98.3 ± 4.5	98.5 ± 6.6	97.8 ± 4.6
Ornithine	99.2 ± 6.0	98.0 ± 3.4	98.6 ± 3.7	97.9 ± 2.9
Adenine	99.3 ± 5.9	97.4 ± 2.3	98.3 ± 1.8	99.1 ± 1.4
Adenine	99.5 ± 4.4	98.1 ± 3.2	98.6 ± 2.6	97.6 ± 3.3
Hypoxanthine	98.6 ± 3.3	97.4 ± 1.5	98.4 ± 1.5	99.1 ± 2.6
Hypoxanthine	99.1 ± 2.2	98.5 ± 7.6	98.1 ± 3.4	97.4 ± 3.2
Acetylcholine	99.2 ± 1.7	98.1 ± 5.3	98.5 ± 4.6	98.0 ± 2.2
Glutamine	98.4 ± 2.6	98.0 ± 0.7	98.6 ± 5.7	97.0 ± 1.2
Glutamine	98.5 ± 3.5	97.4 ± 1.7	98.3 ± 6.6	98.1 ± 2.1
Lysine	98.2 ± 2.6	97.3 ± 6.8	98.5 ± 4.5	98.0 ± 1.9
Lysine	97.5 ± 3.4	97.0 ± 5.5	98.1 ± 3.4	98.6 ± 4.8
Methionine	98.3 ± 4.6	97.1 ± 7.3	98.6 ± 1.7	97.5 ± 5.6
Methionine	97.5 ± 3.6	97.1 ± 6.2	98.3 ± 2.6	99.1 ± 4.4
Histidine	97.8 ± 3.7	96.8 ± 5.3	98.2 ± 3.4	97.4 ± 2.5
Histidine	98.3 ± 4.8	97.1 ± 4.4	98.6 ± 4.5	97.5 ± 3.4
Phenylalanine	98.1 ± 4.9	97.3 ± 5.5	98.7 ± 5.9	98.1 ± 2.3
Phenylalanine	98.0 ± 2.6	96.7 ± 6.2	97.5 ± 3.3	97.6 ± 3.6
Arginine	97.5 ± 3.3	97.1 ± 5.7	98.9 ± 2.2	98.3 ± 2.7
Arginine	98.8 ± 1.7	97.9 ± 7.1	98.1 ± 2.8	97.4 ± 1.8
Citrulline	99.1 ± 2.0	98.3 ± 3.1	98.0 ± 1.6	97.4 ± 2.5
Citrulline	98.3 ± 3.4	98.0 ± 2.2	99.1 ± 8.5	97.5 ± 2.3
Glucosamine	97.9 ± 1.7	98.3 ± 5.6	98.5 ± 7.4	97.1 ± 4.2

Glucosamine	99.3 ± 2.6	98.4 ± 6.5	98.1 ± 4.3	97.5 ± 2.9
Tyrosine	98.6 ± 3.8	98.4 ± 7.7	98.6 ± 3.2	97.6 ± 1.7
Tyrosine	99.1 ± 2.6	98.3 ± 5.4	98.5 ± 2.8	97.2 ± 2.4
N-Acetyl-Glutamine	99.0 ± 1.8	98.6 ± 4.5	98.4 ± 1.7	97.7 ± 3.5
N-Acetyl-Glutamine	98.7 ± 2.1	98.9 ± 3.3	98.5 ± 0.7	97.6 ± 4.6
N-Acetyl-Glutamic Acid	98.5 ± 2.7	98.3 ± 6.5	98.8 ± 1.9	97.5 ± 5.8
N-Acetyl-Glutamic Acid	98.4 ± 3.7	98.9 ± 5.8	99.1 ± 0.8	98.1 ± 6.2
N-Acetyl-Methionine	98.1 ± 2.4	98.6 ± 7.7	98.4 ± 3.6	98.0 ± 4.3
N-Acetyl-Methionine	97.7 ± 1.3	98.3 ± 3.4	99.1 ± 4.5	98.1 ± 2.6
Tryptophan	98.3 ± 2.6	98.6 ± 4.5	97.7 ± 5.4	97.1 ± 1.7
Tryptophan	98.5 ± 3.5	98.1 ± 3.3	98.8 ± 3.3	97.4 ± 8.6
Kynurenine	97.1 ± 4.4	97.5 ± 4.2	98.3 ± 2.2	96.5 ± 7.5
Kynurenine	97.4 ± 2.3	97.8 ± 2.1	98.1 ± 1.1	97.4 ± 4.7
5-OH-Tryptophan	98.1 ± 1.4	98.3 ± 1.3	99.4 ± 2.1	97.1 ± 3.8
5-OH-Tryptophan	98.5 ± 1.6	98.3 ± 2.5	98.6 ± 3.7	98.0 ± 2.6
Cystine	99.3 ± 2.1	99.1 ± 3.1	98.5 ± 2.5	98.5 ± 4.4
Thymidine	99.1 ± 3.0	98.7 ± 2.9	98.6 ± 1.4	98.2 ± 5.2
Thymidine	98.1 ± 2.9	98.5 ± 3.4	99.1 ± 2.6	98.6 ± 6.3
Cytidine	98.5 ± 2.8	98.2 ± 4.3	98.5 ± 3.7	98.5 ± 7.2
Cytidine	99.3 ± 1.7	98.6 ± 6.5	98.0 ± 2.4	98.1 ± 4.3
Biotin	99.3 ± 2.7	99.1 ± 7.7	98.6 ± 4.6	98.2 ± 3.0
Uridine	98.5 ± 3.8	98.8 ± 6.9	99.1 ± 5.5	98.0 ± 0.7
Adenosine	97.4 ± 2.6	98.1 ± 5.3	99.4 ± 4.7	97.3 ± 0.5
2'-Deoxyguanosine	98.1 ± 1.8	98.4 ± 3.2	99.1 ± 2.5	97.1 ± 1.6
Homocystine	97.3 ± 2.5	98.6 ± 2.4	99.1 ± 1.4	97.5 ± 2.5
Guanosine	98.5 ± 3.7	97.9 ± 3.7	98.6 ± 3.6	97.7 ± 4.4
N-Acetyl-Neuraminic Acid	99.0 ± 2.5	98.7 ± 4.5	98.4 ± 4.3	97.0 ± 5.6
N-Acetyl-Neuraminic Acid	98.4 ± 3.6	99.1 ± 7.6	98.6 ± 5.3	97.3 ± 4.5
Riboflavin	97.7 ± 1.7	98.4 ± 1.8	99.1 ± 4.2	97.0 ± 3.6
Folic Acid	98.8 ± 2.3	99.1 ± 2.5	98.5 ± 3.5	97.5 ± 2.4
Glutathione Oxidized	97.4 ± 3.1	98.5 ± 3.6	99.1 ± 3.6	96.8 ± 1.5
Glutathione Oxidized	99.1 ± 2.6	98.8 ± 5.7	98.5 ± 2.9	97.5 ± 3.8
NAD	98.6 ± 1.2	98.8 ± 4.5	99.1 ± 2.1	98.3 ± 4.6
NADH	97.7 ± 6.3	98.3 ± 3.6	98.6 ± 3.7	97.2 ± 5.5
NADP	98.3 ± 8.3	97.4 ± 2.2	99.1 ± 4.2	96.5 ± 6.4
NADPH	97.4 ± 3.5	98.1 ± 5.1	98.5 ± 5.3	98.1 ± 6.6
FAD	98.8 ± 2.6	98.5 ± 7.2	99.1 ± 6.7	95.6 ± 4.3
Glutathione Reduced	98.3 ± 1.4	98.8 ± 5.4	99.1 ± 7.5	98.1 ± 3.2
Methionine Sulfoxide	99.1 ± 2.5	98.1 ± 3.5	98.5 ± 8.7	99.5 ± 2.6
Methionine Sulfoxide	97.7 ± 3.6	98.4 ± 2.6	99.1 ± 1.8	97.6 ± 4.5
N-Acetyl-Cysteine	98.3 ± 4.1	97.9 ± 1.5	98.6 ± 2.5	98.6 ± 5.6

N-Acetyl-Cysteine	97.8 ± 5.1	98.3 ± 3.7	98.4 ± 3.4	98.4 ± 6.5
Homoleucine	98.1 ± 3.2	98.5 ± 4.4	97.6 ± 4.6	97.9 ± 8.8
Cysteine	97.6 ± 2.3	98.1 ± 5.2	98.5 ± 5.5	98.3 ± 3.0
Cysteinyl-Glycine	98.3 ± 3.4	97.7 ± 7.1	98.7 ± 3.7	99.5 ± 4.1
Cysteinyl-Glycine	98.6 ± 1.7	97.6 ± 8.9	98.3 ± 2.8	95.4 ± 3.2
5-Methyl-Cytosine	96.3 ± 3.8	98.1 ± 5.1	97.6 ± 1.7	98.7 ± 2.3
Histamine	97.7 ± 4.9	98.1 ± 6.8	98.4 ± 2.5	99.3 ± 2.4
Histamine	98.1 ± 5.6	98.4 ± 5.6	97.8 ± 3.1	97.6 ± 3.5
Dihydroorotic Acid	98.3 ± 4.5	98.5 ± 4.5	97.6 ± 9.8	98.2 ± 4.5
O-Acetyl-Serine	97.6 ± 3.4	98.1 ± 5.4	98.5 ± 4.5	99.1 ± 5.4
O-Acetyl-Serine	98.6 ± 2.3	98.1 ± 3.3	97.8 ± 3.8	98.3 ± 6.6
Glycolic Acid	98.7 ± 1.2	98.4 ± 2.2	99.1 ± 2.7	99.5 ± 4.5
Pyruvic Acid	98.4 ± 2.4	97.7 ± 1.4	99.2 ± 2.8	98.3 ± 3.3
Lactic Acid	98.1 ± 3.5	98.3 ± 2.7	98.7 ± 3.4	97.6 ± 2.2
GABA	98.5 ± 3.6	98.1 ± 3.7	99.3 ± 1.9	98.9 ± 1.8
Malonic Acid	98.4 ± 2.7	98.6 ± 4.4	98.7 ± 2.3	96.5 ± 2.7
Fumaric Acid	98.8 ± 1.6	98.1 ± 3.2	99.1 ± 3.4	97.2 ± 1.4
Succinic Acid	99.3 ± 3.5	98.8 ± 2.1	98.0 ± 1.4	98.6 ± 3.5
Citraconic Acid	99.5 ± 2.4	98.6 ± 1.7	97.6 ± 2.3	99.4 ± 4.6
Itaconic Acid	98.9 ± 3.3	99.1 ± 1.5	97.5 ± 3.2	97.6 ± 6.5
Glutaric Acid	99.1 ± 4.6	98.4 ± 3.3	98.7 ± 1.4	98.3 ± 5.3
Cinnamic Acid	97.8 ± 5.3	98.6 ± 3.6	99.1 ± 4.7	99.1 ± 7.2
Coumaric Acid	99.1 ± 3.2	98.5 ± 4.9	98.1 ± 5.6	98.5 ± 9.1
Uric Acid	98.9 ± 5.7	98.2 ± 2.4	97.6 ± 2.5	98.1 ± 1.2
Citric Acid	99.3 ± 3.3	98.5 ± 3.5	98.3 ± 1.4	97.9 ± 2.3
Glucuronic Acid	99.6 ± 4.4	99.1 ± 4.7	98.4 ± 3.3	98.8 ± 1.4
Xanthurenic Acid	99.4 ± 2.5	99.0 ± 3.6	98.6 ± 4.2	99.1 ± 4.4
Lactose	99.7 ± 6.2	99.4 ± 3.4	98.4 ± 8.2	98.7 ± 2.7
cGMP	99.5 ± 5.3	98.4 ± 4.3	98.3 ± 5.9	99.3 ± 6.2
cGMP	99.3 ± 3.4	98.6 ± 2.2	99.1 ± 2.1	99.4 ± 5.1
AMP	99.5 ± 1.5	98.4 ± 3.2	98.8 ± 0.7	99.0 ± 6.7
GMP	98.7 ± 2.6	98.0 ± 5.5	99.1 ± 3.4	97.5 ± 5.8
GMP	99.8 ± 8.2	98.1 ± 6.4	98.7 ± 2.5	98.5 ± 4.6
UDP	98.4 ± 5.3	97.5 ± 3.6	98.8 ± 1.6	98.1 ± 3.5
UDP	99.5 ± 4.4	98.1 ± 5.7	99.1 ± 07.5	97.3 ± 4.4
ADP	99.8 ± 3.3	97.9 ± 2.6	98.4 ± 5.4	96.6 ± 2.7
ADP	99.6 ± 4.1	97.6 ± 1.5	98.1 ± 6.3	97.5 ± 1.7
TTP	98.4 ± 2.4	98.1 ± 0.5	99.4 ± 4.2	97.3 ± 2.8
TTP	99.3 ± 1.8	97.7 ± 0.6	98.3 ± 6.0	96.5 ± 3.7
CTP	99.7 ± 2.7	98.1 ± 3.4	98.6 ± 4.9	97.5 ± 4.6
CTP	99.5 ± 3.7	98.4 ± 4.7	98.3 ± 3.4	97.3 ± 5.5
UTP	98.9 ± 5.1	98.1 ± 3.6	99.1 ± 8.5	97.7 ± 6.8
ATP	99.4 ± 6.2	98.3 ± 4.5	98.5 ± 6.6	97.8 ± 4.6
ITP	99.2 ± 6.0	98.0 ± 3.4	98.6 ± 3.7	97.9 ± 2.9

Glucose	99.3 ± 5.9	97.4 ± 2.3	98.3 ± 1.8	99.1 ± 1.4
pGlu	99.5 ± 4.4	98.1 ± 3.2	98.6 ± 2.6	97.6 ± 3.3
pGlu	98.6 ± 3.3	97.4 ± 1.5	98.4 ± 1.5	99.1 ± 2.6
Inositol	99.1 ± 2.2	98.5 ± 7.6	98.1 ± 3.4	97.4 ± 3.2
Homogentisate	99.2 ± 1.7	98.1 ± 5.3	98.5 ± 4.6	98.0 ± 2.2
Homogentisate	98.4 ± 2.6	98.0 ± 0.7	98.6 ± 5.7	97.0 ± 1.2
N-Acetyl-Leucine	98.5 ± 3.5	97.4 ± 1.7	98.3 ± 6.6	98.1 ± 2.1
Azelaic Acid	98.2 ± 2.6	97.3 ± 6.8	98.5 ± 4.5	98.0 ± 1.9
Azelaic Acid	97.5 ± 3.4	97.0 ± 5.5	98.1 ± 3.4	98.6 ± 4.8
CMP	98.3 ± 4.6	97.1 ± 7.3	98.6 ± 1.7	97.5 ± 5.6
Glutamic Acid	97.5 ± 3.6	97.1 ± 6.2	98.3 ± 2.6	99.1 ± 4.4
Aspartic Acid	97.8 ± 3.7	96.8 ± 5.3	98.2 ± 3.4	97.4 ± 2.5
GDP	98.3 ± 4.8	97.1 ± 4.4	98.6 ± 4.5	97.5 ± 3.4
Homovanillate	98.1 ± 4.9	97.3 ± 5.5	98.7 ± 5.9	98.1 ± 2.3
UMP	98.0 ± 2.6	96.7 ± 6.2	97.5 ± 3.3	97.6 ± 3.6
TMP	97.5 ± 3.3	97.1 ± 5.7	98.9 ± 2.2	98.3 ± 2.7

Table S-10. Stability study during autosampler storage. QC samples consisted of spiked cell extract matrix on three different concentration levels (low/mid/high).

Compound	12 h	24 h	36 h	48 h
Glycine	99.3 ± 4.3	98.5 ± 1.3	97.4 ± 5.4	93.3 ± 4.4
Alanine	98.4 ± 3.2	98.0 ± 7.2	96.5 ± 3.5	92.5 ± 5.5
beta-Alanine	98.5 ± 2.6	96.7 ± 8.4	94.3 ± 1.6	91.9 ±3.2
Sarcosine	99.3 ± 3.8	95.6 ± 9.5	92.2 ± 6.7	90.1 ±7.6
Choline	99.6 ± 4.4	96.4 ± 10.3	91.4 ± 2.3	89.7 ±5.4
Serine	97.5 ± 5.3	95.3 ± 8.2	92.2 ± 3.2	90.8 ±1.6
Cytosine	99.3 ± 6.6	96.2 ± 9.4	92.6 ± 4.4	90.1 ± 0.5
Uracil	98.1 ± 4.8	95.6 ± 5.6	92.7 ± 2.5	89.7 ± 3.4
Dihydrouracil	97.6 ± 4.2	95.1 ± 6.5	91.5 ± 5.6	89.5 ± 4.1
Dihydrouracil	99.3 ± 3.4	96.4 ± 7.7	92.7 ± 8.1	90.3 ± 6.8
Proline	98.6 ± 4.1	95.1 ± 8.8	92.1 ± 6.9	90.1 ± 7.8
Betaine	98.2 ± 5.3	95.0 ± 6.9	91.5 ± 5.7	89.6 ± 3.1
Valine	99.7 ± 5.5	96.3 ± 5.1	93.3 ± 1.8	90.2 ± 6.6
Threonine	99.1 ± 6.6	96.4 ± 5.2	93.4 ± 2.5	90.5 ± 4.4
Nicotinamide	99.0 ± 4.3	95.6 ± 4.3	92.2 ± 3.4	89.1 ± 5.6
Thymine	99.5 ± 5.2	96.6 ± 6.4	93.3 ± 6.6	90.4 ± 3.2
Isoleucine	98.0 ± 4.1	96.4 ± 7.6	94.4 ± 3.3	93.2 ± 4.4
Leucine	97.8 ± 5.2	97.0 ± 8.5	92.1 ± 4.4	90.6 ± 3.4
Asparagine	99.3 ± 5.4	96.7 ± 9.2	93.3 ± 5.4	91.4 ± 2.1
Ornithine	98.9 ± 5.5	97.3 ± 5.3	92.2 ± 2.5	90.8 ± 3.4
Ornithine	97.6 ± 4.6	95.6 ± 4.7	92.2 ± 1.3	90.1 ± 6.1
Adenine	96.5 ± 5.7	95.0 ± 5.6	93.1 ± 2.6	92.3 ± 4.5
Adenine	97.3 ± 6.8	95.4 ± 6.5	92.2 ± 0.7	90.8 ± 3.4
Hypoxanthine	98.2 ± 5.9	96.1 ± 7.3	93.1 ± 4.5	91.3 ± 2.1
Hypoxanthine	99.1 ± 4.1	96.4 ± 8.4	92.2 ± 2.3	90.6 ± 7.7
Acetylcholine	98.6 ± 5.6	96.0 ± 8.6	93.1 ± 3.4	90.5 ± 5.5
Glutamine	98.9 ± 3.5	97.2 ± 4.8	93.6 ± 4.6	90.7 ± 4.3
Glutamine	99.1 ± 4.4	96.5 ± 3.0	92.7 ± 5.7	91.3 ± 3.9
Lysine	99.2 ± 5.3	97.1 ± 4.1	93.9 ± 2.6	91.1 ± 0.9
Lysine	98.5 ± 3.2	97.2 ± 4.1	92.5 ± 3.4	88.9 ± 1.1
Methionine	99.1 ± 4.7	98.4 ± 5.2	93.1 ± 4.3	91.8 ± 2.5
Methionine	97.6 ± 4.8	97.0 ± 6.2	92.1 ± 6.4	90.3 ± 3.1
Histidine	96.5 ± 5.2	95.5 ± 2.3	94.5 ± 5.6	91.1 ± 5.4
Histidine	97.2 ± 8.4	95.1 ± 3.4	92.7 ± 7.7	90.5 ± 0.4
Phenylalanine	98.4 ± 5.5	94.8 ± 9.5	92.7 ± 8.8	91.1 ± 1.2
Phenylalanine	99.1 ± 4.6	95.4 ± 7.3	92.9 ± 4.5	90.3 ± 3.3
Arginine	98.5 ± 5.8	95.3 ± 8.6	92.5 ± 3.4	90.6 ± 4.4
Arginine	96.5 ± 4.6	95.3 ± 9.3	92.6 ± 2.3	90.2 ± 5.5
Citrulline	95.6 ± 4.5	94.3 ± 6.2	90.1 ± 1.2	87.6 ± 2.1
Citrulline	97.1 ± 3.4	95.1 ± 5.2	90.1 ± 3.6	88.8 ± 3.1
Glucosamine	98.3 ± 6.3	95.3 ± 4.3	89.5 ± 4.5	88.3 ± 2.2

Glucosamine	97.6 ± 2.2	95.0 ± 3.7	90.2 ± 1.0	89.1 ± 3.3
Tyrosine	95.6 ± 1.9	94.2 ± 7.3	89.5 ± 6.3	88.2 ± 4.1
Tyrosine	98.1 ± 1.0	95.0 ± 6.4	89.7 ± 5.4	87.6 ± 3.3
N-Acetyl-Glutamine	98.0 ± 3.2	94.8 ± 8.5	90.0 ± 4.5	88.9 ± 4.4
N-Acetyl-Glutamine	97.6 ± 8.3	95.3 ± 6.6	91.1 ± 6.7	89.3 ± 2.1
N-Acetyl-Glutamic Acid	99.3 ± 3.4	96.2 ± 5.7	90.7 ± 5.2	89.2 ± .06
N-Acetyl-Glutamic Acid	98.6 ± 4.5	95.4 ± 8.0	90.5 ± 3.2	88.3 ± 5.1
N-Acetyl-Methionine	97.4 ± 5.6	95.3 ± 9.1	90.1 ± 2.1	88.6 ± 3.2
N-Acetyl-Methionine	98.9 ± 6.3	95.2 ± 7.8	89.5 ± 3.3	88.1 ± 4.4
Tryptophan	97.3 ± 5.4	95.6 ± 6.5	89.8 ± 4.4	87.6 ± 3.7
Tryptophan	97.0 ± 4.5	94.8 ± 5.4	89.3 ± 5.5	87.3 ± 6.9
Kynurenine	97.2 ± 5.6	94.3 ± 4.3	88.9 ± 6.6	86.7 ± 5.6
Kynurenine	99.4 ± 6.5	94.0 ± 7.2	89.1 ± 7.8	86.4 ± 6.3
5-OH-Tryptophan	98.6 ± 3.7	93.2 ± 6.1	90.0 ± 3.9	87.7 ± 4.1
5-OH-Tryptophan	90.5 ± 4.9	85.4 ± 5.4	80.3 ± 1.1	73.3 ± 6.2
Cystine	97.6 ± 1.2	95.3 ± 6.6	90.3 ± 1.2	88.1 ± 7.5
Thymidine	89.5 ± 1.3	83.3 ± 8.7	74.2 ± 2.4	67.7 ± 8.2
Thymidine	98.5 ± 5.6	96.1 ± 8.5	91.2 ± 0.5	89.0 ± 9.1
Cytidine	87.3 ± 4.4	80.2 ± 6.3	71.1 ± 1.3	54.4 ± 3.4
Cytidine	86.6 ± 3.5	74.4 ± 5.4	68.8 ± 1.4	52.1 ± 5.5
Biotin	98.2 ± 6.2	96.3 ± 6.3	91.6 ± 0.5	90.0 ± 1.2
Uridine	98.1 ± 5.3	96.3 ± 6.2	91.9 ± 2.6	89.1 ± 3.1
Adenosine	98.6 ± 7.2	96.7 ± 7.1	92.1 ± 3.5	90.4 ± 3.4
2'-Deoxyguanosine	97.5 ± 6.4	95.4 ± 8.1	90.3 ± 4.7	88.4 ± 2.6
Homocystine	99.3 ± 8.3	97.4 ± 4.4	91.4 ± 0.4	89.5 ± 2.7
Guanosine	98.2 ± 9.2	96.1 ± 6.5	90.1 ± 3.6	88.7 ± 4.4
N-Acetyl-Neuraminic Acid	98.1 ± 4.6	96.0 ± 5.6	90.8 ± 0.3	89.8 ± 5.1
N-Acetyl-Neuraminic Acid	99.3 ± 3.5	96.4 ± 7.8	92.7 ± 1.1	90.4 ± 3.2
Riboflavin	98.2 ± 4.3	96.7 ± 7.0	93.1 ± 8.2	91.1 ± 6.5
Folic Acid	97.5 ± 2.5	96.3 ± 6.9	92.4 ± 3.3	90.3 ± 4.2
Glutathione Oxidized	97.6 ± 1.7	96.0 ± 5.2	91.8 ± 0.4	90.2 ± 3.1
Glutathione Oxidized	98.3 ± 6.8	95.8 ± 4.3	91.5 ± 4.5	89.7 ± 8.5
NAD	98.1 ± 5.5	95.9 ± 7.4	90.3 ± 5.6	88.8 ± 6.2
NADH	97.5 ± 4.4	96.1 ± 8.5	92.1 ± 7.9	88.0 ± 3.1
NADP	98.3 ± 8.3	97.0 ± 9.6	90.6 ± 4.9	89.2 ± 1.7
NADPH	97.6 ± 6.7	97.0 ± 5.7	91.4 ± 1.2	89.0 ± 2.5
FAD	98.1 ± 5.5	97.1 ± 6.5	92.5 ± 5.2	90.3 ± 7.4
Glutathione Reduced	97.5 ± 4.4	96.5 ± 6.4	90.3 ± 6.2	90.0 ± 5.2
Methionine Sulfoxide	98.3 ± 3.3	97.2 ± 7.3	90.8 ± 7.1	90.1 ± 4.9
Methionine Sulfoxide	99.1 ± 6.2	98.1 ± 9.2	90.1 ± 4.3	87.7 ± 3.6
N-Acetyl-Cysteine	98.3 ± 8.8	97.1 ± 10.6	93.0 ± 3.4	88.2 ± 2.7

N-Acetyl-Cysteine	97.5 ± 6.5	96.7 ± 6.5	90.5 ± 2.5	88.7 ± 3.1
Homoleucine	96.6 ± 5.3	95.4 ± 7.4	91.4 ± 1.6	87.3 ± 2.5
Cysteine	96.4 ± 1.4	95.0 ± 8.3	91.1 ± 7.7	87.2 ± 3.1
Cysteinyl-Glycine	95.8 ± 5.5	92.2 ± 6.2	90.7 ± 9.8	88.3 ± 1.6
Cysteinyl-Glycine	96.1 ± 6.6	93.1 ± 5.1	91.2 ± 6.2	88.4 ± 4.4
5-Methyl-Cytosine	95.0 ± 7.5	92.5 ± 4.3	90.4 ± 8.3	87.9 ± 5.2
Histamine	94.7 ± 8.3	91.1 ± 3.2	90.5 ± 4.5	88.3 ± 3.5
Histamine	94.2 ± 4.4	92.2 ± 2.4	90.3 ± 10.6	86.4 ± 2.6
Dihydroorotic Acid	94.6 ± 5.5	91.7 ± 1.5	90.1 ± 8.8	87.5 ± 4.1
O-Acetyl-Serine	94.8 ± 2.3	92.4 ± 0.6	90.5 ± 9.4	86.2 ± 3.7
O-Acetyl-Serine	98.1 ± 1.6	97.6 ± 0.7	94.5 ± 4.5	91.3 ± 3.1
Glycolic Acid	97.4 ± 2.4	96.6 ± 3.8	95.3 ± 6.6	92.2 ± 4.2
Pyruvic Acid	98.5 ± 3.5	97.4 ± 4.9	95.1 ± 7.7	92.1 ± 3.0
Lactic Acid	98.5 ± 4.1	96.6 ± 2.2	94.3 ± 8.9	93.1 ± 2.5
GABA	99.3 ± 3.2	98.1 ± 1.1	94.6 ± 4.3	90.2 ± 4.1
Malonic Acid	96.7 ± 2.9	96.0 ± 1.6	95.1 ± 3.2	91.4 ± 3.4
Fumaric Acid	98.5 ± 4.1	97.3 ± 2.7	93.1 ± 6.6	90.1 ± 4.7
Succinic Acid	98.6 ± 5.2	97.1 ± 3.3	95.6 ± 4.3	92.1 ± 3.3
Citraconic Acid	98.8 ± 6.3	97.3 ± 4.2	95.8 ± 7.5	93.2 ± 2.5
Itaconic Acid	97.6 ± 7.2	96.6 ± 3.1	93.1 ± 6.9	90.1 ± 4.8
Glutaric Acid	99.3 ± 8.7	98.3 ± 2.3	97.2 ± 1.4	92.1 ± 3.3
Cinnamic Acid	97.7 ± 4.4	97.0 ± 7.4	94.5 ± 2.6	91.1 ± 2.5
Coumaric Acid	97.5 ± 3.5	96.6 ± 5.5	93.6 ± 7.8	91.6 ± 3.4
Uric Acid	99.3 ± 4.3	98.5 ± 1.3	97.4 ± 5.4	93.3 ± 4.4
Citric Acid	98.4 ± 3.2	98.0 ± 7.2	96.5 ± 3.5	92.5 ± 5.5
Glucuronic Acid	98.5 ± 2.6	96.7 ± 8.4	94.3 ± 1.6	91.9 ±3.2
Xanthurenic Acid	99.3 ± 3.8	95.6 ± 9.5	92.2 ± 6.7	90.1 ±7.6
Lactose	99.6 ± 4.4	96.4 ± 10.3	91.4 ± 2.3	89.7 ±5.4
cGMP	97.5 ± 5.3	95.3 ± 8.2	92.2 ± 3.2	90.8 ±1.6
cGMP	99.3 ± 6.6	96.2 ± 9.4	92.6 ± 4.4	90.1 ± 0.5
AMP	98.1 ± 4.8	95.6 ± 5.6	92.7 ± 2.5	89.7 ± 3.4
GMP	97.6 ± 4.2	95.1 ± 6.5	91.5 ± 5.6	89.5 ± 4.1
GMP	99.3 ± 3.4	96.4 ± 7.7	92.7 ± 8.1	90.3 ± 6.8
UDP	98.6 ± 4.1	95.1 ± 8.8	92.1 ± 6.9	90.1 ± 7.8
UDP	98.2 ± 5.3	95.0 ± 6.9	91.5 ± 5.7	89.6 ± 3.1
ADP	99.7 ± 5.5	96.3 ± 5.1	93.3 ± 1.8	90.2 ± 6.6
ADP	99.1 ± 6.6	96.4 ± 5.2	93.4 ± 2.5	90.5 ± 4.4
TTP	99.0 ± 4.3	95.6 ± 4.3	92.2 ± 3.4	89.1 ± 5.6
TTP	99.5 ± 5.2	96.6 ± 6.4	93.3 ± 6.6	90.4 ± 3.2
CTP	98.0 ± 4.1	96.4 ± 7.6	94.4 ± 3.3	93.2 ± 4.4
CTP	97.8 ± 5.2	97.0 ± 8.5	92.1 ± 4.4	90.6 ± 3.4
UTP	99.3 ± 5.4	96.7 ± 9.2	93.3 ± 5.4	91.4 ± 2.1
ATP	98.9 ± 5.5	97.3 ± 5.3	92.2 ± 2.5	90.8 ± 3.4
ITP	97.6 ± 4.6	95.6 ± 4.7	92.2 ± 1.3	90.1 ± 6.1

Glucose	96.5 ± 5.7	95.0 ± 5.6	93.1 ± 2.6	92.3 ± 4.5
pGlu	97.3 ± 6.8	95.4 ± 6.5	92.2 ± 0.7	90.8 ± 3.4
pGlu	98.2 ± 5.9	96.1 ± 7.3	93.1 ± 4.5	91.3 ± 2.1
Inositol	99.1 ± 4.1	96.4 ± 8.4	92.2 ± 2.3	90.6 ± 7.7
Homogentisate	98.6 ± 5.6	96.0 ± 8.6	93.1 ± 3.4	90.5 ± 5.5
Homogentisate	98.9 ± 3.5	97.2 ± 4.8	93.6 ± 4.6	90.7 ± 4.3
N-Acetyl-Leucine	99.1 ± 4.4	96.5 ± 3.0	92.7 ± 5.7	91.3 ± 3.9
Azelaic Acid	99.2 ± 5.3	97.1 ± 4.1	93.9 ± 2.6	91.1 ± 0.9
Azelaic Acid	98.5 ± 3.2	97.2 ± 4.1	92.5 ± 3.4	88.9 ± 1.1
CMP	99.1 ± 4.7	98.4 ± 5.2	93.1 ± 4.3	91.8 ± 2.5
Glutamic Acid	97.6 ± 4.8	97.0 ± 6.2	92.1 ± 6.4	90.3 ± 3.1
Aspartic Acid	96.5 ± 5.2	95.5 ± 2.3	94.5 ± 5.6	91.1 ± 5.4
GDP	97.2 ± 8.4	95.1 ± 3.4	92.7 ± 7.7	90.5 ± 0.4
Homovanillate	98.4 ± 5.5	94.8 ± 9.5	92.7 ± 8.8	91.1 ± 1.2
UMP	99.1 ± 4.6	95.4 ± 7.3	92.9 ± 4.5	90.3 ± 3.3
TMP	98.5 ± 5.8	95.3 ± 8.6	92.5 ± 3.4	90.6 ± 4.4

Table S-11. MRM transitions ^{13}C labeled metabolites in ESI^+ mode.

Q1	Q3	Metabolite	DP	EP	CE	CXP
78.0	78.0	Glycine	16	10	5	10
93.0	46.0	Alanine	31	10	21	10
93.0	46.1	Sarcosine	31	10	21	10
109.0	62.0	Serine	16	10	15	10
110.0	110.1	Choline	15	10	20	10
121.0	74.0	Proline	26	10	25	10
121.0	74.1	Guanidinoacetic acid	31	10	17	10
123.0	76.0	Valine	31	10	17	10
123.0	123.0	Betaine	31	10	5	10
124.1	77.0	Threonine	49	10	17	10
124.1	77.0	Homoserine	49	10	17	10
129.1	84.1	Nicotinamide	11	10	15	10
137.0	76.0	Asparagine	41	10	21	10
138.0	74.2	Isoleucine	46	10	25	10
138.0	46.0	Leucine	51	10	35	10
138.1	121.0	Ornithine	36	10	10	10
138.1	74.1	Ornithine	36	10	31	10
141.1	141.1	Adenine	16	10	5	10
152.0	135.1	Glutamine	36	10	29	10
152.1	88.1	Glutamine	36	10	10	10
153.1	89.0	Lysine	36	10	29	10
153.1	136.0	Lysine	36	10	10	10
155.0	138.1	Methionine	56	10	15	10
155.0	108.1	Methionine	56	10	10	10
157.0	162.0	Guanine	31	10	29	10
157.0	115.0	Guanine	31	10	25	10
162.0	115.0	Histidine	46	10	21	10
162.0	87.0	Histidine	46	10	25	10
168.2	58.2	2-amino-adipic acid	25	10	28	10
168.2	121.2	2-amino-adipic acid	25	10	14	10
175.1	128.1	Phenylalanine	51	10	11	10
175.1	111.0	Phenylalanine	51	10	15	10
181.0	74.1	Arginine	31	10	39	10
181.0	121.0	Arginine	31	10	10	10
182.0	74.0	Citrulline	36	10	30	10
182.1	165.0	Citrulline	36	10	15	10
191.1	144.2	Tyrosine	46	10	21	10
191.1	174.0	Tyrosine	46	10	10	10
216.0	199.1	Tryptophan	51	10	15	10
216.0	155.1	Tryptophan	51	10	25	10
219.0	155.0	Kynurenine	31	10	25	10
219.0	202.0	Kynurenine	31	10	13	10

230.0	91.0	Cystathionine	36	10	41	10
230.1	138.0	Cystathionine	36	10	10	10
254.1	117.0	Uridine	31	10	15	10
254.1	100.1	Uridine	31	10	15	10
255.0	101.0	Biotin	46	10	43	10
259.1	125.0	gamma Glutamylcysteine	25	10	25	10
279.0	114.1	Inosine	36	10	30	10
279.0	152.0	Inosine	36	10	15	10
294.0	157.0	Guanosine	36	10	19	10
318.0	135.0	Glutathione	71	10	10	10
318.0	184.1	Glutathione	71	10	13	10
399.0	141.1	S-(5'-adenosyl)-homocysteine	51	10	27	10
399.0	139.0	S-(5'-adenosyl)-homocysteine	51	10	27	10
633.1	633.0	Glutathione oxidized	71	10	40	10
685.0	685.0	NAD	24	10	5	10
687.0	687.0	NADH	23	10	5	10
765.1	765.1	NADP	25	10	5	10
767.1	767.1	NADPH	24	10	5	10

Table S-12. MRM transitions ^{13}C labeled metabolites in ESI^- mode.

Q1	Q3	Metabolite	DP	EP	CE	CXP
77.0	77.0	Glycolic Acid	-30	-10	-5	-10
90.0	90.0	Pyruvic acid	-30	-10	-5	-10
92.0	92.0	Lactic Acid	-45	-10	-5	-45
105.0	43.0	Malonic Acid	-25	-10	-36	-10
106.0	106.0	GABA	-10	-10	-5	-10
119.0	74.0	Fumaric Acid	-35	-10	-12	-10
119.0	74.1	Fumaric acid	-35	-10	-12	-10
121.0	76.0	Succinate	-35	-10	-16	-10
136.0	74.0	Aspartate	-15	-10	-33	-10
136.1	91.0	Aspartate	-15	-10	-20	-10
151.0	106.1	Glutamate	-30	-10	-20	-10
181.0	134.1	Aconitic acid	-25	-10	-10	-10
181.0	89.1	Aconitic acid	-25	-10	-18	-10
185.1	92.0	Glucose	-15	-10	-28	-10
185.2	92.1	Glucose	-15	-10	-28	-10
185.2	61.1	Glucose	-15	-10	-13	-10
188.0	79.0	Phosphoglyceric acid	-45	-10	-32	-10
188.0	97.1	Phosphoglyceric acid	-45	-10	-21	-10
197.1	197.0	Citrate	-25	-10	-5	-10
197.1	90.0	Citrate	-25	-10	-12	-10
331.0	79.0	TMP	-65	-10	-44	-10
332.0	79.0	UMP	-60	-10	-60	-10
332.0	79.0	CMP	-75	-10	-62	-10
334.0	79.0	UMP	-60	-10	-60	-10
338.0	338.1	cAMP	-85	-10	-36	-10
340.0	79.0	dAMP	-60	-10	-62	-10
354.1	354.1	cGMP	-21	-10	-5	-10
356.0	79.0	AMP	-73	-10	-65	-10
372.1	79.0	GMP	-65	-10	-62	-10
412.0	159.0	UDP	-60	-10	-25	-10
412.0	79.0	UDP	-60	-10	-76	-10
436.0	79.0	ADP	-75	-10	-25	-10
452.1	159.0	GDP	-70	-10	-25	-10
452.1	79.0	GDP	-70	-10	-82	-10
491.1	159.0	CTP	-44	-10	-27	-10
491.1	79.0	CTP	-44	-10	-52	-10
492.0	159.0	UTP	-47	-10	-23	-10
492.0	79.0	UTP	-47	-10	-38	-10
493.0	79.0	TTP	-60	-10	-60	-10
516.0	159.0	ATP	-70	-10	-25	-10
516.0	79.0	ATP	-70	-10	-90	-10
532.1	79.0	GTP	-60	-10	-90	-10

Table S-13. Metabolites identified in ESI$^+$ ionization mode in various cell numbers.

Metabolite	Q1	Q3	Ret. Time [min]	DP [V]	EP [V]	CE [V]	CXP [V]	Sum Formula	3 x 10^6 cells	1 x 10^6 cells	0.5 x 10^6 cells	1 x 10^5 cells	1 x 10^4 cells
Ethanolamine	62.0	45.0	8.34	31	10	21	10	C2H7NO	✓	✓	✓	✓	✓
Glycine	76.0	76.0	9.61	16	10	5	10	C2H5NO2	✓	x	x	x	x
Trimethylamine-N-oxide	76.1	58.0	8.18	25	10	29	10	C3H9NO	✓	x	x	x	x
Cysteamine	78.0	61.0	3.27	31	10	17	10	C2H7NS	✓	x	x	x	x
Putrescine	89.0	72.0	12.25	31	10	13	10	C4H12N2	✓	✓	✓	✓	x
Alanine	90.0	44.0	8.71	31	10	21	10	C3H7NO2	✓	✓	✓	x	x
beta-Alanine	90.0	73.0	8.21	39	10	25	10	C3H7NO2	✓	x	x	x	x
Sarcosine	90.0	44.0	8.33	31	10	21	10	C3H7NO2	✓	✓	✓	x	x
Cadaverine	103.0	86.0	11.22	26	10	15	10	C5H14N2	✓	✓	✓	✓	✓
Choline	105.0	105.0	4.74	15	10	20	10	C5H14NO	✓	✓	✓	✓	✓
Serine	106.0	60.0	9.95	16	10	15	10	C3H7NO3	✓	✓	✓	✓	x
Hypotaurine	110.0	92.0	8.85	31	10	13	10	C2H7NO2S	✓	x	x	x	x
Cytosine	112.0	95.0	4.8	45	10	25	10	C4H5N3O	✓	✓	x	x	x
Histamine	112.0	112.0	8.6	22	10	5	10	C5H9N3	✓	x	x	x	x
Histamine	112.0	95.0	8.6	22	10	12	10	C5H9N3	✓	x	x	x	x
Uracil	113.0	96.0	4.06	56	10	25	10	C4H4N2O2	✓	x	x	x	x
Uracil	113.0	70.0	4.06	56	10	23	10	C4H4N2O2	✓	x	x	x	x
Creatinine	114.0	86.1	1.99	26	10	10	10	C4H7N3O	✓	✓	x	x	x
Creatinine	114.0	114.0	1.99	26	10	7	10	C4H7N3O	✓	✓	x	x	x
Dihydrouracil	115.0	73.0	2.41	16	10	10	10	C4H6N2O2	✓	x	x	x	x
Dihydrouracil	115.0	115.0	2.41	16	10	5	10	C4H6N2O2	✓	x	x	x	x
Proline	116.0	70.0	7.52	26	10	25	10	C5H9NO2	✓	✓	✓	✓	✓
Betaine	118.0	118.0	6.72	31	10	5	10	C5H11NO2	✓	✓	✓	✓	x
Valine	118.0	72.0	7.31	31	10	17	10	C5H11NO2	✓	✓	✓	✓	✓

Threonine	120.0	74.0	9.11	49	10	17	10	C4H9NO3	✓	✓	✓	✓	✓
Cysteine	122.1	76.1	7.99	25	10	25	10	C3H7NO2S	✓	x	x	x	x
Cysteine	122.1	104.9	7.99	25	10	25	10	C3H7NO2S	✓	x	x	x	x
Nicotinamide	123.0	79.0	6.65	11	10	15	10	C6H6N2O	✓	✓	x	x	x
4-Hydroxybenzaldehyde	123.0	95.1	7.35	25	10	10	10	C7H6O2	✓	x	x	x	x
Nicotinic acid	124.0	80.0	2.4	46	10	31	10	C6H5NO2	✓	✓	✓	x	x
5-Methylcytosine	126.0	126.0	4.9	56	10	5	10	C5H7N3O	✓	x	x	x	x
1-methylhistamine	126.1	82.1	7.07	25	10	25	10	C6H11N3	✓	✓	x	x	x
1-methylhistamine	126.1	68.0	7.07	25	10	25	10	C6H11N3	✓	✓	x	x	x
Thymine	127.0	110.0	2.46	21	10	20	10	C5H6N2O2	✓	x	x	x	x
Pipecolic acid	130.1	70.1	7.65	38	10	22	10	C6H11NO2	✓	✓	✓	✓	x
N-Acetylputrescine	131.0	114.0	6.25	16	10	15	10	C6H14N2O	✓	✓	✓	x	x
Agmatine	131.1	72.1	10.61	25	10	15	10	C5H14N4	✓	✓	✓	✓	x
Agmatine	131.1	114.1	10.61	25	10	10	10	C5H14N4	✓	✓	✓	✓	x
Creatine	132.0	44.0	9.02	51	10	35	10	C4H9N3O2	✓	✓	x	x	x
3-Guanidinopropionic acid	132.0	72.0	8.81	51	10	23	10	C4H9N3O2	✓	✓	x	x	x
Isoleucine	132.0	69.0	6.41	46	10	25	10	C6H13NO2	✓	✓	✓	✓	✓
Leucine	132.0	44.0	6.05	51	10	35	10	C6H13NO2	✓	✓	✓	✓	✓
Asparagine	133.0	74.0	10.1	41	10	21	10	C4H8N2O3	✓	✓	✓	✓	x
Ornithine	133.0	116.0	13.47	36	10	10	10	C5H12N2O2	✓	✓	x	x	x
Ornithine	133.0	70.0	13.47	36	10	31	10	C5H12N2O2	✓	✓	x	x	x
Adenine	136.0	92.0	3.73	16	10	30	10	C5H5N5	✓	✓	✓	✓	x
Adenine	136.0	119.0	3.73	16	10	33	10	C5H5N5	✓	✓	✓	✓	x
2-Phenylacetamide	136.1	91.1	7.39	25	10	20	10	C8H9NO3	✓	✓	x	x	x
Hypoxanthine	137.0	119.0	3.99	61	10	25	10	C5H4N4O	✓	✓	✓	✓	✓
Hypoxanthine	137.0	110.0	3.99	61	10	29	10	C5H4N4O	✓	✓	✓	✓	✓
1-Methylnicotinamide	137.1	94.1	5.57	25	10	30	10	C7H9N2O	✓	✓	✓	✓	✓
Anthranilic acid	138.0	91.9	1.68	31	10	30	10	C7H7NO2	✓	✓	x	x	x

Anthranilic acid	138.0	120.0	1.68	31	10	17	10	C7H7NO2	✓	✓	x	x	x
Trigonelline	138.1	92.1	7.04	25	10	30	10	C7H7NO2	✓	✓	✓	✓	✓
Tyramine	138.1	121.1	3.85	25	10	15	10	C8H11NO	✓	x	x	x	x
Tyramine	138.1	103.1	3.85	25	10	20	10	C8H11NO	✓	x	x	x	x
O-Phosphoethanolamine	142.1	44.2	12.53	25	10	13	10	C2H8NO4P	✓	x	x	x	x
4-Methyl-5-thiazoleethanol	144.8	126.0	6.48	25	10	20	10	C6H9NOS	✓	x	x	x	x
4-Methyl-5-thiazoleethanol	144.8	113.1	6.48	25	10	30	10	C6H9NOS	✓	x	x	x	x
Homoleucine	146.1	86.1	3.03	25	10	15	10	C7H15NO2	✓	✓	✓	✓	✓
Spermidine	146.2	72.1	15.41	50	10	22	10	C7H19N3	✓	✓	✓	✓	✓
Acetylcholine	147.0	88.0	3.03	26	10	20	10	C7NH16O2	✓	✓	x	x	x
Glutamine	147.0	130.0	9.91	36	10	10	10	C5H10N2O3	✓	✓	✓	✓	x
Glutamine	147.0	84.0	9.91	36	10	29	10	C5H10N2O3	✓	✓	✓	✓	x
Lysine	147.0	130.0	13	36	10	10	10	C6H14N2O2	✓	✓	✓	✓	x
Lysine	147.0	84.0	13	36	10	29	10	C6H14N2O2	✓	✓	✓	✓	x
O-Acetyl-serine	148.0	106.1	7.75	26	10	15	10	C5H9NO4	✓	x	x	x	x
O-Acetyl-serine	148.0	88.0	7.75	26	10	15	10	C5H9NO4	✓	x	x	x	x
Methylaspartic acid	148.1	102.0	11.56	25	10	10	10	C5H9NO4	✓	✓	x	x	x
Methylaspartic acid	148.1	88.0	11.56	25	10	10	10	C5H9NO4	✓	✓	x	x	x
p-Coumaraldehyde	149.1	103.1	5.75	25	10	10	10	C9H8O2	✓	x	x	x	x
Methionine	150.0	104.0	6.74	56	10	10	10	C5H11NO2S	✓	✓	✓	✓	✓
Methionine	150.0	133.0	6.74	56	10	15	10	C5H11NO2S	✓	✓	✓	✓	✓
Guanine	152.0	111.0	2.91	31	10	25	10	C5H5N5O	✓	✓	x	x	x
Guanine	152.0	135.0	2.91	31	10	29	10	C5H5N5O	✓	✓	x	x	x
Xanthine	153.0	136.0	2.84	46	10	25	10	C5H4N4O2	✓	✓	x	x	x
Xanthine	153.0	110.0	2.84	46	10	27	10	C5H4N4O2	✓	✓	x	x	x
3-OH-anthranilate	154.3	108.0	8.9	30	10	25	10	C7H7NO3	✓	x	x	x	x
3-OH-anthranilate	154.3	136.2	8.9	30	10	18	10	C7H7NO3	✓	x	x	x	x
Histidine	156.0	83.0	11.49	46	10	25	10	C6H9N3O2	✓	✓	✓	x	x

Histidine	156.0	110.0	11.49	46	10	21	10	C6H9N3O2	✓	✓	✓	x	x
Dihydroorotic acid	158.9	113.1	7.51	25	10	11	10	C5H6N2O4	✓	x	x	x	x
Dihydroorotic acid	158.9	131.0	7.51	25	10	10	10	C5H6N2O4	✓	x	x	x	x
Allantoin	159.0	99.0	16.3	31	10	25	10	C4H6N4O3	✓	x	x	x	x
Allantoin	159.0	116.0	16.3	31	10	11	10	C4H6N4O3	✓	x	x	x	x
Tryptamine	161.0	91.0	3.02	26	10	40	10	C10H12N2	✓	✓	x	x	x
Tryptamine	161.0	144.0	3.02	26	10	15	10	C10H12N2	✓	✓	x	x	x
Carnitine	162.0	85.0	8.78	46	10	30	10	C7H15NO3	✓	✓	x	x	x
Carnitine	162.0	103.0	8.78	46	10	25	10	C7H15NO3	✓	✓	x	x	x
2-amino-adipic acid	162.2	55.2	10.32	25	10	28	10	C6H11NO4	✓	x	x	x	x
2-amino-adipic acid	162.2	116.2	10.32	25	10	14	10	C6H11NO4	✓	x	x	x	x
N-Acetyl-Cysteine	164.1	122.1	4.62	25	10	14	10	C5H9NO3S	✓	x	x	x	x
N-Acetyl-Cysteine	164.1	59.1	4.62	25	10	30	10	C5H9NO3S	✓	x	x	x	x
Phenylalanine	166.0	103.0	5.81	51	10	15	10	C9H11NO2	✓	✓	✓	✓	✓
Phenylalanine	166.0	120.0	5.81	51	10	11	10	C9H11NO2	✓	✓	✓	✓	✓
Methionine sulfoxide	166.2	74.1	9.81	25	10	14	10	C5H11NO3S	✓	✓	x	x	x
Methionine sulfoxide	166.2	55.9	9.81	25	10	25	10	C5H11NO3S	✓	✓	x	x	x
Pyridoxal	168.0	94.0	2.79	31	10	25	10	C8H9NO3	✓	✓	✓	✓	x
Pyridoxal	168.0	150.0	2.79	31	10	17	10	C8H9NO3	✓	✓	✓	✓	x
Norharmane	169.1	142.1	2.17	25	10	12	10	C11H8N2	✓	x	x	x	x
Norharmane	169.1	115.0	2.17	25	10	35	10	C11H8N2	✓	x	x	x	x
Pyridoxamine	169.1	134.0	8.76	25	10	25	10	C8H12N2O2	✓	x	x	x	x
Pyridoxamine	169.1	152.0	8.76	25	10	25	10	C8H12N2O2	✓	x	x	x	x
Cysteic Acid	170.2	124.0	10.4	46	10	10	10	C3H7NO5S	✓	x	x	x	x
Pyridoxine	170.0	134.0	3.04	41	10	25	10	C8H11NO3	✓	✓	✓	✓	✓
Pyridoxine	170.0	152.0	3.04	41	10	19	10	C8H11NO3	✓	✓	✓	✓	✓
Selenocysteine	170.1	123.9	2.79	25	10	20	10	C3H7NO2Se	✓	x	x	x	x
Selenocysteine	170.1	106.9	2.79	25	10	20	10	C3H7NO2Se	✓	x	x	x	x

N-Acetyl-ornithine	175.0	115.3	14.78	31	10	20	10	C7H14N2O3	✓	✓	x	x	x
N-Acetyl-ornithine	175.0	70.0	14.78	31	10	39	10	C7H14N2O3	✓	✓	x	x	x
Arginine	175.0	116.0	12.69	31	10	10	10	C6H14N4O2	✓	✓	✓	✓	✓
Arginine	175.0	70.0	12.69	31	10	39	10	C6H14N4O2	✓	✓	✓	✓	✓
N-Acetyl-aspartic acid	175.9	134.1	8.95	25	10	12	10	C6H9NO5	✓	x	x	x	x
N-Acetyl-aspartic acid	175.9	88.1	8.95	25	10	16	10	C6H9NO5	✓	x	x	x	x
Indole-3-acetic acid	176.2	130.1	1.69	46	10	25	10	C10H9NO2	✓	✓	x	x	x
Citrulline	176.0	70.1	10.45	36	10	30	10	C6H13N3O3	✓	✓	x	x	x
Citrulline	176.0	159.0	10.45	36	10	15	10	C6H13N3O3	✓	✓	x	x	x
N-carbamoyl aspartate	177.1	88.0	8.45	25	10	20	10	C5H8N2O5	✓	x	x	x	x
N-carbamoyl aspartate	177.1	116.0	8.45	25	10	20	10	C5H8N2O5	✓	x	x	x	x
CysteinylGlycine	179.1	162.0	9.6	25	10	12	10	C5H10N2O3S	✓	x	x	x	x
CysteinylGlycine	179.1	76.0	9.6	25	10	18	10	C5H10N2O3S	✓	x	x	x	x
Glucosamine	180.0	144.0	10.28	31	10	13	10	C6H13NO5	✓	x	x	x	x
Glucosamine	180.0	162.0	10.28	31	10	13	10	C6H13NO5	✓	x	x	x	x
Theobromine	181.1	108.0	2.36	25	10	25	10	C7H8N4O2	✓	x	x	x	x
Theobromine	181.1	163.0	2.36	25	10	13	10	C7H8N4O2	✓	x	x	x	x
Tyrosine	182.0	165.0	7.34	46	10	10	10	C9H11NO3	✓	✓	✓	✓	✓
Tyrosine	182.0	136.0	7.34	46	10	21	10	C9H11NO3	✓	✓	✓	✓	✓
Methionine sulfone	182.3	136.0	7.85	25	10	15	10	C5H11NO4S	✓	x	x	x	x
Methionine sulfone	182.3	56.1	7.85	25	10	25	10	C5H11NO4S	✓	x	x	x	x
Selenohomocysteine	184.1	137.9	2.74	25	10	20	10	C4H9NO2Se	✓	x	x	x	x
Selenohomocysteine	184.1	120.9	2.74	25	10	20	10	C4H9NO2Se	✓	x	x	x	x
Se-Methylselenocysteine	184.1	123.0	3	25	10	20	10	C4H9NO2Se	✓	x	x	x	x
Se-Methylselenocysteine	184.1	167.1	3	25	10	20	10	C4H9NO2Se	✓	x	x	x	x
O-Phospho-serine	186.0	70.0	13	36	10	25	10	C3H8NO6P	✓	x	x	x	x
O-Phospho-serine	186.0	88.0	13	36	10	35	10	C3H8NO6P	✓	x	x	x	x
N8-Acetyl-Spermidine	188.2	171.3	10.69	25	10	10	10	C9H21N3O	✓	✓	✓	✓	x

N-Acetyl-glutamine	189.0	84.0	8.16	16	10	28	10	C7H12N2O4	✓	✓	✓	✓	x
N-Acetyl-glutamine	189.0	130.0	8.16	16	10	21	10	C7H12N2O4	✓	✓	✓	✓	x
Nε, Nε, Nε - Trimethyllysine	189.2	130.1	11.67	25	10	10	10	C9H21N2O2	✓	✓	✓	x	x
N-Acetyl-glutamic acid	190.0	130.2	8.42	26	10	20	10	C7H11NO5	✓	✓	x	x	x
N-Acetyl-glutamic acid	190.0	84.0	8.42	26	10	33	10	C7H11NO5	✓	✓	x	x	x
Kynurenic Acid	190.1	146.1	2.78	25	10	20	10	C10H7NO3	✓	x	x	x	x
Kynurenic Acid	190.1	172.0	2.78	25	10	30	10	C10H7NO3	✓	x	x	x	x
N-Acetyl-methionine	192.0	104.0	3.97	21	10	20	10	C7H13NO3S	✓	✓	✓	x	x
N-Acetyl-methionine	192.0	144.0	3.97	21	10	15	10	C7H13NO3S	✓	✓	✓	x	x
Phenylacetylglycine	194.1	76.0	3.33	25	10	10	10	C10H11NO3	✓	x	x	x	x
Phenylacetylglycine	194.1	91.0	3.33	25	10	20	10	C10H11NO3	✓	x	x	x	x
Selenomethionine	198.0	56.4	3.63	25	10	20	10	C5H11NO2Se	✓	x	x	x	x
Selenomethionine	198.0	180.9	3.63	25	10	9	10	C5H11NO2Se	✓	x	x	x	x
Hercynine	198.1	139.1	9.9	25	10	20	10	C9H15N3O2	✓	x	x	x	x
Hercynine	198.1	95.1	9.9	25	10	20	10	C9H15N3O2	✓	x	x	x	x
N, N-Dimethylarginine	203.2	158.1	10.88	25	10	12	10	C8H18N4O2	✓	x	x	x	x
Tryptophan	205.0	146.0	5.7	51	10	25	10	C11H12N2O2	✓	✓	✓	✓	✓
Tryptophan	205.0	188.0	5.7	51	10	15	10	C11H12N2O2	✓	✓	✓	✓	✓
AcetylCarnitine	205.0	84.1	3.3	34	10	19	10	C9H17NO4	✓	✓	x	x	x
AcetylCarnitine	205.0	145.0	3.3	34	10	19	10	C9H17NO4	✓	✓	x	x	x
N-Acetylphenylalanine	208.1	148.1	5.55	25	10	20	10	C11H13NO3	✓	x	x	x	x
N-Acetylphenylalanine	208.1	120.1	5.55	25	10	20	10	C11H13NO3	✓	x	x	x	x
Kynurenine	209.0	146.0	5.84	31	10	25	10	C10H12N2O3	✓	✓	x	x	x
Kynurenine	209.0	192.0	5.84	31	10	13	10	C10H12N2O3	✓	✓	x	x	x
Cyclo(Leu-Pro)	211.1	70.1	1.78	25	10	15	10	C11H18N2O2	✓	✓	x	x	x
Cyclo(Leu-Pro)	211.1	183.1	1.78	25	10	15	10	C11H18N2O2	✓	✓	x	x	x
Panthothenic acid	220.1	90.2	3.93	25	10	15	10	C9H17NO5	✓	✓	✓	✓	✓
Panthothenic acid	220.1	72.2	3.93	25	10	23	10	C9H17NO5	✓	✓	✓	✓	✓

5-Hydroxy-tryptophan	221.0	162.1	7.01	36	10	20	10	C11H12N2O3	✓	x	x	x	x
5-Hydroxy-tryptophan	221.0	204.0	7.01	36	10	15	10	C11H12N2O3	✓	x	x	x	x
GlcNAc	222.0	138.1	6.53	26	10	10	10	C8H15NO6	✓	✓	x	x	x
GlcNAc	222.0	204.0	6.53	26	10	11	10	C8H15NO6	✓	✓	x	x	x
Cystathionine	223.0	134.0	6.48	36	10	10	10	C7H14N2O4S	✓	x	x	x	x
Cystathionine	223.0	88.0	6.48	36	10	41	10	C7H14N2O4S	✓	x	x	x	x
Carnosine	227.0	209.9	12.55	31	10	10	10	C9H14N4O3	✓	x	x	x	x
Carnosine	227.0	110.0	12.55	31	10	33	10	C9H14N4O3	✓	x	x	x	x
2'-deoxycytidine	228.0	94.9	2.36	31	10	40	10	C9H13N3O4	✓	x	x	x	x
2'-deoxycytidine	228.0	112.0	2.36	31	10	15	10	C9H13N3O4	✓	x	x	x	x
Proline-hydroxyproline	229.2	211.1	10.54	25	10	10	10	C5H9NO3	✓	x	x	x	x
Proline-hydroxyproline	229.2	70.1	10.54	25	10	20	10	C5H9NO3	✓	x	x	x	x
Melatonin	233.1	174.3	5.08	30	10	18	10	C13H16N2O2	✓	x	x	x	x
Cystine	241.0	74.0	6.7	46	10	37	10	C6H12N2O4S2	✓	x	x	x	x
Tetrahydrobiopterin	242.1	149.0	7.36	25	10	30	10	C9H15N5O3	✓	x	x	x	x
Tetrahydrobiopterin	242.1	166.1	7.36	25	10	20	10	C9H15N5O3	✓	x	x	x	x
Thymidine	243.0	110.0	2.45	26	10	25	10	C10H14N2O5	✓	x	x	x	x
Thymidine	243.0	127.0	2.45	26	10	15	10	C10H14N2O5	✓	x	x	x	x
Cytidine	244.0	94.8	4.67	26	10	40	10	C9H13N3O5	✓	✓	x	x	x
Cytidine	244.0	112.0	4.67	26	10	19	10	C9H13N3O5	✓	✓	x	x	x
Biotin	245.0	97.0	2.42	46	10	43	10	C10H16N2O3S	✓	✓	x	x	x
Uridine	245.0	113.0	3.98	31	10	15	10	C9H12N2O6	✓	✓	x	x	x
gamma Glutamylcysteine	251.1	122.1	9.46	25	10	25	10	C8H14N2O5S	✓	x	x	x	x
gamma Glutamylcysteine	251.1	130.1	9.46	25	10	30	10	C8H14N2O5S	✓	x	x	x	x
2'-Deoxyadenosine	252.0	235.2	3.91	36	10	10	10	C10H13N5O3	✓	x	x	x	x
2'-Deoxyadenosine	252.0	136.0	3.91	36	10	21	10	C10H13N5O3	✓	x	x	x	x
Linatine	260.1	214.1	2.32	25	10	20	10	C10H17N3O5	✓	x	x	x	x
Linatine	260.1	242.1	2.32	25	10	10	10	C10H17N3O5	✓	x	x	x	x

Biotin sulfoxide	261.1	243.1	5.45	25	10	10	10	C10H16N2O4S	✓	x	x	x	x
Biotin sulfoxide	261.1	215.1	5.45	25	10	20	10	C10H16N2O4S	✓	x	x	x	x
Adenosine	268.0	136.0	4.02	25	10	51	10	C10H13N5O4	✓	✓	✓	✓	x
2'-Deoxyguanosine	268.0	152.0	4.56	41	10	15	10	C10H13N5O4	✓	x	x	x	x
Homocystine	269.0	136.0	4.07	26	10	15	10	C8H16N2O4S2	✓	x	x	x	x
Inosine	269.0	110.0	5.17	36	10	30	10	C10H12N4O5	✓	✓	✓	✓	✓
Inosine	269.0	137.0	5.17	36	10	15	10	C10H12N4O5	✓	✓	✓	✓	✓
Biotin Sulfone	277.1	259.1	3.13	25	10	10	10	C10H16N2O5S	✓	x	x	x	x
Biotin Sulfone	277.1	231.1	3.13	25	10	20	10	C10H16N2O5S	✓	x	x	x	x
Saccharopine	277.1	130.1	2.79	25	10	12	10	C11H20N2O6	✓	x	x	x	x
Saccharopine	277.1	213.1	2.79	25	10	12	10	C11H20N2O6	✓	x	x	x	x
1-Methyladenosine	282.1	150.1	7.08	25	10	40	10	C11H15N5O4	✓	x	x	x	x
Guanosine	284.0	152.0	6.3	36	10	19	10	C10H13N5O5	✓	✓	✓	✓	x
Xanthosine	285.0	136.0	6.28	46	10	30	10	C10H12N4O6	✓	✓	x	x	x
Xanthosine	285.0	153.0	6.28	46	10	17	10	C10H12N4O6	✓	✓	x	x	x
S Methylthioadenosine	298.1	136.0	2.52	25	10	20	10	C11H15N5O3S	✓	x	x	x	x
S Methylthioadenosine	298.1	163.0	2.52	25	10	13	10	C11H15N5O3S	✓	x	x	x	x
S Methylthioinosine	299.1	167.0	2.86	25	10	13	10	C11H14N4O4S	✓	x	x	x	x
S Methylthioinosine	299.1	137.0	2.86	25	10	20	10	C11H14N4O4S	✓	x	x	x	x
d-Sphingosine	300.0	282.0	2.39	31	10	17	10	C18H37NO2	✓	✓	x	x	x
Glutathione	308.1	130.1	11.78	71	10	10	10	C10H17N3O6S	✓	x	x	x	x
Glutathione	308.1	179.1	11.78	71	10	13	10	C10H17N3O6S	✓	x	x	x	x
NANA	310.0	121.0	10.95	31	10	25	10	C11H19NO9	✓	x	x	x	x
NANA	310.0	274.0	10.95	31	10	15	10	C11H19NO9	✓	x	x	x	x
PQQ	331.0	285.0	1.7	51	10	27	10	C14H6N2O8	✓	x	x	x	x
Riboflavin	377.0	243.0	4.63	71	10	35	10	C17H20N4O6	✓	x	x	x	x
S-(5'-adenosyl)-l-homocysteine	385.0	136.1	10.45	51	10	27	10	C14H20N6O5S	✓	x	x	x	x

S-(5'-adenosyl)-l-homocysteine	385.0	134.0	10.45	51	10	27	10	C14H20N6O5S	✓	x	x	x	x
Ergocalciferol	397.4	69.1	1.45	25	10	28	10	C28H44O	✓	x	x	x	x
Ergocalciferol	397.4	379.3	1.45	25	10	12	10	C28H44O	✓	x	x	x	x
S-(5'-adenosyl)-l-methionine	399.0	135.9	13.17	51	10	30	10	C15H22N6O5S	✓	x	x	x	x
S-(5'-adenosyl)-l-methionine	399.0	250.0	13.17	51	10	23	10	C15H22N6O5S	✓	x	x	x	x
Palmitoylcarnitine	400.3	85.0	2.33	25	10	20	10	C23H45NO4	✓	x	x	x	x
Folic acid	442.0	295.0	9.32	41	10	23	10	C19H19N7O6	✓	x	x	x	x
5-Methyl-THF	460.0	311.0	14.27	51	10	29	10	C20H25N7O6	✓	x	x	x	x
5-Methyl-THF	460.0	313.0	14.27	51	10	29	10	C20H25N7O6	✓	x	x	x	x
Glutathione oxidized	613.0	231.0	1.22	71	10	40	10	C20H32N6O12S2	✓	x	x	x	x
Glutathione oxidized	613.0	355.0	1.22	71	10	33	10	C20H32N6O12S2	✓	x	x	x	x
NAD^+	664.4	664.0	14.29	24	10	5	10	C21H27N7O14P2	✓	✓	x	x	x
NAD^+	664.4	136.0	14.29	24	10	39	10	C21H27N7O14P2	✓	✓	x	x	x
NADH	666.0	649.0	13.77	23	10	23	10	C21H29N7O14P2	✓	✓	x	x	x
$NADP^+$	744.0	604.0	12.51	51	10	35	10	C21H29N7O17P3	✓	x	x	x	x
$NADP^+$	744.0	136.0	12.51	51	10	79	10	C21H29N7O17P3	✓	x	x	x	x
NADPH	746.0	509.0	11.57	24	10	23	10	C21H31N7O17P3	✓	x	x	x	x
NADPH	746.1	136.0	11.57	24	10	22	10	C21H31N7O17P3	✓	x	x	x	x
NADPH	746.1	625.0	11.57	24	10	23	10	C21H31N7O17P3	✓	x	x	x	x
FAD	786.0	348.0	11.37	76	10	31	10	C27H33P2N9O15	✓	x	x	x	x

Table S-14. Metabolites identified in ESI^- ionization mode in various cell numbers.

Metabolite	Q1	Q3	Ret. Time [min]	DP [V]	EP [V]	CE [V]	CXP [V]	Sum Formula	3×10^6 Cells	1×10^6 cells	0.5×10^6 cells	1×10^5 cells	1×10^4 cells
Glycolic acid	75.0	75.0	9.41	-30	-10	-5	-10	C2H4O3	✓	x	x	x	x
Pyruvic acid	87.1	87.1	5.27	-30	-10	-5	-10	C3H4O3	✓	x	x	x	x
Lactic acid	89.3	89.3	8.2	-45	-10	-5	-10	C3H6O3	✓	✓	✓	✓	x
gamma-Aminobutyric acid	102.2	102.2	11.3	-10	-10	-5	-10	C4H9NO2	✓	✓	x	x	x
Hydroxybutyric acid	103.1	59.0	8.05	-25	-10	-18	-25	C4H8O3	✓	x	x	x	x
Malonic acid	103.1	41.1	11.94	-25	-10	-36	-10	C3H4O4	✓	x	x	x	x
Fumaric acid	115.2	71.1	13.83	-35	-10	-12	-10	C4H4O4	✓	x	x	x	x
Succinic acid	117.4	73.0	12.73	-35	-10	-16	-10	C4H6O4	✓	x	x	x	x
Taurine	124.1	80.0	9.57	-25	-10	-12	-10	C2H7NO3S	✓	x	x	x	x
Pyroglutamic acid	127.9	83.9	9.73	-25	-10	-13	-10	C5H7NO3	✓	x	x	x	x
Pyroglutamic acid	127.9	81.9	9.73	-25	-10	-17	-10	C5H7NO3	✓	x	x	x	x
Citraconic acid	129.0	85.0	11.66	-15	-10	-14	-10	C5H6O4	✓	✓	✓	x	x
Itaconic acid	129.0	85.0	5.25	-15	-10	-14	-10	C5H6O4	✓	✓	✓	x	x
Oxaloacetic Acid	131.0	87.0	11.68	-15	-10	-10	-10	C4H4O5	✓	x	x	x	x
Aspartic acid	132.2	88.1	15.2	-15	-10	-20	-10	C4H7NO4	✓	✓	✓	x	x
Aspartic acid	132.2	71.3	15.2	-15	-10	-33	-10	C4H7NO4	✓	✓	✓	x	x
Threonic acid	135.2	75.0	10.5	-15	-10	-14	-10	C4H8O5	✓	x	x	x	x
O-Phosphorylethanolamine	140.0	79.0	15.07	-20	-10	-15	-10	C2H8NO4P	✓	x	x	x	x
Octanoic acid	143.1	143.1	2.01	-65	-10	-5	-10	C8H16O2	✓	x	x	x	x
alpha-Ketoglutaric acid	145.0	57.0	12.47	-20	-10	-25	-10	C5H6O5	✓	✓	✓	✓	✓
alpha-Ketoglutaric acid	145.0	101.0	12.47	-20	-10	-12	-10	C5H6O5	✓	✓	✓	✓	✓
N-Acetyl-DL-serine	146.0	128.2	11.53	-15	-10	-20	-10	C5H9NO4	✓	x	x	x	x
Glutamic acid	146.2	131.0	13.26	-30	-10	-10	-10	C5H9NO4	✓	✓	✓	x	x
Glutamic acid	146.2	102.1	13.26	-30	-10	-20	-10	C5H9NO4	✓	✓	✓	x	x

Cinnamic acid	147.1	131.0	3.92	-60	-10	-23	-10	C9H8O2	✓	✓	✓	x	x
Cinnamic acid	147.1	103.0	3.92	-60	-10	-16	-10	C9H8O2	✓	✓	✓	x	x
p-Coumaric acid	163.0	119.1	4.75	-60	-10	-19	-10	C9H8O3	✓	x	x	x	x
Phenylpyruvic acid	163.0	91.1	2.56	-25	-10	-15	-10	C9H8O3	✓	x	x	x	x
Quinolinate	166.5	78.2	2.25	-30	-10	-25	-10	C10H7NO2	✓	x	x	x	x
Quinolinate	166.5	122.0	2.25	-30	-10	-13	-10	C10H7NO2	✓	x	x	x	x
Uric acid	167.0	124.0	11.27	-50	-10	-22	-10	C5H4N4O3	✓	x	x	x	x
Homogentisate	167.0	107.9	4.21	-50	-10	-35	-10	C8H8O4	✓	x	x	x	x
Homogentisate	167.0	123.0	4.21	-50	-10	-23	-10	C8H8O4	✓	x	x	x	x
Dihydroxyacetone phosphate	169.0	79.0	14.29	-40	-10	-36	-10	C3H7O6P	✓	x	x	x	x
Glycerol 3-phosphate	171.0	79.0	14.16	-40	-10	-26	-10	C3H9O6P	✓	x	x	x	x
N-Acetylleucine	172.1	130.1	5.78	-15	-10	-20	-10	C8H15NO3	✓	✓	x	x	x
Shikimic Acid	173.1	119.1	1.52	-75	-10	-10	-10	C7H10O5	✓	x	x	x	x
Shikimic Acid	173.1	93.0	1.52	-75	-10	-15	-10	C7H10O5	✓	x	x	x	x
Aconitic acid	173.0	129.0	13.65	-25	-10	-10	-10	C6H6O6	✓	✓	x	x	x
Aconitic acid	173.0	85.0	13.65	-25	-10	-18	-10	C6H6O6	✓	✓	x	x	x
N-Acetylaspartate	174.2	130.0	13.38	-15	-10	-20	-10	C6H9NO5	✓	x	x	x	x
N-Acetylaspartate	174.2	88.2	13.38	-15	-10	-20	-10	C6H9NO5	✓	x	x	x	x
Allantoic acid	175.0	115.2	10.5	-25	-10	-10	-10	C4H8N4O4	✓	x	x	x	x
Allantoic acid	175.0	132.0	10.5	-25	-10	-12	-10	C4H8N4O4	✓	x	x	x	x
Hippurate	178.1	77.1	5.7	-50	-10	-25	-10	C9H9NO3	✓	x	x	x	x
Hippurate	178.1	134.0	5.7	-50	-10	-16	-10	C9H9NO3	✓	x	x	x	x
Inositol	179.1	179.1	14.09	-25	-10	-5	-10	C6H12O6	✓	x	x	x	x
Inositol	179.1	81.0	14.09	-50	-10	-15	-10	C6H12O6	✓	x	x	x	x
Glucose	179.1	89.1	13.64	-15	-10	-28	-10	C6H12O6	✓	✓	✓	x	x
Glucose	179.1	59.1	13.64	-15	-10	-13	-10	C6H12O6	✓	✓	✓	x	x
Sorbitol	181.1	89.0	9.64	-60	-10	-20	-10	C6H14O6	✓	✓	✓	✓	x
Homovanillate	181.1	137.1	5.77	-50	-10	-12	-10	C9H10O4	✓	x	x	x	x

4-hydroxyphenyllactic acid	181.1	163.0	6.15	-25	-10	-14	-10	C9H10O4	✓	✓	✓	x	x
4-hydroxyphenyllactic acid	181.1	135.1	6.15	-25	-10	-16	-10	C9H10O4	✓	✓	✓	x	x
4-Pyridoxic acid	182.1	108.2	2.34	-40	-10	-21	-10	C8H9NO4	✓	x	x	x	x
4-Pyridoxic acid	182.1	138.0	2.34	-40	-10	-21	-10	C8H9NO4	✓	x	x	x	x
Phosphoglyceric acid	185.0	79.0	9.82	-45	-10	-32	-10	C3H7O7P	✓	x	x	x	x
Phosphoglyceric acid	185.0	97.0	9.82	-45	-10	-21	-10	C3H7O7P	✓	x	x	x	x
Azelaic acid	187.0	169.0	10.8	-50	-10	-22	-10	C9H16O4	✓	x	x	x	x
Azelaic acid	187.0	125.0	10.8	-50	-10	-22	-10	C9H16O4	✓	x	x	x	x
5-Hydroxyindole-3-acetate	190.1	157.2	6.38	-50	-10	-18	-10	C10H9NO3	✓	✓	✓	x	x
5-Hydroxyindole-3-acetate	190.1	146.0	6.38	-50	-10	-16	-10	C10H9NO3	✓	✓	✓	x	x
Citric acid	191.1	191.0	8.32	-25	-10	-5	-10	C6H8O7	✓	x	x	x	x
Citric acid	191.1	87.0	8.32	-25	-10	-12	-10	C6H8O7	✓	x	x	x	x
Glucuronic acid	193.0	113.0	14.12	-45	-10	-18	-10	C6H10O7	✓	x	x	x	x
Gluconic acid	195.0	195.0	11.81	-50	-10	-5	-10	C6H12O7	✓	x	x	x	x
Gluconic acid	195.0	129.0	11.81	-50	-10	-20	-10	C6H12O7	✓	x	x	x	x
Xanthurenic acid	204.0	160.0	6.42	-45	-10	-20	-10	C10H7NO4	✓	✓	x	x	x
Lipoic acid	205.0	171.0	2.56	-45	-10	-12	-10	C8H14O2S2	✓	x	x	x	x
Myristic acid	227.2	227.2	1.76	-15	-10	-5	-10	C14H28O2	✓	x	x	x	x
Neopterin	252.1	252.1	6.63	-40	-10	-5	-10	C9H11N5O4	✓	x	x	x	x
Neopterin	252.1	192.0	6.63	-40	-10	-22	-10	C9H11N5O4	✓	x	x	x	x
Palmitic Acid	255.2	255.2	1.71	-15	-10	-5	-10	C16H32O2	✓	✓	x	x	x
Linoleic acid	279.2	279.2	1.66	-15	-10	-5	-10	C18H32O2	✓	✓	x	x	x
Oleic acid	281.2	281.2	1.72	-15	-10	-5	-10	C18H34O2	✓	✓	x	x	x
Stearic acid	283.3	283.3	1.67	-15	-10	-5	-10	C18H36O2	✓	✓	x	x	x
cTMP	303.2	241.2	6.67	-65	-10	-20	-10	C10H13N2O7P	✓	✓	x	x	x
cTMP	303.2	125.0	6.67	-65	-10	-28	-10	C10H13N2O7P	✓	✓	x	x	x
cCMP	304.0	261.0	5	-70	-10	-20	-10	C9H12N3O7P	✓	x	x	x	x
cCMP	304.0	110.1	5	-23	-10	-5	-10	C9H12N3O7P	✓	x	x	x	x

dCMP	306.1	195.1	13.3	-70	-10	-56	-10	C9H14N3O7P	✓	x	x	x	x
dCMP	306.1	79.0	13.3	-22	-10	-36	-10	C9H14N3O7P	✓	x	x	x	x
Geranyl PP	313.0	79.0	14.65	-25	-10	-45	-10	C10H20O7P2	✓	x	x	x	x
TMP	321.1	79.0	14.91	-65	-10	-44	-10	C10H15N2O8P2	✓	x	x	x	x
TMP	321.1	195.1	14.91	-65	-10	-24	-10	C10H15N2O8P2	✓	x	x	x	x
CMP	322.0	195.1	15.24	-75	-10	-25	-10	C9H14N3O8P	✓	x	x	x	x
CMP	322.0	79.0	15.24	-75	-10	-62	-10	C9H14N3O8P	✓	x	x	x	x
UMP	323.2	195.1	15.77	-60	-10	-25	-10	C9H13N2O9P	✓	x	x	x	x
UMP	323.2	79.0	15.77	-60	-10	-60	-10	C9H13N2O9P	✓	x	x	x	x
cAMP	328.0	107.0	8.1	-85	-10	-36	-10	C10H11N5O6P	✓	✓	x	x	x
cAMP	328.0	134.0	8.1	-85	-10	-36	-10	C10H11N5O6P	✓	✓	x	x	x
dAMP	330.1	134.0	14.28	-60	-10	-20	-10	C10H14N5O6P	✓	x	x	x	x
dAMP	330.1	79.0	14.28	-60	-10	-62	-10	C10H14N5O6P	✓	x	x	x	x
Lactose	341.0	161.0	14.24	-65	-10	-12	-10	C12H22O11	✓	✓	✓	x	x
cGMP	344.0	133.0	10.68	-75	-10	-34	-10	C10H12N5O7P	✓	x	x	x	x
cGMP	344.0	150.0	10.68	-75	-10	-34	-10	C10H12N5O7P	✓	x	x	x	x
AMP	346.1	211.1	13.33	-73	-10	-50	-10	C10H14N5O7P	✓	x	x	x	x
AMP	346.1	79.0	13.33	-73	-10	-65	-10	C10H14N5O7P	✓	x	x	x	x
GMP	362.0	211.1	15.29	-65	-10	-25	-10	C10H14N5O8P	✓	x	x	x	x
GMP	362.0	79.0	15.29	-65	-10	-62	-10	C10H14N5O8P	✓	x	x	x	x
XMP	363.0	151.0	13.11	-35	-10	-25	-10	C10H13N4O9P	✓	x	x	x	x
XMP	363.0	79.0	13.11	-35	-10	-36	-10	C10H13N4O9P	✓	x	x	x	x
Farnesyl Ppi	381.0	79.0	14.61	-25	-10	-45	-10	C15H28O7P2	✓	x	x	x	x
dCDP	386.2	159.0	11.34	-65	-10	-25	-10	C9H15N3O10P2	✓	x	x	x	x
dCDP	386.2	79.0	11.34	-65	-10	-72	-10	C9H15N3O10P2	✓	x	x	x	x
CDP	402.0	159.0	15.91	-65	-10	-25	-10	C9H15N3O11P2	✓	x	x	x	x
CDP	402.0	79.0	15.91	-65	-10	-78	-10	C9H15N3O11P2	✓	x	x	x	x
ADP	426.3	159.0	15.11	-75	-10	-25	-10	C10H15N5O10P2	✓	x	x	x	x

ADP	426.3	79.0	15.11	-75	-10	-88	-10	C10H15N5O10P2	✓	x	x	x	x
CDP-ethanolamine	445.0	79.0	14.52	-45	-10	-82	-10	C11H20N4O11P2	✓	x	x	x	x
dUTP	467.0	159.0	12.23	-24	-10	-25	-10	C9H15N2O14P3	✓	x	x	x	x
dUTP	467.0	79.0	12.23	-24	-10	-44	-10	C9H15N2O14P3	✓	x	x	x	x
TTP	481.0	159.0	14.48	-60	-10	-25	-10	C10H17N2O14P3	✓	x	x	x	x
TTP	481.0	79.0	14.48	-60	-10	-60	-10	C10H17N2O14P3	✓	x	x	x	x
ATP	506.1	159.0	16.14	-70	-10	-25	-10	C10H16N5O13P3	✓	x	x	x	x
ATP	506.1	79.0	16.14	-70	-10	-90	-10	C10H16N5O13P3	✓	x	x	x	x
ITP	507.0	159.0	14.97	-60	-10	-25	-10	C10H15N4O14P3	✓	x	x	x	x
ITP	507.0	79.0	14.97	-60	-10	-90	-10	C10H15N4O14P3	✓	x	x	x	x
UDP-GalNAc	606.2	79.0	15	-85	-10	-85	-10	C17H27N3O17P2	✓	x	x	x	x
UDP-GalNAc	606.2	385.0	15	-85	-10	-38	-10	C17H27N3O17P2	✓	x	x	x	x
CMP-NANA	613.0	79.0	15.3	-60	-10	-85	-10	C20H31N4O16P	✓	x	x	x	x
CMP-NANA	613.0	322.0	15.3	-60	-10	-28	-10	C20H31N4O16P	✓	x	x	x	x

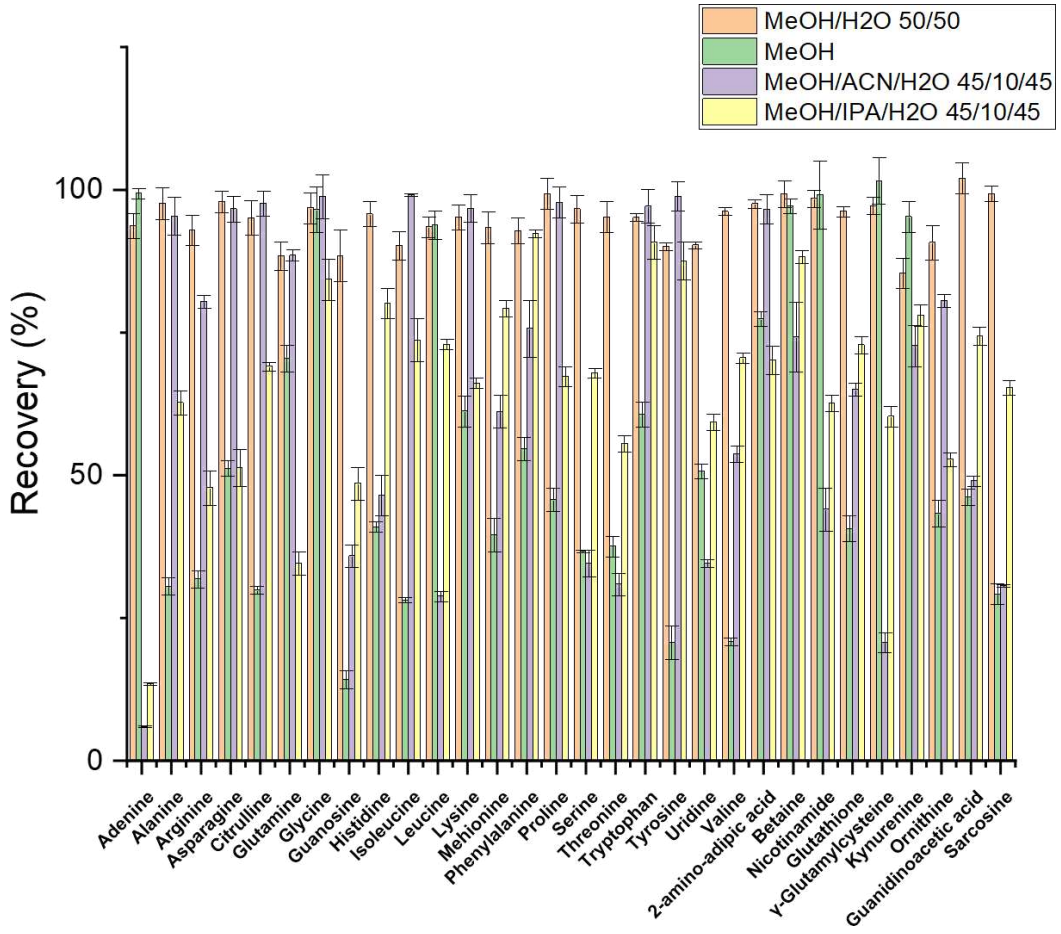

Fig. S-1A. Recovery of ^{13}C labeled metabolites in ESI^+ mode.

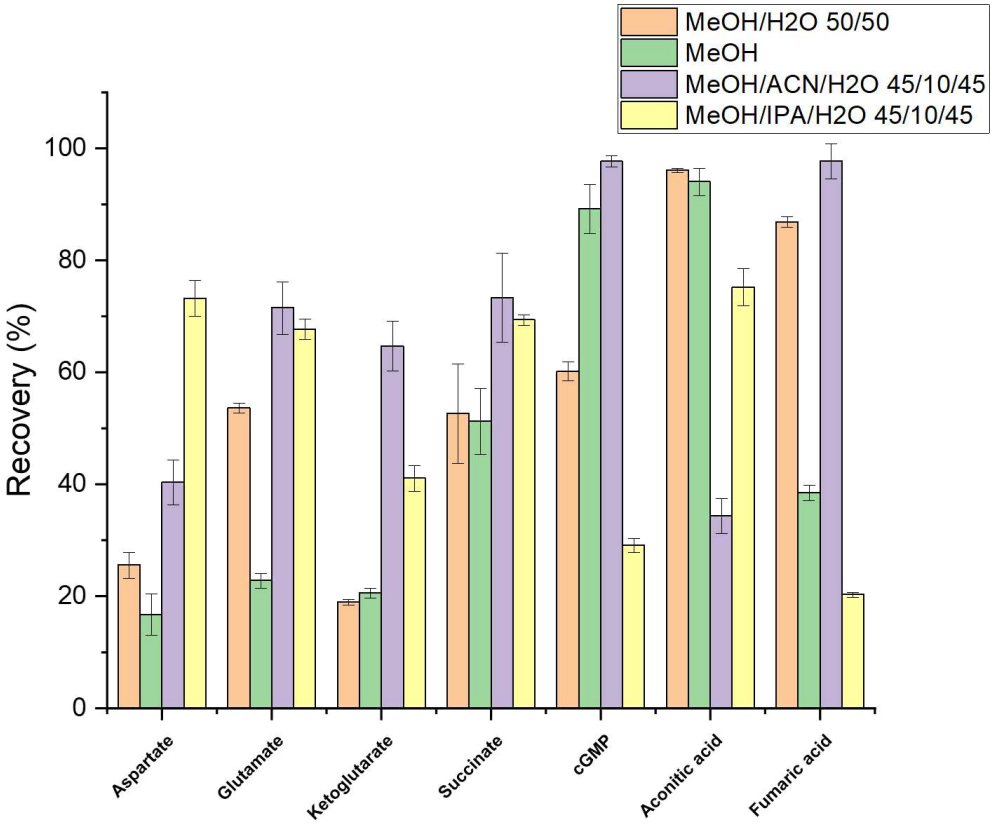

Fig. S-1B. Recovery of ^{13}C labeled metabolites in ESI^- mode.

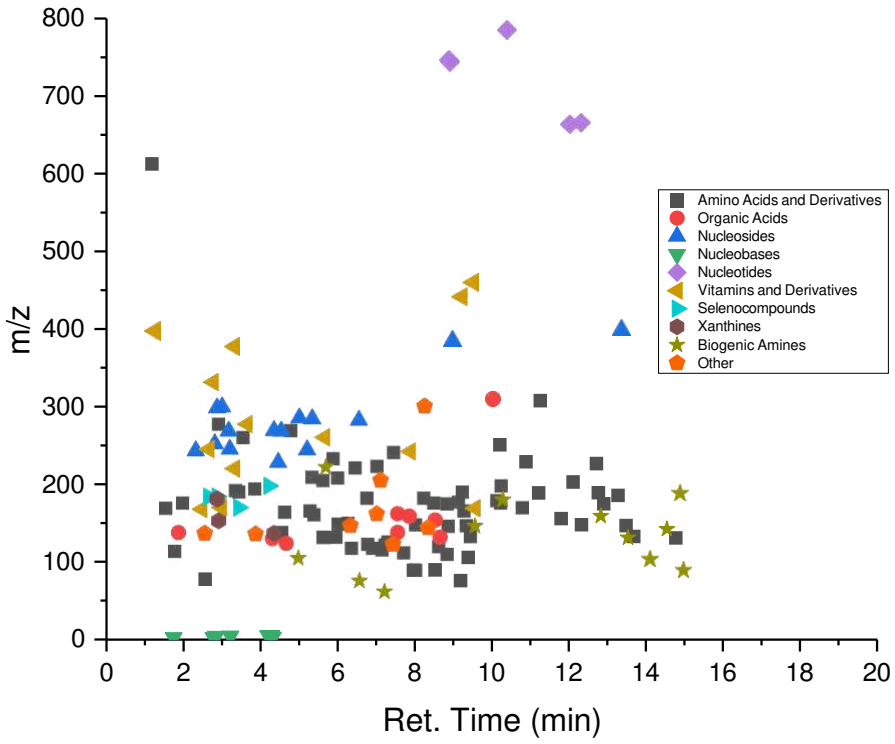

Fig. S-2A. HILIC-Z metabolite distribution in positive ionization mode

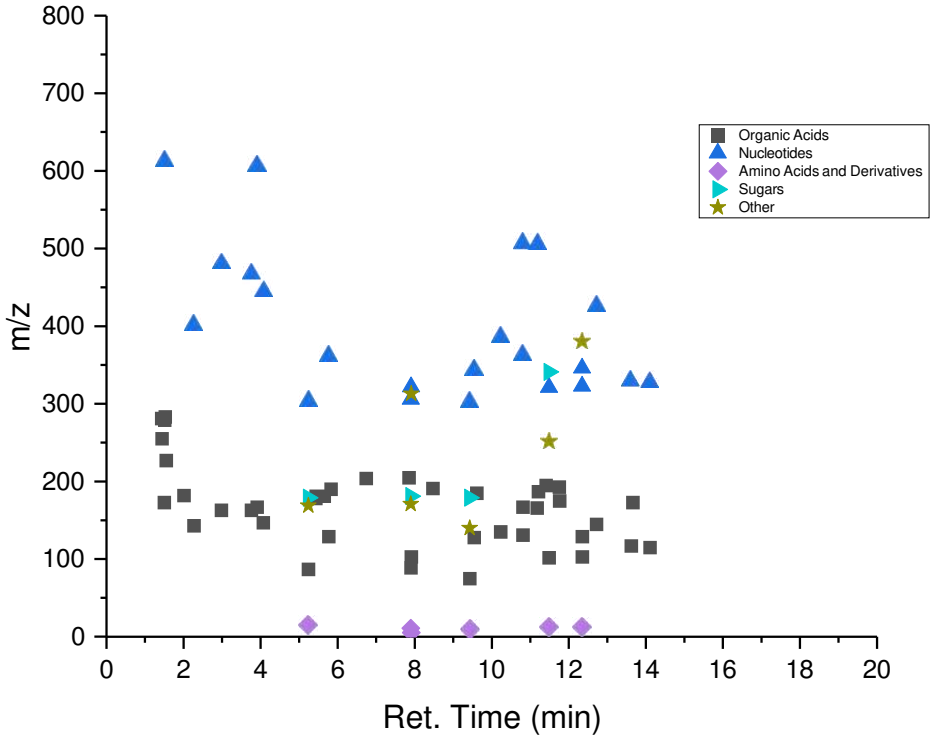

Fig. S-2B. HILIC-Z metabolite distribution in negative ionization mode

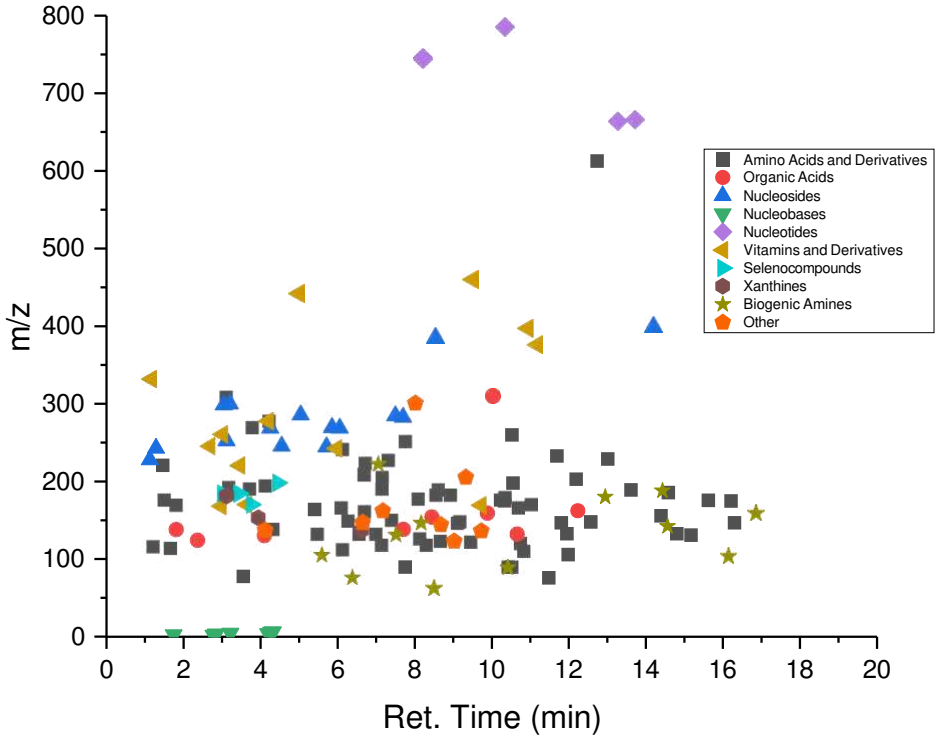

Fig. S-3A. Z-HILIC metabolite distribution in positive ionization mode

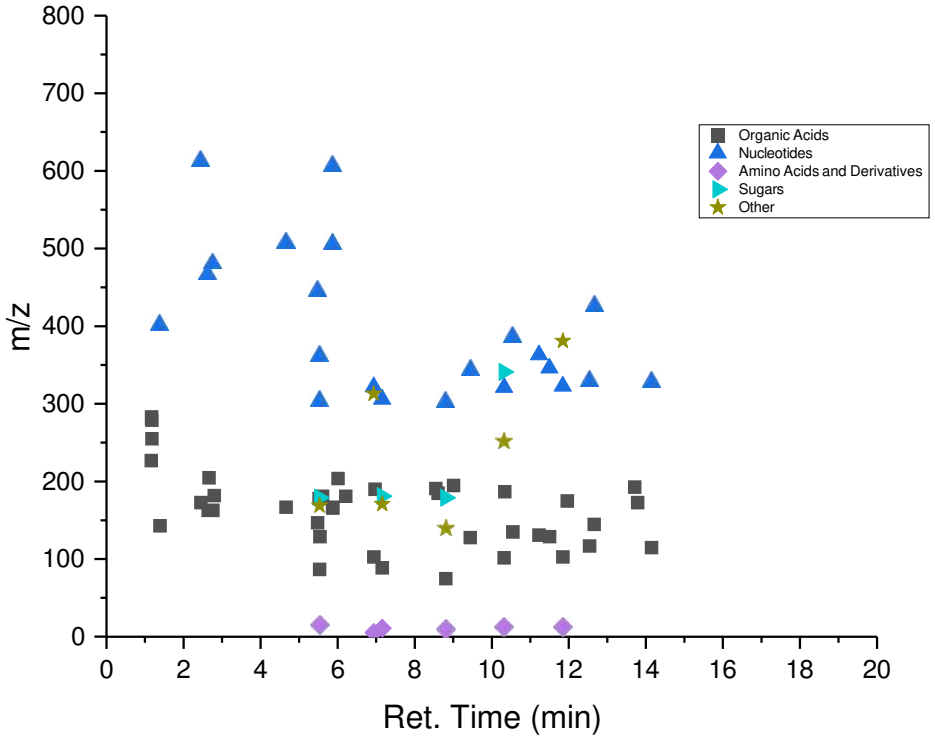

Fig. S-3B. Z-HILIC metabolite distribution in negative ionization mode

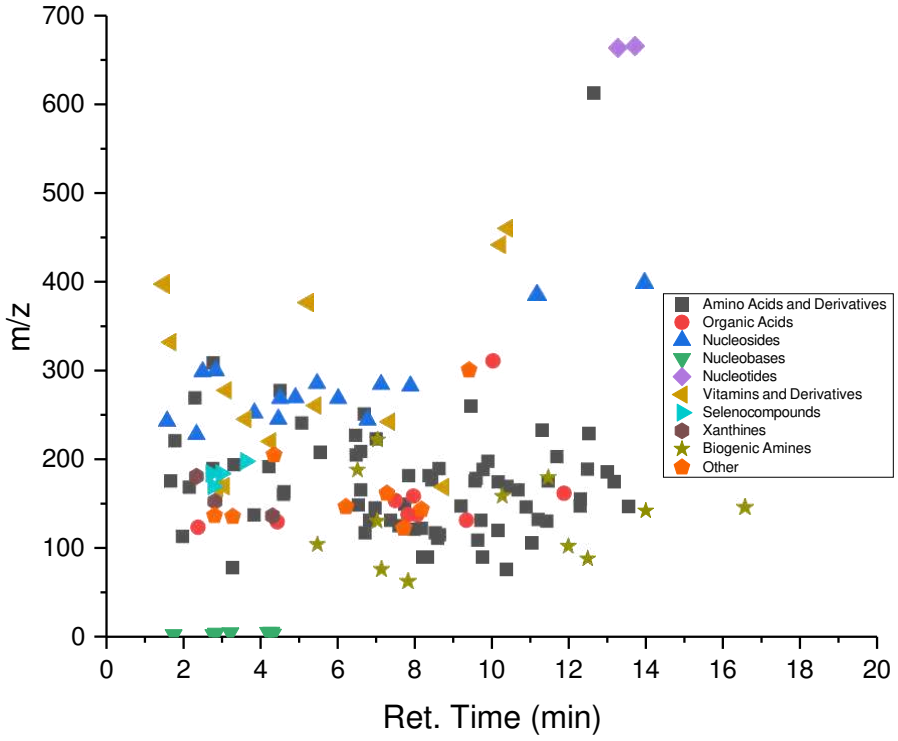

Fig. S-4A. BEH-Amide metabolite distribution in positive ionization mode

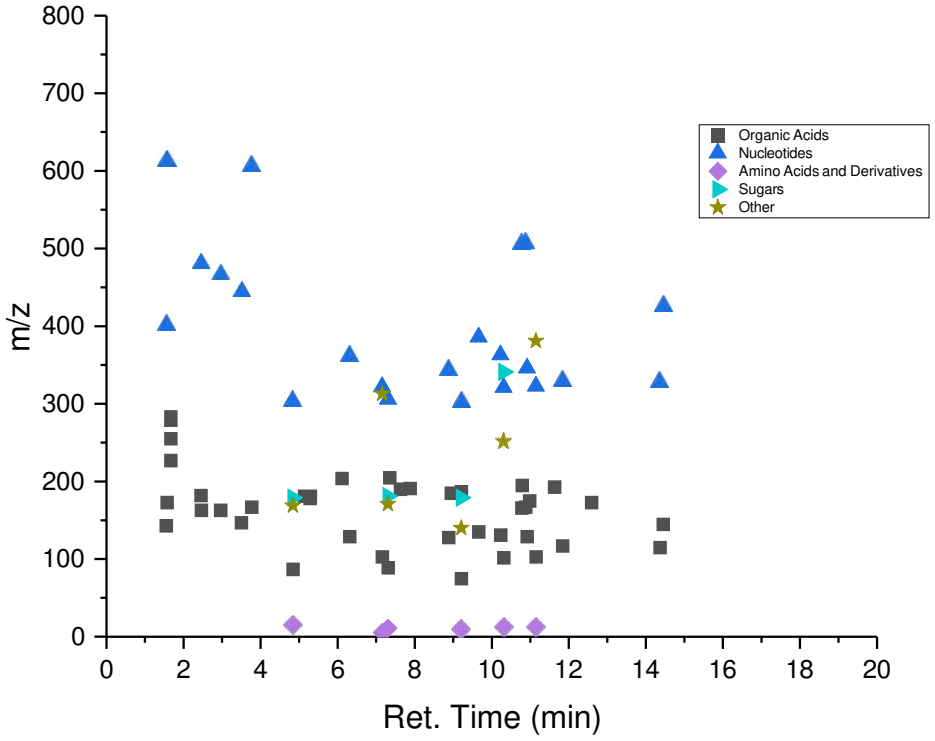

Fig. S-4B. BEH-Amide metabolite distribution in negative ionization mode

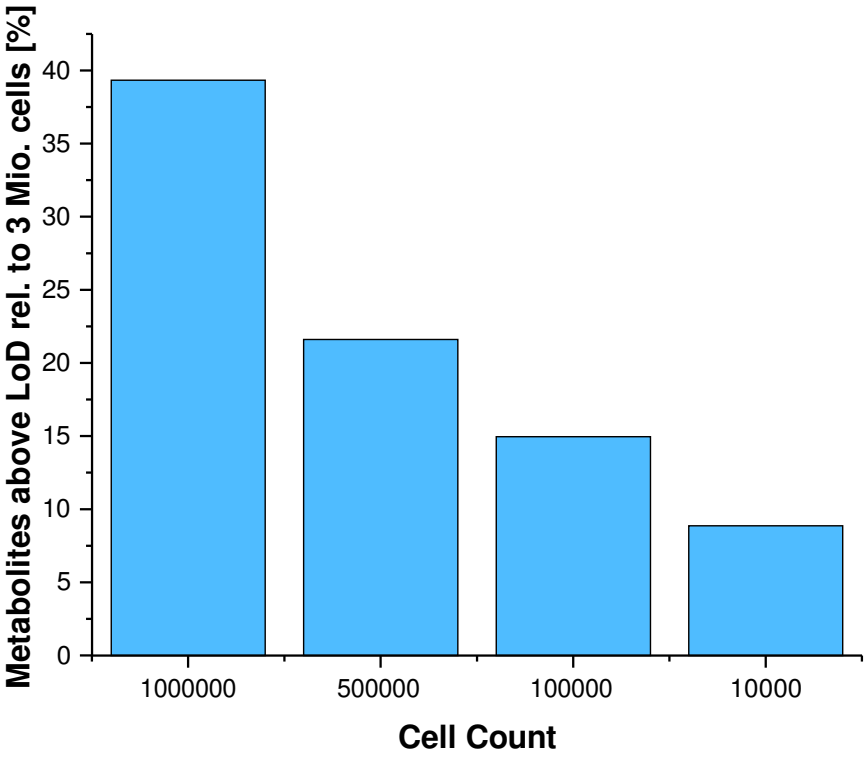

Fig. S-5. Metabolites detected above LoD in five different cell aliquots.

Journal of Chromatography A 1688 (2023) 463727

Contents lists available at ScienceDirect

Journal of Chromatography A

journal homepage: www.elsevier.com/locate/chroma

Isomer selectivity of one- and two-dimensional approaches of mixed-mode and hydrophilic interaction liquid chromatography coupled to tandem mass spectrometry for sugar phosphates of glycolysis and pentose phosphate pathways

Min Su[1], Kristian Serafimov[1], Peng Li, Cornelius Knappe, Michael Lämmerhofer*

Pharmaceutical (Bio-)Analysis, Institute of Pharmaceutical Sciences, University of Tübingen, Auf der Morgenstelle 8, Tübingen 72076, Germany

a r t i c l e i n f o

Article history:
Received 2 August 2022
Revised 16 December 2022
Accepted 17 December 2022
Available online 18 December 2022

Keywords:
Metabolomics
Sugar phosphates
Mixed-mode chromatography
HILIC
Two-dimensional liquid chromatography

a b s t r a c t

In this study, the chromatographic behavior of mixed-mode and hydrophilic interaction liquid chromatography (HILIC) with the mixed-mode HILIC/strong anion-exchange (SAX) column HILICpak VT-50 2D and the two HILIC columns Atlantis Premier BEH Z-HILIC and Acquity Premier BEH Amide was assessed with regard to their separation capability of the metabolites from the glycolysis and pentose phosphate pathways. Chromatographic conditions were evaluated with the aim of achieving separation of the isomeric glycolytic phosphorylated carbohydrate metabolites free from isomeric interferences and thus allowing for selective targeted analysis by liquid chromatography with tandem mass spectrometry (MS/MS) using multiple reaction monitoring acquisition. The effects of pH values (8.0/9.0/10.0) of the ammonium bicarbonate buffer and gradient time were investigated during HILIC-MS/MS analysis, with the optimal conditions found at pH = 10.0. Separation of the pentose phosphate isomers (ribose 5- and 1-phosphate, xylulose 5-phosphate and ribulose 5-phosphate) was achieved on the mixed-mode HILIC/SAX (HILICpak VT-50 2D) column and HILIC BEH Amide column. Column performance was evaluated based on the direct comparison of chromatographic parameters, i.e. peak width at 50% and peak tailing factors of the individual metabolites. Parity plots were generated allowing a direct comparison between the normalized retention times and assessment of orthogonality of all 3 stationary phases evaluated. Separation of 7 biologically relevant hexose monophosphates metabolites turned out to be challenging by HILIC-MS/MS, with the BEH Amide providing the best individual results for such a separation. However, fructose 6-phosphate and glucose 1-phosphate co-eluted. Therefore, an on-line heart-cutting HILIC-Mixed Mode 2D-LC-QToF experiment was conducted, allowing the separation of this critical isomer pair. In this setup, the BEH Amide column in the ^{1}D separated the majority of target metabolites, while a heart-cut of the peak from totally coeluted fructose 6-phosphate and glucose 1-phosphate was separated in the ^{2}D with HILICpak VT50-2D column, thus allowing undisturbed determination of the glycolytic phosphorylated carbohydrate metabolites due to their chromatographic separation from hexose monophosphate metabolites. The assay specificity towards 7 common hexose monophosphates was characterized (glucose 1- and 6-phosphate, galactose 1- and 6-phosphate, fructose 6-phosphate, mannose 1- and 6-phosphate). The selectivity of some rare hexose monophosphates (allose 6-phosphate, tagatose 6-phosphate, sorbose 1-phosphate) was also tested.

© 2022 Elsevier B.V. All rights reserved.

1. Introduction

Sugar phosphates (SPx) are phosphoric acid esters of monosaccharides, which play crucial roles in biological systems. They are the major constituents in the central hub of energy metabolism including glycolysis and pentose phosphate pathway (PPP), whereby the former is feeding into the tricarboxylic acid cycle (TCA) (see Fig. 1, in modified form from KEGG [1]). Thus, SPx participate in generating, storing and transferring energy. They also provide building blocks for key biomolecules such as nucleic acids and polysaccharides. Glycolysis is the conduit of glucose metabolism involving the catabolism of glucose to pyruvate, which is in turn decarboxylated and oxidized to produce acetyl-coenzyme A (CoA) for either further oxidation in the TCA cycle or biosynthesis of cell

* Corresponding author.
E-mail address: michael.laemmerhofer@uni-tuebingen.de (M. Lämmerhofer).
[1] Shared first authorship

https://doi.org/10.1016/j.chroma.2022.463727
0021-9673/© 2022 Elsevier B.V. All rights reserved.

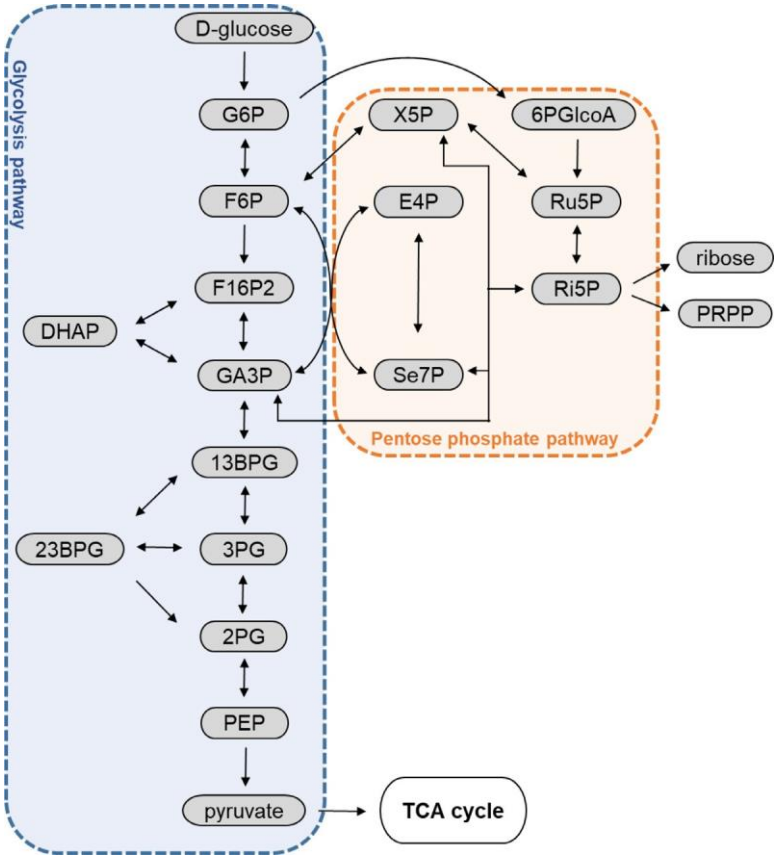

Fig. 1. Sugar phosphates (SPx) and related metabolites of glycolysis pathway and pentose phosphate pathway (in modified form from KEGG [1]).

constituents and metabolites [2]. As alternative pathway to glycolysis, in the irreversible oxidative phase of PPP, ribose 5-phosphate is generated by oxidation of glucose 6-phosphate, and NADPH is formed simultaneously. Subsequently, the reversible non-oxidative stage starts with interconverting SPx into ribose and phosphoribosyl pyrophosphate (PRPP), which are essential precursors of histidine and purine/pyrimidine nucleotides biosynthesis [3]. Increased flux in glycolysis *in vivo* is a biochemical fingerprint of cancer cells [4], as cancer cells can activate glycolysis in the absence of oxygen to meet their high energy demand (switch from aerobic to anaerobic energy production). The phenomenon is also known as The Warburg Effect [5]. According to the studies of Kauffman et al., the levels of SPx in the PPP were measured in cerebral tissue of mice after periods of ischemia, anesthesia by phenobarbital, hyperthermia, hypothermia, and iodoacetate and fluoroacetate way in brain poisoning, and were found altered dramatically [6]. The comprehensive separation of those biologically relevant SPx forms the basis for investigating and monitoring those pathways of central carbon metabolism.

The separation of phosphorylated sugar isomers is extremely challenging and an area of active investigation, and various unique and sensitive techniques have been employed. Generally, the methods of choice for separating the SPx have been mainly capillary electrophoresis (CE) [7,8], gas chromatography (GC) [9,10], and liquid chromatography (LC) [11,12] hyphenated to mass spectrometry (MS) as the detector. Benefiting from the multi-target coverage, sensitivity, robustness, high efficiency, and ease-of-use, LC-MS has emerged as the most powerful technique for profiling SPx benefitting from LC selectivity for isomers [13]. As one of the most important tools in the chromatographer's armory, reversed-phase (RP) suffers drawbacks in SPx separation due to its poor retention of those highly polar metabolites. The state-of-art LC-MS methods establishing separation of SPx involve anion exchange chromatography (AEX) [14–16], hydrophilic interaction liquid chromatography (HILIC) [17], ion pairing RPLC (IP-RPLC) [18,19], and more specifically porous graphitic carbon (PGC) and mixed-mode chromatography (MMC) [20–22]. AEX utilizes the electrostatic interaction between the cationic stationary phase and the oppositely charged phosphorylated carbohydrate analytes for retention, which turned out to be a valuable approach for addressing polar ionic or ionizable metabolites [23]. However, efficient counterions, e g, phosphates, are required for elution. If volatile counterions are used such as ammonium acetate, high concentrations are required which are not well compatible with ESI-MS. To eliminate the ion suppression and ion source contamination resulting from high concentration of buffer additives (electrolytes), the additional setup such as electrolytic suppressor prior to MS is required [16,24]. The hydrophilic interaction between analytes and immobilized thin water layer governs the retention of HILIC [25,26], possibly supported by adsorptive interactions (H-bonding, dipole, electrostatic). Nevertheless, HILIC suffers the drawback of poor peak shape when multiple phosphorylated sugars are of interest. The IP-based methods have the advantage over other chromatography modes that the peak tailing problem, which arises from the strong adhesion of phosphates group to glassware and stainless steel, is to some extent resolved [27–29]. Mathon et al. evaluated methylphosphonic acid as competitive reagent to the HILIC mobile phase to achieve the separation of eight SPx with good efficiency and peak shape [30]; however, ion suppression in ESI-MS is inevitable with this nonvolatile additive. To cope with the above-mentioned analytical challenges in SPx, chemical derivatization-based methods were established [31–35]. In spite of these benefits, they have the disadvantage of being laborious and causing hydrolysis of phosphoester groups in the course of the chemical reaction.

Herein, this study reports two different LC modes, MMC and HILIC, with three different columns, the mixed-mode HILIC/SAX (HILICpak VT-50 2D) and two HILIC hybrid organic/inorganic surface (Premier) technology columns (Z-HILIC and BEH Amide), for separating SPx from pentose phosphate and glycolysis pathway focusing in particular on a thorough investigation of the selectivity between the isomeric/isobaric hexose monophosphates (HMP) and pentose monophosphates (PMP). Besides focusing on optimizing selectivity of critical isomeric peaks of the targeted metabolites (Fig. 1), assay specificity against potential interferences and some other less common isomeric analogs was thoroughly evaluated. Furthermore, peak performances were statistically evaluated as another criterion for column selection. Column coupling was finally evaluated as an option to achieve a full separation of all major biologically important HMPs. While in the above discussed state-of-the-art workflows [13–24] several of the targeted isomeric sugar phosphates showed adequate selectivity, these works fall short in investigating assay specificity for a wide range of potential isomeric interferences. To our knowledge, the present work investigates isomeric selectivity for the largest number of isomeric sugar phosphates including many that can be present in biological samples but are usually ignored. While the present paper does not provide a final validated method, it should raise the awareness that it is insufficient to test selectivity of the glycolytic target isomers (e.g. F6P and G6P) only, but needs thorough assay specificity evaluation towards many other biologically relevant potential isomeric interferences as well.

2. Materials and methods

2.1. Materials

Methanol and acetonitrile of Ultra-LC-MS grade were supplied by Carl Roth (Karlsruhe, Germany). Ammonium formate (NH_4FA), ammonium bicarbonate (NH_4HCO_3), ammonium hydroxide solution (NH_4OH, ~25% NH3), were supplied by Sigma–Aldrich (Taufkirchen, Germany). Ultrapure water for LC-MS was obtained by purification of demineralized water by a Purelab Ultra purification system (ELGA LabWater, Celle, Germany).

2.2. SPx standards

α-D-Glucose 1-phosphate disodium salt hydrate (G1P), D-glucose 6-phosphate sodium salt (G6P), D-fructose 6-phosphate disodium salt hydrate (F6P), D-mannose 6-phosphate disodium salt hydrate (M6P), α-D(+)-mannose 1-phosphate sodium salt hydrate (M1P), α-D-galactose 1-phosphate dipotassium salt pentahydrate (Gal1P), D-galactose 6-phosphate lithium salt (Gal6P), L-sorbose-1-phosphate lithium salt (Sor1P), D-tagatose 6-phosphate lithium salt (Tag6P), D-fructose 1,6-bisphosphate trisodium salt hydrate (F16P2), L-glyceraldehyde-3-phosphate solution (GA3P, 8-12 mg/ml in H_2O), 2,3-bisphospho-D-glycerate (23BPG), D-(−)-3-phosphoglyceric acid disodium salt (3PG), D(+)-2-phosphoglyceric acid sodium salt hydrate (2PG), phospho(enol)pyruvic acid monopotassium salt (PEP), sodium pyruvate (Pyr), sodium L-lactate (Lac), 6-phosphogluconic acid trisodium salt (6PGlcoA), D-xylulose 5-phosphate lithium salt (X5P), D-ribose 5-phosphate disodium (Ri5P), D-ribose 1-phosphate bis(cyclohexylammonium) salt (Ri1P), D-ribulose 5-phosphate disodium salt (Ru5P), and D-sedoheptulose 7-phosphate lithium salt (Se7P) were supplied by Sigma-Aldrich (Taufkirchen, Germany). Glycerone phosphate dilithium salt (dihydroxyacetone phosphate, DHAP) and allose 6-phosphate (A6P) were obtained from BioZol (Eching, Germany). Standards were dissolved in acetonitrile-water (50:50; v/v) to give stock solutions of 100 µg/mL. All solutions were kept at -20°C until further use.

2.3. HPLC-ESI-QTrap-MS/MS analysis with SRM acquisition

Chromatographic separation was performed on a 1290 Infinity UHPLC system (Agilent Technologies, Waldbronn, Germany) with a binary pump (G4220A), multisampler (G7167B) cooled to 4°C, and thermostatted column compartment (G1316A). For detection, the chromatographic system was hyphenated to a 4500 QTrap mass spectrometer equipped with a Turbo V source (Sciex, Framingham, MA, USA) operated by an ESI probe (TurboIonspray) in negative ion mode. Ion source parameters were as follows: nebulizer gas (GS1, zero grade air) 30 psi, heater gas (GS2, zero grade air) 30 psi, curtain gas (CUR, nitrogen) 35 psi, source temperature (TEM) 400°C, ion source voltage -4500 V. SRM transitions and compound dependent parameters for analytes are summarized in Table 1.

The chromatographic separations were performed with three columns under the following conditions:

(1) HILICpak VT-50 2D column (5 µm, 2.0 × 150 mm, Shodex, supplied by Showa Denko Europe, Munich, Germany). Mobile phase A was 20 mM ammonium formate in water, mobile phase B was methanol. The gradient elution (0.0 min, 20% B; 3.0 min, 20% B; 13 min, 5% B; 20 min, 5% B; 20.1 min, 20% B; 30 min, 20% B) was carried out at a flow rate of 0.2 mL/min with a constant column temperature of 60°C. Five µL of mixed and individual standards of 10 HMP (G1P, G6P, F6P, M6P, M1P, Gal1P, Gal6P, Sor1P, Tag6P, and A6P) and 4 pentose sugar phosphates (X5P, Ri5P, Ri1P, and Ru5P) were injected.
(2) Atlantis Premier BEH Z-HILIC column (pre-equipped with a VanGuard FIT guard-column) (1.7 µm, 2.1 × 150 mm, Waters, Eschborn, Germany). Mobile phase A and mobile phase B were adjusted to a pH of 10.0 with ammonia and consisted of 10 mM ammonium bicarbonate in water (mobile phase A) and 10 mM ammonium bicarbonate in water/acetonitrile (10:90; v/v), respectively. The gradient elution (0.0 min, 90% B; 17.0 min 82.5% B; 18.0 min 82.5% B; 18.1 min 90% B; 30.0 min 90% B) was carried out at a flow rate of 0.4 mL min^{-1} and a constant column temperature of 35°C was maintained throughout the entire run. The mixed standards of 22 (SPx and some other) related metabolites (G1P, G6P, F6P, M1P, M6P, Gal1P, Gal6P, X5P, Ri5P, Ri1P, Ru5P, GA3P, DHAP, F16P2, 23BPG, 3PG, 2PG, PEP, Pyr, Lac, 6PGlCoA, and Se7P) were injected. For the total mixture of all analytes after mixing, the solution containing the individual standard stocks was lyophilized and reconstituted in acetonitrile to obtain a solution with a cocncentration of 10 µg mL^{-1}. Injection volume was 5 µL.
(3) Acquity Premier BEH Amide column (1.7 µm, 2.1 × 150 mm, Waters). The chromatographic conditions were the same as the ones for Z-HILIC column specified above. Five µL of the same mixture as the one for Z-HILIC column was injected.

2.4. HILIC-mixed mode heart cutting 2D-LC-QToF-MS

A 1290 Infinity II 2D-LC Solution from Agilent Technologies (Waldbronn, Germany) was used for heart-cutting 2D-LC. The first dimension (^{1}D) LC system consisted of a binary high-pressure gradient UHPLC pump (High Speed Pump, G7120A), a Multisampler (G7167B), a Multicolumn Thermostat (G7116B), a diode array detector (G7117B) with 1 µL flow cell (G4212-60008) and a pressure release kit (G4236-60010) between UV-detector and 2D-interface. The second dimension (^{2}D) LC system comprised a binary high-pressure gradient UHPLC pump (High Speed Pump, G7120A), a valve drive (G1170A) with a 5 position/10 port 2D-LC active solvent modulation (ASM) valve (5067e4266) connected to two 6 position/14 port valve heads (5067e4142) carrying six 40 µL loops each and a multicolumn thermostat (G7116B). Experiments utilizing active solvent modulation (ASM) were performed with the ASM

Table 1
SRM transitions and compound specific MS parameters (dt, dwell time; DP, declustering potential; EP, entrance potential; CE, collision energy; CXP, collision cell exit potential).

SPx	Q1, *m/z*	Q3, *m/z*	Dt, ms	DP, V	EP, V	CE, V	CXP, V
HMP-1	259.3	79	20	-40	-10	-50	-10
HMP-2	259.3	97	20	-40	-10	-22	-10
F16P2-1	339.0	79	20	-10	-10	-70	-10
F16P2-2	339.0	97	20	-10	-10	-23	-15
GA3P/DHAP -1	169.0	79	20	-60	-10	-30	-10
GA3P/DHAP -2	169.0	97	20	-60	-10	-12	-15
3PG/2PG-1	185.0	79	20	-20	-10	-35	-10
3PG/2PG-2	185.0	97	20	-20	-10	-20	-10
PEP-1	167.0	79	20	-30	-10	-50	-10
PEP-2	167.0	97	20	-30	-10	-20	-10
6PGlcoA-1	275.0	79	20	-20	-10	-60	-12
6PGlcoA-2	275.0	97	20	-20	-10	-23	-15
Se7P-1	289.0	79	20	-40	-10	-60	-15
Se7P-2	289.0	97	20	-40	-10	-20	-8
PMP-1	229.0	79	20	-30	-10	-40	-10
PMP-2	229.0	97	20	-30	-10	-15	-15
23BPG-1	265.0	79	20	-40	-10	-50	-15
23BPG-2	265.0	167	20	-40	-10	-16	-10
Pyruvate-1	87.0	32	20	-20	-10	-12	-8
Pyruvate-2	87.0	43	20	-20	-10	-10	-10
Lactate-1	89.0	43	20	-30	-10	-18	-8
Lactate-2	89.0	45	20	-30	-10	-12	-10

factor 5.5 (split ratio 1:4) restriction capillary (85 × 0.12 mm, 0.96 μL). For detection, the effluent from the ^{2}D column was directed to a TripleTOF 5600+ QTOF mass spectrometer from Sciex (Concord, Ontario, Canada). The exact experimental setup is displayed in Fig. 8. The acquisition rates were set to 40 Hz in the ^{1}D for the DAD. MS data acquisition and analysis was performed with Analyst TF 1.7 and PeakView software (Sciex), respectively. Multiple heart-cutting with time-based sampling was chosen as a 2D-LC measurement mode. The BEH Amide 150 × 2.1 mm, 1.7 μm column was used in the first dimension, whereas the HILICpak VT50 2D 150 × 2.0 mm, 5μm was employed as the second dimension column. The sampling table was created beforehand in accordance to a 1D reference chromatogram with the ^{1}D separation method (BEH Amide). Sampling time was 4.8 s. The mixed standard of G1P, F6P, Gal1P, M1P, M6P, G6P and Gal6P was injected and it was prepared from diluting the individual stock solutions with acetonitrile to obtain the concentration of 10 μg mL^{-1}. Multisampler Injection volume was 5 μL and constant column compartment temperature in first dimensions was held at 35 °C, in second dimension the column temperature was 60°C. Chromatographic conditions in both dimensions were as described in section 2.3. During the 2D-LC experiment, the following MS instrument parameters were used: curtain gas (CUR) 30 psi, ion source gas (nebulizing gas; GS1) 50 psi, heater gas (drying gas; GS2) 30 psi, ion spray floating voltage (ISVF) -4500 V, source temperature (TEM) 450°C and declustering potential (DP) 100 V. Data acquisition was performed in information-dependent acquisition (IDA) in high sensitivity mode and the mass range of the TOF-MS full scan comprised m/z 70 - 1000 with an accumulation time of 250 ms and a collision energy (CE) of 5 V. MS/MS in IDA (top 4) was performed with -30 V CE and 20 V CE spread (CES) and an accumulation time of 100 ms. Mass calibration was conducted with the Calibrant Delivery System through the ESI inlet using the negative calibration solution for the SCIEX X500 System.

2.5. Data processing

Analyst 1.7 was employed for data acquisition and LC-MS system control. PeakView 2.2 was used for ion intensities extraction from the raw data files and for further data evaluation. MultiQuant 3.0 and Origin 2021 (OriginLab, Northampton, MA, USA) were used for generating parity plots and distributions of peak widths and tailing factors.

3. Results and discussion

3.1. SPx separation on a mixed-mode column

The mixed-mode HILIC/SAX (Shodex HILICpak VT-50 2D) column was the first one employed in this study for separating SPx. It is packed with 5 μm polymer particles modified with polyvinyl alcohol carrying quaternary ammonium as the basic ion-pairing group. The polymer-based packing material provides decent chemical stability, and furthermore, owing to utilizing PEEK as housing material, this column is able to minimize the adhesion of phosphate groups to the column hardware.

LC conditions were optimized in terms of buffer, organic modifier, and pH value (shown in suppl. Fig. S1 -S3 along with a short description about the optimization) to examine the impact of these factors on the chromatographic separation of SPx. With the optimal chromatographic condition (20 mM NH_4FA in aqueous phase; MeOH as organic modifier, column temperature of 60°C), the mixed-mode column showed reasonable selectivity for several isomers but fell short in separating all ten hexose SPx tested. Fig. 2A and Fig. 2B depict the chromatographic separation of ten hexose SPx as mixed and individual injections, respectively. Considering the relevant glycolytic metabolites G6P and F6P only, they are at least partially separated from each other. However, M6P (described as unique S.cerevisiae (yeast) metabolite [35]) represents an interference for F6P and G6P is only partially resolved from Gal6P. A6P, which coelutes with G6P, should be of less relevance for bioanalysis of mammalian systems as this metabolite is characteristic for E.coli according to PathBank. Similarly, a partial separation of the PMP isomers including Ri5P, X5P, Ru5P, and Ri1P was also achieved with critical isomers for X5P and Ru5P. The mixed injection of those four isomeric pentose SPx is shown in Fig. 2C, while the separation as individual injections are shown in Fig. 2D. All 3 pentose phosphate metabolites from the pentose phosphate pathway (Ri5P, Ru5P, X5P) are partially separated from each other as well as from Ri1P, a metabolite of relevance as intermediate in nucleotide metabolism and biosynthesis, respectively. Other metabolites with more than one polar function such

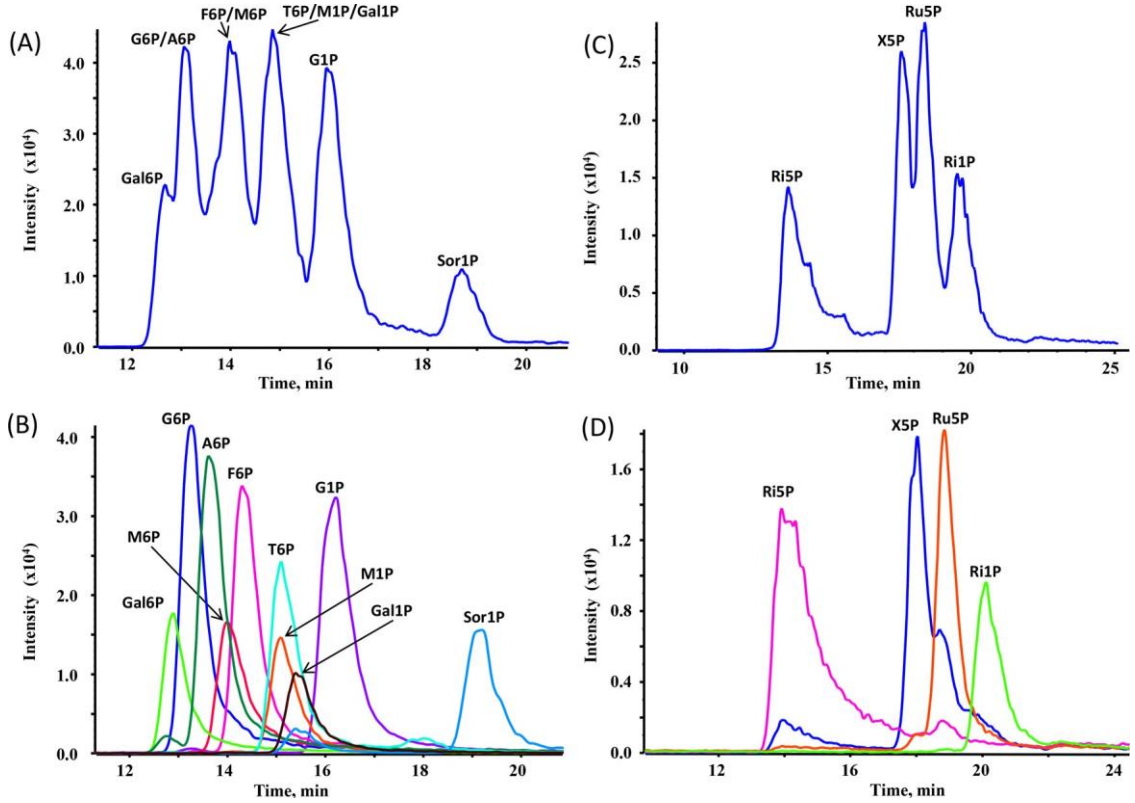

Fig. 2. SPx isomer separations by HILIC/SAX mixed-mode chromatography (HILICpak VT-50 2D column). Chromatograms showing the separation of hexose sugar phosphates as a mixture of all (A) and as individually injected standards (B). Pentose sugar phosphates analogous as a mixture (C) and as individual injections of reference compounds (D) on the mixed mode column. Chromatographic conditions employed were as described in Section 2.3.

as 2,3-BPG could not be eluted even with 90% of aqueous mobile phase. Moreover, the notable peak tailing resulting from the complex retention mechanism (relatively slow kinetics of ion-exchange compared to RPLC) and the peculiarity of phosphorylated carbohydrates was also inevitable. While this HILICpak VT-50 2D mixed-mode column shows exceptional selectivity for the isomers of SPx, it is of disadvantage that this mixed-mode stationary is only available with 5 µm particle diameter and no sub-2µm or core-shell UHPLC version is available which could result in even better resolutions.

3.2. SPx separation on a BEH Z-HILIC column

Based on rugged ethylene bridged hybrid (BEH) silica particles, the new sub-2 µm Atlantis Premier BEH Z-HILIC column is able to maintain high performance from pH 2 -10. This stationary phase was packed into column hardware with metal frits modified with high-performance surface coating, viz. hybrid organic/inorganic surface (Premier) technology, to minimize the interactions of the phosphorylated analytes (such as sugar phosphates) with metal surfaces [36]. It is known that these compounds tend to interact with stainless steel surfaces of LC systems and the inner wall of electrospray probes leading to partly irreversible adsorption and even loss of analytes [27–29]. Hence, better performance, especially less tailing, was expected for the Premier columns.

Three different alkaline buffer pH values (pH 8, 9 and 10) were evaluated in HILIC gradient elution mode on this Z-HILIC column to separate SPx of the central carbon metabolism, in which 10 mM NH_4HCO_3 was used as buffer additive (Fig. S4, S5 and Fig. 3). Under alkaline conditions, α/β-anomer interconversion (of SPx with free hemiacetal function) is fast so that anomers elute in a single peak which simplifies the SPx isomer analysis. Under evaluated conditions, pH 10 gave the best chromatographic separation of HMP isomers. Fig. 3 shows the chromatograms of hexose and pentose SPx at an eluent pH value of 10. A6P, Tag6P and Sorb1P are of less relevance for bioanalysis of mammalian systems, therefore they were not included in this method. Although adequate separation of all hexose SPx was not achieved, as shown in Fig. 3A, there is a full baseline separation between the two glycolytic metabolites G6P and F6P. Unfortunately, Gal6P coelutes with G6P and Gal1P with F6P. G1P is at least partially resolved from F6P. Gal1P is an intermediate in the interconversion of glucose and uridine diphosphate galactose and exists in all living species, including bacteria, plants and humans [35]. The peak shape was significantly improved due to smaller particle diameter (1.7 µm for Z-HILIC vs 5 µm for HILICpak VT-50 2D) presumably also as a result of the Premier column hardware technology. Concerning the isomeric metabolites of pentose SPx, only Ri5P could be fully separated from the other isomers, yet the peak tailing might still slightly interfere in quantitative analysis (Fig. 3C, 3D). Finally, the separation performance of other metabolites of the glycolysis pathway and pentose phosphate pathway was evaluated (Fig. S-6). Except for 3PG all other analytes (pyruvate, lactate, 23PG, 6PGlcoA, 2PG, F16P2, Se7P, PEP, DHAP, and GAP3) showed an acceptable peak shape and eluted within the gradient under these conditions.

3.3. SPx separation on a BEH amide column

The third column evaluated for the separation of the phosphorylated metabolites is a new sub-2 µm UHPLC-HILIC column (Premium BEH Amide) based on the ethylene-bridged hybrid organic/inorganic silica chemistry, which is stable from pH 2-10, with high-performance surface coating of column hardware.

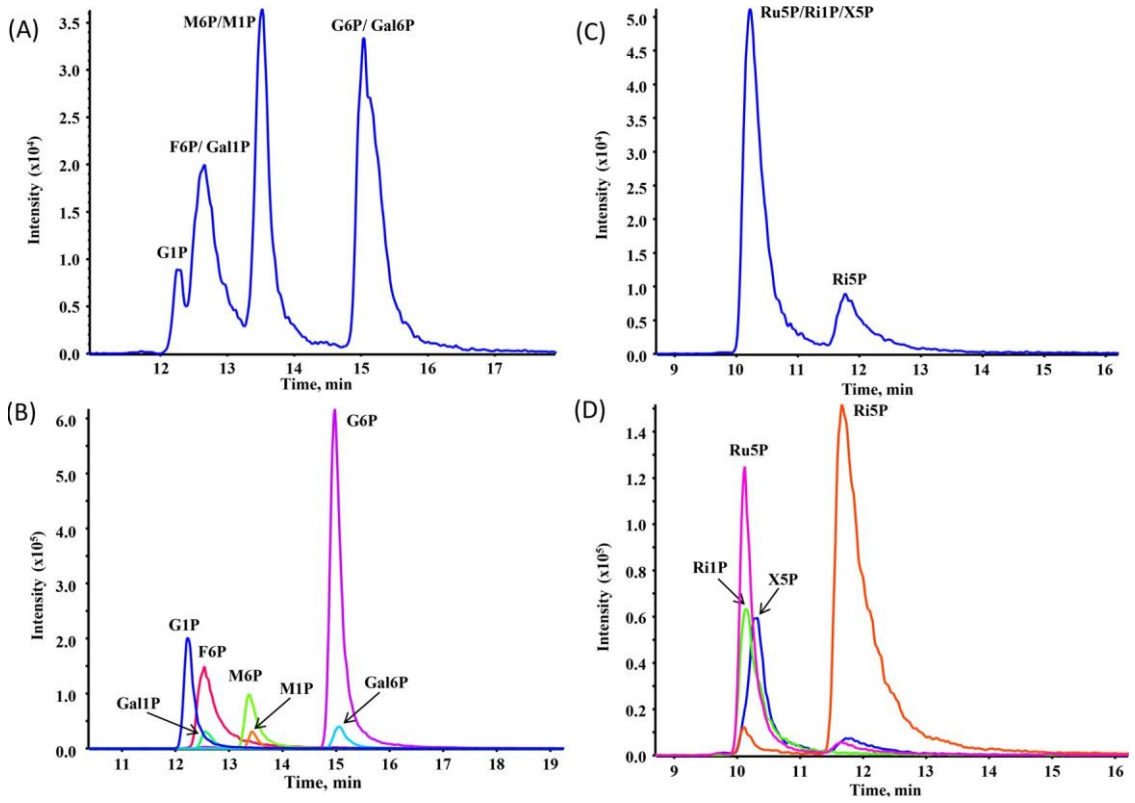

Fig. 3. SPx isomer separations by HILIC (Atlantis Premium BEH Z-HILIC column). Chromatograms showing the separation of hexose sugar phosphates as a mixture of all (A) and as individually injected standards (B). Pentose sugar phosphates analogous as a mixture (C) and as individual injections of reference compounds (D) on BEH Z-HILIC column at a pH value of 10. Chromatographic conditions employed were as described in Section 2.3.

Three different buffer pH values were evaluated to determine the effects on the chromatographic separation of the target metabolites. The pH was adjusted to 8.0, 9.0 or 10.0, whilst the buffer concentration was kept constant at 10 mM NH_4HCO_3 (chromatograms for different pH values are shown in the supplementary material as Fig. S-7, Fig. S-8 and Fig. 8). Optimal chromatographic conditions for the separation of the mixture of the 7 most important isomeric HMPs performed best at a pH value of 10.0 (Fig. 4A). Individual injections of ten HMP metabolite standards with such mobile phase are shown in Fig. 4B. The glycolytic metabolite pairs G6P and F6P were fully separated from each other, yet G1P coeluted with the latter. The two metabolites can only be determined as their sum with this method. Other isomeric glycolysis metabolite pairs such as GAP3/DHAP and metabolite pairs with potential isotopologue interferences such as Pyruvate/Lactate were also examined and fully separated, while simultaneously showing good peak shapes (Fig S-9). Bis-phosphorylated compounds such as 2,3-BPG and F16P2 were successfully eluted during the chromatographic run. It was, however, noticeable that diphosphates provided broader peaks, which can be attributed to the stronger interactions with the stationary phase, column hardware and chromatographic system (associated with slow kinetics). On this column, also 3PG gave acceptable peak shape, at least much better than on Z-HILIC columns (Figure S-9D). Metabolites from the pentose phosphate pathway were also further studied in terms of their chromatographic behavior. Significant improvements in separation of the isobaric Ru5P, X5P, Ri1P and Ri5P, compared to Z-HILIC, was observed by increasing the pH value to 10.0 (Fig. 4C and 4D) and all PMPs were partially resolved from each other. Again, like on the mixed-mode column, the critical isomers was found between Ru5P and X5P, which however, eluted in reversed order compared to HILIC/SAX. For these critical metabolites, the mixed-mode phase gave, however, better resolution. Chromatograms of the separation of the pentose phosphate pathway metabolites at pH 8.0 and 9.0 are further provided in the supplementary section (Fig. S-7B and Fig. S-8B).

3.4. Evaluation of column performance

Having determined the optimal chromatographic conditions for all 3 columns, their performance was compared by statistical evaluation of peak width, peak tailing factors and retention time distributions. Fig. 5A and 5B show violin plots representing the values for peak widths at half maximum and peak tailing factors of the PMPs and HMPs. From Fig. 5A, it becomes evident that the mixed mode column gave much higher peak width values when compared to the Z-HILIC and BEH Amide columns. This is not further surprising as the mixed mode column is based on 5 µm particles while the other two are UHPLC columns based on 1.7 µm BEH particles. The Z-HILIC and BEH Amide both performed relatively similar in terms of peak width, with the BEH Amide providing a slightly narrower distribution yet minimally larger median of the values. Peak tailing factors were also compared between the 3 columns. Both the mixed-mode and Z-HILIC columns provided a wider distribution than BEH Amide. The mixed mode column provided a lower variance, yet the median was higher than for the Z-HILIC column. The BEH Amide column outperformed both in terms of peak symmetry, as it provided the narrowest distribution with less analytes having a peak tailing factor above 1.5.

To assess the complementarity of the individual columns, parity plots for normalized retention times showing their correlations between 2 columns at a time are shown in Fig. 6A, 6B and 6C.

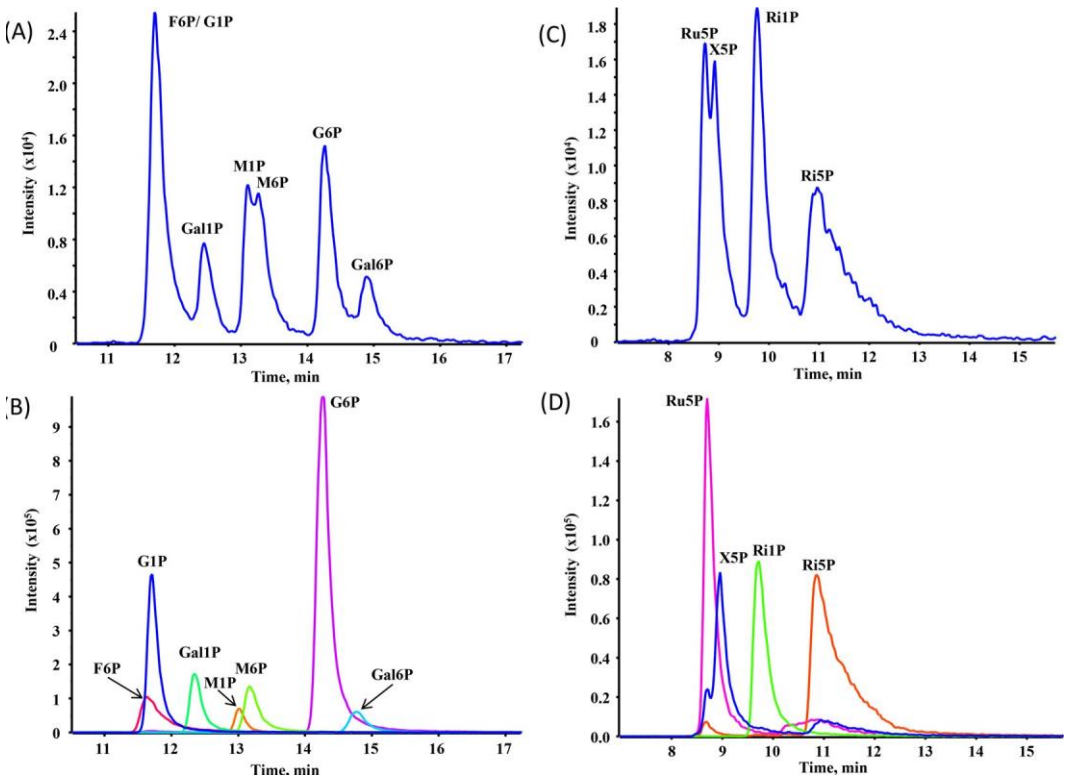

Fig. 4. SPx isomer separations by HILIC (Acquity Premium BEH Amide column). Chromatograms showing the separation of hexose sugar phosphates as a mixture of all (A) and as individually injected standards (B). Pentose sugar phosphates analogous as a mixture (C) and as individual injections of reference compounds (D) on BEH Amide column at a pH value of 10. Chromatographic conditions employed were as described in Section 2.3.

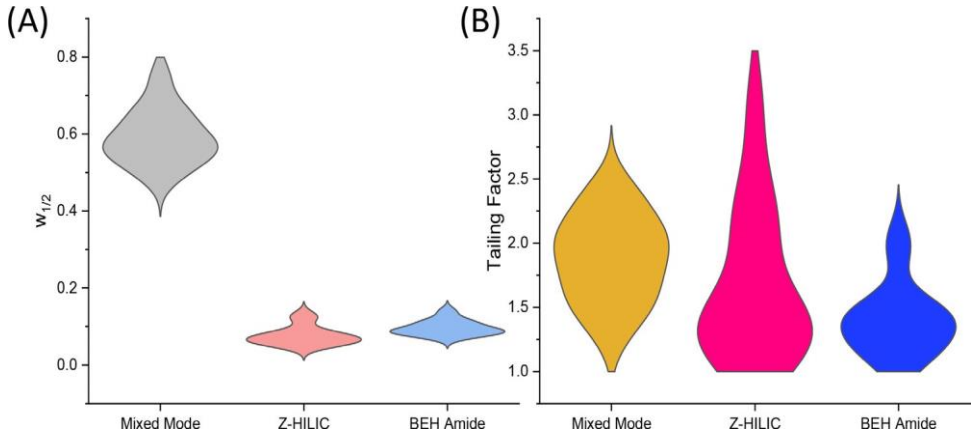

Fig. 5. Chromatographic performance of the evaluated columns for sugar phosphates. (A) Peak widths, (B) peak tailing factors. Chromatographic conditions as described in Section 2.3. Standards used are mentioned in Section 2.2 and the respective sMRM transitions can be found in Table 1.

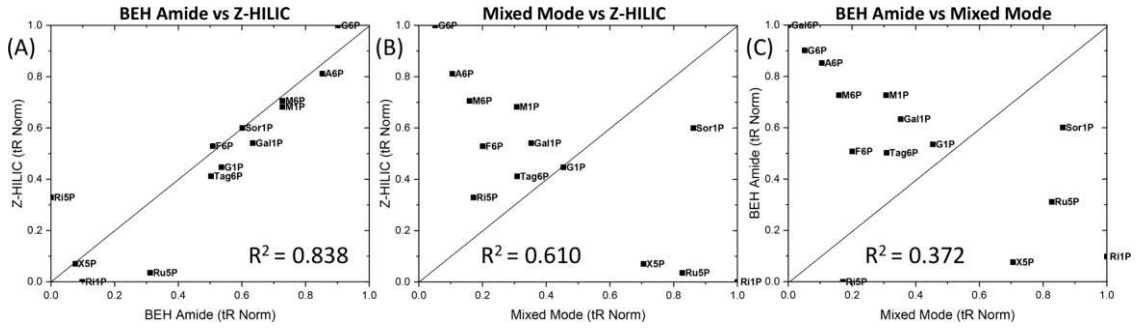

Fig. 6. Stationary phase orthogonality of tested mixed-mode and HILIC columns. Parity plot of normalized retention times on (A) Z-HILIC vs BEH Amide, (B) Z-HLIC vs Mixed Mode, and (C) BEH Amide vs Mixed Mode. Chromatographic conditions as described in Section 2.3.

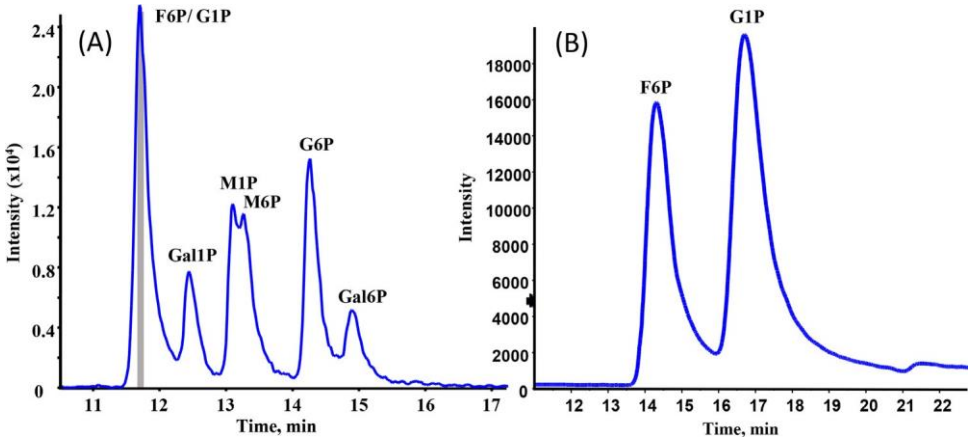

Fig. 7. On-line 2D-LC-QToF separation of F6P and G1P. A) Separation of HMP on the BEH Amide column ([1] D) showing also the heart-cut in the chromatogram (marked in gray). B) Separation ofF6P and G1P, which were co-eluted in the [1] D, but well resolvable on the second dimension HILICpak VT-50 2D column (time-based sampling based on prior [1]D chromatogram). Chromatographic conditions employed as described in 2.3.

Normalized retention times were calculated by eq. 1

$$t_{R,norm} = \frac{tR,x - tR,first}{tR,last - tR,first} \quad (1)$$

Wherein $t_{R,x}$, $t_{R,first}$ and $t_{R,last}$ represent the retention times of the respective SPx peak of interest, of the first and last eluted SPx, respectively. It is interesting to note that the highest correlation is observed between $t_{R,norm}$ of the two HILIC stationary phases, viz. BEH Amide and Z-HILIC (Fig. 6A). Although there is a strong correlation, some minor retention orthogonalities do exist (data points distant from the diagonal parity line). On contrary, the mixed-mode column is quite orthogonal to both HILIC columns and data points scatter distinctly in the 2D-retention space of the two complementary HILIC columns (cf. Fig. 6B and 6C). It may also be a result of the altered pH value in the mixed-mode separation in comparison to the HILIC separations.

Furthermore, gradient elution conditions were optimized with the Z-HILIC and BEH Amide columns, as they proved to be the best regarding chromatographic performance and were considered for further usage. Three different gradient times t_g were tested for both columns (8, 15 and 30 min) with the aim of obtaining higher resolution between the individual HMP peaks. Concerning Z-HILIC column, as shown in Fig. S-10, the increase of t_g yielded a minor improvement in selectivity of HMPs, while the sensitivity decreased. Similar results were observed for the PMPs (Fig. S-11A, Fig. S-11B, Fig. S-11C). For the case of the BEH Amide, it was observed that increasing the t_g provided better resolution between the HMPs, specifically the increase of t_g from 8 to 15 min showed a beneficial effect. Increasing the gradient time from 15 to 30 min led to a further improvement but at expense of run time (Fig. S-12A, Fig. S-12B, Fig. S-12C). PMPs were, however, almost fully baseline separated by increasing t_g to 30 min (Fig. S-13A, Fig. S-13B, Fig. S-13C).

3.5. Separation of HMPs by HILIC-mixed mode-2D-LC-QToF-MS

A multiple heart-cutting 2D-LC method with anion-exchange in the [1]D and porous graphitic carbon column in the [2]D for quantiative analysis of glycolytic metabolites by ESI-MS/MS detection was recently reported [37]. Based on the above experiments and obtained results, we decided to establish an on-line heart cutting HILIC-Mixed Mode 2D-LC-QToF experiment for the simultaneous LC separation of the 7 biologically most relevant HMP isomers. It was shown in Fig. 4A that the Acquity Premier BEH Amide column can resolve all HMP isomers except for F6P and G1P, which coeluted in one peak. This most critical peak pair, on the other hand was separated well on the HILICpak VT-50 2D (Fig. 2A). The latter was preferred over the Z-HILIC column, as better selectivity between the isobaric G1P and F6P was achieved. Hence, the Acquity Premier BEH-Amide and HILICpak VT50-2D columns, were successfully coupled using a 5-position/10-port valve with active solvent modulation (ASM) capability a 2D-LC interface between the two dimensions. This valve was equipped with two loop decks each with six 40 µL sample storage loops. For collecting the entire peak and enhancing the sensitivity, a sample storage loop with larger volume should be used. Alternatively, a new software version allows to simultaneously analyze the entire loop deck at once (multi-inject option). The effect is similar to the use of a larger loop resulting in higher sensitivity. The use of an ASM (active solvent modulation) valve was utilized to minimize solvent incompatibility between [1]D and [2]D, as the conditions between both dimensions differed (basic conditions with ammonium bicarbonate buffer in the [1]D and acidic conditions with ammonium formate in the [2]D). Herein, a 40 µL heartcut of the co-eluting F6P and G1P (first peak in the [1]D separation) (Fig. 7A) was transferred via a time-based heart-cutting experiment into the second dimension with the HILICpak VT50 2D column, which in turn provided the separation of the two compounds that were unresolved in the [1]D (Fig. 7B) (The instrumental setup of the 2D-LC system is shown in Fig. 8). The separation of Gal1P, M1P/M6P, G6P, and Gal6P could be maintained as can be seen in Fig. 7A. Details on the instrumental setup are described in Section 2.4. and the individual chromatographic conditions employed are provided in Section 2.3. The separation of all 7 biologically important HMPs achieved by this 2D-LC separation is shown in Fig. 7A and Fig. 7B (both representing the [1]D and [2]D separation). Using such heart-cutting 2D-LC setup, the glycolytic HMPs, F6P and G6P, can be resolved from potential isomeric interferences G1P, Gal1P, M1P/M6P and Gal6P, making a determination with adequate assay specificity possible. A second critical HMP isomer pair is M1P and M6P. These two compounds were only slightly separated during our experiments (with M1P eluting before M6P as shown in Fig. 7) and it needs further optimization if these isomers are of biological interest. Incomplete separations of carbohydrate isomers and quantifying the sum of specific isomers is quite commonly accepted in metabolomics [38]. Nonetheless, this work was performed to prepare the grounds for the development of an accurate quantitative assay

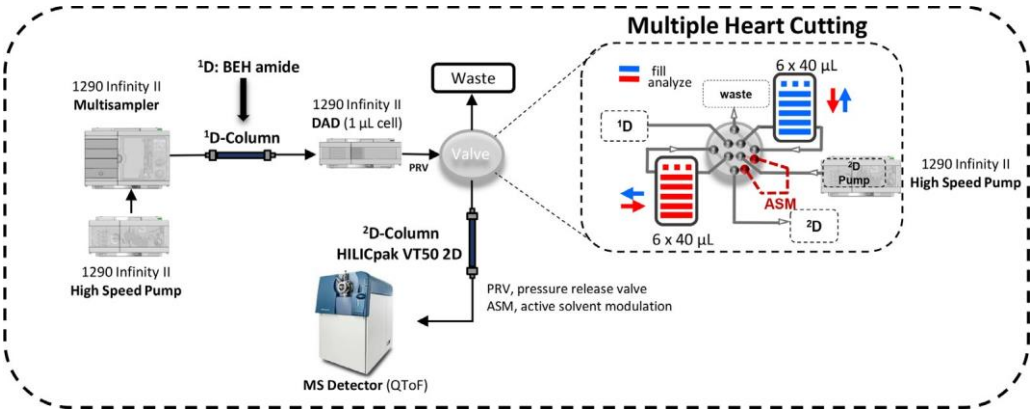

Fig. 8. Experimental setup of the on-line 2D-LC-QToF instrument used for the separation of the critical G1P/F6P isomer pair via HILIC-Mixed Mode-2D-LC-QToF-MS.

for glycolytic metabolites which is the next step of our ongoing research.

4. Conclusions

The analysis of SPx remains challenging due to problems in chromatographic separation and MS detection, including peak tailing, poor chromatographic retention in RP, and the presence of several isomers (i.e. isomeric interferences in the analysis of glycolytic hexose phosphates). In this study, three different LC modes hyphenated to tandem MS for separating SPx from central carbon metabolism were evaluated. The mixed-mode HILIC/SAX column exhibited largely adequate separation for pentose SPx isomers (X5P, Ri5P, Ri1P, and Ru5P) with partial resolution of the critical pair X5P/ Ru5P und full separation of the other two isomers. With Premier coating technology deactivating metal frits and other column hardware surfaces, the two BEH HILIC columns tested (Z-HILIC and Amide) offered largely satisfying peak shapes for SPx yet still significant tailing was observed. The Premier BEH Amide column showed the best behavior at a pH value of 10, at which no anomer peaks were observed, and also satisfactory selectivity except for F6P and G1P. A heartcut of the peak corresponding to those two overlapping metabolites was sampled into a storage and separated by complementary Mixed-mode (HILIC/SAX) LC using a HILIC-Mixed Mode 2D-LC-QToF experiment. Besides, the chromatographic behavior of other critical SPx from the glycolysis and pentose phosphate pathways were evaluated on the Premier BEH Amide column. As a conclusion, based on the currently performed systematic selectivity studies it was possible to derive that i) the Premium BEH Amide column provides the best separation of HMPs and PMPs, ii) the unresolved F6P/G1P critical peak pair can be well resolved on HILIC/SAX mixed-mode column, and iii) a 2D-LC-QToF heart cutting experiment combining the BEH Amide in the ^{1}D and HILICpak VT50-2D column in the ^{2}D allows to establish a method which provide adequate assay specificity to determine the glycolytic metabolites G6P and F6P without interferences from isomer hexose monophosphates. Some further improvements in peak shape should be possible by using biocompatible UHPLC systems or UHPLC instruments with high performance surface coating technology having inactivated surfaces in the flow path. The current work should raise the awareness that in quantitative analysis of glycolytic metabolites a number of isomeric metabolites have to be considered for assay specificity testing and not only the major glycolytic target metabolites G6P and F6P. This work prepared the grounds for a full method development to obtain a robust validated accurate assay for quantitative analysis of glycolytic sugar phosphate metabolites.

Declaration of Competing Interest

The authors declare that they have no known competing financial interests or personal relationships that could have appeared to influence the work reported in this paper.

CRediT authorship contribution statement

Min Su: Investigation, Methodology, Formal analysis, Data curation, Visualization, Writing – original draft, Writing – review & editing. **Kristian Serafimov:** Investigation, Methodology, Formal analysis, Data curation, Visualization, Writing – original draft, Writing – review & editing. **Peng Li:** Supervision, Writing – review & editing. **Cornelius Knappe:** Investigation, Methodology, Writing – review & editing. **Michael Lämmerhofer:** Conceptualization, Methodology, Supervision, Writing – review & editing, Resources, Funding acquisition.

Data availability

The data have been deposited in Mendeley Data and can be accessed under the following doi:10.17632/vw9b87j8k9.1.

Acknowledgments

We are grateful to Agilent Technologies for support of this research by an Agilent Research Award (#4068).

Supplementary materials

The data (i.e. retention times, peak widths, asymmetry factors and tailing factors) have been deposited in the public data repository Mendeley Data and can be accessed under the following doi: 10.17632/vw9b87j8k9.1.

Supplementary material associated with this article can be found, in the online version, at doi:10.1016/j.chroma.2022.463727.

References

[1] H. Ogata, S. Goto, K. Sato, W. Fujibuchi, H. Bono, M. Kanehisa, KEGG: Kyoto encyclopedia of genes and genomes, Nucleic Acids Res. 27 (1999) 29–34, doi:10.1093/nar/27.1.29.

[2] R.A. Harris, Glycolysis Overview, 2nd ed., Elsevier Inc., 2013, doi:10.1016/B978-0-12-378630-2.00044-X.

[3] M.M.C. Wamelink, E.A. Struys, J.H.J. Huck, B. Roos, M.S. Van Der Knaap, C. Jakobs, N.M. Verhoeven, Quantification of sugar phosphate intermediates of the pentose phosphate pathway by LC-MS/MS: application to two new inherited defects of metabolism, J. Chromatogr. B Anal. Technol. Biomed. Life Sci. 823 (2005) 18–25, doi:10.1016/j.jchromb.2005.01.001.

[4] S. Ganapathy-Kanniappan, J.-F.H. Geschwind, Tumor glycolysis as a target for cancer therapy: progress and prospects, 2013. http://www.molecular-cancer.com/content/12/1/152.

[5] M. Lopez-Lazaro, The warburg effect: why and how do cancer cells activate glycolysis in the presence of oxygen? Anticancer. Agents Med. Chem. 8 (2008) 305–312, doi:10.2174/187152008783961932.
[6] F.C. Kauffman, J.G. Brown, J.V. Passonneau, O.H. Lowry, Effects of changes in brain metabolism on levels of pentose phosphate pathway intermediates, J. Biol. Chem. 244 (1969) 3647–3653, doi:10.1016/s0021-9258(18)83418-4.
[7] J.P.M. Hui, J. Yang, J.S. Thorson, E.C. Soo, Selective detection of sugar phosphates by capillary electrophoresis/mass spectrometry and its application to an engineered E. coli host, (n.d.). 10.1002/cbic.200700116.
[8] G. Sonenshein, A.L. Yang, W.C. Sedlak, M. Regnier, F.E. Mosier, N. Ho, N. Adamec, O. Kopka Fiehn, J. Dormann, P. Altmann, T. Trethewey, R.N. Willmitzer, L. Plumb, Metabolomic profiling of anionic metabolites by capillary electrophoresis mass spectrometry, Proc. Natl. Acad. Sci. U.S.A. 5 (2007) 6165–6174, doi:10.1021/ac900675k.
[9] J.Y. Jung, M.K. Oh, Isotope labeling pattern study of central carbon metabolites using GC/MS, J. Chromatogr. B Anal. Technol. Biomed. Life Sci. 974 (2015) 101–108, doi:10.1016/j.jchromb.2014.10.033.
[10] D.B. Chu, C. Troyer, T. Mairinger, K. Ortmayr, S. Neubauer, G. Koellensperger, S. Hann, Isotopologue analysis of sugar phosphates in yeast cell extracts by gas chromatography chemical ionization time-of-flight mass spectrometry, Anal. Bioanal. Chem. 407 (2015) 2865–2875, doi:10.1007/s00216-015-8521-9.
[11] A. Buchholz, R. Takors, C. Wandrey, Quantification of intracellular metabolites in Escherichia coli K12 using liquid chromatographic-electrospray ionization tandem mass spectrometric techniques, Anal. Biochem. 295 (2001) 129–137, doi:10.1006/abio.2001.5183.
[12] P. Vizán, G. Alcarraz-Vizán, S. Díaz-Moralli, J.C. Rodríguez-Prados, M. Zanuy, J.J. Centelles, O. Jáuregui, M. Cascante, Quantification of intracellular phosphorylated carbohydrates in HT29 human colon adenocarcinoma cell line using liquid chromatography-electrospray ionization tandem mass spectrometry, Anal. Chem. 79 (2007) 5000–5005, doi:10.1021/ac070170v.
[13] J.M. Buescher, S. Moco, U. Sauer, N. Zamboni, Ultrahigh performance liquid chromatography-tandem mass spectrometry method for fast and robust quantification of anionic and aromatic metabolites, Anal. Chem. 82 (2010) 4403–4412, doi:10.1021/ac100101d.
[14] A.P. Alonso, R.J. Piasecki, Y. Wang, R.W. LaClair, Y. Shachar-Hill, Quantifying the labeling and the levels of plant cell wall precursors using ion chromatography tandem mass spectrometry, Plant Physiol. 153 (2010) 915–924, doi:10.1104/pp.110.155713.
[15] D.B. Chu, K. Klavins, G. Koellensperger, S. Hann, Speciation analysis of sugar phosphates via anion exchange chromatography combined with inductively coupled plasma dynamic reaction cell mass spectrometry-optimization for the analysis of yeast cell extracts, J. Anal. At. Spectrom. 29 (2014) 915–925, doi:10.1039/c4ja00043a.
[16] S. Hu, J. Wang, E.H. Ji, T. Christison, L. Lopez, Y. Huang, Targeted metabolomic analysis of head and neck cancer cells using high performance ion chromatography coupled with a Q exactive HF mass spectrometer, Anal. Chem. 87 (2015) 6371–6379, doi:10.1021/acs.analchem.5b01350.
[17] E. Iturrospe, K.M. Da Silva, B. Talavera Andújar, M. Cuykx, J. Boeckmans, T. Vanhaecke, A. Covaci, A.L.N. van Nuijs, An exploratory approach for an oriented development of an untargeted hydrophilic interaction liquid chromatography-mass spectrometry platform for polar metabolites in biological matrices, J. Chromatogr. A 1637 (2021) 461807, doi:10.1016/j.chroma.2020.461807.
[18] L. Coulier, R. Bas, S. Jespersen, E. Verheij, M.J. Van Der Werf, T. Hankemeier, Simultaneous quantitative analysis of metabolites using ion-pair liquid chromatography-electrospray ionization mass spectrometry, Anal. Chem. 78 (2006) 6573–6582, doi:10.1021/ac0607616.
[19] J. Wu, Y. Zhang, R. Wiegand, J. Wang, G. Bepler, J. Li, Quantitative analysis of intracellular nucleoside triphosphates and other polar metabolites using ion pair reversed-phase liquid chromatography coupled with tandem mass spectrometry, J. Chromatogr. B Anal. Technol. Biomed. Life Sci. 1006 (2015) 167–178, doi:10.1016/j.jchromb.2015.10.030.
[20] H. Hinterwirth, M. Lämmerhofer, B. Preinerstorfer, A. Gargano, R. Reischl, W. Bicker, O. Trapp, L. Brecker, W. Lindner, Selectivity issues in targeted metabolomics: Separation of phosphorylated carbohydrate isomers by mixed-mode hydrophilic interaction/weak anion exchange chromatography, J. Sep. Sci. 33 (2010) 3273–3282, doi:10.1002/jssc.201000412.
[21] J.H. Knox, B. Kaur, G.R. Millward, Structure and performance of porous graphitic carbon in liquid chromatography, J. Chromatogr. A 352 (1986) 3–25, doi:10.1016/S0021-9673(01)83368-9.
[22] C. Antonio, T. Larson, A. Gilday, I. Graham, E. Bergström, J. Thomas-Oates, Quantification of sugars and sugar phosphates in Arabidopsis thaliana tissues using porous graphitic carbon liquid chromatography-electrospray ionization mass spectrometry, J. Chromatogr. A 1172 (2007) 170–178, doi:10.1016/j.chroma.2007.10.011.
[23] J. Walsby-Tickle, J. Gannon, I. Hvinden, C. Bardella, M.I. Abboud, A. Nazeer, D. Hauton, E. Pires, T. Cadoux-Hudson, C.J. Schofield, J.S.O. McCullagh, Anion-exchange chromatography mass spectrometry provides extensive coverage of primary metabolic pathways revealing altered metabolism in IDH1 mutant cells, Commun. Biol. 3 (2020) 1–12, doi:10.1038/s42003-020-0957-6.
[24] M. Schwaiger, E. Rampler, G. Hermann, W. Miklos, W. Berger, G. Koellensperger, Anion-exchange chromatography coupled to high-resolution mass spectrometry: a powerful tool for merging targeted and non-targeted metabolomics, Anal. Chem. 89 (2017) 7667–7674, doi:10.1021/acs.analchem.7b01624.
[25] B. Buszewski, S. Noga, Hydrophilic interaction liquid chromatography (HILIC)-a powerful separation technique, Anal. Bioanal. Chem. 402 (2012) 231–247, doi:10.1007/s00216-011-5308-5.
[26] P. Hemström, K. Irgum, Hydrophilic interaction chromatography, 2006. 10.1002/jssc.200600199.
[27] A. Wakamatsu, K. Morimoto, M. Shimizu, S. Kudoh, A severe peak tailing of phosphate compounds caused by interaction with stainless steel used for liquid chromatography and electrospray mass spectrometry, J. Sep. Sci. 28 (2005) 1823–1830, doi:10.1002/jssc.200400027.
[28] Y. Asakawa, N. Tokida, C. Ozawa, M. Ishiba, O. Tagaya, N. Asakawa, Suppression effects of carbonate on the interaction between stainless steel and phosphate groups of phosphate compounds in high-performance liquid chromatography and electrospray ionization mass spectrometry, J. Chromatogr. A 1198–1199 (2008) 80–86, doi:10.1016/j.chroma.2008.05.015.
[29] R. Tuytten, F. Lemière, E. Witters, W. Van Dongen, H. Slegers, R.P. Newton, H. Van Onckelen, E.L. Esmans, Stainless steel electrospray probe: a dead end for phosphorylated organic compounds? J. Chromatogr. A 1104 (2006) 209–221, doi:10.1016/j.chroma.2005.12.004.
[30] C. Mathon, G.A. Barding, C.K. Larive, Separation of ten phosphorylated mono- and disaccharides using HILIC and ion-pairing interactions, Anal. Chim. Acta 972 (2017) 102–110, doi:10.1016/j.aca.2017.03.029.
[31] J. Han, V. Tschernutter, J. Yang, T. Eckle, C.H. Borchers, Analysis of selected sugars and sugar phosphates in mouse heart tissue by reductive amination and liquid chromatography-electrospray ionization mass spectrometry, Anal. Chem. 85 (2013) 5965–5973, doi:10.1021/ac400769g.
[32] N. Sheng, H. Zhao, X. Chen, D. Wang, M. Li, Z. Wang, J. Zhang, J. Jiang, A novel derivatization strategy for profiling phosphate ester/anhydride metabolic network and application on glioma rats using HILIC-MS/MS, Talanta 228 (2021) 122238, doi:10.1016/j.talanta.2021.122238.
[33] S. Li, F.L. Liu, Z. Zhang, X.M. Yin, T.T. Ye, B.F. Yuan, Y.Q. Feng, Ultrasensitive determination of sugar phosphates in trace samples by stable isotope chemical labeling combined with RPLC-MS, Anal. Chem. 94 (2022) 4866–4873, doi:10.1021/ACS.ANALCHEM.2C00346.
[34] P. Li, M. Gawaz, M. Chatterjee, M. Lämmerhofer, Targeted profiling of short-, medium-, and long-chain fatty acyl-coenzyme as in biological samples by phosphate methylation coupled to liquid chromatography-tandem mass spectrometry, Anal. Chem. (2021), doi:10.1021/acs.analchem.1c00664.
[35] D.S. Wishart, A. Guo, E. Oler, F. Wang, A. Anjum, H. Peters, R. Dizon, Z. Sayeeda, S. Tian, B.L. Lee, M. Berjanskii, R. Mah, M. Yamamoto, J. Jovel, C. Torres-Calzada, M. Hiebert-Giesbrecht, V.W. Lui, D. Varshavi, D. Varshavi, D. Allen, D. Arndt, N. Khetarpal, A. Sivakumaran, K. Harford, S. Sanford, K. Yee, X. Cao, Z. Budinski, J. Liigand, L. Zhang, J. Zheng, R. Mandal, N. Karu, M. Dambrova, H.B. Schï Oth, R. Greiner, V. Gautam, HMDB 5.0: the human metabolome database for 2022, Nucleic Acids Res. 50 (2022), doi:10.1093/nar/gkab1062.
[36] M. Gilar, M. DeLano, F. Gritti, Mitigation of analyte loss on metal surfaces in liquid chromatography, J. Chromatogr. A 1650 (2021) 462247, doi:10.1016/j.chroma.2021.462247.
[37] K Klavins, DB Chu, S Hann, G. Koellensperger, Fully automated on-line two-dimensional liquid chromatography in combination with ESI MS/MS detection for quantification of sugar phosphates in yeast cell extracts, Analyst 139 (6) (2014) 1512–1520 Mar 21PMID: 24471156, doi:10.1039/c3an01930f.
[38] HF Kvitvang, KA Kristiansen, P. Bruheim, Assessment of capillary anion exchange ion chromatography tandem mass spectrometry for the quantitative profiling of the phosphometabolome and organic acids in biological extracts, J. Chromatogr. A 1370 (2014) 70–79 Nov 28Epub 2014 Oct 20. PMID: 25454131, doi:10.1016/j.chroma.2014.10.029.

Supplementary Material

Isomer selectivity one- and two-dimensional approaches of mixed-mode and hydrophilic interaction liquid chromatography coupled to tandem mass spectrometry for sugar phosphates of glycolysis and pentose phosphate pathways

Min Su[#], Kristian Serafimov[#], Peng Li, Cornelius Knappe, Michael Lämmerhofer *

Institute of Pharmaceutical Sciences, Pharmaceutical (Bio-)Analysis, University of Tübingen, Tübingen, Germany

[#] Shared first authorship

*Author for correspondence:

Prof. Dr. Michael Lämmerhofer

Pharmaceutical (Bio-)Analysis

Institute of Pharmaceutical Sciences

University of Tübingen

Auf der Morgenstelle 8

72076 Tübingen, Germany

T +49 7071 29 78793, F +49 7071 29 4565

e-mail: michael.laemmerhofer@uni-tuebingen.de

Text S1 | liquid chromatographic condition optimization on HILIC/SAX mixed-mode chromatography (HILICpak VT-50 2D column)

LC conditions were optimized in terms of buffer concentration and type, organic modifier, and pH value. When utilizing ammonium acetate instead of ammonium formate as the buffer, most of the HMPs cannot be eluted with the 30 min run time (figure not shown). Four different concentrations of ammonium formate were also tested for gaining a better separation of 3 representative HMPs (G1P, G6P, and F6P). As shown in **Fig S1**, a decreasing buffer concentration attenuated the ionic interaction thus improved the separation of those 3 HMPs. Resulting from the increased retention, HMPs could not be eluted within 30 minutes when utilizing 10 mM NH_4FA (figure not shown). Therefore, 20 mM NH_4FA was selected as final buffer concentration. Concerning the organic modifier, methanol gave better separation of hexose mono-phosphates than acetonitrile (shown in **Fig S2**), therefore methanol was chosen as the organic modifier. The neutral pH value offered the best results compared to acidic and basic conditions, which lost the selectivity of isomeric HMPs due to insufficient retention or broadening of peak width (shown in **Fig S3**).

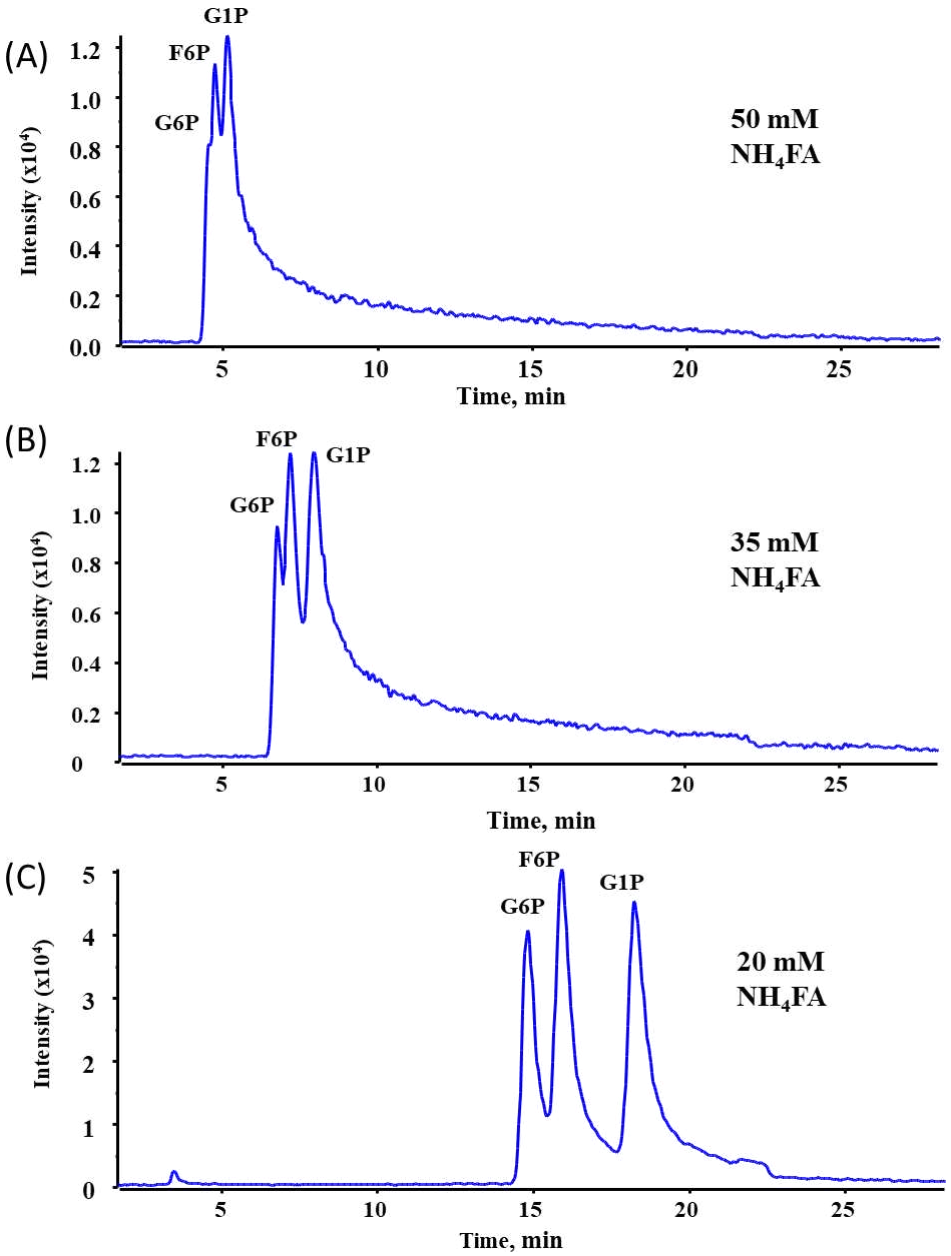

Figure S-1 |

Buffer concentration optimization of SPx on HILIC/SAX mixed-mode chromatography (HILICpak VT-50 2D column). Chromatograms show the results by employing 50 mM (A), 35 mM (B), 20 mM (C) ammonium formate as mobile phase A, respectively. Acetonitrile was used as the mobile phase B. The gradient elution (0.0 min, 20% B; 3.0 min, 20% B; 13 min, 5% B; 20 min, 5% B; 20.1 min, 20% B; 30 min, 20% B) was carried out at a flow rate of 0.2 mL/min. The column temperature kept at 60°C for the whole process. Five µL of mixed solution (standards) of 3 hexose sugar phosphates (G6P, G1P, and F6P) were injected.

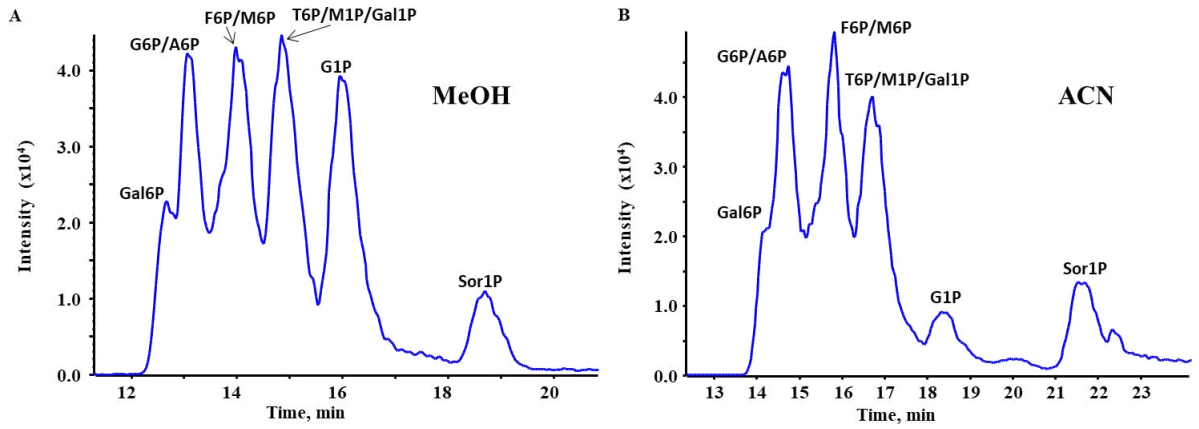

Figure S-2 |

Optimization of HMP separations in terms of organic modifier by HILIC/SAX mixed-mode chromatography (HILICpak VT-50 2D column). Chromatograms (A) and (B) show the results by using 20 mM ammonium formate as mobile phase A, methanol or acetonitrile as mobile phase B, respectively. The gradient elution (0.0 min, 20% B; 3.0 min, 20% B; 13 min, 5% B; 20 min, 5% B; 20.1 min, 20% B; 30 min, 20% B) was carried out at a flow rate of 0.2 mL/min and a constant column temperature of 60°C. Five µL of mixed solution of 10 hexose sugar phosphate standards (Gal6P, G6P, A6P, M6P, F6P, Tag6P, M1P, Gal1P, G1P, and Sor1P) were injected.

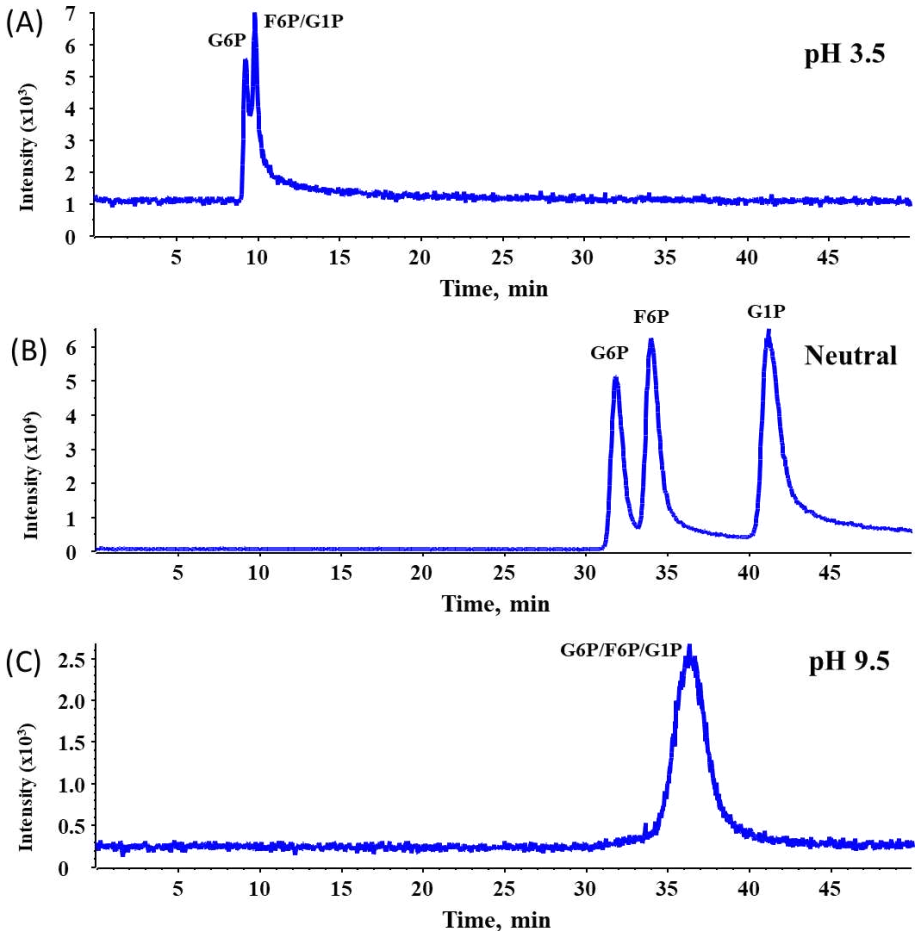

Figure S-3|

pH optimization of SPx separation on HILIC/SAX mixed-mode chromatography (HILICpak VT-50 2D column). Chromatograms (A), (B), and (C) show the results of G6P/F6P/G1P separation by using acidic (pH 3.5), neutral (without pH adjusting), and basic (pH 9.5) mobile phases. 20% ACN in 10 mM NH4FA was used as the mobile phase. The flow rate was 0.2 mL/min and the column temperature kept at 60 °C for the whole run. Five µL of mixed solution of G6P, G1P, and F6P were injected.

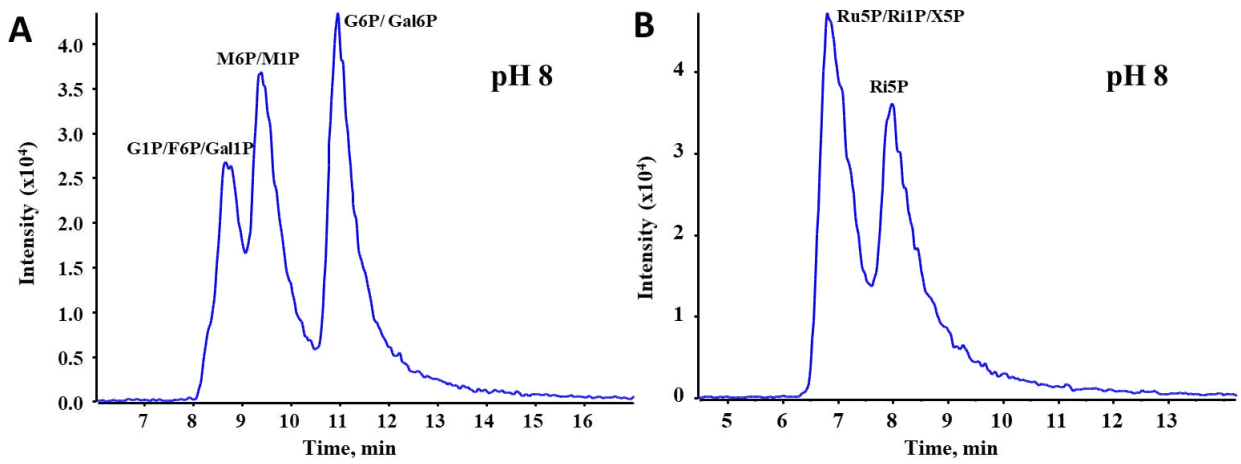

Figure S-4 |

SPx isomer separations by HILIC (Premium BEH Z-HILIC column). Chromatograms showing the separation of hexose (A) and pentose (B) sugar phosphates. pH value was adjusted to 8, other chromatographic conditions employed were as described in section **2.3**. A mixed solution of 7 hexose sugar phosphate standards (Gal6P, G6P, M6P, F6P, M1P, Gal1P, G1P) and 4 pentose sugar phosphate standards (Ru5P, Ri1P, X5P and Ri5P) were injected.

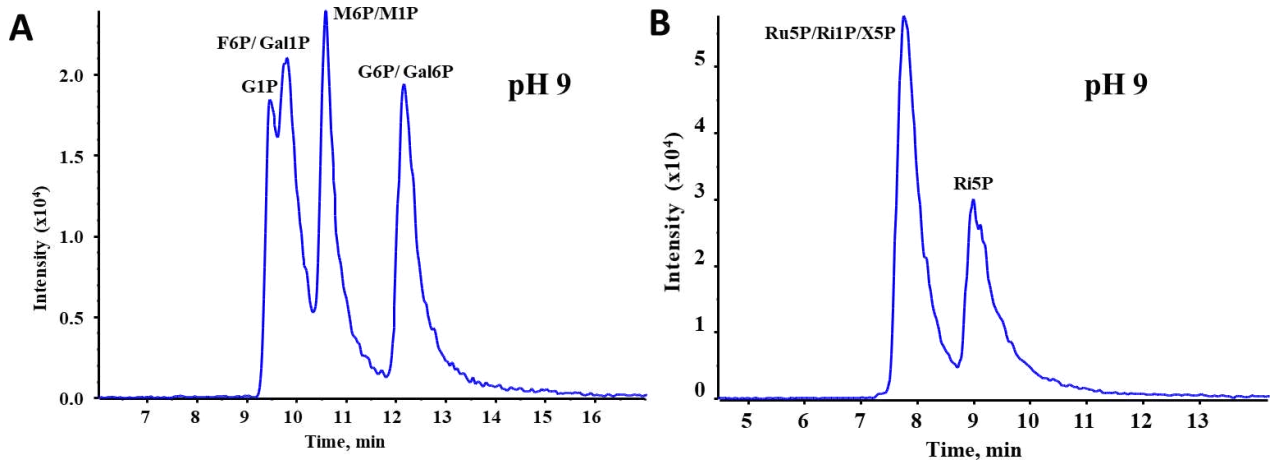

Figure S-5 |

SPx isomer separations by HILIC (Premium BEH Z-HILIC column). Chromatograms showing the separation of hexose (A) and pentose (B) sugar phosphates. pH value was adjusted to 9, other chromatographic conditions employed were as described in section **2.3**. A mixed solution of 7 hexose sugar phosphate standards (Gal6P, G6P, M6P, F6P, M1P, Gal1P, G1P) and 4 pentose sugar phosphate standards (Ru5P, Ri1P, X5P and Ri5P) were injected.

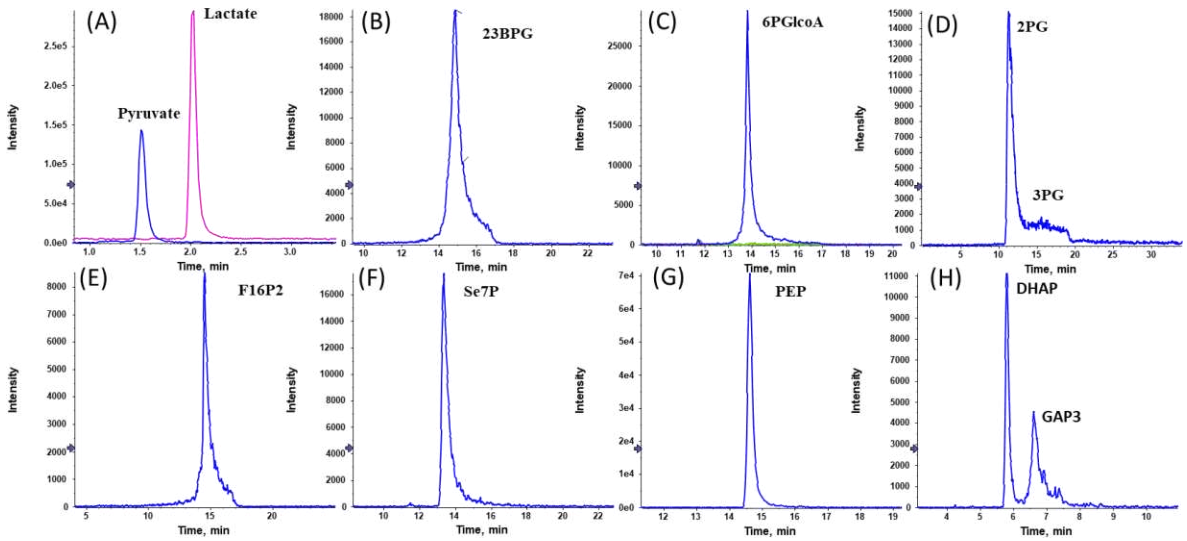

Figure S-6 |

SPx isomer separations by HILIC (Premium BEH Z-HILIC column). Chromatographic conditions employed were as described in section **2.3**. A standard mixture containing all of the compounds annotated in **Table-1** was injected.

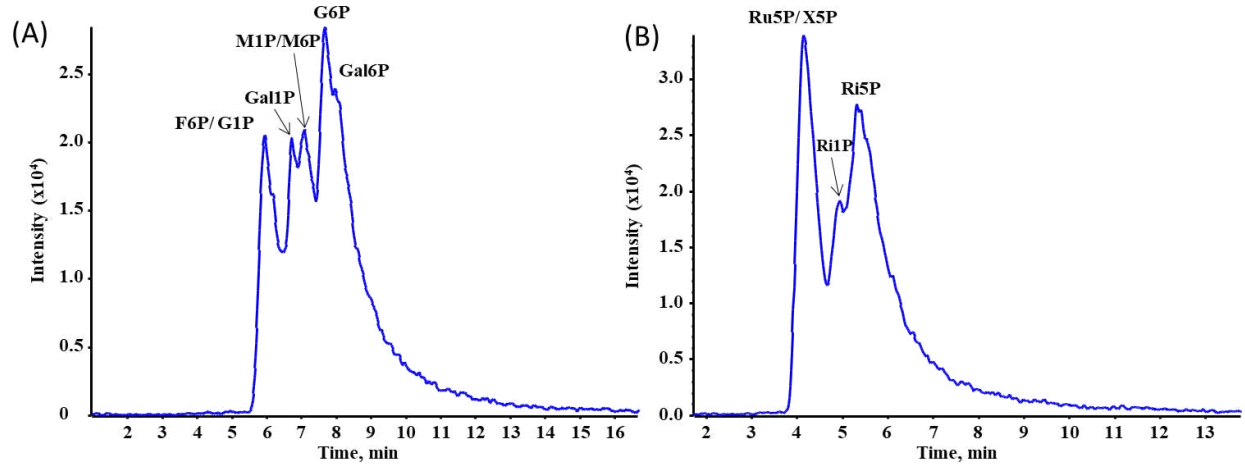

Figure S-7 |

SPx isomer separations by HILIC (Premium BEH Amide column). Chromatograms showing the separation of hexose (A) and pentose (B) sugar phosphates. pH value was adjusted to 8, other chromatographic conditions employed were as described in section **2.3**. A mixed solution of 7 hexose sugar phosphate standards (Gal6P, G6P, M6P, F6P, M1P, Gal1P, G1P) and 4 pentose sugar phosphate standards (Ru5P, Ri1P, X5P and Ri5P) were injected.

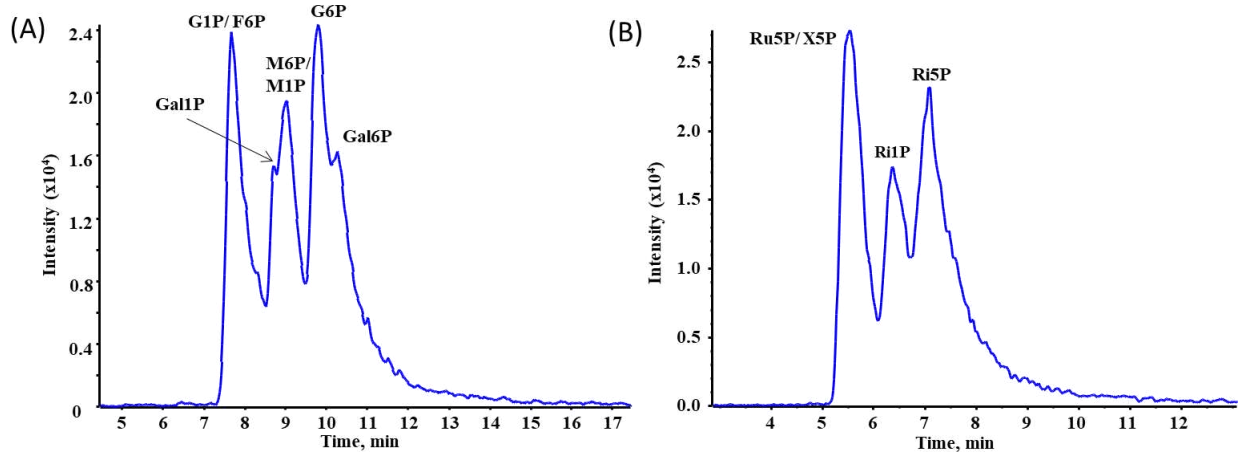

Figure S-8 |

SPx isomer separations by HILIC (Premium BEH Amide column). Chromatograms showing the separation of hexose (A) and pentose (B) sugar phosphates. pH value was adjusted to 9, other chromatographic conditions employed were as described in section **2.3**. A mixed solution of 7 hexose sugar phosphate standards (Gal6P, G6P, M6P, F6P, M1P, Gal1P, G1P) and 4 pentose sugar phosphate standards (Ru5P, Ri1P, X5P and Ri5P) were injected.

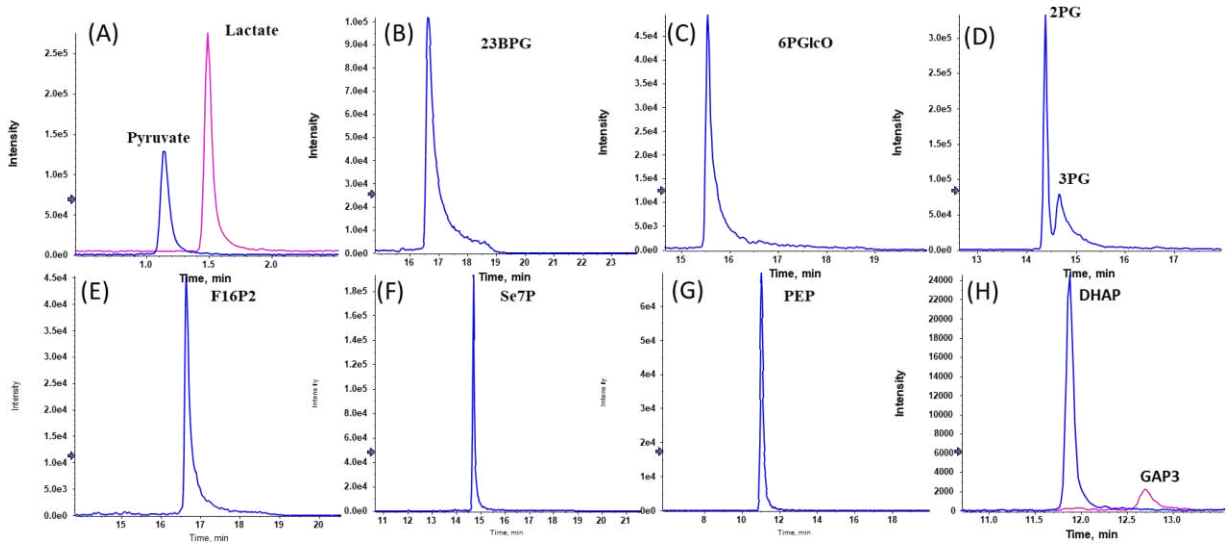

Figure S-9 |

SPx isomer separations by HILIC (Premium BEH Amide column). Chromatographic conditions employed were as described in section **2.3**. A standard mixture containing all of the compounds annotated in **Table-1** was injected.

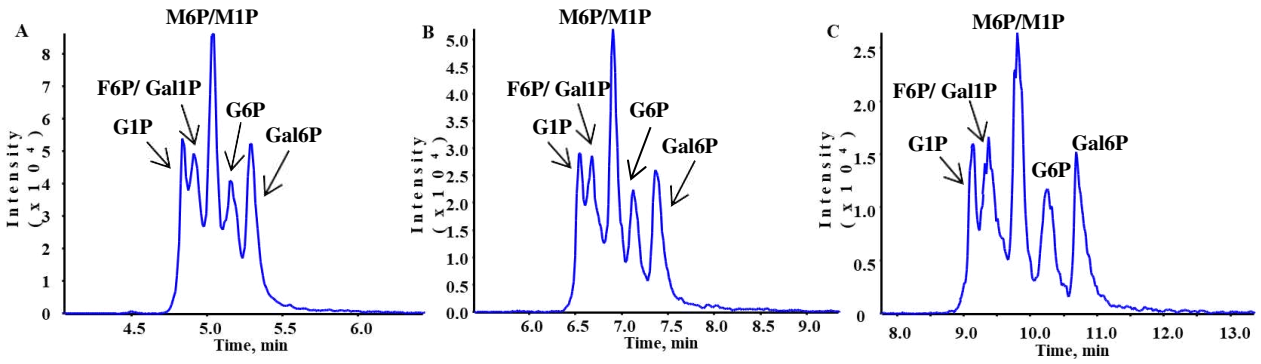

Figure S-10 |

Gradient optimization t_g on the Z-HILIC column with regard to the separation of the hexose monophosphates with t_g 8 min (A), t_g 15 min (B) and t_g 30 min (C). A mixed solution of 7 hexose sugar phosphate standards (Gal6P, G6P, M6P, F6P, M1P, Gal1P, G1P) (Ru5P, Ri1P, X5P and Ri5P) was injected.

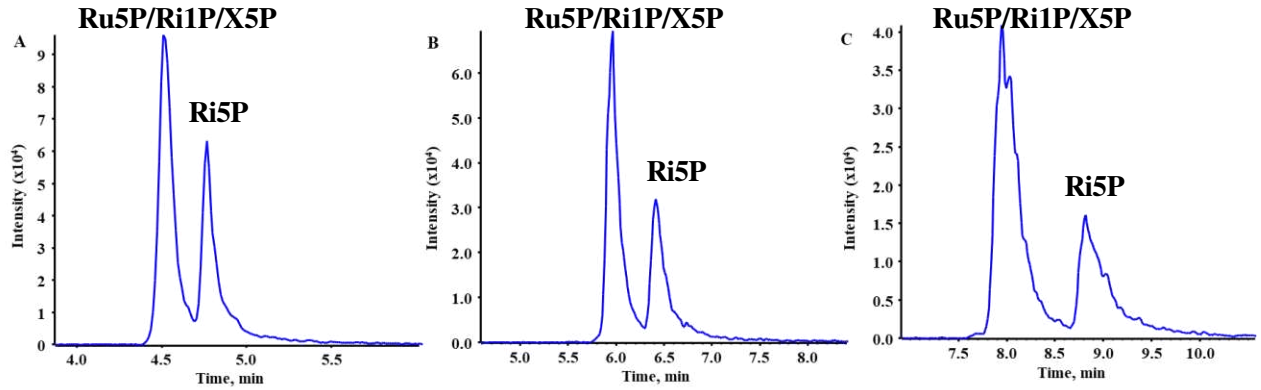

Figure S-11 |

Gradient optimization t_g on the Z-HILIC column with regard to the separation of the pentose monophosphates with t_g 8 min (A), t_g 15 min (B) and t_g 30 min (C). A mixed solution of 4 pentose sugar phosphate standards (Ru5P, Ri1P, X5P and Ri5P) was injected.

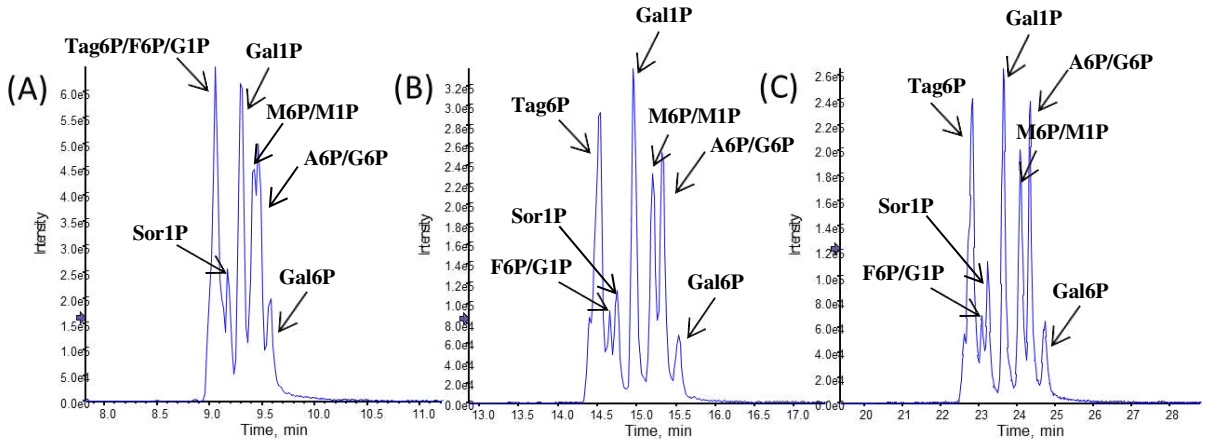

Figure S-12 |

Gradient optimization t_g on the BEH Amide column with regard to the separation of the hexose monophosphates with t_g 8 min (A), t_g 15 min (B) and t_g 30 min (C). A mixed solution of 10 hexose sugar phosphate standards (Gal6P, G6P, A6P, M6P, F6P, Tag6P, M1P, Gal1P, G1P, Sor1P) was injected.

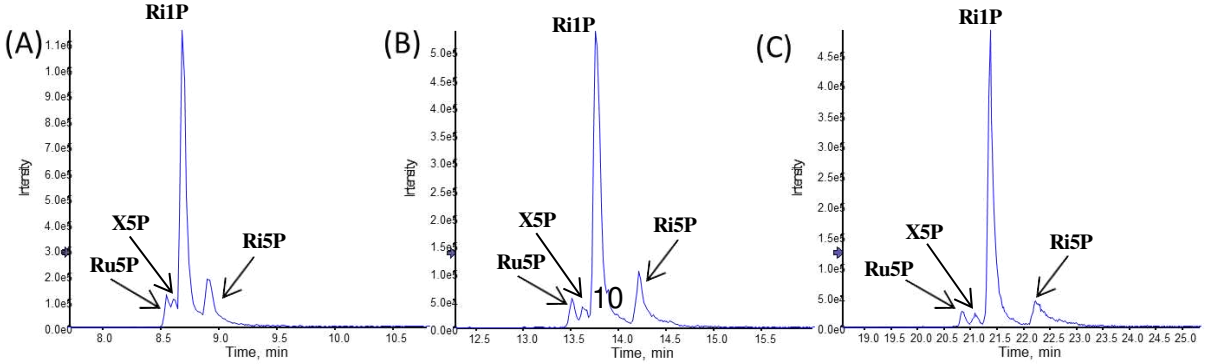

Figure S-13 |

Gradient optimization t_g on the BEH Amide column with regard to the separation of the pentose monophosphates with t_g 8 min (A), t_g 15 min (B) and t_g 30 min (C). A mixed solution of 4 pentose sugar phosphate standards (Ru5P, Ri1P, X5P and Ri5P) was injected.

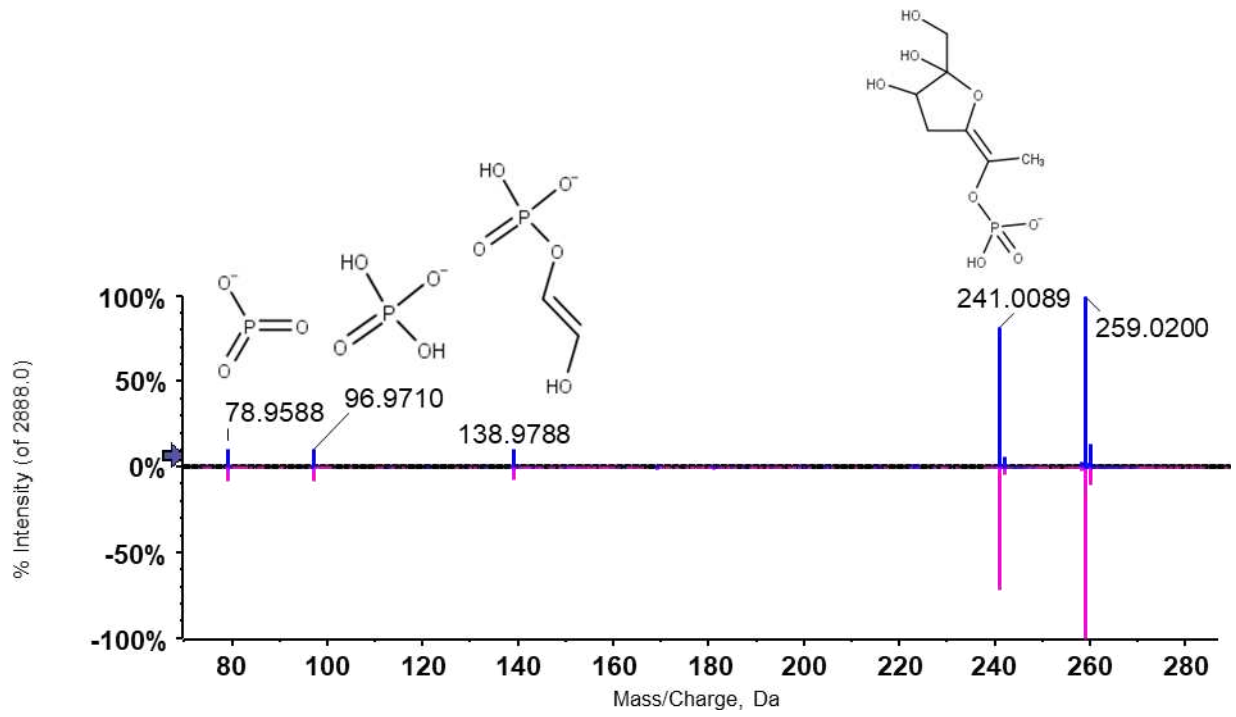

Figure S-14 | MS^2 spectra of G1P (blue) and F6P (pink) acquired via QToF-MS. The comparison shows that the two isomeric compounds have completely identical product ion spectra.

ISSN 1615-9306 · JSSCCJ 47 (1) 2024 · Vol. 47 · No. 1 · January 2024

Journal of SEPARATION SCIENCE

1|2024

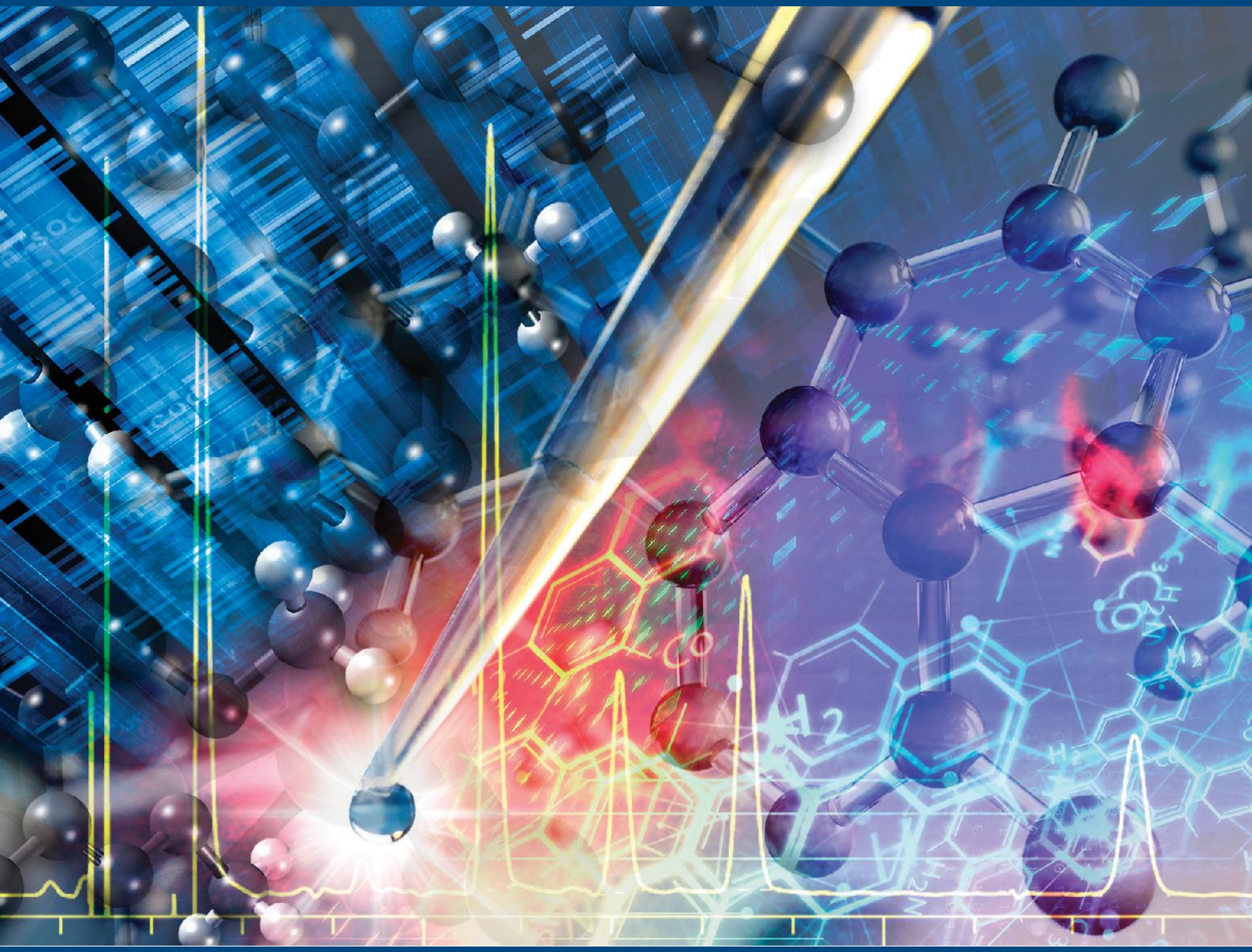

www.jss-journal.com

Methods
Chromatography · Electroseparation

Applications
Biomedicine · Foods · Environment

WILEY VCH

Received: 20 October 2023 | Revised: 20 October 2023 | Accepted: 22 October 2023

DOI: 10.1002/jssc.202300780

JOURNAL OF SEPARATION SCIENCE

RESEARCH ARTICLE

Quantitative analysis of the glutathione pathway cellular metabolites by targeted liquid chromatography-tandem mass spectrometry

Kristian Serafimov | **Yüsra Aydin** | **Michael Lämmerhofer**

Institute of Pharmaceutical Sciences, Pharmaceutical (Bio-)Analysis, University of Tübingen, Tübingen, Germany

Correspondence
Michael Lämmerhofer, Institute of Pharmaceutical Sciences, Pharmaceutical (Bio-)Analysis, University of Tübingen, Auf der Morgenstelle 8, 72076 Tübingen, Germany.
Email: Michael.laemmerhofer@uni-tuebingen.de

Glutathione, its biosynthesis intermediates, and other thiol metabolites are of central relevance for the redox homeostasis of cells. Their analysis is critical due to the facile interconversion of redox pairs during sampling, sample preparation, and data acquisition, in particular in the electrospray ionization interface. In this work, we propose a fast-targeted liquid chromatography-tandem mass spectrometry method to accurately analyze 14 metabolites from the glutathione pathway. *N*-Ethylmaleimide reagent is added with the extraction solvent and instantly stabilizes the thiol-redox state by derivatization. Liquid chromatographic separation of the analytes was performed on a sub-2 μm superficially porous hydrophilic interaction liquid chromatography column with sulfobetaine chemistry. Tandem mass spectrometry with triple-quadrupole mass spectrometry in multiple-reaction monitoring acquisition mode allowed sensitive detection of the targeted metabolites with limits of quantification in the range of 5–25 nM. Run times of 3 min enable a high throughput analysis of cellular samples. For calibration, a ^{13}C-labelled cell extract was used as an internal standard. The method was validated and the concentrations of glutathione and its biosynthesis intermediates were determined in HeLa cells.

KEYW ORDS
glutathione, hydrophilic interaction chromatography, redox homeostasis, tandem mass spectrometry, targeted metabolomics

Article Related Abbreviations: ACN, acetonitrile; BQB, ω-bromoacetonylquinolinium bromide; CysCys, L-cystine dihydrochloride; Cys-Gly-NEM, cysteinyl-glycine-*N*-ethyl-maleimide; Cys-NEM, cysteine-*N*-ethyl-maleimide; Cystath, cystathionine; ER, extraction recovery; ESI, electrospray ionization; Glu, glutamic acid; Glu-Cys-NEM, γ-glutamyl-cystine-*N*-ethyl-maleimide; Gly, glycine; GSH-NEM, glutathione-*N*-ethyl-maleimide; GSSG, glutathione disulfide; HCys-NEM, homocysteine *N*-ethyl-maleimide; HILIC, hydrophilic interaction liquid chromatography; HSer, homoserine; IAM, iodoacetamide; IS, internal standard; LC-MS/MS, liquid chromatography-tandem mass spectrometry; LOD, limit of detection; LOQ, limit of quantification; ME, matrix effect; MeOH, methanol; Met, methionine; NEM, *N*-ethyl-maleimide; PE, process efficiency; Ser, serine; UHPLC, ultra-high-performance liquid chromatography.

This is an open access article under the terms of the Creative Commons Attribution License, which permits use, distribution and reproduction in any medium, provided the original work is properly cited.
© 2023 The Authors. *Journal of Separation Science* published by Wiley-VCH GmbH.

RIGHTSLINK

16159314, 2024, 1, Downloaded from https://analyticalsciencejournals.onlinelibrary.wiley.com/doi/10.1002/jssc.202300780 by Kristian Serafimov - Universitatsbibliothek Tübingen , Wiley Online Library on [26/02/2024]. See the Terms and Conditions (https://onlinelibrary.wiley.com/terms-and-conditions) on Wiley Online Library for rules of use; OA articles are governed by the applicable Creative Commons License

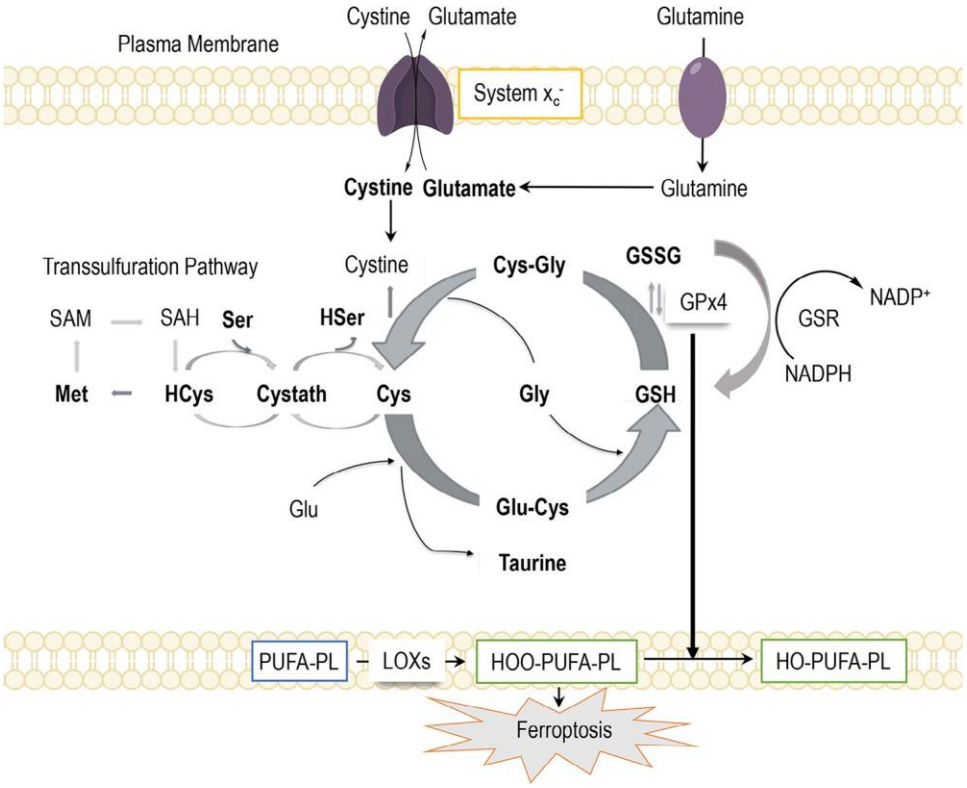

FIGURE 1 Glutathione pathway and its intermediates (target analytes in bold letters) [1, 4]. PUFA-PL (polyunsaturated-fatty-acid-containing phospholipids); LOXs (lipoxygenases); HOO-PUFA-PL (peroxy-polyunsaturated-fatty-acid-containing phospholipid); HO-PUFA-PL (hydroxy-polyunsaturated-fatty-acid-containing phospholipid); GSR (glutathione disulfide reductase); GPx4 (glutathione peroxidase 4).

1 | INTRODUCTION

Metabolites containing sulfur atoms have a special importance for cells of all organisms, as they are involved in numerous vital cellular functions [1]. Glutathione (GSH) is the most abundant intracellular thiol in most mammalian cells and many prokaryotic cells [2]. GSH is found in animal tissues, bacteria, and plants at concentrations ranging from about 0.2 mM to about 10 mM. Reduced GSH and its corresponding glutathione disulfide (GSSG) play an important function in intracellular redox homeostasis keeping the cell in a reducing environment. GSH is a cofactor of glutathione peroxidases GPx which detoxify hydrogen peroxide and lipid peroxides. Amongst them, GPx4, which reduces membrane lipid hydroperoxides, received recently great attention in ferroptosis research, a regulated cell death involving aberrant iron metabolism, GPx4 deficiency, and lipid peroxidation [3] (Figure 1). GSH plays a major role in the detoxification of a variety of xenobiotics (epoxides, electrophiles, and Michael acceptors) by phase II biotransformation forming hydrophilic conjugates [4].

Studies of redox metabolomics require the analysis of reduced GSH and GSSG and their metabolic intermediates (Figure 1). Glutathione, γ-L-glutamyl-L-cysteinylglycine, is a tripeptide formed from the three amino acids cysteine (Cys), glutamic acid (Glu), and glycine (Gly). The unusual γ-peptide bond between Glu and Cys prevents GSH from being hydrolyzed by most peptidases. GSH is less readily oxidized than its precursors Cys and γ-glutamylcysteine (Glu-Cys). GSH is maintained in its thiol form by GSSG reductase (GSR), an NADPH-dependent enzyme (Figure 1). For GSH biosynthesis, Cys is required which entails the uptake of cystine (Cys-Cys) via the cystine-glutamate antiporter (system x_c) into cells followed by reduction to Cys [5]. Cys can also be obtained by the transsulfuration pathway via methionine (Met), homocysteine (HCys), and cystathionine (Cystath) (note: HCys results from Met via *S*-adenosylmethionine after methyl transfer leading to *S*-adenosylhomocysteine and cleavage to HCys; Cystath is obtained from serine [Ser] and HCys which can release Cys by homoserine [HSer] cleavage) (Figure 1). The γ-glutamyl cycle leads to the formation of GSH from Cys via Glu-Cys and is degraded to Cys via cysteinylglycine (Cys-Gly) [1, 6–9].

A number of studies reported targeted liquid chromatography-tandem mass spectrometry (LC-MS/MS) assays for thiol compounds, both in free [10–15] and

RIGHTSLINK

16159314, 2024, 1, Downloaded from https://analyticalsciencejournals.onlinelibrary.wiley.com/doi/10.1002/jssc.202300780 by Kristian Serafimov - Universitatsbibliothek Tübingen , Wiley Online Library on [26/10/2024]. See the Terms and Conditions (https://onlinelibrary.wiley.com/terms-and-conditions) on Wiley Online Library for rules of use; OA articles are governed by the applicable Creative Commons License

derivatized form. Since thiols are prone to oxidation during sample preparation and electrospray ionization, the majority of recent studies focused on thiol analysis after the derivatization of the reactive sulfhydryls. Successful strategies to protect thiols prior to sample preparation and LC-MS/MS analysis of thiol substances comprised iodoacetamide (IAM) alkylation [16, 17], derivatization with *N*-ethylmaleimide in a Michael addition type reaction [18–22] or with *N*-arylmaleimides [23], labeling with 4-fluoro-7-nitro-2,1,3-benzoxadiazole [24, 25], ω-bromoacetonylquinolinium bromide (BQB) [26] or monobromobimane [27]. Besides freezing the redox state of thiol metabolites, derivatization can also have a beneficial impact on liquid chromatographic retention. For example, *N*-ethyl maleimide derivatized hydrophilic thiol metabolites can be sufficiently retained to be analyzed by reversed-phase LC (RPLC) [1]. Using more lipophilic alkyl or aryl substituents on the maleimide, for example, *N*-phenylmaleimide allows for tailoring RP retention [28]. Quinolinium derivatives of thiols were analyzed on an ODS (n-octadecyl-silyl) stationary phase [26] and RPLC analysis of thiols sequentially derivatized with IAM and isopropylchloroformate by use of EZ-FAAST LC/MS amino acid analysis kit was reported as well [29]. On polar RP phases (e.g. HydroRP), thiols have been analyzed also in the underivatized form [11]. However, GSH, other thiol metabolites, their derivatives as well as their precursors and intermediates from the GSH biosynthesis pathway are quite polar in nature. They show favorable characteristics for hydrophilic interaction liquid chromatography (HILIC) [30, 31]. Not surprisingly, HILIC was therefore the method of first choice in the recent literature using Sulfobetaine and Amide column chemistries [1, 23, 25]. The majority of these separations were in the 10 min time scale or had even longer run times. In one study, Forgacsova et al. showed the rapid analysis of 4 thiols by sub-2 μm HILIC-Amide MS/MS in 2.5 min run time. A critical factor in quantitative LC-electrospray ionization-MS (LC-ESI-MS) in the biological matrix is ion suppression and matrix effect (ME), respectively [30]. Stable isotope-labeled internal standards are a good strategy to adequately correct for these MEs. Although they are available for many of the thiol compounds addressed in this study, they have not always been considered before [11, 25]. On the other hand, deuterated internal standard (IS) [23, 29] mixed $^{13}C^{15}N$ labeled metabolites [29], and uniformly labeled ^{13}C-cell extract [1] have been employed for thiol metabolite analysis to compensate for these problems. Also, chemical labeling with light and heavy versions of the derivatization reagent (e.g., BQB for samples and BQB-D7 for standards) was a strategy for ME correction [26].

In this study, the goal was to develop an accurate quantitative LC-ESI-MS/MS assay for the determination of cellular levels of glutathione and its biosynthesis intermediates (Figure 1). To ensure that the cellular redox state of the thiol metabolome is representative of the sample and not artificially altered during sample preparation or ESI process, thiols were derivatized with *N*-ethylmaleimide. Various RP and HILIC columns were screened to evaluate their complementary retention profiles and suitability for targeted thiol metabolomics. To ensure a high sample throughput the goal was to develop a fast assay with run times of less than 5 min. Since superficially porous particle columns have favorable kinetic performance-speed-back pressure characteristics, they have been thoroughly evaluated herein in comparison to sub-2 μm fully porous particle columns with the same and other chemistries. Sub-2 μm superficially porous particle sulfobetaine-based HILIC column, which was not used before for this application, has been finally selected due to its unprecedented speed. A high-throughput quantitative assay was developed, validated, and applied to determine the GSH and thiol metabolite levels in HeLa cells.

2 | EXPERIMENTAL SECTION

2.1 | Materials

For the preparation of mobile phases, the following reagents have been used: MS-grade acetonitrile (ACN) and formic acid (>98%) from Carl Roth. Purified water (18 MΩ cm) was obtained by an ELGA PureLab Ultra purification system and was exclusively used for all steps in which water was required.

In the course of method development, various RP and HILIC columns were screened for their retention profiles of the target analytes. Six different RP columns with different column chemistries were selected for LC-MS measurement: Waters Acquity CSH C18 (150 × 2.1 mm, 1.7 μm), Agilent Zorbax SB-18 (100 × 2.1 mm, 1.8 μm), Waters Acquity HSS T3 (150 × 2.1 mm, 1.8 μm), Waters Acquity Premier BEH Phenyl (150 × 2.1 mm, 1.7 μm), Phenomenex Gemini C18 (150 × 2 mm, 3 μm), Agilent Zorbax Bonus RP (150 × 1.0 mm, 3.0 μm). All columns were equipped with a guard column to extend column lifespan and durability. In the case of HILIC, 4 columns were selected and used during column screening studies: Waters Acquity Premier BEH Amide (150 × 2.1 mm, 1.7 μm), Waters Acquity Premier Z-HILIC (150 × 2.1 mm, 1.7 μm), HILICON iHILIC-Fusion (150 × 2.1 mm, 1.8 μm) and Agilent InfinityLab Poroshell 120 HILIC-Z (50 × 2.1 mm, 1.9 μm). The HPLC crimp neck vials (1.5 mL) and crimp caps were purchased from BGB Analytik.

Ser, Met, HSer, and cysteine hydrochloride monohydrate (Cys) were purchased from TCI-Tokyo Chemical

RIGHTSLINK
16159314, 2024, 1, Downloaded from https://analyticalsciencejournals.onlinelibrary.wiley.com/doi/10.1002/jssc.202300780 by Kristian Serafimov - Universitatsbibliothek Tübingen , Wiley Online Library on [26/10/2024]. See the Terms and Conditions (https://onlinelibrary.wiley.com/terms-and-conditions) on Wiley Online Library for rules of use; OA articles are governed by the applicable Creative Commons License

Industry, and L-cystine dihydrochloride (CysCys) from abcr. Homocysteine (HCys), glutamine (Gln), cystinyl-glycine (CysGly), Glu, L-glutathione oxidized (GSSG), Glu-Cys, Cystath, L-glutathione reduced (GSH), taurine, *N*-ethylmaleimide were obtained from Sigma Aldrich. Uniformly (U-)^{13}C-labeled yeast extract of more than 2 × 10^9 *Pichia pastoris* cells (~15 mg; strain CBS 7435) was obtained from ISOtopic Solutions (Vienna, Austria).

2.2 | Preparation of HeLa cells and extraction

The human cervical HeLa cells adapted to serum-free conditions (AC free, ECACC 08011102) were grown in a humidified incubator at 37 °C with 5% CO_2. Cells were fed with EX-CELL Hela serum-free media (Sigma-Aldrich) with 2 mM L-glutamine (Sigma-Aldrich), 12 U/mL penicillin, and 12 µg/mL streptomycin until the cell density reached around 1 × 10^6.

Cell counting was performed in triplicate with a hemocytometer. Aliquots of 3 × 10^6 HeLa cells were transferred into 15 mL falcon tubes and spun down for 5 min at 100 g. After removing the supernatant, cell pellets were washed twice with ice-cold Dulbecco's phosphate-buffered saline (Sigma-Aldrich) with repeated centrifugation. Cell samples were snap-frozen in liquid nitrogen and kept at −80 °C till use.

Samples were prepared in homogenization tubes (3 × 10^6 HeLa cells). After adding 1 mL of the ice-cold extraction solvent (50 % methanol (MeOH) containing 10 mM *N*-ethyl-maleimide (NEM) and 50 % aqueous 20 mM NH_4FA buffer containing 10 µL internal standard stock solution) and 0.15 g zirconia/glass beads, samples were homogenized at 4 °C for 10 cycles (10 s per cycle, 5687 rcf, pause 30 s) with Precellys Evolution using Cryolys Evolution cooling unit with dry ice cooling (Bertin Technologies). After the cell lysis, the extract was centrifuged at 18 928 rcf for 10 min. The collected supernatants (extracts) were evaporated to dryness overnight under nitrogen using a high-performance evaporator (Genevac EZ-2) (Genevac, Ipswich, UK). The dry residue of the extract was reconstituted in 10 µL water and 90 µL ACN, followed by three cycles of vortexing and sonication (each 30 s). The samples were vortexed, and centrifuged at 18928 rcf for 5 min and the supernatant was further analyzed. The ^{13}C labeled *Pichia pastoris* cell extract stock solution used herein was prepared analogously as the HeLa cell extract, with the difference being the factor 10 larger reconstitution volume (100 µL water/900 µL ACN). The reason for the larger reconstitution volume of the IS stock solution compared to the HeLa cell aliquots was the higher number of *Pichia pastoris* yeast cells (2 × 10^9) compared to the HeLa samples (3 × 10^6).

Four different extraction protocols, which differed in the organic solvent content, were tested in this study regarding their extraction recoveries (ERs). The extraction solvents consisted of MeOH/H_2O with the composition 1. (80/20; v/v); 2. (70/30; v/v); 3. (60/40; v/v/); and 4. (50/50; v/v). Aliquots of washed HeLa cell pellets (each 3 × 10^6 cells) were prepared according to section 2.2. HeLa cell pellets were thawed on ice. Extraction solvents (500 µL MeOH containing 10 mM NEM and 500 µL aqueous 20 mM NH_4FA buffer) were kept on ice before their addition to the cell samples. Evaluation of each extraction protocol's performance was based on the extraction of 6 aliquots of cell samples (pellets from 3 × 10^6 cells). For the determination of metabolite ERs, 3 of these samples were spiked before the extraction (pre-extraction spiking) with 10 µL of aqueous internal standard solution contained in the aqueous buffer extraction solvent (^{13}C-labeled yeast extract of *Pichia pastoris* cells, synonymous with *Komagataella phaffii*), whereas for the other three samples, 10 µL of the aqueous internal standard solution were added as a post-extraction spike. Extraction recoveries were calculated as the ratio of average peak areas for internal standards in the pre-extraction and post-extraction spiked sample.

Supernatants were dried and reconstituted in 10 µL H_2O and 90 µL ACN (containing the post-extraction ^{13}C-IS spike). Three cycles of vortexing and sonication (each 30 s) followed and the samples were centrifuged at 18928 rcf for 5 min with the supernatant further analyzed by ultra-high-performance LC (UHPLC)-ESI-MS/MS. The performance of the distinct extraction solvents was assessed by ERs of the spiked internal standards (^{13}C-cell extract) [33].

2.3 | Instrumentation

The targeted measurements were performed on a UHPLC-ESI-QqQ-MS/MS system. The UHPLC was a 1290 Infinity from Agilent Technologies equipped with a binary pump and thermostated column compartment. The LC was coupled to a Sciex API 4000 mass spectrometer (Sciex). A PAL HTC-xt autosampler from CTC Analytics AG was used for the sample injection and the sample compartment was constantly cooled to 4 °C. MarvelX capillaries from Idex Corporation were installed from autosampler to TCC (250 mm length × 0.075 mm inner diameter). The connection between the column and ion source was a PEEKsil capillary (100 mm length, 50 µm i.d.).

An Eppendorf centrifuge 5415 R was used to centrifuge the cell samples purchased from the Eppendorf AG (Hamburg, Germany).

16159314, 2024, 1, Downloaded from https://analyticalsciencejournals.onlinelibrary.wiley.com/doi/10.1002/jssc.202300780 by Kristian Serafimov - Universitatsbibliothek Tübingen , Wiley Online Library on [26/02/2024]. See the Terms and Conditions (https://onlinelibrary.wiley.com/terms-and-conditions) on Wiley Online Library for rules of use; OA articles are governed by the applicable Creative Commons License

RIGHTSLINK

Unless otherwise specified, chromatographic separation was performed on an Agilent Poroshell 120 HILIC-Z (Waldbronn, Germany) column (50 × 2.1 mm, 1.9 μm). For metabolite analysis in ESI^+ mode, mobile phases A and B were adjusted to a pH of 3.5 with formic acid and consisted of 50 mM ammonium formate in water (A) and 50 mM ammonium formate in ACN-water (90/10, v/v) (B), respectively. Gradient elution was performed as follows (0.0 min, 100% B; 0.4 min 100% B; 1.60 min 70% B; 1.80 min 70% B; 1.81 min 100% B; 3.0 100% B) and was carried out at a flow rate of 1.0 mL/min. A constant column temperature of 35 ˚C was maintained throughout the entire run. The injection volume was 3 μL. The autosampler was kept at 4 ˚C. Ion source parameters were as follows: nebulizer gas (GS1, zero grade air) 30 psi, heater gas (GS2, zero grade air) 90 psi, curtain gas (nitrogen) 30 psi, source temperature 650 ˚C, ion source voltage +5500 V (positive mode). Compound-specific parameters were optimized individually through direct infusion MS (Table 1). A minimum of two MRM transitions (quantifier and qualifier) were monitored except for Gly. Gly does not provide characteristic enough fragment ions, for which reason a pseudo-MRM transition with the precursor ion *m/z* programmed in Q1 and Q3 was employed. It was more reliable in terms of specificity and provided higher signal intensity (the same for corresponding IS (U-^{13}C)-Gly and (U-^{13}C) GSSG which was low abundant). Due to the significant number of transitions monitored simultaneously, the Scheduled-MRM function was enabled. A window of 30 seconds was set around the designated metabolite-specific retention time and the total cycle time was 410 ms. Blank solvents (mobile phases A and B) were injected at the beginning of the chromatographic batch to ensure proper column and system equilibration.

All further data processing steps and evaluations were executed with PeakView 2.2 (Sciex), MultiQuant 3.0 (Sciex), Excel 2016 (Microsoft), and Origin 2021 (OriginLab).

2.4 | Metabolite quantification and method validation

Standard stock solutions (1 mg/mL) were prepared in 50% (v/v) H_2O/MeOH. The stability of the analytes in solution was evaluated and is discussed further in section 3.4.5. Working solutions were obtained by diluting the stock solution to the appropriate concentration with deionized water.

Matrix-matched calibration curves were constructed using weighted least-square linear regression (weighting factor: 1/x) by spiking five different calibrant levels in a standard addition experiment to a pooled HeLa cell extract and by plotting the peak area ratio of analyte to IS versus the nominal concentration of each analyte. The resulting calibration functions were used to determine target analyte concentrations in real samples (HeLa cell extracts). Integration and data processing were conducted with the MultiQuant 3.0 software (Sciex) via an automated algorithm employing a Gaussian smoothing (1 Point), noise percentage of 90%, baseline subtraction window of 0.1 min, and a peak splitting factor of 2. Authentic chemical standards were used to calibrate and validate the methods. For each individual metabolite, the corresponding U^{13}C-labeled metabolite was used as an internal standard (Figure 2). Validation was performed largely in accordance with the FDA guidelines for bioanalytical method validation with some modifications [35]. MEs, ERs, and process efficiencies (PEs) were determined in accordance with the Matuszewski protocol [32] (Table S1), with consideration of the endogenously present metabolite concentrations in the cell extracts, as there is no stripped matrix available. As mentioned above, endogenous levels of the individual metabolites were obtained by LC-MS and standard addition experiments. The determined endogenous concentrations of the individual metabolites were subtracted in the experiments of ME and accuracy determination. Thus, signal suppression or enhancement due to ME was calculated as follows (Equation (1)):

$$ME\% = \frac{A_{spiked} - A_0}{A_{neat}} \quad (1)$$

where A_{spiked} is the area of spiked cell extracts after extraction, A_0 is the peak area of the analyte endogenously present in the extract and A_{neat} is the peak area of the selected metabolite in neat solution. Similarly, individual metabolite accuracies (Acc) were calculated in quality controls as % recovery as follows (Equation (2)):

$$Acc\% = \frac{C_{found} - C_0}{C_{spiked}} \quad (2)$$

With c_{spiked} is the concentration of analyte spiked before extraction to the cell extracts, c_0 the endogenously present amount, and c_{found} the concentration of the selected metabolite found in the spiked sample.

2.5 | Derivatization with *N*-ethyl-maleimide

In order to obtain further information on the reaction process taking place and possible side reactions as well as stability, the NEM-derivatization reaction (Figure 3) was observed over a time-span of 12 hours, based on Cys, GSH, CysGly, GluCys, and HCys (Figure S1). A 1 μg/mL

RIGHTSLINK
16159314, 2024, 1, Downloaded from https://analyticalsciencejournals.onlinelibrary.wiley.com/doi/10.1002/jssc.202300780 by Kristian Serafimov - Universitatsbibliothek Tübingen , Wiley Online Library on [24/10/2024]. See the Terms and Conditions (https://onlinelibrary.wiley.com/terms-and-conditions) on Wiley Online Library for rules of use; OA articles are governed by the applicable Creative Commons License

TABLE 1 Multiple reaction monitoring (MRM) transitions and compound-specific mass spectrometry (MS) parameters.

Compound	Precursor ion (*m/z*)	Product ion (*m/z*)	DP (V)	CE (V)	CXP (V)
Cystine_1	241.0	151.9	36	13	28
Cystine_2	241.0	120.1	36	19	10
Cystine_3	241.0	122.3	36	27	10
GSSG_1	613.4	355.7	35	25	10
GSSG_2	613.4	231.0	35	30	10
GSSG_3	613.4	177.3	35	30	10
GSSG_4	613.4	484.1	35	20	10
Homocys_NEM_1	261.0	56.0	41	43	10
Homocys_NEM_2	261.0	173.1	41	9	8
Homocys_NEM_3	261.0	215.1	41	17	12
GSH_NEM_1	433.2	304.1	51	21	16
GSH_NEM_2	433.2	201.1	51	29	18
GSH_NEM_3	433.2	286.9	51	29	16
GluCys_NEM_1	376.1	247.1	71	21	14
GluCys_NEM_2	376.1	229.9	71	29	12
GluCys_NEM_3	376.1	201.1	71	29	12
Cys_NEM_1	247.1	201.1	71	19	12
Cys_NEM_2	247.1	184.1	61	27	18
Cys_NEM_3	247.1	230.2	71	19	18
Taurine_1	126.0	97.0	26	20	10
Taurine_2	126.0	108.0	26	20	8
Taurine_3	126.0	65.0	26	35	10
Homoser_1	120.1	56.0	16	20	10
Homoser_2	120.1	74.1	16	10	6
Homoser_3	120.1	102.1	16	10	10
Cystathionin_1	223.1	134.1	46	19	12
Cystathionin_2	223.1	88.0	46	39	6
Cystathionin_3	223.1	56.2	46	39	10
Methionine_1	150.1	104.1	16	15	8
Methionine_2	150.1	56.1	16	21	6
Methionine_3	150.1	61.1	16	21	12
Glycine	76.0	76.0	25	5	18
Serine_1	106.0	60.0	20	25	10
Serine_2	106.0	70.0	20	25	10
Serine_3	106.0	88.0	20	25	10
Glu_1	148.1	84.1	20	25	10
Glu_2	148.1	102.0	20	25	10
Glu_3	148.1	56.2	20	25	10
CysGly_NEM_1	304.1	201.0	56	21	12
CysGly_NEM_2	304.1	212.0	56	25	12
CysGly_NEM_3	304.1	158.0	56	35	10
(U-^{13}C) Methionine	155.0	108.1	16	15	10
(U-^{13}C) Cystathionine	230.0	138.0	36	10	10
(U-^{13}C) Homoserine	124.0	77.0	16	10	10
(U-^{13}C) Taurine	128.0	110.1	26	20	10
(U-^{13}C) Cysteine-NEM	250.1	186.1	71	27	10

(Continues)

RIGHTSLINK

16159314, 2024, 1, Downloaded from https://analyticalsciencejournals.onlinelibrary.wiley.com/doi/10.1002/jssc.202300780 by Kristian Serafimov - Universitatsbibliothek Tübingen , Wiley Online Library on [26/02/2024]. See the Terms and Conditions (https://onlinelibrary.wiley.com/terms-and-conditions) on Wiley Online Library for rules of use; OA articles are governed by the applicable Creative Commons License

TABLE 1 (Continued)

Compound	Precursor ion (*m/z*)	Product ion (*m/z*)	DP (V)	CE (V)	CXP (V)
(U-^{13}C) Cystine	247.3	155.0	36	13	10
(U-^{13}C) Glycine	78.1	78.1	25	5	10
(U-^{13}C) GSSG	633.3	633.3	35	5	10
(U-^{13C}) Homocysteine-NEM	265.4	218.1	41	25	10
(U-^{13}C) GSH-NEM	443.2	309.1	51	21	10
(U-^{13}C) GluCys-NEM	384.2	250.1	71	21	10
(U-^{13}C) Serine	109.1	62.1	20	25	10
(U-^{13}C) Glutamic Acid	153.0	106.1	20	25	10
(U-^{13}C) CysGly-NEM	309.1	203.1	56	21	12

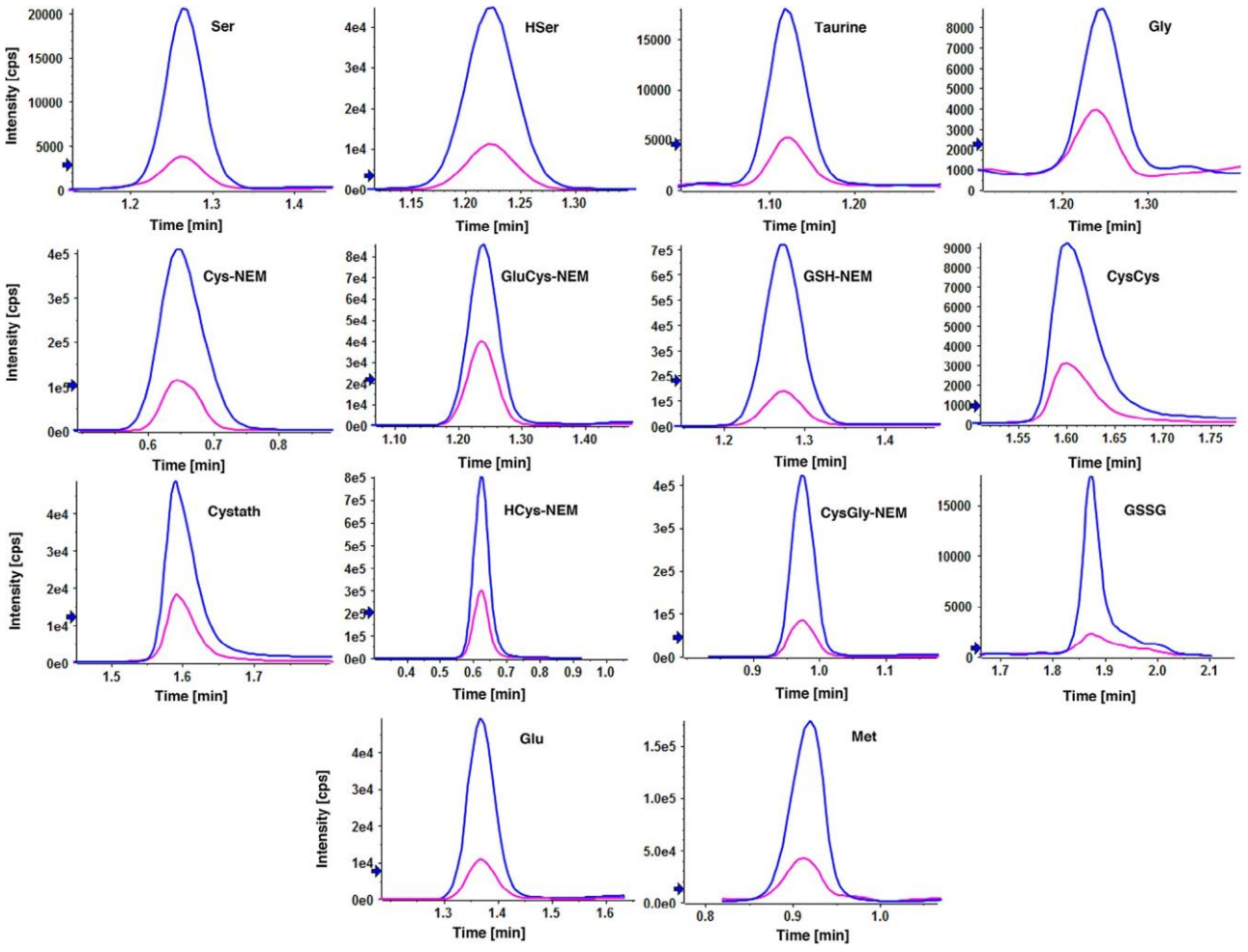

FIGURE 2 Extracted ion chromatograms of metabolites (blue) found in HeLa cell extract and their corresponding U-^{13}C-analogue (pink) from spiked *Pichia pastoris* yeast cell extract under final method conditions. Col. Compartment held at 35˚C. Gradient separation is as follows: 0.0 min, 100% B; 0.4 min 100% B; 1.60 min 70% B; 1.80 min 70% B; 1.81 min 100% B; 3.0 min 100% B. Flow rate adjusted to 1.0 mL min^{-1}. Mobile phases A and B were adjusted to a pH of 3.5 with formic acid and consisted of 50 mM ammonium formate in water (A) and 50 mM ammonium formate in acetonitrile-water (B), respectively.

solution of Cys, GSH, CysGly, GluCys, and HCys was used as a reference, dissolved in 500 µL MeOH and 500 µL of 20 mM aqueous NH_4FA buffer with a pH value of 7.5. In order to quench the reaction, 10 µL of concentrated formic acid was used to stop the reaction process. This is due to the fact that under acidic conditions the amine moiety is protonated, thus not being able anymore to carry out a Michael-addition type reaction.

RIGHTSLINK

16159314, 2024, 1, Downloaded from https://analyticalsciencejournals.onlinelibrary.wiley.com/doi/10.1002/jssc.202300780 by Kristian Serafimov - Universitatsbibliothek Tübingen , Wiley Online Library on [24/10/2024]. See the Terms and Conditions (https://onlinelibrary.wiley.com/terms-and-conditions) on Wiley Online Library for rules of use; OA articles are governed by the applicable Creative Commons License

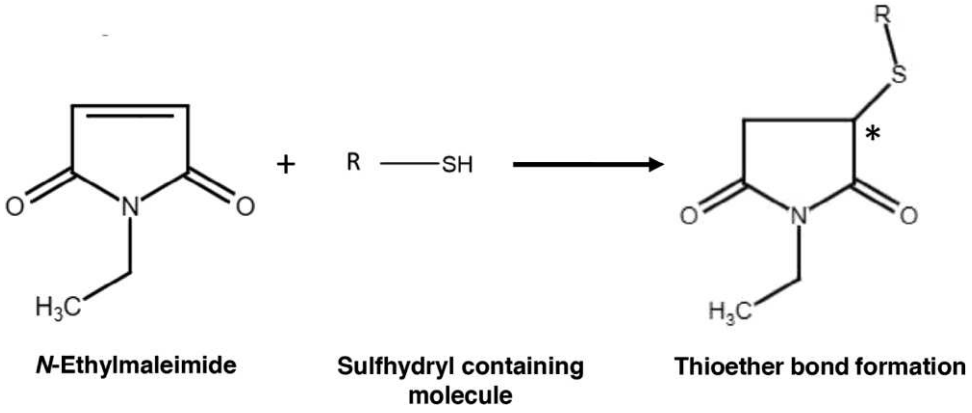

FIGURE 3 Derivatization reaction of sulfhydryl-containing analytes with *N*-Ethyl-Maleimide (NEM) (* indicates new chiral center).

3 | RESULTS AND DISCUSSION

3.1 | Column screening

The first step in method development focused on the selection of a suitable column with sufficient retention and peak shape. For this purpose, a real sample containing the target analytes in the presence of a matrix (cell culture sample) was selected to acquire information about potential interferences. Initially, six different RP columns with various column chemistries were selected for LC-MS column screening. While NEM-derivatized thiol compounds were sufficiently retained, RP did not provide adequate retention for free amino acids especially Glu, Ser, and CysCys, as expected (Figure S2). Therefore, HILIC was further considered and 4 distinct HILIC columns were evaluated, two of them with sulfobetaine chemistry (Z-HILIC, and HILIC-Z), one amide bonded (BEH Amide), and one mixed-mode positive and negative charge-modulated hydroxyethyl amide stationary phase (iHILIC Fusion) [36]. In this screening, mobile phase composition and column compartment temperature were kept constant, whilst for this column screening also the ratio t_g/t_0 was kept constant. Flow rates were adjusted to achieve the same linear velocity for all columns. Acidic conditions were chosen for method development, due to the chemical nature of the target analytes (amino acids and their derivatives), which generally ionize better in ESI^+ mode under acidic pH values. The screening results with these conditions are shown in Figure 4. Some of the NEM-derivatives show double peaks which is due to the generation of the second chiral center (indicated by a * in Figure 3) which leads to the formation of a mixture of two diastereomers that can be separated by RPLC and HILIC.

The column performance was compared by statistical evaluation of peak width, peak tailing factors, and retention time distributions. Figure 5A,B shows violin plots representing the values for peak widths at half maximum and peak tailing factors of the glutathione pathway-related metabolites. The distributions of peak tailing and peak width were compared between the 4 columns. As can be seen in Figure 5A, HILIC-Z provided the narrowest distribution for peak widths with a mode value of 0.05 min (variance between 0.025 and 0.17 min) compared to 0.10 min for iHILIC (0.025–0.30 min), 0.11 min for Z-HILIC (0.07–0.17 min), and 0.17 min (0.03–0.33 min). Distributions of peak tailing factors in Figure 5B clearly indicate less tailing for the core-shell HILIC-Z column with a mode value of 1.1 (variance between 0.9 and 1.2) than iHILIC Fusion with mode of 1.2 (1.05–1.5), BEH Amide with mode of 1.5 (1.1–2.0), and Z-HILIC with a modal value of 1.6 and a wide distribution of tailing factors (1.0–2.0). Due to narrower peaks and lower peak tailing factors the core-shell HILIC-Z was chosen for further method development, which also promised faster separations.

To illustrate retention profiles and to assess the complementarity of the individual columns, parity plots for normalized retention times showing their correlations between 2 columns at a time are shown in Figure 6. Normalized retention times were calculated by Equation (3).

$$t_{R,norm} = \frac{tR, x - tR, first}{tR, last - tR, first} \quad (3)$$

wherein $t_{R,x}$, $t_{R,first}$, and $t_{R,last}$ represent the retention times of the respective metabolite peak of interest, of the first and the last eluted compound, respectively. It is interesting to note that there is the highest correlation and similarity, respectively, between $t_{R,norm}$ of BEH Amide, and Z-HILIC (Figure 6B). The iHILIC-Fusion column provides some orthogonality to both the Z-HILIC and HILIC-Z columns, clearly seen by some minor scatter of the data points in the 2D-retention space (Figure 6A–F). Comparing HILIC-Z (based on superficially porous particles) with Z-HILIC

16159314, 2024, 1, Downloaded from https://analyticalsciencejournals.onlinelibrary.wiley.com/doi/10.1002/jssc.202300780 by Kristian Serafimov - Universitatsbibliothek Tübingen , Wiley Online Library on [26/02/2024]. See the Terms and Conditions (https://onlinelibrary.wiley.com/terms-and-conditions) on Wiley Online Library for rules of use; OA articles are governed by the applicable Creative Commons License

RIGHTSLINK

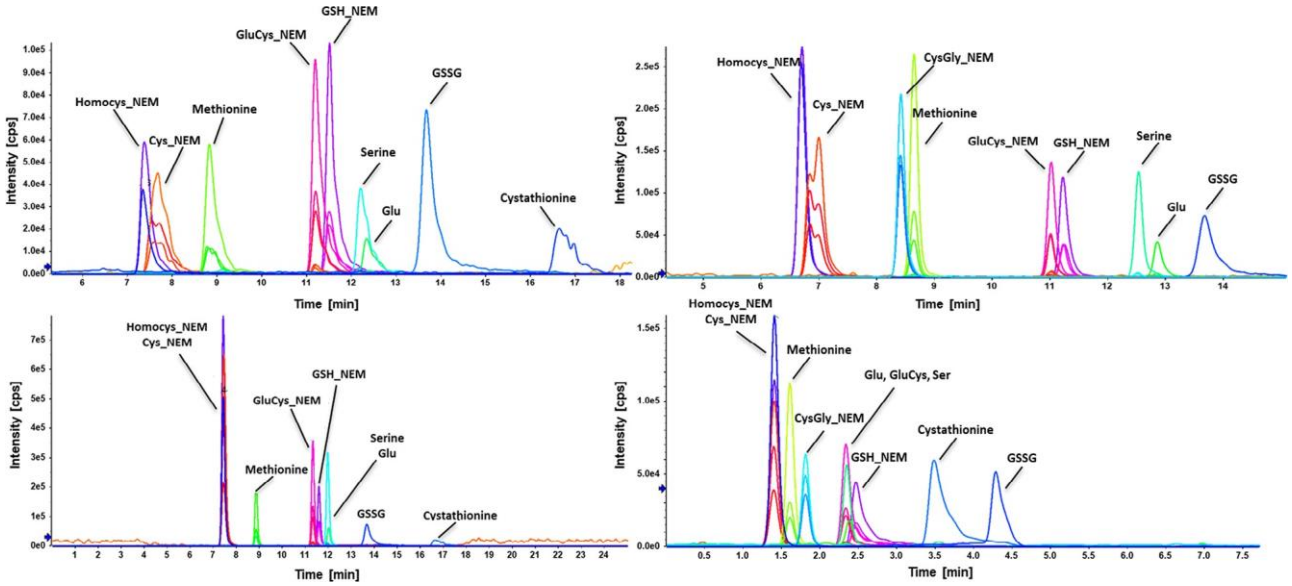

FIGURE 4 Hydrophilic interaction liquid chromatography (HILIC) column screening results. (A) Waters Premier BEH Amide 150 × 2.1 mm, 1.7 μm; (B) Waters Premier Z-HILIC 150 × 2.1 mm, 1.7 μm, (C) HILICON iHILIC-Fusion (+) 150 × 2.1 mm, 1.8 μm, (D) Agilent Poroshell HILIC-Z 50 × 2.1 mm, 1.9 μm. Mobile phase composition is described in section 2.6. A linear gradient from 0% A (aqueous) to 30% A was employed at 0.4 mL min^{-1}, with a method translation tool utilized in order to provide comparable conditions for the individual columns. Column compartment held at 35˚C.

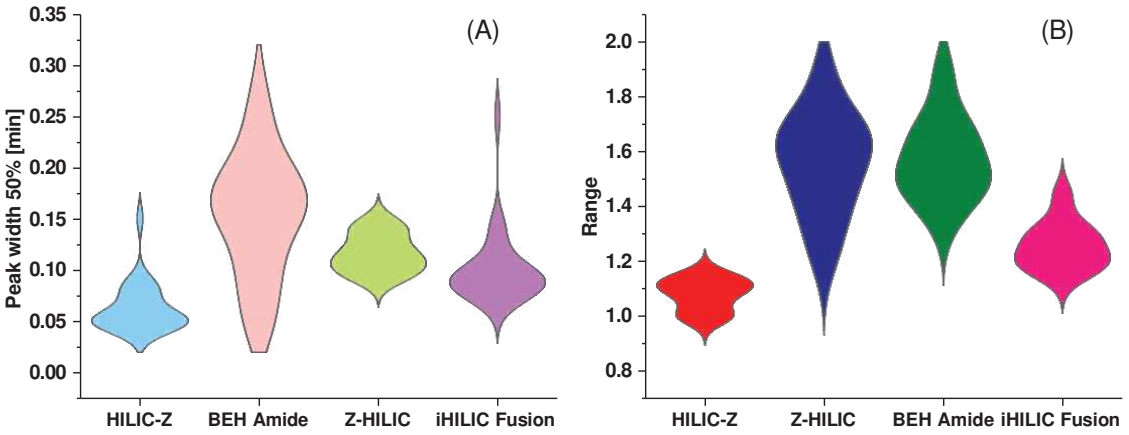

FIGURE 5 Violin plots illustrating column performance in terms of peak widths at half maximum (A) and tailing factors (B) for 1.9 μm superficially porous HILIC-Z column, 1.7 μm fully porous Premier Z-HILIC column, 1.7 μm fully porous Premier BEH-Amide column and 1.8 μm fully porous iHILIC Fusion (+) column.

(based on fully porous particles) both with sulfobetaine chemistry, it turns out that Z-HILIC has larger normalized retention for several analytes (data points below the 45˚ parity line). The RP columns originally considered during method development were also assessed by similarity plots (Figure S3A–O). The complementarity in retention profiles was, however, minor, and free amino acids Cys-Cys, Ser, and Glu were not retained. The above similarity plots are an illustrative representation of relative retention characteristics. To put the complementarity/similarity of normalized retentions into numbers, the Asterisk method for assessing orthogonality has been employed [34]. It characterizes the separation space by 4 axes x- and y-axis, a negative and positive diagonal line. Corresponding Z_1, Z_2, Z_-, and Z_+ values measure the analyte spreading along these axes. The Z-parameters are then bundled into a single A_0 value using eq. 4 which describes the orthogonality (in %) [34].

$$A_0 = \sqrt{Z_- Z_+ Z_1 Z_2} \quad (4)$$

RIGHTSLINK
16159314, 2024, 1, Downloaded from https://analyticalsciencejournals.onlinelibrary.wiley.com/doi/10.1002/jssc.202300780 by Kristian Serafimov - Universitatsbibliothek Tübingen , Wiley Online Library on [26/02/2024]. See the Terms and Conditions (https://onlinelibrary.wiley.com/terms-and-conditions) on Wiley Online Library for rules of use; OA articles are governed by the applicable Creative Commons License

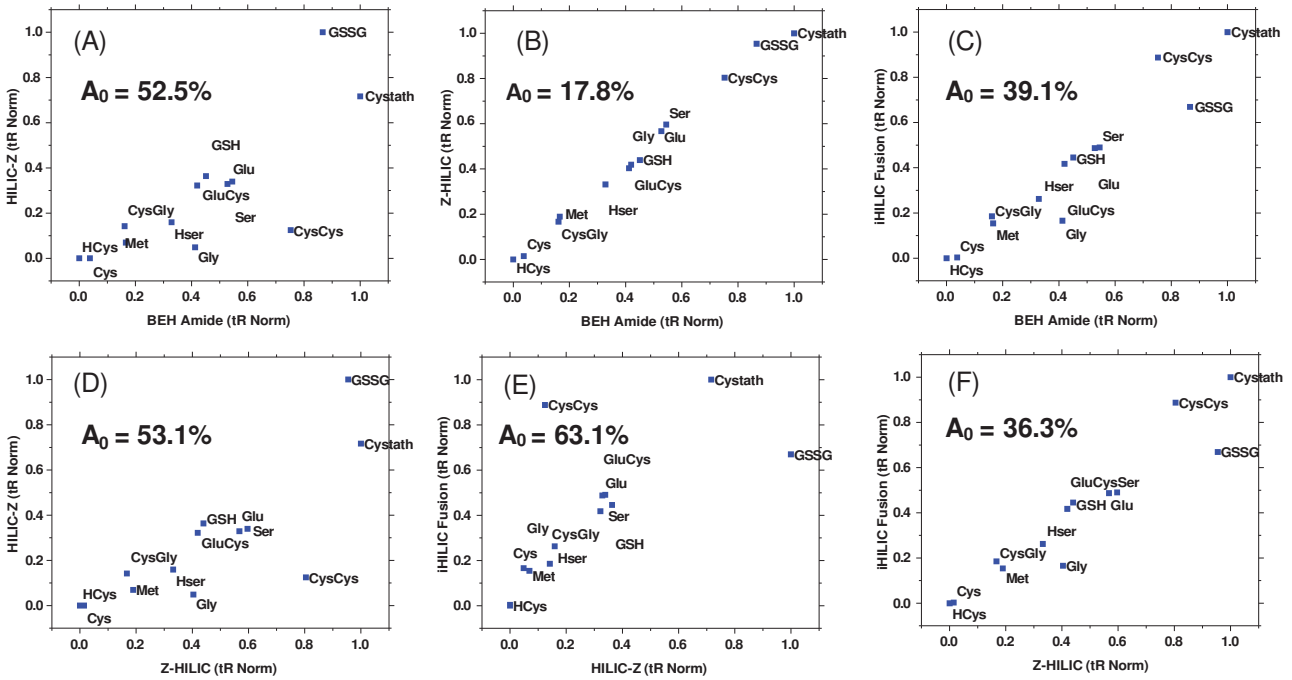

FIGURE 6 Parity-plots for normalized retention times (calculated by Equation (3)) showing the orthogonality between 2 columns, between (A) HILIC-Z and BEH Amide; (B) Z-HILIC and BEH Amide; (C) iHILIC Fusion (+) and BEH Amide; (D) HILIC-Z and Z-HILIC; (E) iHILIC Fusion (+) and HILIC-Z; (F) iHILIC Fusion (+) and Z-HILIC.

The higher A_0 is, the more orthogonal the two compared separations are. Ideally, for two separation systems to be orthogonal, all 4 Z-values should be high, as is the case with, for example, phase system G (HILIC-Z vs. Zorbax RRHD). A value of 100% expresses complete orthogonality. The results obtained for the column orthogonality via the Asterisk method for phase systems involving the HILIC and RP columns screened are summarized in Table 2. Based on the results obtained (A_0 values), it became evident that the highest orthogonality is provided between the sulfobetaine-coated superficially porous HILIC-Z column and the fully porous polar embedded Agilent BonusRP column. Compared to HILIC-Z, Z-HILIC (A_0 = 53%), Amide (A_0 = 53%) and iHILIC-Fusion (A_0 = 63%) are showing moderate orthogonality. Besides giving an overview of the retention profiles of the different tested HILIC columns, the system may also give a hint in which direction to move, when the selectivity of one column is not sufficient.

TABLE 2 Evaluation of retention orthogonality by comparison of the asterisk equation parameters for the following phase systems: (A) BEH Amide versus HILIC-Z; (B) BEH Amide vs Z-HILIC; (C) BEH Amide vs iHILIC-Fusion; (D) HILIC-Z versus Z-HILIC; (E) HILIC-Z versus iHILIC-Fusion; (F) Z-HILIC versus iHILIC-Fusion; (G) HILIC-Z versus Zorbax RRHD; (H) HILIC-Z versus CSH C18; (I) HILIC-Z versus BEH Phenyl; (J) HILIC-Z versus HSS T3; (K) HILIC-Z versus Gemini C18; (L) HILIC-Z versus Bonus RP.

Scenario	A_0 [%]	Z_- [%]	Z_+ [%]	Z_1 [%]	Z_2 [%]
A	53	45.9	63.1	95.6	99.8
B	18	7.7	48.1	95.6	89.3
C	39	25.6	82.6	82.9	87.0
D	53	46.9	63.3	99.6	95.3
E	63	58.9	69.6	99.6	97.2
F	36	25.6	55.5	95.3	97.2
G	73	85.7	87.8	96.4	72.1
H	68	87.3	82.4	96.4	68.6
I	48	66.4	78.3	96.4	47.1
J	69	79.4	90.2	96.4	68.4
K	68	80.5	87.6	96.4	67.3
L	77	94.9	84.6	96.4	77.3

3.2 | Optimization of LC parameters

After column selection, other important influential factors were optimized such as mobile phase composition, gradient profile, column temperature, and flow rate. Initial tested conditions of the method involved mobile phases A and B, which consisted of 20 mM ammonium formate in water (A) and 20 mM ammonium formate in ACN-water (90/10, v/v) (B), respectively, both adjusted to a pH of 3.5 with formic acid, and the gradient elution profile was 0.0 min, 100% B; 1.0 min 100% B; 4.00 min 70% B; 4.50 min 70% B; 4.51 min 100% B; 8.0 min 100% B with a flow rate of 0.4 mL/min. However, problems were faced

16159314, 2024, 1, Downloaded from https://analyticalsciencejournals.onlinelibrary.wiley.com/doi/10.1002/jssc.202300780 by Kristian Serafimov - Universitatsbibliothek Tübingen , Wiley Online Library on [26/02/2024]. See the Terms and Conditions (https://onlinelibrary.wiley.com/terms-and-conditions) on Wiley Online Library for rules of use; OA articles are governed by the applicable Creative Commons License

RIGHTSLINK

with achieving an optimal peak shape, specifically in the case of Cys and GSSG (Figure S4). Therefore, the buffer concentration was increased to 50 mM, and better peak shapes were observed. The final gradient method involved the usage of mobile phases A and B, consisting of 50 mM ammonium formate in water (A) and 50 mM ammonium formate in ACN-water (90/10, v/v) (B), respectively, both adjusted to a pH of 3.5 with formic acid, and the gradient elution profile was 0.0 min, 100% B; 0.4 min 100% B; 1.60 min 70% B; 1.80 min 70% B; 1.81 min 100% B; 3.0 min 100% B (vide infra).

Column temperature was studied in the range of 20 and 40 °C in 5 °C increments. The effect of temperature on retention was negligible (data not shown). The final method involved a constant column oven temperature of 35 °C. Furthermore, the flow rate was optimized as well (Figure S5). Generally, the selection of the flow rate is a compromise between higher peak capacities at high flow rates and higher ESI sensitivity at lower flow rates. A flow rate of 1.0 mL/min was finally selected to enable high throughput for clinical studies (run times 3 min), and scheduled MRM windows of ± 30 s were selected around the set MRM transition (for optimization of MS parameters see Supporting Information and Figures S-6, S-8, and S-9).

3.3 | Optimization of cell extraction protocol

Extraction recovery of polar metabolites from cellular samples is a critical step for the overall performance of a quantitative analytical assay. To limit the co-extraction of proteins, a high organic content in extraction solvent is preferred to efficiently precipitate proteins. However, this may limit the extraction recovery of very polar metabolites. In a series of experiments, the extraction recovery was studied in dependence on the organic content in an aqueous/MeOH mixture of the extraction solvent, and NEM derivatization of thiols was performed to preclude oxidation of free thiols during the sample preparation process. For this purpose, the NEM reagent was added with extraction solvent (500 µL aqueous 20 mM NH_4FA buffer containing the ^{13}C labeled internal standard extract and 500 µL MeOH with a NEM concentration of 10 mM dissolved) to the cell pellets. NEM reacts instantly with the sulfhydryl groups and the derivatized forms are stable over time, measured in our study over 12 h (Figure S1). The extraction process itself was combined with the cell lysis process using a Precellys bead homogenizer with dry ice cooling. After cell lysis, extraction, and centrifugation, the supernatant was removed and evaporated. The residues were re-dissolved in water and diluted with ACN. Possibly co-extracted proteins were precipitated at this point. To ensure no protein precipitates are injected into the UHPLC system, another centrifugation step was introduced before sample injection.

It can be seen that ERs were above 80% for all tested analytes with all extraction solvents tested (Table S2). However, ERs slightly decreased with increasing MeOH content, with the best recoveries being observed with the 50/50 (v/v) MeOH-H_2O mixture (Figure 7). These conditions were further used for metabolite extraction. Previous studies conducted in our laboratory [37], showed that the usage of other extraction solvents, such as IPA or ACN results in lower metabolite recoveries, specifically for amino acids and their derivatives. Therefore, solvents other than MeOH-H_2O mixtures were not re-evaluated.

3.4 | Method validation

The final HILIC method was successfully developed based on the Agilent Poroshell 120 HILIC-Z column, employing acidic conditions (positive ionization mode; pH = 3.5). The corresponding retention times of all metabolites which could reliably and reproducibly be determined with the developed method are given in Table 3.

3.4.1 | Assay specificity

A critical parameter of bioanalytical methods is assay specificity, that is, the ability to differentiate the analytes from components of similar structures present in the respective complex biological matrix. Under the employed chromatographic conditions, all of the redox active analyte pairs, for example, cysteine (Cys-NEM)/cystine (Cys-Cys), GSH-NEM/GSSG, are separated from each other. While this would be critically important in assays analyzing underivatized thiols, here it is beneficial as well because it is known that Michael adduct formation is generally reversible (although not observed herein). In order to enable control of method selectivity, a minimum of 2 MRM transitions were monitored per metabolite. It allowed us to control for interferences by monitoring the ion ratio between the qualifier and quantifier transitions throughout the developed assay. As ion ratios remained constant throughout the analysis of HeLa cell samples (vide infra), it was concluded that isobaric interferences were absent.

3.4.2 | Matrix effects, extraction recoveries, and process efficiencies

MEs, ERs, and PEs were evaluated at an intermediate concentration level (100 ng/mL) of each target analyte by comparison of the peak areas of spiked HeLa cell extract

RIGHTSLINK
16159314, 2024, 1, Downloaded from https://analyticalsciencejournals.onlinelibrary.wiley.com/doi/10.1002/jssc.202300780 by Kristian Serafimov - Universitatsbibliothek Tübingen , Wiley Online Library on [26/02/2024]. See the Terms and Conditions (https://onlinelibrary.wiley.com/terms-and-conditions) on Wiley Online Library for rules of use; OA articles are governed by the applicable Creative Commons License

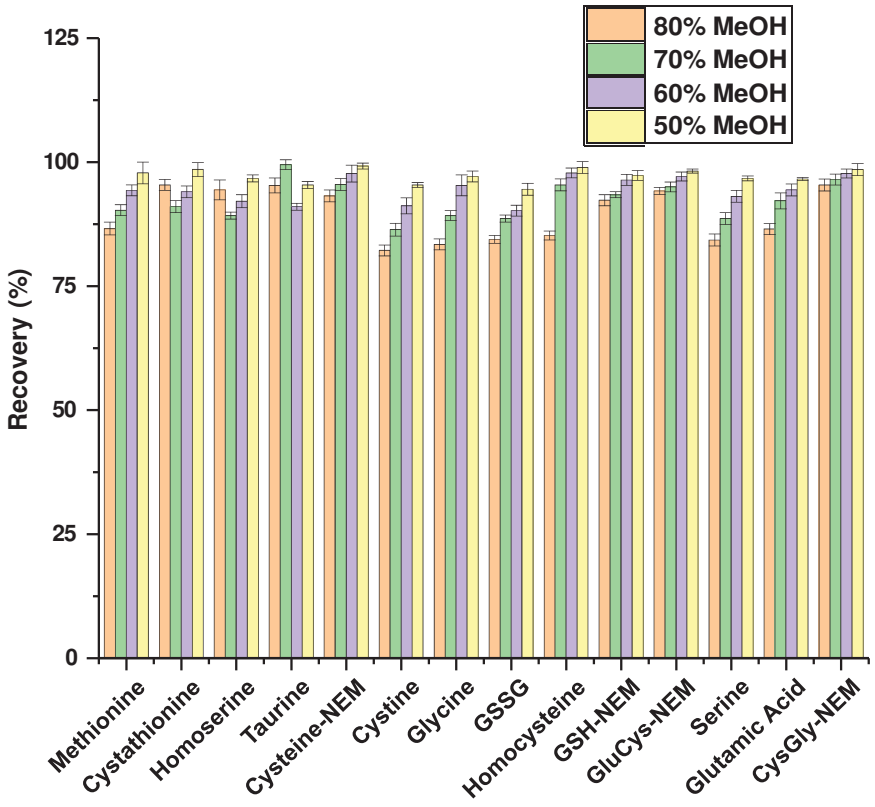

FIGURE 7 Dependence of individual metabolite recoveries on the percentage of MeOH in the extraction solvent MeOH/water (v/v).

(corrected for endogenous levels) versus standard solution. Values close to 100% represent minimum ME, quantitative extraction, and optimal PE, respectively. The results are summarized in Table S1.

MEs ranged between 90.1% (GSH-NEM) and 98.1% (Glycine). It is evident that for the analytes in this study, no significant signal suppression was observed. ERs between 90.6% and 97.6% were found and are in the acceptable range. PE was determined to be between 83.2% and 94.3%. Detailed results for each individual analyte's ME, PE, and ER are provided in Table S1.

3.4.3 | Calibration and method sensitivity

External calibration functions were established by plotting peak area ratios of analytes and their U-^{13}C-labeled internal standards (see Figure 2) versus the concentration of standard solutions. Weighted linear regression (1/x) was used to derive slopes, intercepts, and correlation coefficients of the calibration curves (Table 3). Linearity was evaluated by the correlation coefficients (r) and residual plots (Figure S10) of the external calibration functions for each metabolite and was, as can be seen from Table 3 always $r \geq 0.99$, indicating a good fit. Residual plots and F-values for each target are provided in Figure S10 confirming that the variance can be explained by the linear model. Apart from external calibration, matrix-matched calibration was performed as well by spiking a series of five concentration levels to the biological matrix (HeLa cell extract), as described in section 2.6. Also, the matrix-matched calibration functions showed $r \geq 0.99$). The limits of detection (LODs) and limits of quantification (LOQs), as well as ULOQs (Table 3), were determined through the external calibration function for the individual metabolites as follows:

$$LOD = \frac{3.3 \cdot \sigma}{m}$$

With σ being the standard error of the calibration function's slope and m the slope value itself. Analogous to the LLOQ determination, the following equation was used:

$$LLOQ = \frac{10 \cdot \sigma}{m}$$

Method calibration was performed ranging from the LLOQ to ULOQ value of each metabolite spanning the range for which adequate precision and accuracy were confirmed (Table 3).

3.4.4 | Within-run and between-run accuracy and precision

Precision and accuracy were evaluated and the results are given in Table 3. Within-run and between-run precision

RIGHTSLINK

16159314, 2024, 1, Downloaded from https://analyticalsciencejournals.onlinelibrary.wiley.com/doi/10.1002/jssc.202300780 by Kristian Serafimov - Universitatsbibliothek Tübingen , Wiley Online Library on [26/10/2024]. See the Terms and Conditions (https://onlinelibrary.wiley.com/terms-and-conditions) on Wiley Online Library for rules of use; OA articles are governed by the applicable Creative Commons License

TABLE 3 Data on method validation for the individual metabolites analyzed in positive ionization mode.

Metabolite	t_R [min]	LOD [pmol/mL]	Range		Linearity [r]	Precision [%]			Accuracy [%]			Slope	Intercept	Amount detected [pmol/mL]
			LLOQ [pmol/mL]	ULOQ [nmol/mL]		QC_{low}	QC_{mid}	QC_{high}	QC_{low}	QC_{mid}	QC_{high}			
Glycine	1.25	0.8	5.0	250	0.9992	3.4	4.1	3.0	101.2	109.1	99.5	1.43×10^3	2.72×10^4	50.1 ± 8.6
Methionine	0.92	1.6	7.3	150	0.9991	5.1	4.3	6.1	98.8	104.5	98.8	1.81×10^3	2.04×10^4	120.3 ± 9.4
Cystathionine	1.59	2.2	7.4	300	0.9993	6.5	2.1	4.3	97.7	99.3	97.7	2.12×10^3	3.26×10^4	34.6 ± 3.2
Taurine	1.12	1.3	3.1	200	0.9990	7.7	3.2	2.3	96.5	103.2	98.5	1.93×10^3	3.86×10^4	24.3 ± 1.8
Cys-NEM	0.65	2.7	20	100	0.9990	9.1	2.4	1.7	99.3	108.7	96.5	2.04×10^4	4.17×10^5	257.3 ± 9.9
CysCys	1.60	1.5	4.6	200	0.9990	4.3	2.0	4.0	98.5	91.2	101.3	1.94×10^3	3.56×10^4	60.1 ± 3.2
GSSG	1.87	7.3	20.2	150	0.9998	3.4	1.7	3.4	99.1	95.4	100.4	1.87×10^3	3.82×10^4	34.8 ± 1.2
Homocys-NEM	0.62	3.0	18.4	100	0.9992	5.1	6.3	2.5	96.6	93.2	96.6	2.12×10^4	3.99×10^5	366.9 ± 6.7
GSH-NEM	1.27	5.2	26.3	120	0.9993	3.2	4.5	3.2	98.3	96.7	99.0	2.64×10^4	3.01×10^5	135.5 ± 8.1
GluCys-NEM	1.24	5.3	17.4	100	0.9991	3.0	2.1	2.7	95.6	98.9	98.0	2.02×10^4	3.33×10^5	121.4 ± 4.3
CysGly-NEM	0.97	3.1	16.3	100	0.9994	2.7	5.3	1.6	105.4	98.6	99.1	1.99×10^4	3.76×10^5	360.6 ± 10.5
Serine	1.27	1.0	2.5	200	0.9999	1.8	3.1	1.5	103.2	99.4	104.5	3.01×10^3	3.44×10^4	79.5 ± 4.6
Glutamic Acid	1.37	1.2	3.4	150	0.9993	3.4	2.6	6.4	106.7	98.5	107.6	2.77×10^3	3.78×10^4	565.4 ± 16.6
Homoserine	1.22	2.5	6.5	200	0.9999	2.1	5.4	4.7	101.2	96.5	99.8	1.87×10^3	4.01×10^5	51.9 ± 3.2

16159314, 2024, 1, Downloaded from https://analyticalsciencejournals.onlinelibrary.wiley.com/doi/10.1002/jssc.202300780 by Kristian Serafimov - Universitätsbibliothek Tübingen , Wiley Online Library on [26/10/2024]. See the Terms and Conditions (https://onlinelibrary.wiley.com/terms-and-conditions) on Wiley Online Library for rules of use; OA articles are governed by the applicable Creative Commons License

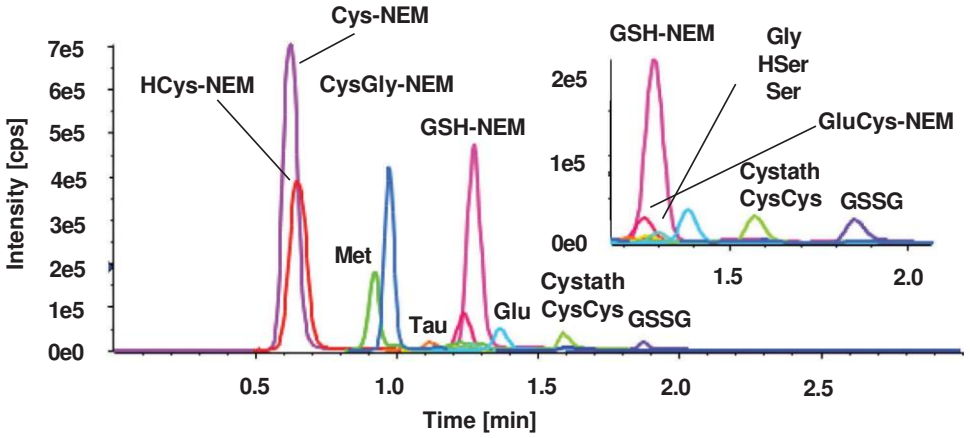

FIGURE 8 Representative chromatogram of target metabolites found in real sample (HeLa cell extract) with the final developed method conditions as mentioned in section **2.6**. For concentrations see Table 3.

and accuracy were assessed in cell-matrix by using three quality controls prepared by spiking cell extract with different concentrations using authentic standards of target analytes at three distinct levels: QC_{Low} (50 ng/mL), QC_{Mid} (100 ng/mL), QC_{High} (200 ng/mL). These three quality controls (QCs) were measured in quintuplicate (n = 5) on three different days to determine the within-run and between-run precision and accuracy, respectively. Endogenous levels determined by the above standard addition experiment were considered in the calculations of accuracies. Precision was below 5% coefficient of variation for the majority of the analytes and below 15% in the entire analyte range, both within-run and between-run. Within- and between-run accuracies showed values in the range between 85% and 115% (assessed as % recovery) in the entire range. This, together with the precision levels found, proved the validity of the developed method.

3.4.5 | Stability

Analyte stability during freeze-thaw cycles and autosampler stability were verified as well. Therefore, fresh QC samples at an intermediate level (100 ng/mL) were prepared and measured in quintuplicate (n = 5) for all stability experiments. A total number of four freeze-thaw cycles were conducted, with the QC samples being kept frozen for 12 h between each cycle. To study extract stability, QCs were reanalyzed and were kept in an autosampler tray (4 ˚C) for 10, 24, and 48 h. All prepared QC samples for stability assays were compared with freshly prepared QCs. The results of the stability tests are summarized in Tables S3 and S4. It becomes evident that the analytes can be considered stable under the evaluated conditions. Changes in analyte concentration for autosampler and freeze/thaw stability were all within common acceptance limits for accuracy (±15%) and hence can be considered sufficiently stable.

3.4.6 | Carryover

To ensure the absence of any carryover, blanks were injected subsequently into a QC at the highest concentration according to the FDA guideline. No carryover was observed and thus the acceptance criteria requested by the FDA guideline for carryover was met.

3.5 | Method application

The validated UHPLC-ESI-MS/MS method was applied to quantify metabolites in a HeLa cell extract (Figure 8). The sample extract was measured in quintuplicate (n = 5). Quantification of the targeted endogenous metabolites was achieved by standard addition with ^{13}C-labeled *Pichia pastoris* (*Komagataella phaffii*) yeast extract included as IS to ensure good precision, correct for sample losses during sample preparation, and correct for MEs. Detailed results are listed in Table 3. Amounts detected varied between 40 and 300 ng/mL for the different analytes (corresponding to 8–200 amol/cell). An additional experiment involving metabolite detectability based on different cell numbers was carried out. Cell aliquots of 1×10^6, 5×10^5, 1×10^5, and 1×10^4 were analyzed with regard to how many metabolites can still be detected in lower cell aliquot numbers. It became evident that close to 50% of the metabolites in this study are below the LOD when the cell count is reduced from 3×10^6 to 1×10^6 (Figure S7).

RIGHTSLINK

16159314, 2024, 1, Downloaded from https://analyticalsciencejournals.onlinelibrary.wiley.com/doi/10.1002/jssc.202300780 by Kristian Serafimov - Universitatsbibliothek Tübingen , Wiley Online Library on [26/02/2024]. See the Terms and Conditions (https://onlinelibrary.wiley.com/terms-and-conditions) on Wiley Online Library for rules of use; OA articles are governed by the applicable Creative Commons License

4 | CONCLUSION

In this study, a targeted metabolomics method focusing on glutathione pathway metabolites was developed and validated, which benefits from the high specificity and sensitivity of UHPLC-MS/MS with scheduled MRM acquisition. A broad column screening was conducted which revealed that optimal results were achieved with the sulfobetaine-modified superficially porous sub-2 μm particle column (HILIC-Z). Thiols were derivatized with *N*-ethylmaleimide before extraction to avoid bias from oxidation of thiol metabolites in the course of sample preparation. Fourteen key metabolites related to the glutathione pathway can be accurately quantified by calibration with authentic standards employing this method. To allow for monitoring assay specificity throughout analytical batches, for the majority of metabolites besides the quantifier transition a qualifier transition was acquired as well. Precision and accuracy were assured by the incorporation of a U-^{13}C-labeled cell extract which enables correction for MEs and analyte losses during sample preparation. The validation confirmed a good performance in terms of precision and accuracy.

Compared to the prior state-of-the-art, our developed method outperformed methods from similar studies and analyte coverage, respectively. Orthmayr et al. [1] have previously developed a chromatographic assay employing NEM derivatization and HILIC, however, our method provides superior throughput with significantly shorter run-times (3 min in comparison to 15 min), coupled with a higher sensitivity through means of the newly developed SPP HILIC-Z column. Other comparable methodologies in the literature such as [11–15] do not employ complete stable isotopic labeling of the target analytes and thus do not correctly compensate for MEs and ion suppression, respectively. They are also not competitive with the high throughput of the currently developed method.

Overall, this newly developed assay provides superior throughput by short run-times, while simultaneously being able to detect low abundant cellular metabolite concentrations of the glutathione pathway.

AC KNO WLEDGMENTS

Open access funding enabled and organized by Projekt DEAL.

CONFLIC T OF INTERES T STATEMENT

The authors declare no conflict of interest.

DATA AVAILABILITY STATEMENT

The data that support the findings of this study are available from the corresponding author upon reasonable request.

OR CID

Michael Lämmerhofer https://orcid.org/0000-0002-1318-0974

REFERENCES

1. Ortmayr K, Schwaiger M, Hann S, Koellensperger G. An integrated metabolomics workflow for the quantification of sulfur pathway intermediates employing thiol protection with N-ethyl maleimide and hydrophilic interaction liquid chromatography tandem mass spectrometry. Analyst 2015;140(22):7687–95. https://doi.org/10.1039/c5an01629k PMID: 26451393
2. Townsend DM, Tew KD, Tapiero H. The importance of glutathione in human disease. Biomed Pharmacother. 2003;57(3-4):145–55. https://doi.org/10.1016/s0753-3322(03)00043-x PMID: 12818476; PMCID: PMC6522248
3. Ursini F, Maiorino M. Lipid peroxidation and ferroptosis: The role of GSH and GPx4. Free Radic Biol Med. 2020;152:175–85. https://doi.org/10.1016/j.freeradbiomed.2020.02.027. Epub 2020 Mar 9. PMID: 32165281
4. Deponte M. Glutathione catalysis and the reaction mechanisms of glutathione-dependent enzymes. Biochim Biophys Acta. 2013;1830(5):3217–66. https://doi.org/10.1016/j.bbagen.2012.09.018. Epub 2012 Oct 2. PMID: 23036594
5. Jiang X, Stockwell BR, Conrad M. Ferroptosis: mechanisms, biology and role in disease. Nat Rev Mol Cell Biol. 2021;22(4):266–82. https://doi.org/10.1038/s41580-020-00324-8. Epub 2021 Jan 25. PMID: 33495651; PMCID: PMC8142022.
6. Hansen RE, Winther JR. An introduction to methods for analyzing thiols and disulfides: reactions, reagents, and practical considerations. Anal Biochem. 2009;394(2):147–58. https://doi.org/10.1016/j.ab.2009.07.051. Epub 2009 Aug 5. PMID: 19664585.
7. Dickinson, DA, Forman HJ. Cellular glutathione and thiols metabolism. Biochem Pharmacol. 2002;64(5-6):1019–26.
8. Hermann, G, Heffeter, P, Kryeziu, K, Berger, W, Hann, S, Koellensperger G. The study of reduced versus oxidized glutathione in cancer cell models employing isotopically labelled standards. Anal Methods. 2014;6(9):3086–94.
9. Oestreicher, J, Morgan B. Glutathione: subcellular distribution and membrane transport. Biochem Cell Biol. 2019;97(3):270–89.
10. Lafaye A, Junot C, Pereira Y, Lagniel G, Tabet JC, Ezan E, et al. Combined proteome and metabolite-profiling analyses reveal surprising insights into yeast sulfur metabolism. J Biol Chem. 2005;280(26):24723–30. https://doi.org/10.1074/jbc.M502285200. Epub 2005 Apr 26. PMID: 15855158.
11. Wu J, Sigler A, Pfaff A, Cen N, Ercal N, Shi H. Development of a HPLC-MS/MS method for assessment of thiol redox status in human tear fluids. Anal Biochem. 2021;629:114295. https://doi.org/10.1016/j.ab.2021.114295. Epub 2021 Jun 26. PMID: 34186074; PMCID: PMC8384703.

RIGHTSLINK

16159314, 2024, 1, Downloaded from https://analyticalsciencejournals.onlinelibrary.wiley.com/doi/10.1002/jssc.202300780 by Kristian Serafimov - Universitatsbibliothek Tübingen , Wiley Online Library on [26/02/2024]. See the Terms and Conditions (https://onlinelibrary.wiley.com/terms-and-conditions) on Wiley Online Library for rules of use; OA articles are governed by the applicable Creative Commons License

12. Zhang YF, Wang Y, Zhang KR, Lei HM, Tang YB, Zhu L. Development and validation of a rapid, robust and sensitive UPLC-QQQ-MS/MS method for simultaneous quantification of GSH metabolism in lung cancer cells. J Chromatogr B Analyt Technol Biomed Life Sci. 2020;1148:122145. https://doi.org/10.1016/j.jchromb.2020.122145. Epub ahead of print. PMID: 32434102.
13. Robin S, Leveque N, Courderot-Masuyer C, Humbert P. LC-MS determination of oxidized and reduced glutathione in human dermis: a microdialysis study. J Chromatogr B Analyt Technol Biomed Life Sci. 2011;879(30):3599–606. https://doi.org/10.1016/j.jchromb.2011.09.052. Epub 2011 Oct 6. PMID: 22019294.
14. Carroll D, Howard D, Zhu H, Paumi CM, Vore M, Bondada S, et al. Simultaneous quantitation of oxidized and reduced glutathione via LC-MS/MS: An insight into the redox state of hematopoietic stem cells. Free Radic Biol Med. 2016;97:85–94. https://doi.org/10.1016/j.freeradbiomed.2016.05.005. Epub 2016 May 19. PMID: 27212018; PMCID: PMC4996720.
15. Petrova B, Warren A, Vital NY, Culhane AJ, Maynard AG, Wong A, et al. Redox metabolism measurement in mammalian cells and tissues by LC-MS. Metabolites. 2021;11(5):313. https://doi.org/10.3390/metabo11050313 PMID: 34068241; PMCID: PMC8153172
16. Smythe CV. The Reaction of Iodoacetate and of Iodoacetamide with various sulfhydryl groups, with urease, and with yeast preparations. J Biol Chem. 1936;114:601–12.
17. Horak J, Lämmerhofer M. Stereoselective separation of underivatized and 6-aminoquinolyl-N-hydroxysuccinimidyl carbamate derivatized amino acids using zwitterionic quinine and quinidine type stationary phases by liquid chromatography-high resolution mass spectrometry. J Chromatogr A. 2019;1596:69–78. https://doi.org/10.1016/j.chroma.2019.02.060. Epub 2019 Feb 26. PMID: 30837161.
18. Steghens JP, Flourié F, Arab K, Collombel C. Fast liquid chromatography-mass spectrometry glutathione measurement in whole blood: micromolar GSSG is a sample preparation artifact. J Chromatogr B Analyt Technol Biomed Life Sci. 2003;798(2):343–49. https://doi.org/10.1016/j.jchromb.2003.10.007 PMID: 14643515
19. Seiwert B, Karst U. Simultaneous LC/MS/MS determination of thiols and disulfides in urine samples based on differential labeling with ferrocene-based maleimides. Anal Chem. 2007;79(18):7131–38. https://doi.org/10.1021/ac071016b. Epub 2007 Aug 17. PMID: 17705399.
20. D'Agostino LA, Lam KP, Lee R, Britz-McKibbin P. Comprehensive plasma thiol redox status determination for metabolomics. J Proteome Res. 2011;10(2):592–603. https://doi.org/10.1021/pr100771g. Epub 2010 Nov 29. PMID: 21053925.
21. Giustarini D, Dalle-Donne I, Milzani A, Fanti P, Rossi R. Analysis of GSH and GSSG after derivatization with N-ethylmaleimide. Nat Protoc. 2013;8(9):1660–69. https://doi.org/10.1038/nprot.2013.095. Epub 2013 Aug 1. PMID: 23928499.
22. Jiao Z, Lu Z, Peng Y, Xu C, Lou Y, Wang G, et al. A quantitative metabolomics assay targeting 14 intracellular metabolites associated with the methionine transsulfuration pathway using LC-MS/MS in breast cancer cells. J Chromatogr B Analyt Technol Biomed Life Sci. 2022;1205:123314. https://doi.org/10.1016/j.jchromb.2022.123314. Epub 2022 Jun 2. PMID: 35772357.
23. Forgacsova A, Galba J, Mojzisova J, Mikus P, Piestansky J, Kovac A. Ultra-high performance hydrophilic interaction liquid chromatography—triple quadrupole tandem mass spectrometry method for determination of cysteine, homocysteine, cysteinylglycine and glutathione in rat plasma. J Pharm Biomed Anal. 2019;164:442–51. https://doi.org/10.1016/j.jpba.2018.10.053. Epub 2018 Nov 1. PMID: 30447532.
24. Pucciarini L, Saluti G, Galarini R, Carotti A, Macchiarulo A, Rudaz S, et al. Optimized one-pot derivatization and enantioseparation of cysteine: application to the study of a dietary supplement. J Pharm Biomed Anal. 2020;180:113066. https://doi.org/10.1016/j.jpba.2019.113066. Epub 2019 Dec 23. PMID: 31891875.
25. Onozato M, Kobata K, Sakamoto T, Ichiba H, Fukushima T. LC-MS/MS analysis of thiol-containing amino acids in exosomal fraction of serum. J Chromatogr Sci. 2020;58(7):636–40. https://doi.org/10.1093/chromsci/bmaa028 PMID: 32577740
26. Wang YL, Zhu QF, Cheng LM, Wang ST, Qin SS, Zheng SJ, et al. Stable isotope labeling—dispersive solid phase extraction—liquid chromatography—tandem mass spectrometry for quantitative analysis of transsulfuration pathway thiols in human serum. J Chromatogr B Analyt Technol Biomed Life Sci. 2018;1083:12–19. https://doi.org/10.1016/j.jchromb.2018.02.036. Epub 2018 Feb 28. PMID: 29518632.
27. Sun Y, Yao T, Guo X, Peng Y, Zheng J. Simultaneous assessment of endogenous thiol compounds by LC-MS/MS. J Chromatogr B Analyt Technol Biomed Life Sci. 2016;1029-1030:213–21. https://doi.org/10.1016/j.jchromb.2016.06.024. 2016 Jul 12. PMID: 27442797.
28. Enomoto AC, Schneider E, McKinnon T, Goldfine H, Levy MA. Validation of a simplified procedure for convenient and rapid quantification of reduced and oxidized glutathione in human plasma by liquid chromatography tandem mass spectrometry analysis. Biomed Chromatogr. 2020;34(9):e4854. https://doi.org/10.1002/bmc.4854. Epub 2020 Jun 28. PMID: 32302415; PMCID: PMC7507186.
29. Suh JH, Kim R, Yavuz B, Lee D, Lal A, Ames BN, et al. Clinical assay of four thiol amino acid redox couples by LC-MS/MS: utility in thalassemia. J Chromatogr B Analyt Technol Biomed Life Sci. 2009;877(28):3418–27. https://doi.org/10.1016/j.jchromb.2009.06.041. Epub 2009 Jul 2. PMID: 19616487; PMCID: PMC3077474.
30. Jiang X, Wang Y, Liu J. Comprehensive characterization of amino acids and water-soluble vitamins in a pentylenetetrazole-induced seizures rat model. J Sep Sci. 2023;46(9):e2201004. https://doi.org/10.1002/jssc.202201004. Epub 2023 Mar 3. PMID: 36841992.
31. Zhang J, Lu Q, Xin L, Lou Y, Xiao W, Wang Z, et al. A liquid chromatography-mass spectrometry untargeted urinary metabonomics combined with quantitative analysis of seven amino acids biomarkers on yaobitong capsule in the intervention of rheumatoid arthritis rats. J Sep Sci. 2022;45(23):4209–23. https://doi.org/10.1002/jssc.202200654. Epub 2022 Oct 17. PMID: 36200630.
32. Matuszewski, BK, Constanzer M, Chavez-Eng C. Strategies for the assessment of matrix effect in quantitative bioanalytical methods based on HPLC– MS/MS. Anal Chem. 2003;75(13):3019–30.

RIGHTSLINK

16159314, 2024, 1, Downloaded from https://analyticalsciencejournals.onlinelibrary.wiley.com/doi/10.1002/jssc.202300780 by Kristian Serafimov - Universitatsbibliothek Tübingen , Wiley Online Library on [26/02/2024]. See the Terms and Conditions (https://onlinelibrary.wiley.com/terms-and-conditions) on Wiley Online Library for rules of use; OA articles are governed by the applicable Creative Commons License

33. Causon, TJ, Hann S Review of sample preparation strategies for MS-based metabolomic studies in industrial biotechnology. Analytica Chimica Acta. 2016;938:18–32.
34. Camenzuli M, Schoenmakers PJ. A new measure of orthogonality for multi-dimensional chromatography. Anal Chim Acta. 2014;838:93–101. https://doi.org/10.1016/j.aca.2014.05.048. Epub 2014 Jun 2. PMID: 25064248.
35. FDA, U.S. Department of Health and Human Services. Bioanalytical method validation guidance for industry 1043. 2018. https://www.fda.gov/files/drugs/published/Bioanalytical-Method-Validation-Guidance-for-Industry.pdf
36. Gilar M, Berthelette KD, Walter TH. Contribution of ionic interactions to stationary phase selectivity in hydrophilic interaction chromatography. J Sep Sci. 2022;45(17):3264–75. https://doi.org/10.1002/jssc.202200165. Epub 2022 Apr 7. PMID: 35347885; PMCID: PMC9545918.
37. Serafimov K, Lämmerhofer M. Metabolic profiling workflow for cell extracts by targeted hydrophilic interaction liquid chromatography-tandem mass spectrometry. J Chromatogr A. 2022;1684:463556. https://doi.org/10.1016/j.chroma.2022.463556. Epub 2022 Oct 8. PMID: 36265203.

SUPPORTING INFORMATION

Additional supporting information can be found online in the Supporting Information section at the end of this article.

How to cite this article: Serafimov K, Aydin Y, Lämmerhofer M. Quantitative analysis of the glutathione pathway cellular metabolites by targeted liquid chromatography-tandem mass spectrometry. J Sep Sci. 2024;47:2300780. https://doi.org/10.1002/jssc.202300780

16159314, 2024, 1, Downloaded from https://analyticalsciencejournals.onlinelibrary.wiley.com/doi/10.1002/jssc.202300780 by Kristian Serafimov - Universitatsbibliothek Tübingen , Wiley Online Library on [26/10/2024]. See the Terms and Conditions (https://onlinelibrary.wiley.com/terms-and-conditions) on Wiley Online Library for rules of use; OA articles are governed by the applicable Creative Commons License

RIGHTSLINK

Supporting information

Quantitative analysis of the glutathione pathway metabolites by targeted liquid chromatography – tandem mass spectrometry in HeLa cells

Kristian Serafimov[a], Yüsra Aydin, Michael Lämmerhofer[a]*

[a] Institute of Pharmaceutical Sciences, Pharmaceutical (Bio-)Analysis, University of Tübingen, Auf der Morgenstelle 8, 72076 Tübingen, Germany

Corresponding Authors:

Prof. Michael Lämmerhofer

Email: Michael.laemmerhofer@uni-tuebingen.de; Telephone: +49 7071 29 78793; Fax: +49 7071 29 4565

Contents

Table S-1. Matrix effects (ME), extraction recoveries (ER) and process efficiencies (PE) values in percentage of 14 analyzed metabolites.

Compound	ME	ER	PE
Glycine	98.1	96.1	94.3
Methionine	94.2	95.3	89.8
Cystathionine	90.4	94.4	85.3
Homoserine	90.5	93.5	84.6
Taurine	94.7	97.6	92.4
Cys-NEM	96.5	94.7	91.4
CysCys	95.4	91.3	87.1
GSSG	97.3	92.1	89.6
Homocys-NEM	92.2	93.0	85.7
GSH-NEM	90.1	92.1	83.0
GluCys-NEM	91.8	90.6	83.2
Serine	92.4	94.5	87.3
Glutamic Acid	93.5	92.4	86.4
CysGly-NEM	97.7	93.3	91.2

Table S-2. Extraction recoveries investigated with U^{13}C metabolites.

Compound	MeOH / H_2O (50/50)	MeOH / H_2O (60/40)	MeOH / H_2O (70/30)	MeOH / H_2O (80/20)
(U-^{13}C) Methionine	97.8 ± 1.3	94.3 ± 1.1	90.3 ± 1.1	86.6 ± 2.2
(U-^{13}C) Cystathionine	98.5 ± 1.1	94.0 ± 1.2	91.0 ± 1.2	85.4 ± 1.4
(U-^{13}C) Homoserine	96.7 ± 2.0	92.1 ± 0.7	89.2 ± 1.3	84.4 ± 0.7
(U-^{13}C) Taurine	95.4 ± 1.5	91.0 ± 1.0	88.5 ± 0.7	85.3 ± 0.7
(U-^{13}C) Cysteine-NEM	99.2 ± 1.2	97.7 ± 1.2	95.5 ± 1.7	93.2 ± 0.6
(U-^{13}C) Cystine	95.4 ± 1.1	91.2 ± 1.3	86.4 ± 1.6	82.2 ± 0.5
(U-^{13}C) Glycine	97.1 ± 1.1	95.3 ± 1.0	89.2 ± 2.1	83.4 ± 1.1
(U-^{13}C) GSSG	94.5 ± 0.8	90.2 ± 0.7	88.6 ± 1.1	84.4 ± 1.2
(U-^{13}C) Homocysteine-NEM	98.9 ± 0.9	97.8 ± 1.2	95.4 ± 1.0	85.2 ± 1.2
(U-^{13}C) GSH-NEM	97.3 ± 1.1	96.4 ± 0.6	93.4 ± 1.1	92.3 ± 1.0
(U-^{13}C) GluCys-NEM	98.2 ± 0.7	97.1 ± 1.0	95.0 ± 0.9	94.2 ± 0.4
(U-^{13}C) Serine	96.7 ± 1.2	93.1 ± 1.2	88.6 ± 1.2	84.3 ± 0.5
(U-^{13}C) Glutamic Acid	96.6 ± 1.1	94.4 ± 1.6	92.2 ± 1.2	86.5 ± 0.3
(U-^{13}C) CysGly-NEM	98.5 ± 1.2	97.7 ± 1.1	96.5 ± 0.9	95.4 ± 1.2

Table S-3 Freeze-thaw analyte stability. QC sample consisted of spiked cell extract matrix on mid concentration level (100 ng mL^{-1}).

Compound	1 Cycle	2 Cycles	3 Cycles	4 Cycles
Glycine	97.7%	99.5%	98.4%	96.4%
Methionine	101.2%	99.6%	98.7%	97.5%
Homoserine	99.3%	97.2%	96.5%	98.6%
Taurine	99.3%	98.5%	97.7%	98.5%
Cysein-NEM	99.5%	99.3%	98.5%	97.6%
Cystine	98.5%	99.1%	99.3%	97.5%
GSSG	99.1%	98.4%	98.0%	99.7%
Homocystein-NEM	98.7%	99.1%	99.3%	98.5%
GSH-NEM	99.1%	98.7%	98.5%	99.6%
GluCys-NEM	97.6%	96.5%	95.7%	95.3%
Serine	99.1%	98.5%	98.9%	96.4%
Glutamic Acid	95.6%	96.0%	97.7%	98.3%
CysGly-NEM	99.3%	98.5%	97.4%	96.5%

Table S-4 Stability study during autosampler storage. QC sample consisted of spiked cell extract matrix on mid concentration level (100 ng mL^{-1}).

Compound	12 h	24 h	36 h	48 h
Glycine	102.5%	98.5%	97.6%	94.4%
Methionine	99.7%	98.5%	94.3%	90.1%
Homoserine	98.5%	97.5%	94.5%	90.3%
Taurine	99.5%	97.6%	95.4%	93.2%
Cys-NEM	98.2%	97.6%	94.4%	94.2%
CysCys	99.3%	98.5%	97.4%	95.5%
GSSG	99.2%	96.5%	94.5%	91.2%
Homocys-NEM	98.5%	97.7%	92.2%	93.4%
GSH-NEM	98.7%	97.6%	95.4%	91.2%
GluCys-NEM	99.4%	97.6%	98.1%	95.4%
Serine	98.9%	97.6%	96.2%	94.3%
Glutamic Acid	99.3%	98.5%	96.5%	95.4%
CysGly-NEM	98.5%	97.7%	97.3%	94.3%

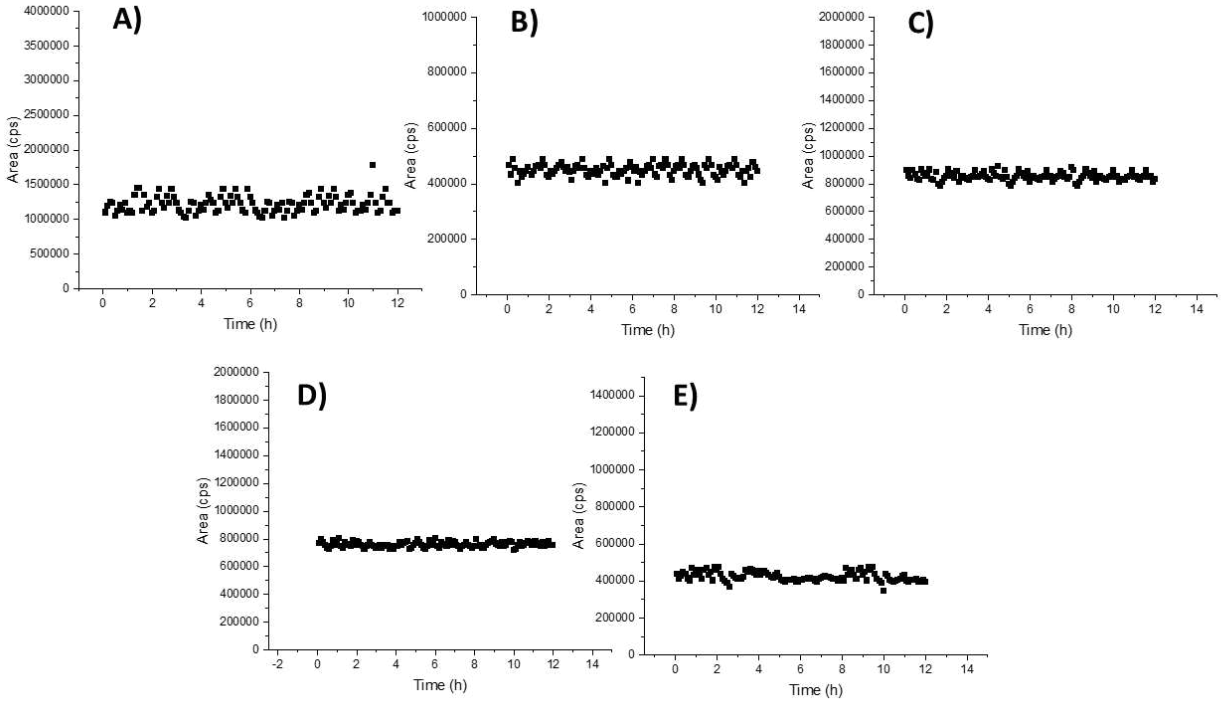

Figure S-1. Reaction kinetics monitored over 12 hours. A) Cys; B) GSH; C) CysGly; D) GluCys; E) Hcys

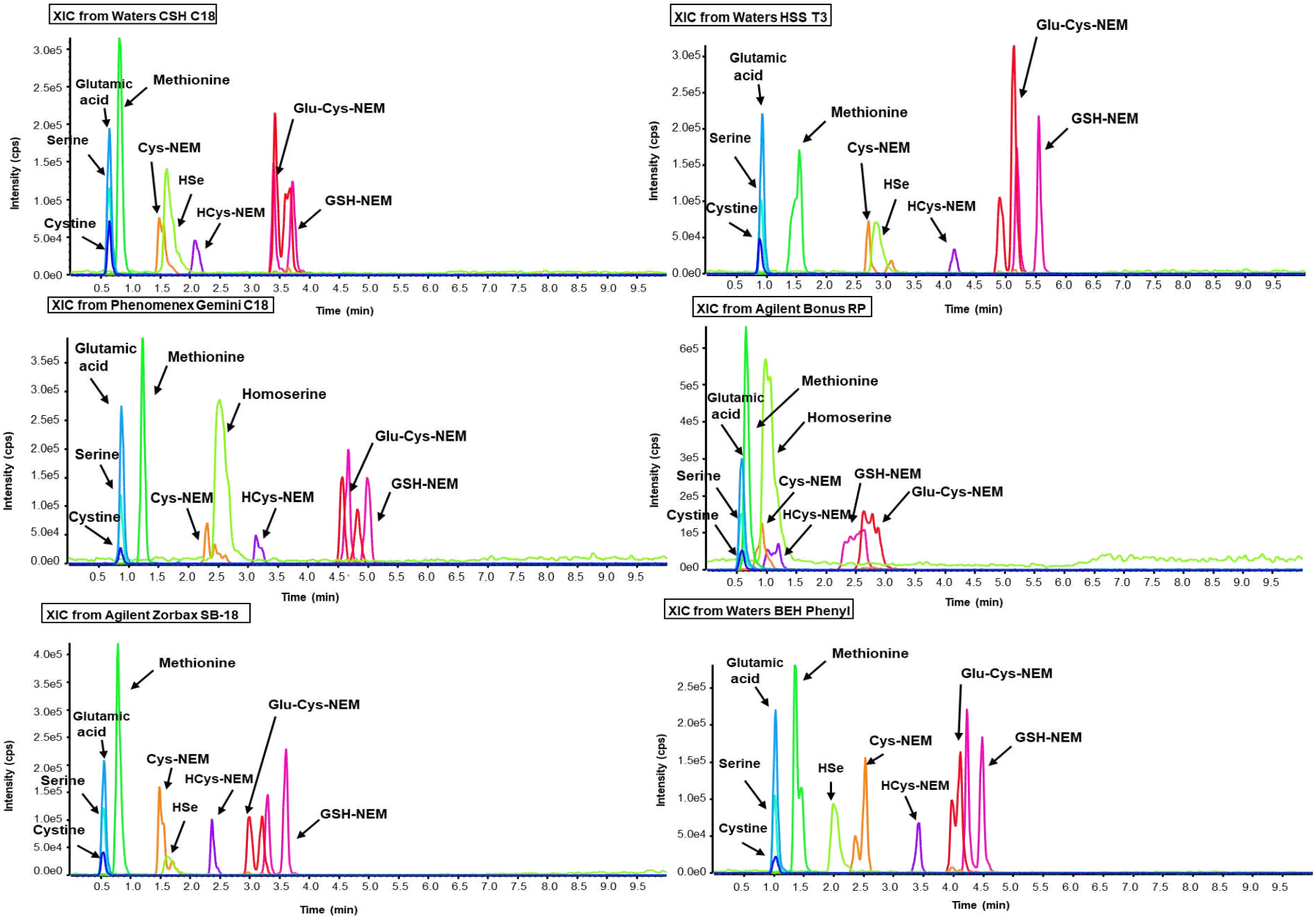

Figure S-2. RP column screening results. Mobile phase conditions 0.1% FA in H_2O and ACN. A linear gradient was employed 3-10% organic modifier B, with the individual method transferred in order to have comparable conditions for all columns via a method translation tool. Column compartment held at 35°C.

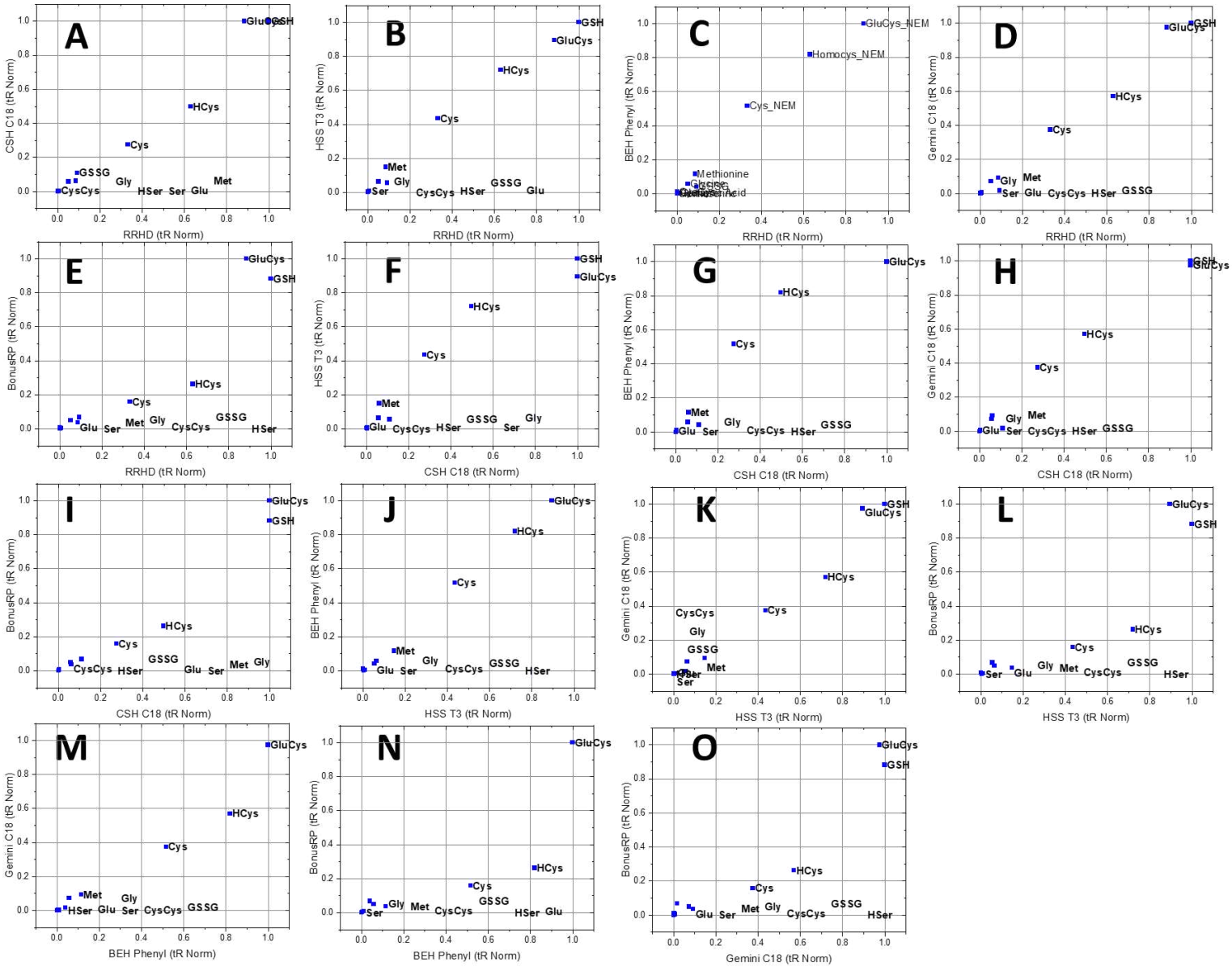

Figure S-3. Parity-plots for normalized retention times (calculated by eq. 1) showing the orthogonality between RP columns tested; between A) Zorbax RRHD and CSH C18; B) Zorbax RRHD and HSS T3; C) Zorbax RRHD and BEH Phenyl; D) Zorbax RRHD and Gemini C18; E) Zorbax RRHD and BonusRP; F) CSH C18 and HSS T3; G) CSH C18 and BEH Phenyl; H) CSH C18 and Gemini C18; I) CSH C18 and Bonus RP; J) HSS T3 and BEH Phenyl; K) HSS T3 and Gemini C18; L) HSS T3 and BonusRP; M) BEH Phenyl and Gemini C18; N) BEH Phenyl and BonusRP; O) Gemini C18 and BonusRP

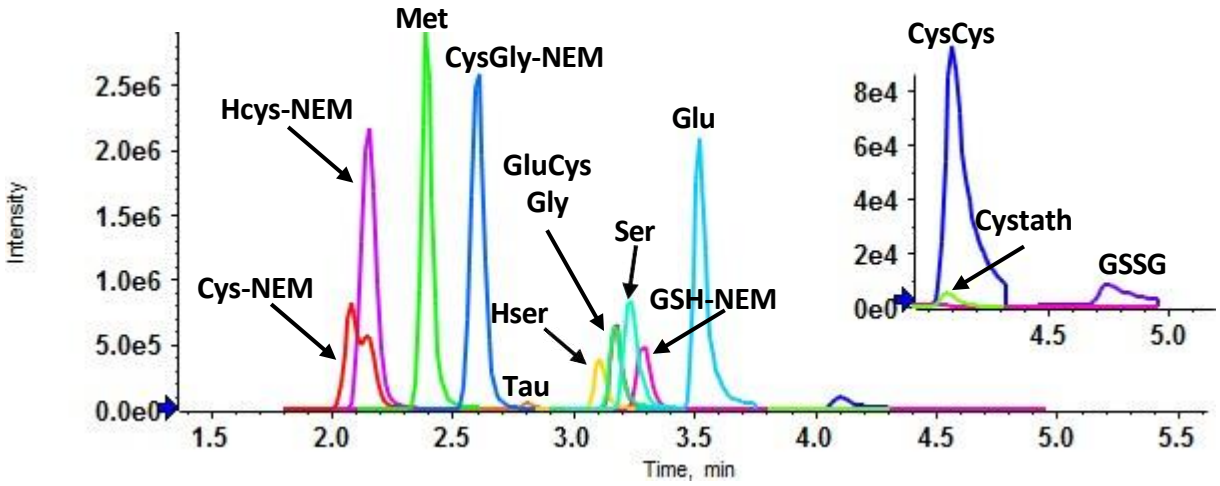

Figure S-4. Real sample chromatogram obtained with the initial developed method conditions described in section **3.1.** Col. Compartment held at 35°C. Gradient separation as follows: 0.0 min 100% B, 4.0 min 70% B; 4.5 min 70% B; 4.51 min 100% B; 8.0 min 100% B. Flow rate adjusted to 0.4 mL min^{-1}. Mobile phases A and B were adjusted to a pH of 3.5 with formic acid and consisted of 20 mM ammonium formate in water (A) and 20 mm ammonium formate in acetonitrile-water (90/10, v/v) (B), respectively.

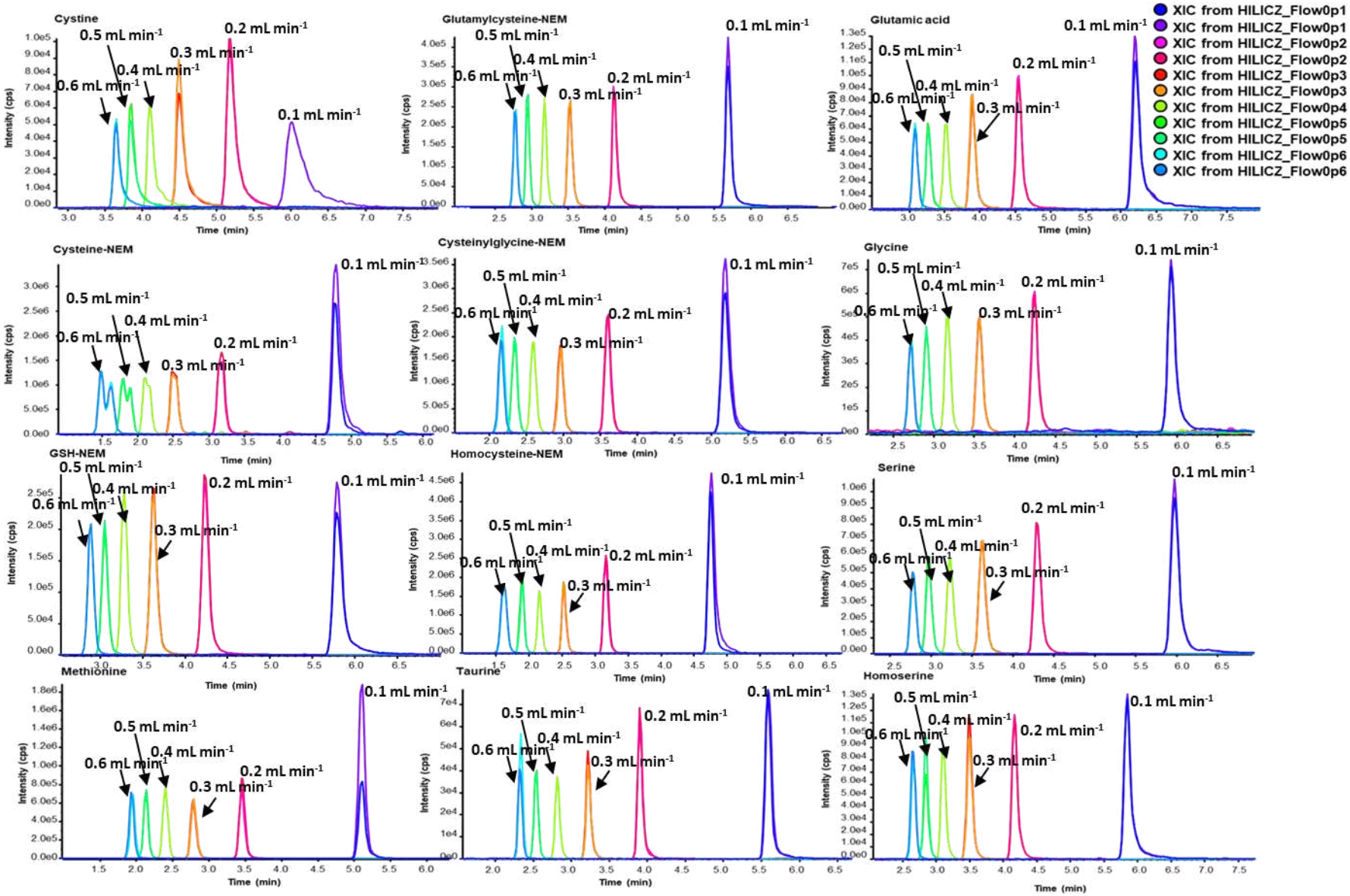

Figure S-5. LC flow rate optimization study. Individual flow rates in different colors. Individual flow rates listed above each sMRM transition.

Optimization of MS source parameters

MS source parameters (GS1, GS2 and TEM) were individually optimized and carefully selected to ensure the highest sensitivity. **Figure S-5, S-7** and **S-8** illustrate the effect of each source setting on every metabolite's signal. It is evident that optimal conditions were achieved at higher TEM values (temperature of TurboIonSpray TIS probe) and GS2 values (heater gas of TIS probe). The higher the TEM value, the more effective the nebulization process, thus resulting in a higher sensitivity, similar as for GS2.

The effect of the ion source temperature on the metabolites' signal was studied (**Figure S-5**). Seven different TEM values were programmed and their effect individually observed (350/400/450/500/550/600/650°C). Generally, higher source temperatures are required when working with high aqueous conditions, in order to provide optimal nebulization. As our method employs HILIC, high temperatures should generally not be required, as the mobile phase used is predominantly made out of organic solvents. However, we found an optimal signal to noise value at a source temperature of 650°C

Another source parameter investigated was GS1, which is the nebulizing gas. A constant steady stream of nitrogen, in our case zero-grade-air, is infused into the ion-source, aiding the ESI-droplet build-up and following nebulization. **Figure S-7** provides an overview of the effect of GS1 on the individual S/N ratio of each relevant metabolite analyzed in this study. It became evident, that a value of 30 psi provided the best results. Values close to 10 psi provided lower metabolite intensity, as did higher values above 30 psi as well. A lower signal intensity due to lower GS1 values can be explained due to the fact that the nebulization process is not efficient enough, thus resulting in lower S/N values. Higher GS1 values can hamper signal intensity, as they can contribute to degradation processes inside the ion-source.

The final source parameter requiring further optimization is the GS2 value. GS2, also called the heater gas, represents a steady constant flow of nitrogen, in our case zero-grade-air, which is infused to the ion-source, with the objective of keeping the temperature inside constant and equally distributed. **Figure S-8** provides an overview of how GS2 plays a role in the S/N of each individual metabolite inspected throughout this study. It is evident that the higher the GS2 value is, the better the signal intensity. This can be attributed to the fact that the nebulization process is more efficient, when the GS2 stream is at a higher psi value, as in this case 70 psi

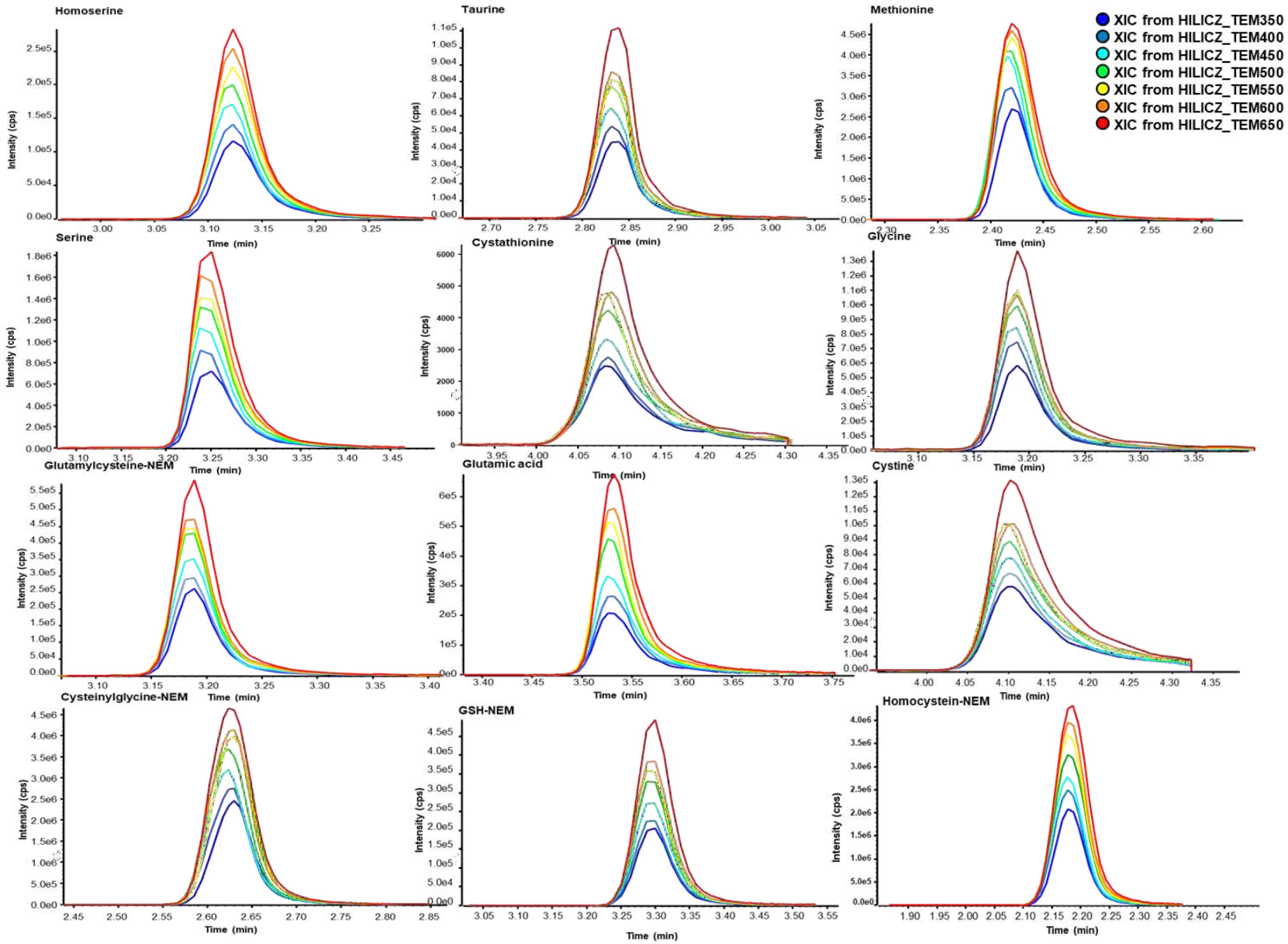

Figure S-6. MS Source Temperature (TEM) effect on analyte S/N values. Individual TEM values in different colours.

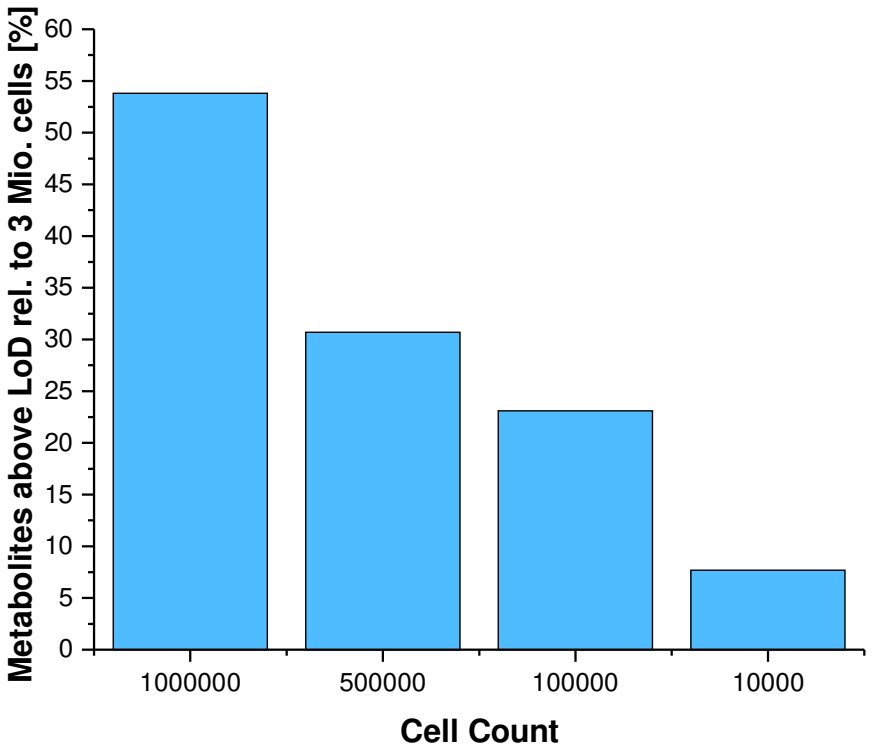

Figure S-7. Target metabolites detected above LoD relative to $3x10^6$ cells.

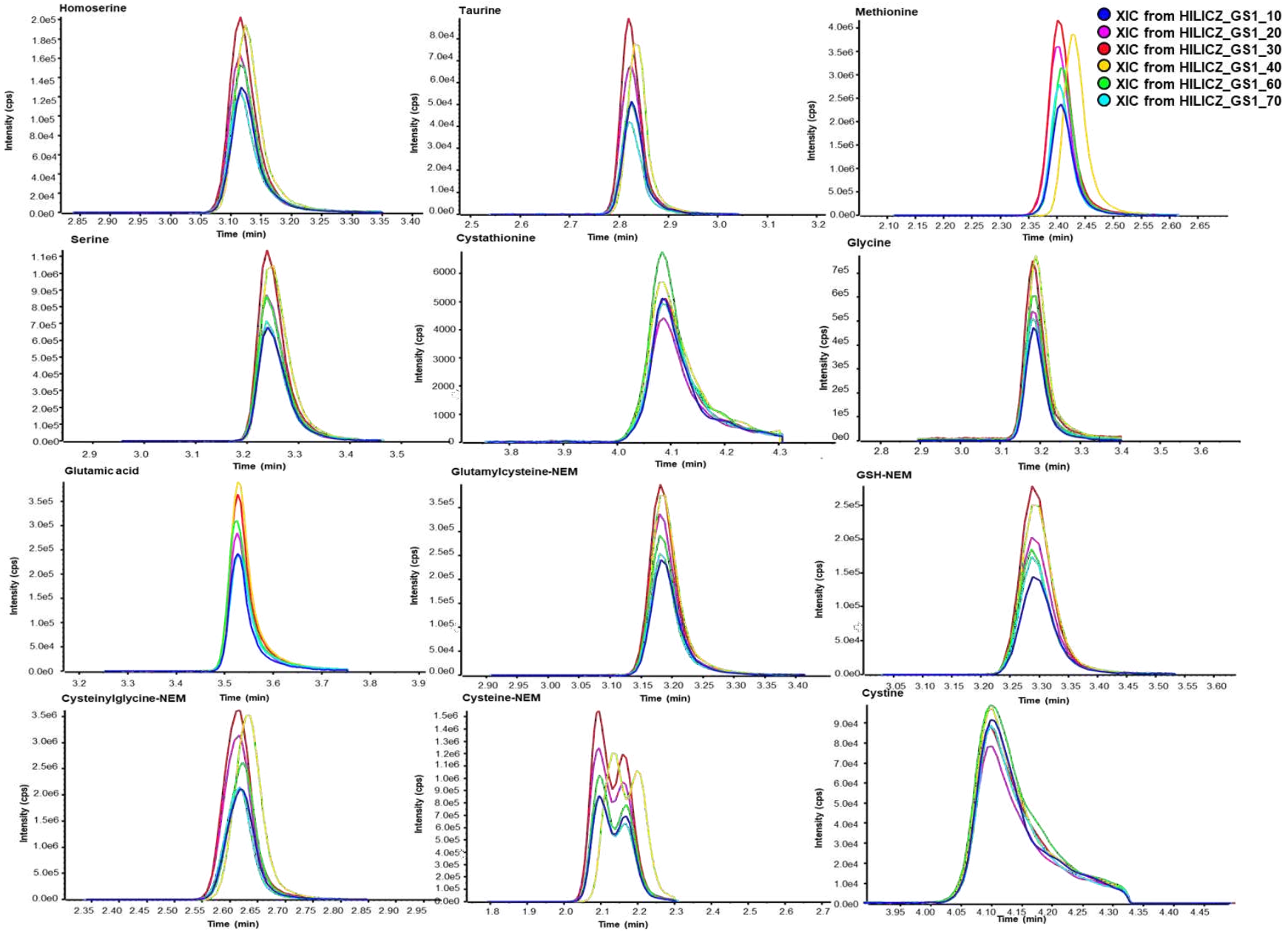

Figure S-8. MS Source nebulizer gas (GS1) effect on analyte S/N values. Individual psi values in different colours.

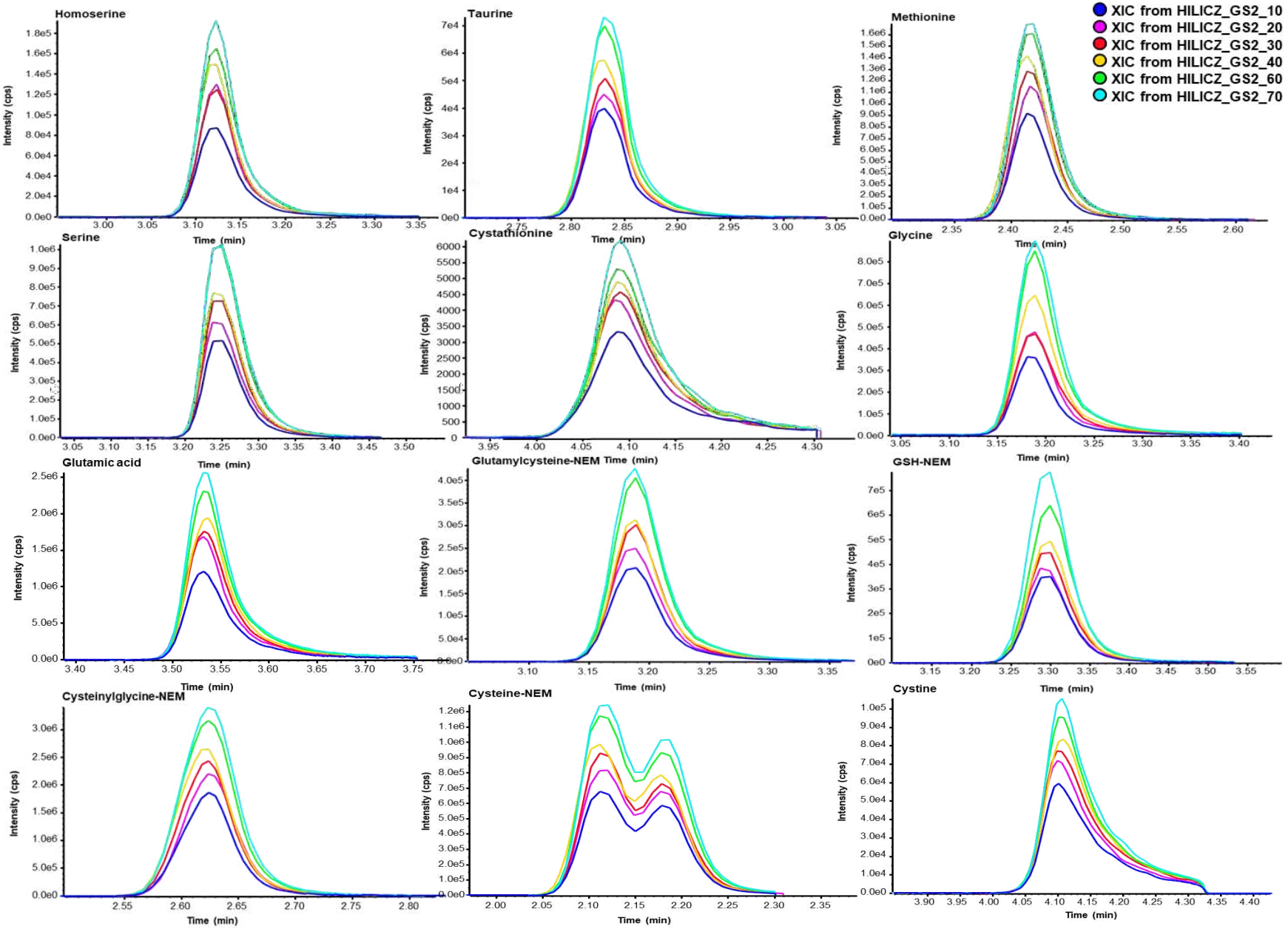

Figure S-9. MS Source temperature gas (GS2) effect on analyte S/N values. Individual psi values in different colours.

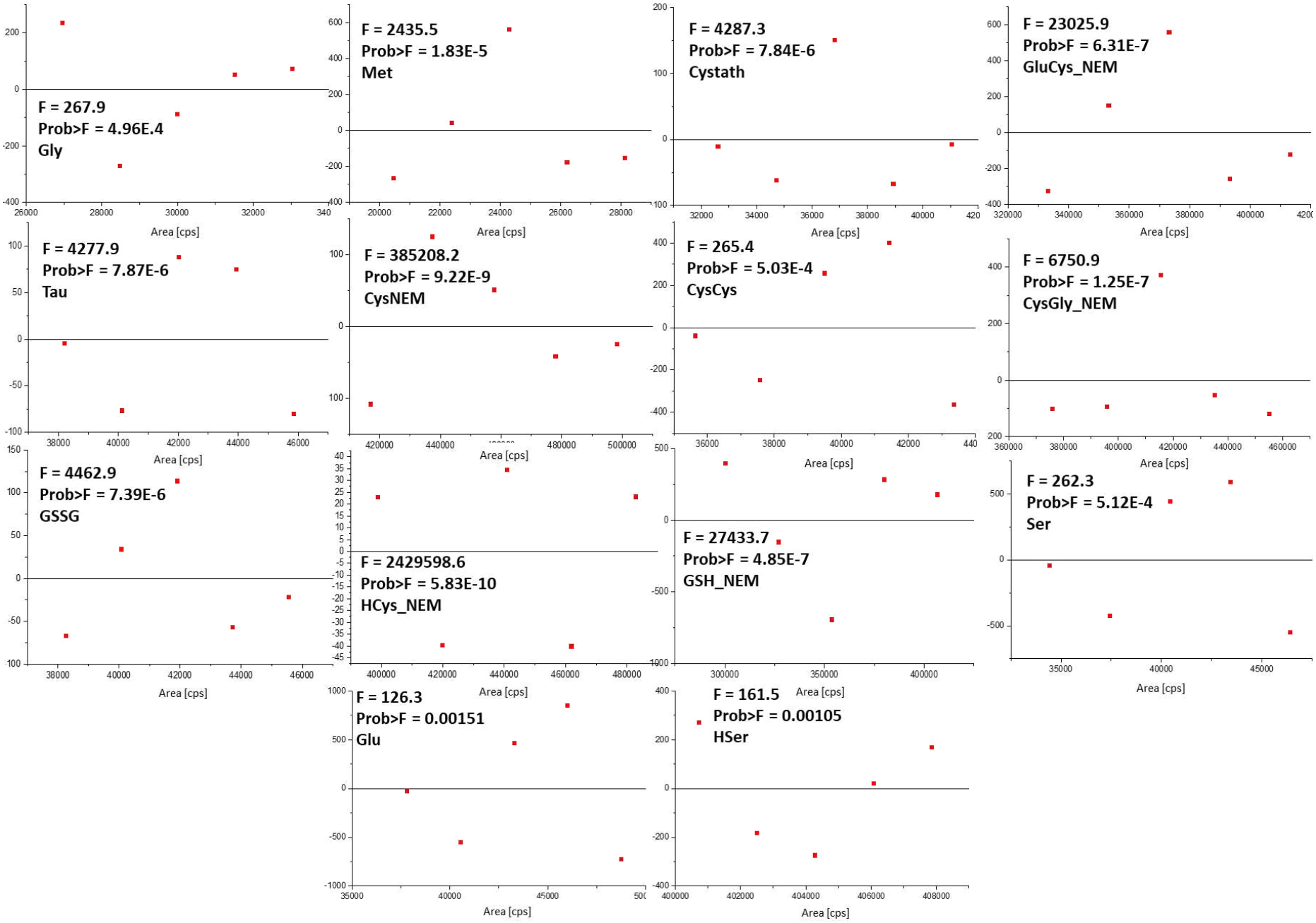

Figure S-10. Residual plots (fitted Y in area [cps]) and F-Values obtained for the linear calibration series of each individual target metabolite. Prob>F is used to assess the whole model test i.e. whether the null hy^{1}p^{5}othesis can be rejected. Values below p = 0.05 conclude that the variables are significantly related with the output, i.e. that the values obtained attain to the linear model.

Journal of Chromatography A 1730 (2024) 465060

Contents lists available at ScienceDirect

Journal of Chromatography A

journal homepage: www.elsevier.com/locate/chroma

Solving the retention time repeatability problem of hydrophilic interaction liquid chromatography

Kristian Serafimov [1], Cornelius Knappe [1], Feiyang Li, Adrian Sievers-Engler, Michael Lämmerhofer [*]

Institute of Pharmaceutical Sciences, Pharmaceutical (Bio-)Analysis, University of Tübingen, Auf der Morgenstelle 8, 72076 Tübingen, Germany

ARTICLE INFO

Keywords:
HILIC
Metabolomics
Peptide
Oligonucleotide
Liquid chromatography-mass spectrometry

ABSTRACT

Hydrophilic interaction (liquid) chromatography (HILIC) has become the first choice LC mode for the separation of hydrophilic analytes. Numerous studies reported the poor retention time repeatability of HILIC. The problem was often ascribed to slow equilibration and insufficient re-equilibration time to establish the sensitive semi-immobilized water layer at the interface of the polar stationary phase and the bulk mobile phase. In this study, we compare retention time repeatability in HILIC for borosilicate glass and PFA (co-polymer of tetrafluoroethylene and perfluoroalkoxyethylene) solvent bottles. During this study, we observed peak patterns shifting towards higher retention times (for metabolites and peptides) and lower retention times (oligonucleotide sample) with ongoing analysis time when standard borosilicate glass bottles were used as solvent reservoirs. It was hypothesized that release of ions (sodium, potassium, borate, etc.) from the borosilicate glass bottles leads to alterations (thickness and electrostatic screening effects) in the semi-immobilized water layer which is adsorbed to the polar stationary phase surface under acetonitrile-rich eluents in HILIC with concomitant shifts in retention. When PFA solvent bottles were employed instead of borosilicate glass, retention time repeatability was greatly improved and changed from average 8.4 % RSD for the tested metabolites with borosilicate glass bottles to 0.14 % RSD for the PFA solvent bottles (30 injections over 12 h). Similar improvements were observed for peptides and oligonucleotides. This simple solution to the retention time repeatability problem in HILIC might contribute to a better acceptance of HILIC, especially in fields like targeted and untargeted metabolomics, peptide and oligonucleotide analysis.

1. Introduction

Reversed-phase HPLC has become the preferred analytical technique for the analysis of organic molecules in fields like pharmaceutical and food analysis [1,2]. Besides excellent resolving power for molecules differing in lipophilicity, it provides robust and highly repeatable separations. However, highly polar molecules like metabolites, small hydrophilic peptides and oligonucleotides are often not sufficiently retained and separated. For this reason, hydrophilic interaction liquid chromatography (HILIC) is the favorable technique nowadays for hydrophilic analytes. The term HILIC has been coined by Andrew Alpert and he showed already in his landmark paper from 1990 that it has exceptional selectivity for amino acids, peptides, oligonucleotides, carbohydrates, organic acids, bases and metabolites [3]). It alleviates pre-column derivatization for enabling RPLC separation and makes the addition of MS-contaminating ion-pairing agents unnecessary [4,5]. The exceptional power of HILIC in various fields including metabolomics has been demonstrated in numerous studies and reviews [6–16]. Part of the great success of HILIC is a wide choice of distinct, nowadays also stable HILIC stationary phases with wide flexibility in the surface chemistry and hence selectivity. According to the ionic character of the functional group being present on the stationary phase surface they can be classified either as neutral phases (amide, diol), charged phases (amino, silica) or zwitterionic phases (e.g., sulfobetaine-modified) [17]. As orthogonal separation principle to RP, HILIC is also of high interest in multidimensional liquid chromatographic separations [18–20].

Although the retention and separation mechanism in HILIC is less clear than in RPLC, a significant gain in the understanding has been seen in the last decade due to a number of seminal fundamental works [21]. Like hypothesized in prior work on carbohydrates separation with

* Corresponding author.
E-mail address: Michael.laemmerhofer@uni-tuebingen.de (M. L¨ammerhofer).
[1] Shared first authorship

https://doi.org/10.1016/j.chroma.2024.465060
Received 22 April 2024; Received in revised form 5 June 2024; Accepted 7 June 2024
Available online 8 June 2024
0021-9673/© 2024 The Author(s). Published by Elsevier B.V. This is an open access article under the CC BY license (http://creativecommons.org/licenses/by/4.0/).

3-aminopropylsilica and acetonitrile-water eluents, it was already claimed by Alpert in his paper from 1990 that 'the stationary phase retains a semi-immobilized layer of mobile phase enriched with water. Chromatography of carbohydrates involves partitioning between this stagnant aqueous layer and the bulk of the (mostly organic) mobile phase. It would be reasonable to suppose that the partition mechanism advanced for the chromatography of carbohydrates represents the mechanism of HILIC fractionations of other classes of polar solutes as well' [3]. Several studies have been published in following years with the aim to support the existence of a 'semi-immobilized' water layer which dynamically changes its thickness and structure as the composition of the mobile phase is altered [24–26]. As a matter of consequence, hydrophilic analytes are stronger retained as the thickness of the water layer increases (due to increase in phase ratio), unless ionic interactions between analyte-adsorbent take over a dominant role. McCalley and Neue showed 'that about 4–13 % of the pore volume of a silica phase is occupied by a water-rich layer when using acetonitrile–water containing 95–70 % (v/v) acetonitrile' [25]. Tallarek and coworkers studied interface behavior of water-acetonitrile mixtures (with 2 to 30 % water) on HILIC surfaces (diol-silica and plain silica) by molecular dynamics simulations [27]. Their results suggest a rigid layer of bound water molecules adsorbed directly at the silica surface (immediate region containing almost exclusively water as measured by radial number density profiles of water oxygen) is surrounded by an interstitial diffuse layer of water molecules. The adjacent interface region showed a high water density towards the immediate region before it declined gradually into the bulk region, where the water (oxygen) number density profiles matched those of the bulk solvent composition.

Experimental support for the surface-adsorbed water layer model comes from excess adsorption isotherm measurements [28,29] which also explain well the changing water-layer density and structure, respectively, with increasing water content in the HILIC eluent. Between 10 and 30 % water in ACN the excess adsorbed amount of water reaches typically a maximum while it declines strongly above 30 % water in the eluent. Temperature also affects the water shell which is typically thicker at low temperature. The effect of salts in the HILIC eluent are complicated, due to their distinct solvation, kosmotropic-chaotropic effects and superimposed attractive-repulsive charge modulations [29]. Results by Alpert suggested that well hydrated eluent ions promote partitioning of charged solutes (less of neutral solutes) into the immobilized aqueous layer in HILIC, while poorly hydrated eluent ions have the opposite effect [29]. It was concluded that chaotropic ions, which are poorly hydrated, tend to partition into the predominantly organic mobile phase in HILIC and kosmotropic ions into the aqueous layer. In other studies, it was demonstrated that retention of neutral solutes increased at higher buffer concentration, which is usually attributed to the salt increasing the volume of the aqueous layer on the stationary phase [25]. This effect can be measured with toluene that cannot penetrate the water layer and is increasingly excluded from the pores with higher buffer concentration, and also as the polarity of the stationary phase increases [25]. Besides partitioning between adsorbed water layer and bulk mobile phase, polar analytes can also directly interact with the ligands and silica backbone of the stationary phases under HILIC conditions through hydrogen-bonding, dipole-dipole interactions and ionic interactions (with dissociated silanols and/or charged groups of the immobilized ligands if present). Hence, a mixed-mode mechanism of partitioning and adsorption is commonly accepted in HILIC nowadays [26]. Knowledge of the above dependencies seem to be of importance to design robust separations in HILIC. While the fundamentals of HILIC retention mechanisms look complicated, practice of HILIC has put forth numerous advantages such as excellent selectivity for hydrophilic compounds, good peak shapes, higher sensitivity in ESI-MS, and so forth [23]). In spite of many successful HILIC separations, HILIC has still a poor reputation. Various authors reported poor run-to-run repeatability in HILIC [30]. Tacitly, it is often assumed that the repeatability problem arises from slow column re-equilibration in gradient HILIC. For this reason, several authors performed rigorous studies on partial and full re-equilibration in HILIC as a potential solution to the problem [22,23,31,32]. In particular for metabolomics (addressing a majority of acidic metabolites), other authors suggest the use of anion-exchange chromatography (hyphenated with mass spectrometry via suppressor technology) to overcome the repeatability problem observed in HILIC-based metabolomics [33,34]. Comparison of HILIC-MS and anion-exchange-suppressor-ESI-MS (AEX-MS) by McCullagh and coworkers provided significantly less retention time variance for AEX-MS compared to HILIC-MS [33]. Analytical methods, in which ion concentrations are critical, are typically using plastic bottles as eluent reservoirs, like in ion-chromatography or ICP-MS to avoid background ion contamination. Hence, it might be supposed that in above cited AEX-MS experiments by McCullagh plastic bottles were used for the eluent and borosilicate glass bottles, which are standard for HPLC instruments, for HILIC. Indeed, there is an application note from Agilent Technologies which recommends the used of Nalgene FEP bottles for the mobile phase reservoirs in HILIC in order to avoid the negative effect of sodium ions [35]. However, no comparison with borosilicate glass bottles was shown and this application note may not be known to a wider community of HILIC users.

For this reason, the objective in this work is to elucidate the effect of using plastic (PFA) instead of borosilicate glass bottles for HILIC experiments. Retention time repeatability of polar metabolites (in untargeted urinary metabolomics), peptides and oligonucleotide test samples was documented for bringing the advantage of plastic bottles in HILIC separations to the attention of a wider community of researchers. A discussion of the observed effects with interpretation in view of HILIC mechanisms is given.

2. Experimental

2.1. Materials

Formic acid, acetic acid, acetonitrile and methanol of Ultra LC-MS grade were supplied by Carl Roth (Karlsruhe, Germany). Ammonium hydroxide solution (Suprapur® quality 28.0 - 30.0 % NH_3 basis) was purchased from Sigma-Aldrich (Merck, Taufkirchen, Germany). Deionized water was purified by a Purelab ultrapurification system (ELGA LabWater, Celle, Germany). All metabolite standards and Teicoplanin (T0578) used in this study were provided by Sigma-Aldrich (Merck). The antisense (single) strand of Patisiran was synthesized by Oligo Sigma (Merck, Munich, Germany) and purchased as desalted raw products without any pre-purification. Stock solutions of the individual standards were prepared in glass vials at concentrations of 1 mg mL^{-1} (50/50 MeOH/H_2O) and used for further dilution. The individual stocks were stored at −80 °C until use. PFA co-polymer (tetrafluoroethylene and perfluoroalkoxyethylene) bottles were supplied by AHF Analysentechnik (Tübingen, Germany). Glass mobile phase solvent bottles were of Duran® borosilicate glass and were provided by Schott AG (Mainz, Germany).

2.2. Metabolomics and oligonucleotide instrumentation

LC-MS analysis of metabolites in urine and of oligonucleotides was performed using an Agilent 1290 Infinity I series LC system from Agilent Technologies (Waldbronn, Germany) equipped with a binary pump, thermostated column compartment and an HTC-xt PAL (CTC Analytics AG, Zwingen, CH) autosampler hyphenated to a TripleTOF 5600+ mass spectrometer with DuoSpray Source, operated in TurboIonSpray mode, from Sciex (Ontario, Canada). The LC system was coupled to a Sciex CDS (calibrant-delivery-sytem) for mass calibration. All analytical hardware was standard and not equipped with biocompatible flow path.

2.3. Peptide analysis instrumentation

LC-UV chromatograms were acquired using an Agilent Technologies 1290 Infinity II 2D-LC system. The system consisted of two 1290 Infinity II High Speed (binary) pumps (G7120A), a 1290 Infinity II Multisampler (G7167B), two 1290 Infinity II Multicolumn thermostat compartments (G7116B), a 1290 Infinity II diode array UV absorbance detector (G7117B) and three 1290 Infinity II Valve Drives (G1170A). Both pumps were utilized with the 100 μL JetWeaver. A Max-Light Cell (G4212−6008) with 10 mm path length and V(σ) = 1 μL was used. The flow cell of the ^{1}D UV detector was protected by a pressure relief kit (G4236−60,010). Valve drives were equipped with two deck valve heads and an ASM valve head (G4243A, G4242A) to enable Multiple-Heartcutting (MHC) 2D-LC or Selective Comprehensive 2D LC (sLCxLC) with 40 μL sample loops. In addition, column selector valve heads (G4234C) were installed in both Multicolumn thermostat compartments implementing the option for column screening. The 2D-LC system was coupled to a Sciex CDS (calibrant-delivery-sytem) and further to a Sciex TripleTOF 5600+ system with DuoSpray source electrospray-ionization. All analytical hardware was standard and not equipped with biocompatible flow path. The 2D-HPLC system was operated using Agilent OpenLab CDS ChemStation Edition Rev.C.01.10 and the mass spectrometer was controlled by Sciex Analyst TF 1.8.1.

2.4. Urine sample preparation

Pooled urine (first morning mid-stream) (from volunteers with informed consent), stored at 4 °C until use, was used for sample preparation. As urine is susceptible for bacterial growth, a 0.22 μm sterile filter was used to filter the samples. Samples were then centrifuged at 4 °C, 20,784 rcf x 15 min to remove cell debris and unwanted precipitants. Each 1 mL sample aliquot was preserved at −80 °C until further metabolomic analysis. Samples were freeze dried in a Labconco (Kansas City, MO, USA) FreeZone 4.5 L Benchtop Freeze Dry System for 24 h and subsequently reconstituted in 100 μL water and 900 μL acetonitrile. Three cycles of vortexing and sonication (each 30 s) were conducted following sample centrifugation at 18,928 rcf for 5 min and analysis of the supernatant.

2.5. Metabolomics methodology

A Premier BEH Amide column (150×2.1 mm, 1.7 μm) provided by Waters (Eschborn, Germany) was used for the chromatographic separation. During analysis of metabolites in ESI^{+} mode, mobile phases A and B were set to a pH of 3.5 with formic acid and included 20 mM ammonium formate in water and water/acetonitrile (10/90; v/v), respectively. In negative ionization mode (ESI^{-}), the chromatographic conditions were different. Mobile phase A and B were set to a pH of 7.5 with acetic acid and included 20 mM ammonium acetate in water and water/acetonitrile (10/90; v/v), respectively. Gradient elution was identical for both ionization modes (0.0 min, 100 % B; 13 min 70 % B; 15 min 70 % B; 15.1 min 100 % B; 20 min 100 % B) and was adjusted to a flow rate of 0.25 mL min^{-1} and a constant column compartment temperature of 35 °C was maintained throughout the entire analytical run. Injection volume was 5 μL. The autosampler was kept at 4 °C. The experimental MS-setup involved a TOF-MS survey scan for precursor detection in the mass range of *m/z* 60−1000 (ESI^{+}) and *m/z* 70−900 (ESI^{-}), respectively. In order to ensure comprehensive recording of MS/MS spectra, SWATH acquisition was implemented with a collision energy of ± 30 V and a collision energy spread of ± 20 V. Twenty SWATH-MS/MS experiments were created for both positive and negative ion mode (Table S-1). Variable SWATH window widths were optimized by swathTUNER based on preliminary measurements using DDA [37]. Experimental parameters in SWATH were as follows - accumulation time was set to 30 ms. The total cycle time summed up to 750 ms. The MS instrument was run in high sensitivity mode achieving a TOF-MS resolution of 30,000 (FWHM @ *m/z* 829.5393) and a SWATH-MS/MS resolution of 15,000 (FWHM @ *m/z* 397.2122). Ion source parameters were the following: nebulizer gas (GS1, zero grade air) 50 psi, heater gas (GS2, zero grade air) 30 psi, curtain gas (CUR, nitrogen) 30 psi, source temperature (TEM) 450 °C, ion source voltage +5500 V (positive mode) and −4500 V (negative mode). Samples were initially analyzed in positive and then in negative ionization mode. A Calibrant Delivery System by Sciex was used to provide mass calibration before every analytical run and the analytical system was controlled by the Analyst 1.7 TF software (AB Sciex, Darmstadt, Germany).

2.6. Peptide analysis methodology

The principal components of the mixture of Teicoplanin (1 mg/mL in ACN/H_2O (80:20 v/v)) were separated in the first dimension on a Waters Premier BEH Amide column (150×2.1, 1.7 μm) and analysed by UV detection. Mobile phase A consisted of water with 10 mM ammonium acetate and mobile phase B of water in acetonitrile (5:95, v/v). Injection volume was 1 μL. An extensive long ^{1}D gradient was used due to the long ^{2}D run times. The gradient elution profile was 0.0 min, 100% B, 0.5 ml/min; 30 min, 64% B, 0.5 ml/min; 30.01 min, 0% B, 0.3 ml/min; 42.1 min, 100%, 0.3 ml/min; 42.11 min, 100% B, 0.3 ml/min; 54.2 min, 100% B, 0.3 ml/min; 54.21 min, 100% B, 0.05 ml/min; 199.99 min, 100% B, 0.05 ml/min; 200 min, 100% B, 0.5 ml/min; 206 min, 100% B, 0.5 ml/min. The temperature of the column was kept at 50 °C and a multisampler temperature of 4 °C was programmed. A sampling rate of 80 Hz and a wavelength of 254 nm were used for UV detection.

2.7. Oligonucleotide analysis methodology

Oligonucleotide separation was performed on a Waters (Eschborn, Germany) Premier BEH Amide column (50×2.1 mm, 1.7 μm) in ESI^{-} mode. Mobile phases A and B were adjusted to a pH of 9.0 with acetic acid and consisted of 15 mM ammonium acetate (water/acetonitrile 30/70 mobile phase A) and 15 mM ammonium acetate in water (mobile phase B). The gradient elution profile was (0.0 min, 100 % A; 10 min 40 % A; 10.01 min 100 % A; 20.0 min 100 % A) and was carried out at a flow rate of 0.25 mL min^{-1} and a constant column temperature of 30 °C was maintained throughout the entire run. The injection volume was 5 μL. The autosampler was kept at 4 °C. The MS experiment consisted of a TOF-MS survey scan for precursor detection in the mass range of *m/z* 100−2000. MS/MS spectra were recorded in DDA acquisition mode, with a collision energy of −35 V and a declustering potential (DP) value of −100 V. The total cycle time summed up to 1.25 s. The MS instrument was run in high sensitivity mode achieving a TOF-MS resolution of 30,000 (FWHM @ *m/z* 829.5393) and a MS/MS resolution of 15,000 (FWHM @ *m/z* 397.2122). Ion source parameters were as follows: nebulizer gas (GS1, zero grade air) 80 psi, heater gas (GS2, zero grade air) 80 psi, curtain gas (CUR, nitrogen) 40 psi, source temperature (TEM) 450 °C, ion source −4500 V (negative mode).

2.8. Data processing and evaluation

All further data processing steps and evaluations were executed with MS-DIAL, PeakView 2.2 (Sciex), MultiQuant 3.0 (Sciex), Excel 2016 (Microsoft, Redmond, WA, USA), Origin 2021 (OriginLab, Northampton, MA, USA), and R Studio 1.4.1717 (R Foundation for Statistical Computing, Vienna, Austria).

3. Results

3.1. Retention time repeatability of metabolites in urinary metabolomics analysis

A pooled human urine sample (pooled urine QC sample) was subjected to gradient HILIC-MS analysis by untargeted SWATH-MS

detection once with common borosilicate glass bottles and once with PFA bottles as solvent reservoirs for both A and B channel. The sample was injected 30-times ($n = 20$) over a period of 12 h for each glass and PFA bottles. It allowed to extract chromatograms of numerous metabolites of different physicochemical character in terms of ionization state (anionic, cationic, zwitterionic) and hydrophilicity range (log D at mobile phase pH) to cover a wide molecular space. Fig. 1 shows overlays of representative chromatograms of tryptophan, ethylmalonic acid, and 1-methyl-adenosine recorded with the glass bottles. It can be seen that with the borosilicate glass bottles there is a significant drift of retention from the first injection to the last injection regardless what is the analyte character. Table S-2 gives the statistics for the retention time distributions of representative analytes with glass bottles used during analysis. It can be seen that in all cases evaluated the drift in retention leads to longer retention times and the chemical properties of the selected metabolites (acidic, basic or zwitterionic) play no crucial role in the drift pattern, as the phenomenon observed is identical.

The corresponding results for the PFA solvent bottles are shown in Fig. 2 (exemplified for citrulline, tryptophan, ethylmalonic acid, methionine, carnitine and 1-methyl-adenosine). Retention time data are summarized in Table S-3 for a wider set of analytes. Fig. 3 shows the distributions of the RSD values of retention times as a comparison between PFA and glass bottles, with the difference between both being striking. It is evident that the RSD values obtained during measurements with glass bottles as mobile phase storage vessels are much higher than the ones obtained with PFA bottles. The choice of buffer anion, formate versus acetate, is not making a difference. Comparison of results from 2 different ionization modes with ammonium formate as additive in ESI^+ and ammonium acetate in ESI^- under otherwise identical conditions showed the same results. It can be concluded that the use of PFA bottles reduced the retention time variance significantly. The%RSDs with PFA solvent bottles are now in a range (on average 0.14 % RSD versus 8.4 % with borosilicate glass bottles) which are commonly observed in RPLC.

3.2. Retention time repeatability of 2D-LC peptide analysis

2D-LC has become an accepted routine technology in pharmaceutical analysis to resolve complex mixtures or combine orthogonal selectivities from two columns when one dimension cannot solve the problem. Furthermore, the ^{2}D has served as a tool to desalt MS-incompatible ^{1}D separations before ESI-MS detection. This is of particular interest also for complex therapeutic peptide samples. Various 2D-LC modalities are available, viz. (multiple) heart cutting, selective comprehensive and full comprehensive [38,39]. There are various critical factors in 2D-LC for the successful implementation and retention time repeatability of the ^{1}D separation is one for (multiple) heartcutting 2D-LC. If retention time of a peak of interest to be sampled into the second dimension is shifted, the center of the peak (in case of a slight t_R shift) or the peak entirely (in case of severe drift) may be missed and hence transfer into the second dimension was not adequate leading to sensitivity loss or complete loss of a peak. Stoll and co-worker already showed (for HILIC×HILIC) that with quite short (<<10 min) re-equilibration times separation repeatability can be excellent, even when full column equilibration actually takes longer time [32]. The repeatability of separation was improved at higher flow rate.

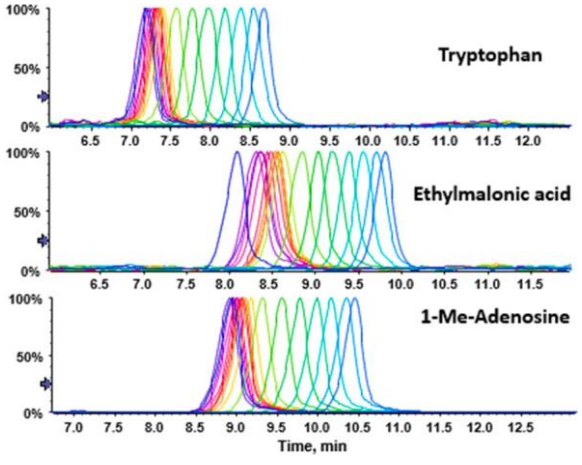

Fig. 1. Representative chromatograms of test solutes from successively injected metabolomics urine QC samples measured over 12 h ($n = 30$) with mobile phase stored in (Duran) borosilicate glass bottles. Blue to red colour shift represents $n = 1$ to $n = 10$, red to yellow $n = 10$ to $n = 23$, yellow to green-blue $n = 23$ to $n = 30$. Pattern follows the trend that with progressive injection time an increase in retention time is observed (for corresponding retention time data see Table S2 of the supplementary material).

The goal of our study was to establish a multiple heart cutting method for Teicoplanin. Teicoplanin is a macrocyclic glycopeptide antibiotics which is produced by fermentation by *Actinoplanes teichomiceticus*. The pharmacopeia specifies 6 major components (A2−2 as the main peak, A2−1, A2−3, A2−4, A2−5 and A3−1) and 2 minor components (A2−1a, A2−1b) (European Pharmacopeia 10.0). They differ by their fatty acid side chains on the amino sugar residue. A3−1 lacks the amino sugar residue at which different fatty acids are attached in the other components. Besides there are several microcomponents present. Methods for quality control are mostly based on RPLC and often employ phosphate buffers. Here, it was of interest to establish a complementary LC method based on HILIC as a first dimension (^{1}D) separation. Fig. 3A shows the ^{1}D-HILIC-UV runs of 18 consecutive injections using borosilicate glass bottles as solvent reservoir. As can be seen there is a significant drift in the peaks, again to longer retention times with higher injection number. For the main A2−2 peak (largest peak in the chromatogram), a mean t_R of 20.980 (±0.077) min was observed corresponding to 0.37 % RSD. While this looks at first glance not too bad, it is evident that such a ^{1}D LC method would not be suitable for time-based multiple heart cutting. Better retention time repeatability is required. The same set of experiments was repeated with PFA bottles as solvent reservoirs in A and B channel. It is evident from Fig. 3B that the repeatability was greatly improved. A mean t_R of 20.436 (±0.009) min was observed corresponding to 0.045 % RSD. The repeatability gain was the same for the other peaks in the HILIC chromatogram. This robust, highly repeatable separation makes time-based multiple heart cutting possible.

3.3. Repeatability in oligonucleotide analysis

HILIC is gaining increasing interest for the separation of oligonucleotide and it was of interest whether retention time repeatability can be improved for this type of solutes as well. The antisense (single) strand of the siRNA Patisiran (the API of Onpattro) was employed as test sample. The repeated injection ($n = 7$) on the HILIC Amide column showed a mean t_R of 5.824 (±0.043) min corresponding to 0.738 % RSD for the borosilicate glass bottles and a mean t_R of 5.794 (±0.016) min corresponding to 0.276 % RSD for the PFA bottles (Fig. 5). Again, a significant improvement of t_R-repeatability can be observed with the PFA bottles also for oligonucleotides. However, for the tested oligonucleotide the retention drift is different than for the other analytes: Retention time decreases with increasing injection order. It is also noticeable that the peak area declines with every injection, both for glass and PFA bottles. It may be related to the fact that glass (instead of plastic) inserts to vials were used for the sample and only ultrapure water to dissolve the analyte. Possibly, more oligonucleotide adsorbs to the glass wall the longer the sample is standing. Analyses with glass bottles were performed first which explains the smaller peaks for the PFA bottles. It is further striking that the overlaid curves in Fig 4B with the PFA bottles look like a loading study with perfect match of the rear end of the peaks as commonly observed in adsorption isotherm measurements following the Langmuir model. If we omit the two first

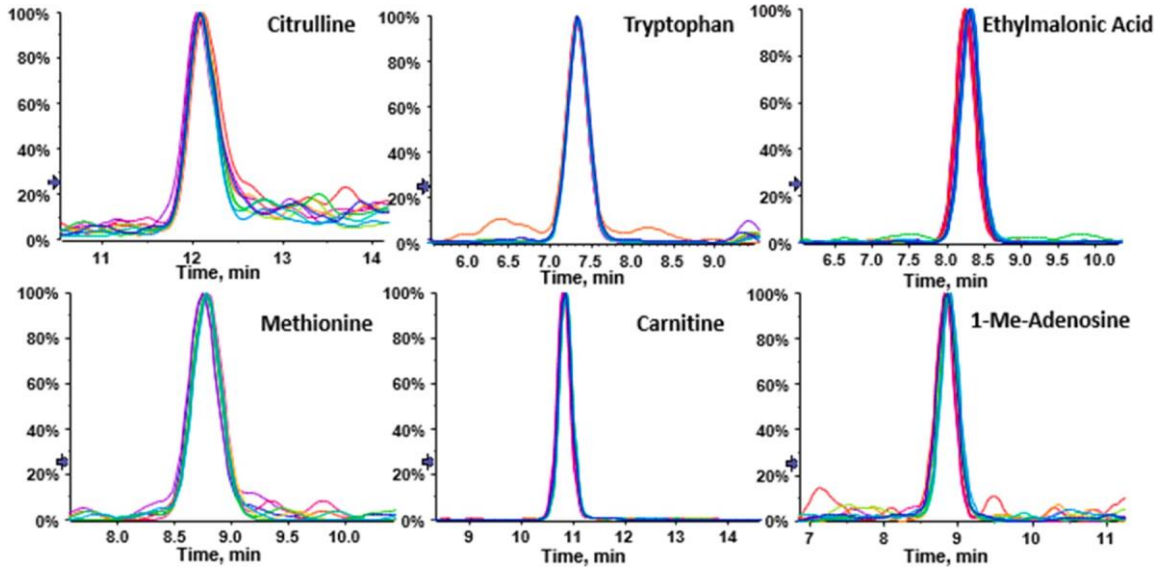

Fig. 2. Representative chromatograms of test solutes from successively injected metabolomics urine QC samples measured over 12 h (n = 30) with mobile phase stored in PFA plastic bottles.

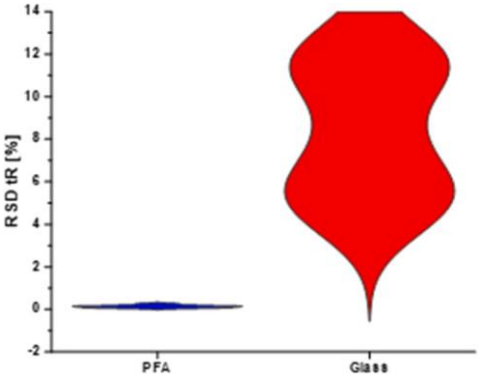

Fig. 3. Violin plot representing the distribution of% RSD values as a comparison between PFA and glass bottle usage during analysis.

injections with the PFA bottles, after which the concentration does not change much anymore, the retention time repeatability is even better, i. e. a mean t_R of 5.803 (±0.003) min was observed corresponding to 0.054 % RSD. This confirms that PFA bottles are also advantageous for HILIC of oligonucleotides.

3.4. Discussion

HILIC was repeatedly reported to suffer from poor run-to-run retention time repeatability [32] which makes problems for its acceptance in untargeted analysis, metabolomics, quality control laboratories, and so forth. Intuitively, it was supposed that the problem is caused by slow re-equilibration to re-establish the complex structured "semi--immobilized" water layer consisting of a strongly bound inner water layer adjacent to the polar stationary phase and a diffusive aqueous layer between this fixed layer and the bulk organic eluent phase [27,30]. Supposedly, the problem exists due to the fact that under typical experimental conditions (gradient HILIC) reequilibration of the stationary phase is not sufficiently achieved. In a number of studies, controlled re-equilibration could at least partly alleviate or at least abate the problem [21]. Agilent Technologies has published a HILIC application note in which they used Nalgene FEP bottles as solvent reservoirs [36]. No comparative data on the effect of these plastic bottles compared to glass bottles on retention time repeatability are given. Since this application note is not widely known, we provide here a comparative study on borosilicate glass and plastic solvent bottles for HILIC separations of 3 different sets of analytes.

HPLC instruments are typically supplied with Duran borosilicate glass bottles as mobile phase reservoirs. It is composed of SiO_2, B_2O_3, Na_2O/K_2O, and Al_2O_3 (81:13:4:2; approximate weight%). Their use in various modes of LC including HILIC is not much questioned. Borosilicate glass is highly resistant to water, neutral and acidic (buffer) solutions, yet a slight release of monovalent ions takes place (protons diffuse into the glass network and ion-exchange takes place releasing Na^+ or K^+ ions) [39]. Furthermore, borosilicate glass bottles can also release boron, silicate, calcium and aluminium ions [40,41–44]. A thin layer of impervious silica gel is subsequently formed on the glass surface (dissolution-reprecipitation mechanism). It slows down further attack of the glass surface. Moreover, glass dissolution (corrosion) is preferred under basic conditions [45]. This phenomenon of borosilicate glass corrosion is a result of the formation of the passivating gel layer on the glass surface [41]. In detail, when solvent and glass are in contact, the hydrolysis rate of B-O-Si linkages and the diffusion rate of the reactants (e.g. water molecules) and the reaction products (B_{aq}, Ca_{aq}) through the closed pores in the gel layer try to reach an equilibrium [41]. These mechanisms remain poorly understood and are highly dependent on factors such as time, exact glass composition, pH, temperature, solvent, and even ions already present in the solvent. We assume that different solvents, buffers and modifiers, which are commonly used in HILIC, disturb such equilibria and cause therefore not only ion release but also ion replacement by hydrogenated species (e.g. Na^+ by H^+) [44].

The release of monovalent ions such as Na^+ into the mobile phase has no significant influence on retention of lipophilic compounds in RPLC. However, in LC modes that are sensitive for varying ion concentrations such as in ion-exchange chromatography and obviously also HILIC, the glass corrosion with its release of ions into the mobile phase has a significant implication on the sensitive stationary phase-mobile phase partitioning equilibria. Na^+ ions are known to be strongly solvated while ammonium ions are poorly solvated [29]. It has been shown by Alpert that, when the cation in the HILIC mobile phase (pH 2.5) with neutral PolyHydroxyethyl A column was exchanged, retention of a peptide increased in the order of $NH_4^+ < Na^+ < Li^+$ [29]. This alteration of retention on a neutral stationary phase may be attributed to a thicker solvent shell on the stationary phase surface in this same order, thus

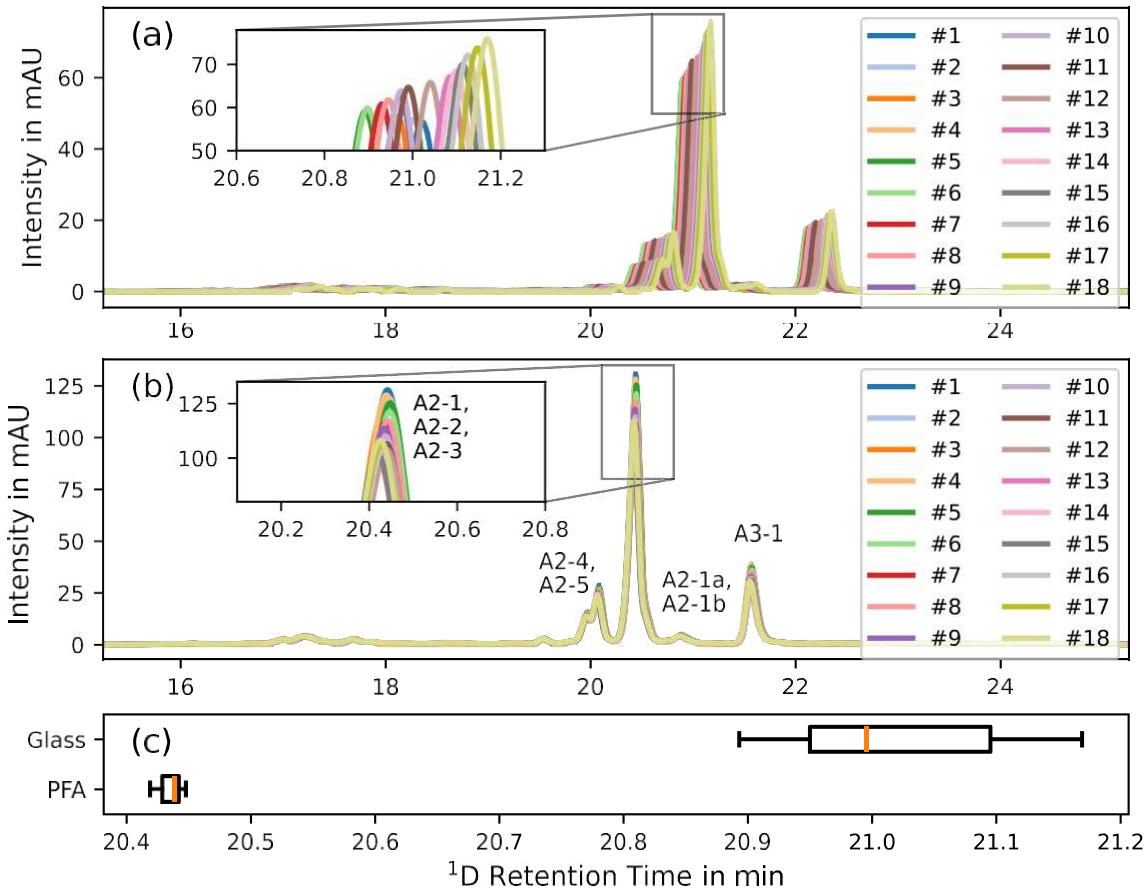

Fig. 4. Representative chromatograms of successively injected teicoplanin test sample solution and comparison of PFA vs glass bottles. (a) UV chromatogram with (Duran) borosilicate glass bottles, shift to higher retention times. (b) UV chromatograms with PFA, no shift. (c) Boxplot shows better repeatability for PFA bottles.

increasing the phase ratio and hence retention. As the thickness of the solvation shell of the respective cation increases, the solvated cation has a stronger propensity to be distributed into the semi-immobilized solvent shell which then gets thicker and causes stronger retention of analytes. Sodium released from the borosilicate glass into the mobile phase is a strongly solvated ion, thus may slowly accumulate in the aqueous layer during HILIC analysis due to its poor thermodynamic solubility in acetonitrile-rich eluent. For keeping electroneutrality, less solvated ammonium ions may be exchanged into the bulk mobile phase due to its better thermodynamic solvation quality in the acetonitrile-rich eluent. This successive restructuring of the aqueous layer of the neutral stationary phase (BEH Amide) with increasing injection number (as more Na^+ ions are released from the glass surface) could explain the increasing retention of the polar metabolites (at pH 3.5) (Fig. 1) and of the peptide sample (under weakly acidic conditions; pH 5.4) (Fig. 4a).

To detect sodium in the system, ion currents for sodium acetate clusters were extracted from the injections of the peptide samples (Fig. 4). As can be seen from Fig. 6, sodium which was well retained elutes as a sharp zone from the HILIC column. Like the peptide sample, also the sodium peak shows increasing retention times and poor retention time repeatability upon repeated injection with the borosilicate glass bottles. In contrast, with the PFA bottle only the first injection is slightly shifted (blue line in Fig. 6) while in general the sodium acetate peaks exhibit stable retention with the PFA bottle (black peaks in Fig. 6). Whether the sodium originates from the teicoplanin sample or from sharp elution of the sodium which was continuously released from the borosilicate bottles and trapped on the HILIC stationary phase until the elution strength is high enough to elute sodium remains unclear.

For the oligonucleotide sample (pH 9), the trend was different. With increasing injection number retention decreased with borosilicate glass bottles (Fig. 5a). Obviously, the above hypothesis does not explain the retention shifts of the oligonucleotide test sample. A possible explanation is an altered retention mechanism. Oligonucleotides elute at much higher water content (here > 30 %). This has been discussed also by D'Atri and coworkers [46]. As can be derived from excess (water) adsorption isotherm measurements [28,29] the water layer on the surface is destabilized above 30 % water in the eluent and disappears at around 50 %. Partitioning may no longer be of relevance. As discussed above, Na^+ is stronger solvated than NH_4^+. It may therefore have lower effective charge density. While NH_4^+ has a stronger charge screening effect on both the oligonucleotide and the negatively charged silanols (at pH 9), release of Na^+ from the glass bottle to the mobile phase may slightly change the screening effect of electrostatics. If NH_4^+ is replaced by Na^+ (less charge density), repulsive electrostatics between negatively charged silanols and olignucleotide gets stronger leading to less retention. This hypothesis reflects the experimental trend.

On the other hand, also borate ion release from borosilicate glass bottles into the mobile phase could have an influence on HILIC retention repeatability. Nagasathiya et al. explained the formation of a stable complex of borate and tartaric acid $[(C_4H_4O_6)_2B]$- and blamed the borosilicate glass solvent bottles as source of boron ions [40]. Likewise, Nishikaze et al. concluded that storage of trifluoroacetic acid (TFA) in borosilicate glass bottles causes boron contamination and recommended the use of PFA bottles [47] In addition, Kozono et al. stated the release of boron ions into alcohols from PYREX® glass [48]. Moreover, polyborate formation has also been described and confirmed by ESI-FTICR-MS by Gaspar et al. [41] Borate ions released into the acetonitrile-rich mobile phase tend to be distributed into the aqueous layer of the polar

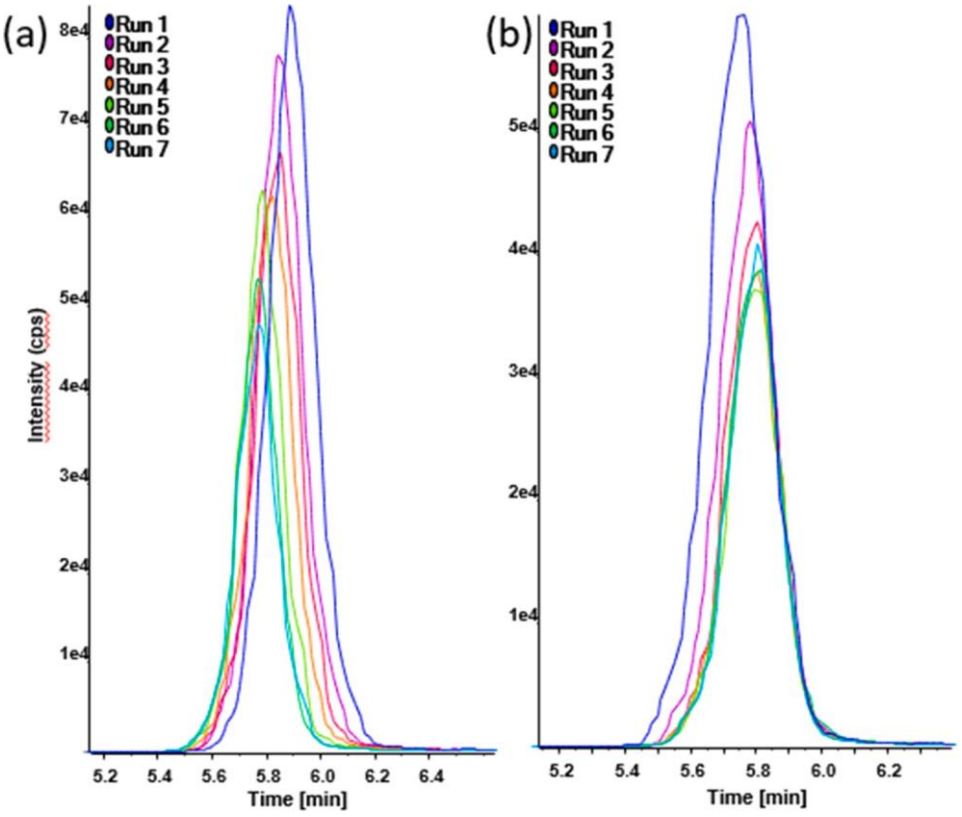

Fig. 5. Extracted ion chromatogram (*m/z* 1330.7748) of oligonucleotide antisense strand of patisiran. Direct comparison between (a) (Duran) borosilicate glass and (b) PFA plastic bottles for storage of mobile phases.

stationary phase due to its poor solubility in solutions with high acetonitrile content. Boric acid may, depending on the pH, exist as a distribution of distinct borate species [42]. At low pH (conditions of ESI^+ metabolomics; pH 3.5), it exists as neutral orthoboric acid ($B(OH)_3$), in the intermediate pH range (conditions of peptide separation, pH 5.4 and ESI^- metabolomics, pH 7.5) as pentaborate as well as triborate and at high pH (pH 9 and above; conditions of oligonucleotide separation) as tetraborate, triborate dianion, and borate anion. These borate species may carry water molecules into the semi-immobilized water layer which swells and gets thicker, thereby increasing the phase ratio and retention, as seen for metabolites (Fig. 1) and peptide (Fig. 4a). The solubility of boric acid in water increases with the addition of chaotropic salts, while it decreases with kosmotropic salts [42]. Hence, the buffer/salt ions in the mobile phase may modulate the effect. The accumulation of negatively charged borate anions at high pH (pH 9) in the semi-immobilized aqueous layer of the stationary phase in the course of the oligonucleotide separations may, on the other hand, also explain increasingly reduced retention times due to increasing electrostatic repulsion with the negatively charged oligonucleotide. Although no borate was detected in this work with glass bottles, in a recent study with borosilicate glass bottles we could detect bis(glycerol)borate in a sample that contained free glycerol but no borate according to ICP-MS (see suppl. material Fig. S1). It is supposed that borate was present, in traces at least, due to release of boron species from the borosilicate glass bottles into the eluent. Other species released from borosilicate glass could contribute in a similar way. Which ion effect is prevailing remains open at this point. The use of the PFA solvent bottles did not suffer from the retention time repeatability problem, as no ions are released into the mobile phase and the ion concentration hence stays constant. For this reason, the sensitive structure of the stationary phase and semi-immobilized aqueous layer, respectively, is not disturbed leading to stable retention times (Figs. 2, 4b, and 5b). PFA is a copolymer of TFE (Tetrafluoroethylene) and perfluoroethers. According to vendor specifications, PFA is already used in the employed instrument for internal tubings in the degasser because it is a gas permeable material. Also other fluoropolymers are used in the instrument such as FEP (fluorinated ethylene propylene) (tubing between solvent bottles, shutoff valves, solvent selection valves and degasser chambers), PEEK (inlets), FEP (tubings), ETFE (Ethylene tetrafluoroethylene) (fittings). Changing the solvent bottle material from borosilicate glass to FEP or PFA reduces the number of materials that come in contact with the eluent, because FEP or PFA is already used in the pump. PFA is stable against common HPLC solvents except for some halogenated solvents. It does not contain plasticizers. PFA bottles fulfill the FDA requirements for food and pharma industry (21CFR177.1550, 21CFR175.300, 21CFR175.105, 21CFR176.170, 21CFR176.180). DuPont, which is one manufacturer of PFA pellets, describe that their product DuPont Teflon PFA 450 HP "contains no additives and is designed for hostile chemical environments where purity in the parts-per-billon range is needed" [49]. Biron described food contact and medical grades for PFA [50]. Nevertheless, low extractable fluorides are generally described for PFAS. If antioxidants or lubricants are used and if or how the bottles are cleaned, depends on the exact process and falls under proprietary information. Contaminations on the surface can be easily removed by cleaning with LC-MS grade solvents. This is routinely done, when preparing mobile phases. To summarize, we did not have any notice during our experiments that PFA pollutes the MS and we did not see any changes in the background signals of the mass spectrometer during use.

TFA can also be used as additive without problems. Boiling HNO_3 or H_2SO_4 can be employed to wash the PFA bottles. Chemically, PFA is absolutely stable at common temperatures, yet elevated temperatures (>200 °C) have to be avoided and sharp objects are problematic. We consider both FEP and PFA to be suitable materials for solvent bottles in HILIC. However, PFA has slight advantages in terms of polymer purity

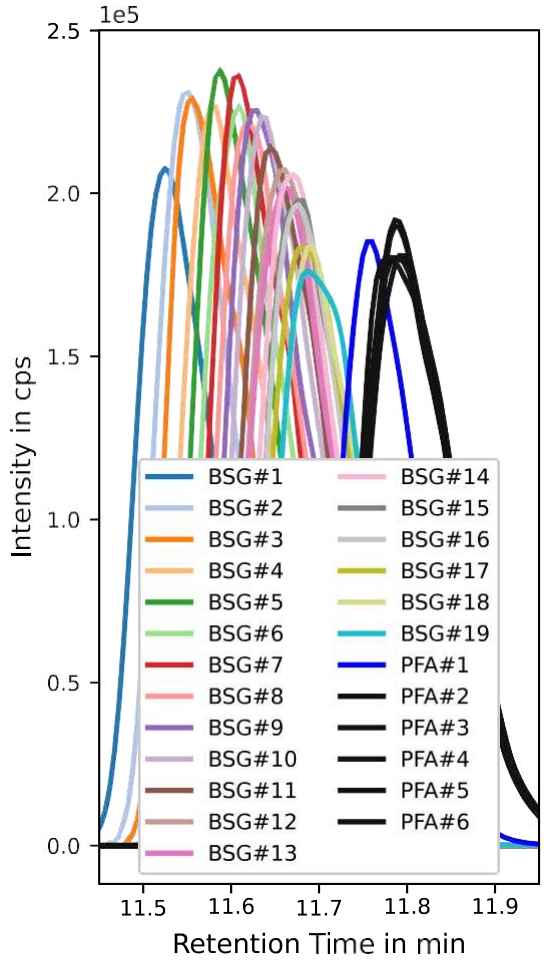

Fig. 6. Extracted ion chromatogram (EIC) of sodium acetate cluster $(CH_3COONa)_1$ Na^+ of Teicoplanin sample. Sodium acetate cluster $(CH_3COONa)_nNa^+$ with n = 1−18 are detectable. Measured EICs with PFA bottles are blue (first measurement) and black (the following) coloured.

and smoother surface texture, but the disadvantage of higher initial cost.

In summary, in accordance with our results, we postulate that the storage of an eluent in borosilicate glass bottles changes the exact composition of the eluent over time, resulting in changes in the hydrophilic layer in HILIC and thus causes retention time shifts and repeatability problems.

4. Conclusion

In this study, retention time repeatability under gradient HILIC conditions (Premier BEH Amide column) was thoroughly investigated using three different sets of analytes (urinary metabolites, peptides, and oligonucleotides). The effect of standard borosilicate glass bottles and PFA bottles as the mobile phase storage vessels on retention time drifts was compared. It became evident that retention time shifts are significant when borosilicate bottles are employed. For the polar metabolites and the peptides, a shift pattern towards stronger retention with increasing analysis time was observed. In contrast, for the oligonucleotide sample the opposite trend was found, i.e. lower retention with higher injection number. It was hypothesized that release of sodium, potassium, borate and other species from the borosilicate glass leads to changes in the semi-immobilized water layer structure and thickness at the interface of the HILIC stationary phase. The altered phase ratio and electrostatic screening effects may lead to shifted retention times compromising retention time repeatability in (gradient) HILIC. This phenomenon can easily be circumvented by use of plastic bottles as solvent reservoirs. Herein, we used PFA bottles instead of borosilicate glass bottles for the eluents. Retention times of urinary metabolites, peptides and oligonucleotides were highly reproducible with RSDs < 0.2 %. PFA is resistant to common HPLC solvents and additives (TFA), highly pure and does not contaminate the ion source. It is a simple solution to replace borosilicate by PFA bottles to solve the commonly reported HILIC retention time repeatability problem. Further improvements in repeatability are envisaged if solvents with even better quality e.g. electrochemical grade are employed which are not supplied in glass bottles but plastic containers. However, for cost reasons it was not considered herein. Future research should also have a look into the effect of aging of the glass bottles and its effect on retention time repeatability addressing the question whether in aged glass bottles the release of ions levels off after a certain time. Moreover, it could be interesting to study the effect of integrating an ion suppressor between pump and injector which removes sodium and potassium cations or a borate ion trap column as suggested recently for improving peak shapes in carbohydrate analysis of some analytes such as mannose [51]. If these strategies along with the use of glass bottles solve the retention time repeatability problem as well, it would be an indirect confirmation for the above hypotheses.

Declaration of competing interest

The authors declare that they have no known competing financial interests or personal relationships that could have appeared to influence the work reported in this paper.

Acknowledgments

The authors are grateful to Dr. Tom van de Goor (Agilent Technologies) for valuable discussions. We are also grateful to Agilent Technologies for support of this research by 2D-LC instrumentation through an Agilent Research Award (#4068 and #4610). The authors thank Dr. Stephan Buckenmaier from Agilent Technologies, Waldbronn, Germany, for technical advice and valuable discussions.

Supplementary materials

Supplementary material associated with this article can be found, in the online version, at doi:10.1016/j.chroma.2024.465060.

References

[1] W.B. Dunn, D. Broadhurst, P. Begley, E. Zelena, S. Francis-McIntyre, N. Anderson, M. Brown, J.D. Knowles, A. Halsall, J.N. Haselden, A.W. Nicholls, I.D. Wilson, D. B. Kell, R. Goodacre, The Human Serum Metabolome (HUSERMET) Consortium, Procedures for large-scale metabolic profiling of serum and plasma using gas chromatography and liquid chromatography coupled to mass spectrometry, Nat. Protoc. 6 (2011) 1060−1083, https://doi.org/10.1038/nprot.2011.335.

[2] E.J. Want, P. Masson, F. Michopoulos, I.D. Wilson, G. Theodoridis, R.S. Plumb, J. Shockcor, N. Loftus, E. Holmes, J.K. Nicholson, Global metabolic profiling of animal and human tissues via UPLC-MS, Nat. Protoc. 8 (2013) 17−32, https://doi.org/10.1038/nprot.2012.135.

[3] A.J. Alpert, Hydrophilic-interaction chromatography for the separation of peptides, nucleic acids and other polar compounds, J. Chromatogr. 499 (1990) 177−196, https://doi.org/10.1016/s0021-9673(00)96972-3.

[4] F. Michopoulos, N. Whalley, G. Theodoridis, I.D. Wilson, T.P. Dunkley, S. E. Critchlow, Targeted profiling of polar intracellular metabolites using ion-pair-high performance liquid chromatography and -ultra high performance liquid chromatography coupled to tandem mass spectrometry: applications to serum, urine and tissue extracts, J. Chromatogr. A 1349 (2014) 60−68, https://doi.org/10.1016/j.chroma.2014.05.019.

[5] F. Li, M. L¨ammerhofer, Impurity profiling of siRNA by two-dimensional liquid chromatography-mass spectrometry with quinine carbamate anion-exchanger and ion-pair reversed-phase chromatography, J. Chromatogr. A 1643 (2021) 462065, https://doi.org/10.1016/j.chroma.2021.462065.

[6] Y. Gagnebin, J. Pezzatti, P. Lescuyer, J. Boccard, B. Ponte, S. Rudaz, Toward a better understanding of chronic kidney disease with complementary chromatographic methods hyphenated with mass spectrometry for improved polar

metabolome coverage, J. Chromatogr. B Analyt. Technol. Biomed. Life. Sci. 1116 (2019) 9–18, https://doi.org/10.1016/j.jchromb.2019.03.031.
[7] B. Preinerstorfer, S. Schiesel, M. La¨mmerhofer, W. Lindner, Metabolic profiling of intracellular metabolites in fermentation broths from beta-lactam antibiotics production by liquid chromatography-tandem mass spectrometry methods, J. Chromatogr. A 1217 (3) (2010) 312–328, https://doi.org/10.1016/j.chroma.2009.11.051.
[8] C. Virgiliou, I. Sampsonidis, H.G. Gika, N. Raikos, G.A. Theodoridis, Development and validation of a HILIC-MS/MS multitargeted method for metabolomics applications, Electrophoresis 36 (18) (2015) 2215–2225, https://doi.org/10.1002/elps.201500208. Erratum in: Electrophoresis. 2016 Jul;37(14):2113.
[9] C. Virgiliou, H.G. Gika, G.A Theodoridis, HILIC-MS/MS multi-targeted method for metabolomics applications, Method. Mol. Biol. 1738 (2018) 65–81, https://doi.org/10.1007/978-1-4939-7643-0_5.
[10] S.U. Bajad, W. Lu, E.H. Kimball, J. Yuan, C. Peterson, J.D. Rabinowitz, Separation and quantitation of water soluble cellular metabolites by hydrophilic interaction chromatography-tandem mass spectrometry, J. Chromatogr. A 1125 (1) (2006) 76–88, https://doi.org/10.1016/j.chroma.2006.05.019.
[11] F. Fei, D.M. Bowdish, B.E. McCarry, Comprehensive and simultaneous coverage of lipid and polar metabolites for endogenous cellular metabolomics using HILIC-TOF-MS, Anal. Bioanal. Chem. 406 (15) (2014) 3723–3733, https://doi.org/10.1007/s00216-014-7797-5.
[12] K. Klavins, H. Drexler, S. Hann, G. Koellensperger, Quantitative metabolite profiling utilizing parallel column analysis for simultaneous reversed-phase and hydrophilic interaction liquid chromatography separations combined with tandem mass spectrometry, Anal. Chem. 86 (9) (2014) 4145–4150, https://doi.org/10.1021/ac5003454.
[13] K. Serafimov, M. La¨mmerhofer, Metabolic profiling workflow for cell extracts by targeted hydrophilic interaction liquid chromatography-tandem mass spectrometry, J. Chromatogr. A 1684 (2022) 463556, https://doi.org/10.1016/j.chroma.2022.463556.
[14] M. Su, K. Serafimov, P. Li, C. Knappe, M. L¨ammerhofer, Isomer selectivity of one- and two-dimensional approaches of mixed-mode and hydrophilic interaction liquid chromatography coupled to tandem mass spectrometry for sugar phosphates of glycolysis and pentose phosphate pathways, J. Chromatogr. A 1688 (2023) 463727, https://doi.org/10.1016/j.chroma.2022.463727.
[15] P. Kozlik, R. Goldman, M. Sanda, Hydrophilic interaction liquid chromatography in the separation of glycopeptides and their isomers, Anal. Bioanal. Chem. 410 (20) (2018) 5001–5008, https://doi.org/10.1007/s00216-018-1150-3.
[16] I. Kohler, M. Verhoeven, R. Haselberg, A.F.G. Gargano, Hydrophilic interaction chromatography − mass spectrometry for metabolomics and proteomics: state-of-the-art and current trends, Microchem. J. (2022), https://doi.org/10.1016/j.microc.2021.106986.
[17] B. Buszewski, S. Noga, Hydrophilic interaction liquid chromatography (HILIC)—a powerful separation technique, Anal. Bioanal. Chem. 402 (2012) 231–247, https://doi.org/10.1007/s00216-011-5308-5.
[18] D.R. Stoll, D.C. Harmes, G.O. Staples, O.G. Potter, C.T. Dammann, D. Guillarme, A. Beck, Development of comprehensive online two-dimensional liquid chromatography/mass spectrometry using hydrophilic interaction and reversed-phase separations for rapid and deep profiling of therapeutic antibodies, Anal. Chem. 90 (9) (2018) 5923–5929, https://doi.org/10.1021/acs.analchem.8b00776.
[19] M. Grübner, A. Dunkel, F. Steiner, T. Hofmann, Systematic evaluation of liquid chromatography (LC) column combinations for application in two-dimensional LC metabolomic studies, Anal. Chem. 93 (37) (2021) 12565–12573, https://doi.org/10.1021/acs.analchem.1c01857.
[20] F. Cacciola, K. Arena, F. Mandolfino, D. Donnarumma, P. Dugo, L. Mondello, Reversed phase versus hydrophilic interaction liquid chromatography as first dimension of comprehensive two-dimensional liquid chromatography systems for the elucidation of the polyphenolic content of food and natural products, J. Chromatogr. A 1645 (2021) 462129, https://doi.org/10.1016/j.chroma.2021.462129.
[21] D.V. McCalley, Understanding and manipulating the separation in hydrophilic interaction liquid chromatography, J. Chromatogr. A 1523 (2017) 49–71, https://doi.org/10.1016/j.chroma.2017.06.026.
[22] H. Vl˘ckova´, K. Je˘zkova´, K. St˘etkov´a, H. Tom˘sikov´a, P. Solich, L. Nov´akov´a, Study of the retention behavior of small polar molecules on different types of stationary phases used in hydrophilic interaction liquid chromatography, J. Sep. Sci. 37 (11) (2014) 1297–1307, https://doi.org/10.1002/jssc.201400020.
[23] D.V. McCalley, A study of column equilibration time in hydrophilic interaction chromatography, J. Chromatogr. A 1554 (2018) 61–70, https://doi.org/10.1016/j.chroma.2018.04.016.
[24] N.P. Dinh, T. Jonsson, K. Irgum, Water uptake on polar stationary phases under conditions for hydrophilic interaction chromatography and its relation to solute retention, J. Chromatogr. A 1320 (2013) 33–47, https://doi.org/10.1016/j.chroma.2013.09.061.
[25] D.V. McCalley, U.D. Neue, Estimation of the extent of the water-rich layer associated with the silica surface in hydrophilic interaction chromatography, J. Chromatogr. A 1192 (2) (2008) 225–229, https://doi.org/10.1016/j.chroma.2008.03.049.
[26] Y. Guo, A survey of polar stationary phases for hydrophilic interaction chromatography and recent progress in understanding retention and selectivity, Biomed. Chromatogr. 36 (4) (2022) e5332, https://doi.org/10.1002/bmc.5332.
[27] S.M. Melnikov, A. Ho¨ltzel, A. Seidel-Morgenstern, U. Tallarek, A Molecular Dynamics Study on the Partitioning Mechanism in Hydrophilic Interaction Chromatography, Angewand. Chem. Int. Edit. 51 (25) (2012) 6251–6254, https://doi.org/10.1021/acs.jpcc.6b03799.
[28] F. Gritti, J. Sehajpal, J. Fairchild, Using the fundamentals of adsorption to understand peak distortion due to strong solvent effect in hydrophilic interaction chromatography, J. Chromatogr. A 1489 (2017) 95–106, https://doi.org/10.1016/j.chroma.2017.02.003.
[29] S. Noga, S. Bocian, B. Buszewski, Hydrophilic interaction liquid chromatography columns classification by effect of solvation and chemometric methods, J. Chromatogr. A 1278 (2013) 89–97, https://doi.org/10.1016/j.chroma.2012.12.077.
[30] A.J. Alpert, Effect of salts on retention in hydrophilic interaction chromatography, J. Chromatogr. A 1538 (2018) 45–53, https://doi.org/10.1016/j.chroma.2018.01.038.
[31] J. Walsby-Tickle, J. Gannon, I. Hvinden, C. Bardella, M. Abboud, A. Nazeer, D. Hauton, E. Pires, T. Cadoux-Hudson, C. Schofield, J. S. O. McCullagh, Anion-exchange chromatography mass spectrometry provides extensive coverage of primary metabolic pathways revealing altered metabolism in IDH1 mutant cells, Commun. Biol. 3 (2020) 247, https://doi.org/10.1038/s42003-020-0957-6.
[32] C. Seidl, D.S. Bell, D.R. Stoll, A study of the re-equilibration of hydrophilic interaction columns with a focus on viability for use in two-dimensional liquid chromatography, J. Chromatogr. A 1604 (2019) 460484, https://doi.org/10.1016/j.chroma.2019.460484.
[33] D.V. McCalley, Managing the column equilibration time in hydrophilic interaction chromatography, J. Chromatogr. A 1612 (2020) 460655, https://doi.org/10.1016/j.chroma.2019.460655.
[34] J. Walsby-Tickle, J. Gannon, I. Hvinden, C. Bardella, M.I. Abboud, A. Nazeer, D. Hauton, E. Pires, T. Cadoux-Hudson, C.J. Schofield, J.S.O. McCullagh, Anion-exchange chromatography mass spectrometry provides extensive coverage of primary metabolic pathways revealing altered metabolism in IDH1 mutant cells, Commun. Biol. 3 (1) (2020) 247, https://doi.org/10.1038/s42003-020-0957-6.
[35] M. Schwaiger, E. Rampler, G. Hermann, W. Miklos, W. Berger, G. Koellensperger, Anion-Exchange Chromatography Coupled to High-Resolution Mass Spectrometry: a Powerful Tool for Merging Targeted and Non-targeted Metabolomics, Anal. Chem. 89 (14) (2017) 7667–7674, https://doi.org/10.1021/acs.analchem.7b01624.
[36] Yannell E.K., Hsiao J., Cuthberson D. Mastering HILIC-Z Separation for Polar Analytes. Agilent Technologies Application Note Omics.
[37] Y. Zhang, A. Bilbao, T. Bruderer, J. Luban, C. Strambio-De-Castillia, F. Lisacek, G. Hopfgartner, E. Varesio, The use of variable Q1 isolation windows improves selectivity in LC-SWATH-MS acquisition, J. Proteome. Res. 14 (10) (2015) 4359–4371, https://doi.org/10.1021/acs.jproteome.5b00543.
[38] D.R. Stoll, P.W. Carr, Two-dimensional liquid chromatography: a state of the art tutorial, Anal. Chem. 89 (1) (2017) 519–531, https://doi.org/10.1021/acs.analchem.6b03506.
[39] B.W.J. Pirok, A.F.G. Gargano, P.J. Schoenmakers, Optimizing separations in online comprehensive two-dimensional liquid chromatography, J. Sep. Sci. 41 (1) (2018) 68–98, https://doi.org/10.1002/jssc.201700863.
[40] K. Nagasathiya, C. Brinda, M. Parani, M. Vairamani, Artifacts from methanol stored in borosilicate glass bottles during electrospray ionization mass spectrometric analysis, Rapid. Commun. Mass. Spectrom. 28 (20) (2014) 2227–2230, https://doi.org/10.1002/rcm.7009.
[41] S. Gin, X. Guo, J.M. Delaye, F. Angeli, K. Damodaran, V. Testud, J. Du, S. Kerisit, S. Kim, Insights into the mechanisms controlling the residual corrosion rate of borosilicate glasses, npj. Mater. Degrad. 4 (2020) 41, https://doi.org/10.1038/s41529-020-00145-2.
[42] G.H. Green, C. Blincoe, H.J. Weeth, Boron contamination from borosilicate glass, J. Agric. Food. Chem. 24 (6) (1976) 1245–1246, https://doi.org/10.1021/jf60208a016.
[43] I. Selman, J. Rees, J Dilnot, Liberation of boron from 'Pyrex' and 'Hysil' glass in relation to plant growth in water culture, Nature 173 (1954) 957–958, https://doi.org/10.1038/173957b0.
[44] S. Manikandan, Jagannath, V.K. Shrikhande, G Kothiyal, Degradation behaviour of borosilicate glass: some studies, Anti-Corros. Method. Mater. 53 (2006) 303–309, https://doi.org/10.1108/00035590610692581.
[45] T. Geisler, A. Janssen, D. Scheiter, T. Stephan, J. Berndt, A. Putnis, Aqueous corrosion of borosilicate glass under acidic conditions: a new corrosion mechanism, J. Non. Cryst. Solid. 356 (28–30) (2010), https://doi.org/10.1016/j.jnoncrysol.2010.04.033.
[46] H. Lardeux, D. Guillarme, V. D' Atri, Comprehensive evaluation of zwitterionic hydrophilic liquid chromatography stationary phases for oligonucleotide characterization, J. Chromatogr. A 1690 (2023) 463785, https://doi.org/10.1016/j.chroma.2023.463785.
[47] T. Nishikaze, S. Kawabata, K. Tanaka, Boron forms unexpected glycopeptide derivatives during MALDI-MS experiment, J. Mass. Spectrom. 48 (9) (2013) 1005–1009, https://doi.org/10.1002/jms.3246.
[48] S. Kozono, S. Takahashi, H. Haraguchi, Determination of boron in high-purity tantalum materials by on-line matrix separation/inductively coupled plasma mass spectrometry, Analyst 127 (7) (2002) 930–934, https://doi.org/10.1039/b201019b.
[49] Product information of DuPont Teflon PFA 440 HP; https://www-eng.lbl.gov/~shuman/NEXT/MATERIALS&COMPONENTS/HV/PFA_440.pdf.
[50] M. Biron, Thermoplastics and Thermoplastic Composites, Elsevier, 2012. ISBN: 978-1-4557-7898-0.
[51] Antec Scientific, BIT − Borate Ion Trap. https://antecscientific.com/products/columns/borate-ion-trap/.

Supporting information

Solving the retention time repeatability problem of hydrophilic interaction liquid chromatography

Kristian Serafimov[#], Cornelius Knappe[#] , Fei-Yang Li, Adrian Sievers-Engler , Michael Lämmerhofer

Shared first authorship

Institute of Pharmaceutical Sciences, Pharmaceutical (Bio-)Analysis, University of Tübingen, Auf der Morgenstelle 8, 72076 Tübingen, Germany

Corresponding Authors:
Prof. Michael Lämmerhofer
Email: Michael.laemmerhofer@uni-tuebingen.de;

Contents

Table S-1. SWATH MS Experiment Design

Experiment	*m/z* range	
	Positive mode	**Negative mode**
TOF-MS	60 - 1000	70 – 900
SWATH-MS/MS 1	59.5 – 83.6	69.5 – 143.5
SWATH-MS/MS 2	82.6 – 132.6	142.5 – 167.5
SWATH-MS/MS 3	131.6 – 166.6	166.5 – 199.7
SWATH-MS/MS 4	165.6 – 202.6	198.7 – 241.7
SWATH-MS/MS 5	201.6 – 259.6	240.7 – 269.7
SWATH-MS/MS 6	258.6 – 289.6	268.7 – 286.6
SWATH-MS/MS 7	288.6 – 315.7	285.6 – 301.7
SWATH-MS/MS 8	314.7 – 329.5	300.7 – 332.6
SWATH-MS/MS 9	328.5 – 369.9	331.6 – 346.6
SWATH-MS/MS 10	368.9 – 429.5	345.6 – 349.6
SWATH-MS/MS 11	428.5 – 478.8	348.6 – 379.8
SWATH-MS/MS 12	477.8 – 550.0	378.8 – 436.7
SWATH-MS/MS 13	549.0 – 596.5	435.7 – 510.6
SWATH-MS/MS 14	595.5 – 623.9	509.6 – 577.8
SWATH-MS/MS 15	622.9 – 677.7	576.8 – 632.3
SWATH-MS/MS 16	676.7 – 721.1	631.3 – 688.7
SWATH-MS/MS 17	720.1 – 760.1	687.7 – 741.0
SWATH-MS/MS 18	759.1 – 810.1	740.0 – 791.1
SWATH-MS/MS 19	809.1 – 876.6	790.1 – 841.1
SWATH-MS/MS 20	875.6 – 1000.5	840.1 – 900.5

Table S-2. Retention time mean values and standard deviations for representative urinary metabolites analysed (glass bottles used as mobile phase reservoirs).

Metabolite	Mode	*Statistical Values*			*Individual Injections*				
		Mean t_R [min]	SD t_R [min]	RSD t_R [%]	t_{R1} [min]	t_{R5} [min]	t_{R10} [min]	t_{R15} [min]	t_{R20} [min]
Citrulline	ESI^-	12.92	± 0.71	5.48	12.12	12.23	12.86	13.43	13.98
Tryptophan	ESI^+	7.80	± 0.40	5.12	7.33	7.45	7.78	8.01	8.44
Decanoyl-Carnitine	ESI^+	4.82	± 0.35	7.34	4.48	4.52	4.67	4.98	5.43
Methionine	ESI^+	9.16	± 0.39	4.26	8.78	8.85	9.02	9.32	9.85
Carnitine	ESI^+	11.38	± 0.46	4.02	10.85	10.93	11.32	11.77	12.02
1-Methyl-Adenosine	ESI^+	9.46	± 0.53	5.59	8.91	8.98	9.32	9.76	10.33
Ethylmalonic Acid	ESI^-	9.06	± 0.54	5.93	8.48	8.52	8.92	9.56	9.80
Pyroglutamic acid	ESI^-	8.44	± 0.46	5.43	7.98	8.06	8.21	8.83	9.14
Hypoxanthine	ESI^-	3.87	± 0.34	8.75	3.59	3.54	3.67	4.18	4.37
Xanthine	ESI^-	5.79	± 0.48	8.22	5.24	5.46	5.55	6.19	6.50
Homogentisic acid	ESI^-	4.55	± 0.52	11.4	4.06	4.10	4.26	5.04	5.31
Creatinine	ESI^+	4.06	± 0.44	10.92	3.55	3.71	3.86	4.48	4.68
Creatine	ESI^+	5.01	± 0.60	12.02	4.40	4.51	4.67	5.59	5.87
Glutamine	ESI^+	5.41	± 0.63	11.58	4.81	5.01	5.15	5.49	6.58
Phenylalanine	ESI^+	5.96	± 0.70	11.69	5.20	5.49	5.52	6.62	6.96
Uric acid	ESI^+	4.57	± 0.51	11.13	4.06	4.16	4.26	5.04	5.31
Caffeic acid	ESI^+	4.78	± 0.63	13.27	4.16	4.23	4.42	5.37	5.70

Table S-3. Retention time mean values and standard deviations for representative urinary metabolites analysed (PFA bottles used as mobile phase reservoirs).

Metabolite	Mode	*Statistical Values*			*Individual Injections*				
		Mean t_R [min]	SD t_R [min]	RSD t_R [%]	t_{R1} [min]	t_{R5} [min]	t_{R10} [min]	t_{R15} [min]	t_{R20} [min]
Citrulline	ESI^-	12.22	± 0.009	0.07	12.23	12.21	12.22	12.23	12.21
Tryptophan	ESI^+	7.37	± 0.012	0.16	7.38	7.35	7.36	7.37	7.38
Decanoyl-Carnitine	ESI^+	4.55	± 0.012	0.26	4.54	4.54	4.55	4.57	4.54
Methionine	ESI^+	8.81	± 0.006	0.07	8.81	8.80	8.81	8.82	8.81
Carnitine	ESI^+	10.91	± 0.008	0.07	10.92	10.92	10.91	10.90	10.92
1-Methyl-Adenosine	ESI^+	8.92	± 0.012	0.13	8.93	8.93	8.92	8.90	8.91
Ethylmalonic Acid	ESI^-	8.45	± 0.006	0.07	8.45	8.44	8.45	8.46	8.45
Pyroglutamic acid	ESI^-	8.02	± 0.005	0.06	8.02	8.01	8.02	8.02	8.01
Hypoxanthine	ESI^-	3.64	± 0.005	0.13	3.64	3.64	3.65	3.65	3.64
Xanthine	ESI^-	5.2	± 0.005	0.09	5.20	5.21	5.20	5.21	5.20
Homogentisic acid	ESI^-	4.11	± 0.005	0.12	4.10	4.11	4.10	4.11	4.11
Creatinine	ESI^+	3.45	± 0.009	0.26	3.48	3.47	3.46	3.48	3.46
Creatine	ESI^+	4.32	± 0.008	0.19	4.33	4.33	4.33	4.31	4.32
Glutamine	ESI^+	4.69	± 0.008	0.17	4.70	4.68	4.70	4.70	4.69
Phenylalanine	ESI^+	5.09	± 0.008	0.16	5.10	5.09	5.10	5.08	5.10
Uric acid	ESI^+	4.1	± 0.006	0.15	4.10	4.11	4.10	4.10	4.09
Caffeic acid	ESI^+	4.11	± 0.006	0.15	4.12	4.11	4.10	4.11	4.11

Table S-4. Retention time mean values and standard deviations for teicoplanin (PFA bottles used as mobile phase reservoirs).

Peptide	Bottle	*Statistical Values*			*Individual Injections*				
		Mean t_R [min]	SD t_R [min]	RSD t_R [%]	t_{R1} [min]	t_{R5} [min]	t_{R10} [min]	t_{R15} [min]	t_{R18} [min]
A_{2-3}	BSG^-	21.014	0.090	0.43	21.021	20.893	20.974	21.113	21.169
A_{3-1}	BSG	22.221	0.083	0.37	22.244	22.107	22.176	22.311	22.353
A_{2-3}	PFA	20.435	0.009	0.04	20.442	20.447	20.438	20.419	20.426
A_{3-1}	PFA	21.565	0.007	0.03	21.568	21.575	21.568	21.558	21.556

Table S-5. Retention time mean values and standard deviations for oligonucleotide sample (PFA bottles used as mobile phase reservoirs).

	Borosilicate glass	PFA
	t_R (min)	t_R (min)
Run 1	5.900	5.758
Run 2	5.855	5.787
Run 3	5.846	5.802
Run 4	5.825	5.800
Run 5	5.788	5.801
Run 6	5.776	5.806
Run 7	5.776	5.807
Mean (min)	**5.824**	**5.794**
sd (min)	**0.047**	**0.017**
RSD %	**0.803**	**0.299**

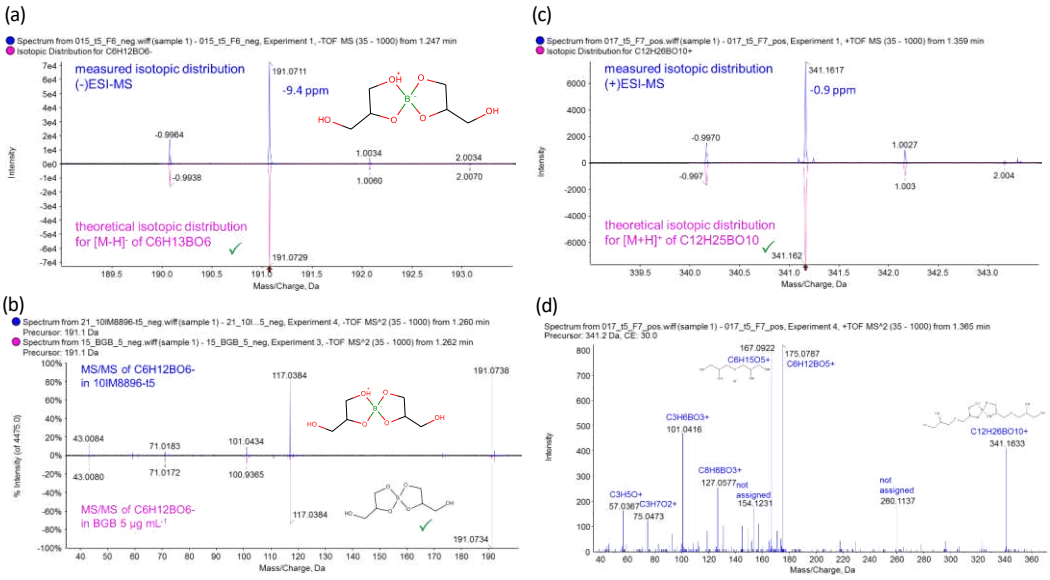

Fig. S1: MS1 (a,c) and MS2 (b,d) spectra (QTOF) of bis(glycerol)borate (a,b) and bis(diglycerol)borate under HILIC conditions in a sample which contained glycerol and diglycerol impurities, but no borate according to ICP-MS. Bis(glycerol)borate standard Almabor® 4410 was supplied by Anderson Development, USA, for verification of the structural annotation.

analytical chemistry

pubs.acs.org/ac Article

Comprehensive Coverage of Glycolysis and Pentose Phosphate Metabolic Pathways by Isomer-Selective Accurate Targeted Hydrophilic Interaction Liquid Chromatography-Tandem Mass Spectrometry Assay

Kristian Serafimov and Michael Lämmerhofer*

Cite This: https://doi.org/10.1021/acs.analchem.4c03490 Read Online

ACCESS | Metrics & More | Article Recommendations | Supporting Information

ABSTRACT: The accurate liquid chromatography-tandem mass spectrometry analysis of phosphorylated isomers from glycolysis and pentose phosphate pathways is a challenging analytical problem in metabolomics due to extraction problems from the biological matrix, adherence to stainless steel surfaces leading to tailing in LC, and incomplete separation of hexose and pentose phosphate isomers. In this study, we present a targeted HILIC-ESI-MS/MS method based on a BEH amide fully porous 1.7 μm particle column with an inert surface coating of column hardware and multiple reaction monitoring (MRM) acquisition fully covering the glycolysis and pentose phosphate pathway metabolites. To minimize contact of the phosphorylated analytes with stainless steel surfaces, a μ-ESI-MS probe with a hybrid electrode made of PEEKsil was employed. Optimized HILIC gradient elution conditions with 100 mM ammonium formate (pH 11) provided the separation of hexose monophosphate and pentose phosphate isomers. To ensure good retention time repeatability in HILIC, perfluoroalkoxy alkane bottles were used for the mobile phase (with sd over 60 runs between 0.01 and 0.02 min). For the quantitative assay, the U-^{13}C-labeled cell extract was spiked prior to extraction by metal oxide-based affinity chromatography (MOAC) with TiO_2 beads. The concentrations of the 24 targets were quantified in HeLa and human embryonic kidney (HEK293) cells. Erastin-induced ferroptosis in HEK293 cells was accompanied by enhanced levels of fructose-1,6-bis-phosphate, 2- and 3-phosphoglycerate, and 2,3-bis-phosphoglycerate.

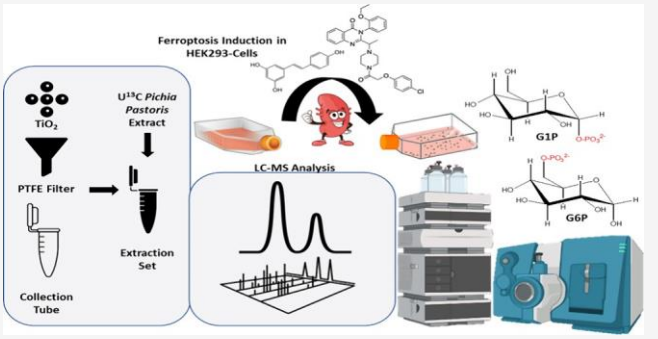

Glycolysis is a central metabolic pathway in cells. This catabolic process converts glucose to pyruvate for the generation of ATP. Several glycolytic metabolites can enter anabolic pathways that provide NADPH and building blocks, such as the pentose phosphate pathway (PPP) (Figure 1). Both processes together are part of central carbon metabolism and play a critical role in cellular energy production. For this reason, it is desirable in targeted and untargeted metabolomics to have a comprehensive coverage over the metabolites of both metabolic processes complementing general metabolomics assays.[1−4] Chemically, the vast majority of the metabolites of glycolysis and PPP are sugar phosphates (SPx) and phosphorylated monosaccharides, respectively, including triose-, tetrose-, pentose-, hexose-, and heptosephosphates (Figure 1).

From an analytical viewpoint, these phosphorylated carbohydrates, such as nucleotides[10] and inositolphosphates,[6] represent a major challenge. They are extremely hydrophilic and not sufficiently retained and resolved on reversed-phase (RP) stationary phases. The retention problem can be solved through the use of ion-pairing agents in the mobile phase, with a detrimental effect on electrospray ionization efficiency and contamination problems of the ion source.[7] Another concept to overcome the problem is precolumn derivatization, e.g., with 3-aminomethylpyridine, 3-amino-9-ethylcarbazole, and other phosphoramides.[21−25] Alkylation of phosphates is another popular strategy, e.g., phosphate methylation with trimethylsilyl diazomethane[6,25] or 8-(diazomethyl)quinoline[26] leading to improved chromatographic performance and sufficient retention on RP columns. Permethylation like in glycan analysis is not an option, as the phosphate group is not stable enough under alkaline permethylation conditions. Molecular isomerism is another problem. There are numerous isomeric species among SPx metabolites (e.g., F6P/G6P; 2PG/3PG;

Received: July 6, 2024
Revised: October 11, 2024
Accepted: October 12, 2024

Downloaded via UNIV TUEBINGEN on October 26, 2024 at 15:57:23 (UTC).
See https://pubs.ac articles.

ACS Publications
© XXXX The Authors. Published by American Chemical Society

https://doi.org/10.1021/acs.analchem.4c03490
Anal. Chem. XXXX, XXX, XXX−XXX

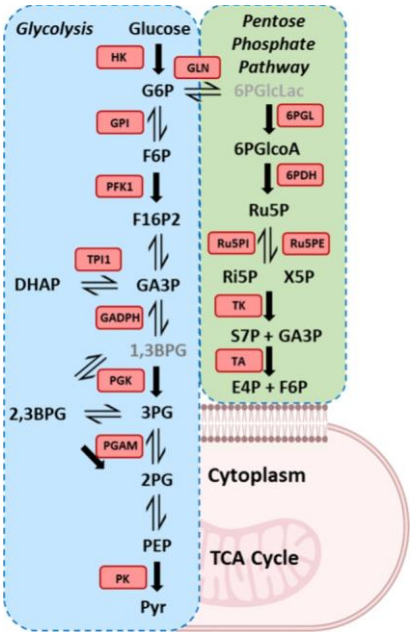

Figure 1. Schematic overview of the glycolytic pathway. HK (hexokinase), GPI (glucose-6-phosphate isomerase), PFK1 (phosphofructokinase 1), TPI1 (triosephosphate isomerase 1), GADPH (glyceraldehyde 3-phosphate dehydrogenase), PGK (phosphoglycerate Kinase), PGAM (phosphoglycerate mutase), PK (phosphokinase), 6PGL (6-phosphogluconatlactonase), 6PDH (6-phosphogluconate dehydrogenase), Ru5PI (ribulose-5-phosphate isomerase), Ru5PE (ribulose-5-phosphate enolase), TK (transketolase), TA (transaldolase). Metabolites in gray font are currently not covered by the developed method. Other abbreviations can be found in the Supporting Information.

Ri5P/Ru5P/Xu5P) for which even tandem mass spectrometry fails to provide adequate assay specificity due to identical precursor ions and nearly identical product ion spectra with only slight differences in the relative intensities of fragment ions.[34] Moreover, an anomeric hydroxyl group at carbon 1 of phosphorylated carbohydrates (e.g., hexose 6-phosphates) gives rise to interconversion between α- and β-anomers, which presents another level of complexity due to an increase in the number of isomers and peaks that must be resolved.[18] The interconversion kinetics can be significantly accelerated at high pH and high temperature owing to the lower energy barrier of interconversion, which may lead to peak coalescence of the anomers simplifying LC separation. Phosphorylated compounds have a further tendency to adsorb onto glass and stainless-steel surfaces. For this reason, silanized glass vials may be advantageous during sample preparation, especially for low-abundance phosphorylated metabolites. On the other hand, stainless-steel surfaces found in standard LC systems may lead to peak tailing and unsatisfactory performance.[8,9] The addition of methylphosphonic acid, medronic acid, or pyrophosphoric acid in μM quantities to the mobile phase has been suggested to alleviate the peak tailing problem due to strong metal surface interactions for phosphorylated metabolites.[31,34] However, this problem has been largely solved by new innovative column technology with polymer-deactivated stainless steel surfaces and coated column hardware, respectively (including frits) (e.g., MaxPeak High Performance Surfaces, HPS).[20] Hydrophilic phosphorylated metabolites can also cause issues during sample preparation due to their limited stability and poor extraction efficiency with organic solvents, leading to low recoveries. As alternatives to reversed-phase LC with ion-pair agents or precolumn derivatization, gas chromatography with chemical ionization time-of-flight mass spectrometry involving two-step online derivatization (ethoximation followed by trimethylsilylation), which resulted in unfavorable double peaks due to *cis*−*trans* isomers of resultant oxime ethers, was employed.[12] Due to the negative charges of the metabolites, capillary electrophoresis coupled to mass spectrometry has been considered a successful strategy for the metabolomic profiling of anionic metabolites including SPx.[10,11] The lack of robustness and limited availability of CE-MS instrumentation, as well as expertise, prevent the widespread acceptance of this technique. For this reason, liquid chromatography tandem mass spectrometry has established itself as the preferred method for the analysis of these molecules. To overcome the poor retention in conventional RP chromatography, a porous graphitic carbon (PGC) column has been employed for SPx due to the high polarity of these compounds.[13] It showed adequate retention but limited resolution for G6P/G1P/F6P, while other hexosephosphate isomers were not evaluated. Moreover, the retention time repeatability of PGC chromatography is known to be poor. LC-MS with a charged surface hybrid CSH phenyl-hexyl column, representing a kind of mixed-mode phase with a polycationic surface and phenylhexyl RP ligands, showed good peak shapes for anionic metabolites as well as resolution of isomers like citric acid and isocitric acid, but only a few selected sugar phosphates were tested; no isomer separation of hexose monophosphates was demonstrated.[19] Silica-based RP/WAX mixed-mode chromatography revealed good selectivity for the isomers of SPx, yet weakly acidic eluents also provided anomer selectivity.[18] Anomer interconversion was studied, and it was found that anomerization (mutarotation) kinetics at 35 °C is in the min time scale, like LC separation, leading to plateaus between anomer peaks. It makes the LC separation of SPx more complicated. Hydrophilic interaction chromatography (HILIC) is a preferred LC separation method in metabolomics.[50−65] For this purpose, among others, the usage of amide stationary phases has already been deployed for the separation of metabolites for roughly two decades.[50−54] Mostly, weakly acidic or neutral mobile phases have been employed in HILIC metabolomics studies with amide phases.[36,50−54] Only few studies suggested amide (typically pH-stable bridged ethylene hybrid-based) or amine stationary phases under alkaline conditions (with a mobile phase pH of 9 or 10).[50,55−58] However, the performance in terms of peak shape and tailing was critical, and assay specificity for glycolytic metabolites, including potential interferences from other pathways, was typically not reported in these studies and therefore uncertain.[40−48] Yet, HILIC has recently been more thoroughly evaluated for SPx isomer separation.[14,15,31] Eight phosphorylated sugars could be separated by HILIC with good peak shape due to the use of methylphosphonic acid as an additive in the mobile phase, which counteracted the metal−phosphate interaction that leads to peak tailing.[14,15,31,33,35] However, several of the critical isomers could not be separated, e.g., G1P/G6P/F6P, and several of the hexose phosphate isomers were not evaluated for assay specificity. HILIC/anion-exchange LC-MS was reported for 27 central carbon metabolites, but isomer selectivity for all hexose phosphates was not revealed.[37] Overall, it seems that anion exchange chromatography (AEX) using a gradient of hydroxide ions for

https://doi.org/10.1021/acs.analchem.4c03490
Anal. Chem. XXXX, XXX, XXX−XXX

elution combined with an ion-suppressor to achieve compatibility with ESI-MS (IC-MS) is the method with the broadest coverage so far.[16,17,36] It has been claimed that it has much better retention time repeatability compared to HILIC.[36] Last but not least, more complicated 2D-LC setups were also evaluated to achieve a full separation of a complex mixture of SPx.[20,30] Overall, there has been a lot of research on the analysis of sugar phosphates, and many incremental improvements have been made over time. However, each of these approaches has some limitations. The goal of this study was to present an improved robust HILIC-ESI-MS/MS method for accurate quantification of all metabolites of the glycolysis and pentose phosphate pathways, overcoming peak shape and retention time repeatability problems (ascribed to HILIC) and securing assay specificity for the isomers while also considering potential interferences from other pathways, such as mannose and lactose metabolism.

EXPERIMENTAL SECTION

Materials. Acetonitrile and methanol (MeOH) of ultra LC-MS grade and zirconia/glass beads were purchased from Carl Roth (Karlsruhe, Germany). Ammonium hydroxide solution (NH_4OH, ~30% NH_3), ammonium formate (NH_4FA), hydrochloric acid (HCl, ACS reagent, 37%), hydrogen chloride solution (HCl, 3 M in methanol), and acetic acid (AA) were supplied by Sigma-Aldrich (Taufkirchen, Germany). Deionized water (H_2O) was purified by a Purelab Ultra purification system (ELGA LabWater, Celle, Germany). Uniformly (U) ^{13}C-labeled yeast extract of more than 2×10^9 *Pichia pastoris* cells (~15 mg; strain CBS 7435) was obtained from ISOtopic Solutions (Vienna, Austria).[26−29] All standards and cell culture materials used in this study were provided by Sigma-Aldrich (Merck).

Cell Culture. The human cervical HeLa cells adapted to serum-free conditions (AC free, ECACC no. 08011102) were grown in a humidified incubator at 37 °C with 5% CO_2. Cells were fed with EX-CELL Hela serum-free medium (Sigma-Aldrich) with 2 mM L-glutamine (Sigma-Aldrich), 12 U mL^{-1} penicillin, and 12 μg mL^{-1} streptomycin until the cell density reached around 1×10^6. Human embryonic kidney (HEK293) cells were grown in stable cell DMEM/F12 medium (Sigma-Aldrich) supplemented with 10% fetal bovine serum, 12 U mL^{-1} penicillin, and 12 μg mL^{-1} streptomycin until the cell density reached around 1×10^6. Cells were maintained at 37 °C with 5% CO_2. To induce ferroptosis, HEK293 cells were incubated with 10 μM erastin and incubated for 24 h. Cell counting was performed in triplicate with a hemocytometer. The culture medium was removed. Cells were washed and quenched by the addition of ice-cold phosphate buffered saline to the adherent cell flask, and the flask was immersed in liquid nitrogen for 1 min. Cells were gently removed with a scraper, transferred in Falcon tubes, and centrifuged at 100 g for 5 min at 4 °C, and the leftover supernatant was removed, immersed in liquid N_2 once more after centrifugation, and then kept for further storage at −80 °C until extraction and analysis.

Standard Solutions. Standard stock solutions of the individual target analytes (1 mg mL^{-1}) were prepared in water/methanol (50:50; v/v). Working solutions were obtained by diluting the stock solution to an appropriate concentration with deionized water.

Sample Preparation and Metabolite Extraction. Sample preparation and (glycolytic and pentosephosphate) metabolite extraction were adapted from a protocol we reported previously for inositol phosphates.[5,6] Around 5 mg of TiO_2 was transferred into centrifuge filter units after consecutive washing with 300 μL of cold H_2O and cold 1 M perchloric acid (PA) solution. Cell samples were prepared in homogenization tubes (e.g., 3×10^6 HeLa cells). After adding 50 μL of the internal standard stock solution, 300 μL of prechilled 1 M PA solution, and 0.15 g of zirconia/glass beads, samples were homogenized at 4 °C for 10 cycles (10 s per cycle, 6800 rpm, pause 30 s) with a Precellys Evolution high-performance cell lyser using a Cryolys Evolution cooling unit with dry ice cooling (Bertin Technologies, France). The samples were spun down for 5 min (16000 g at 4 °C). The supernatant was transferred into the centrifuge filter units with washed TiO_2. After the mixture was shaken for 15 min (1400 rpm at 4 °C), followed by a centrifugation step (3500 g at 4 °C for 1 min), the filtrate was discarded. The homogenization and loading steps were repeated once. For the washing step of the loaded TiO_2 beads, 300 μL of cold 100 mM aqueous HCl solution was added. After shaking (1400 rpm at 4 °C for 1 min) and centrifugation (3500 g at 4 °C for 1 min), the filtrate was discarded. The washing step was repeated once. 200 μL of 10% (v/v) NH_4OH solution was added for elution of the analytes from the TiO_2 beads. After shaking (1400 rpm at 4 °C for 5 min) and centrifugation (3500 g at 4 °C for 1 min), the filtrate containing the (phosphorylated and other) metabolites was transferred into fresh tubes. After the elution step was repeated once, the filtrates were combined. Samples were evaporated for further analysis under nitrogen using a high-performance evaporator (Genevac EZ-2) (Genevac, Ipswich, UK) and reconstituted in 100 μL of ACN/H_2O (50/50; v/v).

UHPLC-QTRAP-MS with MRM Acquisition. Chromatographic separation was performed on a 1290 Infinity UHPLC system (Agilent Technologies, Waldbronn, Germany) with an Acquity Premier BEH Amide fully porous sub-2 μm particle column (150 × 2.1 mm, 1.7 μm, Waters) equipped with a guard column. Mobile phases A and B were adjusted to a pH of 11.0 with formic acid and consisted of 100 mM ammonium formate in water (A) and water/acetonitrile (10:90; v/v) (B), respectively. Mobile phases were prepared in perfluoroalkoxy alkane (PFA) polymer bottles provided by AHF Analysentechnik (Tübingen, Germany). The gradient elution (0.0 min, 90% B; 12.0 min, 85% B; 20.0 min, 80% B; 20.1 min, 90% B; 25.0 min, 90% B) was carried out at a flow rate of 0.4 mL min^{-1} and a constant column temperature of 35 °C. The injection volume was 3 μL. MS detection was conducted with the above chromatographic system hyphenated to a QTRAP 4500 mass spectrometer with a Turbo V source (Sciex, Framingham, MA, USA) operated with the μESI hybrid electrode probe (50 μm id) made of PEEKsil in the negative mode. Connection to the chromatographic column was conducted with peek-lined 150 mm × 50 μm MarvelXACT capillaries (IDEX Health & Science, Lake Forest, IL, USA). Ion source parameters were as follows: curtain gas (N_2) 30 psi, nebulizer gas (zero grade air) 40 psi, heater gas (zero grade air) 70 psi, ion source voltage −4500 V, and source temperature 500 °C. MRM transitions and compound-dependent parameters for analytes and internal standards are summarized in Table S1.

Calibration and Method Validation. Matrix effect (ME), extraction recovery (ER), and process efficiency (PE) were evaluated according to protocols published by Matuszewski and co-workers.[32] ME was determined at three concentration levels by comparing the response of standards spiked to the

https://doi.org/10.1021/acs.analchem.4c03490
Anal. Chem. XXXX, XXX, XXX−XXX

HeLa cell matrix after extraction (postextraction spiked) and that in solution as follows:

$$\mathrm{ME}\% = \frac{A_{\mathrm{spiked}} - A_0}{A_{\mathrm{neat}}} \quad (1)$$

where A_{spiked} is the area of the postextraction spiked cell extracts, A_0 the peak area of the analyte endogenously present in the cell extract (determined by standard addition), and A_{neat} is the peak area of the selected metabolite in neat solution. Analogously, ER and PE were determined from a concentration series of pre-extraction spiked versus postextraction spiked HeLa cell samples and pre-extraction spiked versus neat standard solution, respectively. External calibration functions were established by plotting peak area ratios of analytes and their internal standards versus the concentration of standard solutions (1, 50, 100, 500, and 1000 ng mL^{-1}) to determine LoDs and LoQs. Apart from external calibration, matrix-matched calibration was performed as well by spiking a series of 5 concentration levels (1, 50, 100, 500, and 1000 ng mL^{-1}) to the biological matrix (3×10^6 HeLa cells). Weighted linear regression ($1/x^2$) was used for both external and matrix-matched calibration curves. Linearity was evaluated by the determination coefficients (r^2) of the matrix matched calibration functions for each metabolite. As acceptance criteria, back-calculations of the concentrations of the nonzero calibrators regarding their nominal concentrations (spiked concentrations; endogenous amount as predetermined via LC-MS and standard-addition-corrected) should be in at least 75% of calibrator levels ±15%. Further evaluation and validation of the developed method, including between- and within-run accuracy and precision, were carried out in HeLa cells according to the FDA guidelines for bioanalytical method validation with some modifications. LoDs and LoQs were determined through the external calibration function for the individual metabolites as follows:

$$\mathrm{LoD} = \frac{3.3x\sigma}{m} \quad (2)$$

With σ being the standard error of the calibration function's slope and m being the slope value itself. Analogously, to determine the LoQ, the following equation was used:

$$\mathrm{LoQ} = \frac{10x}{\sigma}{m} \quad (3)$$

Individual metabolite accuracies (ACCs) were calculated with quality controls (QCs) obtained by spiking HeLa cells at three concentration levels corrected for endogenous levels as % recovery as follows:

$$ACC\% = \frac{c_{\mathrm{found}} - c_0}{c_{\mathrm{spiked}}} \quad (4)$$

where c_{spiked} is the concentration spiked to HeLa cells, c_0 is the endogenously present amount (determined by standard addition), and c_{found} is the concentration of the selected metabolite found in the spiked sample.

Data Processing. Analyst 1.7 with Analyst Device Driver was utilized for data acquisition and system control. PeakView ver. 2.2 was used for manual data evaluation. MultiQuant 3.0 was employed for peak integration, linear regression ($1/x^2$ as weight), and concentration calculation. Statistical analysis and visualization were performed withR (R Foundation for Statistical Computing, Vienna, Austria).

RESULTS AND DISCUSSION

Optimization of HILIC Separation Conditions. A number of studies evaluated HILIC for the separation of SPx. However, none fully succeeded in the complete separation of all glycolytic metabolites and their isomers with good peak shape (without tailing) and adequate assay specificity for other isomeric metabolites that are not part of the glycolysis or pentose phosphate pathway. Hence, in this study, HILIC method optimization also addressed a few hardware details besides the column and mobile phase conditions. For example, instead of a standard Turbo V ion source with a stainless steel probe, a μESI probe was employed. The column was attached to the chromatographic system using peek-lined 150 mm × 50 μm MarvelXACT capillaries, and postcolumn tubing connections from the column to the μESI probe were made from PEEKsil. These modifications were made to minimize extra-column volumes and contact of the analytes with metal surfaces. To document the gain in performance and peak shape, respectively, by avoiding the contact of the analytes with a stainless-steel surface, the chromatograms of PEP, F16P2, 6PGlocA, and PRPP acquired with the stainless steel standard ESI probe and the PEEKsil probe were compared, as shown in Figure S1. It is evident that tailing has been effectively reduced with the PEEKsil probe. An ACQUITY Premier BEH Amide column with MaxPeak High Performance Surface (HPS) hardware technology was employed for this work. The mitigation of analyte loss, especially of phosphorylated solutes like nucleotides and oligonucleotides, was already recently demonstrated.[49] Otherwise, a standard UHPLC system was used throughout this work. Further improvements in peak shape and sensitivity should therefore be possible with a bioinert system. To validate assay specificity, some isomeric hexose and pentose phosphates (M1P/M6P, Gal1P/Gal6P, and Ru1P), which are not part of the glycolysis and pentose phosphate pathways, were included during method development to secure their adequate separation in the final method. A total of 24 target metabolites were finally selected to be accurately analyzed by the UHPLC-QqQ-MS/MS method. Next, elution conditions were optimized focusing specifically on the choice of buffer salt, buffer concentration, and pH value adjustment. Preliminary tests showed that BEH Amide is favorable over Z-HILIC, with zwitterionic sulfobetaine stationary phase surface bonding, and that ammonium formate (NH_4FA) provides slightly better sensitivity compared to ammonium acetate (NH_4Ac) (Table S2). NH_4FA was chosen for further method development as an additive. Initially, the effect of the pH value was investigated, and the focus was on the hexose phosphates, which were the most challenging isomer separations. A high pH is preferred for reducing sugar phosphates like G6P to promote fast anomer interconversion (relative to the chromatographic time scale) and avoid individual separated anomer peaks. BEH amide is stable up to pH 11 and hence is favorable for this application. Tests were performed with 50 mM NH_4FA buffer at four distinct pH values (pH 8.0, 9.0, 10.0 and 11.0). Other chromatographic conditions (t_G, flow rate, and column compartment temperature) were kept constant. Figure S2A−D shows a gradual improvement of peak symmetry as the pH increased from 8 to 11. It is also evident that with lower pH values several peaks of the hexose phosphate isomers overlap, and a full separation can be achieved at pH 11 only. Corresponding chromatographic data for this optimization are provided in Table S3. Further

https://doi.org/10.1021/acs.analchem.4c03490
Anal. Chem. XXXX, XXX, XXX−XXX

optimization involved the study of various buffer concentrations (10, 50, and 100 mM NH_4FA, always adjusted to 11.0). While with 10 mM NH_4FA severe peak tailing over 2 min prevented full baseline separation (Figure S3A), significantly less tailing was observed with 50 mM NH_4FA (Figure S3B). However, the glycolytic metabolite F6P was still not fully baseline-separated from G1P. The remaining glycolytic metabolite G6P was fully separated from other isomeric interferences (Gal6P/GalP/M6P/M1P). A further increase of the buffer concentration to 100 mM NH_4FA at a pH value of 11.0 allowed nearly baseline separation of the critical peak pair F6P/G1P and full baseline separation of the other hexose phosphates (Figure 2 and S3C).

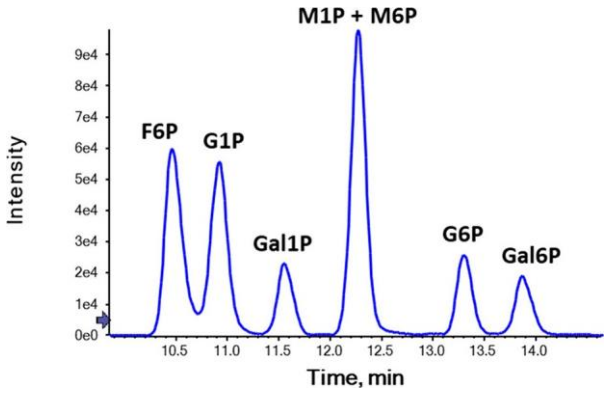

Figure 2. Extracted ion chromatogram and isomer separation of HMP analytes found in the HeLa cell sample extract (3×10^6 cells) with optimized method conditions.

M1P and M6P are not separated by these conditions yet can be determined as their sum. The glycolytic metabolite pairs G6P and F6P are sufficiently resolved for their quantitative analysis. Peak tailing could be eliminated with 100 mM NH_4FA (pH 11), yielding peak widths for the individual HMPs of approximately 0.2 min. It turns out that there are still adverse phosphate−surface interactions despite the polymer-coated column hardware and frits; however, they can be properly disrupted by high ionic strength. Further chromatographic data on this optimization are provided in Table S4. Using these optimized conditions for hexose monophosphates, pentose phosphates and the other glycolytic and PPP metabolites were evaluated regarding isomer separation and peak shape (Figure 3).

The four pentose phosphates are also separated. Ru5P and Xu5P were only partially separated, while Ru1P and Ri5P are fully baseline-separated. This separation should be suitable to allow at least an estimation of Ru5P and Xu5P, while the other two pentose phosphates can be determined without assay specificity compromises. Moreover, all the other target metabolites also show satisfactory peak shapes, and other critical isomeric peak pairs were fully resolved (2PG and 3PG, GA3P and DHAP). Pyr and Lac, which must be separated to avoid M + 2 isotopologue overlap, were fully baseline-resolved. The method also covers several bis-phosphates (F16P2 and 2,3PG), as well as PRPP with phosphate at the 5-position and a pyrophosphate group in position 1 of ribose. They exhibit symmetric peaks as well, and all target metabolites can be separated within 20 min.

Mass Spectrometry. A tandem MS method with MRM acquisition was established for detection that was beneficial owing to its robustness, sensitivity, and wide linear range. SPx and other glycolytic metabolites were recorded in negative ESI-MS. Single deprotonated molecules were selected as precursor ions and two product ions for each target metabolite. For SPx, the more intensive product ion with m/z 79 (PO_3^-) was a quantifier ion, and m/z 97 ($H_2PO_4^-$) was a qualifier ion transition (see Table S1). For 23PG, m/z 167.0 (from neutral loss of phosphoric acid) was monitored as the qualifier ion. For pyruvate and lactate, their neutral loss product ions of CO_2 served as qualifier ions, while m/z 32 and 43 were the quantifier ions for pyruvate and lactate. Contrary to our previous method involving phosphate and carboxylate methylation, which failed to detect G1P, GA3P, DHAP, pyruvate, and lactate after methylation,[25] all 24 targets were detectable in the relevant concentration range by this new

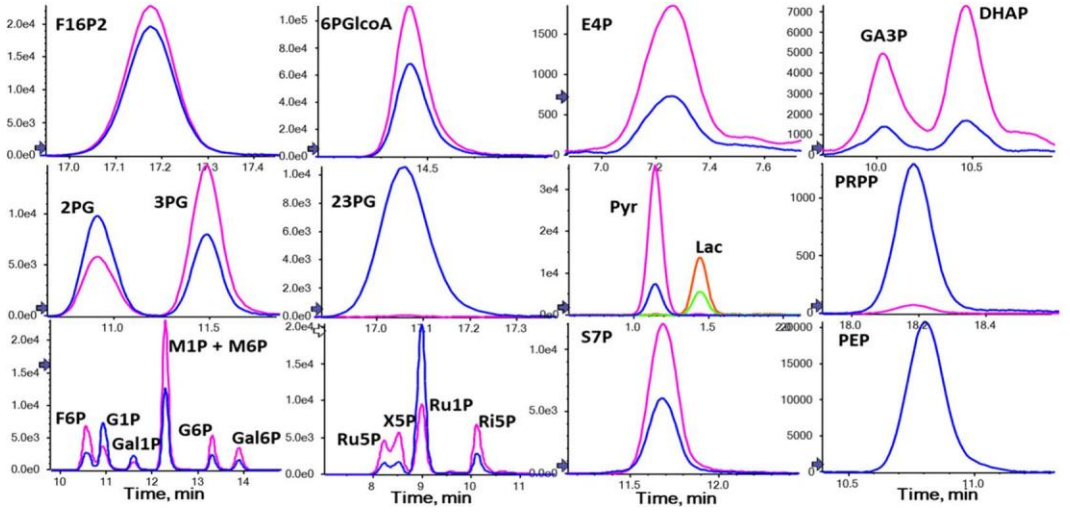

Figure 3. Extracted ion chromatograms of each individual metabolite found in the HeLa cell sample extract (3×10^6 cells). The blue line indicates the noncarbon labeled metabolite, and the pink line indicates the U-^{13}C-carbon labeled metabolite (with the exception of the U-^{13}C-labeled lactate labeled in red). All U-^{13}C-labeled analogs could be detected in the U-^{13}C-labeled cell extract except for PEP, for which U^{13}C-PRPP was used as the IS.

https://doi.org/10.1021/acs.analchem.4c03490
Anal. Chem. XXXX, XXX, XXX−XXX

HILIC method. MRM transitions and compound-specific MS parameters specified in Table S1 were employed for further method development.

Sample Preparation. A critical aspect in SPx analysis is efficient extraction from the biological material with good recovery after sampling and quenching of metabolism (see Figure S4; best quenching performance with liquid N_2 as assessed by the highest energy charge according to eq S1). The phosphorylated compounds strongly bind to proteins and other solid material as well as surfaces of glass vials, which may easily lead to extraction losses. Typically, a strong acid is required for liquid extraction. However, with an HCl-containing solvent mixture (often a first choice), there is a certain risk for hydrolytic cleavage and phosphate migration. Weaker acids like acetic acid, trichloroacetic acid, or perchloric acid are therefore often used for this reason. On the other hand, metal oxide-based affinity chromatography (MOAC) has been suggested for the extraction of phosphopeptides, phosphoproteins, and phosphorylated metabolites as well.[42] It worked well for extraction of inositol phosphates and was therefore adopted herein.[10] A U-^{13}C-labeled cell extract was first added to cell samples to compensate for losses and variances during the multiple steps of sample preparation. Next, homogenization and protein precipitation with 1 M perchloric acid (PA) were carried out in homogenization tubes using zirconia/glass beads. The supernatant was loaded onto the TiO_2 beads, which were filled into a homemade extraction cartridge equipped with a centrifuge filter with acid-resistant hydrophilic polytetrafluoroethylene (PTFE). The filtrate was discarded, and the beads washed with cold HCl. Finally, the SPx were eluted from the TiO_2 beads with 10% (v/v) ammonia solution, and the filtrate was evaporated to dryness and then reconstituted for LC analysis. This protocol provided good extraction recoveries (vide infra). The main benefit of TiO_2 extraction is purification of the primary PA extract. After protein precipitation with PA, the supernatant is used for TiO_2 extraction, which removes interfering components and reduces matrix effects. The extent of enrichment depends on the number of cells initially used to prepare the sample. In general, the MOAC with TiO_2 ensures a high extraction recovery (together with prior perchloric acid extraction and protein precipitation). PA ensures that the analytes are released from proteins and are available for extraction from the supernatant of this step by MOAC with TiO_2. Extraction recoveries larger than 65% can be achieved, and losses are properly corrected for by the U-^{13}C-labeled IS.

Method Performance. Method validation was performed with HeLa cells as the matrix. Matrix effects (ME), extraction recoveries (ER), and process efficiency (PE) were evaluated at three different concentration levels according to Matuszewski.[36] ME was assessed by comparing peak areas of postextraction spiked HeLa cells, corrected for endogenous levels determined by standard addition series, with those of corresponding standard solutions. Table S5 shows that ion suppression was observed during analysis with MEs ranging between 78.8% and 89.4%. When peak areas were corrected by U-^{13}C-labeled IS, the minor ion suppression could be successfully corrected, with MEs ranging between 96% and 103% (Table S6). ER was assessed by comparison of peak areas of pre-extraction spiked and postextraction spiked HeLa cells at three concentration levels. Table S7 (without IS correction) and Table S8 (with IS correction) provide the obtained ERs with the optimized MOAC extraction protocol. PE values (from comparison of peak areas of pre-extraction spiked HeLa cells and corresponding standard solutions) without U-^{13}C-internal standard correction are provided in Table S9, and those after U-^{13}C-internal standard correction are provided in Table S10, which ranged between 84% and 95%. From these results, it can be concluded that the ^{13}C-labeled cell extract for compensation of analyte loss during sample preparation provides adequate performance of this assay for all analytes, and it was used in the following validation. Matrix-matched calibration (corrected for endogenous levels as determined by standard addition) was employed and provided $r^2 > 0.99$ for all 24 target metabolites (Table S11). Back-calculations of the concentrations of the nonzero calibrators regarding their nominal concentrations (i.e., spiked concentrations after correction for endogenous concentrations) were always less than ±15% of calibrator levels (Table S9). Next, both inter- and intraday precision and accuracy were determined with QCs at three distinct levels. Precision was always below 10% RSD for all analytes throughout the validation sequence (Tables S12 and S13). Intra- and interday accuracies performed well across the entire validation series, with recovery values ranging between 90% and 105% (calculated after the correction of endogenous levels) (Tables S14 and S15). Based on these results, it is shown that this method is reliable for SPx quantification in biological samples.

HILIC Retention Time Repeatability. HILIC has a reputation of poor retention time repeatability. McCullagh and co-workers performed a comparison of HILIC-MS with IC-MS and found significantly less retention time variance for IC-MS (sd on average ±0.04 min) than HILIC-MS (sd ±0.2 min).[36] For this reason, the retention time repeatability of the developed assay was investigated. We observed stable retention times (sd of 0.01−0.02 min) over $n = 60$ sample injections (with a total analysis time of 25 h) (Figure 4).

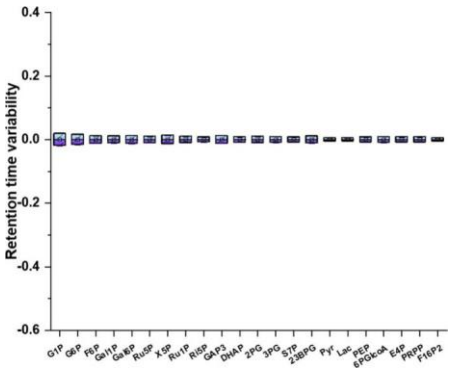

Figure 4. HILIC retention time repeatability study carried out in this work. A total of $n = 60$ samples (25 h estimated) were analyzed with the experimental setup described in the manuscript. Retention time variability in minutes of the individual metabolites listed as SD is shown.

As can be derived from Table S16A and B, the retention time fluctuations were minimal and even less than those for IC-MS reported by McCullagh.[36] At this point, it must be emphasized that we used PFA solvent bottles instead of the more common borosilicate glass.[38] Borosilicate glass bottles as solvent reservoirs release ions (Na^+, K^+, and borate) that lead to restructuring of the semi-immobilized water layer on the stationary phase surface in the course of an analytical batch, leading to shifts in retention time and poor retention time

https://doi.org/10.1021/acs.analchem.4c03490
Anal. Chem. XXXX, XXX, XXX−XXX

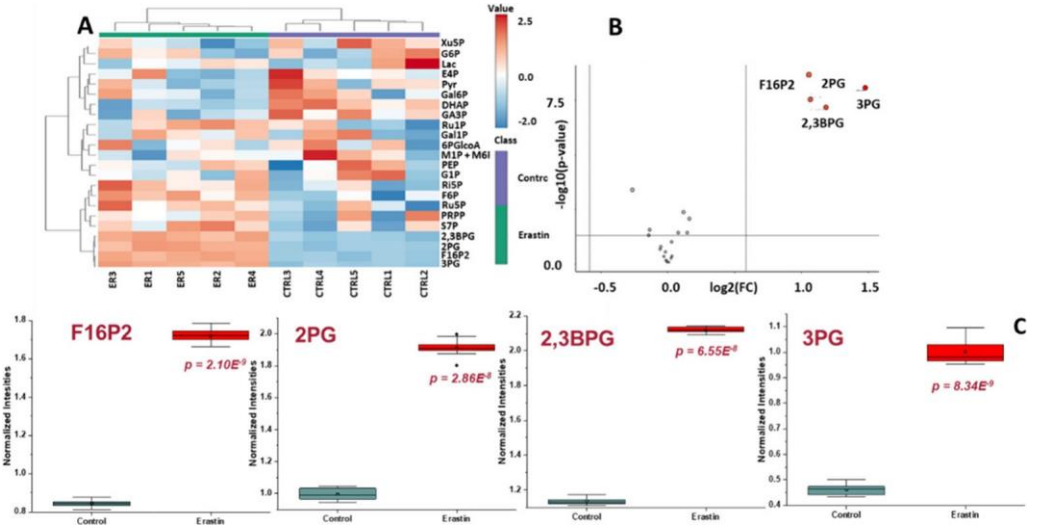

Figure 5. Metabolic profiles in HEK293 cells (3×10^6) upon erastin treatment ($n = 5$). Features were autoscaled, and the Ward clustering method was performed. (A) Heatmaps displaying an overview of metabolite abundance distribution, with comparison between erastin-induced ferroptotic cell samples (ER) versus the control (CTRL). (B) Volcano plots showing the comparison between ferroptosis-induced (erastin) samples and the control (p-value threshold 0.05). (C) Representative boxplots of significantly increased metabolites (2PG, 3PG, 2,3BPG, and F16P2) found in HEK293 cell extract samples in which ferroptosis was induced compared to untreated ones (control).

repeatability. With PFA bottles, the ion concentration in the solvent reservoirs stays constant and hence no retention shifts are observed.[43] A comparison between glass and PFA solvent bottles with E4P as a representative example can be found in Figure S5. It can be seen that there is a significant drift of retention when a standard borosilicate glass bottle is used as a mobile phase reservoir. Together with optimized eluent conditions, coated column hardware, the PEEKsil μESI probe, and PFA bottles, these aspects prove important points for an optimized method for phosphorylated compounds with symmetrical peaks, stable retention times, and robust analysis.

Applications. After method establishment and validation, we applied this targeted LC-MS/MS assay to profile SPx and other glycolytic metabolites in cultured HeLa cells to document the applicability to real samples. The results are given in Table S17. All target metabolites were detected above their LoQ values. Their concentrations ranged between 8 and 216 nM in the dried extract of 3×10^6 HeLa cells (reconstituted by 100 μL of ACN/water (50:50; v/v); corresponding to 2−82 fmol per cell). The highest concentration was found for lactic acid (215.9 ± 8.8 nM; corresponding to 71.9 ± 2.9 fmol per cell). G6P and F6P were measured at 34.3 ± 2.3 nM (11.4 ± 0.8 fmol per cell) and 38.2 ± 3.2 nM (12.7 ± 1.1 fmol per cell), respectively, and F16P2 was determined at a concentration of 55.7 ± 4.1 nM (18.6 ± 1.4 fmol per cell). This confirmed the applicability of our method. Finally, the applicability of our assay was further assessed by studying glycolysis and PPP metabolic processes under ferroptotic cell death.[39] For this purpose, erastin was used to induce ferroptosis in HEK293 cells, an immortalized human embryonic kidney cell line (see the Experimental section for detailed conditions). Erastin inhibits the cystine−glutamate antiporter system X_c, leading to cysteine deprivation and cellular deficiency to synthesize the antioxidant glutathione.[44] It is accompanied by reactive oxygen species (ROS) accumulation due to mitochondrial dysfunction and causes an avalanche of metabolic alterations. Figure 5A shows the heat map of the glycolysis and PPP metabolites of a two-group comparison (erastin-induced ferroptosis vs control, i.e., untreated HEK293 cells) (for concentrations see Table S18). Cluster analysis provides a classification according to the two groups based on the glycolytic and PPP metabolite concentration levels. A volcano plot in Figure 5B generated by comparing metabolite levels of these two groups by univariate statistics reveals that the glycolytic metabolites F16P2, 2PG, 2,3BPG, and 3PG were significantly upregulated (p-value of <0.05) with a fold-change of >2 in the erastin-induced ferroptosis group (Table S19). Enhanced glycolysis in cells with ferroptosis was further confirmed by the enhanced glucose uptake (see Figure S6).

CONCLUSIONS

The accurate and robust analysis of sugar phosphates (SPx) by LC-MS/MS remains a challenging analytical task in metabolomics despite many advances. Full coverage of the glycolytic and PPP metabolites in a single quantitative analytical run with an adequately validated assay specificity is still difficult to achieve. Problems include peak tailing, poor chromatographic retention in RP, contaminations from ion-paring agents in ion-pair RPLC, limited repeatability in HILIC, anomerization of reducing sugar phosphates, and the presence of several isomers (isomeric interferences in the analysis of glycolytic hexose phosphates from other pathways like lactose and mannose metabolism also have to be considered), which are indistinguishable by MS. In this study, we present a HILIC method hyphenated to tandem MS for separating SPx from central carbon metabolism (glycolysis and PPP) that overcomes the above-mentioned problems. A BEH Amide HILIC column with MaxPeak High Performance Surface-coated column hardware (stainless steel tube and metal frits) operated at high pH (pH 11) and high ionic strength (100 mM ammonium formate) with a negative acetonitrile (HILIC) gradient provided full peak coalescence of anomers, full isomer separation (except for M1P/M6P, which eluted as a single peak but without interference with other hexose monophosphate peaks) and hence adequate assay specificity for G6P and F6P, and symmetrical peaks. Additionally, other

https://doi.org/10.1021/acs.analchem.4c03490
Anal. Chem. XXXX, XXX, XXX−XXX

critical isomeric peak pairs such as 2PG/3PG, GA3P/DHAP, and the redox-active lactate/pyruvate (M + 2) peaks were fully baseline-resolved. Bis-phosphorylated compounds such as F16P2 and 2,3BPG and even a pyrophosphorylated metabolite (PRPP) could be determined with good peak shapes. Due to the use of PFA plastic bottles as solvent reservoirs (instead of borosilicate glass bottles), retention time repeatability was excellent in contrast to what is reported in the literature. The validated assay was used to analyze the glycolysis and PPP metabolites in different biological matrices (HeLa cells and kidney embryonic cells) using UHPLC-QTrap-MRM acquisition. To our knowledge, the current developed method is the first comprehensive workflow based on HILIC-ESI-MS/MS fully covering the glycolysis and pentose phosphate pathway that does not need derivatization, system passivation, or the addition of EDTA or methylphosphonic acid to the eluent and has solved (i) the isomer selectivity problem,(ii) the poor peak shape problem of phosphorylated polar metabolites, and (iii) the run-to-run repeatability problem in HILIC.

ASSOCIATED CONTENT

Supporting Information

The Supporting Information is available free of charge at https://pubs.acs.org/doi/10.1021/acs.analchem.4c03490.

Information and data on chromatographic parameters such as ME, PE, ER; assay validation data values, i.e., precision, accuracy, calibration, LoD, and LoQ; results of the retention time repeatability study in HILIC; quantification results in HeLa and HEK293 cell culture extracts; fold change and statistical values for significant metabolites in the ferroptosis HEK293 model; further chromatographic data obtained during method optimization and development, i.e., peak tailing, peak widths, and retention times dependent on pH and buffer additive concentration; and figures displaying the effect of pH and buffer additive concentration on the chromatographic separation (PDF)

AUTHOR INFORMATION

Corresponding Author

Michael Lämmerhofer − *Institute of Pharmaceutical Sciences, Pharmaceutical (Bio-)Analysis, University of Tübingen, 72076 Tübingen, Germany;* orcid.org/0000-0002-1318-0974; Email: michael.laemmerhofer@uni-tuebingen.de

Author

Kristian Serafimov − *Institute of Pharmaceutical Sciences, Pharmaceutical (Bio-)Analysis, University of Tübingen, 72076 Tübingen, Germany*

Complete contact information is available at: https://pubs.acs.org/10.1021/acs.analchem.4c03490

Notes

The authors declare no competing financial interest.

REFERENCES

(1) Girel, S.; Guillarme, D.; Fekete, S.; Rudaz, S.; González-Ruiz, V. *J. Chromatogr. A* 2023, *1697*, No. 463994.
(2) Lioupi, A.; Virgiliou, C.; Walter, T. H.; Smith, K. M.; Rainville, P.; Wilson, I. D.; Theodoridis, G.; Gika, H. G. *J. Chromatogr. A* 2022, *1672*, No. 463013.
(3) Serafimov, K.; Lämmerhofer, M. *J. Chromatogr. A* 2022, *1684*, No. 463556.
(4) Diamantidou, D.; Sampsonidis, I.; Liapikos, T.; Gika, H.; Theodoridis, G. *J. Chromatogr. A* 2023, *1690*, No. 463779.
(5) Straube, H.; Witte, C. P.; Herde, M. *Cells* 2021, *10* (3), 689.
(6) Li, P.; Gawaz, M.; Chatterjee, M.; Lämmerhofer, M. *Anal. Chim. Acta* 2022, *1191*, No. 339286.
(7) Coulier, L.; Bas, R.; Jespersen, S.; Verheij, E.; van der Werf, M. J.; Hankemeier, T. *Anal. Chem.* 2006, *78* (18), 6573−6582.
(8) Wakamatsu, A.; Morimoto, K.; Shimizu, K.; Kudoh, S. *J. Sep. Sci.* 2005, *28*, 1823−1830.
(9) Tuytten, R.; Lemiere, F.; Witters, E.; Van Dongen, W.; Slegers, H.; Newton, R. P.; Van Onckelen, H.; Esmans, E. L. *J. Chromatogr. A* 2006, *1104*, 209−221.
(10) Hui, J. P. M.; Yang, J.; Thorson, J. S.; Soo, E. C. *ChemBiochem* 2007, *8*, 1180−1188.
(11) Soga, T.; Igarashi, K.; Ito, C.; Mizobuchi, K.; Zimmermann, H. P.; Tomita, M. *Anal. Chem.* 2009, *81*, 6165−6174.
(12) Chu, D. B.; Troyer, C.; Mairinger, T.; Ortmayr, K.; Neubauer, S.; Koellensperger, G.; Hann, S. *Anal. Bioanal. Chem.* 2015, *407*, 2865−2875.
(13) Antonio, C.; Larson, T.; Gilday, A.; Graham, I.; Bergstrom, E.; Thomas-Oates, J. *J. Chromatogr. A* 2007, *1172*, 170−178.
(14) Hemstrom, P.; Irgum, K. *J. Sep. Sci.* 2006, *29*, 1784−1821.
(15) Jandera, P.; Janas, P. *Anal. Chim. Acta* 2017, *967*, 12−32.
(16) Schwaiger, M.; Rampler, E.; Hermann, G.; Miklos, W.; Berger, W.; Koellensperger, G. *Anal. Chem.* 2017, *89*, 7667−7674.
(17) Chu, D. B.; Klavins, K.; Koellensperger, G.; Hann, S. *J. Anal. At. Spectrom.* 2014, *29*, 915−925.
(18) Hinterwirth, H.; Lämmerhofer, M.; Preinerstorfer, B.; Gargano, A.; Reischl, R.; Bicker, W.; Trapp, O.; Brecker, L.; Lindner, W. *J. Sep. Sci.* 2010, *33*, 3273−3282.
(19) Smith, K. M.; Wilson, I. D.; Rainville, P. D. *Anal. Chem.* 2021, *93*, 1009−1015.
(20) Su, M.; Serafimov, K.; Li, P.; Knappe, C.; Lämmerhofer, M. *J. Chromatogr. A* 2023, *1688*, No. 463727.
(21) Yang, W.-C.; Sedlak, M.; Regnier, F. E.; Mosier, N.; Ho, N.; Adamec, J. *Anal. Chem.* 2008, *80*, 9508−9516.
(22) Han, J.; Tschernutter, V.; Yang, J.; Eckle, T.; Borchers, C. H. *Anal. Chem.* 2013, *85*, 5965−5973.
(23) Sheng, N.; Zhao, H.; Chen, X.; Wang, D.; Li, M.; Wang, Z.; Zhang, J.; Jiang, J. *Talanta* 2021, *228*, No. 122238.
(24) Zeng, H.; Qi, C. B.; Liu, T.; Xiao, H. M.; Cheng, Q. Y.; Jiang, H. P.; Yuan, B. F.; Feng, Y. Q. *Anal. Chem.* 2017, *89*, 4153−4160.
(25) Li, P.; Su, M.; Chatterjee, M.; Lämmerhofer, M. *Anal. Chim. Acta* 2022, *1221*, No. 340099.
(26) Luo, X. T.; Cai, B. D.; Jiang, H. P.; Xiao, H. M.; Yuan, B. F.; Feng, Y. Q. *J. Chromatogr. A* 2019, *1592*, 82−90.
(27) Haberhauer-Troyer, C.; Delic, M.; Gasser, B.; Mattanovich, D.; Hann, S.; Koellensperger, G. *Anal. Bioanal. Chem.* 2013, *405* (6), 2031−9.
(28) Serafimov, K.; Aydin, Y.; Lämmerhofer, M. *J. Sep. Sci.* 2024, *47* (1), No. 2300780.
(29) Wasito, H.; Hermann, G.; Fitz, V.; Troyer, C.; Hann, S.; Koellensperger, G. *Anal. Bioanal. Chem.* 2022, *414* (15), 4359−4368.
(30) Klavins, K.; Chu, D. B.; Hann, S.; Koellensperger, G. *Analyst* 2014, *139* (6), 1512−20.
(31) Mathon, C.; Barding, G. A., Jr.; Larive, C. K. *Anal. Chim. Acta* 2017, *972*, 102−110.
(32) Matuszewski, B. K.; Constanzer, M. L.; Chavez-Eng, C. M. *Anal. Chem.* 2003, *75* (13), 3019−30.
(33) Ross, K. L.; Dalluge, J. J. *Anal. Chem.* 2009, *81* (10), 4021−6.
(34) Hsiao, J. J.; Potter, O. G.; Chu, T. W.; Yin, H. *Anal. Chem.* 2018, *90* (15), 9457−9464.
(35) Koley, S.; Chu, K. L.; Gill, S. S.; Allen, D. K. *J. Exp. Bot.* 2022, *73* (9), 2938−2952.
(36) Walsby-Tickle, J.; Gannon, J.; Hvinden, I.; Bardella, C.; Abboud, M. I.; Nazeer, A.; Hauton, D.; Pires, E.; Cadoux-Hudson, T.; Schofield, C. J.; McCullagh, J. S. O. *Commun. Biol.* 2020, *3*, 247.
(37) Si-Hung, L.; Troyer, C.; Causon, T.; Hann, S. *Talanta* 2019, *205*, No. 120147.

(38) Serafimov, K.; Knappe, C.; Li, F.; Sievers-Engler, A.; Lämmerhofer, M. *J. Chromatogr. A* 2024, *1730*, No. 465060.
(39) Jiang, X.; Stockwell, B. R.; Conrad, M. *Nat. Rev. Mol. Cell. Biol.* 2021, *22* (4), 266−282.
(40) Tian, Y.; Wan, N.; Zhang, H.; Shao, C.; Ding, M.; Bao, Q.; Hu, H.; Sun, H.; Liu, C.; Zhou, K.; Chen, S.; Wang, G.; Ye, H.; Hao, H. *Nat. Chem. Biol.* 2023, *19* (12), 1480−1491.
(41) Michopoulos, F.; Whalley, N.; Theodoridis, G.; Wilson, I. D.; Dunkley, T. P.; Critchlow, S. E. *J. Chromatogr A* 2014, *1349*, 60−8.
(42) Patel, J. H.; Ong, D. J.; Williams, C. R.; Callies, L. K.; Wills, A. E. *Cell Rep.* 2022, *41* (4), No. 111552.
(43) Zheng, J.; Yang, J.; Liang, X.; Fang, M.; Wang, Y. *Talanta* 2024, *266*, No. 125074.
(44) Shestov, A. A.; Liu, X.; Ser, Z.; Cluntun, A. A.; Hung, Y. P.; Huang, L.; Kim, D.; Le, A.; Yellen, G.; Albeck, J. G.; Locasale, J. W. *Elife* 2014, *3*, No. e03342.
(45) TeSlaa, T.; Bartman, C. R.; Jankowski, C. S. R.; Zhang, Z.; Xu, X.; Xing, X.; Wang, L.; Lu, W.; Hui, S.; Rabinowitz, J. D. *Cell Metab.* 2021, *33* (2), 367−378.
(46) Kim, G. D.; Qiu, D.; Jessen, H. J.; Mayer, A. *mBio* 2023, *14* (3), No. e00102-23.
(47) Zhu, B.; Wei, H.; Wang, Q.; Li, F.; Dai, J.; Yan, C.; Cheng, Y. *Talanta* 2018, *179*, 615−623.
(48) Cluntun, A. A.; Huang, H.; Dai, L.; Liu, X.; Zhao, Y.; Locasale, J. W. *Cancer Metab.* 2015, *3*, 10.
(49) DeLano, M.; Walter, T. H.; Lauber, M. A.; Gilar, M.; Jung, M. C.; Nguyen, J. M.; Boissel, C.; Patel, A. V.; Bates-Harrison, A.; Wyndham, K. D. *Anal. Chem.* 2021, *93*, 5773−5781.
(50) Bajad, S. U.; Lu, W.; Kimball, E. H.; Yuan, J.; Peterson, C.; Rabinowitz, J. D. *J. Chromatogr. A* 2006, *1125* (1), 76−88.
(51) Tolstikov, V. V.; Fiehn, O. *Anal. Biochem.* 2002, *301* (2), 298−307.
(52) Guo, K.; Ji, C.; Li, L. *Anal. Chem.* 2007, *79* (22), 8631−8638.
(53) Gika, H. G.; Theodoridis, G. A.; Vrhovsek, U.; Mattivi, F. *J. Chromatogr. A* 2012, *1259*, 121−127.
(54) Tsugawa, H.; Cajka, T.; Kind, T.; Ma, Y.; Higgins, B.; Ikeda, K.; Kanazawa, M.; Van der Gheynst, J.; Fiehn, O.; Arita, M. *Nat. Meth.* 2015, *12* (6), 523−526.
(55) Contrepois, K.; Jiang, L.; Snyder, M. *Mol. Cell. Prot.* 2015, *14* (6), 1684−1695.
(56) Sillner, N.; Walker, A.; Harrieder, E. M.; Schmitt-Kopplin, P.; Witting, M. *J. Chromatogr. B* 2019, *1109*, 142−148.
(57) Cajka, T.; Hricko, J.; Rudl Kulhava, L.; Paucova, M.; Novakova, M.; Kuda, O. *Int. J. Mol. Sci.* 2023, *24* (3), 1987.
(58) Spagou, K.; Tsoukali, H.; Raikos, N.; Gika, H.; Wilson, I. D.; Theodoridis, G. *J. Sep. Sci.* 2010, *33* (6−7), 716−727.
(59) Kohler, I.; Verhoeven, M.; Haselberg, R.; Gargano, A. *Microchem. J.* 2022, *175*, No. 106986.
(60) Lee, H. J.; Kremer, D. M.; Sajjakulnukit, P.; Zhang, L.; Lyssiotis, C. A. *Metabolomics* 2019, *15* (7), 103.
(61) Fu, X.; Deja, S.; Kucejova, B.; Duarte, J. A. G.; McDonald, J. G.; Burgess, S. C. *Anal. Chem.* 2019, *91* (9), 5881−5887.
(62) Chen, J.; Hou, W.; Han, B.; Liu, G.; Gong, J.; Li, Y.; Zhong, D.; Liao, Q.; Xie, Z. *Anal. Bioanal. Chem.* 2016, *408* (10), 2527−2542.
(63) Paglia, G.; Hrafnsdóttir, S.; Magnúsdóttir, M.; Fleming, R. M.; Thorlacius, S.; Palsson, B. Ø.; Thiele, I. *Anal. Bioanal. Chem.* 2012, *402* (3), 1183−1198.
(64) García-Cañaveras, J. C.; Donato, M. T.; Castell, J. V.; Lahoz, A. *J. Proteome Res.* 2011, *10* (10), 4825−4834.
(65) Nelson, D.; Xu, N.; Carlson, J. *Scand. J. Clin. Lab. Invest.* 2012, *72* (6), 441−446.

https://doi.org/10.1021/acs.analchem.4c03490
Anal. Chem. XXXX, XXX, XXX−XXX

Supporting information

Comprehensive coverage of glycolysis and pentose phosphate metabolic pathways by isomer-selective accurate targeted hydrophilic interaction liquid chromatography-tandem mass spectrometry assay

Kristian Serafimov[a], Michael Lämmerhofer[a]*

[a] Institute of Pharmaceutical Sciences, Pharmaceutical (Bio-)Analysis, University of Tübingen, Auf der Morgenstelle 8, 72076 Tübingen, Germany

***Authors for correspondence:**

Prof. Michael Lämmerhofer
Pharmaceutical (Bio-)Analysis
Institute of Pharmaceutical Sciences
University of Tuebingen
Auf der Morgenstelle 8
72076 Tuebingen, Germany
T +49 7071 29 78793
e-mail: michael.laemmerhofer@uni-tuebingen.de
http://www.bioanalysis.uni-tuebingen.de/

Content

Table S1: MRM transitions and compound specific MS parameters (Dt, dwell time; DP, declustering potential; EP, entrance potential; CE, collision energy; CXP, collision cell exit potential).

SPx	Q1, *m/z*	Q3, *m/z*	Dt, ms	DP, V	EP, V	CE, V	CXP, V
HMP-1	259.3	79.0	20	-40	-10	-50	-10
HMP-2	259.3	97.0	20	-40	-10	-22	-10
F16P2-1	339.0	79.0	20	-10	-10	-70	-10
F16P2-2	339.0	97.0	20	-10	-10	-23	-15
GA3P/DHAP -1	169.0	79.0	20	-60	-10	-30	-10
GA3P/DHAP -2	169.0	97.0	20	-60	-10	-12	-15
3PG/2PG-1	185.0	79.0	20	-20	-10	-35	-10
3PG/2PG-2	185.0	97.0	20	-20	-10	-20	-10
PRPP-1	389.1	79.0	20	-40	-10	-35	-10
PRPP-2	389.1	97.0	20	-40	-10	-15	-10
E4P-1	199.0	79.0	20	-40	-10	-35	-10
E4P-2	199.0	97.0	20	-40	-10	-15	-10
PEP-1	167.0	79.0	20	-30	-10	-50	-10
PEP-2	167.0	97.0	20	-30	-10	-20	-10
6PGlcoA-1	275.0	79.0	20	-20	-10	-60	-12
6PGlcoA-2	275.0	97.0	20	-20	-10	-23	-15
S7P-1	289.0	79.0	20	-40	-10	-60	-15
S7P-2	289.0	97.0	20	-40	-10	-20	-8
PMP-1	229.0	79.0	20	-30	-10	-40	-10
PMP-2	229.0	97.0	20	-30	-10	-15	-15
23BPG-1	265.0	79.0	20	-40	-10	-50	-15
23BPG-2	265.0	167.0	20	-40	-10	-16	-10
Pyruvate-1	87.0	32.0	20	-20	-10	-12	-8
Pyruvate-2	87.0	43.0	20	-20	-10	-10	-10
Lactate-1	89.0	43.0	20	-30	-10	-18	-8
Lactate-2	89.0	45.0	20	-30	-10	-12	-10
$U^{13}C$-HMP	265.3	79.0	20	-40	-10	-50	-10
$U^{13}C$-F16P2	345.0	79.0	20	-10	-10	-70	-10
$U^{13}C$-GA3P/DHAP	172.0	79.0	20	-60	-10	-30	-10
$U^{13}C$-3PG/2PG	188.0	79.0	20	-20	-10	-35	-10
$U^{13}C$-PEP	170.0	79.0	20	-30	-10	-50	-10
$U^{13}C$-6PGlcoA	281.0	79.0	20	-20	-10	-60	-12
$U^{13}C$-Se7P	296.0	79.0	20	-40	-10	-60	-15
$U^{13}C$-PMP	234.0	79.0	20	-30	-10	-40	-10
$U^{13}C$-23BPG	268.0	79.0	20	-40	-10	-50	-15
$U^{13}C$-Pyruvate	90.0	32.0	20	-20	-10	-12	-8
$U^{13}C$-Lactate	92.0	43.0	20	-30	-10	-18	-8

Table S2 | Instrumental detection (LoD, eq 2) and quantification limits (LoQ, eq. 3) determined with standard diluton series using 2 distinct buffer additves and gradient profile as specified (0.0 min, 90% B; 12.0 min, 15% B; 20.0 min, 20% B; 20.1 min, 10% B; 25.0 min, 10% B).

SPx	LoD NH_4FA* [nmol/L]	LoD NH_4Ac [nmol/L]	LoQ NH_4FA* [nmol/L]	LoQ NH_4Ac [nmol/L]
HMP	1.2 ± 0.2	2.7 ± 0.2	5.7 ± 0.5	8.3 ± 0.2
PMP	2.0 ± 0.3	3.1 ± 0.2	6.2 ± 0.5	9.3 ± 0.3
GA3P	1.5 ± 0.1	2.8 ± 0.3	4.5 ± 0.4	8.5 ± 0.4
DHAP	1.9 ± 0.1	2.4 ± 0.2	5.9 ± 0.3	7.6 ± 0.5
2PG	1.3 ± 0.3	2.5 ± 0.3	4.2 ± 0.2	8.2 ± 0.2
3PG	1.5 ± 0.2	2.4 ± 0.2	4.5 ± 0.4	7.7 ± 0.4
2,3BPG	1.7 ± 0.2	3.0 ± 0.2	3.6 ± 0.2	6.1 ± 0.5
Pyr	2.6 ± 0.3	3.6 ± 0.2	8.4 ± 0.3	11.4 ± 0.7
Lac	2.7 ± 0.2	3.5 ± 0.1	8.6 ± 0.3	10.9 ± 0.4
E4P	2.0 ± 0.1	2.6 ± 0.2	6.1 ± 0.5	8.5 ± 0.2
6PGlcoA	1.8 ± 0.3	3.2 ± 0.3	5.6 ± 0.3	9.9 ± 0.3
S7P	2.0 ± 0.3	3.1 ± 0.4	6.1 ± 0.4	10.2 ± 0.3
F16P2	2.9 ± 0.5	3.7 ± 0.5	8.7 ± 0.6	11.9 ± 0.5
PEP	1.4 ± 0.2	3.1 ± 0.3	4.3 ± 0.4	9.9 ± 0.2
PRPP	1.3 ± 0.1	2.4 ± 0.1	3.9 ± 0.1	8.3 ± 0.3

***** final method conditions

Table S3 | Retention times, peak widths at half height and tailing factors for the individual metabolites obtained for the method development conditions according to Figure S-1 (50 mM ammonium formate)

Metabolite	t_R pH 8.0 [min]	Peak Width pH 8.0 [min]	Tailing Factor pH 8.0	t_R pH 9.0 [min]	Peak Width pH 9.0 [min]	Tailing Factor pH 9.0	t_R pH 10.0 [min]	Peak Width pH 10.0 [min]	Tailing Factor pH 10.0	t_R pH 11.0 [min]	Peak Width pH 11.0 [min]	Tailing Factor pH 11.0
G6P	10.81	0.25	1.89	9.85	0.24	1.66	9.34	0.23	1.59	11.47	0.22	1.56
G1P	8.93	0.24	1.66	8.06	0.21	1.54	8.58	0.21	1.67	8.81	0.20	1.45
Gal1P	9.95	0.24	1.94	8.54	0.22	1.72	8.76	0.24	1.74	9.64	0.18	1.39
Gal6P	10.34	0.23	2.01	9.27	0.23	1.81	9.48	0.19	1.69	12.01	0.24	1.44
M1P + M6P	8.85	0.25	1.82	8.31	0.24	1.66	8.96	0.22	1.92	11.28	0.21	1.42
F6P	9.44	0.25	1.64	8.92	0.25	1.56	8.55	0.26	1.44	8.68	0.19	1.31
Ru1P	6.56	0.24	1.55	6.43	0.22	1.34	6.87	0.23	1.28	7.01	0.23	1.24
Ri5P	7.75	0.25	1.93	7.52	0.26	1.45	7.65	0.25	1.32	7.98	0.22	1.34
Xu5P	6.45	0.25	1.82	6.31	0.25	1.52	6.58	0.24	1.44	6.24	0.25	1.32
Ru5P	6.21	0.24	1.74	6.12	0.23	1.53	6.44	0.22	1.37	6.01	0.20	1.26
GA3P	8.86	0.25	1.61	8.60	0.24	1.48	8.34	0.25	1.56	8.10	0.19	1.41
DHAP	8.99	0.24	1.64	8.71	0.25	1.50	8.51	0.23	1.42	8.38	0.24	1.35
2PG	9.43	0.23	1.89	9.21	0.22	1.35	9.32	0.20	1.46	8.94	0.17	1.36
3PG	9.78	0.23	1.78	9.44	0.20	1.48	9.55	0.21	1.35	9.32	0.19	1.27
2,3BPG	15.87	0.13	2.21	15.45	0.09	1.77	15.62	0.08	1.38	15.12	0.07	1.27
Pyr	1.13	0.05	1.15	1.14	0.05	1.11	1.11	0.05	1.14	1.14	0.05	1.01
Lac	1.32	0.06	1.18	1.28	0.05	1.21	1.30	0.06	1.23	1.35	0.06	1.15
E4P	10.38	0.24	1.67	9.96	0.22	1.56	10.00	0.20	1.35	9.89	0.18	1.45
6PGlcoA	13.01	0.23	2.25	12.88	0.20	2.03	12.77	0.21	1.88	12.57	0.19	1.76
S7P	10.34	0.26	2.01	10.22	0.23	1.76	10.01	0.22	1.56	9.89	0.21	1.42
F16P2	16.89	0.15	2.45	16.44	0.10	1.87	15.76	0.08	1.34	15.31	0.08	1.22
PEP	9.43	0.23	1.67	9.25	0.19	1.38	9.18	0.17	1.22	8.99	0.18	1.18
PRPP	17.33	0.24	3.43	17.12	0.15	3.02	16.44	0.13	2.56	16.23	0.13	2.45

Table S4 | Retention times, peak widths and tailing factors for the individual metabolites obtained for the method development conditions according to Figure S-2. Gradient profile as specified 0.0 min, 90% B; 12.0 min, 15% B; 20.0 min, 20% B; 20.1 min, 10% B; 25.0 min, 10% B.

Metabolite	t_R 10 mM NH_4FA [min]	Peak Width 10 mM NH_4FA [min]	Tailing Factor 10 mM NH_4FA	t_R 50 mM NH_4FA [min]	Peak Width 50 mM NH_4FA [min]	Tailing Factor 50 mM NH_4FA	t_R 100 mM NH_4FA [min]*	Peak Width 100 mM NH_4FA [min]*	Tailing Factor 100 mM NH_4FA*
G6P	9.31	0.24	2.12	11.47	0.22	1.76	13.88	0.14	1.50
G1P	7.32	0.23	2.34	8.81	0.20	1.95	10.51	0.13	1.08
Gal1P	8.45	0.25	2.55	9.64	0.18	1.89	11.57	0.10	0.82
Gal6P	10.20	0.28	2.43	12.01	0.24	1.94	13.30	0.21	1.46
M1P + M6P	8.82	0.26	2.76	11.28	0.21	2.02	12.27	0.11	1.16
F6P	7.77	0.24	2.65	8.68	0.19	2.12	10.90	0.19	1.38
Ru1P	6.02	0.28	1.94	7.01	0.23	1.56	8.95	0.17	1.14
Ri5P	7.12	0.27	1.88	7.98	0.25	1.45	10.06	0.20	1.36
Xu5P	5.65	0.29	1.92	6.24	0.24	1.41	8.44	0.20	1.12
Ru5P	5.32	0.30	2.12	6.01	0.22	1.62	8.19	0.21	0.85
GA3P	7.15	0.26	1.99	8.10	0.23	1.66	10.02	0.19	1.24
DHAP	7.34	0.27	1.86	8.38	0.24	1.54	10.52	0.23	1.20
2PG	7.66	0.29	2.12	8.94	0.24	1.34	10.90	0.14	1.29
3PG	7.95	0.28	2.08	9.32	0.23	1.22	11.53	0.15	0.88
2,3BPG	13.54	0.17	1.87	15.12	0.14	1.54	17.04	0.05	0.70
Pyr	1.13	0.06	1.08	1.14	0.05	1.01	1.15	0.04	0.96
Lac	1.38	0.07	1.01	1.35	0.04	0.98	1.42	0.05	1.55
E4P	8.30	0.25	1.78	9.89	0.22	1.54	11.72	0.18	1.30
6PGlcoA	10.98	0.24	2.12	12.57	0.20	1.81	14.46	0.13	1.65
S7P	8.85	0.27	2.21	9.89	0.21	1.33	11.71	0.13	0.81
F16P2	14.14	0.18	2.34	15.31	0.12	1.45	17.20	0.05	1.12
PEP	7.94	0.24	2.45	8.99	0.18	1.18	10.81	0.14	0.99
PRPP	14.93	0.16	3.12	16.23	0.12	2.67	18.19	0.09	2.17

*optimized final conditions

Table S5 | Matrix effect (ME) of SPx and extended metabolites without internal standard correction (Hela cells as matrix, n = 5).

ME, %	QC_{low}	QC_{mid}	QC_{high}
G6P	80.1 ± 1.5	79.7 ± 3.0	81.2 ± 1.1
G1P	80.5 ± 2.1	87.6 ± 2.3	80.6 ± 3.0
Gal1P	79.8 ± 1.4	79.4 ± 3.2	80.7 ± 2.2
Gal6P	85.6 ± 2.2	81.5 ± 2.6	82.5 ± 2.3
M1P + M6P	88.4 ± 1.3	79.8 ± 3.5	82.9 ± 3.4
F6P	80.3 ± 1.7	79.6 ± 3.6	80.6 ± 3.1
Ru1P	90.5 ± 1.6	86.9 ± 2.5	83.7 ± 1.0
Ri5P	90.1 ± 2.4	85.6 ± 2.9	84.5 ± 2.5
Xu5P	85.3 ± 1.5	83.7 ± 3.4	82.3 ± 2.4
Ru5P	83.0 ± 2.8	84.9 ± 2.3	83.0 ± 2.2
GA3P	86.2 ± 2.5	78.8 ± 3.0	82.6 ± 1.5
DHAP	85.7 ± 2.2	80.1 ± 2.1	84.9 ± 1.6
2PG	81.9 ± 2.4	80.4 ± 3.2	82.5 ± 1.2
3PG	80.9 ± 1.0	81.9 ± 2.7	82.1 ± 2.1
2,3BPG	80.8 ± 1.1	86.6 ± 2.5	83.0 ± 2.3
Pyr	87.5 ± 2.2	80.8 ± 1.9	81.9 ± 3.0
Lac	89.4 ± 2.5	88.9 ± 2.5	86.7 ± 2.3
E4P	82.7 ± 2.6	80.3 ± 3.4	89.6 ± 2.6
6PGlcoA	83.5 ± 1.4	85.0 ± 1.5	83.9 ± 2.7
S7P	79.9 ± 1.5	82.1 ± 2.9	84.4 ± 2.3
F16P2	86.9 ± 1.7	85.7 ± 2.3	85.2 ± 1.1
PEP	86.3 ± 1.6	75.9 ± 2.2	86.8 ± 1.6
PRPP	82.6 ± 1.9	82.5 ± 1.6	85.5 ± 1.0

The concentrations of QC_{low}, QC_{mid}, and QC_{high} were 25 ng/mL, 250 ng/mL, and 500 ng/mL respectively.

Table S6 | Matrix effect (ME) of SPx and extended metabolites with internal standard correction (Hela cells as matrix, n = 5).

ME, %	QC_{low}	QC_{mid}	QC_{high}
G6P	98.7 ± 1.2	94.2 ± 3.5	97.5 ± 1.4
G1P	97.1 ± 2.2	97.3 ± 2.4	98.0 ± 3.7
Gal1P	97.1 ± 1.8	95.2 ± 3.3	98.2 ± 2.1
Gal6P	95.4 ± 2.1	94.3 ± 2.7	102.4 ± 2.6
M1P + M6P	98.9 ± 1.4	97.5 ± 3.3	98.3 ± 3.3
F6P	98.4 ± 1.2	99.6 ± 3.1	108.2 ± 3.2
Ru1P	97.7 ± 1.1	96.5 ± 2.8	96.8 ± 1.9
Ri5P	98.4 ± 2.3	95.4 ± 2.2	97.3 ± 2.8
X5P	95.4 ± 1.6	93.2 ± 3.1	96.6 ± 2.5
Ru5P	93.3 ± 2.2	94.0 ± 2.9	95.1 ± 2.3
GA3P	96.3 ± 2.9	98.2 ± 3.1	96.0 ± 1.8
DHAP	95.7 ± 2.4	97.5 ± 2.2	99.1 ± 1.7
2PG	97.1 ± 2.5	96.2 ± 3.1	95.4 ± 1.8
3PG	95.4 ± 1.7	97.2 ± 2.4	99.7 ± 2.3
2,3BPG	94.3 ± 1.8	96.1 ± 2.8	99.3 ± 2.5
Pyr	97.3 ± 2.3	95.6 ± 1.8	96.2 ± 3.4
Lac	96.2 ± 2.2	98.5 ± 2.1	94.3 ± 2.5
E4P	98.4 ± 2.7	96.7 ± 3.2	99.3 ± 2.8
6PGlcoA	103.1 ± 1.8	95.4 ± 1.8	102.5 ± 3.2
S7P	94.4 ± 1.4	103.1 ± 2.6	97.6 ± 3.1
F16P2	96.6 ± 1.1	95.4 ± 2.1	94.1 ± 1.7
PEP	102.4 ± 1.2	95.7 ± 2.5	96.3 ± 2.1
PRPP	94.3 ± 1.3	101.8 ± 1.5	95.7 ± 1.8

The concentrations were the same as in Table S4.

Table S7 | Extraction recovery (ER) of SPx and extended metabolites in this method without internal standard correction (Hela cells as matrix, n = 5).

ER, %	QC_{low}	QC_{mid}	QC_{high}
G6P	70.2 ± 1.4	67.2 ± 1.2	65.6 ± 2.6
G1P	73.1 ± 2.5	66.4 ± 1.4	68.7 ± 3.6
Gal1P	71.6 ± 2.1	73.6 ± 2.5	66.3 ± 1.7
Gal6P	72.4 ± 3.3	74.5 ± 1.6	67.5 ± 2.0
M1P + M6P	65.3 ± 4.6	73.8 ± 3.5	74.8 ± 3.3
F6P	69.9 ± 1.5	66.9 ± 2.4	67.9 ± 1.5
Ru1P	66.7 ± 2.2	73.9 ± 2.9	69.9 ± 2.2
Ri5P	65.8 ± 3.1	76.9 ± 3.5	73.3 ± 2.3
Xu5P	67.5 ± 2.6	75.6 ± 1.4	72.5 ± 2.0
Ru5P	68.1 ± 1.3	67.5 ± 3.3	74.6 ± 1.4
GA3P	70.0 ± 3.4	68.8 ± 2.6	76.3 ± 1.6
DHAP	72.7 ± 2.5	69.5 ± 2.7	75.4 ± 1.4
2PG	69.5 ± 3.6	72.4 ± 1.5	75.6 ± 1.5
3PG	71.6 ± 2.7	68.6 ± 1.1	76.5 ± 2.3
2,3BPG	72.7 ± 2.1	77.7 ± 2.4	73.9 ± 3.2
Pyr	94.6 ± 3.3	95.5 ± 2.5	91.1 ± 1.6
Lac	95.9 ± 3.6	93.8 ± 2.6	92.0 ± 1.4
E4P	71.3 ± 2.4	70.6 ± 3.5	75.0 ± 1.7
6PGlcoA	76.3 ± 3.3	68.3 ± 1.4	73.5 ± 2.1
S7P	75.6 ± 3.7	76.9 ± 1.3	76.4 ± 2.0
F16P2	71.5 ± 2.5	73.5 ± 2.1	70.3 ± 1.1
PEP	76.1 ± 1.8	74.4 ± 2.7	72.1 ± 2.4
PRPP	68.7 ± 1.9	75.9 ± 1.5	74.7 ± 2.3

The concentrations were the same as in Table S4.

Table S8 | Extraction recovery (ER) of SPx and extended metabolites in this method with internal standard correction (Hela cells as matrix, n = 5).

ER, %	QC_{low}	QC_{mid}	QC_{high}
G6P	88.5 ± 1.1	87.7 ± 1.4	89.2 ± 2.1
G1P	89.3 ± 2.4	86.6 ± 1.9	88.4 ± 3.2
Gal1P	87.4 ± 2.3	85.4 ± 2.1	86.5 ± 1.8
Gal6P	86.6 ± 3.2	88.3 ± 1.1	87.4 ± 2.1
M1P + M6P	88.1 ± 4.1	89.1 ± 3.2	89.2 ± 3.2
F6P	89.1 ± 1.7	86.5 ± 2.3	87.5 ± 1.4
Ru1P	86.4 ± 2.4	83.4 ± 2.7	89.1 ± 2.7
Ri5P	85.4 ± 3.2	86.7 ± 3.3	86.9 ± 2.5
X5P	87.7 ± 2.9	89.1 ± 1.5	86.3 ± 3.0
Ru5P	88.4 ± 1.8	87.7 ± 3.2	87.1 ± 1.3
GA3P	90.1 ± 3.1	88.3 ± 2.2	91.1 ± 1.2
DHAP	92.2 ± 2.2	89.2 ± 2.9	93.2 ± 1.7
2PG	89.1 ± 3.2	92.1 ± 1.8	90.3 ± 1.8
3PG	91.3 ± 2.8	93.2 ± 1.9	92.2 ± 2.1
2,3BPG	92.2 ± 2.9	94.3 ± 2.1	93.3 ± 3.1
Pyr	94.4 ± 3.2	95.4 ± 2.2	91.2 ± 1.8
Lac	95.4 ± 3.3	93.2 ± 2.6	92.4 ± 1.5
E4P	87.7 ± 2.1	90.3 ± 3.0	89.6 ± 1.4
6PGlcoA	90.1 ± 3.2	92.2 ± 1.9	93.1 ± 2.4
S7P	89.3 ± 3.3	86.6 ± 1.4	91.1 ± 2.3
F16P2	91.2 ± 2.1	93.4 ± 2.1	90.2 ± 1.2
PEP	86.6 ± 1.5	89.2 ± 2.4	92.2 ± 3.2
PRPP	88.5 ± 1.3	89.1 ± 1.6	94.5 ± 2.7

The concentrations were the same as in Table S4.

Table S9 | Process efficiency (PE) of SPx and extended metabolites in this method without internal standard correction (Hela cells as matrix, n = 5).

ER, %	QC_{low}	QC_{mid}	QC_{high}
G6P	56.2 ± 1.1	53.6 ± 1.6	53.3 ± 1.6
G1P	58.8 ± 1.6	58.2 ± 1.5	55.4 ± 1.5
Gal1P	57.1 ± 1.3	58.4 ± 1.4	53.5 ± 1.4
Gal6P	62.0 ± 0.7	60.7 ± 1.3	55.7 ± 1.2
M1P + M6P	57.7 ± 1.4	58.9 ± 1.6	62.0 ± 1.8
F6P	56.1 ± 2.1	53.3 ± 1.8	54.7 ± 1.6
Ru1P	60.4 ± 1.2	64.2 ± 2.2	58.5 ± 2.1
Ri5P	59.3 ± 1.5	65.8 ± 2.4	61.9 ± 1.9
Xu5P	57.6 ± 1.4	63.3 ± 0.9	59.7 ± 2.0
Ru5P	56.5 ± 1.3	57.3 ± 1.6	61.9 ± 1.4
GA3P	60.3 ± 1.2	54.2 ± 1.5	63.0 ± 1.5
DHAP	62.3 ± 1.6	55.7 ± 1.8	64.0 ± 1.4
2PG	56.9 ± 1.7	58.2 ± 2.0	62.4 ± 2.5
3PG	57.9 ± 1.6	56.2 ± 2.1	62.8 ± 0.8
2,3BPG	58.7 ± 1.5	67.3 ± 1.6	61.3 ± 1.3
Pyr	82.8 ± 1.2	77.2 ± 1.5	74.6 ± 1.6
Lac	85.7 ± 1.6	83.4 ± 1.4	79.8 ± 1.7
E4P	59.0 ± 1.9	56.7 ± 1.3	67.2 ± 1.5
6PGlcoA	63.7 ± 1.6	58.1 ± 1.1	61.7 ± 1.2
S7P	60.4 ± 1.5	63.1 ± 0.9	64.5 ± 1.3
F16P	62.1 ± 1.4	63.0 ± 1.6	59.9 ± 0.7
PEP	65.7 ± 1.6	56.5 ± 1.7	62.6 ± 1.0
PRPP	56.7 ± 1.8	62.6 ± 1.5	63.9 ± 0.9

The concentrations were the same as in Table S4.

Table S10 | Process efficiency (PE) of SPx and extended metabolites in this method with internal standard correction (Hela cells as matrix, n = 5).

ER, %	QC_{low}	QC_{mid}	QC_{high}
G6P	87.5 ± 1.2	87.1 ± 1.2	90.3 ± 1.5
G1P	88.7 ± 2.1	86.4 ± 1.3	86.0 ± 1.6
Gal1P	85.1 ± 0.9	85.3 ± 0.8	85.8 ± 1.7
Gal6P	87.6 ± 3.2	86.8 ± 1.5	86.9 ± 1.4
M1P + M6P	88.4 ± 2.1	87.5 ± 1.6	91.1 ± 2.1
F6P	88.1 ± 2.2	85.9 ± 1.2	90.2 ± 2.2
Ru1P	85.8 ± 1.6	81.5 ± 1.1	89.3 ± 2.3
Ri5P	84.6 ± 1.4	88.5 ± 1.1	85.9 ± 0.9
X5P	86.5 ± 1.3	92.1 ± 2.4	85.7 ± 0.8
Ru5P	88.7 ± 1.9	87.6 ± 2.5	85.8 ± 1.4
GA3P	90.3 ± 0.8	86.9 ± 2.3	90.4 ± 1.3
DHAP	91.9 ± 2.0	88.4 ± 2.8	94.3 ± 1.2
2PG	88.1 ± 2.0	91.4 ± 0.6	88.8 ± 1.1
3PG	90.1 ± 1.8	94.3 ± 0.8	91.8 ± 2.4
2,3BPG	94.1 ± 1.5	93.9 ± 1.4	91.9 ± 1.8
Pyr	97.4 ± 1.5	95.5 ± 1.3	90.4 ± 1.5
Lac	96.4 ± 1.3	92.4 ± 1.6	90.1 ± 1.4
E4P	86.8 ± 1.2	92.2 ± 1.5	88.3 ± 1.3
6PGlcoA	89.7 ± 1.7	91.1 ± 1.7	95.1 ± 1.2
S7P	91.2 ± 2.4	85.7 ± 2.1	89.7 ± 0.9
F16P	92.2 ± 2.3	92.8 ± 2.0	88.8 ± 1.3
PEP	84.8 ± 2.2	87.7 ± 1.5	92.5 ± 1.2
PRPP	83.4 ± 1.3	81.9 ± 1.6	90.4 ± 2.2

The concentrations were the same as in Table S4.

Table S11 | Calibration values for final method conditions (r^2-value) and percent found of nominal calibrator concentration.

Calibrator concentration accuracy [%]	1 ng/mL	50 ng/mL	100 ng/mL	500 ng/mL	1 µg/mL	r2-Value matrix-matched calibration
G6P	86.4 ± 0.8	88.4 ± 2.4	101.2 ± 2.3	88.3 ± 2.2	103.2 ± 3.3	0.9916
G1P	87.9 ± 1.2	87.5 ± 2.0	100.9 ± 2.1	89.5 ± 3.2	98.3 ± 2.1	0.9893
Gal1P	85.4 ± 1.2	92.3 ± 3.2	96.7 ± 1.6	102.3 ± 1.7	104.5 ± 1.6	0.9965
Gal6P	85.1 ± 0.3	94.5 ± 1.6	99.5 ± 2.2	110.6 ± 3.4	99.3 ± 0.9	0.9945
M1P + M6P	88.6 ± 2.2	102.3 ± 2.7	107.8 ± 1.7	104.3 ± 3.5	87.9 ± 1.2	0.9967
F6P	87.3 ± 1.6	105.6 ± 2.5	110.3 ± 2.3	85.8 ± 2.5	93.3 ± 0.8	0.9926
Ru1P	89.0 ± 2.3	109.3 ± 0.9	102.4 ± 0.9	88.6 ± 0.9	92.1 ± 1.4	0.9957
Ri5P	88.2 ± 3.2	110.4 ± 0.8	105.6 ± 1.0	93.2 ± 1.2	91.5 ± 1.0	0.9975
Xu5P	86.3 ± 1.1	99.5 ± 0.7	98.5 ± 1.2	92.4 ± 0.6	102.3 ± 0.4	0.9977
Ru5P	90.5 ± 2.2	96.3 ± 2.1	97.3 ± 1.1	95.6 ± 2.2	105.6 ± 0.5	0.9969
GA3P	94.3 ± 2.1	95.3 ± 3.5	90.6 ± 0.4	98.8 ± 1.7	99.6 ± 1.3	0.9975
DHAP	91.2 ± 3.3	91.2 ± 2.1	98.2 ± 0.3	102.3 ± 2.0	104.5 ± 2.0	0.9996
2PG	86.0 ± 1.6	94.3 ± 0.8	88.6 ± 2.2	110.7 ± 2.5	96.5 ± 1.8	0.9993
3PG	85.2 ± 0.9	96.7 ± 1.3	91.4 ± 3.3	105.4 ± 1.5	94.3 ± 2.2	0.9991
2,3BPG	88.3 ± 0.8	99.2 ± 1.2	92.5 ± 2.2	108.6 ± 1.3	89.1 ± 3.1	0.9929
Pyr	90.3 ± 1.1	104.3 ± 3.2	94.6 ± 1.5	113.6 ± 0.4	103.4 ± 2.2	0.9919
Lac	91.2 ± 1.0	107.8 ± 4.0	104.3 ± 1.3	87.7 ± 0.5	105.6 ± 1.8	0.9971
E4P	87.2 ± 0.3	112.3 ± 0.6	109.8 ± 1.2	94.5 ± 1.6	112.3 ± 1.4	0.9943
6PGlcoA	85.6 ± 0.5	101.2 ± 0.9	110.3 ± 0.7	99.6 ± 2.7	87.7 ± 2.1	0.9929
S7P	88.4 ± 2.2	89.5 ± 1.1	112.5 ± 2.5	102.3 ± 0.9	103.3 ± 1.7	0.9954
F16P2	89.2 ± 3.3	93.4 ± 2.2	99.1 ± 2.6	99.2 ± 0.7	102.6 ± 0.9	0.9912
PEP	88.3 ± 2.6	95.5 ± 1.3	90.6 ± 0.9	105.4 ± 1.6	105.4 ± 2.0	0.9954
PRPP	86.5 ± 1.3	96.7 ± 1.2	87.6 ± 0.8	88.6 ± 2.1	105.4 ± 0.4	0.9988

Table S12 | Intra – day precision (as % RSD) (Hela cells as matrix, n = 5).

Precision, %	QC_{low}	QC_{mid}	QC_{high}
G6P	6.6 ± 1.2	5.5 ± 0.8	4.3 ± 0.9
G1P	6.1 ± 0.9	6.1 ± 0.5	5.1 ± 1.5
Gal1P	5.4 ± 0.8	6.4 ± 0.4	3.2 ± 0.7
Gal6P	6.2 ± 1.1	7.7 ± 1.9	4.8 ± 1.2
M1P + M6P	7.7 ± 1.3	4.6 ± 1.3	5.4 ± 0.6
F6P	8.1 ± 0.9	5.1 ± 1.7	6.1 ± 0.5
Ru1P	4.3 ± 0.7	6.9 ± 2.1	5.8 ± 1.3
Ri5P	6.8 ± 1.4	8.3 ± 1.9	6.6 ± 1.2
Xu5P	7.9 ± 1.2	3.3 ± 0.4	7.1 ± 0.9
Ru5P	8.9 ± 2.1	4.4 ± 0.3	4.3 ± 1.0
GA3P	10.1 ± 2.6	5.5 ± 0.4	3.8 ± 0.7
DHAP	9.4 ± 1.5	2.8 ± 0.2	6.6 ± 0.5
2PG	5.6 ± 0.6	3.5 ± 0.2	7.7 ± 2.1
3PG	6.1 ± 0.5	4.1 ± 0.3	8.1 ± 1.9
2,3BPG	7.7 ± 0.4	6.1 ± 1.2	5.4 ± 1.2
Pyr	4.4 ± 0.3	7.8 ± 1.4	5.5 ± 0.7
Lac	5.1 ± 0.6	6.1 ± 1.5	6.6 ± 1.1
E4P	6.6 ± 0.5	5.4 ± 0.9	4.4 ± 0.9
6PGlcoA	5.8 ± 0.4	6.6 ± 1.6	3.2 ± 0.4
S7P	4.9 ± 0.3	3.1 ± 0.7	6.5 ± 0.8
F16P2	6.6 ± 1.3	5.4 ± 0.9	7.7 ± 1.4
PEP	8.1 ± 1.7	5.4 ± 2.1	7.7 ± 0.6
PRPP	6.5 ± 1.5	5.4 ± 2.4	3.2 ± 1.2

The concentrations were the same as in Table S4.

Table S13 | Inter – day precision (as % RSD) (Hela cells as matrix, n = 5).

Precision, %	QC_{low}	QC_{mid}	QC_{high}
G6P	6.9 ± 1.2	5.6 ± 1.0	4.9 ± 0.9
G1P	7.2 ± 2.1	6.3 ± 1.1	5.7 ± 1.1
Gal1P	5.4 ± 0.9	6.2 ± 0.7	4.4 ± 1.2
Gal6P	4.5 ± 1.2	8.2 ± 1.6	5.4 ± 0.7
M1P + M6P	6.6 ± 0.7	5.5 ± 1.0	6.3 ± 1.2
F6P	8.8 ± 1.4	5.7 ± 1.2	7.4 ± 1.0
Ru1P	5.6 ± 0.6	7.7 ± 0.9	6.3 ± 0.9
Ri5P	7.7 ± 0.9	8.8 ± 1.3	6.5 ± 2.1
Xu5P	6.1 ± 1.0	4.3 ± 0.6	7.4 ± 2.4
Ru5P	5.4 ± 1.1	5.5 ± 0.4	5.3 ± 0.4
GA3P	8.8 ± 1.2	6.7 ± 0.3	4.5 ± 1.2
DHAP	9.1 ± 1.0	3.3 ± 0.3	7.3 ± 1.3
2PG	6.6 ± 2.1	4.1 ± 1.2	6.5 ± 0.9
3PG	7.1 ± 0.6	5.5 ± 1.1	7.9 ± 1.2
2,3BPG	6.8 ± 2.6	6.8 ± 0.9	6.6 ± 1.3
Pyr	4.1 ± 1.4	8.8 ± 1.2	8.2 ± 1.2
Lac	4.9 ± 1.0	7.2 ± 1.1	6.0 ± 0.7
E4P	6.1 ± 0.9	5.6 ± 1.0	5.2 ± 0.6
6PGlcoA	5.5 ± 0.5	7.3 ± 0.9	4.1 ± 1.2
S7P	5.4 ± 1.2	4.3 ± 1.2	7.8 ± 1.3
F16P2	6.1 ± 2.3	5.4 ± 1.8	7.7 ± 1.8
PEP	8.8 ± 1.3	6.1 ± 1.1	9.3 ± 1.2
PRPP	4.4 ± 1.2	2.1 ± 0.5	5.5 ± 1.7

The concentrations were the same as in Table S4.

Table S14 | Intra – day accuracy (as determined by % recovery) (Hela cells as matrix, n = 5).

Accuracy, %	QC_{low}	QC_{mid}	QC_{high}
G6P	99.3 ± 3.3	97.6 ± 5.4	93.3 ± 1.8
G1P	95.4 ± 4.1	103.3 ± 3.4	104.3 ± 4.1
Gal1P	90.3 ± 3.2	98.6 ± 4.2	95.5 ± 2.9
Gal6P	105.4 ± 4.1	102.1 ± 3.3	98.8 ± 3.4
M1P + M6P	103.2 ± 2.8	96.6 ± 2.9	92.2 ± 3.4
F6P	89.3 ± 1.9	103.3 ± 2.6	94.3 ± 2.7
Ru1P	92.2 ± 2.8	95.5 ± 3.7	101.2 ± 3.4
Ri5P	91.1± 3.4	97.7 ± 4.3	90.2 ± 3.7
Xu5P	88.4 ± 4.0	90.3 ± 3.2	88.4 ± 2.3
Ru5P	90.3 ± 2.4	98.8 ± 4.5	94.4 ± 2.8
GA3P	93.3 ± 2.8	102.2 ± 3.2	97.7 ± 1.9
DHAP	95.5 ± 3.9	100.3 ± 4.1	93.3 ± 2.3
2PG	98.8 ± 3.1	95.5 ± 5.4	92.2 ± 1.9
3PG	100.2 ± 2.7	104.3 ± 4.8	94.4 ± 1.9
2,3BPG	97.7 ± 3.2	98.8 ± 3.1	90.2 ± 2.1
Pyr	106.7 ± 4.1	102.2 ± 3.9	96.6 ± 2.3
Lac	107.7 ± 5.3	98.8 ± 3.3	94.3 ± 3.1
E4P	104.3 ± 4.9	94.4 ± 3.0	91.1 ± 2.7
6PGlcoA	98.8 ± 1.7	95.5 ± 2.8	93.3 ± 3.2
S7P	96.6 ± 3.2	98.9 ± 3.2	98.5 ± 3.3
F16P2	98.8 ± 3.4	97.7 ± 2.1	101.2 ± 4.4
PEP	103.3 ± 4.6	95.5 ± 3.3	98.1 ± 4.1
PRPP	93.3 ± 1.1	98.2 ± 1.5	95.4 ± 1.7

The concentrations were the same as in Table S4.

Table S15 | Inter – day accuracy (as determined by % recovery) (Hela cells as matrix, n = 5).

Accuracy, %	QC_{low}	QC_{mid}	QC_{high}
G6P	95.4 ± 3.3	97.7 ± 2.7	98.3 ± 2.5
G1P	96.5 ± 3.1	95.4 ± 3.2	98.1 ± 3.1
Gal1P	93.2 ± 2.8	98.3 ± 3.3	96.5 ± 3.2
Gal6P	96.7 ± 4.1	95.4 ± 1.9	98.1 ± 2.2
M1P + M6P	98.9 ± 3.2	101.1 ± 3.2	99.3 ± 2.4
F6P	101.2 ± 3.3	99.3 ± 2.9	98.2 ± 1.8
Ru1P	93.2 ± 2.8	94.4 ± 3.2	97.6 ± 2.7
Ri5P	93.1 ± 3.8	95.5 ± 2.4	96.7 ± 3.2
Xu5P	92.2 ± 2.9	93.2 ± 2.7	95.4 ± 3.1
Ru5P	90.4 ± 2.7	96.6 ± 2.9	91.2 ± 2.0
GA3P	88.8 ± 3.1	95.4 ± 3.1	96.7 ± 2.9
DHAP	91.1 ± 2.8	94.3 ± 3.2	95.9 ± 1.5
2PG	95.4 ± 3.1	97.7 ± 2.8	98.3 ± 1.2
3PG	99.2 ± 3.5	98.4 ± 2.9	96.3 ± 1.1
2,3BPG	101.1 ± 2.9	93.3 ± 2.4	96.6 ± 2.3
Pyr	104.3 ± 3.1	98.2 ± 2.5	95.3 ± 2.0
Lac	102.2 ± 2.8	98.1 ± 2.7	94.1 ± 3.1
E4P	99.7 ± 3.0	94.4 ± 2.6	95.5 ± 3.2
6PGlcoA	96.6 ± 1.8	96.6 ± 3.2	97.7 ± 2.1
S7P	98.3 ± 1.4	97.7 ± 4.1	96.6 ± 2.2
F16P2	103.3 ± 5.6	98.8 ± 4.1	93.3 ± 2.1
PEP	101.1 ± 2.5	98.3 ± 2.9	98.3 ± 2.3
PRPP	88.9 ± 2.1	93.2 ± 2.2	95.6 ± 2.7

The concentrations were the same as in Table S4.

Table S16A | Retention time repeatability of target analytes over 60 injections (over 25 hour estimated).

Inj Nr.	G1P [min]	G6P [min]	F6P [min]	Gal1P [min]	Gal6P [min]	Ru5P [min]	Xu5P [min]	Ru1P [min]	Ri5P [min]	GAP3 [min]	DHAP [min]
1	10.49	13.85	10.92	11.59	13.31	8.2	8.46	8.96	10.07	10.04	10.5
2	10.54	13.89	10.92	11.58	13.32	8.18	8.44	8.95	10.06	10.02	10.52
3	10.55	13.88	10.91	11.56	13.32	8.19	8.45	8.94	10.05	10.02	10.5
4	10.51	13.87	10.91	11.57	13.32	8.21	8.46	8.96	10.07	10.04	10.52
5	10.52	13.88	10.92	11.59	13.31	8.2	8.45	8.94	10.06	10.01	10.52
6	10.5	13.9	10.93	11.57	13.3	8.19	8.44	8.95	10.06	10.02	10.51
7	10.49	13.86	10.94	11.55	13.3	8.21	8.45	8.96	10.05	10.04	10.5
8	10.49	13.88	10.92	11.57	13.3	8.21	8.46	8.94	10.07	10.04	10.5
9	10.52	13.88	10.91	11.59	13.31	8.2	8.42	8.96	10.06	10.04	10.5
10	10.51	13.88	10.9	11.57	13.3	8.19	8.44	8.95	10.06	10.02	10.52
11	10.48	13.89	10.9	11.58	13.3	8.18	8.42	8.95	10.06	10.01	10.5
12	10.52	13.9	10.9	11.57	13.31	8.2	8.46	8.93	10.06	10.02	10.52
13	10.53	13.87	10.9	11.59	13.34	8.18	8.43	8.95	10.05	10.01	10.51
14	10.5	13.88	10.9	11.57	13.3	8.19	8.44	8.94	10.07	10.04	10.5
15	10.49	13.86	10.9	11.58	13.31	8.2	8.43	8.96	10.07	10.01	10.5
16	10.51	13.84	10.91	11.59	13.3	8.18	8.46	8.95	10.07	10.02	10.5
17	10.48	13.86	10.93	11.58	13.29	8.19	8.44	8.94	10.05	10.02	10.51
18	10.5	13.87	10.92	11.59	13.31	8.2	8.43	8.96	10.06	10.04	10.51
19	10.52	13.9	10.92	11.58	13.34	8.18	8.46	8.93	10.05	10.02	10.52
20	10.49	13.88	10.92	11.59	13.31	8.2	8.44	8.96	10.07	10.04	10.51
21	10.49	13.85	10.92	11.59	13.31	8.2	8.46	8.96	10.07	10.04	10.5
22	10.54	13.89	10.92	11.58	13.32	8.18	8.44	8.95	10.06	10.02	10.52
23	10.55	13.88	10.91	11.56	13.32	8.19	8.45	8.94	10.05	10.02	10.5
24	10.51	13.87	10.91	11.57	13.32	8.21	8.46	8.96	10.07	10.04	10.52
25	10.52	13.88	10.92	11.59	13.31	8.2	8.45	8.94	10.06	10.01	10.52
26	10.5	13.9	10.93	11.57	13.3	8.19	8.44	8.95	10.06	10.02	10.51
27	10.49	13.86	10.94	11.55	13.3	8.21	8.45	8.96	10.05	10.04	10.5
28	10.49	13.88	10.92	11.57	13.3	8.21	8.46	8.94	10.07	10.04	10.5
29	10.52	13.88	10.91	11.59	13.31	8.2	8.42	8.96	10.06	10.04	10.5
30	10.51	13.88	10.9	11.57	13.3	8.19	8.44	8.95	10.06	10.02	10.52
31	10.48	13.89	10.9	11.58	13.3	8.18	8.42	8.95	10.06	10.01	10.5
32	10.52	13.9	10.9	11.57	13.31	8.2	8.46	8.93	10.06	10.02	10.52
33	10.51	13.88	10.9	11.57	13.3	8.19	8.44	8.95	10.06	10.02	10.52
34	10.48	13.89	10.9	11.58	13.3	8.18	8.42	8.95	10.06	10.01	10.5
35	10.52	13.9	10.9	11.57	13.31	8.2	8.46	8.93	10.06	10.02	10.52
36	10.53	13.87	10.9	11.59	13.34	8.18	8.43	8.95	10.05	10.01	10.51
37	10.5	13.88	10.9	11.57	13.3	8.19	8.44	8.94	10.07	10.04	10.5
38	10.49	13.86	10.9	11.58	13.31	8.2	8.43	8.96	10.07	10.01	10.5
39	10.51	13.84	10.91	11.59	13.3	8.18	8.46	8.95	10.07	10.02	10.5
40	10.48	13.86	10.93	11.58	13.29	8.19	8.44	8.94	10.05	10.02	10.51
41	10.5	13.87	10.92	11.59	13.31	8.2	8.43	8.96	10.06	10.04	10.51
42	10.52	13.9	10.92	11.58	13.34	8.18	8.46	8.93	10.05	10.02	10.52
43	10.49	13.85	10.92	11.59	13.31	8.2	8.46	8.96	10.07	10.04	10.5
44	10.54	13.89	10.92	11.58	13.32	8.18	8.44	8.95	10.06	10.02	10.52
45	10.55	13.88	10.91	11.56	13.32	8.19	8.45	8.94	10.05	10.02	10.5
46	10.51	13.87	10.91	11.57	13.32	8.21	8.46	8.96	10.07	10.04	10.52

47	10.52	13.88	10.92	11.59	13.31	8.2	8.45	8.94	10.06	10.01	10.52
48	10.5	13.9	10.93	11.57	13.3	8.19	8.44	8.95	10.06	10.02	10.51
49	10.49	13.86	10.94	11.55	13.3	8.21	8.45	8.96	10.05	10.04	10.5
50	10.49	13.88	10.92	11.57	13.3	8.21	8.46	8.94	10.07	10.04	10.5
51	10.52	13.88	10.91	11.59	13.31	8.2	8.42	8.96	10.06	10.04	10.5
52	10.51	13.88	10.9	11.57	13.3	8.19	8.44	8.95	10.06	10.02	10.52
53	10.48	13.89	10.9	11.58	13.3	8.18	8.42	8.95	10.06	10.01	10.5
54	10.52	13.9	10.9	11.57	13.31	8.2	8.46	8.93	10.06	10.02	10.52
55	10.53	13.87	10.9	11.59	13.34	8.18	8.43	8.95	10.05	10.01	10.51
56	10.5	13.88	10.9	11.57	13.3	8.19	8.44	8.94	10.07	10.04	10.5
57	10.49	13.86	10.9	11.58	13.31	8.2	8.43	8.96	10.07	10.01	10.5
58	10.51	13.84	10.91	11.59	13.3	8.18	8.46	8.95	10.07	10.02	10.5
59	10.48	13.86	10.93	11.58	13.29	8.19	8.44	8.94	10.05	10.02	10.51
60	10.5	13.87	10.92	11.59	13.31	8.2	8.43	8.96	10.06	10.04	10.51
MEAN [min]	**10.51**	**13.88**	**10.91**	**11.58**	**13.31**	**8.19**	**8.44**	**8.95**	**10.06**	**10.03**	**10.51**
SD [min]	**0.02**	**0.02**	**0.01**	**0.01**	**0.01**	**0.01**	**0.01**	**0.01**	**0.01**	**0.01**	**0.01**
RSD [%]	**0.18**	**0.12**	**0.11**	**0.10**	**0.09**	**0.13**	**0.16**	**0.11**	**0.07**	**0.12**	**0.08**

Table S16B | Retention time repeatability of target analytes over 60 injections (over 25 hour estimated).

Inj Nr.	S7P [min]	2,3BPG [min]	Pyr [min]	Lac [min]	PEP [min]	6PGlcoA [min]	E4P [min]	PRPP [min]	F16P2 [min]	2PG [min]	3PG [min]
1	11.72	17.05	1.15	1.43	10.83	14.46	11.72	18.2	17.2	10.92	11.53
2	11.71	17.03	1.14	1.42	10.82	14.45	11.71	18.21	17.19	10.9	11.51
3	11.71	17.03	1.14	1.43	10.81	14.46	11.7	18.2	17.19	10.91	11.52
4	11.7	17.05	1.15	1.43	10.83	14.45	11.7	18.2	17.2	10.91	11.51
5	11.72	17.05	1.15	1.43	10.83	14.46	11.71	18.22	17.2	10.9	11.53
6	11.7	17.03	1.15	1.43	10.83	14.46	11.72	18.21	17.19	10.92	11.52
7	11.71	17.02	1.15	1.43	10.81	14.43	11.7	18.2	17.2	10.92	11.51
8	11.7	17.02	1.14	1.43	10.82	14.45	11.7	18.22	17.2	10.91	11.51
9	11.72	17.04	1.14	1.42	10.82	14.44	11.71	18.21	17.2	10.9	11.53
10	11.71	17.04	1.15	1.42	10.81	14.46	11.72	18.19	17.2	10.9	11.53
11	11.71	17.02	1.15	1.42	10.83	14.44	11.7	18.2	17.2	10.91	11.52
12	11.7	17.05	1.15	1.42	10.81	14.45	11.71	18.19	17.19	10.92	11.5
13	11.72	17.05	1.15	1.42	10.82	14.44	11.7	18.2	17.2	10.89	11.51
14	11.71	17.05	1.14	1.42	10.82	14.46	11.72	18.2	17.2	10.9	11.52
15	11.71	17.03	1.14	1.42	10.83	14.44	11.72	18.2	17.19	10.9	11.52
16	11.72	17.05	1.14	1.43	10.82	14.45	11.72	18.2	17.2	10.92	11.53
17	11.7	17.04	1.15	1.43	10.83	14.45	11.72	18.21	17.19	10.92	11.52
18	11.72	17.05	1.14	1.43	10.81	14.46	11.71	18.19	17.2	10.89	11.53
19	11.72	17.04	1.15	1.43	10.83	14.46	11.71	18.21	17.19	10.91	11.51
20	11.72	17.05	1.15	1.43	10.83	14.46	11.72	18.2	17.19	10.92	11.53
21	11.72	17.05	1.15	1.43	10.83	14.46	11.72	18.2	17.2	10.92	11.53
22	11.71	17.03	1.14	1.42	10.82	14.45	11.71	18.21	17.19	10.9	11.51
23	11.71	17.03	1.14	1.43	10.81	14.46	11.7	18.2	17.19	10.91	11.52
24	11.7	17.05	1.15	1.43	10.83	14.45	11.7	18.2	17.2	10.91	11.51
25	11.72	17.05	1.15	1.43	10.83	14.46	11.71	18.22	17.2	10.9	11.53
26	11.7	17.03	1.15	1.43	10.83	14.46	11.72	18.21	17.19	10.92	11.52
27	11.71	17.02	1.15	1.43	10.81	14.43	11.7	18.2	17.2	10.92	11.51
28	11.7	17.02	1.14	1.43	10.82	14.45	11.7	18.22	17.2	10.91	11.51
29	11.72	17.04	1.14	1.42	10.82	14.44	11.71	18.21	17.2	10.9	11.53
30	11.71	17.04	1.15	1.42	10.81	14.46	11.72	18.19	17.2	10.9	11.53
31	11.71	17.02	1.15	1.42	10.83	14.44	11.7	18.2	17.2	10.91	11.52
32	11.7	17.05	1.15	1.42	10.81	14.45	11.71	18.19	17.19	10.92	11.5
33	11.71	17.04	1.15	1.42	10.81	14.46	11.72	18.19	17.2	10.9	11.53
34	11.71	17.02	1.15	1.42	10.83	14.44	11.7	18.2	17.2	10.91	11.52
35	11.7	17.05	1.15	1.42	10.81	14.45	11.71	18.19	17.19	10.92	11.5
36	11.72	17.05	1.15	1.42	10.82	14.44	11.7	18.2	17.2	10.89	11.51
37	11.71	17.05	1.14	1.42	10.82	14.46	11.72	18.2	17.2	10.9	11.52
38	11.71	17.03	1.14	1.42	10.83	14.44	11.72	18.2	17.19	10.9	11.52
39	11.72	17.05	1.14	1.43	10.82	14.45	11.72	18.2	17.2	10.92	11.53
40	11.7	17.04	1.15	1.43	10.83	14.45	11.72	18.21	17.19	10.92	11.52
41	11.72	17.05	1.14	1.43	10.81	14.46	11.71	18.19	17.2	10.89	11.53
42	11.72	17.04	1.15	1.43	10.83	14.46	11.71	18.21	17.19	10.91	11.51
43	11.72	17.05	1.15	1.43	10.83	14.46	11.72	18.2	17.2	10.92	11.53
44	11.71	17.03	1.14	1.42	10.82	14.45	11.71	18.21	17.19	10.9	11.51
45	11.71	17.03	1.14	1.43	10.81	14.46	11.7	18.2	17.19	10.91	11.52
46	11.7	17.05	1.15	1.43	10.83	14.45	11.7	18.2	17.2	10.91	11.51
47	11.72	17.05	1.15	1.43	10.83	14.46	11.71	18.22	17.2	10.9	11.53
48	11.7	17.03	1.15	1.43	10.83	14.46	11.72	18.21	17.19	10.92	11.52

49	11.71	17.02	1.15	1.43	10.81	14.43	11.7	18.2	17.2	10.92	11.51
50	11.7	17.02	1.14	1.43	10.82	14.45	11.7	18.22	17.2	10.91	11.51
51	11.72	17.04	1.14	1.42	10.82	14.44	11.71	18.21	17.2	10.9	11.53
52	11.71	17.04	1.15	1.42	10.81	14.46	11.72	18.19	17.2	10.9	11.53
53	11.71	17.02	1.15	1.42	10.83	14.44	11.7	18.2	17.2	10.91	11.52
54	11.7	17.05	1.15	1.42	10.81	14.45	11.71	18.19	17.19	10.92	11.5
55	11.72	17.05	1.15	1.42	10.82	14.44	11.7	18.2	17.2	10.89	11.51
56	11.71	17.05	1.14	1.42	10.82	14.46	11.72	18.2	17.2	10.9	11.52
57	11.71	17.03	1.14	1.42	10.83	14.44	11.72	18.2	17.19	10.9	11.52
58	11.72	17.05	1.14	1.43	10.82	14.45	11.72	18.2	17.2	10.92	11.53
59	11.7	17.04	1.15	1.43	10.83	14.45	11.72	18.21	17.19	10.92	11.52
60	11.72	17.05	1.14	1.43	10.81	14.46	11.71	18.19	17.2	10.89	11.53
MEAN [min]	**11.71**	**17.04**	**1.15**	**1.43**	**10.82**	**14.45**	**11.71**	**18.2**	**17.2**	**10.91**	**11.52**
SD [min]	**0.01**	**0.01**	**0.01**	**0.01**	**0.01**	**0.01**	**0.01**	**0.01**	**0.01**	**0.01**	**0.01**
RSD [%]	**0.07**	**0.07**	**0.43**	**0.35**	**0.08**	**0.06**	**0.07**	**0.05**	**0.03**	**0.09**	**0.08**

Table S17 | SPx and extended metabolites in glycolysis and pentose phosphate pathways quantified in $3x10^6$ Hela Cells n = 5. Matrix-matched calibration (HeLa cells) corrected for endogenous levels.

SPx	Concentration* [nmol/L]	Amount per cell [fmol/cell]
G6P	34.3 ± 2.3	11.4 ± 0.8
G1P	71.2 ± 3.2	23.7 ± 1.1
Gal1P	26.1 ± 1.1	8.7 ± 0.4
Gal6P	17.1 ± 0.7	5.7 ± 0.2
M1P + M6P	73.9 ± 4.5	24.6 ± 1.5
F6P	38.2 ± 3.2	12.7 ± 1.1
Ru1P	110.5 ± 6.7	36.8 ± 2.2
Ri5P	23.6 ± 1.6	7.9 ± 0.5
Xu5P	11.6 ± 0.6	3.9 ± 0.2
Ru5P	12.5 ± 1.2	4.2 ± 0.4
GA3P	14.7 ± 1.3	4.9 ± 0.4
DHAP	14.4 ± 1.6	4.8 ± 0.5
2PG	22.1 ± 0.6	7.4 ± 0.2
3PG	14.3 ± 0.4	4.8 ± 0.1
2,3BPG	10.8 ± 0.3	3.6 ± 0.1
Pyr	140.1 ± 5.6	46.7 ± 1.9
Lac	215.9 ± 8.8	71.9 ± 2.9
E4P	13.1 ± 1.0	4.4 ± 0.3
6PGlcoA	101.9 ± 3.2	34.0 ± 1.1
S7P	21.1 ± 1.4	7.0 ± 0.5
F16P2	55.7 ± 4.1	18.6 ± 1.4
PEP	15.5 ± 2.1	5.2 ± 0.7
PRPP	8.4 ± 0.2	2.8 ± 0.1

*In reconstituted sample: Dried MOAC extract reconstituted in ACN/H_2O (50/50; v/v)

Table S18 | SPx and extended metabolites in glycolysis and pentose phosphate pathways quantified in $3x10^6$ HEK293 cells n=5. Matrix-matched calibration (HEK293 cells) corrected for endogenous levels. Cell volume determined by Coulter Counting at 1570 μm^3 ± 24.7 μm^3.

SPx	Ferroptosis induced* [nmol/L]	Ferroptosis induced, per cell [fmol/cell]	Ferroptosis induced, per cell volume [pmol/μm^3]	Control* [nmol/L]	Control, per cell [fmol/cell]	Control, per cell [pmol/μm^3]
G6P	32.4 ± 0.8	10.8 ± 0.3	20.6 ± 0.7	33.2 ± 0.4	11.1 ± 0.1	21.1 ± 0.1
G1P	50.8 ± 1.2	16.9 ± 0.4	32.4 ± 0.4	52.8 ± 3.4	17.6 ± 1.1	33.6 ± 0.2
Gal1P	22.4 ± 1.0	7.5 ± 0.3	14.3 ± 0.2	20.5 ± 1.6	6.8 ± 0.5	13.1 ± 0.1
Gal6P	21.3 ± 0.9	7.1 ± 0.3	13.6 ± 0.1	20.2 ± 1.1	6.7 ± 0.4	12.9 ± 0.3
M1P + M6P	63.4 ± 3.2	21.1 ± 1.1	40.4 ± 0.3	65.5 ± 5.6	21.8 ± 1.9	41.7 ± 0.2
F6P	37.1 ± 2.6	12.4 ± 0.9	23.6 ± 0.2	32.4 ± 3.2	10.8 ± 1.1	20.6 ± 0.1
Ru1P	87.9 ± 5.4	29.3 ± 1.8	56.0 ± 0.1	85.8 ± 7.1	28.6 ± 2.4	54.6 ± 0.5
Ri5P	21.2 ± 2.6	7.1 ± 0.9	13.5 ± 0.1	17.9 ± 2.3	6.0 ± 0.8	11.4 ± 0.1
Xu5P	8.8 ± 1.4	2.9 ± 0.5	5.6 ± 0.1	9.6 ± 0.6	3.2 ± 0.2	6.1 ± 0.1
Ru5P	9.7 ± 1.3	3.2 ± 0.4	6.2 ± 0.2	9.4 ± 0.3	3.1 ± 0.1	6.0 ± 0.1
GA3P	14.3 ± 0.7	4.8 ± 0.2	9.1 ± 0.1	13.7 ± 0.2	4.6 ± 0.1	8.7 ± 0.1
DHAP	13.1 ± 0.6	4.4 ± 0.2	8.3 ± 0.2	14.1 ± 0.4	4.7 ± 0.1	9.0 ± 0.2
2PG	21.7 ± 0.5	7.2 ± 0.2	13.8 ± 0.1	10.4 ± 0.5	3.5 ± 0.1	6.6 ± 0.1
3PG	15.2 ± 0.3	5.1 ± 0.2	9.7 ± 0.1	5.8 ± 0.3	1.9 ± 0.1	3.7 ± 0.1
2,3BPG	11.4 ± 0.3	3.8 ± 0.1	7.3 ± 0.1	4.9 ± 0.2	1.6 ± 0.1	3.1 ± 0.1
Pyr	151.3 ± 7.7	50.4 ± 2.6	96.4 ± 0.3	156.1 ± 8.9	52.0 ± 3.0	99.4 ± 0.6
Lac	207.1 ± 9.4	69.0 ± 3.1	131.9 ± 0.4	214.5 ± 9.6	71.5 ± 3.2	136.6 ± 0.5
E4P	12.2 ± 1.1	4.1 ± 0.4	7.8 ± 0.5	11.6 ± 0.2	3.9 ± 0.1	7.4 ± 0.1
6PGlc	81.9 ± 3.2	27.3 ± 1.1	52.2 ± 0.3	83.8 ± 5.6	27.9 ± 1.9	53.4 ± 0.1
S7P	19.8 ± 2.1	6.6 ± 0.7	12.6 ± 0.2	18.8 ± 0.3	6.3 ± 0.1	12.0 ± 0.1
F16P2	49.5 ± 3.2	16.5 ± 1.1	31.5 ± 0.1	26.1 ± 1.2	8.7 ± 0.4	16.6 ± 0.1
PEP	17.1 ± 0.7	5.7 ± 0.2	10.9 ± 0.1	18.1 ± 1.2	6.0 ± 0.4	11.5 ± 0.1
PRPP	8.9 ± 0.2	3.0 ± 0.1	5.7 ± 0.1	8.3 ± 0.6	2.8 ± 0.2	5.3 ± 0.1

*In reconstituted sample: Dried MOAC extract reconstituted in ACN/H_2O (50/50; v/v)

Table S19 | Fold change and statistical significance in ferroptosis model ($3x10^6$ HEK293 cells). Comparison between ferroptosis (erastin) group and control.

SPx	Fold Change	Log2(FC)	p-value (corr.)
2PG	2.09	1.47	$2.8625E^{-8}$
3PG	2.78	1.18	$8.3404E^{-9}$
2,3BPG	2.27	1.06	$6.5528E^{-8}$
F16P2	2.07	1.05	$2.1071E^{-9}$

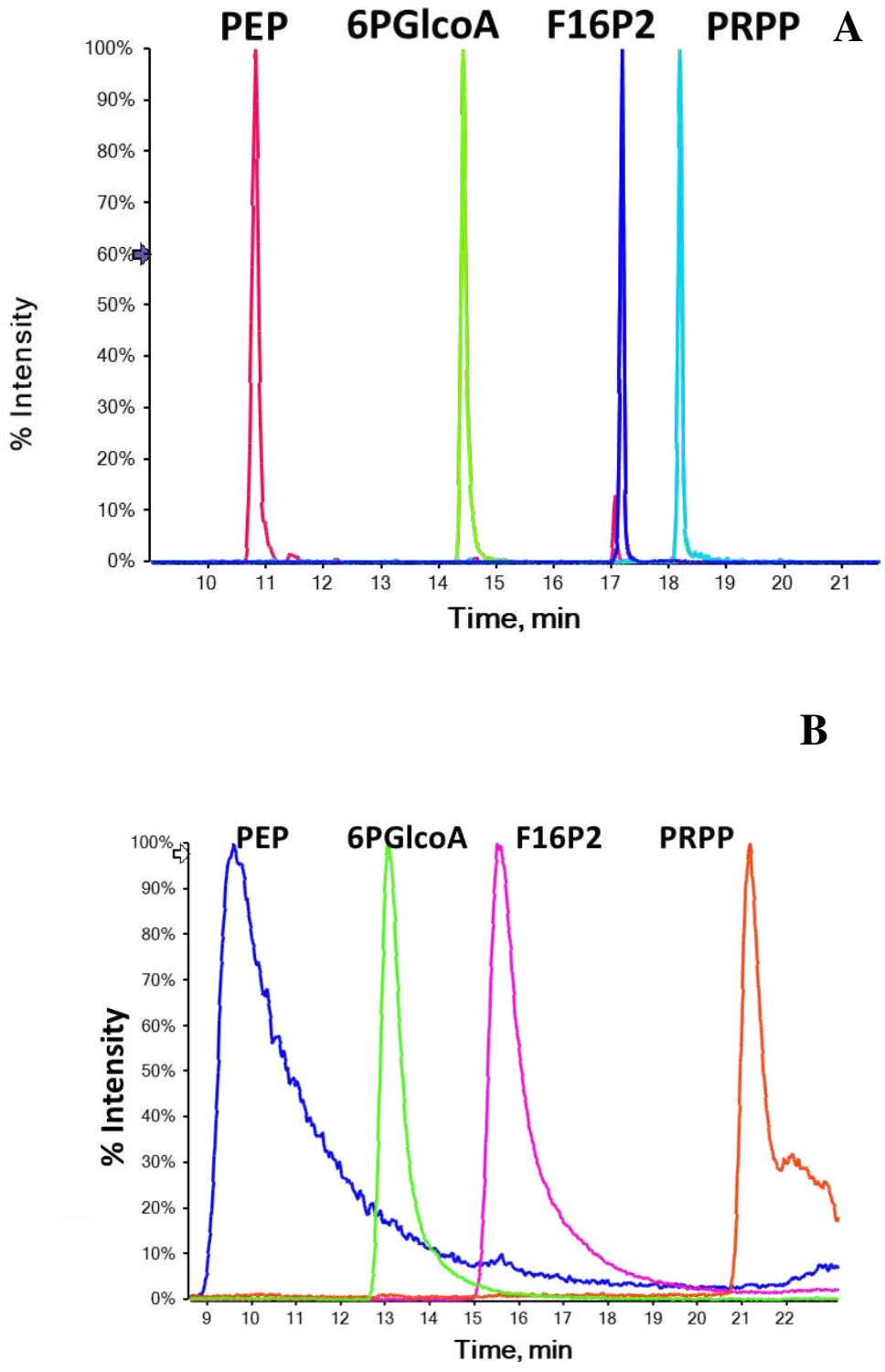

Figure S1 | Comparative chromatograms of PEP, 6PGlcoA, F16P2 and PRPP using the optimized method conditions with (A) a standard stainless steel ESI-probe and (B) a PEEKsil probe as described in the main document.

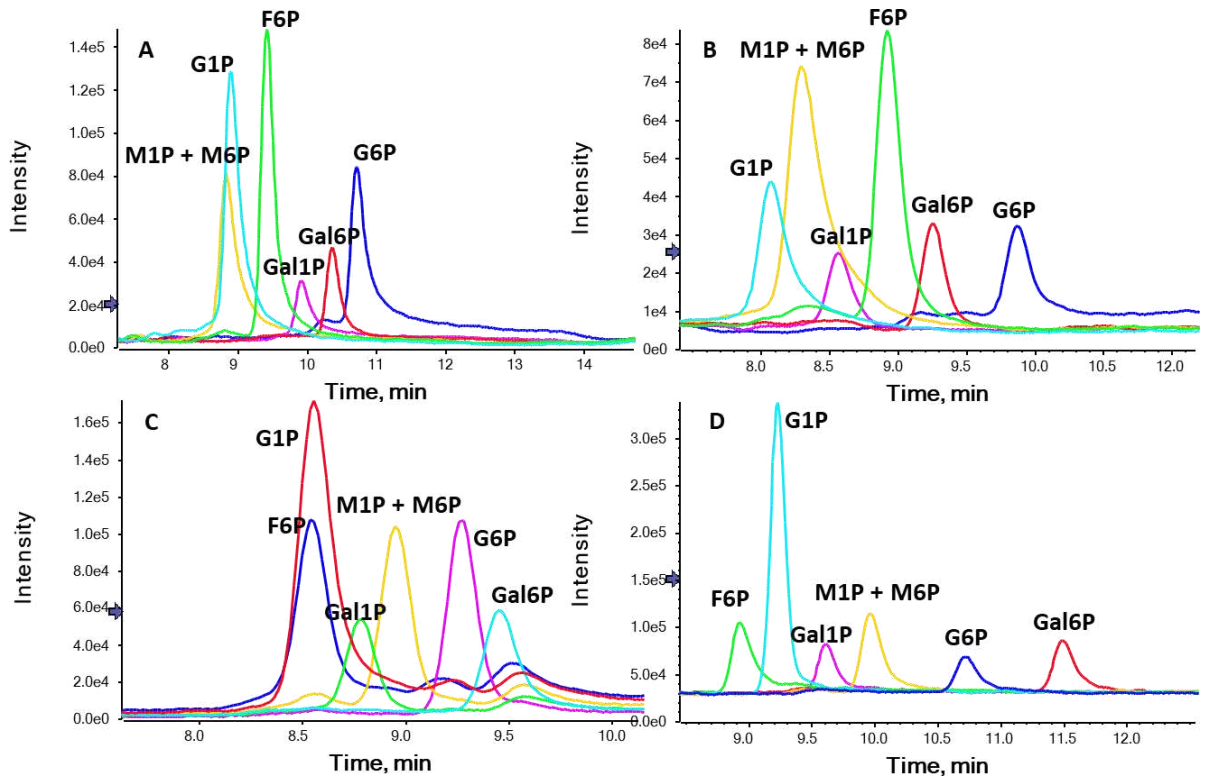

Figure S2 | Effect of buffer pH value on peak shapes of HMP analytes. A) pH adjusted to 8.0. B) 9.0. C) 10.0. D) 11.0. Buffer concentration constant for all 4 at 50 mM NH_4FA. Gradient profile as specified 0.0 min, 90% B; 12.0 min, 15% B; 20.0 min, 20% B; 20.1 min, 10% B; 25.0 min, 10% B.

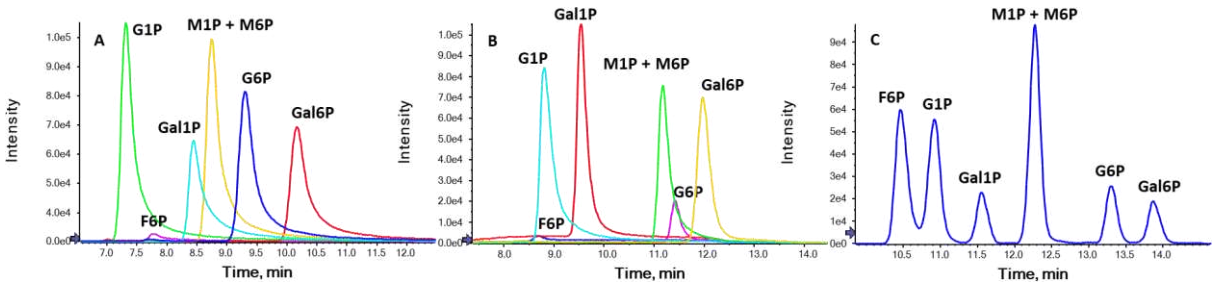

Figure S3 | Effect of buffer concentration on peak shapes of HMP analytes. pH value adjusted to 11.0. A) Buffer concentration 10 mM NH_4FA. B) 50 mM NH_4FA. C) Final method conditions 100 mM. Gradient profile as specified 0.0 min, 90% B; 12.0 min, 15% B; 20.0 min, 20% B; 20.1 min, 10% B; 25.0 min, 10% B.

Evaluation of Quenching Conditions

We conducted an additional experiment providing further insight into different quenching possibilities of our adherent cell culture. The following options were more closely evaluated – quenching with hot-air using a hot-air-blower, quenching with organic solvent i.e. -80°C methanol and acetonitrile, quenching with AMBIC buffer and quenching by our current method with ice-cold PBS and liquid nitrogen. The efficiency of each quenching protocol was put into comparison by using the energy charge (EC) values, calculated as:

$$EC = \frac{ATP+0.5ADP}{ATP+ADP+AMP} \quad \text{(S1)}$$

After quenching and extraction, the samples were analyzed for the adenylate charge molecules AMP/ADP/ATP via the discussed method. The relative distribution of AMP/ADP/ATP for each protocol is provided in **Figure S-5** together with the calculated energy charge.

The results obtained were interesting. Beginning with the assumption that all samples coming from the same cell culture have the same EC, possible differences that would be observed are to be attributed to incomplete quenching of the metabolic processes and ongoing consumption of ATP, thus resulting in increased ADP and AMP concentrations and a reduced EC. From **Figure S-5** it is evident that the maintenance of metabolites was best in the case of the protocol currently used by us in this study i.e. ice-cold PBS and liquid nitrogen, followed by the protocols utilizing MeOH, ACN and AMBIC buffer, which yielded approximately similar results and the hot-air quenching technique delivering the least satisfactory results

Further information regarding each individual quenching/harvesting protocol is as follows:

1) Ice-cold PBS and liquid nitrogen protocol (current protocol)

The culture media was removed. Cells were washed and quenched by the addition of ice-cold phosphate buffered saline to the adherent cell flask and the flask was immersed in liquid nitrogen for 1 minute. Cells were gently removed with a scraper, transferred in Falcon tubes, centrifuged at 100 g, 5 min, 4°C, the leftover supernatant removed, immersed in liquid N2 once more after centrifugation and then kept for further storage at -80°C until extraction and analysis.

2) Hot-air blower quenching

The culture media was removed. Cells were washed once with ice-cold phosphate buffered saline to the adherent cell flask. Quenching was performed with hot air for 5 s using the hot-air blower. Cell flask was then immersed in liquid nitrogen and the cells were gently removed with a scraper and transferred in Falcon tubes, centrifuged at 100 g, 5 min, 4°C and the leftover supernatant removed, the pellet then once more snap frozen in liquid nitrogen after centrifugation and then kept for further storage at -80°C until extraction and analysis.

3) Organic solvent quenching (methanol)

The culture media was removed. Cells were washed once with ice-cold phosphate buffered saline. 5 mL of quenching solution (-80°C methanol) were added and kept on the cells for 5 minutes. The quenching solution was then removed and the flask was immersed in liquid nitrogen for 1 minute and the cells were gently removed with a scraper and transferred in Falcon tubes. Centrifugation was conducted at 100g for 5min at 4°C, the leftover supernatant removed and the cell pellet once more snap frozen in liquid nitrogen and then kept for further storage at -80°C until extraction and analysis.

4) Organic solvent quenching (acetonitrile)

The culture media was removed. Cells were washed once with ice-cold phosphate buffered saline. 5 mL of quenching solution (-80°C acetonitrile) were added and kept on the cells for 5 minutes. The quenching solution was then removed and the flask was immersed in liquid nitrogen for 1 minute and the cells were gently removed with a scraper and transferred in Falcon tubes. Centrifugation was conducted at 100g for 5min at 4°C, the leftover supernatant removed and the cell pellet once more snap frozen in liquid nitrogen and then kept for further storage at -80°C until extraction and analysis.

5) AMBIC quenching (ammonium bicarbonate)

The culture media was removed. Cells were washed once with ice-cold phosphate buffered saline. 5 mL of quenching solution (-80°C 0.85% (w/v) ammonium bicarbonate pH 7.4) were added and kept on the cells for 5 minutes. The quenching solution was then removed and the flask was immersed in liquid nitrogen for 1 minute and the cells were gently removed with a scraper and transferred in Falcon tubes. Centrifugation was conducted at 100g for 5min at 4°C, the leftover supernatant removed and the cell pellet once more snap frozen in liquid nitrogen and then kept for further storage at -80°C until extraction and analysis.

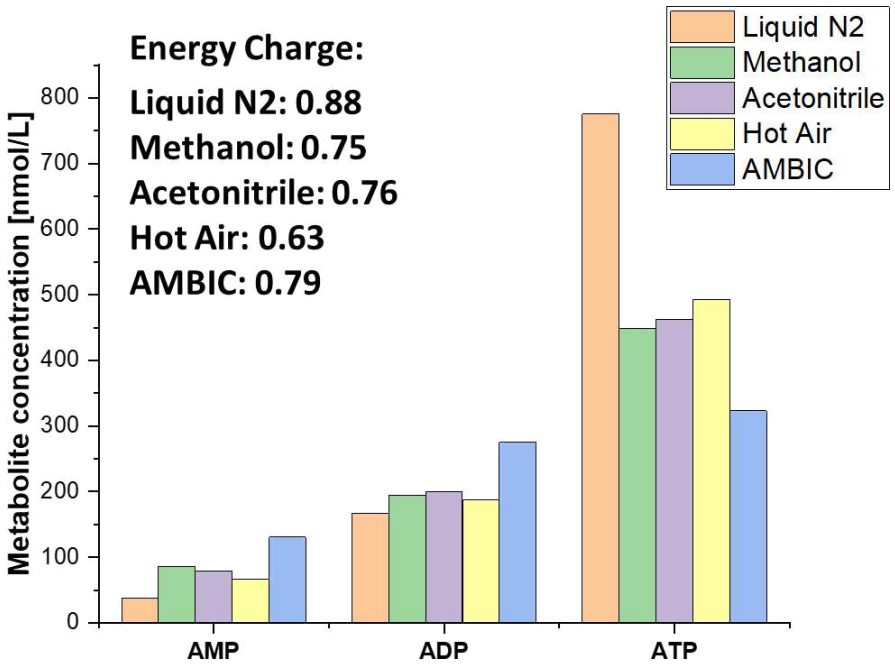

Figure S4 | Energy charge and adenylate metabolite concentrations obtained during the comparative study of metabolism quenching. Five individual protocols tested as labeled.

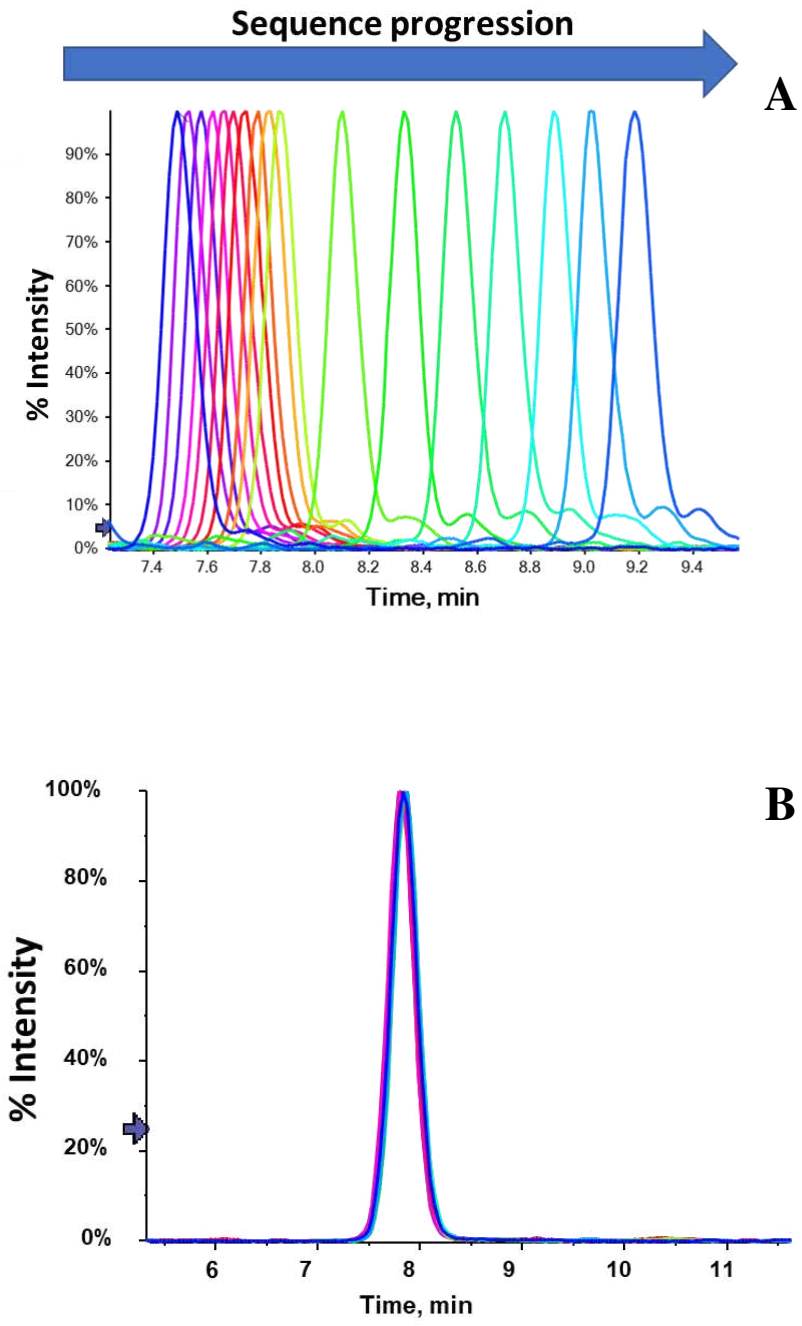

Figure S5 | A) HILIC retention time shift observed when using classic borosilicate bottles instead of PFA bottles. E4P chosen as representative example, method conditions as described in the main document. E4P detected in HeLa cell sample. Retention time towards higher t_R values observed with progressing sequence duration. B) Samples over 25 hours, E4P as example, with PFA bottles as a comparison, no t_R shift observed.

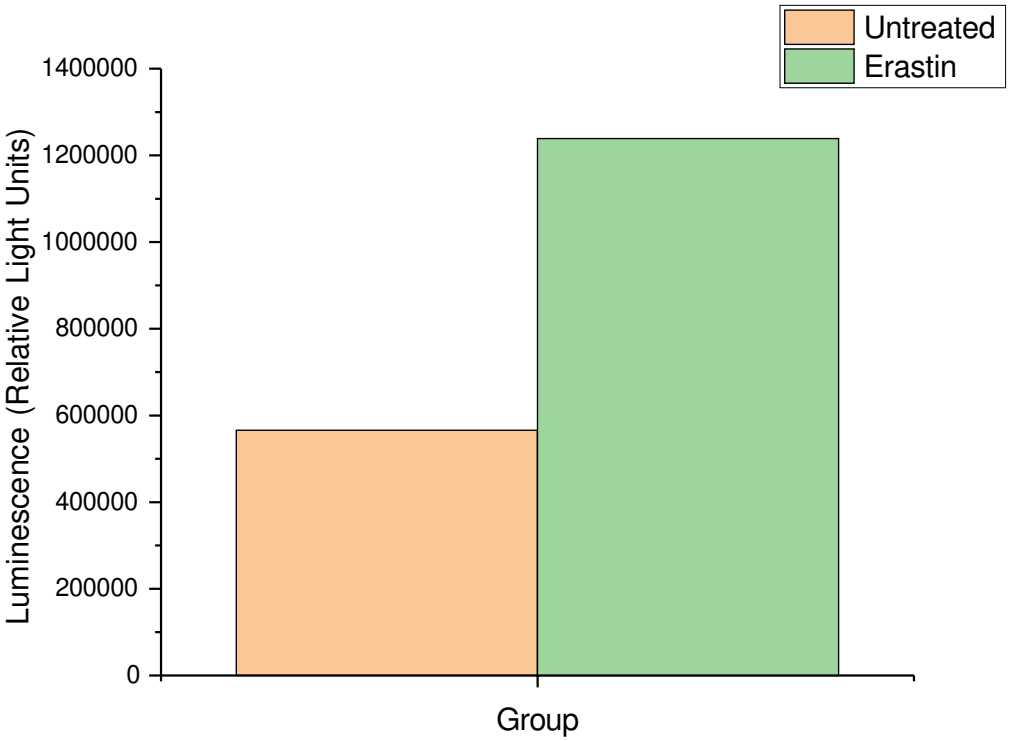

Figure S6 | Results obtained from the Glucose-Uptake-Go Assay. It determines the amount 2-deoxy-glucose that is taken up by the cells. The assay involved the addition of two buffers - the addition of the stop Buffer stops 2-deoxy-glucose transport, lyses cells, destroys any NADPH within the cells and inactivates proteins. The addition of the neutralization buffer neutralizes the solution before addition of the 2-deoxy-glucose-6-phosphate detection reagent. The glucose-6-phosphate dehydrogenase (G6PDH) within the reagent oxidizes 2-deoxy-glucose-6-phosphate (2DG6P) to 6-phosphodeoxygluconate (6PDG) and reduces $NADP^+$ to NADPH. The reductase uses the NADPH to convert the proluciferin to luciferin, which is then used by luciferase to produce light. The detection then is photometric.

List of Abbreviations

2PG	2-Phosphoglycerate
3PG	3-Phosphoglycerate
2,3BPG	2,3-Bisphosphoglycerate
6PGlcoA	6-Phosphogluconate
CE	Collision energy
CUR	Curtain gas
DHAP	Dihydroxyacetone phosphate
DP	Declustering potential
EIC	Extracted ion chromatogram
E4P	Erythrose-4-phosphate
F6P	Fructose-6-phosphate
F16P2	Fructose-1,6-bisphosphate
FDA	U.S. Food and Drug Administration
GA3P	Glyceraldehyde 3-phosphate
G1P	Glucose-1-phosphate
G6P	Glucose-6-phosphate
Gal1P	Galactose-1-phosphate
Gal6P	Galactose-6-phosphate
GS1	Nebulizer gas
GS2	Heater gas
HMP	Hexose monophosphate
IS	Internal standard
Lac	Lactate
M1P	Mannose-1-phosphate
M6P	Mannose-6-phosphate
ME	Matrix effect
PE	Process efficiency
PEP	Phosphoenol pyruvate
PMP	Pentose monophosphate
PRPP	5-Phosphoribosyl 1-pyrophosphate
Pyr	Pyruvate
RE	Recovery

Ru1P	Ribulose-1-phosphate
Ri5P	Ribose-5-phosphate
ROS	Reactive oxygen species
Ru5P	Ribulose-5-phosphate
S7P	Seduheptulose-7-phosphate
TEM	Source temperature
Xu5P	Xylulose-5-phosphate

Targeted and untargeted urinary metabolomics of alkaptonuria patients using ultra high-performance liquid chromatography-tandem mass spectrometry

Kristian Serafimov[a], Johanna Ruth Tischlarik[b,c], Michael Lämmerhofer[a]*

[a] Institute of Pharmaceutical Sciences, Pharmaceutical (Bio-)Analysis, University of Tübingen, Auf der Morgenstelle 8, 72076 Tübingen, Germany

[b] Department of Pharmacology, Experimental Therapy and Toxicology, Institute of Experimental and Clinical Pharmacology and Pharmacogenomics, and ICePhA Mouse Clinic, University of Tübingen, Wilhelmstraße 56, D-72074 Tübingen, Germany

[c] Gene Therapy for Hearing Impairment Group, Department of Otolaryngology - Head & Neck Surgery, University of Tübingen Medical Center, Elfriede-Aulhorn-Straße 5, D-72076 Tübingen, Germany

Corresponding Authors:

Prof. Michael Lämmerhofer

Email: Michael.laemmerhofer@uni-tuebingen.de; Telephone: +49 7071 29 78793; Fax: +49 7071 29 4565

Abstract

Alkaptonuria (AKU) is a rare autosomal-recessive disease which is characterized through black urine and ochronosis. It is caused by deficiency of the enzyme Homogentisate 1,2-dioxygenase in the Phenylalanine/Tyrosine degradation pathway which leads to the accumulation of Homogentisic acid (HGA). Urine was provided by AKU patients and healthy controls. Several different methods were developed in this study each with a specific goal: 1) A simple and inexpensive RP-UHPLC-UV method for routine monitoring of HGA as a key metabolite employing a Phenylhexyl stationary phase chemistry. Validation was performed in accordance to FDA guidelines and method selectivity was further evaluated via on-line high-resolution sampling 2D-LC-QToF-MS, coupling the Phenylhexyl phase in the first dimension with a C18 phase in the second dimension. 2) A targeted and accurate RP-UHPLC-MRM-QTrap assay, providing quantitative analysis of the relevant pathway metabolites based on a Phenylhexyl stationary phase, and 3) an untargeted HILIC-UHPLC-QToF-MS/MS method with SWATH acquisition employing a sulfobetaine-type HILIC-Z superficially porous particle column, with the aim of uncovering more details about the metabolic profile of this genetic disorder. Untargeted analysis allowed to annotate 204 metabolites detected in positive and negative ESI mode in total. Two separate LC methods were employed, differing in their conditions depending on the ionization mode (20 mM ammonium formate as buffer additive adjusted to a pH = 3.5 with formic acid in ESI^+ mode and 20 mM ammonium acetate adjusted to a pH = 7.5 with acetic acid in ESI^- mode). By effectively combining the aforementioned methods, a comprehensive workflow was developed, allowing the effective analysis of both patient and control urine samples.

1. Introduction

Alkaptonuria is a rare autosomal-recessive disease occurring in 1 in 100,000 – 250,000 births [**1**]. The disease is characterized through darkened urine, premature spondyloarthropathy and ochronosis. AKU is caused by deficiency of the enzyme Homogentisate 1,2-dioxygenase in the Phenylalanine/Tyrosine degradation pathway (**Figure 1**).

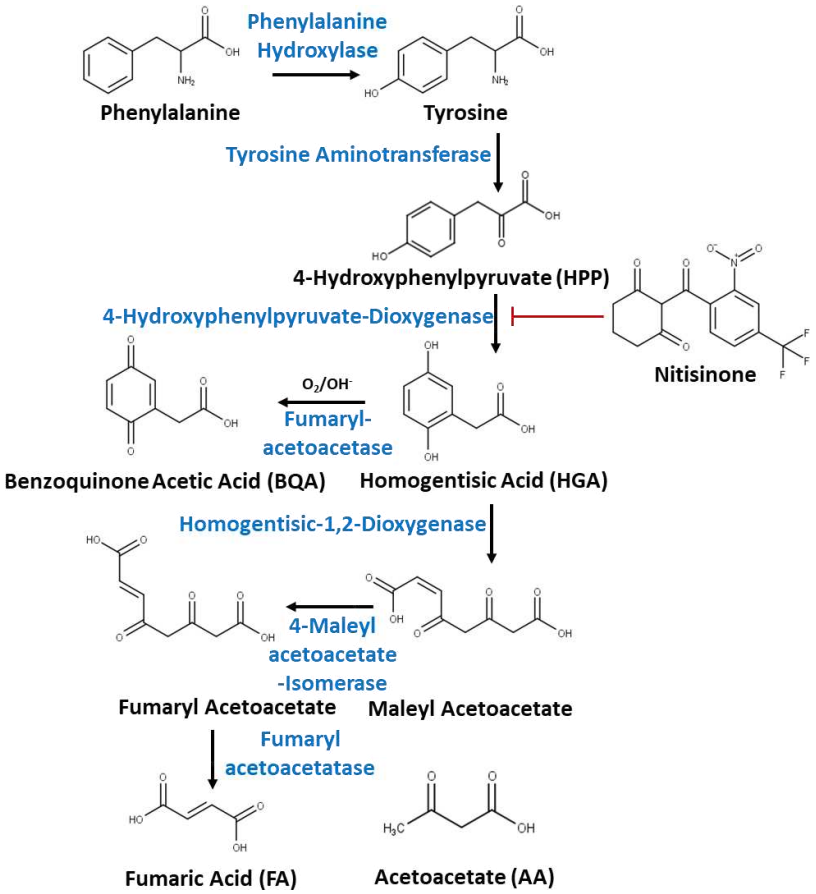

Figure 1. Phenylalanine and Tyrosine degradation pathway with regard to its defect in AKU.

Under normal physiological conditions, the enzyme converts Homogentisic acid (HGA) into Maleylacetoacetate (MAA). Instead of forming MAA, HGA accumulates. HGA gets oxidized into Benzoquinone acetic acid (BQA), which in turn easily polymerizes. The exact structure of the resultant polymer and pigment, respectively, is unknown [**2**]. The accumulated HGA and resultant polymer, respectively, is then deposited in connective tissues, leading to further complications associated with the disease's progression. Depending on where the mutation is on the deficient enzyme's structure, the severity of the disease differs [**3**]. The enzyme is predominantly expressed in the prostate, small intestine, colon, kidney, and liver, as well as in osteoarticular compartment cells (chondrocytes, synoviocytes, and osteoblasts) [**4**]. Clinical features are darkened or blackened urine after exposure to air caused by the oxidation of HGA to BQA. This is often the first symptom and can already be seen in AKU-affected children, although it is often only discovered years later at diagnosis of the disease. In clinical practice, the test for HGA in urine is the gold-standard assay for diagnosing AKU with the amount of

homogentisic acid in the 24-hour urine is detected via gas chromatography-mass spectrometry (GC-MS) analysis [**5**]. The amount of HGA excreted each day in patients with AKU is usually between 1 and 8 grams. Based on the results obtained, the diagnosis and evaluation of the disease is established on the AKU Severity Score Index (AKUSSI) [**6**]. Methods described in the literature involving LC-MS [**7**] are also available as a diagnostic tool, via the accurate quantitative analysis of HGA. Recent advances in diagnosis include the usage of dried urine paper spots for the determination of HGA with colorimetric assays, which involve the usage of dried HGA paper spots with known concentration and their color development in alkali and the following comparison with the unknown sample [**8**]. Capillary electrophoresis (CE) has been reported in the literature as a reliable method in combination with filter paper collection of urine for the determination of organic acids [**9**]. The goal of this study was i) to develop a simple and cheap method for routine monitoring of HGA levels in patients without complicated LC-MS instrumentation to assess the effect of diet and therapeutic treatments, ii) to develop an accurate targeted LC-MS/MS assay to monitor the relevant pathway metabolites for the same purpose, and iii) to identify by untargeted metabolomics other possibly relevant or interesting metabolites which are regulated significantly in AKU patients and have received less attention previously. Urine as a convenient biofluid which can be obtained by non-invasive sampling was employed for this study. It requires sample normalization as described e.g. [**10**]. Creatinine was employed herein for this purpose. UV detection and analysis of HGA has been described previously in the literature with a RP-LC C18 column in urine of AKU patients, as aromatic acids like HGA show reasonable retention on common C18 columns [**11-15**]. However, for convenient extension of the target analyte set to other metabolites of the pathway, a phenylhexyl-modified sub-2µm fully porous silica particle column was selected in this study, which is an aspect not previously discussed in other studies. While in metabolomics HILIC [**16-19**] and RPLC with C18 [**19**] and pentafluorophenyl-phases [**20-22**] are dominating the field, phenylhexyl is less commonly applied in metabolomics. In the case of the untargeted metabolomics analysis performed here, new insights can be offered into unknown metabolic alterations and therefore help to generate new hypothesis. Hence, more and more studies showed its potential for the identification and characterization of inborn errors of metabolism [**23,24**], including very few also to address specific questions in context of AKU [**25,26**]. Untargeted metabolomics was used to follow the metabolite changes in nitisinone-treated patients [**27-29**]. Untargeted LC-QTOF-MS metabolomics methodology recently was

applied for the investigation of the indolepyruvate pathway which employed a mixed-mode C18-PFP column [**30**]. New methodologies, e.g. NMR vs LC-MS/MS [**27**] or data-dependent [**27**] vs data-independent acquisition (DIA) LC-MS/MS workflows (in this work), may reveal new insights into compensatory pathways and specific metabolite patterns not in the primary focus. In view of this, we utilized here HILIC-UHPLC-ESI-QTOF-MS/MS by DIA with SWATH to establish digital maps of urinary AKU patient metabolomes vs those of healthy volunteers as controls, which has not yet been described from an analytical and experimental setpoint. In order to cover a wider range of polar metabolites, we employed in this work HILIC with a sulfobetaine HILIC-Z core-shell column, as an advancement of our targeted HILIC metabolomics platform [**31**]. It has a good chance to be complementary to above referenced RPLC assays. All samples were injected twice, ESI^+ and ESI^- modes, with adjusted conditions in terms eluent pH to optimize ionization efficiency for each mode. Data-independent acquisition (DIA) by SWATH-MS, as described in the experimental section, may also lead to new discoveries, as MS/MS are available for all precursor ions and do not depend on MS1 information, unlike in DDA which often fails to trigger MS/MS experiments for low abundant metabolites.

2. Experimental

2.1. Materials

Formic acid, acetic acid, acetonitrile and methanol of Ultra LC-MS grade were supplied by Carl Roth (Karlsruhe, Germany). Creatinine-d3, 4-hydroxyphenyl pyruvic acid, homogentisic acid, fumaric acid, acetoacetate, nitisinone, phenylalanine, tyrosine, trifluoroacetic acid and ammonia solution (25% of Suprapur quality) were purchased from Sigma-Aldrich (Merck, Taufkirchen, Germany). Deionized water was purified by a Purelab ultrapurification system (ELGA LabWater, Celle, Germany). The uniformly $U^{13}C,^{15}N$-labelled amino acid metabolomics mix used as internal standard was provided by Cambridge Isotope Laboratories (Eurisotop, Saarbrücken, Germany).

2.2. Urine sample preparation

Urine samples were collected from 10 male healthy volunteers (control group) and 4 alkaptonuria patients (3 male and 1 female as case group). Volunteers and patients were instructed to stay sober until sample donation. Second morning urine (mid-stream) was

collected. As urine represents a medium susceptible to bacterial growth, a 0.22 µm sterile filter was used to filter the samples. Argon was introduced to each sample aliquot of 1 mL and frozen at -80°C until further metabolomic analysis. For untargeted HILIC-UHPLC-QTOF-MS/MS metabolomics analysis, samples were freeze dried in a Labconco (Kansas City, MO, USA) FreeZone 4.5 L Benchtop Freeze Dry System for 24 h. Before freeze-drying, the isotope labeled internal standards were added to each sample (U-^{13}C,^{15}N-labelled amino acid mix and creatinine-d3). After freeze-drying, the samples were reconstituted in 100 µL water and 900 µL acetonitrile. Samples were then centrifuged at 4°C, 13000 rpm x 15 min to remove cell debris and unwanted precipitants. In addition, a 50 µL aliquot of each urine sample was pipetted into an Eppendorf tube to prepare a pooled quality control (QC) sample for validation of the experimental precision, repeatability and stability in the untargeted metabolomics approach.

2.3. Standard solutions

Standard stock solutions of the individual target analytes (HGA, Tyr, Phe, HPP, Acetoacetate, Fumaric Acid) (1 mg mL^{-1}) were prepared in water/methanol (50:50; v/v). Stability of the analytes in solution was evaluated and is discussed further in section **4.2** and **4.3**. Working solutions were obtained by diluting the stock solution to the appropriate concentration with deionized water and in the case of HILIC – dilution was performed with acetonitrile.

2.4. Methods

2.4.1. UHPLC-UV method for homogentisic acid analysis in urine samples

A general overview of the workflow and methods applied herein is provided in **Figure 2**.

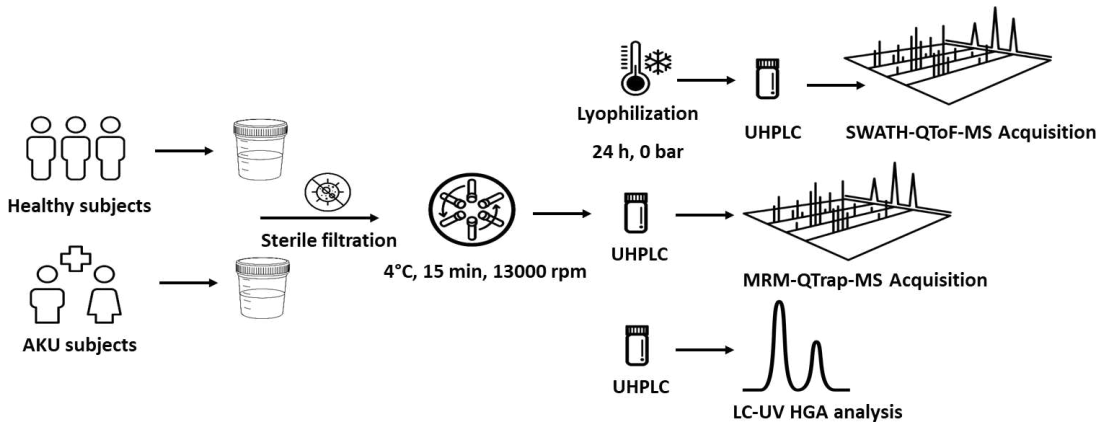

Figure 2. Schematic representation of the workflow employed in the LC analysis of urine samples.

LC-UV measurements were conducted on a 1290 Infinity series liquid chromatography system from Agilent Technologies (Waldbronn, Germany). The system consisted of a binary pump, a thermostatted column compartment (TCC), a diode array detector (DAD) and an autosampler. The system was equipped with an ultralow dispersion kit. This included a Max-Light ultralow dispersion cartridge flow cell (inner volume 0.6 µL) and an ultralow dispersion needle seat assembly. MarvelX capillaries from Idex Corporation (Lake Forest, Illinois, USA) were installed from autosampler to TCC (350 mm length x 0.075 mm inner diameter) and from TCC to DAD (250 mm x 0.075 mm). Chromatographic separation was achieved by an Acquity Premier BEH Phenyl column (150 x 2.1 mm, 1.7 µm) from Waters (Eschborn, Germany). Mobile Phase A consisted of 0.1% TFA in H_2O, whereas mobile phase B consisted of 0.1% TFA in methanol. A linear gradient was employed from 3% B at 0 min to 100% mobile phase B in 11 min, with a subsequent change to starting conditions in 0.1 min and a re-equilibration step of 4.9 min, resulting in a total analysis time of 15 min. The column compartment was held constant at 35°C during the entire chromatographic run. The flow rate was set to 0.4 mL min^{-1}. The method was largely validated in accordance to the FDA guideline for bioanalytical method validation with some modifications [**32**]. LoDs and LoQs were

determined through the external calibration function for the individual metabolites as follows:

$$LoD = \frac{3.3\,x\,\sigma}{m} \quad (1)$$

With σ being the standard error of the calibration function's slope and m the slope value itself. Analogous for the LoQ determination, the following equation was used:

$$LoQ = \frac{10\,x\,\sigma}{m} \quad (2)$$

(**Table S-1**). QC samples were used to determine within-day and between-day precision and accuracy (**Table S-1**). Freeze-thaw HGA stability was also evaluated, with a total number of 4 freeze-thaw cycles conducted, with the QC sample (100 ng mL^{-1}) being kept frozen for 12 hours between each cycle (**Table S-1**) and no carryover was observed (blank injection post highest concentration QC sample). As there is no HGA stripped matrix available, accuracy values were calculated in quality controls (pool of urine of healthy volunteers) as % recovery as follows:

$$ACC\% = \frac{c_{found} - c_0}{c_{spiked}} \quad (3)$$

With c_{spiked} is the concentration of spiked urine sample, c_0 the endogenously present amount and c_{found} the concentration of the selected metabolite found in the spiked sample. Matrix-matched calibration curves (with correction for endogenous amount present as there was no stripped matrix available) were constructed using weighted least-square linear regression (weighting factor: $1/x^2$) by spiking five different calibrant levels (100 ng mL^{-1}; 250 ng mL^{-1}; 500 ng mL^{-1}; 750 ng mL^{-1} and 1000 ng mL^{-1}) to a pooled urine sample and by plotting the peak area versus the nominal concentration of each analyte. With the final validated method, the patient samples from our cohort were analyzed for HGA and the values obtained are provided in **Table S-2**.

2.4.2. 2D-LC-QTOF-MS/MS with high-resolution sampling for peak purity testing of the homogentisic acid peak

A 1290 Infinity II 2D-LC Solution from Agilent Technologies (Waldbronn, Germany) was used for high-resolution sampling 2D-LC. The first dimension (^{1}D) LC system consisted of a binary high pressure gradient UHPLC pump (High Speed Pump, G7104A), a Multisampler (G7167B), a Multicolumn Thermostat (G7116B), a diode array detector (G7117B) with 1 µL flow cell (G4212-60008) and a pressure release kit (G4236-60010)

between UV-detector and 2D-interface. The second dimension (^{2}D) LC system was comprised of a binary high-pressure gradient UHPLC pump (High Speed Pump, G7104A, a valve drive (G1170A) with a 5 position/10 port 2D-LC active solvent modulation (ASM) valve (5067e4266) connected to two 6 position/14 port valve heads (5067e4142) carrying six 40 µL loops each and a multicolumn thermostat (G7116B). Experiments utilizing active solvent modulation (ASM) were performed with the ASM factor 5 (split ratio 1:4) restriction capillary (85×0.12 mm, 0.96 µL). For detection, the effluent from the ^{2}D column was directed to a TripleTOF 5600+ QTOF mass spectrometer from Sciex (Concord, Ontario, Canada). The acquisition rates were set to 40 Hz in the ^{1}D for the DAD, and 40 Hz for the DAD detector in the ^{2}D, respectively. The 2D-chromatographic data from the UV detectors were processed with Open Lab CDS Rev. C.01.07 SR4 from Agilent Technologies. MS data acquisition and analysis was performed with Analyst TF 1.7 and PeakView software (Sciex), respectively. Sampling time in the ^{1}D was 0.08 min for the respective peak. Individual cuts taken from the first dimension were collected in the 40 µL sample loops and stored until the ^{2}D system was ready for the analysis of the next fraction. The operation of the multiple heart cutting interface was fully automated using the high-resolution sampling functionality of the 1290 Infinity II 2D-LC Solution system. The Acquity Premier BEH Phenyl (150 x 2.1 mm, 1.7 µm) column was used in the first dimension, whereas an Agilent Eclipse Zorbax Plus C18 (50 x 3.0 mm, 1.8 µm) was employed as the second dimension column. Chromatographic conditions in the first dimension were as described in section **2.2.3.**, whereas 0.1% formic acid in H_2O and methanol, respectively, was used in the second dimension. The following gradient profile as used in the second dimension: 0 min 5% B, 0.5 min 5% B, 1.5 min 80% B, 1.8 min 80% B, 1.81 min 5% B, 2.5 min 5% B. The column compartment in the second dimension was held at 35°C and the flow rate was 1.0 mL min^{-1}. The total analysis time in the second dimension was 2.5 min. During the 2D-LC-MS experiment, the following MS instrument parameters were used: both polarities were employed in separate runs, curtain gas (CUR) 30 psi, ion source gas (nebulizing gas; GS1) 30 psi, heater gas (drying gas; GS2) 70 psi, ion spray floating voltage (ISVF) +5500 V (positive mode) and -4500 V (negative mode), source temperature (TEM) 650° C and declustering potential (DP) +/-100 V. Data acquisition was performed by information-dependent acquisition (IDA) in high sensitivity mode and the mass range of the TOF-MS full scan comprised *m/z* 70 - 1000 with an accumulation time of 250 ms and a collision energy (CE) of +/-5 V. MS/MS in IDA (top 4) was performed with +/-30 V

CE and 20 V CE spread (CES) and an accumulation time of 100 ms. Mass calibration was conducted with the Calibrant Delivery System through the APCI inlet using the positive calibration solution for the SCIEX X500 System. Further details on the 2D-LC-MS heart cutting experiment are provided in **Table S-3**.

2.4.3. Targeted analysis of the relevant alkaptonuria metabolites by UHPLC-ESI-QTrap-MS/MS

Targeted LC-MS analysis was performed using a 1290 Infinity UHPLC system from Agilent Technologies equipped with a binary pump, thermostated column compartment hyphenated to a QTRAP 4500 mass spectrometer with a TurboIonSpray source from Sciex. Metabolites from the Phenylalanine and Tyrosine catabolic pathway were analysed as targets. Chromatographic separation was achieved by an Acquity Premier BEH Phenyl column (150 x 2.1 mm, 1.7 µm) from Waters (Eschborn, Germany). Mobile phase A consisted of 0.1% FA in H_2O, whereas mobile phase B consisted of 0.1% FA in methanol. A linear gradient was employed from 3% B at 0 min to 100% mobile phase B at 15 min, back to starting conditions in 0.1 min and a re-equilibration step of 4.9 min, resulting in a total analysis time of 20 min. The column compartment was maintained at 35°C during the measurement. A flow rate of 0.4 mL min^{-1} was adjusted. Injection volume was 5 µL. The autosampler was kept at 4°C. Ion source parameters were as follows: nebulizer gas (GS1, zero grade air) 30 psi, heater gas (GS2, zero grade air) 70 psi, curtain gas (CUR, nitrogen) 30 psi, source temperature (TEM) 650 °C, ion source voltage +5500 V (positive mode) and -4500 V (negative mode). Polarity switching was employed with a settling time of 50 ms between positive and negative ion modes. Compound specific parameters were optimized individually through direct infusion MS and are reported in **Table S-4**. Due to the significant number of transitions monitored simultaneously, the Scheduled-MRM function was enabled. A window of 60 seconds was set around the designated metabolite specific retention time. Blank solvents (mobile phase A and B) were injected in the beginning of the chromatographic batch to ensure proper column and system equilibration. The method was validated largely according to the FDA guideline for bioanalytical method validation with some modifications. Quantitative results from patient samples (**Table S-**5), range, LoD, LoQ and within- and between-day precision and accuracy, matrix effects for the relevant metabolites were determined (**Table S-6**) and freeze-thaw stability evaluated (**Table S-7**). A fresh QC sample 100 ng mL^{-1} QC_{Mid})

was prepared and measured in quintuplicate (n = 5). A total number of 4 freeze-thaw cycles were conducted, with the QC sample being kept frozen for 12 hours between each cycle. A minimum of 2 MRM transitions per metabolite were monitored, in order to enable the assessment of the method's selectivity by monitoring of ion ratios. Matrix-matched calibration curves (with correction for endogenous amount present as there was no stripped matrix available) were constructed using weighted least-square linear regression (weighting factor: $1/x^2$) by spiking five different calibrant levels (10 ng mL^{-1}; 50 ng mL^{-1}; 100 ng mL^{-1}; 250 ng mL^{-1} and 500 ng mL^{-1}) to a pooled urine sample and by plotting the peak area versus the nominal concentration of each analyte. Integration and data processing were conducted with the MultiQuant 3.0 software (Sciex) via an automated algorithm employing a Gaussian smoothing (1 Point), noise percentage of 90%, baseline subtraction window of 0.1 min and a peak splitting factor of 2. Excel 2021 (Microsoft, Redmond, WA; USA) and Origin 2017 (OriginLab, Northampton, MA, USA) were used for further data processing. Matrix effects, extraction recoveries, and process efficiencies were determined in accordance to the Matuszewski protocol [**33**] **(Table S-6)**, with consideration of the endogenously present metabolite concentrations, as there was no stripped matrix available. Pre-determination of the individual metabolites was conducted via LC-MS and standard addition. The endogenous levels were considered during matrix effect and accuracy determination. Thus, signal suppression or enhancement due to matrix effect was calculated as follows:

$$ME\% = \frac{A_{spiked} - A_0}{A_{neat}} \quad (4)$$

Where A_{spiked} is the area of spiked urine sample, A_0 the peak area of the analyte endogenously present and A_{neat} being the peak area of the selected metabolite in neat solution. Similarly, individual metabolite accuracies (Acc) were calculated in matrix-matched quality controls as % recovery in accordance to equation 3 above in section **2.4.1**. External calibration functions were established by plotting the peak area ratios of the individual target metabolites and internal standard versus the concentration of the solutions. Weighted linear regression ($1/x^2$) was used to derive slopes, intercepts and correlation coefficients of the calibration curves. Matrix-matched calibration was also performed by performing a spiking experiment series of the target analytes to the biological matrix. LoDs and LoQs were determined through the external calibration function for the individual metabolites as stated in equation 1 and 2, section **2.4.1**.

2.4.4. Untargeted analysis by UHPLC-ESI-QTOF-MS/MS with SWATH Acquisition

For untargeted analysis, a 1290 Infinity UHPLC System from Agilent Technologies (Waldbronn, Germany) equipped with a binary pump, thermostated column compartment and a HTC-xt PAL (CTC Analytics AG, Zwingen, CH) autosampler was hyphenated to a TripleTOF 5600+ mass spectrometer with DuoSpray Source from Sciex (Ontario, Canada). An Agilent Poroshell 120 HILIC-Z column (150 x 2.1 mm, 2.7 µm), equipped with a guard-column, was used for the HILIC separation. Depending on the electrospray ionization mode, pH and buffer of the mobile phase were adjusted. For positive ionization mode, mobile phase A was composed of 20 mM NH_4FA in H_2O, pH = 3.5 and mobile phase B of 20 mM NH_4FA in H_2O/ACN (10/90; v/v), pH = 3.5 and a linear gradient was applied from 0% A to 30% A in 13 min. For negative ionization mode, the gradient profile remained the same, however, mobile phase conditions differed – mobile phase A (20 mM NH_4Ac in H_2O, pH = 7.5) and mobile phase B (20 mM NH_4Ac in H_2O/ACN 10/90, v/v, pH = 7.5). An isocratic hold for 2 min at 30% A at the end of the gradient was added to allow late eluting compounds to be eluted within the gradient. Re-equilibration for 10 min afterwards resulted in a total chromatographic run time of 25 min. The flow rate was set to 250 µL min^{-1} and a constant column compartment temperature of 35°C was maintained throughout the chromatographic run. A 5 µL sample volume was injected and samples were maintained at 4°C in the autosampler during the analytical sequence.

MS data acquisition was done in data-independent acquisition (DIA) mode with SWATH. Each MS-cycle consisted of a TOF-MS survey scan for precursor ion detection in the mass range of *m/z* 70-1000 and the accumulation time of the MS1-experiment was set to 100 ms. For comprehensive recording of MS/MS spectra, SWATH acquisition was utilized with a collision energy (CE) of ±30 V and a collision energy spread (CES) of ± 20 V. A total number of 25 consecutive SWATH-MS/MS experiments were created for both positive and negative ion mode covering the precursor ion range from *m/z* 70 - 1000. The variable SWATH window widths, i.e. the variable precursor ion isolation windows, were optimized for each ionization mode by swathTUNER based on corresponding IDA experiments (*vide infra*) [**34**]. The accumulation time was set to 30 ms. The total cycle time summed up to 850 ms. The MS/MS experiments were run in high sensitivity mode achieving a TOF-MS resolution of 30,000 (FWHM @ m/z 829.5393) and a SWATH-MS/MS resolution of 15,000 (FWHM @ m/z 397.2122). Ion source parameters were as

follows: nebulizer gas (GS1, zero grade air) 30 psi, heater gas (GS2, zero grade air) 70 psi, curtain gas (CUR, nitrogen) 30 psi, source temperature (TEM) 650 °C, ion source voltage +5500 V (positive mode) and -4500 V (negative mode). The data inputs for the swathTUNER were acquired from preliminary measurements of urine samples using information-dependent acquisition (IDA) and the resultant TOF-MS survey scan data in each mode. Samples were first analyzed in positive and subsequently in negative ionization mode. Blank solvents (mobile phase A and B) were measured at the beginning of each analytical sequence, followed by 10 QC samples to ensure system equilibration. Mass calibration was performed before every 5th run via the Calibrant Delivery System. The analytical system was controlled by the Analyst 1.7 TF software.

2.5. Data processing (untargeted analysis).

Data processing of untargeted analysis data was performed with MS-DIAL (version 4.7.0) [**35**]. PeakView 2.2 (Sciex), MultiQuant 3.0 (Sciex), Excel 2021 (Microsoft, Redmond, WA, USA), Origin 2021 (OriginLab, Northampton, MA, USA), and R Studio 1.4.1717 (R Foundation for Statistical Computing, Vienna, Austria). MS-DIAL was used for peak finding, blank subtraction, feature alignment, normalization, MS/MS spectral deconvolution and metabolite identification by spectral matching with library spectra (*Riken Institute*, *All Public MS/MS*) containing over 290.000 and 36.000 metabolites in positive and negative ionization mode, respectively. Authentic chemical standards were used, when available, to confirm certain putative identification results through retention time (RT), precursor mass and MS/MS spectrum match. The quality of the reported identifications is indicated in suppl. **Table S-8** and **Table S-9** as suggested by the MSI consortium [**36**]. Level one is attributed to compounds which were identified by matching of the retention time, MS and MS/MS spectra to an authentic chemical standard. Level two indicates structural annotations based on matching of MS and MS/MS spectra to those found in MS spectral libraries, thus annotating such compounds only in a putative manner. A total score of 80% was set as a criterium for initial automated metabolite annotation. Further detailed information on the experimental design and data processing with MS-DIAL is provided in **Table S-10** and **Table S-11**. For statistical analysis, the freely available online platform MetaboAnalyst **[37]** was utilized. Thus, data were normalized to the creatinine content in the samples (determined previously via LC-MS)

and then LOWESS normalized, log transformed. T-Tests (adjusted for multiple hypothesis testing using false discovery rate FDR < 0.05) were used to compare metabolites between AKU and control groups. FDR adjustment was used in all statistical significance tests. Fold change calculation was based on the normalized peak areas of each metabolite. Orthogonal projections to latent structures-discriminant analysis (OPLS-DA) models with pareto-scaling, principal component analysis (PCA) and pathway analysis were also performed using MetaboAnalyst.

3.. Results and discussion

3.1. UHPLC-UV method for HGA analysis in urine samples

For routine monitoring of Alkaptonuria patients' urine samples a straightforward LC-UV method for HGA analysis was developed. Its selectivity may benefit from additional aromatic interactions superimposed upon classical hydrophobic interactions in RPLC. Thus, MeOH was selected as organic modifier for gradient elution which does not disrupt such π-π-interactions. A chromatogram obtained of an AKU patient urine sample is shown in **Figure 3A**, with the HGA peak annotated, and a chromatogram of a healthy patient in **Figure 3B**.

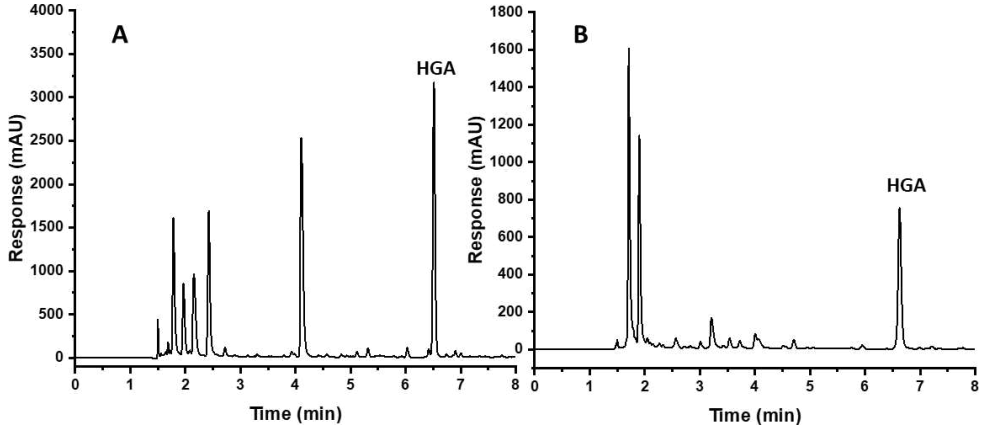

Figure 3: Chromatogram of unspiked urine representing a AKU patient (A) and a healthy patient (B) at a wavelength of 230 nm. Detection via LC-UV on an Agilent 1290 system using an Acquity Premier Phenyl-Hexyl (150 x 2.1 mm, 1.7 µm) column. Peak of HGA marked.

It can be seen that HGA gives a symmetrical narrow peak on the phenylhexyl column with given conditions and is well retained and separated from potential interferences which elute in the early part of the chromatogram. With the developed LC-UV method, the patient samples from our n=4 cohort were quantified for HGA. The results obtained are provided in **Table S-2**. The results for HGA are provided in µmol HGA per mmol Creatinine as the standard for AKU in scientific literature (values for AKU reported between 1134 – 2504 µmol/mmol creatinine according to HMDB). It is evident that the values obtained correspond with the literature values for HGA, with a lower value obtained for Patient C, due to the intake of Nitisinone.

To validate assay specificity of HGA, peak purity testing by diode array detection was supported by heart-cutting 2D-LC-UV-ESI-QToF-MS. The HGA peak from a pooled urine sample heart-cut (1 fraction total) was transferred into the second dimension, in which the fraction was separated again by complementary LC (Zorbax Eclipse Plus C18 with gradient elution by water/methanol containing 0.1% formic acid). The 2nd dimension LC comprised both UV and ESI-QToF-MS in data dependent (IDA) acquisition mode. **Figure S-1A** shows the heart-cut and **Figure S-1B** the ^{2}D UV chromatogram of the cut from the HGA peak. The cut peak corresponding to HGA did not show other peaks in the 2nd dimension chromatogram indicating absence of interferences and high peak purity in the 1st dimension, confirmed through comparison of the UV-spectra with a reference HGA standard (see **Figure S-2)**. The MS/MS-spectrum of HGA was also successfully acquired via HR-MS with no other interfering ions detected during the IDA-QToF acquisition. (**Figure S-2**). The results of the peak purity testing showed adequate assay specificity. The LC-UV method was then validated (for results see **Table S-1**). Calibration (matrix matched) was performed and the details on the HGA calibration functions (i.e. slope and intercept, r^2 coefficients and calibrator back calculations) are provided in **Table S-1**. LoD and LoQ for HGA were determined as described in section **2.4.1.** through the calibration function. Back-calculations of the concentrations of the non-zero calibrators with regard to their nominal concentrations (i.e. spiked concentrations after correction for endogenous) was always < ±15% of calibrator levels. Within-run and between runs precision and accuracy were evaluated in urine as matrix by using quality control samples in 3 different concentrations. The following spiking levels to pooled urine from healthy volunteers have been employed: QC_{Low} (50 ng mL^{-1}), QC_{Mid} (100 ng mL^{-1}), QC_{High} (500 ng mL^{-1}). These three QCs were measured in quintuplicate (n = 5) on three different days to determine the within-run and between runs

precision and accuracy, respectively. Precision results for HGA were always below 5% CV, both within-run and between runs. Within-run and between runs accuracy showed values in the range between 85 and 115% (assessed as % recovery) (see eq. 1). Freeze-thaw stability was evaluated based on QC_{Mid} (100 ng mL^{-1}), and showed results as reported in **Table S-1**. There was no change in the % recovery even after 4 freeze-thaw cycles indicating sufficient stability when no more than 4 freeze thaw cycles are applied. Carryover was also studied, with blank injections subsequently to the highest concentrated QC sample of HGA. No carryover was observed, thus confirming proper performance of the method.

3.2. Targeted analysis of AKU metabolic network by UHPLC-ESI-QTRAP-MS/MS

For investigations with a closer look into the Tyr degradation pathway related to AKU, as an extension, but requiring more advanced instrumentation, a targeted assay for accurate quantitative analysis of 7 out of the 9 metabolites of the metabolic AKU network was developed. Fumaryl and maleyl acetoacetate were not included because of lack of authentic standards. MRM transitions for the targeted UHPLC-MS/MS analysis were optimized with standards by direct infusion MS. A minimum of 2 MRM transitions (qualifier and quantifier) were monitored for the AKU metabolites, in order to allow for within-run assay specificity evaluation and verification of absence of matrix interferences by monitoring the specific qualifier-quantifier ion peak area ratios. **Table S-4** summarizes acquired precursor and product ions of the target metabolites, as well as the compound-specific, optimized MS/MS parameters, including DP, EP, CE and CXP. As described in section **2.2.2.**, polarity switching was employed: amino acids and their derivative were detected in positive ionization mode, whilst organic acids better ionized in negative ion mode. The LC method was based on the sub-2µm phenylhexyl phase which was also employed for UV. The elution conditions were slightly adapted by replacing 0.1% TFA for 0.1% formic acid as additive and slightly adjusting the gradient profile. All target analytes, organic acids and amino acids as well, were sufficiently retained on the phenylhexyl phase (see **Table S-6** for retention times) and showed good peak shapes (**Figure 4**).

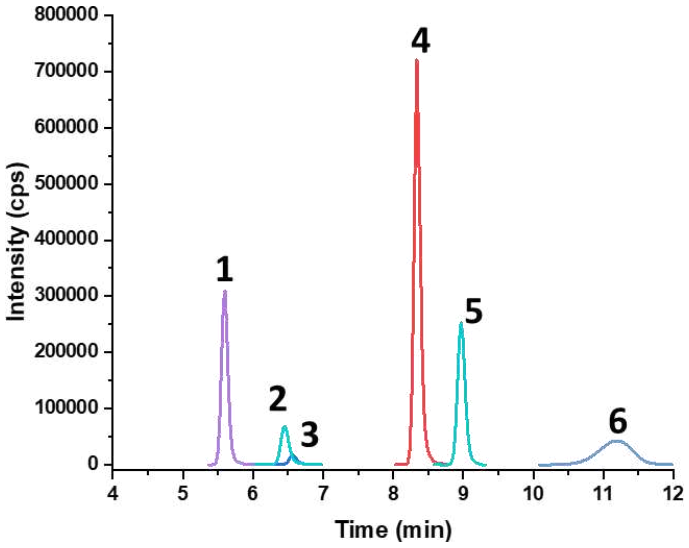

Figure 4: XICs of analytes detected in a pooled urine sample during UHPLC-QTrap-MRM acquisition. 1) Tyrosine; 2) Fumaric Acid; 3) Acetoacetate; 4) Phenylalanine; 5) HGA; 6) HPP

Matrix effects (ME), extraction recoveries (ER) and process efficiencies (PE) of each target analyte were evaluated via a QC sample (10 ng mL^{-1}). Values close to 100% represent minimum matrix effect, quantitative extraction and optimal process efficiency, respectively. MEs ranged between 88.4% (Phenylalanine) and 101.6% (Fumaric acid). ER were between 88.5% and 97.7% which is in the acceptable range. PE was determined to be between 78.8% and 99.3%. Detailed results for each individual analyte's ME, PE and RE are provided in **Table S-6**. Detailed information on each individual analyte's calibration functions (i.e. correlation coefficient, slope and intercept of the matrix matched calibration fuctions), LoD and LoQ are also provided in **Table S-6**. Within-run and between runs precision and accuracy were evaluated in urine as matrix by using quality control samples spiked at 3 different concentrations: QC_{Low} (10 ng mL^{-1}), QC_{Mid} (100 ng mL^{-1}), QC_{High} (500 ng mL^{-1}). The results are shown in **Table S-6.** These three QCs were measured in quintuplicate (n = 5) on three different days. Precision was below 5% CV for all of the analytes, both within-run and between runs. Within-run and between runs accuracies showed values in the range between 85 and 115% (assessed as % recovery) in the entire range. Freeze-thaw analyte stability was evaluated as well and all were within common acceptance limits for accuracy (±15 %). (**Table S-7**). Calibration

functions showed $r^2 \geq 0.99$ and back-calculations of the concentrations of the non-zero calibrators with regard to their nominal concentrations (i.e. spiked concentrations after correction for endogenous) was always < ±15% of calibrator levels. Based on these results, it is evident that the analytes can be considered stable if not more than 4 freeze-thaw cycles are performed. To ensure absence of any carryover, blanks were injected subsequently to a QC or a calibrant at highest concentration according to the FDA guideline. No carryover was observed and thus the acceptance criteria requested by the FDA guideline for carryover was met. Representative EICs of metabolites relevant to the AKU pathway were extracted and are shown in **Figure 4** in a pooled urine QC sample containing both healthy and AKU patient urine. With the results obtained for this method, we performed a quantification of the patient samples from our study for the key metabolites in the pathway. The results obtained are listed in **Table S-5**. It is evident that the results obtained for HGA with our LC-UV assay correspond to the obtained results with our targeted LC-MS acquisition. Patient C once more shows lower HGA values due to the administration of Nitisinone, whilst having higher HPP values, as expected, due to the conversion of HPP to HGA being blocked. The values obtained for HGA correspond to those known already in the literature, with reference ranges for HGA in urine reported between 1134 – 2504 µmol/mmol creatinine, according to HMDB.

3.3. Untargeted analysis by UHPLC-ESI-QTOF-MS/MS with SWATH Acquisition

In total, 204 metabolites were successfully annotated by the described untargeted analysis approach with MS-DIAL data processing. The detailed information on all the detected metabolites is provided in **Table S-8** (positive ion mode) and **Table S-9** (negative ion mode) in the supporting information of this study, with each table providing information on the retention time and accurate *m/z* of each individual compound. After data pre-processing as described in the experimental section, features displaying RSD-values above 15% based on QC samples were omitted. Samples were normalized by the creatinine content to account for varying dilution. Resultant data were LOWESS normalized and log-transformed prior to further statistical evaluation. Multivariate and univariate statistical analysis was performed to extract the molecular features significantly regulated. First, non-supervised PCA was conducted to analyze the global metabolic profiles in the different groups. As shown in **Figure S-3A and S-3B,** the

samples were clustered even by non-supervised statistics into two fully separated classes corresponding to the healthy volunteers and AKU patient groups in both positive and negative ionization modes. Subsequently, supervised OPLS-DA models were generated, which showed enhanced between-group separation between the AKU and control groups in score plots of both ionization modes (**Figure 5A and 5B).**

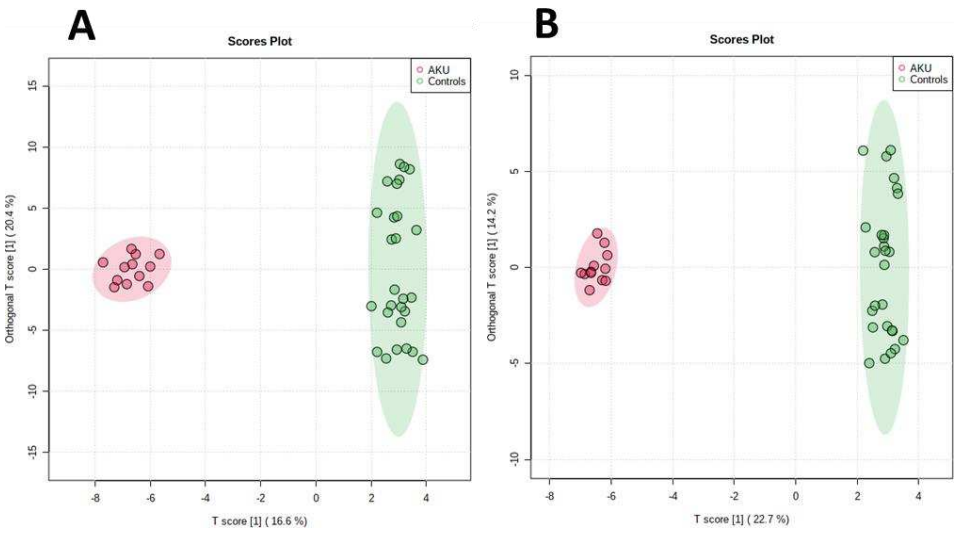

Figure 5. OPLS-DA model in positive (A) and negative (B) ionization mode obtained from patient and control sample set. The x-axis and y-axis indicate the first principal component and second principal component, respectively.

Candidate metabolites with a *p*-value (pFDR < 0.05) and fold changes > 2.0 identified by univariate statistics and Volcano plots (*p*-value adjusted FDR) were considered to be potential biomarkers (**Figure 6A and 6B;** full statistical data can be found in suppl. **Tables S-10** and **S-11**). It is evident that differences are observed between both sample groups. In the peak lists of **Table S-8** and **S-9** as well as the Volcano plots (**Figure 6A and 6B**), a number of exogenic compounds and their metabolites (e.g. caffeine, theophylline, theanine, salicylic acid, ascorbic acid) show up which are not related to AKU but to diet and drug intake (they have not been removed). Furthermore, in the Volcano plot of **Figure 6A** (positive mode), amino acids, vitamins, indole derivatives, glycine conjugates, purine and pyrimidine bases, and phenylpropanoids. Most of these metabolites are upregulated, while acylcarnitines (see also suppl. **Figure S-4**), Phe, cadaverine, choline and *N*-acetyllysine were found to be downregulated in AKU compared to healthy controls. It can be partly explained by the diet of AKU patients

which consume less meat. In the Volcano plot separately generated for the negative mode (**Figure 6B**), HGA and other metabolites of the Tyr degradation pathway, organic acids including those of the TCA cycle, phenylpropanoids, Trp and indole metabolites are significantly upregulated, glutamine, glutaric acid, and hippurate are significantly downregulated.

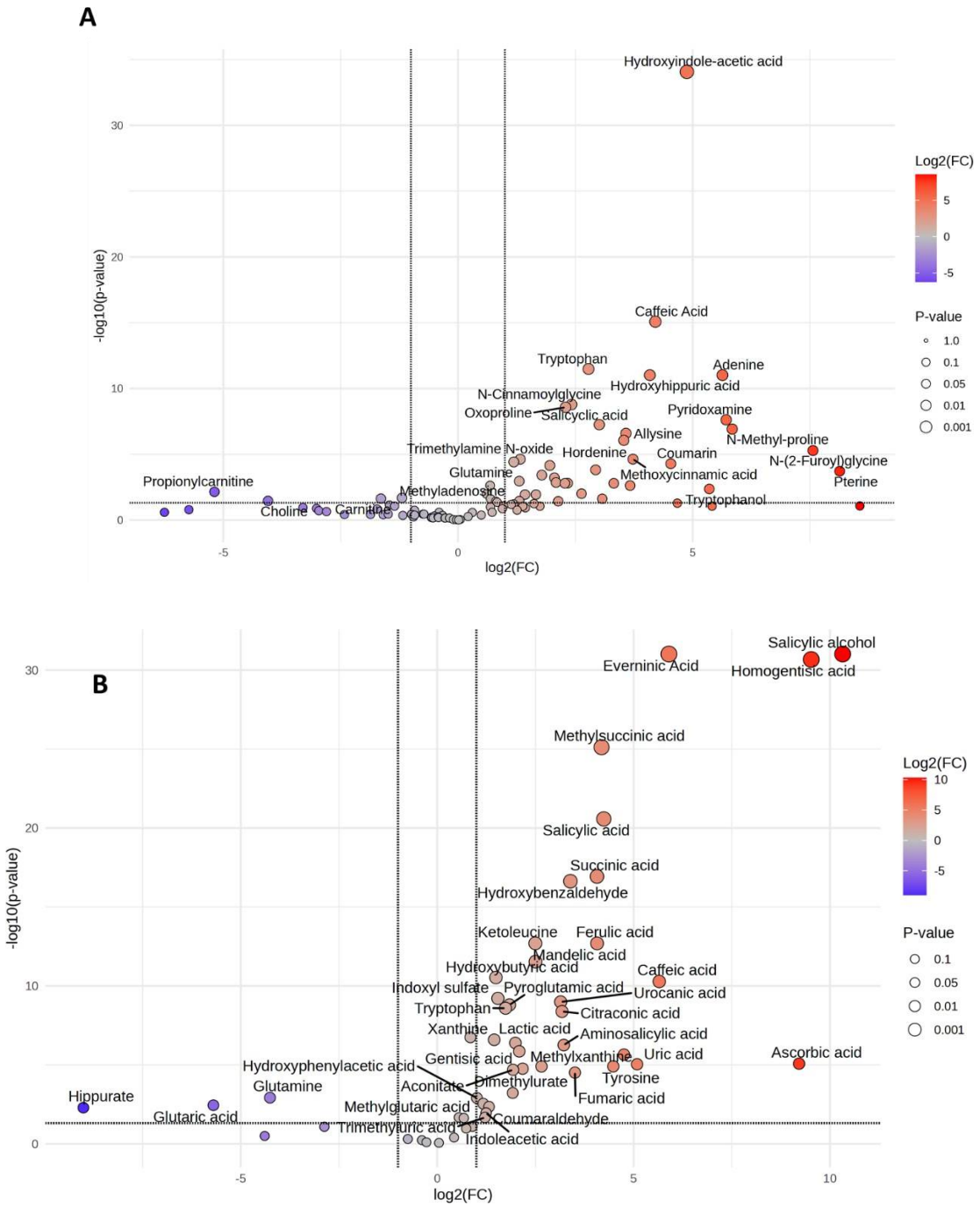

Figure 6. Volcano plots with metabolites identified in ESI^+ (A) and ESI^- (B) mode. Significantly upregulated metabolites in AKU group marked in red. P-Value (FDR adjusted) threshold 0.05. Fold Change threshold 2.0.

Pathway analysis was then conducted using MetaboAnalyst. As expected, it showed a significantly enriched pathway for the Tyrosine metabolism (as indicated by the large -log(p) value on the y-axis) and also a relatively large pathway impact from topology analysis (**Figure 7**). Besides, several other amino acid metabolism pathways with significant impact were indicated by this pathway analysis. This pathway analysis not only confirmed previously discussed Tyr, purine and TCA (citrate) cycle pathway perturbations [**26**] as well as Trp metabolism [**30**], but gave further insights in more complex metabolic alterations.

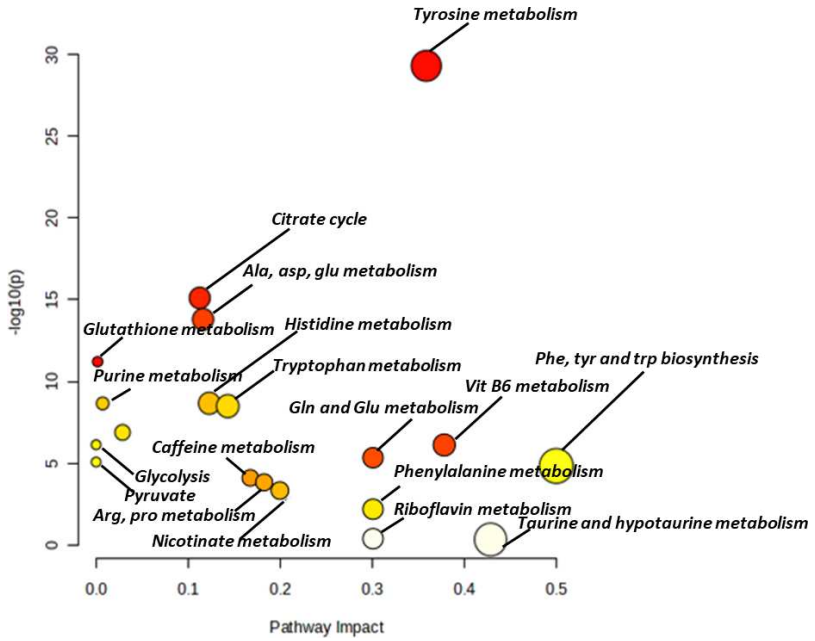

Figure 7: Pathway analysis results.

4. Conclusion

This study aimed at providing a set of methods for having a closer look into the alterations of the metabolite profiles of alkaptonuria patients. It was based on i.) a cheap straightforward reversed-phase UHPLC-UV method with sub-2µm phenylhexyl column for monitoring of the primary AKU key metabolite HGA, ii) a targeted reversed-phase UHPLC-ESI-QTrap-MS/MS method based on MRM acquisition with sub-2µm

phenylhexyl column for monitoring of the key metabolic pathway related to tyrosine degradation, and iii) an untargeted metabolomics method based on sulfobetaine-type core-shell particle-based HILIC-UHPLC-ESI-QTOF-MS/MS with data-independent SWATH acquisition for global metabolite profiling. Besides analysing the changes in the well-known key metabolites by the two targeted assays in urine of patients with alkaptonuria, the untargeted assay allowed to explore the biomarkers and metabolic pathways associated with the disease, leading to a deeper understanding of the AKU metabolic network and related pathways. The developed methods provided a broad metabolite coverage, successfully detecting over 200 metabolites stemming from various pathways. While on the one hand the detected metabolic changes of the Tyrosine metabolism where well known and in agreement with former studies, in this work also other metabolic pathways were significantly perturbed, as found by untargeted metabolomics and pathway analysis, such as Trp metabolism, Gln and Glu metabolism, His metabolism, Phe/Tyr/Trp biosynthesis, citrate cycle, vitamin B6 metabolism, Arg and Pro metabolism, and the nicotinate metabolism. The developed method provided a broad metabolite coverage, successfully detecting over 200 metabolites stemming from various pathways. Our developed diagnostic LC-UV method provides adequate run-times and sensitivities, coupled with selective analysis, thus making it a powerful tool for the clinical monitoring of this metabolic disorder. Overall, it can be considered that the proposed workflow and developed methods can be successfully utilized for both the comprehensive and specific analysis of metabolites in AKU urine patient samples.

Conflict of interest statement

The authors declared no conflicts of interest.

[1] Tharini G, Ravindran V, Hema N, Prabhavathy D, Parveen B. Alkaptonuria. Indian J Dermatol. 2011 Mar;56(2):194-6. doi: 10.4103/0019-5154.80415.

[2] Chow, Wing Ying, et al. "Pigmentation chemistry and radical-based collagen degradation in alkaptonuria and osteoarthritic cartilage." Angewandte Chemie International Edition 59.29 (2020): 11937-11942.

[3] Titus, G., Mueller, H., Burgner, J. et al. Crystal structure of human homogentisate dioxygenase. Nat Struct Mol Biol 7, 542–546 (2000)

[4] Ascher DB, Spiga O, Sekelska M, Pires DEV, Bernini A, Tiezzi M, Kralovicova J, Borovska I, Soltysova A, Olsson B, Galderisi S, Cicaloni V, Ranganath L, Santucci A, Zatkova A. Homogentisate 1,2-dioxygenase (HGD) gene variants, their analysis and genotype-phenotype correlations in the largest cohort of patients with AKU. Eur J Hum Genet. 2019 Jun;27(6):888-902. doi: 10.1038/s41431-019-0354-0.

[5] Sharabi AF, Goudar RB. Alkaptonuria. 2023 Aug 8. In: StatPearls [Internet]. Treasure Island (FL): StatPearls Publishing; 2024 Jan–.

[6] Langford B, Besford M, Hall A, Eddowes L, Timmis O, Gallagher JA, Ranganath L. Alkaptonuria Severity Score Index Revisited: Analysing the AKUSSI and Its Subcomponent Features. JIMD Rep. 2018;41:53-62. doi: 10.1007/8904_2018_98.

[7] Hughes AT, Milan AM, Christensen P, Ross G, Davison AS, Gallagher JA, Dutton JJ, Ranganath LR. Urine homogentisic acid and tyrosine: simultaneous analysis by liquid chromatography tandem mass spectrometry. J Chromatogr B Analyt Technol Biomed Life Sci. 2014 Jul 15;963:106-12. doi: 10.1016/j.jchromb.2014.06.002.

[8] Jacomelli G, Micheli V, Bernardini G, Millucci L, Santucci A. Quick Diagnosis of Alkaptonuria by Homogentisic Acid Determination in Urine Paper Spots. JIMD Rep. 2017;31:51-56. doi: 10.1007/8904_2016_554.

[9] Barbas C, García A, de Miguel L, Simó C. Evaluation of filter paper collection of urine samples for detection and measurement of organic acidurias by capillary electrophoresis. J Chromatogr B Analyt Technol Biomed Life Sci. 2002 Nov 15;780(1):73-82. doi: 10.1016/s1570-0232(02)00415-4.

[10] Gagnebin Y, Tonoli D, Lescuyer P, Ponte B, de Seigneux S, Martin PY, Schappler J, Boccard J, Rudaz S. Metabolomic analysis of urine samples by UHPLC-QTOF-MS: Impact of normalization strategies. Anal Chim Acta. 2017 Feb 22;955:27-35. doi: 10.1016/j.aca.2016.12.029.

[11] K. Contrepois, L. Jiang, M. Snyder, Optimized analytical procedures for the untargeted metabolomic profiling of human urine and plasma by combining hydrophilic interaction (HILIC) and reverse-phase liquid chromatography (RPLC)–mass spectrometry, Mol. Cell. Proteomics 14 (2015) 1684–1695, https://doi.org/10.1074/mcp.M114.046508.

[12] J. Ivanisevic, Z.-J. Zhu, L. Plate, R. Tautenhahn, S. Chen, P.J. O'Brien, C.H. Johnson, M.A. Marletta, G.J. Patti, G. Siuzdak, Toward 'omic scale metabolite profiling: a dual separation-mass spectrometry approach for coverage of lipid and central carbon metabolism, Anal. Chem. 85 (2013) 6876–6884, https://doi.org/10.1021/ac401140h.

[13] K. Spagou, I.D. Wilson, P. Masson, G. Theodoridis, N. Raikos, M. Coen, E. Holmes, J.C. Lindon, R.S. Plumb, J.K. Nicholson, E.J. Want, HILIC-UPLC-MS for exploratory urinary metabolic profiling in toxicological studies, Anal. Chem. 83 (2011) 382–390, https://doi.org/10.1021/ac102523q.

[14] J. Chen, W. Wang, S. Lv, P. Yin, X. Zhao, X. Lu, F. Zhang, G. Xu, Metabonomics study of liver cancer based on ultra performance liquid chromatography coupled to mass spectrometry with HILIC and RPLC separations, Anal. Chim. Acta 650 (2009) 3–9, https://doi.org/10.1016/j.aca.2009.03.039.

[15] J. Chen, L. Zhou, X. Zhang, X. Lu, R. Cao, C. Xu, G. Xu, Urinary hydrophilic and hydrophobic metabolic profiling based on liquid chromatography-mass spectrometry methods: differential metabolite discovery specific to ovarian cancer, ELECTROPHORESIS 33 (2012) 3361–3369, https://doi.org/10.1002/elps.201200140.

[16] Begou O, Gika HG, Wilson ID, Theodoridis G. Hyphenated MS-based targeted approaches in metabolomics. Analyst. 2017 Aug 21;142(17):3079-3100. doi: 10.1039/c7an00812k.

[17] Virgiliou C, Sampsonidis I, Gika HG, Raikos N, Theodoridis GA. Development and validation of a HILIC-MS/MS multitargeted method for metabolomics applications. Electrophoresis. 2015 Sep;36(18):2215-2225. doi: 10.1002/elps.201500208. Erratum in: Electrophoresis. 2016 Jul;37(14):2113.

[18] Virgiliou C, Gika HG, Theodoridis GA. HILIC-MS/MS Multi-Targeted Method for Metabolomics Applications. Methods Mol Biol. 2018;1738:65-81. doi: 10.1007/978-1-4939-7643-0_5.

[19] Serafimov, K., Aydin, Y., & Lämmerhofer, M. (2024). Quantitative analysis of the glutathione pathway cellular metabolites by targeted liquid chromatography-tandem mass spectrometry. Journal of separation science, 47(1), e2300780. https://doi.org/10.1002/jssc.202300780

[19] Chen S, Kong H, Lu X, Li Y, Yin P, Zeng Z, Xu G. Pseudotargeted metabolomics method and its application in serum biomarker discovery for hepatocellular carcinoma based on ultra high-performance liquid chromatography/triple quadrupole mass spectrometry. Anal Chem. 2013 Sep 3;85(17):8326-33. doi: 10.1021/ac4016787.

[20] Zanella D, Liden T, York J, Franchina FA, Focant JF, Schug KA. Exploiting targeted and untargeted approaches for the analysis of bacterial metabolites under altered growth conditions. Anal Bioanal Chem. 2021 Sep;413(21):5321-5332. doi: 10.1007/s00216-021-03505-2.

[21] Preinerstorfer B, Schiesel S, Lämmerhofer M, Lindner W. Metabolic profiling of intracellular metabolites in fermentation broths from beta-lactam antibiotics production by liquid chromatography-tandem mass spectrometry methods. J Chromatogr A. 2010 Jan 15;1217(3):312-28. doi: 10.1016/j.chroma.2009.11.051.

[22] Harrieder EM, Kretschmer F, Böcker S, Witting M. Current state-of-the-art of separation methods used in LC-MS based metabolomics and lipidomics. J Chromatogr B Analyt Technol Biomed Life Sci. 2022 Jan 1;1188:123069. doi: 10.1016/j.jchromb.2021.123069.

[23] Ismail IT, Showalter MR, Fiehn O. Inborn Errors of Metabolism in the Era of Untargeted Metabolomics and Lipidomics. Metabolites. 2019 Oct 21;9(10):242. doi: 10.3390/metabo9100242. Erratum in: Metabolites. 2020 Jan 06;10(1):E25. doi: 10.3390/metabo10010025.[24] Almontashiri NAM, Zha L, Young K, Law T, Kellogg MD, Bodamer OA, Peake RWA. Clinical Validation of Targeted and Untargeted Metabolomics Testing for Genetic Disorders: A 3 Year Comparative Study. Sci Rep. 2020 Jun 10;10(1):9382. doi: 10.1038/s41598-020-66401-2. Erratum in: Sci Rep. 2020 Jul 7;10(1):11160. doi: 10.1038/s41598-020-68532-y.

[25] Norman BP, Davison AS, Ross GA, Milan AM, Hughes AT, Sutherland H, Jarvis JC, Roberts NB, Gallagher JA, Ranganath LR. A Comprehensive LC-QTOF-MS Metabolic Phenotyping Strategy: Application to Alkaptonuria. Clin Chem. 2019 Apr;65(4):530-539. doi: 10.1373/clinchem.2018.295345.

[26] Norman BP, Davison AS, Hughes JH, Sutherland H, Wilson PJ, Berry NG, Hughes AT, Milan AM, Jarvis JC, Roberts NB, Ranganath LR, Bou-Gharios G, Gallagher JA. Metabolomic studies in the inborn error of metabolism alkaptonuria reveal new

biotransformations in tyrosine metabolism. Genes Dis. 2021 Feb 22;9(4):1129-1142. doi: 10.1016/j.gendis.2021.02.007.

[27] Davison AS, Norman BP, Ross GA, Hughes AT, Khedr M, Milan AM, Gallagher JA, Ranganath LR. Evaluation of the serum metabolome of patients with alkaptonuria before and after two years of treatment with nitisinone using LC-QTOF-MS. JIMD Rep. 2019 May 31;48(1):67-74. doi: 10.1002/jmd2.1204

[28] Grasso D, Geminiani M, Galderisi S, Iacomelli G, Peruzzi L, Marzocchi B, Santucci A, Bernini A. Untargeted NMR Metabolomics Reveals Alternative Biomarkers and Pathways in Alkaptonuria. Int J Mol Sci. 2022 Dec 13;23(24):15805. doi: 10.3390/ijms232415805.

[29] Ranganath LR, Milan AM, Hughes AT, Dutton JJ, Fitzgerald R, Briggs MC, Bygott H, Psarelli EE, Cox TF, Gallagher JA, Jarvis JC, van Kan C, Hall AK, Laan D, Olsson B, Szamosi J, Rudebeck M, Kullenberg T, Cronlund A, Svensson L, Junestrand C, Ayoob H, Timmis OG, Sireau N, Le Quan Sang KH, Genovese F, Braconi D, Santucci A, Nemethova M, Zatkova A, McCaffrey J, Christensen P, Ross G, Imrich R, Rovensky J. Suitability Of Nitisinone In Alkaptonuria 1 (SONIA 1): an international, multicentre, randomised, open-label, no-treatment controlled, parallel-group, dose-response study to investigate the effect of once daily nitisinone on 24-h urinary homogentisic acid excretion in patients with alkaptonuria after 4 weeks of treatment. Ann Rheum Dis. 2016 Feb;75(2):362-7. doi: 10.1136/annrheumdis-2014-206033.

[30] Gertsman I, Gangoiti JA, Nyhan WL, Barshop BA. Perturbations of tyrosine metabolism promote the indolepyruvate pathway via tryptophan in host and microbiome. Mol Genet Metab. 2015 Mar;114(3):431-7. doi: 10.1016/j.ymgme.2015.01.005.

[31] Serafimov K, Lämmerhofer M. Metabolic profiling workflow for cell extracts by targeted hydrophilic interaction liquid chromatography-tandem mass spectrometry. J Chromatogr A. 2022 Nov 22;1684:463556. doi: 10.1016/j.chroma.2022.463556.

[32] FDA U.S. Department of Health and Human Services, Bioanalytical Method Validation Guidance for Industry 1043, U.S. Dep. Heal. Hum. Serv.Food Drug Adm, 2018, pp. 1e41. https://www.fda.gov/files/drugs/published/Bioanalytical-Method-Validation-Guidance-for-Industry.pdf

[33] Matuszewski BK, Constanzer ML, Chavez-Eng CM. Strategies for the assessment of matrix effect in quantitative bioanalytical methods based on HPLC-MS/MS. Anal Chem. 2003 Jul 1;75(13):3019-30. doi: 10.1021/ac020361s.

[34] Zhang Y, Bilbao A, Bruderer T, Luban J, Strambio-De-Castillia C, Lisacek F, Hopfgartner G, Varesio E. The Use of Variable Q1 Isolation Windows Improves Selectivity in LC-SWATH-MS Acquisition. J Proteome Res. 2015 Oct 2;14(10):4359-71. doi: 10.1021/acs.jproteome.5b00543.

[35] Tsugawa H, Cajka T, Kind T, Ma Y, Higgins B, Ikeda K, Kanazawa M, VanderGheynst J, Fiehn O, Arita M. MS-DIAL: data-independent MS/MS deconvolution for comprehensive metabolome analysis. Nat Methods. 2015 Jun;12(6):523-6. doi: 10.1038/nmeth.3393.

[36] Sumner LW, Amberg A, Barrett D, Beale MH, Beger R, Daykin CA, Fan TW, Fiehn O, Goodacre R, Griffin JL, Hankemeier T, Hardy N, Harnly J, Higashi R, Kopka J, Lane AN, Lindon JC, Marriott P, Nicholls AW, Reily MD, Thaden JJ, Viant MR. Proposed minimum reporting standards for chemical analysis Chemical Analysis Working Group (CAWG) Metabolomics Standards Initiative (MSI). Metabolomics. 2007 Sep;3(3):211-221. doi: 10.1007/s11306-007-0082-2.

[37] Xia J, Wishart DS. Metabolomic data processing, analysis, and interpretation using MetaboAnalyst. Curr Protoc Bioinformatics. 2011 Jun;Chapter 14:Unit 14.10. doi: 10.1002/0471250953.bi1410s34.

Figure captions

Fig. 1

Phenylalanine and Tyrosine degradation pathway. In AKU, an inborn genetic deficiency of the enzyme Homogentisate 1,2-dioxygenase leads to accumulation of HGA.

Fig. 2

Schematic representation of the workflow employed in this study.

Fig. 3

LC-UV chromatogram of urine sample of an AKU patient (A) and of a healthy control (B) at a wavelength of 230 nm. Column, Acquity Premier Phenyl-Hexyl (150 x 2.1 mm, 1.7 µm). Peak of HGA annotated.

Fig. 4

EICs of analytes detected in a pooled urine sample during UHPLC-QTrap-MRM acquisition. 1) Tyrosine; 2) Fumaric Acid; 3) Acetoacetate; 4) Phenylalanine; 5) HGA; 6) HPP.

Fig. 5

OPLS-DA model in positive (A) and negative (B) ionization mode obtained from patient and control sample set. The x-axis and y-axis indicate the first principal component and second principal component, respectively.

Fig. 6

Volcano plots (AKU vs control) with metabolites identified in ESI^+ (A) and ESI^- (B) mode. Significantly upregulated metabolites in AKU group marked in red. P-Value (FDR adjusted) threshold 0.05. Fold Change threshold 2.0.

Fig. 7

Pathway analysis results.

Supplementary Material

Targeted and untargeted urinary metabolomics of alkaptonuria patients using ultra high-performance liquid chromatography-tandem mass spectrometry

Kristian Serafimov[a], Johanna Ruth Tischlarik[b], Michael Lämmerhofer[a]*

[a] Institute of Pharmaceutical Sciences, Pharmaceutical (Bio-)Analysis, University of Tübingen, Auf der Morgenstelle 8, 72076 Tübingen, Germany

[b] Department of Pharmacology, Experimental Therapy and Toxicology, Institute of Experimental and Clinical Pharmacology and Pharmacogenomics, and ICePhA Mouse Clinic, University of Tübingen, Wilhelmstraße 56, D-72074 Tübingen, Germany

[c] Gene Therapy for Hearing Impairment Group, Department of Otolaryngology - Head & Neck Surgery, University of Tübingen Medical Center, Elfriede-Aulhorn-Straße 5, D-72076 Tübingen, Germany

Corresponding Authors:

Prof. Michael Lämmerhofer

Email: Michael.laemmerhofer@uni-tuebingen.de; Telephone: +49 7071 29 78793; Fax: +49 7071 29 4565

Table S-1: Data on method validation for the determination of HGA by LC-UV.

Metabolite	t_R [min]	LOD [nmol/mL]	LOQ [nmol/mL]	ULOQ [nmol/mL]	Linearity [r]	Backcalc. [%] Cal. Lvl1/2/3/4/5**	Slope	Intercept	Precision [QC_{low}/$_{mid}$/$_{high}$]* [%]	Accuracy [QC_{low}/$_{mid}$/$_{high}$]* [%]	Freeze-Thaw Stability*** [%]
HGA	6.71	33.3	137.4	2973.5	0.9976	94.5/102.3/99.2/95.4/98.3	1.91×10^1	3.73×10^2	4.4/3.0/2.3	98.3/101.2/95.4	98.2 ± 3.3

*** QC_{low}/$_{mid}$/$_{high}$ correspond to 50/100/500 ng mL^{-1}**

Lvl1/2/3/4/5 correspond to matrix matched calibration conc. levels of 100 ng mL^{-1}; 250 ng mL^{-1}; 500 ng mL^{-1}; 750 ng mL^{-1} and 1000 ng mL^{-1}

***** Freeze-thaw-stability presented as a mean value from all 4 cycles based on QC_{mid} (100 ng mL^{-1})***

Table S-2. Patient sample quantification data on HGA obtained with the developed LC-UV method. Sample values for HGA in µmol HGA per mmol Creatinine.

Compound	HGA [µmol/mmol Creatinine]
Patient A	1804.9 ± 64.9
Patient B	2656.2 ± 30.1
Patient C	102.9 ± 13.5
Patient D	2462.7 ± 53.1

Table S-3. 2D-LC-MS experiment heart cut sampling details.

Cut #	^{1}D Cut start [min]	Sampling time [min]	Mode	^{2}D Run start [min]	Deck	^{1}D Ret. time [min]	Loop	Cut group
1	6.50	0.08	Time	4.08	A	6.53	1	0

Table S-4. MRM transitions of AKU key metabolites fo UHPLC-ESI-QTRAP-MS/MS with polarity switching. A minimum of 2 MRM transitions were measured (1 being the qualifier and 2 the quantifier transition.

Metabolite	**Q1** *m/z*	**Q3** *m/z*	**DP** **[V]**	**EP** **[V]**	**CE** **[V]**	**CXP** **[V]**
HGA_1	167.8	123.8	-60	-10	-14	-10
HGA_2	167.8	108.9	-60	-10	-32	-10
HPP	178.7	71.0	-40	-10	-12	-10
HPP_2	178.7	107.0	-40	-10	-12	-10
Fumaric Acid	115.0	71.0	-35	-10	-12	-10
Acetoacetate	101.0	57.0	-40	-10	-8	-10
Acetoacetate_2	101.0	101.0	-40	-10	-5	-10
BQA_1	165.0	121.0	-60	-10	-8	-10
BQA_2	165.0	147.0	-60	-10	-8	-10
Phenylalanine	166.0	103.0	51	10	15	10
Phenylalanine_2	166.0	120.0	51	10	11	10
Tyrosine	182.0	165.0	46	10	10	10
Tyrosine_2	182.0	136.0	46	10	21	10
Creatinine-d3	117.2	117.2	25	10	5	10
13C,15N Tyrosine_IS	192.1	98.1	46	10	10	10
13C,15N Phenylalanine_IS	176.1	98.1	51	10	15	10

Table S-5. Patient sample quantification data on HGA obtained with the developed LC-MS method. Sample values for HGA in µmol HGA per mmol Creatinine.

	Patient A	**Patient B**	**Patient C**	**Patient D**
HGA [µmol/mmol creatinine]	1652.2 ± 16.5	2721.3 ± 44.3	1365.2 ± 32.2	2346.8 ± 39.5
Tyr [µmol/mmol creatinine]	21.6 ± 2.5	23.9 ± 1.9	18.5 ± 0.9	20.6 ± 3.4
Phe [µmol/mmol creatinine]	11.5 ± 0.8	14.4 ± 1.2	12.2 ± 1.1	13.4 ± 1.2
FA [µmol/mmol creatinine]	23.1 ± 0.7	36.1 ± 2.1	9.2 ± 0.8	28.9 ± 2.2
AA [µmol/mmol creatinine]	113.6 ± 11.1	86.7 ± 9.8	47.7 ± 3.2	124.3 ± 6.7
HPP [µmol/mmol creatinine]	188.5 ± 16.7	189.1 ± 20.4	588.9 ± 39.5	192.1 ± 22.1

Table S-6: Method validation data for AKU key metabolites by UHPLC-ESI-QTrap-MS/MS with MRM-acquisition.

Metabolite	t_R [min]	LOD [pmol/mL]	LOQ [pmol/mL]	ULOQ [nmol/mL]	Linearity [r]	Backcalc. [%] Cal. Lvl1/2/3/4/5**	Slope	Intercept	Precision [$QC_{low}/_{mid}/_{high}$] [%]*	Accuracy [$QC_{low}/_{mid}/_{high}$] [%]*	ME [%]	ER [%]	PE [%]	Freeze-thaw-stability*** [%]
HGA	9.01	43.4	144.5	11.9	0.9946	89.2/93.4/90.5/104.5/100.3	6.09×10^2	1.17×10^4	6.2/4.1/5.9	98.9/102.3/91.6	93.4	91.2	85.2	98.2 ± 2.1
Tyrosine	5.58	29.3	90.5	8.3	0.9978	90.4/95.6/93.2/100.4/98.9	1.03×10^4	9.94×10^4	5.8/4.7/2.4	98.3/102.4/87.6	99.2	88.5	87.8	97.8 ± 1.2
Phenylalanine	9.28	30.9	88.4	12.1	0.9987	87.4/93.8/104.5/110.1/92.1	9.80×10^3	2.63×10^3	3.2/4.1/4.4	95.4/98.6/87.1	88.4	89.1	78.8	97.2 ± 1.6
HPP	11.23	34.4	106.6	16.6	0.9983	103.2/100.5/98.6/89.6/94.3	6.75×10^3	4.92×10^4	5.4/3.2/5.2	90.3/92.1/103.5	99.7	92.5	92.2	97.9 ± 2.3
Fumaric Acid	6.53	89.6	263.6	30.2	0.9938	105.4/100.3/98.5/88.4/93.2	1.37×10^4	3.48×10^5	6.1/4.6/4.9	91.3/95.2/97.3	101.6	97.7	99.3	98.2 ± 0.9
Acetoacetate	6.53	128.3	281.1	29.4	0.9985	96.6/102.3/105.4/97.3/96.6	1.11×10^3	3.66×10^2	5.2/3.2/5.1	89.2/90.4/101.2	97.3	95.5	92.9	98.0 ± 1.3

* **$QC_{low}/_{mid}/_{high}$ correspond to 10/100/500 *ng mL^{-1}***

Lvl1/2/3/4/5 correspond to matrix matched calibration conc. levels of 10 ng mL^{-1}; 50 ng mL^{-1}; 100 ng mL^{-1}; 250 ng mL^{-1} and 500 ng mL^{-1}

**** Freeze-thaw-stability presented as a mean value from all 4 cycles based on QC_{mid} (50 ng mL^{-1}). Individual values in Table S-5***

Table S-7. Freeze-thaw analyte stability determined by targeted LC-QTrap-MS analysis. QC sample consisted of spiked urine (100 ng mL^{-1}).

Compound	1 Cycle	2 Cycles	3 Cycles	4 Cycles
HGA	98.9 ± 5.7	98.2 ± 2.4	97.6 ± 2.5	98.1 ± 1.2
Tyrosine	99.3 ± 3.3	98.5 ± 3.5	98.3 ± 1.4	97.9 ± 2.3
Phenylalanine	99.6 ± 4.4	99.1 ± 4.7	98.4 ± 3.3	98.8 ± 1.4
HPP	99.4 ± 2.5	99.0 ± 3.6	98.6 ± 4.2	99.1 ± 4.4
Fumaric Acid	99.7 ± 6.2	99.4 ± 3.4	98.4 ± 8.2	98.7 ± 2.7
Acetoacetate	99.5 ± 5.3	98.4 ± 4.3	98.3 ± 5.9	99.3 ± 6.2

Table S-8. Metabolites identified in ESI$^+$ ionization mode.

Compound	Precursor ion [m/z]	Adduct	t_R [min]	Sum formula	Mass error [ppm]	Identification Level	logP value	HMDB ID
Ethanolamine	62.0600	$[M+H]^+$	8.34	C2H7NO	0.5	2	-1.51	HMDB0000149
Trimethylamine N-oxide	76.0756	$[M+H]^+$	2.46	C3H9NO	-2.9	2	-2.57	HMDB0000925
GABA	104.0706	$[M+H]^+$	8.5	C4H9NO2	0.9	1	-3.17	HMDB0000112
N,N-Dimethylglycine	104.0706	$[M+H]^+$	7.36	C4H9NO2	2.1	1	-1.70	HMDB0000092
Choline	105.1148	$[M+H]^+$	5.47	C5H14NO	1.1	1	-3.60	HMDB0000097
Diethanolamine	106.0862	$[M+H]^+$	6.60	C4H11NO2	1.2	2	-1.43	HMDB0004437
Cytosine	112.0505	$[M+H]^+$	6.19	C4H5N3O	2.2	1	-1.73	HMDB0004437
Histamine	112.0869	$[M+H]^+$	5.17	C5H9N3	-1.2	1	-0.70	HMDB0000870
Uracil	113.0345	$[M+H]^+$	2.49	C4H4N2O2	-1	1	-1.07	HMDB0000300
Creatinine	114.0661	$[M+H]^+$	4.67	C4H7N3O	-2.1	1	-1.76	HMDB0000562
Proline	116.0706	$[M+H]^+$	2.86	C5H9NO2	1.4	1	-2.70	HMDB0251528
Glycocyamine	118.0611	$[M+H]^+$	10.66	C3H7N3O2	-0.9	2	-3.10	HMDB0000128
Valine	118.0862	$[M+H]^+$	7.34	C5H11NO2	-2.6	1	-2.26	HMDB0000883
Threonine	120.0655	$[M+H]^+$	4.14	C4H9NO3	0	1	-2.94	HMDB0000167
Phenylacetaldehyde	121.0647	$[M+H]^+$	5.64	C8H8O	-2.7	2	1.78	HMDB0006236
Nicotinamide	123.0552	$[M+H]^+$	2.21	C6H6N2O	2	1	-0.37	HMDB0001406
Taurine	126.0219	$[M+H]^+$	8.49	C2H7NO3S	1.2	1	-2.60	HMDB0000251
5-Methylcytosine	126.0661	$[M+H]^+$	6.72	C5H7N3O	0.6	1	-0.63	HMDB0002894
Oxoproline	130.0498	$[M+H]^+$	6.42	C5H7NO3	1.8	2	-1.30	HMDB0304793
Pipecolinic acid	130.0862	$[M+H]^+$	7.76	C6H11NO2	2.9	2	-2.31	HMDB0000070
N-Acetylputrescine	131.1178	$[M+H]^+$	7.96	C6H14N2O	-1.4	1	-0.84	HMDB0002064
Creatine	132.0767	$[M+H]^+$	9.39	C4H9N3O2	-2.1	1	-2.90	HMDB0000064
Leucine	132.1019	$[M+H]^+$	7.87	C6H13NO2	-0.6	1	-1.52	HMDB0000687
Isoleucine	132.1019	$[M+H]^+$	9.01	C6H13NO2	-0.9	1	-1.71	HMDB0000172
Adenine	136.0617	$[M+H]^+$	4.07	C5H5N5	-2.8	1	-0.09	HMDB0000034
Hypoxanthine	137.0457	$[M+H]^+$	4.89	C5H4N4O	2	1	-1.11	HMDB0000157

Methylnicotinamide	137.0787	$[M+H]^+$	6.43	C7H9N2O	-1.8	2	-4.30	HMDB0000699
Tyramine	138.0913	$[M+H]^+$	4.77	C8H11NO	2.7	2	-0.14	HMDB0000306
Proline betaine	144.1019	$[M+H]^+$	12.43	C7H13NO2	2.2	2	-3.90	HMDB0004827
Indole-carboxaldehyde	146.0600	$[M+H]^+$	5.41	C9H7NO	-0.6	2	1.68	HMDB0029737
Allysine	146.0811	$[M+H]^+$	3.07	C6H11NO3	-1.2	2	-2.20	HMDB0001263
Guanidinobutanoic acid	146.0924	$[M+H]^+$	8.55	C5H11N3O2	-1.3	1	-1.50	HMDB0003464
Deoxycarnitine	146.1175	$[M+H]^+$	9.01	C7H15NO2	-0.1	2	-3.20	HMDB0001161
Acetylcholine	146.1254	$[M+H]^+$	3.99	C7H16NO2	0.4	1	-4.20	HMDB0000895
Coumaric acid	165.0546	$[M+H]^+$	2.54	C9H8O3	2.8	2	1.83	HMDB0001713
Glutamine	147.0764	$[M+H]^+$	6.22	C5H10N2O3	0.6	1	-3.64	HMDB0000641
Methyloxyindole	148.0756	$[M+H]^+$	2.24	C9H9NO	0	2	1.55	HMDB0004096
Methyladenine	150.0774	$[M+H]^+$	7.15	C6H7N5	-1.5	2	-0.31	HMDB0011600
N-Acetylhistamine	154.0974	$[M+H]^+$	5.35	C7H11N3O	-0.7	1	-1.20	HMDB0013253
Histidine	156.0767	$[M+H]^+$	12.89	C6H9N3O2	2.8	1	-3.32	HMDB0000177
Homostachydrine	158.1175	$[M+H]^+$	6.86	C8H15NO2	0.7	2	-3.40	HMDB0033433
Aminovaleric acid betaine	160.1332	$[M+H]^+$	8.96	C8H17NO2	-0.6	2	-3.50	HMDB0240732
Indole-carboxylic acid	162.0549	$[M+H]^+$	6.28	C9H7NO2	0.5	1	1.99	HMDB0003320
Carnitine	162.1124	$[M+H]^+$	9.28	C7H15NO3	2.2	1	-4.90	HMDB0000062
Nicotine	163.1229	$[M+H]^+$	4.26	C10H14N2	-1.8	2	1.16	HMDB0243542
Phenylalanine	166.0862	$[M+H]^+$	7.52	C9H11NO2	2.8	1	-1.38	HMDB0000159
Methylxanthine	167.0563	$[M+H]^+$	2.54	C6H6N4O2	0.4	2	-0.40	HMDB0010738
Pyridoxal	168.0655	$[M+H]^+$	8.66	C8H9NO3	2.2	2	0.02	HMDB0001545
Uric acid	169.0356	$[M+H]^+$	8.24	C5H4N4O3	2	1	-2.17	HMDB0000289
Pyridoxine	170.0811	$[M+H]^+$	3.15	C8H11NO3	0.8	1	-0.77	HMDB0000239
Methylhistidine	170.0924	$[M+H]^+$	14.52	C7H11N3O2	0	2	-3.10	HMDB0000001
Indoleacetic acid	176.0706	$[M+H]^+$	7.07	C10H9NO2	-1.9	2	1.87	HMDB0000197
Cotinine	177.1022	$[M+H]^+$	1.95	C10H12N2O	0.1	2	0.07	HMDB0001046
Nicotine-N-oxide	179.1178	$[M+H]^+$	5.78	C10H14N2O	-3	2	1.17	HMDB0001497
Hippuric acid	180.0655	$[M+H]^+$	4.31	C9H9NO3	-1.3	2	0.31	HMDB0000714
Glucosamine	180.0866	$[M+H]^+$	6.32	C6H13NO5	2.3	1	-2.70	HMDB0001514

Caffeic acid	181.0495	$[M+H]^+$	4.55	$C_9H_8O_4$	-1.5	2	1.15	HMDB0001964
Theobromine	181.0720	$[M+H]^+$	2.03	$C_7H_8N_4O_2$	0.6	2	-0.78	HMDB0002825
Theophylline	181.0720	$[M+H]^+$	4.61	$C_7H_8N_4O_2$	0.6	2	-0.02	HMDB0001889
Tyrosine	182.0811	$[M+H]^+$	7.66	$C_9H_{11}NO_3$	-2.9	1	-2.26	HMDB0000158
Pyridoxic acid	184.0604	$[M+H]^+$	6.80	$C_8H_9NO_4$	1.5	2	-0.08	HMDB0000017
N-Acetyllysine	189.1233	$[M+H]^+$	9.26	$C_8H_{16}N_2O_3$	2.6	1	-2.50	HMDB0000446
Dimethoxycinnamic acid	209.0804	$[M+H]^+$	3.97	$C_{11}H_{12}O_4$	-0.7	2	1.82	HMDB0034315
Hydroxyindole-acetic acid	192.0655	$[M+H]^+$	3.04	$C_{10}H_9NO_3$	-0.7	2	1.28	HMDB0000763
Caffeine	195.0876	$[M+H]^+$	1.69	$C_8H_{10}N_4O_2$	1.8	1	-0.07	HMDB0001847
Salicyluric Acid	196.0604	$[M+H]^+$	4.11	$C_9H_9NO_4$	-0.6	2	0.95	HMDB0000840
Hydroxyhippuric acid	196.0604	$[M+H]^+$	6.31	$C_9H_9NO_4$	2.2	2	0.95	HMDB0006116
Dimethylurate	197.0669	$[M+H]^+$	3.19	$C_7H_8N_4O_3$	1.7	2	-0.52	HMDB0001857
Dimethylarginine	203.1502	$[M+H]^+$	11.99	$C_8H_{18}N_4O_2$	-1.3	2	-2.90	HMDB0003334
Indole-butanoic acid	204.1019	$[M+H]^+$	3.77	$C_{12}H_{13}NO_2$	-0.3	2	2.30	HMDB0002096
O-Acetyl-carnitine	204.1230	$[M+H]^+$	7.64	$C_9H_{17}NO_4$	1.8	1	-2.40	HMDB0240773
Tryptophan	205.0971	$[M+H]^+$	7.27	$C_{11}H_{12}N_2O_2$	0.8	1	-1.06	HMDB0000929
N-Cinnamoylglycine	206.0811	$[M+H]^+$	3.82	$C_{11}H_{11}NO_3$	-1	2	1.42	HMDB0011621
Trimethyluric acid	211.0825	$[M+H]^+$	2.31	$C_8H_{10}N_4O_3$	2.2	2	-0.37	HMDB0002123
N-Acetylarginine	217.1295	$[M+H]^+$	11.4	$C_8H_{16}N_4O_3$	-1.7	1	-1.70	HMDB0004620
Propionylcarnitine	218.1386	$[M+H]^+$	6.56	$C_{10}H_{19}NO_4$	1.7	2	-2.30	HMDB0000824
Pantothenic acid	220.1179	$[M+H]^+$	5.10	$C_9H_{17}NO_5$	-2.1	1	-1.10	HMDB0000210
Butyryl carnitine	232.1543	$[M+H]^+$	5.72	$C_{11}H_{21}NO_4$	-0.4	2	-2.10	HMDB0002013
Indole-acetyl-alanine	247.1077	$[M+H]^+$	4.22	$C_{13}H_{14}N_2O_3$	-0.3	2	1.19	HMDB0304378
Tryptophan betaine	247.1441	$[M+H]^+$	4.79	$C_{14}H_{18}N_2O_2$	-1.8	2	-0.54	HMDB0061115
Phenylacetylglutamine	265.1182	$[M+H]^+$	5.57	$C_{13}H_{16}N_2O_4$	1.5	1	-0.35	HMDB0006344
Caffeoylcholine	266.1465	$[M+H]^+$	4.99	$C_{14}H_{20}NO_4$	-2.1	2	-0.43	-
Adenosine	268.1040	$[M+H]^+$	5.07	$C_{10}H_{13}N_5O_4$	-2.1	1	-1.05	HMDB0000050
N-Acetylcarnosine	269.1244	$[M+H]^+$	11.21	$C_{11}H_{16}N_4O_4$	-1.2	2	-0.93	HMDB0255058
Coumaroyl agmatine	277.1659	$[M+H]^+$	5.55	$C_{14}H_{20}N_4O_2$	-1.3	2	1.54	-
Methyladenosine	282.1196	$[M+H]^+$	7.45	$C_{11}H_{15}N_5O_4$	-2.1	2	-1.80	HMDB0243935

N-Acetylcytidine	286.1033	$[M+H]^+$	3.74	$C_{11}H_{15}N_3O_6$	-2.4	2	-1.40	HMDB0005923
Methylguanosine	298.1146	$[M+H]^+$	4.51	$C_{11}H_{15}N_5O_5$	-2.2	2	-1.80	HMDB0001563
Dimethylguanosine	312.1302	$[M+H]^+$	4.35	$C_{12}H_{17}N_5O_5$	-2.8	2	-1.80	HMDB0001961
Riboflavin	377.1455	$[M+H]^+$	3.85	$C_{17}H_{20}N_4O_6$	-1.7	1	-1.46	HMDB0000244
Cadaverine	103.1229	$[M+H]^+$	16.55	$C_5H_{14}N_2$	0.3	2	-0.27	HMDB0002322
Hordenine	166.1226	$[M+H]^+$	6.43	$C_{10}H_{15}NO$	0.2	2	1.76	HMDB0004366
N-(2-Furoyl)glycine	170.0447	$[M+H]^+$	7.23	$C_7H_7NO_4$	-0.8	2	0.10	HMDB0000439
Pterine	164.0566	$[M+H]^+$	7.12	$C_6H_5N_5O$	1.1	2	-0.86	HMDB0000802
Pyridoxamine	169.0971	$[M+H]^+$	8.34	$C_8H_{12}N_2O_2$	1.6	2	-1.20	HMDB0001431
Tryptophanol	191.1178	$[M+H]^+$	6.65	$C_{11}H_{14}N_2O$	-2.1	2	0.75	HMDB0244977

Table S-9. Metabolites identified in ESI$^-$ ionization mode.

Compound	Precursor ion [m/z]	Adduct	t_R [min]	Sum formula	Mass error [ppm]	Identification Level	logP value	HMDB ID
Glycolic acid	75.0087	$[M-H]^-$	9.41	C2H4O3	1.2	1	-1.11	HMDB0000115
Lactic acid	89.0244	$[M-H]^-$	8.32	C3H6O3	2.2	1	-0.47	HMDB0000190
Fumaric acid	115.0036	$[M-H]^-$	14.82	C4H4O4	-2.6	1	0.46	HMDB0000134
Succinic acid	117.0193	$[M-H]^-$	13.33	C4H6O4	0	1	-0.59	HMDB0000254
Hydroxyvaleric acid	117.0557	$[M-H]^-$	5.80	C5H10O3	1.4	1	0.04	HMDB0000531
Hydroxybenzaldehyde	121.0295	$[M-H]^-$	6.04	C7H6O2	-0.9	1	1.27	HMDB0011718
Salicylic alcohol	123.0451	$[M-H]^-$	5.79	C7H8O2	-2.6	1	1.03	-
Phosphoethanolamine	124.0169	$[M-H]^-$	8.90	C2H8NO3P	0	2	-1.50	HMDB0000224
Pyroglutamic acid	128.0353	$[M-H]^-$	8.90	C5H7NO3	2.9	1	-0.89	HMDB0000267
Itaconic acid	129.0193	$[M-H]^-$	12.15	C5H6O4	-2.8	1	0.35	HMDB0002092
Citraconic acid	129.0193	$[M-H]^-$	5.21	C5H6O4	-1.2	1	0.35	HMDB0000634
Ketoleucine	129.0557	$[M-H]^-$	3.04	C6H10O3	2.1	1	0.82	HMDB0000695
Isoleucine	130.0873	$[M-H]^-$	7.00	C6H13NO2	-0.1	1	-1.70	HMDB0000172
Leucine	130.0873	$[M-H]^-$	6.08	C6H13NO2	-0.7	1	-1.52	HMDB0000687
Methylsuccinic acid	131.0349	$[M-H]^-$	11.60	C5H8O4	2.7	1	0.13	HMDB0001844
Glutaric acid	131.0349	$[M-H]^-$	10.72	C5H8O4	2.8	1	-0.29	HMDB0000661
Hydroxy-methylpentanoate	130.0653	$[M-H]^-$	3.59	C6H11O3	2.2	2	0.54	-
Hypoxanthine	135.0312	$[M-H]^-$	2.93	C5H4N4O	0.7	1	-0.55	HMDB0000157
Salicylic acid	137.0244	$[M-H]^-$	5.32	C7H6O3	2.2	1	2.26	HMDB0001895
Urocanic acid	137.0356	$[M-H]^-$	5.15	C6H6N2O2	-3	2	0.22	HMDB0000301
Amino-methylhexanoic acid	144.1030	$[M-H]^-$	3.54	C7H15NO2	2.3	2	2.22	HMDB0031595
Methylglutaric acid	145.0506	$[M-H]^-$	12.18	C6H10O4	-1.5	2	0.33	HMDB0000752
Coumaraldehyde	147.0451	$[M-H]^-$	3.61	C9H8O2	0.6	2	2.06	HMDB0040986
Xanthine	151.0261	$[M-H]^-$	4.50	C5H4N4O2	-2.9	2	-0.65	HMDB0000292
Mandelic acid	151.0400	$[M-H]^-$	6.52	C8H8O3	1.5	2	0.62	HMDB0000703

Hydroxyphenylacetic acid	151.0400	$[M-H]^-$	3.19	C8H8O3	2.6	2	0.75	HMDB0000020
Gentisic acid	153.0193	$[M-H]^-$	5.01	C7H6O4	0.4	2	1.74	HMDB0000152
Dihydroxybenzoic acid	153.0193	$[M-H]^-$	3.49	C7H6O4	1.5	2	0.86	HMDB0013677
Hydroxymethylglutaric acid	161.0455	$[M-H]^-$	12.6	C6H10O5	-2.1	2	-0.75	HMDB0000355
Phenyllactic acid	165.0557	$[M-H]^-$	3.71	C9H10O3	-2.1	2	1.83	HMDB0000779
Homogentisic acid	167.0349	$[M-H]^-$	5.66	C8H8O4	-1.2	1	0.86	HMDB0000130
Vanillic acid	167.0349	$[M-H]^-$	6.83	C8H8O4	2.2	2	1.43	HMDB0000484
Pyridoxine	168.0666	$[M-H]^-$	2.76	C8H11NO3	-1.5	1	-0.77	HMDB0000239
Aconitate	173.0091	$[M-H]^-$	12.84	C6H6O6	-1.2	2	-0.14	HMDB0000072
Methoxyindole-carbaldehyde	174.0560	$[M-H]^-$	3.55	C10H9NO2	1.1	2	1.22	-
Ascorbic acid	175.0248	$[M-H]^-$	9.36	C6H8O6	1.2	1	-1.90	HMDB0000044
Caffeic acid	179.0349	$[M-H]^-$	7.59	C9H8O4	-1.8	2	1.15	HMDB0001964
Methyl vanillate	181.0506	$[M-H]^-$	5.37	C9H10O4	-0.6	2	1.52	HMDB0240266
Everninic Acid	181.0506	$[M-H]^-$	2.70	C9H10O4	2.8	2	1.55	-
Harman	181.0771	$[M-H]^-$	3.28	C12H10N2	2	2	3.10	HMDB0035196
Azelaic acid	187.0975	$[M-H]^-$	10.95	C9H16O4	0.8	1	1.57	HMDB0000784
Kynurenic acid	188.0353	$[M-H]^-$	4.17	C10H7NO3	0	1	1.16	HMDB0000715
Ferulic acid	193.0506	$[M-H]^-$	7.55	C10H10O4	0.1	2	1.51	HMDB0000954
Harmol	197.0720	$[M-H]^-$	3.35	C12H10N2O	-3	2	1.70	HMDB0034217
Indoxyl sulfate	212.0023	$[M-H]^-$	3.76	C8H7NO4S	-1.3	2	1.29	HMDB0000682
Uridine	243.0622	$[M-H]^-$	5.50	C9H12N2O6	-0.7	1	-1.98	HMDB0000296
Hydroxybutyric acid	103.0403	$[M-H]^-$	6.53	C4H8O3	-0.3	2	-0.51	HMDB0000710

Table S-10. MS Experiment Design

Experiment	*m/z* range	
	Positive mode	**Negative mode**
TOF-MS	70 - 1000	70 – 1000
SWATH-MS/MS 1	69.5 – 100.2	69.5 – 135.4
SWATH-MS/MS 2	99.2 – 122.6	134.4 – 163.3
SWATH-MS/MS 3	121.6 – 139.6	162.3 – 187.6
SWATH-MS/MS 4	138.6 – 156.6	186.6 – 204.4
SWATH-MS/MS 5	155.6 – 171.6	203.4 – 228.5
SWATH-MS/MS 6	170.6 – 189.6	227.5 – 254.9
SWATH-MS/MS 7	188.6 – 206.5	253.9 – 282.6
SWATH-MS/MS 8	205.5 – 222.6	281.6 – 311.5
SWATH-MS/MS 9	221.6 – 241.6	310.5 – 327.7
SWATH-MS/MS 10	240.6 – 259.6	326.7 – 346.6
SWATH-MS/MS 11	258.6 – 277.7	345.6 – 364.6
SWATH-MS/MS 12	276.7 – 300.6	363.6 – 379.7
SWATH-MS/MS 13	299.6 – 317.7	378.7 – 395.6
SWATH-MS/MS 14	316.7 – 332.3	394.6 – 411.7
SWATH-MS/MS 15	331.3 – 352.6	410.7 – 429.7
SWATH-MS/MS 16	351.6 – 371.6	428.7 – 447.7
SWATH-MS/MS 17	370.6 – 390.8	446.7 – 477.7
SWATH-MS/MS 18	389.8 – 411.7	476.7 – 508.7
SWATH-MS/MS 19	410.7 – 433.7	507.7 – 536.6
SWATH-MS/MS 20	432.7 – 465.5	535.6 – 571.7
SWATH-MS/MS 21	464.5 – 509.3	570.7 – 616.7
SWATH-MS/MS 22	508.3 – 555.7	615.7 – 669.6
SWATH-MS/MS 23	554.7 – 624.7	668.6 – 743.7
SWATH-MS/MS 24	623.7 – 729.2	742.7 – 843.1
SWATH-MS/MS 25	728.2 – 1000.5	842.1 – 1000.5

Table S-11. MS Dial Processing Settings

Parameter	Setting	
	Positive mode	**Negative mode**
Data collection range	0.5 – 19 min	0.5 – 19 min
Mass range	70 - 1000	70 – 1000
MS^1 Tolerance	0.01 Da	0.01 Da
MS/MS Tolerance	0.025 Da	0.025 Da
Smoothing level	2	2
Minimum peak width	5	5
Minimum peak height [cps]	100	100
Mass slice width	0.1 Da	0.1 Da

Table S-12. Statistics on significantly regulated metabolites (AKU vs control) detected in ESI^+ mode.

Metabolite	Fold Change	log2(FC)	p-value(FDR)	-log10(p-value)
Dimethoxycinnamic acid	3.78E+02	8.56E+00	1.45E-06	5.84E+00
5-Methylcytosine	4.85E+00	2.28E+00	1.88E-05	4.73E+00
Adenine	4.97E+01	5.63E+00	6.85E-17	1.62E+01
Allysine	1.19E+01	3.58E+00	6.71E-06	5.17E+00
Cadaverine	3.03E-01	-1.72E+00	2.00E-02	1.70E+00
Caffeic Acid	1.84E+01	4.20E+00	4.26E-09	8.37E+00
Choline	6.05E-02	-4.05E+00	5.23E-03	2.28E+00
Cytosine	3.45E+00	1.79E+00	1.22E-03	2.91E+00
Diethanolamine	5.05E+00	2.34E+00	2.59E-04	3.59E+00
Dimethylurate	4.39E+00	2.14E+00	2.10E-02	1.68E+00
Glutamine	2.28E+00	1.19E+00	3.54E-04	3.45E+00
Glycocyamine	3.88E+00	1.96E+00	9.65E-05	4.02E+00
Hordenine	1.16E+01	3.53E+00	2.54E-10	9.60E+00
Hydroxyhippuric acid	1.70E+01	4.09E+00	4.43E-13	1.24E+01
Hydroxyindole-acetic acid	2.94E+01	4.88E+00	6.85E-17	1.62E+01
Tryptophan betaine	2.27E+00	1.18E+00	1.20E-03	2.92E+00
Indole-acetyl-alanine	7.63E+00	2.93E+00	4.52E-09	8.34E+00
Indoleacetic acid	2.55E+01	4.67E+00	2.09E-05	4.68E+00
Isoleucine	8.41E+00	3.07E+00	1.45E-06	5.84E+00
Methylxanthine	4.26E+01	5.41E+00	1.59E-07	6.80E+00
Dimethylguanosine	4.15E+00	2.05E+00	1.12E-04	3.95E+00
N-(2-Furoyl)glycine	1.89E+02	7.56E+00	3.60E-12	1.14E+01
N-Acetylarginine	1.27E+01	3.67E+00	3.41E-06	5.47E+00
N-Acetylcytidine	2.47E+00	1.31E+00	7.17E-04	3.14E+00
N-Acetyllysine	1.43E-01	-2.80E+00	1.02E-04	3.99E+00
N-Cinnamoylglycine	5.35E+00	2.42E+00	4.96E-08	7.30E+00
Nicotinamide	2.20E+00	1.14E+00	4.90E-03	2.31E+00
Oxoproline	4.89E+00	2.29E+00	1.12E-07	6.95E+00
Phenylalanine	2.75E-01	-1.86E+00	1.16E-03	2.94E+00
Pipecolinic acid	4.26E+00	2.09E+00	1.39E-05	4.86E+00
Proline	3.35E+00	1.75E+00	1.06E-02	1.97E+00
Propionylcarnitine	2.74E-02	-5.19E+00	1.07E-08	7.97E+00
Pterine	2.80E+02	8.13E+00	3.18E-06	5.50E+00
Pyridoxamine	5.25E+01	5.71E+00	3.18E-17	1.65E+01
Salicyclic acid	8.06E+00	3.01E+00	2.08E-05	4.68E+00
Theophylline	6.20E+00	2.63E+00	3.90E-06	5.41E+00
Trimethylamine N-oxide	2.51E+00	1.33E+00	7.06E-05	4.15E+00
Trimethylurate	9.98E+00	3.32E+00	6.47E-05	4.19E+00
Tryptophan	6.87E+00	2.78E+00	1.07E-08	7.97E+00
Tryptophan betaine	2.40E+00	1.26E+00	2.16E-04	3.66E+00
Tryptophanol	4.09E+01	5.35E+00	6.71E-06	5.17E+00

Table S-13. Statistics on significantly regulated metabolites (AKU vs control) detected in ESI^- mode.

Metabolite	Fold Change	log2(FC)	p-value (FDR)	-log10(p-value)
Salicylic alcohol	1.28E+03	1.03E+01	1.11E-22	2.20E+01
Homogentisic acid	7.35E+02	9.52E+00	5.87E-19	1.82E+01
Salicylic acid	1.89E+01	4.24E+00	1.01E-18	1.80E+01
Everninic Acid	5.96E+01	5.90E+00	1.09E-18	1.80E+01
Succinic acid	1.68E+01	4.07E+00	1.44E-18	1.78E+01
Catechol	8.00E+00	3.00E+00	1.09E-13	1.30E+01
Hydroxybenzaldehyde	1.05E+01	3.39E+00	6.23E-13	1.22E+01
Caffeic acid	5.03E+01	5.65E+00	2.69E-11	1.06E+01
Methylsuccinic acid	1.82E+01	4.18E+00	1.87E-10	9.73E+00
Citraconic acid	9.04E+00	3.18E+00	3.63E-08	7.44E+00
Urocanic acid	8.83E+00	3.14E+00	3.71E-08	7.43E+00
Ferulic acid	1.68E+01	4.07E+00	1.10E-07	6.96E+00
Ketoleucine	5.65E+00	2.50E+00	1.10E-07	6.96E+00
Ascorbic acid	5.93E+02	9.21E+00	1.34E-06	5.87E+00
Xanthine	2.74E+00	1.45E+00	1.34E-06	5.87E+00
Indoxyl sulfate	2.92E+00	1.54E+00	3.38E-06	5.47E+00
Hippurate	1.94E-03	-9.01E+00	1.25E-05	4.90E+00
Uric acid	3.40E+01	5.09E+00	1.56E-05	4.81E+00
Gentisic acid	4.25E+00	2.09E+00	1.73E-05	4.76E+00
Lactic acid	3.97E+00	1.99E+00	2.08E-05	4.68E+00
Mandelic acid	5.66E+00	2.50E+00	2.60E-05	4.59E+00
Hydroxybutyric acid	2.82E+00	1.49E+00	2.84E-05	4.55E+00
Pyroglutamic acid	3.58E+00	1.84E+00	5.12E-05	4.29E+00
Tyrosine	2.23E+01	4.48E+00	1.82E-04	3.74E+00
Aconitate	3.81E+00	1.93E+00	1.82E-04	3.74E+00
Hydroxymethylglutaric acid	4.52E+00	2.18E+00	2.49E-04	3.60E+00
Glutaric acid	1.93E-02	-5.70E+00	6.67E-04	3.18E+00
Fumaric acid	1.14E+01	3.51E+00	2.03E-03	2.69E+00
Tryptophan	3.34E+00	1.74E+00	2.71E-03	2.57E+00
Hydroxyphenylacetic acid	2.02E+00	1.01E+00	3.58E-03	2.45E+00
Coumaraldehyde	2.50E+00	1.32E+00	3.84E-03	2.42E+00
Methylglutaric acid	2.25E+00	1.17E+00	9.05E-03	2.04E+00
Kynurenic acid	2.60E-02	-5.26E+00	1.61E-02	1.79E+00

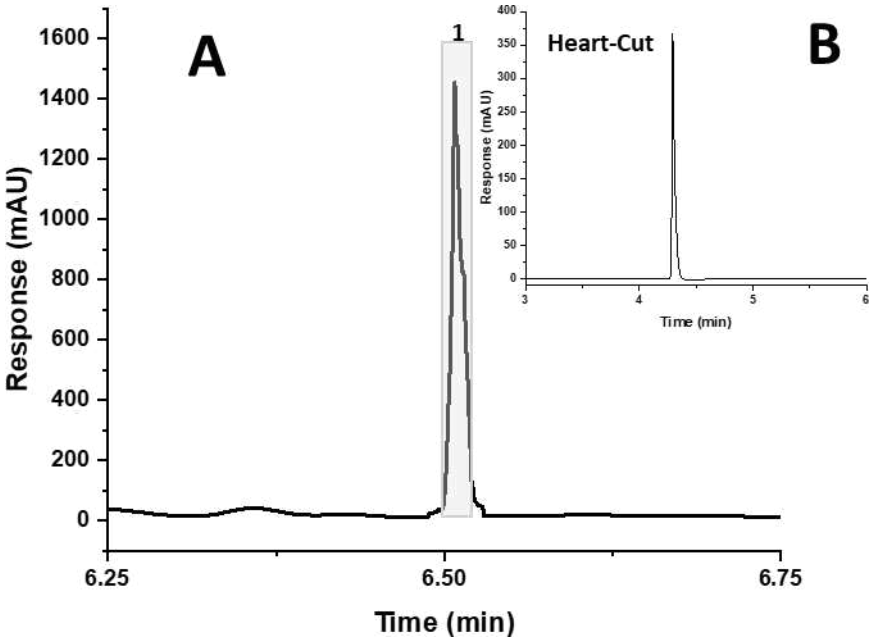

Figure S-1. LC-UV Chromatogram of HGA acquire during sample measurement via 2D-LC-QToF in the first dimension (1D). Heart cut labeled (1) and the LC-UV chromatogram acquired from heart cut during the second dimension (2D) labeled (Heart-Cut).

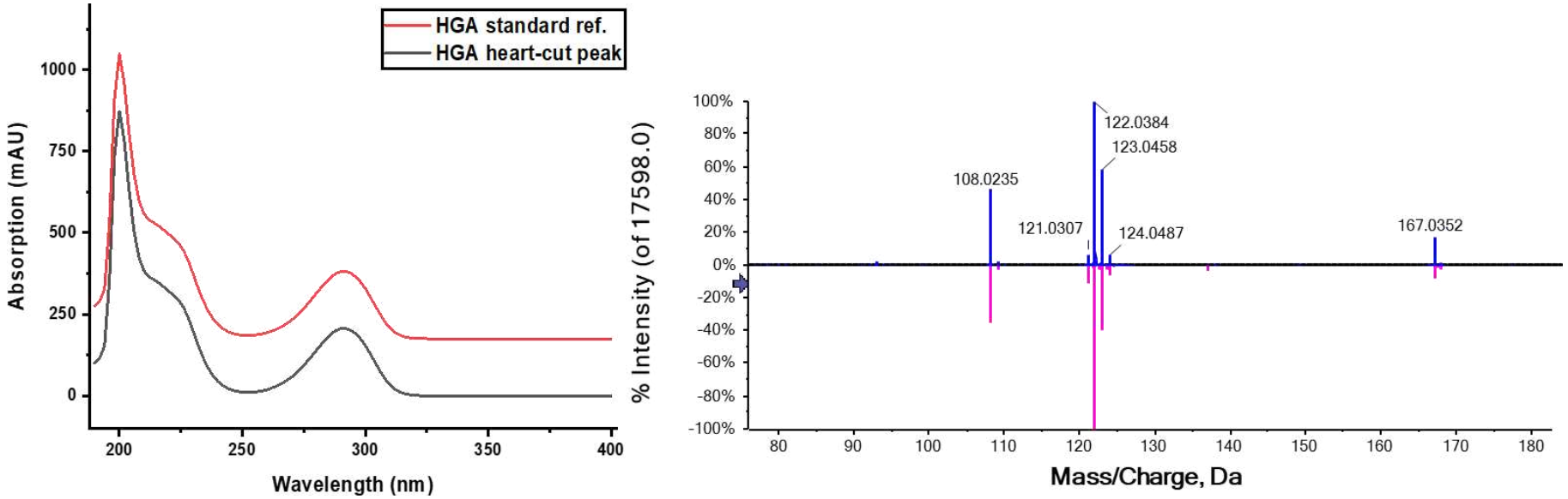

Figure S-2. UV spectra of HGA reference standard and HGA isolated peak via 2D-LC and MS2 Spectrum of HGA acquired during 2D-LC-UV-ESI-QToF-MS (blue colour) versus standard reference HGA spectrum (pink).

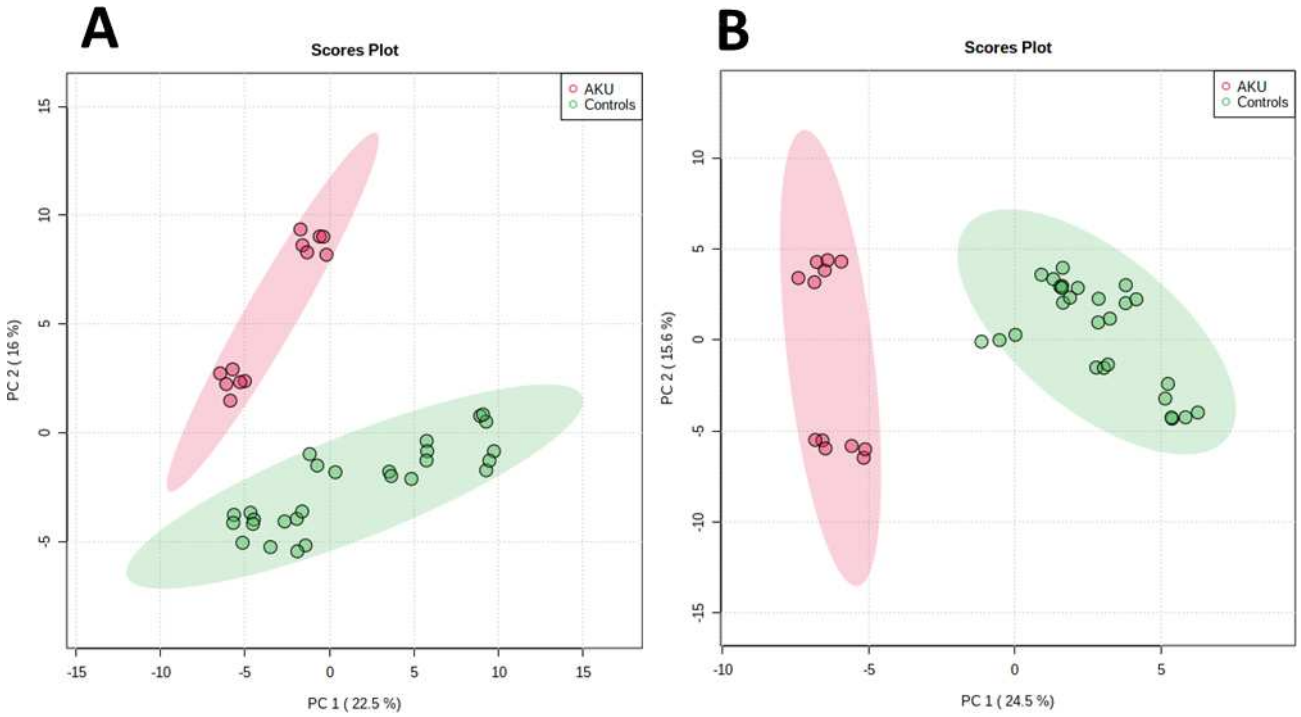

Figure S-3. Principal component analysis (PCA) of urine metabolome positive mode (A) and negative mode (B) UHPLC-HILIC-QToF-MS

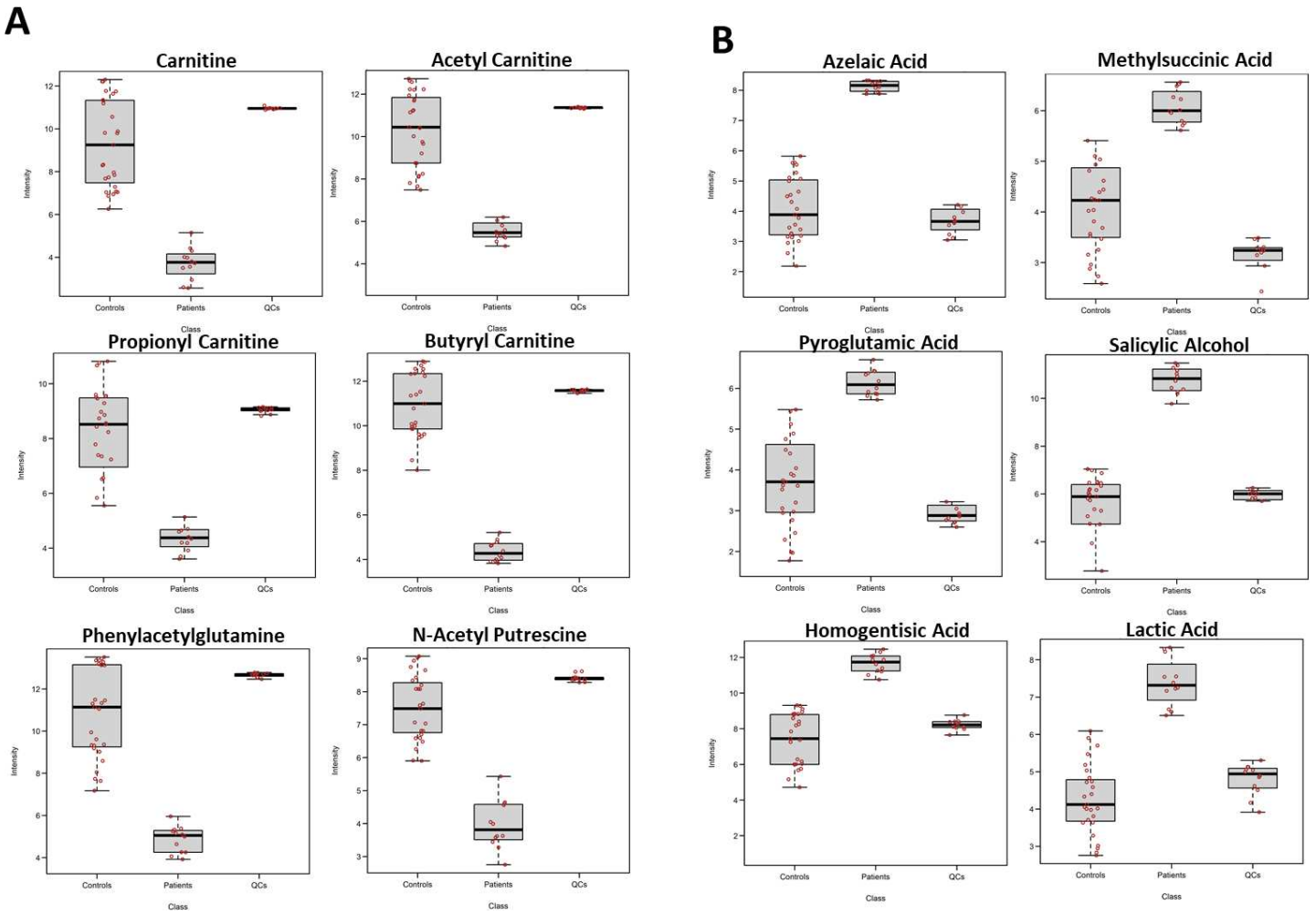

Figure S-4. Box plots of metabolites detected in ESI positive (A) and negative (B) ionization mode showing a significant statistical difference ($p < 0.05$) between both cohorts.

6. Acknowledgements

I would like to thank a significant amount of people who contributed to this thesis in various ways throughout the last years.

First of all, I deeply thank my supervisor Prof. Dr. Michael Lämmerhofer for giving me the opportunity to work in his group and for his endless support throughout my PhD thesis. Apart from the multitude of challenging and interesting research projects he provided, his endless support and guidance throughout the entire process contributed to a wonderful scientific environment during the years the work on this thesis was conducted. His trust and guidance are aspects I will forever be grateful for.

I would also like to thank Prof. Dr. Stefan Laufer for the second supervision and the evaluation of my thesis.

Many thanks go to Dr. Adrian Sievers-Engler, not only for his lovely sense of humour and daily dose of sarcasm, but for him acting as a mentor and sharing his vast knowledge and experience with me about analytical chemistry. Adrian was always there when I faced trouble in technical and analytical aspects and is one of the most important people who helped me pull through with any challenges that involved analytical chemistry.

I am very grateful for my former colleagues, specifically my office buddies Adrian Brun, Dr. Xiaoqing Fu and Min Su, as well as Matthias Olfert, Peng Li and Ryan Karongo for the good time we had. Furthermore, I would like to appreciate the work of our secretaries, without whom I would have never been able to find my way around the system – Michaela Friedrichs and Eveline Wachendorfer.

A special thank you goes to all of my close friends who were there for me during good and bad times.

Finally, I wish to thank my parents, Silvia and Georgi, for giving me the possibility of a new life by coming to Germany and making this entire scientific adventure possible. My brother, Andrian, for being the person by my side and able to rely on him about everything at any time. Without them and their support, the accomplished so far would have merely remained a dream.

“Where ignorance is bliss, ´tis folly to be wise.”

Thomas Gray